



**Cranial Form Evolution and Functional Adaptations to Diet
among Papionins: A Comparative Study combining Quantitative
Genetics, Geometric Morphometrics, and Finite Element Analysis**

António Miguel Guarita Pires Rosa Prôa

Submitted in partial fulfilment of the requirements for the degree of

Doctor of Philosophy in Human Sciences

The University of Hull *and* The University of York

The Hull York Medical School

July 2013

Abstract

This thesis aims to study the evolution of cranial form and its biomechanical adaptation to the function of feeding in papionins, a group of primates with well-established phylogeny, large variations in cranial form, and well known ecologies and diets. The thesis firstly tests the hypothesis of evolutionary divergence of papionin cranial forms by random genetic drift with a quantitative genetic model (previously tested for acceptable type I error rates); if rejected, different cranial forms should reflect adaptations to the particular biomechanical demands of different diets. To study those adaptations, hypotheses about the cranial biomechanical performance under biting loads are then formulated in terms of the diet of each papionin species and tested using 3D finite element models and geometric morphometrics. Large scale deformations and cranial form are assessed using landmarks distributed over the cranium, and local strain distributions are assessed visually. Lastly, the association between cranial form, biomechanical parameters and diet among papionin species is tested using partial least squares. Results show that papionin cranial forms did not diverge by random genetic drift alone and thus adaptation must have occurred. When testing for biomechanical adaptation to biting, there are differences in cranial deformations between durophagous and graminivorous species, each with particular adaptations in the cranium that are thus apparent in cranial strains and deformations. Another striking result is that male and female crania of a single species (eating the same foods) deform similarly, albeit having different forms. The cranium of the phylogenetic outgroup *Macaca* deforms differently from all other papionins, but generally cranial deformations do not follow the phylogenetic relationship among papionins. Finally, a statistically significant association is found between cranial form and cranial deformations, and between diet and cranial form. Bite force and deformations show a less clear association with diet.

Table of Contents

Abstract	2
Table of Contents	3
List of Figures	7
List of Tables	10
Acknowledgements	15
Author's Declaration	17
Chapter 1. Introduction and Background	19
1.1. Motivation and Objectives	19
1.2. Form and Function	21
1.2.1. Evolution of Form and Function	22
1.2.2. Analysis of Form and Function	26
1.2.3. Material Properties and Architecture of Bone	28
1.2.4. Functional Adaptation of Bone	31
1.2.5. Biomechanics of Support and Movement	34
1.2.6. Form, Function and Size	35
1.3. Papionin Biology	36
1.3.1. Papionin Evolution and Classification	37
1.3.2. Papionin Distribution and Ecology	39
1.3.3. Papionin Diets and Feeding Strategies	41
1.3.4. Papionin Anatomical Terminology	46
1.3.5. Papionin Cranial Form and Anatomy	47
1.3.6. Papionin Masticatory Muscle Anatomy	49
1.4. Adaptations to Diet and Cranial Form Evolution	52
1.4.1. Concept of Adaptation	52
1.4.2. Physical Properties of Foods	54
1.4.3. Papionin Cranial Adaptations to Diet	55
1.4.4. Functional Hypotheses of Papionin Cranial Form Evolution	59
1.5. Summary	63

Chapter 2. Overview of Methods	64
2.1. Introduction	64
2.2. Quantitative Genetic Analysis	64
2.3. Geometric Morphometric Analysis	66
2.3.1. Landmarks.....	66
2.3.2. Shape and Form	68
2.3.3. Procrustes Superimposition: Generalized Procrustes Analysis.....	69
2.3.4. The Thin-plate Spline.....	72
2.4. Finite Element Analysis.....	74
2.4.1. Pre-processing: Finite Element Model Building.....	76
2.4.2. Pre-processing: Material Properties and Boundary Conditions.....	77
2.4.3. Solution and Post-processing.....	78
2.4.4. Validation and Sensitivity	79
2.5. Landmark-based Deformations Analysis	81
2.5.1. Landmark Displacement in Finite Element Analysis.....	81
2.5.2. Scaling to Bite Force.....	83
2.5.3. Visualizing Deformation	84
2.6. Multivariate Statistical Analysis.....	84
2.6.1. Principal Components Analysis	85
2.6.2. Partial Least Squares Analysis	85
2.6.3. Statistical Significance Tests.....	86
2.7. Summary	87
Chapter 3. Simulating Type I Error Rates for Testing Random Genetic Drift with Phenotypic Covariance Matrices.....	88
3.1. Introduction	88
3.2. Material and Methods.....	92
3.2.1. Simulation Model 1.....	93
3.2.2. Simulation Model 2.....	94
3.2.3. Simulation Model 3.....	95
3.2.4. Simulation Model 4.....	96
3.2.5. Simulation Model 5.....	97
3.2.6. Genetic Drift Test.....	99
3.3. Results	100
3.4. Discussion	107

Chapter 4. Testing the Role of Random Genetic Drift in the Evolutionary Divergence of Papionin Crania.....	112
4.1. Introduction	112
4.2. Material and Methods.....	114
4.2.1. Sample Data Set	114
4.2.2. Genetic Drift Test.....	116
4.3. Results	118
4.4. Discussion	119
Chapter 5. Building Three-dimensional Models of Papionin Crania for Finite Element Analysis.....	121
5.1. Introduction	121
5.2. Building 3D Models of Papionin Crania.....	125
5.2.1. Sample Specimens	125
5.2.2. Image Segmentation.....	126
5.2.3. Boundary Conditions	128
5.3. Model solution: bite force and landmarks.....	134
5.3.1. Maximum Bite Force	136
5.3.2. Landmarks and Visualizing Deformations.....	136
5.4. Discussion	140
Chapter 6. Testing the Effects of Model Building Decisions on the Results of Finite Element Analysis.....	143
6.1. Introduction	143
6.2. Material and Methods.....	146
6.2.1. Differences in Internal Architecture.....	146
6.2.2. Differences in Jaw Joint Constraint	147
6.2.3. Differences in Estimated Muscle Force	148
6.3. Results	149
6.3.1. Differences in Internal Architecture.....	150
6.3.2. Differences in Jaw Joint Constraint	153
6.3.3. Differences in Estimated Muscle Force	156
6.4. Discussion	159

Chapter 7. Comparative Studies of Cranial Biomechanical Performance under Biting Loads among Papionins	162
7.1. Introduction	162
7.2. Material and Methods.....	167
7.3. Results	169
7.3.1. Among Durophagous Genera.....	169
7.3.2. Omnivorous <i>versus</i> Graminivorous	174
7.3.3. Male <i>versus</i> Female.....	179
7.3.4. Durophagous <i>versus</i> Graminivorous.....	182
7.3.5. All Models.....	187
7.4. Discussion	190
 Chapter 8. The Association between Diet, Cranial Form, Maximum Bite Force, and Cranial Deformations in Papionins	194
8.1. Introduction	194
8.2. Material and Methods.....	195
8.3. Results	197
8.3.1. Diet <i>versus</i> Cranial Form	199
8.3.2. Diet <i>versus</i> Maximum Bite Force	201
8.3.3. Diet <i>versus</i> Cranial Deformations.....	203
8.3.4. Cranial Form <i>versus</i> Maximum Bite Force.....	206
8.3.5. Cranial Form <i>versus</i> Cranial Deformations	208
8.4. Discussion	210
 Chapter 9. Conclusion.....	212
9.1. Summary of Key Findings	212
9.2. Implications for Future Research	215
 Literature Cited	220
Appendix A. Complete Taxonomy of Papionins.....	256
Appendix B. R Functions used in Chapters 3 and 4	258
Appendix C. Published Research Paper.....	262
Appendix D. Strain values from Chapter 6.....	274
Appendix E. Strain values from Chapter 7	289

List of Figures

Figure 1.1. Load-deformation curve	29
Figure 1.2. Major stresses shown on a cat humerus.....	31
Figure 1.3. Consensus phylogenetic tree of the papionin monkeys.....	38
Figure 1.4. Geographic distribution of the papionin species used in this study	40
Figure 1.5. Representation of the skull of an adult male <i>Papio</i> sp.	48
Figure 1.6. Masticatory muscle anatomy of an adult male <i>Papio</i> sp.	50
Figure 2.1. Procrustes superimposition: the three steps.....	71
Figure 2.2. A schematic simplification of steps in finite element analysis (FEA).....	75
Figure 3.1. Simulation of genetic drift in four populations.....	98
Figure 3.2. Type I error rates for the simulated analyses with varying sample sizes and t/N_e ratios (drift intensities).....	101
Figure 3.3. Type I error rates for the simulated analyses with varying sample sizes and t/N_e ratios (drift intensities)	103
Figure 3.4. Slopes (β) of the Ackermann and Cheverud test	106
Figure 3.5. Type I error rates for the simulated analyses under model 4 with varying $\sigma^2_{\max E}/\sigma^2_{\max G}$, sample sizes and t/N_e ratios (drift intensities).....	111
Figure 4.1. Set of 46 landmarks on the midline and left side showed on the surface of a male <i>Theropithecus gelada</i> cranium	116
Figure 4.2. Phylogenetic tree showing the 6 analyses performed.....	118
Figure 5.1. Origin and insertion of the temporal muscle	123
Figure 5.2. Left panel: Origin and insertion of the masseter muscle in a specimen of <i>Macaca mulatta</i> ; right panel: Coronal section at the ramus of the mandible	124
Figure 5.3. Origin and insertion of the medial pterygoid muscle	124
Figure 5.4. Anatomical cross sectional area (ACSA) of the temporal muscle.....	129
Figure 5.5. Estimation of the anatomical cross sectional area (ACSA) of the masseter muscle	131
Figure 5.6. Estimation of the anatomical cross sectional area (ACSA) of the medial pterygoid muscle	131
Figure 5.7. Example of a fully built FEA model before solution.....	133
Figure 5.8. Results of a finite element analysis	137

Figure 5.9. PCA showing cranial deformations after bites	139
Figure 6.1. Cross-section through two differently built models	147
Figure 6.2. Von Mises' strain contour plots of the male <i>Theropithecus gelada</i> : filled, unfilled, and modified jaw joint constraint	151
Figure 6.3. PCA of deformations with the two models of <i>Theropithecus gelada</i> with different internal architecture, filled and unfilled, among other species models	152
Figure 6.4. Displacement (deformation plus rigid body motions) when the model is (A) constrained in all three axes in both sides of the jaw joint, and (B) constrained in the working side only in the vertical axis	154
Figure 6.5. PCA of deformations with the two models of <i>Theropithecus gelada</i> with different jaw joint constraints, among other species models	155
Figure 6.6. Von Mises' strain contour plots of the male <i>Theropithecus gelada</i> model with ACSA muscle forces and two other load cases	157
Figure 6.7. PCA of deformations with the <i>Theropithecus gelada</i> model loaded with different muscle load cases (Table 6.1) and showed among other species models.....	158
Figure 7.1. The crania of male and female of two species of long-faced papionins.....	164
Figure 7.2. Von Mises' strain contour plots of three cranial models of durophagous genera: <i>Cercocebus</i> , <i>Lophocebus</i> and <i>Mandrillus</i>	171
Figure 7.3. Cranial deformations among durophagous genera visualized using PCA of size-and-shape variables.....	172
Figure 7.4. Visualization of differences in deformations due to two bites (I1 and M3) between specimen pairs.....	173
Figure 7.5. Von Mises' strain contour plot of omnivorous (<i>P. anubis</i> , <i>P. hamadryas</i>) and graminivorous species (<i>T. gelada</i>)	176
Figure 7.6. Cranial deformations between omnivorous (<i>P. anubis</i> , <i>P. hamadryas</i>) and graminivorous species (<i>T. gelada</i>) visualized using PCA of size-and-shape variables	177
Figure 7.7. Visualization of differences in deformations due to two bites (I1 and M3) between specimen pairs.....	178
Figure 7.8. Von Mises' strain contour plots of models representing male (m) and female (f) of the species <i>P. anubis</i> and <i>T. gelada</i>	180
Figure 7.9. Cranial deformations between male and female in two papionin species (<i>P. anubis</i> and <i>T. gelada</i>) visualized using PCA of size-and-shape variables	181
Figure 7.10. Von Mises' strain contour plot of the durophagous species <i>Cercocebus torquatus</i> and the graminivorous species <i>Theropithecus gelada</i> (male).....	184

Figure 7.11. Cranial deformations between the durophagous species <i>Cercocebus torquatus</i> and the graminivorous species <i>Theropithecus gelada</i> (male) visualized using PCA of size-and-shape variables.....	185
Figure 7.12. Visualization of differences in deformations due to two bites (I1 and M3) between specimen pairs.....	186
Figure 7.13. Summary of Von Mises' strain contour plots of all models.....	188
Figure 7.14. Cranial deformations of the whole sample visualized using PCA of size-and-shape variables	189
Figure 8.1. Scatter plot of the 9 principal component score vectors that describe cranial deformations of the whole sample visualized using a PCA.....	198
Figure 8.2. PLS analysis of cranial form and dietary categories	200
Figure 8.3. PLS analysis of maximum bite force and diet.....	202
Figure 8.4. PLS analysis of cranial deformations and diet	204
Figure 8.5. Visualization of deformations between the two extremes of deformation along PLS1	205
Figure 8.6. PLS analysis of maximum bite force and cranial form	207
Figure 8.7. PLS analysis of cranial deformations and cranial form.....	209
Figure 9.1. Cranial deformations excluding landmarks on the zygomatic arch of the whole sample visualized using a preliminary PCA of size-and-shape variables	217

List of Tables

Table 1.1 Dietary categorization of papionin species used in this study	45
Table 3.1. Type I error rates for the genetic drift test using simulation model 5 (1000 repetitions).....	107
Table 4.1. Landmarks used for the random genetic drift test.....	115
Table 5.1. Dry crania specimens used to build models.	126
Table 5.2. Computerized tomography (CT) image resolution.	127
Table 5.3. Estimated muscle anatomical cross-sectional area (ACSA) and muscle forces.	132
Table 5.4. Estimated anterior and posterior temporal parameters.....	132
Table 5.5a. Bite forces and jaw joint reaction forces, as computed from FEA.....	135
Table 5.5b. Bite forces and jaw joint reaction forces (continued).....	135
Table 5.6. Landmarks for deformations analyses used in subsequent chapters.	138
Table 6.1. Muscle force magnitudes of different load cases of the same model.....	148
Table 6.2. Bite forces and jaw joint reaction forces of the models in this chapter.	149
Table 7.1. Cranium and rostrum lengths of the models	167
Table 8.1. Proportion of each food category consumed per species	197
Table 8.2. Singular values with P-values, percentage of total covariance explained by each axis, and pairwise correlations of PLS scores between cranial form and diet with P-values.....	199
Table 8.3. Singular values with P-values, percentage of total covariance explained by each axis, and pairwise correlations of PLS scores between maximum bite force and diet with P-values.....	201
Table 8.4. Singular values with P-values, percentage of total covariance explained by each axis, and pairwise correlations of PLS scores between cranial deformations and diet with P-values.....	203
Table 8.5. Singular values with P-values, percentage of total covariance explained by each axis, and pairwise correlations of PLS scores between maximum bite force and cranial form with P-values	206

Table 8.6. Singular values with P-values, percentage of total covariance explained by each axis, and pairwise correlations of PLS scores between cranial deformations and cranial form with P-values	208
Table D.1. Maximum (ϵ_1) and minimum (ϵ_3) principal strain values at the location of 70 landmarks during first incisor (I1) bite load for the filled, unfilled and jaw joint constraint sensitivity tests	275
Table D.2. Maximum (ϵ_1) and minimum (ϵ_3) principal strain values at the location of 70 landmarks during second incisor (I2) bite load for the filled, unfilled and jaw joint constraint sensitivity tests	276
Table D.3. Maximum (ϵ_1) and minimum (ϵ_3) principal strain values at the location of 70 landmarks during first premolar (P3) bite load for the filled, unfilled and jaw joint constraint sensitivity tests	277
Table D.4. Maximum (ϵ_1) and minimum (ϵ_3) principal strain values at the location of 70 landmarks during second premolar (P4) bite load for the filled, unfilled and jaw joint constraint sensitivity tests	278
Table D.5. Maximum (ϵ_1) and minimum (ϵ_3) principal strain values at the location of 70 landmarks during first molar (M1) bite load for the filled, unfilled and jaw joint constraint sensitivity tests	279
Table D.6. Maximum (ϵ_1) and minimum (ϵ_3) principal strain values at the location of 70 landmarks during second molar (M2) bite load for the filled, unfilled and jaw joint constraint sensitivity tests	280
Table D.7. Maximum (ϵ_1) and minimum (ϵ_3) principal strain values at the location of 70 landmarks during third molar (M3) bite load for the filled, unfilled and jaw joint constraint sensitivity tests	281
Table D.8. Maximum (ϵ_1) and minimum (ϵ_3) principal strain values at the location of 70 landmarks during first incisor (I1) bite load for the varying muscle force load cases sensitivity tests	282
Table D.9. Maximum (ϵ_1) and minimum (ϵ_3) principal strain values at the location of 70 landmarks during second incisor (I2) bite load for the varying muscle force load cases sensitivity tests	283
Table D.10. Maximum (ϵ_1) and minimum (ϵ_3) principal strain values at the location of 70 landmarks during first premolar (P3) bite load for the varying muscle force load cases sensitivity tests.....	284

Table D.11. Maximum (ϵ_1) and minimum (ϵ_3) principal strain values at the location of 70 landmarks during second premolar (P4) bite load for the varying muscle force load cases sensitivity tests.....	285
Table D.12. Maximum (ϵ_1) and minimum (ϵ_3) principal strain values at the location of 70 landmarks during first molar (M1) bite load for the varying muscle force load cases sensitivity tests	286
Table D.13. Maximum (ϵ_1) and minimum (ϵ_3) principal strain values at the location of 70 landmarks during second molar (M2) bite load for the varying muscle force load cases sensitivity tests.....	287
Table D.14. Maximum (ϵ_1) and minimum (ϵ_3) principal strain values at the location of 70 landmarks during third molar (M3) bite load for the varying muscle force load cases sensitivity tests	288
Table E.1. Maximum (ϵ_1) and minimum (ϵ_3) principal strain values at the location of 70 landmarks during first incisor (I1) bite load for the 3 models of durophagous species	290
Table E.2. Maximum (ϵ_1) and minimum (ϵ_3) principal strain values at the location of 70 landmarks during second incisor (I2) bite load for the 3 models of durophagous species	291
Table E.3. Maximum (ϵ_1) and minimum (ϵ_3) principal strain values at the location of 70 landmarks during first premolar (P3) bite load for the 3 models of durophagous species	292
Table E.4. Maximum (ϵ_1) and minimum (ϵ_3) principal strain values at the location of 70 landmarks during second premolar (P4) bite load for the 3 models of durophagous species	293
Table E.5. Maximum (ϵ_1) and minimum (ϵ_3) principal strain values at the location of 70 landmarks during first molar (M1) bite load for the 3 models of durophagous species	294
Table E.6. Maximum (ϵ_1) and minimum (ϵ_3) principal strain values at the location of 70 landmarks during second molar (M2) bite load for the 3 models of durophagous species	295
Table E.7. Maximum (ϵ_1) and minimum (ϵ_3) principal strain values at the location of 70 landmarks during third molar (M3) bite load for the 3 models of durophagous species	296
Table E.8. Maximum (ϵ_1) and minimum (ϵ_3) principal strain values at the location of 70 landmarks during first incisor (I1) bite load for the 3 models of baboon species.....	297
Table E.9. Maximum (ϵ_1) and minimum (ϵ_3) principal strain values at the location of 70 landmarks during second incisor (I2) bite load for the 3 models of baboon species	298

Table E.10. Maximum (ϵ_1) and minimum (ϵ_3) principal strain values at the location of 70 landmarks during first premolar (P3) bite load for the 3 models of baboon species	299
Table E.11. Maximum (ϵ_1) and minimum (ϵ_3) principal strain values at the location of 70 landmarks during second premolar (P4) bite load for the 3 models of baboon species	300
Table E.12. Maximum (ϵ_1) and minimum (ϵ_3) principal strain values at the location of 70 landmarks during first molar (M1) bite load for the 3 models of baboon species	301
Table E.13. Maximum (ϵ_1) and minimum (ϵ_3) principal strain values at the location of 70 landmarks during second molar (M2) bite load for the 3 models of baboon species	302
Table E.14. Maximum (ϵ_1) and minimum (ϵ_3) principal strain values at the location of 70 landmarks during third molar (M3) bite load for the 3 models of baboon species	303
Table E.15. Maximum (ϵ_1) and minimum (ϵ_3) principal strain values at the location of 70 landmarks during first incisor (I1) bite load for the models of male and female <i>P. anubis</i> and <i>T. gelada</i> species	304
Table E.16. Maximum (ϵ_1) and minimum (ϵ_3) principal strain values at the location of 70 landmarks during second incisor (I2) bite load for the models of male and female <i>P. anubis</i> and <i>T. gelada</i> species	305
Table E.17. Maximum (ϵ_1) and minimum (ϵ_3) principal strain values at the location of 70 landmarks during first premolar (P3) bite load for the models of male and female <i>P. anubis</i> and <i>T. gelada</i> species	306
Table E.18. Maximum (ϵ_1) and minimum (ϵ_3) principal strain values at the location of 70 landmarks during second premolar (P4) bite load for the models of male and female <i>P. anubis</i> and <i>T. gelada</i> species	307
Table E.19. Maximum (ϵ_1) and minimum (ϵ_3) principal strain values at the location of 70 landmarks during first molar (M1) bite load for the models of male and female <i>P. anubis</i> and <i>T. gelada</i> species	308
Table E.20. Maximum (ϵ_1) and minimum (ϵ_3) principal strain values at the location of 70 landmarks during second molar (M2) bite load for the models of male and female <i>P. anubis</i> and <i>T. gelada</i> species	309
Table E.21. Maximum (ϵ_1) and minimum (ϵ_3) principal strain values at the location of 70 landmarks during third molar (M3) bite load for the models of male and female <i>P. anubis</i> and <i>T. gelada</i> species	310

Table E.22. Maximum (ϵ_1) and minimum (ϵ_3) principal strain values at the location of 70 landmarks during first incisor (I1) bite load for the models of a durophagous, a graminivorous and <i>Macaca</i> species	311
Table E.23. Maximum (ϵ_1) and minimum (ϵ_3) principal strain values at the location of 70 landmarks during second incisor (I2) bite load for the models of a durophagous, a graminivorous and <i>Macaca</i> species	312
Table E.24. Maximum (ϵ_1) and minimum (ϵ_3) principal strain values at the location of 70 landmarks during first premolar (P3) bite load for the models of a durophagous, a graminivorous and <i>Macaca</i> species	313
Table E.25. Maximum (ϵ_1) and minimum (ϵ_3) principal strain values at the location of 70 landmarks during second premolar (P4) bite load for the models of a durophagous, a graminivorous and <i>Macaca</i> species	314
Table E.26. Maximum (ϵ_1) and minimum (ϵ_3) principal strain values at the location of 70 landmarks during first molar (M1) bite load for the models of a durophagous, a graminivorous and <i>Macaca</i> species	315
Table E.27. Maximum (ϵ_1) and minimum (ϵ_3) principal strain values at the location of 70 landmarks during second molar (M2) bite load for the models of a durophagous, a graminivorous and <i>Macaca</i> species	316
Table E.28. Maximum (ϵ_1) and minimum (ϵ_3) principal strain values at the location of 70 landmarks during third molar (M3) bite load for the models of a durophagous, a graminivorous and <i>Macaca</i> species	317

Acknowledgements

When I came to the Hull York Medical School (HYMS), at the University of York, in November 2009, I knew I was starting an entirely new stage of my life, a stage strewn with actors who would either take off their masks before me or wear them at all times. I had the good fortune of having the maskless by far outrank the masked on this stage. I wish to thank them from the bottom of my heart, and as the curtain closes, I offer a grand round of applause:

To my supervisors, Paul O'Higgins and Leandro Monteiro, who not only made me learn (almost from scratch) everything I have put into this thesis, they were also always kind and fair, and a model for my future career. Also to the chair of my thesis advisory pannel, Sarah Elton, sharp and strict; and to Samuel Cobb, who always had a wise counsel (and always made available his tremendous library).

To the Programa Doutoral em Biologia Computacional 2008 (PDBC), where I learned immensely and made friends for life. It was one of the best social experiences I ever had. To the Director of PDBC, Jorge Carneiro, without whom being chosen for PDBC and then doing a PhD in York would not have been possible. And to Manuela Cordeiro, whose assistance with the all-prevailing paperwork of PDBC and PhD was invaluable in so many occasions. Also to the Instituto Gulbenkian de Ciência (IGC) for hosting PDBC in such an engaging science environment, and to the IGC people for making it so.

To the funding agency, Fundação para a Ciência e a Tecnologia, Portugal, for providing me (through PDBC) with sufficient funds (bolsa de doutoramento SFRH/BD/33852/2009) to come and do PhD research in HYMS.

To colleagues of every order who were part of the Centre for Anatomical and Human Sciences (CAHS) while I was in HYMS, some of whom I now call friends: Laura Fitton (who taught me everything I know about finite element analysis), Jason Dunn (also an irreplaceable flat mate), Viviana Toro Ibacache, Carlo Meloro, Hester Baverstock, Eline van Asperen, Ekaterina Bulygina Stansfield, Erica Kempf, Thomas Needs, Anthony Walmsley, Karen Swan, Han Cao, Elizabeth Kerr, Ricardo Godinho, Philip Cox, Andrew McIntosh, Thomas Püschel, Philip Morris. And to visitors in CAHS, who one way or another were part of my PhD experience and made me carry

on: Laurent Puymeraill, Fabio Di Vincenzo, Sarah DeGroot, Iannis Sarris, Jasmina Ludoški, Andrei Evteev, Olga Nanova, Wataru Yano, Debora Martínez Salmerón; and our yearly delightful visitors Charles Oxnard and Nick Milne. And to our most excellent administrative staff, Roxana Freeman, Jackie Houlton, Elaine Brookes, Gill Pulpher, Lauren Mathews, Kit Fan, Victoria Hill and the rest of HYMS staff.

It is only fair to acknowledge also the people who wrote several software packages I used extensively and without which I could have not accomplished my PhD: Helgi Gunarsson (EVAN Toolbox), Jun Fen Liu and Michael Fagan (VOX-FE), the people who developed Avizo, ImageJ, Microsoft Office 2010, Mendeley, Open Office, Putty, Past, the R environment and many of its functions. And also our IT officers in HYMS Jeffrey Barber and Ade Hollingsworth.

To the people I have met and befriended while a PhD student in York, even if not connected directly with the PhD: Beatrice Demarchi, Flora Gröning, Ashley Coutu, Richard Palliser, Jos Woolley, Karine Taché, Holly Wright, Ralf Bockmann, Igor Gutiérrez Zugasti, André Colonese, Grazia Sciacchitano, Stefania Merlo Perring, Hannah Koon, Akis Nezis, Richard Allen, David Broughton, Adele Meloro.

To Sara Melo, who was with me through a large part of my PhD, and put up with me through the brightest and darkest periods of this play. And to our friends, who we would not have met if not in York: André Freire, Artur Gomes, Luís Rodrigues, Pedro Ribeiro, Benjamin Craddock, Maria Matos Silva, Manuel Sarmento, Pedro Silva, Pedro Burmester Campos, Frank Soboczanski.

To my friends outside York, longtime friends or more recent acquaintances that quickly became part of my life, all of whom made bearable being on this PhD stage and made me carry on: Luís Luz, Liliana Ribeiro dos Santos, Carlos Afonso, Liliana Pereira, Cláudia Martinho, Tiana Gonçalves, Filipa Barbosa, Rui Costa, Márcio Baptista, Sophia Eloi, Andrea Quatorze, Joana Ferreira, Diana Martins, Helena Alcobia, Carla Pedro.

Lastly (as they are first), to my parents and sister, cousins, uncles and aunts: they know who they are, because I have no others.

Author's Declaration

I confirm that this work is original and that if any passage(s) or diagram(s) have been copied from academic papers, books, the internet or any other sources these are clearly identified by the use of quotation marks and the reference(s) is fully cited. I certify that, other than where indicated, this is my own work and does not breach the regulations of HYMS, the University of Hull or the University of York regarding plagiarism or academic conduct in examinations. I have read the HYMS Code of Practice on Academic Misconduct, and state that this piece of work is my own and does not contain any unacknowledged work from any other sources.

“É bem possível que a pele de Salomão não pudesse resistir por muito tempo à acção concertada de três dentaduras treinadas no duro ofício de comer o que aparece para sobreviver.”

José Saramago, in *A Viagem do Elefante* (2008)

Chapter 1. Introduction and Background

1.1. Motivation and Objectives

Understanding the evolution and ecology of organisms and making predictions of behavioural habits in living and extinct taxa requires an understanding of the true relationship between form and function, which has always been difficult to establish (Wroe 2010). In order to study that relationship, an understanding of a wide range of disciplines is required, from evolution and development to statistics, biomechanics and physical properties of materials.

The overall objective of this thesis is to understand the evolution of cranial form and its biomechanical adaptation to the function of feeding, using papionins as a model system. The particular biological system under study here is the papionin cranium. Papionins are a group of primates with well-established phylogeny, varying cranial form and known dietary strategies. Primate crania, in general, have different forms and each form is thought to have evolved for a different function, while constrained by their close phylogenetic relationships. Papionins, as a primate group, share a recent common ancestor and have the same gross musculo-skeletal anatomy, yet present different cranial forms and different diets. It is to be expected that the cranium of papionin species should have diverged and adapted to eat the different diets and, therefore, that each cranial form is the effect of adaptation to diet and not of random processes such as random genetic drift. Given the considerable evidence of dental (Hayes, Freedman, & Oxnard 1990) and morphological (Frost *et al.* 2003; Leigh 2006; Dunn 2011) variation in papionins, it seems indeed possible that some of this variation is adaptive and relates to dietary differences.

However, it is not always easy to know for certain whether a particular trait evolved as an adaptation to a function. Natural selection could not be nearly as pervasive as previously thought (Gould & Lewontin 1979). Testing diversification by random genetic drift, then, is a useful starting point in the study of evolutionary variation. Initially in this thesis it is hypothesised that if random genetic drift was not the single driver of papionin cranial form evolution, the form of each papionin cranium

might reflect adaptation to the particular biomechanical demands of different dietary strategies. In other words, it is only reasonable to ask if the cranium is adapted to diet after random genetic drift have been eliminated as the sole cause of evolutionary divergence. Though a straightforward goal, the steps along the way are complex. First, the null hypothesis that random genetic drift was the single evolutionary process responsible for the cranial morphology of papionins is tested with a quantitative genetic model. To achieve such a goal, a simulation test on the validity of the quantitative genetic model to accommodate type I error rate within acceptable brackets for biological interpretation of results is first performed. Then, when satisfied that the error does stay within acceptable limits, the quantitative genetic model is applied to a papionin sample, and when the null hypothesis of random genetic drift is rejected a more adaptive interpretation of cranial form is favoured.

Following from the results of the initial evolutionary tests, hypotheses about the mechanical performance of the cranium are formulated in terms of the type of foods eaten by each papionin species. Feeding is a fundamental animal behaviour. For this reason much of the morphological variation in an adaptive radiation tends to be interpreted as trophic adaptation (Schluter 2000). In numerous primates, dietary differentiation has been associated with morphological adaptation (Ravosa 1990; Daegling 1992; Singleton 2005; Taylor 2006). Indeed, Herring (1993) claims that the extent to which the mammalian cranium adapts dynamically during food manipulation has not yet been appreciated. Research into the relationship between feeding biomechanics and cranial morphology has focused on the role of loading regimens in shaping cranial adaptation, and how stresses are dissipated through the cranium (Chalk *et al.* 2011). Differences in how the cranium resists load biomechanically (*i.e.* deforms) are hypothesised as indicating differences in feeding strategies. However, the relationship between cranial deformations (here meaning only changes in size and shape, not translations or rotations) arising from biting and feeding (loading regimens) has never been formally assessed. While the deformations of the cranium are unlikely to be selected for in an evolutionary sense, cranial form interacts with loading (here due to biting) to cause deformations of the cranium. In turn, these deformations lead to ontogenetic adaptations of bony form and structure and, as such, are a possible indicator of feeding mechanism and dietary strategy.

Mechanical performance hypotheses are tested using three-dimensional (3D) finite element models and geometric morphometrics. Biomechanical parameters estimated from finite element analysis (FEA; such as bite force, nodal displacements,

global deformations and resulting local strains) are here used as a measure of function. Finite element analysis provides a powerful approach to evaluating cranial deformation in response to masticatory loads (Chalk *et al.* 2011). The basis of finite element method is a virtual 3D model obtained from a series of image slices of the real object. With the increase in computational power, building 3D models has not only become possible but also common. Models are built to simulate real or create artificial situations with which “to increase knowledge and insight about reality, and to estimate or predict variables of interest” (Nigg & Herzog 2006). In studying the cranium of papionin monkeys, particularly biomechanical parameters when biting loads are applied, leading to deformation, models are the best solution: valuable (and many times unique) museum specimens that cannot be replaced are best tampered with inside the computational space, than in a real biomechanics laboratory. The damaging or destruction of the specimens would also render the reproducibility of experiments impossible.

Subsequently, towards the end of the thesis, hypotheses that both maximum bite force and cranial deformations under biting load among papionin species, as resulting from FEA, are associated with cranial form and diet, and these two are associated with each other, are also tested using multivariate statistics.

In this first chapter, attention is given to a review on the evolution and analysis of form and function, on the material properties and functional adaptation of bone (the key material in the cranium, and of great interest when testing cranial biomechanical performance under biting), on the biomechanics of support and movement, and on issues relating form, function and size. A review of papionin evolution, classification, ecology, diet, cranial and muscular anatomy is also provided, since this group of organisms is the system under study here. An appraisal of topics such as the concept of adaptation, the physical properties of food items and functional hypotheses of papionin adaptation to feeding is also outlined towards the end of the chapter.

1.2. Form and Function

Can function be predicted from form? Many attempts have been made to answer that question (Lauder 1995; Alexander 2006; Hutchinson 2012). Yet, so far no straightforward and convincing answer has been provided. Differences in form alone are

often interpreted as differences in function (van der Meijden, Kleinteich, & Coelho 2012, which states that in scorpions, shape types can be an approximation to biomechanical performance).

How to measure the relationship between form and function? The main assumption behind a possible answer is that structures are adapted in some way to some function, and that they are reasonably efficient at performing that function (Benton 2005). Every structure and each organizational level may be associated with specific functional properties (Liem *et al.* 2001). Bones, as structures, should then provide much information about function, such as locomotion or mastication (Herring 1993; Benton 2005). There are muscle scars on bone surfaces, and bony processes where muscles attach: muscles are an indicator of strength, leading to inferences about locomotion or other functions (Benton 2005). Cranial skeletal structures should be associated with functional properties of muscle (Herzog 2006).

In this section (1.2) and its subsections, a review of several aspects concerning form and function is provided, including the evolution and analysis of form and function, the material properties and functional adaptation of bone (the key material of interest throughout this thesis), the biomechanics of support and movement, and also issues relating form, function and size.

1.2.1. Evolution of Form and Function

The *form* of an organism is a phenotype resulting from the sum of its genotype, its development, and the environment it occupies (Equations 1.1 and 1.2); *function* can be defined as any effect that a given form performs (Wolff 1991). In a purely adaptationist view, every structure has been said to exist because it performs (or has performed in the phylogenetic past of an organism) a function (Liem *et al.* 2001). Surviving, meaning an organism being able to pass on its genes, is the key to the understanding of biological form and function, suggesting that that a particular form-function combination can be seen as an *adaptation* (see concept of adaptation in Section 1.4.1) to a particular role, making the organism adapted to a particular environment, increasing its fitness (Wolff 1991).

Form evolves because there is *variation* in form within a population. Phenotypic variation in form can be described by phenotypic evolutionary theory, the basic principles of quantitative genetics, and can be summarized in the equation

$$P = G + E \quad (1.1)$$

The phenotypic value (P) is the combined effect of the genotypic value (G) and the environmental deviation (E). The genotypic value itself is the sum of all the genetic effects, which can be classified as additive ones and dominant ones (Falconer & Mackay 1996). The previous equation can then be written

$$P = A + D + I + E \quad (1.2)$$

with A being the additive genetic effect, D the dominant genetic effect and I the interaction between the genetic effects and the environmental one. The contributions of each effect cannot be determined in a single individual, but can be estimated for the whole population by estimating the variances of each genetic effect (Falconer & Mackay 1996; Ridley 2004; further developed in Gillespie 2004):

$$V_P = V_A + V_D + V_I + V_E \quad (1.3)$$

The proportion of the total phenotypic variance V_P that is explained by the genetic variance V_G (and therefore inherited from the parent population) is called the *heritability* (Falconer & Mackay 1996). Considered in a broad sense, estimating the heritability of a trait will use the total genetic variance: $H^2 = V_G/V_P$. But in a narrow sense will only use the additive variance: $h^2 = V_A/V_P$. The latter is very useful for evolutionary studies because it gives an indication of how the mean z of a trait will respond to selection in

$$\Delta z = h^2 S \quad (1.4)$$

the so called *breeder's equation*, where S is the deviation of the population mean from the parental population mean $S = z_t - z_0$ (Falconer & Mackay 1996).

The course of evolution of the average phenotype in a population in response to natural or artificial selection is determined by the additive genetic variance and

covariance between traits (Lande 1980a; Roff 2002). The evolutionary importance of covariation between characters in populations and its connection with correlated responses to natural or artificial selection has been apparent ever since Darwin (1859), and especially since Mendel's (1866) work revealed the underlying genetic mechanisms (Lande 1979). Knowledge of genetic correlations (and covariances) is, thus, crucial for an understanding of evolution through correlated responses to selection (Cheverud 1988). One of the basic principles in quantitative genetics is that the correlated response of a trait to selection on another trait is proportional to the genetic correlation between both traits (Zeng 1988). The quantitative analysis of the evolution of a vector \mathbf{z} of traits requires two sets of parameters, the heritabilities (h^2) of the traits and the correlations between each pair (Roff 1995). These correlations are made up of two elements, the genetic correlation (r_G), which is the correlation of the breeding values, and the environmental correlation (r_E), which is the correlation of environmental deviations plus non-additive genetic deviations (Roff 1995; Falconer & Mackay 1996). Estimating r_G , unfortunately, requires extremely large sample sizes to minimize the error and increase the statistical power of the analysis (Roff 1995). The phenotypic correlation (r_P) is more easily measured than r_G or r_E and is a simple function of the two: $r_P = r_G\sqrt{(h_i^2 h_j^2)} + r_E\sqrt{[(1 - h_i^2)(1 - h_j^2)]}$, simplified above as $P = G + E$ (Roff 1995).

For a phenotype comprising multiple traits (such as the form of an organism), the single-generation response to selection is given by the multivariate version (Lande 1979) of the above mentioned breeder's equation,

$$\Delta\mathbf{z} = \beta\mathbf{G} \quad (1.5)$$

where \mathbf{z} is a vector of phenotypic means, β is the vector of directional selection gradients, and \mathbf{G} is the genetic variance-covariance matrix. β can be considered the multivariate counterpart of the single-trait narrow sense heritability h^2 . When the mean values of two traits i and j are plotted against each other the slope of the line is $\Delta z_i / \Delta z_j = h_i^2 S / h_j^2 S = h_i(V_{Ai}/V_P)S / [h_j(V_{Aj}/V_P)S] = (h_i/h_j)(V_{Ai}V_P/V_{Aj}V_P)$, which written in matrix notation is $\Delta\mathbf{z} = \beta\mathbf{G}$ (Lande 1979).

When this multivariate equation is extrapolated over many generations to reconstruct the evolutionary history or to predict the future trajectory of a phenotype, it constitutes a bridge between microevolutionary processes and macroevolutionary patterns (Lande 1979; Jones, Arnold, & Bürger 2003). That extrapolation is, however, only possible if \mathbf{G} remains relatively constant over long spans of evolutionary time

(Jones *et al.* 2003). This not being the case, understanding selection over evolutionary time is impossible within the existing quantitative genetics theory framework (Jones *et al.* 2003). Understanding how \mathbf{G} changes over evolutionary time has been the focus of many studies (*e.g.* Jones *et al.* 2003, using stochastic simulations). Arnold *et al.* (2008) review the literature on the evolution and stability of the \mathbf{G} matrix. The ultimate forces that contribute to the structure of \mathbf{G} are recombination, mutation, genetic drift and selection (Griswold, Logsdon, & Gomulkiewicz 2007).

Natural selection does not operate on traits themselves, but rather on their functional consequences (Arnold 1983). One variant is selected if it confers an enhanced capacity, which in turn leads to a greater evolutionary fitness by increasing survival, mating success, or fecundity (Losos 2011). Investigating whether the trait actually produces a predicted increase in functional capability and a consequent increase in fitness of a population has been a common test of hypothesis in the field of biomechanics and physiology (Losos 2011). Nevertheless, in the same way that phenotypically different taxa can perform the same function in a way that their fitnesses are the same (see, for example, the phenotype-fitness map concept in Bull, Heineman, & Wilke 2011), taxa which are phenotypically similar may differ substantially in functional ability (Losos 2011).

Even if a trait confers increased functional capacities, it may not be favoured by natural selection, because such an increase will have to prove advantageous in terms of fitness (increased survival or reproductive success) (Futuyma 2009). Losos (2011) mentions the example of *Anolis* lizards (found in Irschick & Losos 1998), which rarely jump, so that an increase in maximal jumping ability would not provide any useful benefit. So the best way to study the functional adaptation of a structure is to investigate an increase in functional capability of the structure that actually results in an increase in fitness; and the best way to measure fitness is to study the organism in its natural environment (Greene 1986; Hertz, Huey, & Garland 1988; Irschick & Garland 2001). Yet, there is not a single phenotypic solution for an environmental problem, but rather multiple solutions. For example, predators preying on toxic prey may evolve resistance to the toxin or avoid eating the part of the body that contains it (Losos 2011). These are what can be called *trade-offs*, and they often result in different phenotypes having the same fitness in a particular environment (Losos 2011).

In biomechanics, attention has been paid to the phenomenon of many-to-one relationships between morphology and performance (Losos 2011). Many-to-one relationships mean that, for any structural system in which parts interact to produce a

function, the same functional capacity may be produced by different combinations of traits, for the different parts (Alfaro, Bolnick, & Wainwright 2004, 2005; Vanhooydonck *et al.* 2006; Wainwright 2007; Young, Sweeney, & Badyaev 2010). Fitton *et al.* (in prep.) demonstrate that, even though the durophagous papionin species *Cercocebus* has lower strains in the face during premolar biting, the omnivorous species *Macaca* is able to produce the bite forces needed to eat hard foods as well, although its cranial biomechanical performance is not optimized for this (see more details in Section 1.3).

The interrelationships among form, function, evolution, and environment are complex and difficult to understand (Wolff 1991) and their analysis requires a particular set of skills, which are discussed in the next subsection.

1.2.2. Analysis of Form and Function

Quoting Herzog (2006), “morphology is the science of structure and form without regarding function.” Consequently, functional morphology can be considered morphology with function added, that is, it is the science of interpreting function from morphology (Dullemeijer 1980; Ashley-Ross & Gillis 2002; Benton 2005), and functional anatomy investigates the performance of structures within organisms (Liem *et al.* 2001). Since the form of a structure is linked to its function, form and function will always have a strong association with each other (Wolff 1991; Liem *et al.* 2001; Boyd & Nigg 2006). To understand how a particular form with a particular function works it is necessary to analyse an organism as a whole, with its physiology and behaviour apparent (Dullemeijer 1980; Liem *et al.* 2001). For example, Dial *et al.* (1991), studying bird flight, discovered that the flight muscles perform differently than predicted on the basis of a static examination of bird anatomy. Notwithstanding, inferring function from form, for example in fossil organisms, is a widely used approach, even when (or precisely because, in the case of fossils) no other biological information is available (Lauder 1995).

Studying form requires an early and comprehensive description of the structures that comprise it, eventually applying the comparative method to determine how universal those structures are (Wolff 1991). Comparative anatomy attempts to trace the evolutionary history of organisms (Liem *et al.* 2001), so that it can be known whether organisms have similar traits for similar functions, different traits for similar functions,

or similar traits for different functions. The comparative method can thus track evolutionary change along lineages and can be used to study adaptation (Harvey & Pagel 1991). One difficulty, though, lies in the assumption of independent evolution of a structure in several lineages, which requires counting of the number of independent convergent evolutionary events by which that structure evolved (analysed by phylogenetically independent contrasts, a method for incorporating phylogeny into statistical analysis by estimating values at nodes, Felsenstein 1985). Such information is not only hard to gather, the true independence of structure evolution is only apparent and not real, since every lineage will always be linked (tracing back for long enough) by a common ancestor. The assumption of independence, however, is found to be sufficient to approach the convergent evolution of many structures (Futuyma 2009).

Although modern-age comparative anatomy is a discipline dating back at least to the 18th century, making it one of the oldest areas of the Natural Sciences, a surprising amount of research in comparative anatomy is still to be undertaken (Liem *et al.* 2001), with much to be learned from simple observational analysis (*e.g.* Curtis *et al.* 2011). A goal of functional anatomists is to find the connections between one form and its function, but a functional analysis is not just about describing a form and its function (Liem *et al.* 2001). Such an analysis is only complete when it leads to an understanding of how that form evolved within a population (phylogenetics): Losos (2011), for example, found that the shape of the head in lizards primarily reflects phylogeny, regardless of what they eat. Phylogeny can be studied by including fossils in the analysis of a particular structure, tracking the evolutionary changes along the lineage (Dullemeijer 1980; Harvey & Pagel 1991; Liem *et al.* 2001). How an individual develops within its own lifetime (ontogeny) is also very important and can be achieved by studying the different developmental stages of an individual, bearing in mind that in living organisms a function such as feeding must always be performed even when the form of the structure performing it is not yet fully mature (Liem *et al.* 2001).

Thorough anatomical knowledge is always needed in order to generate testable hypotheses of function. Once these hypotheses are generated, functional analysis can begin (Liem *et al.* 2001). One such approach in studying function is the use of mechanical models, where biological structures (often bones but not only) are compared with mechanical devices (such as levers or pulleys) and calculations made of the forces acting on them (Benton 2005; Kerr 2010).

Comparative analysis of form and function is complex: different organisms may do similar things in different ways; no one kind of organism has all the structural

modifications that are associated with its habitat; and one kind of organism may have not one but several specializations (Bock & von Wahlert 1965; Hildebrand & Goslow 2001). Additionally, organisms can have behaviours that cannot be discerned by the analysis of structure alone (e.g. Cypher, Murdoch, & Ralls 2004). Conversely, some organisms may fail to function in ways for which they seem to be structurally adapted (Swartz 1993; Hildebrand & Goslow 2001). This often happens due to phylogenetic constraints, which are a result of the phylogenetic history a species or group of related species that make certain evolutionary pathways not likely to be followed (Ligon 1992; definition of phylogenetic constraint reviewed by McKittrick 1993). Although functions may be studied in isolation, it is the integration of all functions of a given form into a cohesive unit that serves the purpose of survival (Wolff 1991).

Nevertheless, determining the principal habits of a vertebrate from its structure is rarely difficult (Rubin & Lanyon 1982; Hildebrand & Goslow 2001; van der Meijden *et al.* 2012), and is often the only way to infer the ecological behaviours of a fossil species (e.g. Strait *et al.* 2009). The arrangement of cranial bones can be interpreted in terms of the stresses and strains acting in different directions (Benton 2005), and understanding the properties of bone as a biological tissue is thus key to understand the form and mechanical function of bone structures such as the cranium.

1.2.3. Material Properties and Architecture of Bone

In vertebrate animals, the materials of the body that provide support and movement are bone, cartilage, muscle, tendon, and ligament (Rogers 1992; Hildebrand & Goslow 2001). Three important properties of living supporting tissues are not shared by any material available to an architect or an engineer: (1) they all grow without interruption of function; (2) they are capable of adjusting to circumstance; and (3) they are durable for an entire lifetime of use (Hildebrand & Goslow 2001). In this thesis, bone alone is the supporting material of interest.

Stress is force per unit area (Hildebrand & Goslow 2001; Kerr 2010). Biting on food exerts a stress on the teeth and jaws (Liem *et al.* 2001). Stress is expressed in kilograms per square centimetre, or Newtons per square metre, or Pascals.

Load is a general term referring to any force that is applied to a solid object (Hildebrand & Goslow 2001; Kerr 2010). It can be assessed quantitatively by

computing the sum of all forces and moments applied to that object (Boyd & Nigg 2006). When any load is applied to an object, deformation occurs, meaning a change in length, volume, or angle (Hildebrand & Goslow 2001; see definitions of two kinds of deformation in Section 2.5). Deformations can be measured globally (of the object as a whole; O'Higgins *et al.* 2011, 2012; see also Section 2.5), but is more often measured using *strains* that describe deformations locally (at a particular point in the object). For a change in length, strain equals that change in length divided by the original length (Hildebrand & Goslow 2001; Truesdell & Noll 2004). Because strain is a ratio it has no units. However the vectors of principal strains at a point collectively describe changes in size and shape at that point. For materials with homogenous and isotropic material properties, strain is directly proportional to stress (Figure 1.1). Strain levels in stiff materials such as bone are typically measured in terms of microstrain (Shrive 2006).

In mechanical terms, the application of a load results in stresses and strains in the structure, defined by the formulae:

$$\sigma = F/A \quad (1.6)$$

$$\epsilon = \Delta L/L_0 \quad (1.7)$$

where σ is stress, F is force, A is area, ϵ is strain, ΔL is change in length, and L_0 is the original length (Richmond *et al.* 2005). By convention, positive strain is stretching (tension), and negative strain is compression (Richmond *et al.* 2005; Figure 1.1).

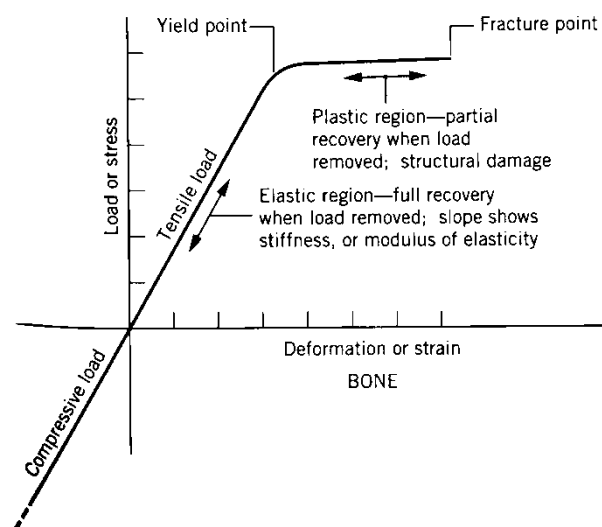


Figure 1.1. Load-deformation curve. Adapted from Hildebrand & Goslow (2001).

Deformation may be permanent or temporary: the capacity of a material to return completely to its original shape after a load is removed is called elasticity (Hildebrand & Goslow 2001; Truesdell & Noll 2004). The ratio of stress to strain (the slope of the regression of strain on stress) is a measure of stiffness and is called the modulus of elasticity or Young's modulus (Hildebrand & Goslow 2001; Kerr 2010; further discussed in Subsection 2.4.2). It has the same units as stress.

Figure 1.2 exemplifies compression, tension, shear force, and torsion on a cat humerus. *Compression* is the application of pushing forces to different points on a material; *tension*, by contrast, is the application of pulling forces on a material; *shearing* forces are directed so as to displace layers of the material parallel to each other; and *torsion* is the twisting of a material due to an applied torque (Beer, Johnston, & DeWolf 1992). As a matter of curiosity, fresh compact bone has compressive strength of 1330 to 2100 kg/cm², tensile strength of 620 to 1050 kg/cm², and shear strength of 500 to 1176 kg/cm² (Hildebrand & Goslow 2001).

In order to save on weight, bulk, and metabolic requirements, the supportive elements of the body provide adequate strength with minimum material (Hildebrand & Goslow 2001). This principle is important when the focus of the analysis is the skeleton. Bones are not solid, but neither are they hollow. Cortical or compact bone is the solid, dense material comprising the walls of diaphyses and external surfaces of bones (reviewed by Boyd & Nigg 2006). Flat bones, such as the ones making the cranial vault, are made of two layers of cortical bone with trabecular bone (called diploe) in between (reviewed by Boyd & Nigg 2006). Trabecular, cancellous or spongy bone is formed by thin bony spicules and plates, called *trabeculae*, that have been observed to orient themselves primarily in the direction of the forces applied to the bone (Boyd & Nigg 2006). Trabeculae are thus organized to withstand mechanical loads while minimizing the weight of the bone (Boyd & Nigg 2006).

Bones can resist bending if the longer dimension is parallel to the load, as is exemplified by a beam supported only at the edges (Hildebrand & Goslow 2001). Beam-like bones withstand bending in one plane; hollow cylindrical bones withstand bending in several planes (Hildebrand & Goslow 2001). The mandible at the level of the teeth, for example, can be regarded as a bony beam turned on edge to the muscles acting on it (*e.g.* Smith 1978; Bucinell *et al.* 2010). The zygomatic arch has been regarded in the same way (*e.g.* Preuschoft *et al.* 1986; Herring *et al.* 1996), but this view has been recently disputed (Curtis *et al.* 2011) and the structure is now starting to be compared more to an arch than to a beam. Evidence suggests that the zygomatic arch bears

compressive forces, being stabilized during biting by the tensioning of the temporal fasciae opposing the pulling of the masseter muscle on the other direction (Curtis *et al.* 2011).

Where several bones function as a unit in sustaining usual loads (such as in the cranium), trabeculae also traverse those bones as a unit (Hildebrand & Goslow 2001). Sutures and joints also play an important role in skeletal adaptation to load, mainly by modifying stresses (Jaslow 1990; Herring & Teng 2000; Hildebrand & Goslow 2001; Rafferty, Herring, & Marshall 2003; Herring 2008; Bright 2012). Bone can thus be adapted to load as a result of a repetitive, mechanical function.

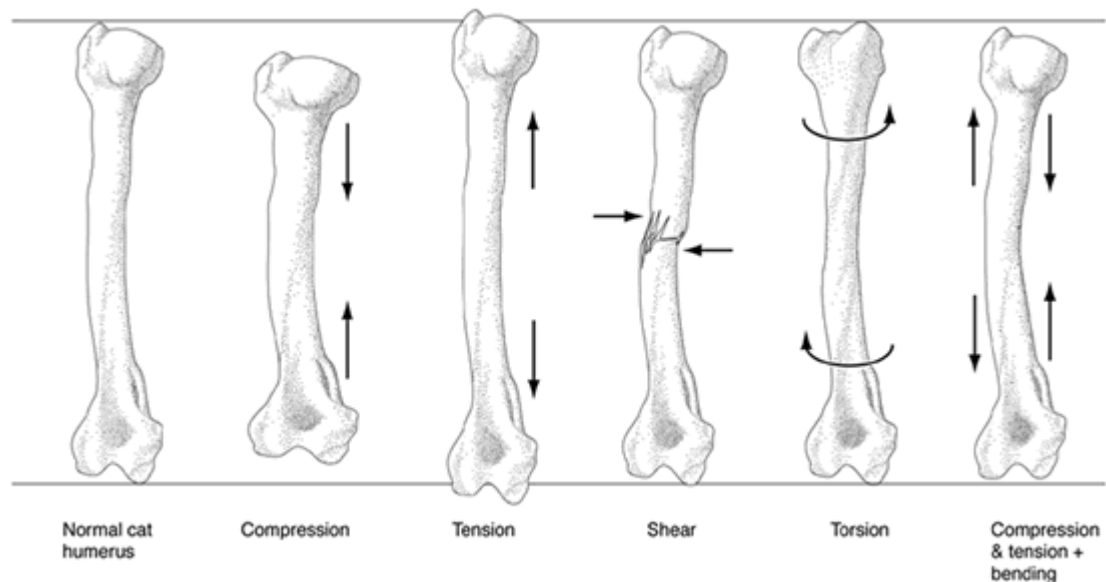


Figure 1.2. Major stresses shown on a cat humerus: compression, tension, shear force, and torsion. Stresses are shown by arrows and the resulting strains by deformation of the bone. Adapted from Liem *et al.* (2001).

1.2.4. Functional Adaptation of Bone

An animal inherits the transmissible, genetic form of its skeleton, but its detailed form is determined by its mechanical use (Hildebrand & Goslow 2001). Galileo Galilei (1638) was among the first to recognize the relation between mechanical forces and skeletal morphology (mentioned by Ruff 2008). Julius Wolff (1892) promulgated his

“law” that states that mechanical loading influences bone structure, meaning that bone is functionally adapted to its mechanical environment during life (Ruff 2008). Ruff (2008) suggests that the expression “bone functional adaptation” should be substituted for “Wolff’s law”. As mentioned before (Subsections 1.2.1 and 1.2.2), form is often hypothesised as the consequence of function, constrained by phylogeny. Particularly, skeletal form is perceived as a compromise between mechanics and other influences (Ruff, Holt, & Trinkaus 2006). Because bone can adapt to load, the skeleton preserves in its form the particular mechanical loadings to which it was subjected during the lifetime of an individual, allowing inferences about the behaviours that produced those loadings (Ruff 2008). The concept of adaptation on a population level is dealt with in Subsection 1.4.1.

The configuration and thickness of bones and the patterns of their trabeculae are established only as the young animal moves about while growing, and they are modified if changes in the distribution of mass or in behaviour alter usual loads (Hildebrand & Goslow 2001). To understand how structural elements of the body are constructed for maximum effectiveness one has to consider the transmission of forces within solid objects. Any force applied to a solid object is opposed by an equal force in the opposite direction. Within that object, units of force have the same magnitude and direction as the externally applied forces: the path followed by those units of force as they pass along an object are called stress lines (Hildebrand & Goslow 2001; Currey 2002; Alexander 2005). Thorough discussion of stress lines is provided by Buckland-Wright (1978), following research on cat crania.

Responses of bone to factors that generate adaptive tissue responses (namely exercise and disuse) are two (Currey 2002; Zernicke, Judex, & Lorincz 2006): bone can respond to stimuli by triggering (1) *remodelling* or (2) *modelling* events. In both, resorption of bone tissue is followed by subsequent bone formation which, in modelling, alters the shape and size of the bone structure, whereas in remodelling it does not (Bromage 1986; Bromage & Boyde 2008).

Remodelling affects all surfaces of the bone, including the internal body of the bone (Currey 2002) but does not alter its form. It plays a role in maintaining stable blood calcium levels: calcium stored in bone is released into the blood stream if levels are too low, and captured into bone (or excreted) if levels are too high. This calcium shifting in and out of bones is ultimately what makes bone remodel and this plays a role in maintaining skeletal mechanical integrity. Remodelling is responsible for all events that occur within the cortical bone (intracortical), and does not change the overall shape

of the particular bone (Zernicke *et al.* 2006). Functional adaptation of bone requires the remodelling of existing bone (Prendergast & Taylor 1994; Hildebrand & Goslow 2001). Since bone tissues are unavoidably linked to their mechanical, biochemical, and electrical environment they can modify their structure and composition in response to changes in their mechanical loading environment (Zernicke *et al.* 2006). When physical stimuli are increased through activity, bone can be removed from one place and deposited where it is most needed to accommodate the new loading levels. In contrast, when no loads are applied, bone can be reabsorbed as the skeleton adapts to the decreasing loading regime (Zernicke *et al.* 2006).

Modelling acts exclusively on endosteal and periosteal surfaces, and therefore can change the shape (and size) of the bone. Bone can be added or removed from these surfaces, but bone resorption is not followed by formation on the same surface (Zernicke *et al.* 2006). Modelling is associated with changes during growth, while most changes happening after skeletal maturation are due to remodelling in response to mechanical usage (Zernicke *et al.* 2006).

In spite of it all, heredity has been shown to be the principal determinant of bone mineral density, although half of its variance is influenced by other factors like physical exercise: in humans, the skeletal response to exercise varies with age and physiological status (competitive runners, Lane *et al.* 1986, Bembien *et al.* 2004; young adults, Friedlander *et al.* 1995; studies on pre-menarcheal girls, Morris *et al.* 1997; Forwood & Burr 1993 provide an earlier review of skeletal responses to exercise in humans). Bone mass gained during exercise is largely temporary and is lost quickly if the exercise programme is discontinued (Dalsky *et al.* 1988; Michel *et al.* 1991; Nordström *et al.* 2005). It is generally understood that exercise effects are local and site-specific (*e.g.* running does not cause a change in the humerus; Zernicke *et al.* 2006), but Lieberman (1996) found that exercised pigs and armadillos, when compared to control individuals, had an increase in cortical bone thickness not only on the weight-supporting limb bones, but also in the cranial vault, particularly in the nuchal region (which is also stressed during running).

Frost (1964, 1987) and Rubin (1984) proposed that bone attempts to keep strains within a narrow and beneficial range, rather than to minimize strains within its matrix. This has been supported by experimental data demonstrating that peak bone strains are similar in a variety of vertebrate species (buffalo, elephant, mouse, human, turkey), ranging from 2000 to 3500 microstrain (Rubin & Lanyon 1982; Burr *et al.* 1996): dynamic strain similarity (Rubin & Lanyon 1984). Removing mechanical stimuli results

in bone loss; recovery of bone does not occur as rapidly as loss of bone (Tuukkanen, Peng, & Väänänen 1994, in rats). Recovery of cortical bone takes longer than that of trabecular bone (Lane *et al.* 1996).

Bone can only adapt to load if the application of that load is continuous or repetitive on a long-term basis. Such loads can be originated either from support or repetitive movement, which are regulated by the principles of biomechanics.

1.2.5. Biomechanics of Support and Movement

Biomechanics is the science of applying the principles of mechanics to living systems (Hatze 1974; Liem *et al.* 2001; Alexander 2005), principles that are important when analysing musculo-skeletal systems, as is the case in this thesis with the masticatory system. It thus deals with forces acting on bodies and structures.

Mechanical force is an interaction between bodies that results in a change in motion of all the interacting bodies (Kerr 2010). Forces are vector quantities because they have a direction as well as a magnitude (Liem *et al.* 2001). The direction of the force is the vectorial component of a force, while the magnitude (amount, quantity, number) is the scalar component of a force (Kerr 2010). Forces can also cause a change in form of a body (Kerr 2010; see also Subsections 1.2.3 and 1.2.4). In musculo-skeletal systems forces are generated by the pulling of contracting muscles.

Muscles produce three types of contractions (Faulkner 2003; Kerr 2010): (1) concentric contraction, muscle shortening; (2) eccentric contraction, muscle lengthening while tense; or (3) static or isometric contraction, remaining at the same length while tense. Muscles always pull, never push, on bone, and they can only produce one type of contraction at a time (Kerr 2010). The point of application (expressed by Cartesian coordinates) of a muscle force is the point where the muscle force is applied, which is the tendinous attachments on the bone (Osborn 1995; Kerr 2010). An important mechanical feature of the force generated by most skeletal muscles is that it is applied at a distance from the centre of a joint (fulcrum, or hinge); this creates *moment* or *torque* (Ross 2008; Kerr 2010). The magnitude of the moment is the product of the applied force and its perpendicular distance from the fulcrum (this distance also known as the moment or the lever arm): $Moment = force \text{ (N)} \times lever \text{ arm (m)}$ (levers in the musculo-skeletal system are reviewed by Kerr 2010). The magnitude of the pull corresponds, in

general, to the size of the muscle, *i.e.*, its physiological cross-sectional area (Patel *et al.* 2002; Taylor & Vinyard 2004; Kerr 2010; Myatt *et al.* 2012), which is discussed thoroughly in Chapter 5.

If forces are the interaction between bodies and can influence their form, the size of those bodies must also play a role. A final consideration in this Section 1.2 refers to the relationship between form, function and size and how scaling has been measured and described in relation to animal morphology.

1.2.6. Form, Function and Size

Size has a deep influence on form and function. One reason is that surface and volume do not increase linearly when dimensions increase. *Scaling* is then defined as the relationship between body proportions and body size among related and similarly shaped organisms (Thompson 1942; Gould 1966; Hildebrand & Goslow 2001). When growth results in no change in proportions it is said to be *isometric*: the large animal has exactly the same proportions as the small animal (Gould 1966; Hildebrand & Goslow 2001; Liem *et al.* 2001). In most animal lineages, however, growth is constrained by developmental processes and mechanisms, by form and by function, and is not isometric; it is said to be *allometric* (Gould 1966; Hildebrand & Goslow 2001). Allometry is the study of the association between form and size (Hildebrand & Goslow 2001). Allometry relates to both ontogeny and phylogeny and is an important concept in relation to structure since it is considered to be of adaptive value (Cheverud 1982; Klingenberg 1998; Hildebrand & Goslow 2001; Mitteroecker *et al.* 2004; Leigh 2006). The allometric equation $y = bx^a$ gives an adequate line of best fit (regression) that represents the relationship between dimensions of two structures of the same animal body (Gould 1966; Hildebrand & Goslow 2001), where the intercept is zero in both dimensions. The parameter b changes the slope of the line; x and y are the linear measurements; and a is the exponent slope of the line.

The selective advantages of a large size are (1) decreased predation probability; (2) the ability to roam over large areas in search of water, food, shelter, or breeding areas; (3) generating and using energy relatively more slowly so relatively little food is required per unit of body weight; and (4) a low surface-to-volume ratio enables the animal to store heat more effectively (Hildebrand & Goslow 2001; Fernandez-Duque

2011; Cowgill *et al.* 2012). But still more food is needed to fuel a bigger size, which is costly for the animal. This means that there is a trade-off between size and function: an animal can only grow in size as much as it can support such a metabolism, meaning that the energy of fitness gains of a larger size must be higher than the energy or fitness cost of maintaining a larger size. The necessary trade-off between overall size and the required energy intake to maintain it might have an impact on cranial form, particularly at the food processing stage.

In papionins, differences in body size among species are apparent and related to differences in cranial form (Ravosa 1990), and the way the cranium behaves mechanically during food processing. Section 1.3 discusses aspects of papionin biology such as evolution, ecology, diet and anatomy, which are important for an understanding of their cranial evolution and adaptation to feeding, later to be analysed in this thesis.

1.3. Papionin Biology

Papionin monkeys have been extensively used for testing many biomechanical hypotheses (*e.g.* Hylander 1975; Oyen, Walker, & Rice 1979; Ravosa 1991a; b; Ravosa & Profant 2000), particularly because they have physiological, ecological, cultural and evolutionary connections with humans. For example, since the early 1960s papionins have been considered an especially useful system for modelling human evolution (reviewed by Cachel 2006). Jolly (2001) proposes that analogies between early hominin evolution and papionin evolution can be made that are more useful than analogies with the great apes. In terms of diet, papionins are less specialized than apes, and that could explain why they survived the climatic changes that drastically reduced hominoid diversity, 15-20 million years ago (Fleagle 1999; molecular data suggest that hominoids and cercopithecoids diverged around 23–30 million years ago, Steiper, Young, & Sukarna 2004; a recently found fossil corroborates a divergence at 25.2 million years ago, Stevens *et al.* 2013). Papionin dietary habits range from marked specialization to generalist feeding; their cranial form is also diverse enough to allow for speculation about its adaptive history, particularly whether diet (through masticatory function) did play or, better still, *is playing* a role in the evolution and mechanical performance of the papionin cranium.

In the following subsections, a review of aspects of papionin biology is provided, including papionin evolution and classification, distribution and ecology, diet and feeding strategies, cranial form and anatomy, and masticatory muscle anatomy.

1.3.1. Papionin Evolution and Classification

The earliest fossil findings attributed to the Superfamily Cercopithecoidea are dated from 19 to 12.5 million years ago (Benefit & McCrossin 2002). They were found in the African deposits of Wadi Moghara, Egypt, a faunal deposit of early Miocene mammals known since the 19th century (Miller 1999). They are currently classified as members of the Family Victoriapithecidae, sister taxon to the Family Cercopithecidae, including two genera, *Victoriapithecus* and *Prohylobates* (Leakey 1985). They are described as having a *Macaca*-like cranium with a long and low calvarium and moderately long snout (Benefit & McCrossin 2002).

In the middle Miocene, cercopithecoids seem to have been a well-established group, although not a taxonomically diverse one, but in the late Miocene and Plio-Pleistocene a radiation of the Family Cercopithecidae can be seen in the fossil record (Foley 1993). The recency of this radiation obscures the clear demarcation of extant species into subgroups since they did not have a long, independent branch evolution (Jablonski 2002). There are, nevertheless, several proposed divisions of the family into subfamilies and tribes using varying criteria (*e.g.* Jolly 1966, 1970; Fleagle 1999). One such subgroup is the Tribe Papionini.

Extant members of the Tribe Papionini are classified in 7 genera (see Appendix A for a complete taxonomy of extant papionins within the Order Primates). Phenetic classifications based on morphological characters have traditionally clustered the large-bodied and long-faced genera, *Mandrillus* and *Papio* (Delson 1975, 1993; Groves 1978) together, and the small-bodied and short-faced genera, *Cercocebus* and *Lophocebus*, also together (even in the same genus, *Cercocebus*; Delson 1975), while outgrouping the small-bodied genus *Macaca* and the large-bodied genus *Theropithecus* (Jolly 1966; Delson 1975). Szalay and Delson (1979) later understood that the genus *Macaca* was the sister group of the rest of the papionins, and that *Theropithecus* was in fact closer to *Papio* and only functionally different from it. Recently, Gilbert (2007, 2008) rejected

the taxonomic separation of papionins into short-faced and long-faced genera on the grounds of cranio-mandibular morphology alone.

Recent molecular cladistic classifications (Disotell, Honeycutt, & Ruvolo 1992; Disotell 1994, 1996; Harris & Disotell 1998; Harris 2000; Tosi *et al.* 2003; Zinner *et al.* 2012) helped to clarify the intergeneric relationships within the Tribe Papionini. The consensus molecular phylogeny groups the genera *Papio*, *Lophocebus* and *Theropithecus* together, in a yet unresolved trichotomy, while grouping the genera *Mandrillus* and *Cercocebus* as sister taxa, and *Macaca* as an outgroup (Figure 1.3). This will be the phylogenetic tree used throughout this thesis as a framework assumption for every analysis.

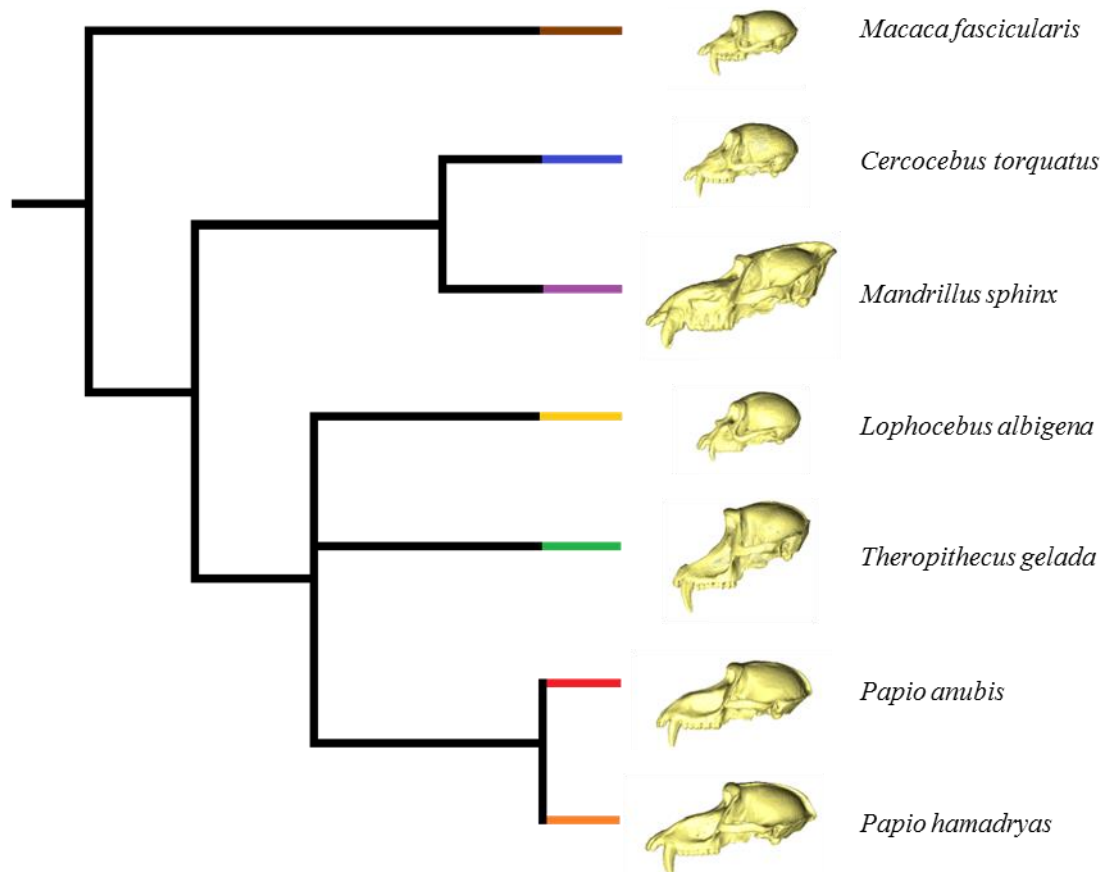


Figure 1.3. Consensus phylogenetic tree of the papionin monkeys as resulting from molecular cladistic analyses, showing male crania of the 7 species used in this study.

Goodman *et al.* (1998) go so far as to place *Mandrillus* in the genus *Cercocebus*, calculating its separation from the main branch as having happened only 4 million years ago; these authors claim the same time of separation for *Theropithecus* and *Papio*, with a similar classification of *Theropithecus* under genus *Papio*. A few cases of interbreeding have indeed been observed between *Theropithecus gelada* and *Papio* species (*anubis* and *hamadryas*), but these are considered to be infrequent (Jolly *et al.* 1997). *Papio* species, on the other hand, are known to interbreed producing fertile offspring in border regions, where the geographic range of one species overlaps with another: in the so-called hybrid zones (Groves 2001; Dunn 2011). This has brought some authors (Thorington & Groves 1970; Groves 2001, p. 237) to the suggestion that *Papio* species should in fact be considered subspecies, unifying all or most into the species *Papio hamadryas*. This view, however, is not yet widespread. Conversely, doubts about the monophyly of *Macaca* as a genus have been raised (Groves 1989), but were dismissed after molecular studies (Morales & Melnick 1998; Tosi, Morales, & Melnick 2000; Tosi *et al.* 2003). Nevertheless, the genus is frequently divided into four species-groups for pragmatic purposes (see Groves 2001 for the distinctions among them and the rationale for this division). *Macaca* is a very old genus, having separated from the other papionins about 7 million years ago (Stewart & Disotell 1998).

There are 5 species of *Papio*, 23 of *Macaca*, 2 of *Mandrillus*, 3 of *Lophocebus*, 6 of *Cercocebus*, and a single species of *Theropithecus* (Groves 2001). This makes 40 species attributed to the Tribe Papionini, plus the recently classified single species (*R. kipunji*, Jones *et al.* 2005) belonging to the genus *Rungwecebus* (Davenport *et al.* 2006). *Rungwecebus* is a disputed genus: it was created based on two sightings in Africa, in 2003 and 2004, but it is thought to be a hybrid between *Papio* and *Lophocebus*. Should it be confirmed as a new sister genus, it should be included in their phylogenetic group.

In the next subsection, papionin geographic distribution and habitat ecology is shown before turning to a detailed account of the diet and feeding habits of the species used in this thesis.

1.3.2. Papionin Distribution and Ecology

Papionin monkeys are mostly African species. The exception is the genus *Macaca*, which has a much wider distribution, from North Africa to Southeast Asia,

with a small population of the North African species *M. sylvanus* living in Gibraltar (Europe); the genus *Papio* also occurs outside Africa in Southern Arabia (IUCN 2011).

They occur in a range of habitats from tropical rainforest to desert savannah. Genera *Cercocebus*, *Lophocebus*, *Mandrillus*, and *Rungwecebus* are rainforest dwellers, (IUCN 2011). Of interest for this study are the species *Cercocebus torquatus* which occurs along the West African coast from West Nigeria to Sette Camma on the Gabon coast; *Lophocebus albigena* which occurs from Southern Cameroon, inland to the Oubangui, and South into Gabon; and *Mandrillus sphinx* which occurs between the River Sanga in Cameroon and the River Kouilou in Congo (Groves 2001). Even though the habitat of *M. sphinx* is rainforest, it is basically a terrestrial species (Hoshino 1985).

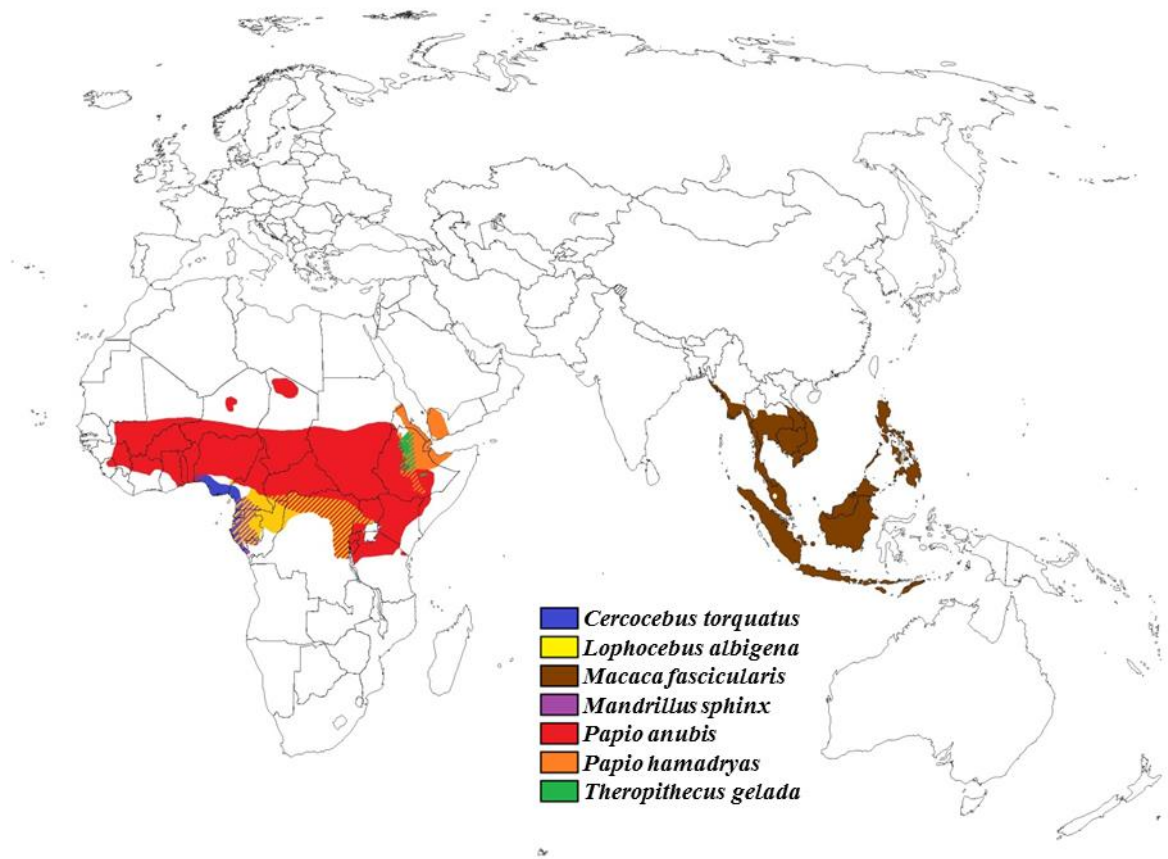


Figure 1.4. Geographic distribution of the papionin species used in this study. Blue, *Cercocebus torquatus*; yellow, *Lophocebus albigena*; brown, *Macaca fascicularis*; purple, *Mandrillus sphinx*; red, *Papio anubis*; orange, *Papio hamadryas*; and green, *Theropithecus gelada*. Data taken from IUCN (2011).

The genera *Papio* and *Theropithecus* include savannah dwelling animals (IUCN 2011). *Papio hamadryas* occurs in the arid zone of northern Ethiopian lowlands, eastwards into Northern Somalia, with populations across the Red Sea in the Southern tip of the Arabian Peninsula (Groves 2001; IUCN 2011). The geographic range of *Papio anubis* is spread longitudinally from Southern Mali and East Guinea-Conakry to Ethiopia, Kenya and North Tanzania, with population patches on the Sahara Desert (IUCN 2011). *Theropithecus gelada* occurs in high grasslands in Tigre, Begemdir, Wolle, and Shoa Provinces of Ethiopia (Groves 2001).

The genus *Macaca* is the most diverse of all genera, occurring in forest, savannah and other habitats; *Macaca fascicularis*, the macaque species of interest for this thesis, occurs in Southeast Asia, from coastal Myanmar, southwards to the Lesser Sunda Islands of Indonesia and Timor-Leste, and eastwards to South Vietnam and the Philippines, mostly in rainforest (IUCN 2011).

Figure 1.4 shows the geographic distribution of the papionin species considered in this study. Occasionally, *P. anubis* and *T. gelada* are sympatric in some areas and can interbreed (Jolly *et al.* 1997), yet present niche separation (Dunbar & Dunbar 1974a). *P. hamadryas* occupies semi-desert habitats, too arid for other papionin species (Dunbar & Dunbar 1974b). As mentioned before, overlapping areas where *Papio* species interbreed are called hybrid zones (Groves 2001; Dunn 2011).

1.3.3. Papionin Diets and Feeding Strategies

Papionins show considerable dietary variation among genera and even among species within a single genus. While a description of the dietary intake of every species in the Tribe Papionini is superfluous here, a detailed review of the diet and feeding strategies of species sampled for this thesis is necessary.

Primate diets can be categorized as primary and secondary (Fitton 2007). Food items consumed throughout the year and considered the most important part of the diet are called the primary diet. Food items available to eat during seasons of the year when primary food resources are scarce are called secondary foods or *fallback foods* (Marshall & Wrangham 2007; Marshall *et al.* 2009). These, although not much consumed throughout the year even if available, may be the most critical food items in the whole diet: the opportunity (and ability) of an individual to consume them may be

the key to its survival into the next primary food abundance season (Fitton 2007). Fallback foods are at least as likely to exert a strong selective pressure on cranial form as primary foods.

The species *Cercocebus torquatus* feeds on fruits and seeds (Jones & Sabater Pi 1968; Mitani 1991; Wieczkowski 2009), and also on young leaves, shoots, flowers, gum, and insects (Mitani 1989). *Cercocebus* is strongly dependent on fruits (60 to 80% of their diet; Mitani 1989) and is known for regularly consuming extremely hard nuts and seeds found on the forest floor. Discarding of seeds (spitting seeds) is a rare occurrence (Wieczkowski 2009). Interestingly, in Côte d'Ivoire, *Cercocebus* are most easily located by the loud sound of cracking nuts with their teeth (Fleagle & McGraw 1999). Food items described by Wieczkowski (2009) include unripe fruit, ripe fruit, unripe seeds, ripe seeds, and dry seeds. The fruits included in its diet soften and the seeds harden as they ripen (Wieczkowski 2009). *Cercocebus* were recorded eating unripe and ripe seeds when they discarded the pulp from unripe and ripe fruit, respectively (Wieczkowski 2009). Not related to *C. torquatus* but interesting to note is that Shah (2003) found that *C. agilis* fed on harder diet items than did its sympatric species *Lophocebus albigena*.

Species of the genus *Lophocebus* have been observed eating hard items, especially seeds (Horn 1987; Lambert *et al.* 2004). Lambert *et al.* (2004) describe the species *Lophocebus albigena* as a hard object consumer, just like *Cercocebus*. Nevertheless they found *L. albigena* eats a wide variety of diet items, including a high percentage of soft ripe fruit in its annual diet (Lambert *et al.* 2004). Fruit makes up to 33% of its diet, and seeds up to 29% (Poulsen, Clark, & Smith 2001). Ham (1994, cited in Tutin *et al.* 1997) found the following numbers: 24% fruits, 41.4% seeds, 4.5% leaves, 1.6% pith, 3.3% flowers, and 25.3% animal matter. Poulsen, Clark and Smith (2001) also consider *L. albigena* as a largely frugivorous animal (plant species consumption correlating with their fruit production), yet eating a wide range of other plant foods such as seeds, leaves and flowers. It relies mostly on the latter two during the season with less fruit abundance, a period where the diversity of food items consumed increases (Poulsen *et al.* 2001). As mentioned above, *L. albigena* is found to feed on less hard items than its sympatric species *C. agilis* (Shah 2003). It also frequently searches for invertebrate prey, especially ants, ant larvae, and caterpillars (Poulsen *et al.* 2001).

Yeager (1996) considers *Macaca fascicularis* as primarily frugivorous, fruits occupying 66.7% of diet. Yet it is omnivorous in also consuming leaves (17.2%),

flowers (8.9%), insects (4.1%), and other foods, such as seeds and even bark, as primary diet (Yeager 1996). It eats insects, stems, leaves, and dipterocarp seeds as fallback foods during periods and in regions where no fruits are available (Berenstain 1986). While having the ability to exploit a variety of food sources during periods of food scarcity, *M. fascicularis* appears to be highly selective: if fruits are available, they are readily preferred over other foods (Ungar 1995; Yeager 1996). Corlett and Lucas (1990) even go so far as to say the species omnivory is imposed by geographical food availability, rather than by food choice. This species has been observed fishing, but this foraging behaviour is considered to be rare (Stewart *et al.* 2008). Even if not very often, it eats crabs (Swindler 2002), hence it being called the “crab-eating macaque,” and has been observed using stone tools to open nuts, oysters, other bivalves, and various types of sea snails (Gumert, Kluck, & Malaivijitnond 2009).

The genus *Mandrillus* is known to eat hard seeds, like its sister taxon *Cercocebus* (Rogers *et al.* 1996; Fleagle & McGraw 1999). Both genera can be said to be omnivorous with a high percentage of fruit in their diet (Astaras, Mühlenberg, & Waltert 2008). *Mandrillus* eats food that naturally falls to the ground (Norris 1988). The study group described by Norris (1988) obtained most of their food (mostly fruit and seeds) from the ground. Once the fruit fell, generally into water, it remained there for several days where it softened, and *Mandrillus* readily ate it (Norris 1988). Yet, the seasonal availability of many of these arboreal foods needs to be stressed (Norris 1988). Folivory is a relatively small part of their diet (Norris 1988). *Mandrillus* feeds on fallen seeds and monocotyledonous plant leaves more frequently in the minor fruiting season than in the major fruiting season (Hoshino 1985; Astaras *et al.* 2011). Still, seeds are the most frequently consumed food item, especially the ones from *Sacoglottis gabonensis*, a large tree which characterizes the forest in Campo Animal Reserve, Cameroon (Hoshino 1985). Individuals in Hoshino (1985) study field ate the pulp of *S. gabonensis*, which was observed to be their most important food from August to October. Hard nuts and seeds that can lay on the forest floor without decomposing are the major food sources of *Mandrillus sphinx* in Cameroon during the dry season when fruits are scarce (Fleagle & McGraw 1999). Crushed seeds were found frequently in the faeces of *M. sphinx* (Hoshino 1985). The same type of forest utilization and feeding has been reported for the congeneric species *M. leucophaeus* (Gartlan & Struhsaker 1972; Astaras *et al.* 2008). Lahm (1986) lists the stomach contents of *M. sphinx* as fruits, seeds, invertebrates, bark, leaves, stems, residual proportions of fibre, and some earth and fungi. Lahm (1986) also found that the kernel of the nut-like fruit *Coula edulis* is

consumed, but the hard covering is discarded, and that while small and medium-sized fruits with abundant small seeds were usually consumed whole; apparently, ripe fruits are mostly preferred. The majority of identified fruit species (88%) were small to medium-sized (Lahm 1986). Tutin *et al.* (1997) found that in Lope Reserve, Gabon, the diet of the *M. sphinx* was composed of 46.7% fruits, 34.4% seeds, 5.7% leaves, 5.7% pith, 0.8% flowers, 4.9% animals, and 1.6% other.

Most *Papio* species are generalist omnivores with seasonal and regional variations in diet (Norris 1988; Hill & Dunbar 2002). *P. anubis* primarily forages on the ground (Aldrich-Blake *et al.* 1971; Rowe 1996) and feeds on grass, tubers, bulbs, corms, rhizomes, flowers, fruit, leaves, seeds, and tree gum (Aldrich-Blake *et al.* 1971; Harding 1976). It supplements its diet with meat and other animal matter (Melnick & Pearl 1987). It preys opportunistically on *Chlorocebus aethiops*, infant gazelles, hares (Rowe 1996), and is known to eat dead birds, insects and other invertebrates, and eggs (Aldrich-Blake *et al.* 1971). Dunbar and Dunbar (1974a) found that *P. anubis* diet comprises 54.9% fruits and seeds, 32% leaves, 7.5% flowers, 2.7% insects, 1.7% roots and bulbs, and 0.7% bark. Young leaves, fruits and flowers are consumed during the rainy season, while roots and tubers are an important food source during the dry season (Barton & Whiten 1993).

P. hamadryas eats mainly dry leaves, flowers, beans, and berries from the plant genera *Acacia*, *Dobera*, and *Grewia* (Stammbach 1987). Grass seeds and *Acacia* flowers seem to be its preferred food during the rainy season, complementing its diet with dug-out roots and tubers (Stammbach 1987). Swedell (2002) found that the main food items eaten during the whole year were the nuts of doum palm trees (*Hyphaene thebaica*) and the leaves, flowers, pods and seeds of *Acacia senegal* and *A. mellifera*, as well as grass seeds, blades and flowers, *A. nubica* leaves and seeds, *Grewia tenax* berries, grass roots, *A. tortilis* seeds, and sap from *A. senegal*. Schreier (2010) observations seem to corroborate the previous ones: palm forest *P. hamadryas* at Filoha, Ethiopia, fed most frequently on the seeds, leaves and flowers of *A. senegal* (23.5%) and doum palm fruit (*H. thebaica*; 21.2%). The flowers, leaves and seeds of *Tribulus cistoides* comprised at least 10.1% of its feeding budget, and no other plant species contributed more than 8% of the feeding budget (Schreier 2010). Hill and Dunbar (2002) calculated from the literature a diet comprised of 45% fruits, 28% leaves, and 22% flowers for *P. hamadryas*. Wieczkowski (2009) found that members of the genus *Papio* do not appear to discard fruit pulp to feed on unripe and ripe seeds like

Cercocebus and *Lophocebus* do. Swedell (2002) also observed *P. hamadryas* adult individuals eating hares on three occasions.

Theropithecus gelada is unique in being an almost exclusive graminivore: it feeds on grass (Dunbar & Dunbar 1974a; Iwamoto 1979). Individual *T. gelada* grazes sitting upright and plucking grass blades and seeds from the ground using their hands (Dunbar & Dunbar 1974a), not using their teeth in grazing, like other animals. Grass blades constitute 96.9% of its diet (Dunbar & Dunbar 1974a), especially grasses of the species *Danthonia subulata*, *Festuca abyssinica*, and *Poa simensis* (Iwamoto 1979). It complements its diet with stems, roots, flowers, seeds, tubers, and rhizomes from herbs, trees, and shrubs, and was also observed eating insects (Iwamoto 1979). Because this diet is of low nutritional value, *T. gelada* spends a significant portion of the day feeding and foraging, from 50 to 75% of the day (Iwamoto & Dunbar 1983), and even up to 79.9% (Kawai & Iwamoto 1979).

Table 1.1 Dietary categorization of papionin species used in this study

Species	Predominant Foods (%)	Dietary Categories
<i>Cercocebus torquatus</i>	fruits (60-80%)	Frugivory, Durophagy
<i>Lophocebus albigena</i>	fruits (33%) seeds (29%)	Frugivory, Durophagy
<i>Macaca fascicularis</i>	fruits and seeds (66.7%) leaves (17.2%) flowers (8.9%)	Frugivory, Omnivory
<i>Mandrillus sphinx</i>	fruits (46.7%) seeds (34.4%)	Frugivory, Durophagy
<i>Papio anubis</i>	fruits and seeds (54.9%) leaves (32%) flowers (7.5%)	Frugivory, Omnivory
<i>Papio hamadryas</i>	fruits and seeds (45%) leaves (28%) flowers (22%)	Folivory, Omnivory
<i>Theropithecus gelada</i>	grass (96.9%)	Graminivory

The dietary and feeding habits of the genus *Rungwecebus* are little known and, since the genus will not be part of the study sample, this will not be dealt with here. Table 1.1 summarises the percentage of predominant food and the attributed dietary categories of each of the above mentioned species. To understand how these different types of diet impacted on the adaptation of the cranium, first the cranial anatomy has to be known. Descriptions of papionin cranium and muscle anatomy follow next.

1.3.4. Papionin Anatomical Terminology

A brief technical note is useful before advancing to description of papionin cranial form and anatomy. When needed, terms describing the relative position and orientation of skeletal structures throughout this thesis follow Hillson (1992) and Fleagle (1999). The *median sagittal plane* is the imaginary plane that divides the skeleton into two equal halves, left and right. As Hillson (1992) writes, every bone has six surfaces that can be described as *medial* (facing towards the median sagittal plane), *lateral* (facing away from the median sagittal plane), *cranial* or *proximal* (facing towards the front of the skull), *caudal* or *distal* (facing towards the tip of the tail), *dorsal* (facing towards the dorsum), and *ventral* (facing towards the belly). The cranium is described as *anterior* (to the front of the cranium), *posterior* (to the back of the cranium), *lateral* (either side, right or left), *superior* (upper part) and *inferior* (lower part). Terms describing more than one surface or their orientation are eventually used, for example, disto-medial, which describes a distal position on the medial plane.

Body movement is described as *flexion* (in general, two parts of the body moving towards each other), opposing *extension* (two parts of the same body moving away from each other); *protraction* (a structure moving forward), opposing *retraction* (a structure moving backwards); *abduction* (movement away from the midline), opposing *adduction* (movement toward the midline) (Liem *et al.* 2001). Movement direction is described in terms of orientation, for example, a muscle can pull infero-superiorly, meaning a movement from the lower part to the upper part, or even in a direction as complicated as inferoanterior-superoposterior, meaning a pull from the lower part of the front to the upper part of the back.

1.3.5. Papionin Cranial Form and Anatomy

The papionin *skull*, like any other mammalian skull, is exceedingly variable with regard to strength and proportions, and yet very conservative with regard to the basic plan of a vault containing the brain and a face containing most of the sensory organs and feeding organs (Hildebrand & Goslow 2001). Figure 1.5 shows a depiction of the skull of an adult male papionin specimen representing genus *Papio*. The skull can be said to consist of two parts, the *mandible* (jaw bone) and the *cranium* (braincase and face) (White, Black, & Folkens 2012). This thesis will be concerned with the cranium only. As with all other vertebrates, the cranium of papionins protects and supports the brain and the sense organs, and is also used in food gathering and processing (De Iuliis & Pulerà 2011). The facial region, or *splanchnocranium* (Fleagle 1999), includes the nose, orbits, and upper jaw, while the *calvarium* (White *et al.* 2012) includes the braincase (neurocranium) and ear (De Iuliis & Pulerà 2011), thus excluding the face.

The adult papionin cranium, as any typical primate cranium, has 27 bones (including the ear bones, excluding the mandible) plus occasional sutural bones, which are irregular ossicles occurring along sutures (White *et al.* 2012). The calvarium is made up of the frontal (*os frontale*), occipital (*os occipitale*), sphenoid (*os sphenoidale*) and the paired parietal (*os parietale*) and temporal (*os temporale*), as seen in Figure 1.5 (Fleagle 1999; White *et al.* 2012). On the external surface of the side wall of the cranium, papionins (and all catarrhines) have the frontal bone contacting the sphenoid bone, thus separating the zygomatic bone anteriorly from the parietal bone posteriorly (Fleagle 1999). The auditory region shows a tubular *external auditory meatus* (*meatus acusticus externus*, Figure 1.5), formed by the laterally extending tympanic bone (Fleagle 1999). On either side of the cranium, dorsal to the posterior teeth, are the *orbits*, and posterior to each orbit there is the *temporal fossa*, where the temporal muscle takes part of its origin (De Iuliis & Pulerà 2011). The temporal fossa evolved from a depressed region on the early synapsid cranium (MacLean 1990), that is why it is called a *fossa* despite having a convex floor in most mammals (including Primates). Infero-lateral to the orbits there is the *zygomatic arch* (*arcus zygomaticus*, Figure 1.5), formed by the jugal or zygomatic bone (*os zygomaticum*, Figure 1.5) and the temporal bone (De Iuliis & Pulerà 2011). Inferiorly, on the basicranium, the sphenoid bone forms thin *pterygoid plates* (not shown in Figure 1.5), where the pterygoid muscles attach (De Iuliis & Pulerà 2011). The nasal region consists of a large nasal chamber, in part filled by delicate scrolls of bone, the turbinates or conchae, which are outgrowths from the

inside walls of the maxillae, nasals, and ethmoids (Hildebrand & Goslow 2001). They are interpreted as an adaptation to endothermy, serving to warm, humidify and clean inspired air before it goes into the lungs (Hildebrand & Goslow 2001). The interorbital region is narrow, and the lacrimal canal is formed by both the maxillary and the lacrimal bones (Fleagle 1999).

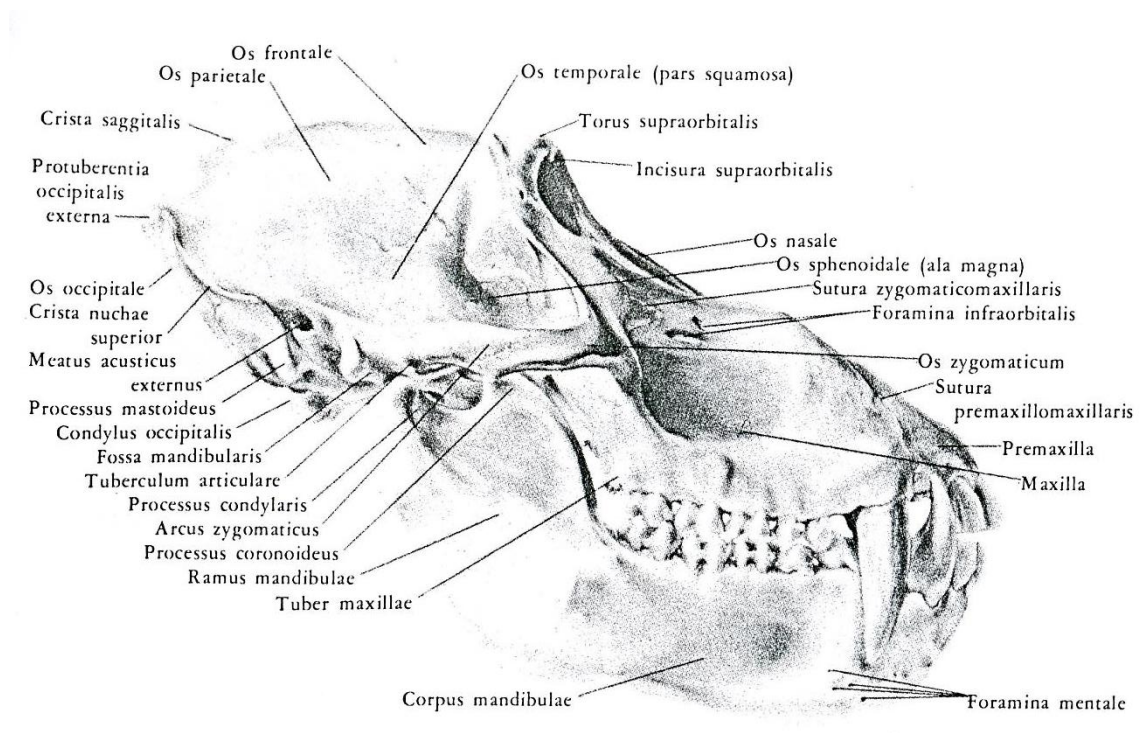


Figure 1.5. Representation of the skull of an adult male *Papio sp.* shown in lateral view. Adapted from Swindler & Wood 1973. See text for more details.

Primates have generally 4 types of teeth: incisors, canines, premolars and molars. Papionins have 2 incisors, 1 canine, 2 premolars and 3 molars per quadrant (Figure 1.5, dental formula 2.1.2.3/2.1.2.3; Fleagle 1999). The molar teeth in papionins are specialized, with the anterior two cusps and the posterior two cusps aligned to form two ridges, or lophs (Fleagle 1999). The canines are dagger-like, but smaller in females than in males, and sharpened by a narrow anterior lower premolar (Fleagle 1999). Broad incisors and molars with high crowns and relatively low cusps are generally found in frugivores and thus considered dietary adaptations to eating fruit (Fleagle 1999). Pirie (1978) found that tooth area may in part be related to the amount of food ingested, having found relatively large molars in leaf-eating primates, and in the grass-eating

Theropithecus; relatively small molars in insectivore primates and in one frugivore (*Ateles*). She suggested that the amount of mastication required to break down the preferred food is one factor in determining the most adaptive tooth size. Additionally, allometric analysis of primate post-canine dentition has revealed that there is a remarkably close correlation between tooth size and body size and very slight deviations from this general trend seem to relate closely to known dietary preferences (Pirie 1978). Nevertheless, she posits that the amount of mastication required by the preferred food item may be more important in determining the adaptive value of tooth size than the specific type of food eaten (Pirie 1978).

As for the particular differences in cranial anatomy among the papionin species sampled for this study, according to Groves (2001) the only real morphological similarity between *Cercocebus* and *Lophocebus* is the depth of the suborbital fossae, which is thought to be convergent as a result of facial shortening. Groves (1978) summarizes the differences between the genera *Lophocebus* and *Cercocebus*, and was the first to separate the two groups at the genus level. *Mandrillus* is a long-faced species like *Papio*, but its cranium is distinguished from the latter genus by its paranasal ridges, combination of large incisors and relatively small postcanine teeth, posteriorly convergent tooth rows, shelflike superior temporal lines overlying the origins of the temporal muscle (Groves 2001). *Theropithecus* can be differentiated from *Papio* by small incisors and larger, high-crowned postcanine teeth with accessory cusps and much reduced molar flare, and relatively shorter but deep face (Groves 2001).

1.3.6. Papionin Masticatory Muscle Anatomy

Of the three muscle types found in primates and other mammals (non-striated, skeletal, and cardiac), biomechanics is mostly concerned with skeletal muscle that is not controlled by the autonomic nervous system but is under direct voluntary control (Herzog 2006). The mammalian head has a large number of specialized muscles, but only four paired muscles are involved in mastication (Rogers 1992; Snell 1995), attaching the mandible to the base of the cranium. These might have played a role in the biomechanical performance and the adaptive evolution of the cranium. They are jointly called *adductors of the mandible* (Hildebrand & Goslow 2001), and in primates and other mammals they are individually named temporal, masseter, medial pterygoid, and

lateral pterygoid muscles. Figure 1.6 shows a depiction of the masticatory muscle anatomy of an adult male specimen of the genus *Papio* sp.

The fan-shaped temporal muscle (*musculus temporalis*), with its posterior fibres running almost horizontally forward and the anterior fibres running vertically downwards (Rogers 1992), originates on the braincase and sagittal crest, when it exists (Hildebrand & Goslow 2001). It runs from the lateral surface of the cranium (temporal fossa) between the superior and inferior temporal lines, and from the strong fascia which covers its superficial surface (Figure 1.6). Its fibres converge on both the outside and inside of the coronoid process of the mandible, passing deep to the zygomatic arch (Rogers 1992; Hildebrand & Goslow 2001). The deep portion of the temporal, attaching the sphenoid to the mandible, was recognized as a separate muscle, *musculus sphenomandibularis* (Dunn *et al.* 1996), but that has been refuted on the grounds that it is simply the deep portion of temporal (Türp, Cowley, & Stohler 1997). The temporal closes the jaw (Hildebrand & Goslow 2001).

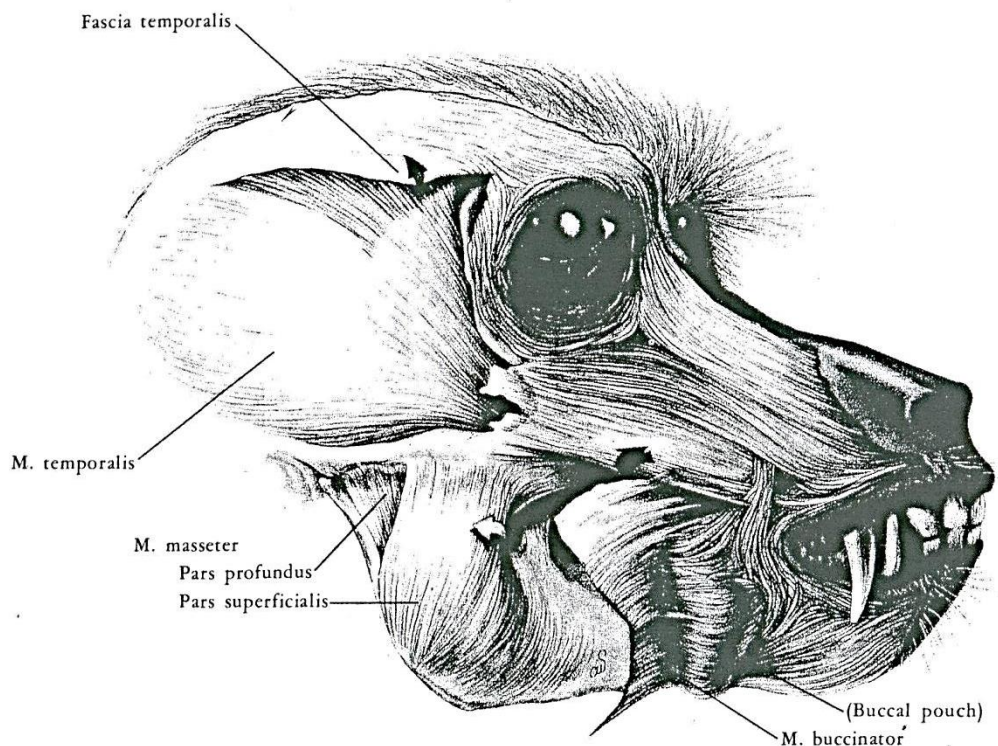


Figure 1.6. Masticatory muscle anatomy of an adult male *Papio* sp. shown in lateral view. Adapted from Swindler & Wood 1973. See text for more details.

The rectangular masseter muscle (*musculus masseter*) is attached to the zygomatic arch, its fibres running downwards and slightly posteriorly to insert on the lateral surface of the ramus, from the base of the coronoid process down to the gonial angle of the mandible (Rogers 1992; Hildebrand & Goslow 2001). It can be differentiated into a superficial portion and deep portion (Swindler & Wood 1973). Masseter is thought to have evolved from a portion of the temporal, while both of these muscles evolved from the *musculus adductor mandibulae* that existed in basal synapsids (Liem *et al.* 2001). This anatomical change during evolution increased bite force and allowed control over the movements of the mandible needed to position the teeth for cutting and masticating food (Liem *et al.* 2001). The masseter also closes the jaw (Hildebrand & Goslow 2001).

The medial pterygoid muscle (*musculus pterygoideus medialis*) runs from the medial side of the lateral pterygoid plate (Rogers 1992). In humans a superficial slip arises from the maxillary tuberosity, a rounded projection behind the third upper molar tooth. Both parts pass downwards, posteriorly and laterally to insert into the deep surface of the mandible, in the roughened area near the gonial angle of the mandible (Rogers 1992). The lateral pterygoid muscle (*musculus pterygoideus lateralis*) also has two parts: the larger, inferior part arises from the lateral side of the lateral pterygoid plate; the superior part arises from the inferior surface of the greater wing of the sphenoid. Both pass almost horizontally backwards to insert into the anterior surface of the disc of the temporo-mandibular joint and into the neck of the mandible. The lower part lies between the two parts of the medial pterygoid muscle (Rogers 1992). Both types of pterygoid close the jaw and pull it medially (Hildebrand & Goslow 2001).

More detailed descriptions and illustrations of the anatomy of masticatory muscles in papionins can be found in Chapter 5 (Section 5.1). In the next section, several issues related to papionin adaptation to masticatory function that contribute for its better understanding are discussed, as well as some functional hypotheses about papionin cranial biomechanics.

1.4. Adaptations to Diet and Cranial Form Evolution

Changes in the form of the cranium can often be understood in terms of adaptation to achieve a stronger bite at the front of the mouth, or to perform an efficient grinding system at the back or the mouth, or to other types of feeding (Benton 2005). The different cranial forms observed among papionins could mean (if neutral evolution is excluded) that each species has adapted to different masticatory performance.

This section (1.4) reviews issues concerning papionin cranial adaptation to feeding, starting with the concept of adaptation (and adaptations, which are slightly different), moving on to physical properties of food items, a description of papionin adaptations to feeding, and finally some functional hypotheses about papionin adaptations to feeding.

1.4.1. Concept of Adaptation

Section 1.2.4 describes how bone can functionally adapt under mechanical loads during the lifetime of an individual. Yet, on a populational level, adaptation has been a widely discussed and controversial topic. Indeed, it is a highly complex concept in any field of biology. Primatologists, for instance, have generally paid little attention to the definition of adaptation and have used the term broadly as an equivalent of behaviour (Ross *et al.* 2002). Persistent questions about which there is disagreement include the very definition of adaptation (Ross *et al.* 2002).

Adaptation can be defined both as a trait and as a process (Wolff 1991; Ross *et al.* 2002; Futuyma 2009). As a trait, *an adaptation* becomes fixed in a population by natural selection because of the effect on its ability to perform a particular function, *i.e.*, a trait that confers a significant selective advantage through the improvement in such function (and which still performs that function) (Ross *et al.* 2002; Futuyma 2009). Most of the time a direct relationship between a trait and its natural selective fixation cannot be proved, which means in practical terms that adaptations are often simply traits that perform a particular function (Ross *et al.* 2002). As a process, *adaptation* refers to genetic change in a population through natural selection, or more accurately it refers to changes in gene frequency that can improve survival and reproduction of that

population in its environment (Futuyma 2009). The process of adaptation necessarily happens over long periods of time, which means it has a historical component: a character state can be better adapted in relation to its ancestral state (Futuyma 2009). Some authors prefer a more non-historical definition, where the extent of adaptation is assessed only among populations in a given environment, not in relation to their ancestral population (*e.g.* Reeve & Sherman 1993).

The two definitions of adaptation are nevertheless interrelated. Since not all traits are adaptations (Futuyma 2009), and gene frequency is ultimately dependent on the number of traits that can confer an adaptive advantage (reviewed by Gillespie 2004), recognizing whether a trait is an adaptation or not is essential to the understanding of adaptation as a process. Considering a particular trait as an adaptation depends on the criteria an author chooses to define adaptation. For example, some of Kay's (1984) criteria for considering a morphological trait as an adaptation include (1) it having the same adaptive role in every extant species that possesses it; (2) no evidence that it evolved, in the same lineage, to perform a different role; and (3) it having a functional relationship to an adaptive role. Otherwise, a trait might have evolved neutrally (by random genetic drift), rather than by natural selection (Futuyma 2009), and thus is not explicitly adapted to a function, but able to perform it due to chance alone. It could also be linked to another trait that is actually the adaptation and evolve with it, or simply exist because of its phylogenetic history (Futuyma 2009). As such, some authors believe it is better not to assume *a priori* that a trait is an adaptation, but discern first whether evidence favours that interpretation or not (Williams 1996).

In papionin populations, many traits that are generally considered adaptations to feeding or, better said, to intra-oral food processing (such as length of the snout, tooth surface or muscle cross-sectional area; see Subsection 1.4.3) are related to the physical properties of food stuffs. For example, large maxillary and mandibular fourth premolars are used to crush seeds in *Cercocebus*, Fleagle & McGraw 2002; see Section 1.4.3). A hard food difficult to break open requires masticatory adaptations different to those required for a tough and fibrous food. A brief discussion of physical properties of foods will follow.

1.4.2. Physical Properties of Foods

The physical properties of different kinds of foods are not entirely well known, but it is established that they affect mastication and intra-oral processing (Hildebrand & Goslow 2001), and cranial form adapts in response to loads generated by intra-oral food processing. Thus the material properties of a given food (and not the foods *per se*; Yamashita 1998; Lucas 2004; Dunn 2011) are important determinants of how the cranial skeleton is loaded during food processing. In order to be of any metabolic value, food items have to be acquired and processed before their nutrients can be released and become available for assimilation (Ungar 2010). Their physical properties govern how they are processed by a masticatory system, *e.g.* the size and shape of a food item can limit ingestion, as well as its toughness (Ungar 2010). Surface area and volume are also important in determining the probability of food-tooth contact during mastication, and the number of chews needed before swallowing (Ungar 2010). Abrasiveness is another important property: many plant foods have silica crystals both endogenously and adherent to the external surface (Ungar 2010). These particles are responsible for much tooth wear in mammals (Baker, Jones, & Wardrop 1959).

The physical properties of wild animal foods are often disregarded by field researchers and unreported, limiting our ability to generate hypotheses of biomechanical adaptation that can be tested in laboratory. Field researchers are more interested in food chemical contents such as total tannins, phenolic or alkaloids (Whiten *et al.* 1991; Cowlshaw 1997) or the spread of resources (Barton, Byrne, & Whiten 1996). Fortunately, Lucas (2004) provides an extensive list of properties of food items, such as toughness and hardness, and even Young's modulus when available in the literature.

The mechanical behaviour of a material when a force is applied to it is best described by its mechanical properties (Ungar 2010). Two of them are stiffness and strength (Lucas 2004). Stiffness is related to elasticity, *i.e.* Young's modulus (see Subsections 1.2.3 and 2.4.2), while strength is the force required to cause a fracture. Another property is toughness, which is defined as the resistance of a solid to fracture (crack propagation); tough objects are more resistant than brittle ones (Ungar 2010). The latter will deform little and fracture at low strains. One other property is hardness: according to Lucas (2004) it is not a property in itself, but a concept that means resistance to deforming under indentation. As such, hardness is an indirect measurement of the yield stress of a solid (Lucas 2004): the stress required to initiate fracture (Ungar 2010).

For instance, roots and tubers are quite variable in toughness and stiffness (Dominy *et al.* 2008). Also, as Barton (1989) points out, the rather broad term “fruit” includes fleshy, sugary storage structures; drier, less digestible nuts; fruit-like vegetable matter; and seeds... In most studies, the consumed fruits reported include seeds, yet these have different properties, and primates that are seed crushers have different morphologies from seed spitters or swallowers (Lucas 2004).

While each dietary item has its own physical properties, certain generalisations can be made. For instance leaves are a very tough food (Lucas 2004; Wright *et al.* 2008), meaning that a large amount of energy is required to digest them and extract their nutrients. Young leaves are less tough than old leaves (Lucas 2004). Fruits (diverse as they can be) are typically not tough, though they may be rather stiff (Williams, Wright, & Truong 2005) necessitating a high bite force to break them. Corms, bulbs and rhizomes have a higher Young’s modulus than leaves or fruits, while all three have a higher toughness than fruits (Dunn 2011). However, rhizomes are tougher and stiffer than all other foods (Dunn 2011). Thus while there is considerable variation in physical properties between the categories of diet, there is also confounding variation within categories. Both are likely to influence cranial form via biomechanical adaptations.

The papionin species have cranial traits that are often interpreted as adaptations to masticatory function (intra-oral food processing) on a basis of comparative anatomy (*e.g.* Fleagle & McGraw 2002). The following section describes aspects of morphology that have been hypothesised to be adaptations to feeding in papionins.

1.4.3. Papionin Cranial Adaptations to Diet

Typical vertebrate adaptations to feeding can be roughly categorized as adaptations to a diet with particular physical properties: (1) hard foods; (2) turgid, brittle and varied foods; (3) tough and fibrous foods; and (4) tough and soft foods (Hildebrand & Goslow 2001). An inspection of their diets (see Section 1.3.3 above) suggests that papionin genera can be included in the first three food categories.

The genera *Cercocebus*, *Lophocebus* and *Mandrillus* are generally understood to be durophagous (Gartlan & Struhsaker 1972; Hoshino 1985; Horn 1987; Rogers *et al.* 1996; Fleagle & McGraw 1999; Lambert *et al.* 2004; Astaras *et al.* 2008; summarized in Table 1.1), meaning they often rely on hard foods (particularly as fallback sources of

nutrients). Durophagous animals crush or crack hard nuts, shells, woody seeds, *etc.*, to make digestible food available (Hildebrand & Goslow 2001). Anatomical traits that can be adaptations to crush or crack foods, such as powerful jaws and teeth with large, plate-like or even flat surfaces (Hildebrand & Goslow 2001), are thus to be expected on those three papionin genera. A comparative analogy can be made with hyenas that crack open hard bones to reach the bone marrow; their adaptations include extra heavy jaws and teeth, enormous adductor muscles and sagittal crest; also an early closure of cranial sutures (Hildebrand & Goslow 2001).

Fleagle and McGraw (1999, 2002) describe both genera *Cercocebus* and *Mandrillus* as having relatively large upper and lower posterior premolars that resemble the first molar in size, claiming this as an adaptation for cracking open hard nuts. *Cercocebus* on its own has been described as having adaptations for feeding on tough-skinned fruits and on hard nuts and seeds, including large incisors that can accommodate wear from puncturing tough-skinned fruit (Hylander 1975), thick molar enamel to withstand the stress of crushing forces (Kay 1981), large maxillary and mandibular second premolars (P4) to increase surface area to crush seeds (Fleagle & McGraw 2002), and a shortened face that increases bite force (Singleton 2004). The genus *Mandrillus* has, like *Cercocebus*, cranio-mandibular traits that can be interpreted as suited to cracking open hard seeds and nuts, especially when the genus is known to exploit hard seeds as a dietary niche (Fleagle & McGraw 1999). Both *Cercocebus* and *Mandrillus* have been reported to eat the pith and bark of various grasses and they may also use their premolars for stripping these foods (Harrison 1988). Yet, Astaras *et al.* (2008) found no evidence of dietary specialization in the genus *Mandrillus* for hard decaying seeds on the forest floor, as Fleagle and McGraw's (1999) morphological analysis suggests. Conversely, species of the genus *Lophocebus* are also reported to eat hard nuts such as palm nuts (Subsection 1.3.3), but Fleagle and McGraw (2002) find they lack the enlarged premolars of *Cercocebus*. Although *Mandrillus* is of larger size than the other two durophagous species, the ability to deal with foods of equivalent mechanical properties requires equality of performance irrespective of size.

The *Papio* species and *Macaca* are good examples of feeders on turgid, brittle and varied foods: they are omnivorous, feeding on dry leaves, flowers, seeds, fruits, berries, roots and tubers, bark, tree gum and bulbs (Aldrich-Blake *et al.* 1971; Harding 1976; Stambach 1987; Yeager 1996; summarized in Table 1.1). Foods like the cells of fruits and berries (turgid) or large seeds and nuts (brittle) must be burst open or fractured to prepared them to digestion, an action that is more effectively performed by

crushing and rolling by a tooth combination resembling a mortar and pestle: a low cone on one tooth fits into a basin on an opposing tooth (Hildebrand & Goslow 2001). Most frugivorous animals (like fruit bats), and granivorous (like squirrels), have postcanine teeth with such a design (Hildebrand & Goslow 2001). Like other animals with a varied diet, the omnivorous *Papio* and *Macaca* have varied teeth that are not specialized solely for shearing or grinding, the postcanine teeth are moderately broad, with low cusps and basins suitable for crushing (Hildebrand & Goslow 2001). *P. anubis* supplements its diet with meat and other animal matter (Melnick & Pearl 1987), which are tough and soft foods (Lucas 2004), but does so only in an opportunistic manner with perhaps little effect on the cranial morphology.

The genus *Theropithecus*, among all papionin genera, is exclusively graminivorous (Dunbar & Dunbar 1974a; Iwamoto 1979; summarized in Table 1.1), with traits that can be considered adaptations to feeding on tough, fibrous foods, such as leaves, stems, roots and other vegetable material (Lucas 2004). Animals that eat them are said to be herbivorous (Hildebrand & Goslow 2001); if they specialize in grass, they are said to be graminivorous. Most mammalian herbivores crush and grind food with their postcanine teeth, while their anterior teeth are instead specialized for shearing, gnawing, or cropping; the two sets of teeth can be separated by a toothless space called the diastema (Hildebrand & Goslow 2001). Postcanine teeth are broad and similar to one another, with premolars often resembling molars (Hildebrand & Goslow 2001). *Theropithecus* has no clear diastema, but is found to have wider condylar heads (Bouvier 1986b; Jablonski 1993), a trait related to feeding mainly on leaves and grasses, food items that require greater masticatory effort, particularly lateral movements of the mandible (Hylander 1992). The genus *Theropithecus* exhibits a somewhat shorter face (when compared with similar-sized papionins, like *Papio* sp.) but also a relatively longer masseter lever arms, higher jaw joints, and other cranial specializations similar to colobines (that also have a longer masseter lever arm and shorter face, interpreted as adaptations to efficiently processing a tougher leaf and seed diet; Hylander 1979a) (Jolly 1970; Jablonski 1993; Ravosa 1996). *Theropithecus*, as is the case for other graminivorous animals, needs to produce large amounts of effort to masticate their tough and fibrous foods, while requiring only minimal amounts of gape (Fitton 2007).

Major anatomical differences among papionins concern mainly the length of the rostrum, with larger sized species having longer snouts, suggesting an allometric component in that trait. Another particular difference is the existence of a maxillary sinus in the genus *Macaca*, common in most Old World monkeys, humans, greater apes,

and various New World monkeys (Ankel-Simons 2007), but not found in any of the other papionins. The presence of a supra-orbital torus has also been controversially associated with feeding as an adaptation to withstand masticatory loads (Hylander, Picq, & Johnson 1991a; b, with *in vivo* experiments). The very existence of a supra-orbital torus on primate species has puzzled researchers for some time. Some have argued that it is an adaptation to anterior dental loading, preventing the deformation of the glabellar region when incisor-bite forces are applied (Endo 1966, 1970; Oyen *et al.* 1979; Oyen & Russell 1982; Russell 1982, 1985). The torus would also prevent bending of the inter-orbital and dorsal orbit in the frontal plane (a region that would suffer from greater stress during incision than during mastication) due to bilateral contraction of the adductor muscles (Endo 1966, 1970; Oyen *et al.* 1979; Oyen & Russell 1982; Russell 1982, 1985). Russell (1985), in her review of the supra-orbital torus, suggested that its formation occurs in primates that lack a more vertically-oriented frontal bone (all except humans), precisely to oppose the anterior dental loads transmitted superiorly. Oyen *et al.* (1979), studying baboons, suggest that an enlarged supra-orbital torus is a response to an increase in jaw-adductor force levels, which is required to compensate changes in the elongation of the incisor load arm relative to the masseter arm, in order to maintain similar incisor-bite forces. However, this was shown to be a spurious correlation reflecting increases in overall skull size during growth (Ravosa 1991b). Hylander *et al.* (1991a; b) *in vivo* results offer mixed support for the anterior dental loading model, because while circum-orbital strain directions during incision are as predicted by the model, since there is the occurrence of a significant strain gradient, this indicates that the supra-orbital torus is overbuilt to counter routine masticatory loads. Circum-orbital strain levels during incision are not higher than those produced during mastication, which goes against the anterior dental loading model (Hylander *et al.* 1991a; b; Hylander & Johnson 1992; Hylander & Ravosa 1992).

Are these adaptations in papionins actually related to feeding? If they are, *how* are they related to it? There have been a number of hypotheses generated to try and answer those questions, many of them biomechanical or functional. The most relevant to papionins are discussed next.

1.4.4. Functional Hypotheses of Papionin Cranial Form Evolution

Understanding of the functional determinants of primate cranial form has benefited greatly from experimental studies (Luschei & Goodwin 1974; McNamara 1974; Hylander 1979a; b; c, 1984, 1985; Hylander & Bays 1979; Bouvier & Hylander 1981; Hylander, Johnson, & Crompton 1992; Hylander *et al.* 1998; Hylander, Johnson, & Crompton 1987; Hylander *et al.* 1991a; Dechow & Carlson 1990), while understanding of the functional bases of cranio-dental variation have been enhanced by morphological studies of cercopithecoid subfamilies (Hylander 1975; Kay 1978; Kay & Hylander 1978; Bouvier 1986a; b; Ravosa 1991c, 1996, 1988, 1990, 1991a; b; Lucas & Teaford 1994). The primate mandibular form has also been the subject of extensive work in the same way (*e.g.* Hylander 1977; Hylander & Johnson 1994; Marinescu, Daegling, & Rapoff 2005; Gröning *et al.* 2009; Panagiotopoulou, Kupczik, & Cobb 2011a; Daegling *et al.* 2011; Gröning, Fagan, & O'Higgins 2011; de Jong, Korfage, & Langenbach 2011). The macaque and baboon primate groups have been more extensively used for testing many biomechanical hypotheses (*e.g.* Hylander 1975; Oyen, Walker, & Rice 1979; Ravosa 1991a; b; Ravosa & Profant 2000).

At the simplest level, there are four main recognized hypotheses that characterize how loading regimens act on the primate cranial skeleton (Chalk *et al.* 2011): (1) bending in the frontal plane; (2) bending in the sagittal plane; (3) dorso-ventral shear of the face relative to braincase; and (4) torsion of the face on the braincase about the antero-posterior axis of the skull.

Bending in the frontal plane is the result of inferiorly directed temporal and masseteric forces applied to the lateral aspects of the orbits and zygomatic arches, and of superiorly directed forces when biting on the anterior dentition (Endo 1966, 1970; Russell 1985; Hylander *et al.* 1991a; b). Following Hylander *et al.* (1991a), when the supra-orbital region is modelled as a simple beam, it is predicted that tensile strains are perpendicular to the mid-sagittal plane of the cranium, and the strain magnitudes are predicted to be highest in the dorsal inter-orbital region. The superiorly directed bite force is expected to yield compressive strain concentrations parallel to the mid-sagittal plane of the cranium (Endo 1966, 1970; Hylander *et al.* 1991a; b).

Bending in the sagittal plane is predicted to be due to superiorly directed bite forces at the teeth and joint reaction forces at the temporo-mandibular joint, combined with inferiorly directed masticatory muscle forces (Hylander *et al.* 1991a). The simple geometric cranial model of a beam with triangular cross section predicts tensile strains

to occur along the palate, the pterygoid processes and the zygomatic arches; compressive strains should be concentrated in the dorsal face, including the maxilla and inter-orbital region (Hylander *et al.* 1991a). Both tensile and compressive strains are predicted to be oriented parallel to the sagittal plane (Hylander *et al.* 1991a).

Dorso-ventral shearing is caused by the inferiorly-directed masticatory muscle forces and the superiorly directed bite and temporo-mandibular joint reaction forces, resulting in the displacement of the facial skeleton superiorly relative to the braincase (Chalk *et al.* 2011). The displacement of the face in the sagittal plane is resisted by bone in that plane. Tensile strains are expected to occur in the dorsal and ventral aspects of the face, with rostral regions experiencing higher strains relative to areas with thicker bone such as the supra-orbital torus. Dorso-ventral shearing is also predicted to cause shear in the lateral surfaces of the rostrum and orbits (Preuschoft *et al.* 1986; Hylander *et al.* 1991a).

Twisting of the face on the braincase about the antero-posterior axis of the cranium is due to the torsional moments of the balancing side muscle force and bite force exceeding the working side muscle force, during unilateral mastication (Greaves 1985, 1995). The face is modeled as a cylinder that twists, and tensile and compressive strain orientations are predicted to be 45° to the twisting axis (*i.e.*, the long-axis of the cranium) (Greaves 1985, 1995; Hylander *et al.* 1991a; Ross 2001, 2008), meaning that the directions of tensile and compressive strains should present the reverse pattern when molar biting and chewing shifts from one side of the face to the other (Greaves 1985, 1995). This hypothesis has been tested experimentally on *P. anubis*, *M. fascicularis* (Hylander *et al.* 1991a; b), and on *Cercopithecus aethiops* (Oyen & Tsay 1991): forces experienced during molar biting and mastication produce a net twisting (torsion) of the facial skeleton about the antero-posterior axis of the cranium (Greaves 1985, 1995), affecting especially the circum-orbital region. While *Papio* and *Macaca* show this characteristic reversal pattern predicted in the theory, circum-orbital strain directions are the opposite of what would be expect, with the working-side browridge experiencing compression during molar biting, not tension (Hylander *et al.* 1991a; b; Hylander & Johnson 1992; Hylander & Ravosa 1992).

These hypotheses were first formulated when strain gauges were the only way to study biomechanical problems and deformations were hard to observe as a whole. Nowadays, other than testing a single biomechanical hypothesis about how a real cranium deforms, computational methods such as finite element analysis are more commonly used because they allow for a visualization of a virtual cranium deforming

after load (Chalk *et al.* 2011). Like shape, deformations are complex and likely involve various combinations of bending, shearing and twisting at the same time.

When speaking of bite force, moving the muscle resultant force closer to the dentition increases the length of the lever arm producing a higher bite force (Osborn 1987; Greaves 2009). Higher bite force also arises when moving the bite point closer to the temporo-mandibular joint, which decreases the length of the load arm. From this follows that, all other factors being equal, relatively shorter rostrums increase the mechanical advantage of the jaw muscles, particularly over the anterior dentition, and increases the efficiency of the muscle force transferred to the dentition (Osborn 1987; Dumont 1997) allowing for an increase in biting force capacity, at the expense of a larger gape (Fitton 2007). Using allometric analysis, Ravosa (1990) investigated the functional significance of differences in facial form between cercopithecines and colobines. Results indicated that there is a stronger positive allometry in the cercopithecine facial skeleton, when compared with colobines (Ravosa 1990). When the angle between the maxilla and the mandible, during maximum jaw opening, is similar, a long face facilitates both an increased gape so the animal can accommodate larger canines, such as found in cercopithecines (Ravosa 1990). They also have a large gonial angle, allowing for the increase in gape by increasing the distance between upper and lower canines, for a set amount of mandibular retraction (Ravosa 1990).

These functional aspects of the cercopithecine cranial form could indicate cranial adaptation to a particular biomechanical loading. Intra-oral food processing when feeding is a source of repetitive loading to the cranium, and the papionin cranium, as discussed in Subsection 1.4.3, is often described as having adaptations to particular types of food, making diet an important factor that could have contributed to the present cranial form in those primates. Since different papionin species occupy different ecological and dietary niches and, thus, respond to different selective pressures, differences in cranial form are often assumed (Hayes *et al.* 1990; Ravosa 1990; Daegling 1992; Frost *et al.* 2003; Singleton 2005; Taylor 2006; Leigh 2006; Dunn 2011) to reflect adaptations in each papionin cranial form to their functional demands, constrained by phylogeny (Fitton 2007).

But is the papionin cranial form adapted at all? It is conceivable that, because it is a relatively recent group (see Subsection 1.3.1), their phenotype did not have time to adapt, and the presently observed form is but the result of random processes such as genetic drift. In other words, is it admissible to discuss adaptation of form to something when there is no certainty about the rejection of random factors producing that form?

Only if random genetic drift is not the single driver of papionin cranial form evolution should its form reflect adaptation that could be interpreted as adaptation to the particular biomechanical demands of different dietary strategies. The necessary test on whether random genetic drift alone is responsible for a phenotypic trait can be performed with the help of a quantitative genetic model

If the outcome of the test is that random genetic drift is not the single driver of cranial evolution, discussing cranial adaptation to diet then becomes acceptable, and how it happened can be approached. One hypothesis is that if a species is particularly specialized in feeding on one food item (for example hard foods, rather than tough, fibrous foods; see Subsection 1.4.2), then its cranium will have adapted to the biomechanical demands that processing that food item for nutrients requires. This is relevant, for example, for the specialist graminivorous species *Theropithecus gelada* (Dunbar & Dunbar 1974a), and even for the durophagous species *Cercocebus torquatus*, *Lophocebus albigena* and *Mandrillus sphinx*, that, although feeding on softer foods often, they rely on vitally important hard fallback foods for survival in the dry season (see Subsections 1.3.3 and 1.4.3). Intra-specific differences in cranial form are also interesting in studying cranial adaptation to food processing, for if a male and a female of the same species show great differences in the form of the cranium while eating the same diet (see Subsection 1.3.3). Their cranium should be adapted in the same way to that diet, even if there are differences in form.

Biomechanical adaptation can be measured in terms of local strains, global deformations, and force magnitudes with the help of powerful computational methods such as finite element analysis. The results can be compared statistically using geometric morphometrics and multivariate methods, and then related to diet and cranial form. If cranial form has not evolved randomly and is indeed adapted to diet, some degree of association must necessarily exist between diet and biomechanical traits such as deformation and bite force.

1.5. Summary

In summary, the relationship between form and function is of paramount importance for the understanding of phenotypic evolution of biological organisms. The evolution of cranial form can be studied with established quantitative genetic theory, and its function can be understood through biomechanics. If random processes (like genetic drift) are not the key driver of form, then (selection towards adaptive) function can be assumed to be. Papionins, on account of their biology and evolutionary relationship to humans, are almost uniquely positioned to be used as a model system in studies of form evolution and biomechanical adaptation. Diet remains a recognised adaptive pressure in the evolution of all vertebrates, possibly making masticatory function responsible for the form of the cranium in papionins. The studies in this thesis, then, consider papionin cranial form evolution and its functional adaptations to diet, under an evolutionary framework.

The following chapter provides an overview of the methods used throughout the thesis. Chapters 3 and 4 concern a test on the divergence of the papionin cranium by the action of a random genetic drift. Chapters 5, 6 and 7 relate respectively to building 3D models, sensitivity analyses, and dietary adaptation hypotheses using biomechanical parameters estimated from the 3D models using finite element analysis. Finally, Chapter 8 tests the association between diet, cranial form and several parameters estimated with finite element analysis and geometric morphometrics. Chapter 9 will summarize the major findings and suggest future research.

Chapter 2. Overview of Methods

2.1. Introduction

This chapter provides an overview of the most important methods used throughout this thesis. These are quantitative genetic analysis, geometric morphometric analysis, finite element analysis, landmark-based deformation analysis and multivariate statistical analysis. The material used and samples range from simulated data to three-dimensional (3D) landmarks to computerized tomography scans. Each one will be described in detail in the chapters where they are used. Additionally, the quantitative genetic model used in Chapters 3 and 4 is described in more detail in these chapters.

2.2. Quantitative Genetic Analysis

Quantitative genetics was developed initially by Fisher (1918), Wright (1921a; b; c; d; e, 1922) and Haldane (1932) when progress in the field of population genetics (the study of genetic variation between individuals; Conner & Hartl 2004) encountered limitations in dealing with complex, multivariate traits. Very often phenotypic traits are not discrete but continuous, caused by additive genetic variation at multiple loci (Falconer & Mackay 1996; Roff 1997). Those traits (for example, shape or form) vary continuously within a population and in a single environment, and their evolution is best studied using the quantitative genetic framework (Lande 1979, 1980a; b; Lande & Arnold 1983; Lofsvold 1986, 1988; Zeng 1988; comprehensive reviews can be found in Falconer & Mackay 1996; Roff 1997; Lynch & Walsh 1998; a simpler introduction is provided by Conner & Hartl 2004).

Quantitative genetics works with the population variance (both genotypic and phenotypic) to estimate the heritability of continuous traits (see Subsection 1.2.1). Empirical applications of quantitative genetics rely on field or laboratory estimates of heritabilities, additive genetic variances and covariances, and regression of trait means

against fitness parameters (Schlichting & Pigliucci 1998). In real outbreeding species, heritability and additive genetic variance can be estimated with methods such as offspring-parent regression, full-sibling and half-sibling analyses (Conner & Hartl 2004). Estimating additive genetic variance is central when studying the connection between neutral microevolutionary processes and macroevolutionary patterns (Lande 1980b; Arnold, Pfrender, & Jones 2001; Jones *et al.* 2003; Bégin & Roff 2004) because it is thought to determine both the response to selection and the pattern of neutral divergence, at least among populations over a small time scale (Lande 1980b; Felsenstein 1988; Zeng 1988). In evolutionary divergence studies, the expected pattern of phenotypic divergence among populations caused by random genetic drift in correlated traits can be used as a null hypothesis to test for neutral evolution (Lande 1979, 1980b).

In addition to single continuous traits in a single environment, quantitative genetics can deal with multiple continuous traits in multiple environments. It can be utilized to take the correlation among traits into account in such studies, including the relationship between genotype and phenotype among multiple traits (Conner & Hartl 2004; Gillespie 2004; see also Section 1.2.1). Quantitative trait loci (QTL) mapping has also been used to study traits that have polygenic effects as a complement to purely statistical quantitative genetics because it is closer to the actual mechanisms underlying quantitative traits (Roff 1997; Schlichting & Pigliucci 1998; Conner & Hartl 2004).

Although quantitative genetics cannot be inherently right or wrong because it is mathematically consistent, criticism of the quantitative genetics framework has been based mainly on discrepancies between its theoretical assumptions and the reality of natural populations (reviewed by Schlichting & Pigliucci 1998). Any type of continuous traits can be used in quantitative genetic analysis, since the method uses the correlation and the variance-covariance matrix among traits. In Chapters 3 and 4 of this thesis all data, simulated or real, are landmark coordinates describing form, a type of multivariate data developed in the field of geometric morphometrics, which will be discussed in the next section.

2.3. Geometric Morphometric Analysis

Morphometric analysis is the statistical study of shape and size variation and their covariations with other variables (Claude 2008). Formally, it is a subfield of statistics (Mitteroecker & Gunz 2009). *Shape* is commonly described as the geometric property of an object invariant under scaling, rotation, or translation. *Size* is a scalar, based on distances or coordinates of points specified on the object. An object can have other attributes that are not shape properties, like colour or texture (Claude 2008). In the 1980s, morphometrics went through a major “revolution” (Rohlf & Marcus 1993) with the development of coordinate-based methods, generalised Procrustes analyses, the associated discovery of the statistical theory of shape, and the computational realization of transformation grids using the thin-plate spline, effectively inaugurating the field of *geometric morphometrics* (reviews on the whole geometric morphometric method can be found in Rohlf & Marcus 1993; Bookstein 1998; O’Higgins 2000; Adams, Rohlf, & Slice 2004; Zelditch *et al.* 2004; Slice 2005; Mitteroecker & Gunz 2009).

Geometric morphometrics is, thus, the statistical analysis of shape based on Cartesian landmark coordinates (Mitteroecker & Gunz 2009). All objects have a shape, and since they are everywhere, natural or man-made, collecting geometric information has become routine (Dryden & Mardia 1998). Following Kendall (1984) and Dryden and Mardia (1998) the notation used here will be that there are k landmarks in m dimensions, usually $k \geq 3$ and $m = 2$ or $m = 3$. The concept and nature of landmarks is discussed next, with the connection between shape and size and superimposition methods being discussed later. This section ends with a review on the thin-plate spline.

2.3.1. Landmarks

A landmark is reference point on an object. To be useful in comparing objects, landmarks must correspond, *i.e.* be equivalent, among them (Dryden & Mardia 1998). The shape of an object is described by a finite number of landmarks (Dryden & Mardia 1998). In the literature there have been various synonyms for landmarks, including vertices, anchor points, sites, *etc.* (Dryden & Mardia 1998). Geometric morphometric analyses depend entirely on the definition of equivalent landmarks between forms (Oxnard & O’Higgins 2009).

There are three types of landmarks. *Anatomical* landmarks are reference points that correspond between organisms in some meaningful way, usually in terms of biological derivation, either in terms of development or of phylogeny – the landmarks are called *homologous* (Dryden & Mardia 1998; but see discussion below). *Mathematical* landmarks are reference points located on an object according to a mathematical or geometrical property of the object, *e.g.* a point of maximum curvature or an extreme point (Claude 2008). *Pseudo*-landmarks are constructed points on an organism, located either around the outline or in between anatomical or mathematical landmarks (Dryden & Mardia 1998).

Another classification assigns landmarks to a further three types. Type I landmarks are discrete juxtaposition of tissues, or sufficiently small features to be defined by a single point (Bookstein 1991a; reviewed by Claude 2008). Type II landmarks are defined by local properties, such as maximal curvatures, where homology may have weaker biological grounds (Claude 2008). Type III landmarks are extremal points that can correspond to an end-points of diameters, a centroid, or an intersection between inter-landmark segments; they are constructed on a curve geometrically (Dryden & Mardia 1998; Claude 2008).

Anatomical landmarks are usually of type I or II, and mathematical landmarks are usually of type II or III. Pseudo-landmarks are commonly taken equally spaced along outlines between pairs of landmarks of type I or II, and in this case they are type III (Dryden & Mardia 1998). Type I landmarks are the easiest to locate and the most reliable for biological studies (Dryden & Mardia 1998).

Geometric morphometrics is based on landmarks as well as on Cartesian coordinates, but landmarks must be equivalent in some meaningful sense. Traditionally, that equivalence is called “homology”, a concept that is far from established and irrefutable in biology. Three classical definitions of homology coexist, depending on the origin of the landmark: structural/functional, developmental, and phylogenetic/evolutionary. Initially, Owen (1848) defined homology as a “structural correspondence,” as opposed to analogy, a “non-correspondent similarity” (Mitteroecker 2007). Furthermore, homology in genetics refers, somewhat inaccurately, to the similarity in DNA or protein sequences (see a good review of the concept of homology in fields other than geometric morphometrics in Hall 1994). Oxnard and O’Higgins (2009), rather than use the word homology prefer to speak simply about the equivalence or correspondence of landmarks, which varies depending on whether the question of interest is about function, development or phylogeny.

In fact, the morphometric toolkit does not implicate *a priori* choice of any specific definition of homology *per se*, rather the choice of landmarks determines the kind of information that is equivalent across the observed forms (Mitteroecker 2007). Any choice of landmarks should be driven by the hypothesis under test, and situations are common where landmarks on the same structure are deemed equivalent or not according to the question being asked (Oxnard & O'Higgins 2009). The selection of the equivalence that corresponds to the actual scientific question thus belongs to the researcher (Mitteroecker 2007).

There is a further type of landmark in the geometric morphometric toolkit: the *sliding semi-landmark*, which is located on a curve or surface and allowed to slide a small distance with respect to another equivalent curve (Dryden & Mardia 1998). The concept of sliding semi-landmarks was invented to extend landmark-based statistics from fixed landmarks to equivalent smooth curves and surfaces. It was first developed and applied to two-dimensional outlines by Bookstein (1997). Thus, assuming that the curves in different specimens will be equivalent according to the hypothesis being tested, a whole sample of semi-landmarks placed on a curve or surface is made to slide on that curve or surface iteratively, with reference to true landmarks, and the configuration of landmarks and semi-landmarks on the (current iteration) consensus form (Oxnard & O'Higgins 2009). As such, the resulting semi-landmarks (after sliding) respect point equivalences between forms in the sense that these are embodied in the true landmarks, minimizing error between specimens (Oxnard & O'Higgins 2009).

2.3.2. Shape and Form

In everyday language, the word shape usually refers to the appearance of an object (Dryden & Mardia 1998). In morphometrics, the term *shape* is used to designate the geometric information present in a landmark configuration that is independent of the overall position (location), size (scale) and orientation of an object (Dryden & Mardia 1998; Mitteroecker & Gunz 2009). Two objects have the same shape if they can be translated, scaled and rotated with respect to each other so that they match exactly (Dryden & Mardia 1998). In practice, researchers who are interested in comparing two objects with different shapes require a way of measuring shape and some notion of

distance between two shapes, as well as methods for the statistical analysis of shape (Dryden 1989; Bookstein 1991a; Dryden & Mardia 1998).

Apart from comparing shapes alone, retaining scale information (size) as well as the shape of an object is often of great interest (Dryden & Mardia 1998). Thus, the term *form* denotes the geometric information that is independent only of the position (location) and orientation of an object (Dryden & Mardia 1998), that is to say it comprises both the shape and the size of an object (Mitteroecker & Gunz 2009). Two objects have the same form if they can be translated and rotated to each other so that they match exactly (Dryden & Mardia 1998). Some hypotheses about evolution or development (like heterochrony) require explicit size and shape for an empirical assessment of how these relate (Klingenberg 1998; Mitteroecker 2007).

One method to compare shapes is called two-point shape coordinates or *Bookstein shape coordinates* (Bookstein 1991b). Translation, scaling and rotation the triangle ABC until A has coordinates (0,0) and B (1,0), the coordinates of C describe the shape of the triangle, and are therefore the shape coordinates of the said triangle (Mitteroecker & Gunz 2009). Progress in the analysis of shape, however, lead to the development of Procrustes superimposition, which was found to be a more general way to compute shape coordinates with clear advantages over Bookstein shape coordinates (such minimizing the distance between configurations, Zelditch *et al.* 2004). The Procrustes superimposition is described in the next subsection.

2.3.3. Procrustes Superimposition: Generalized Procrustes Analysis

To compare different shapes it is not enough just to measure their landmark configurations; these also need to match in a logical way. This matching of landmark configurations is called superimposition because the configurations are placed on top of each other (Zelditch *et al.* 2004). Several superimposition methods are available, but the Procrustes superimposition is the most extensively used, and will be the only one used in this thesis. The method earned its name by analogy with the Greek myth of Procrustes, a character who would fit his guests to a bed by stretching them or cutting their legs (Zelditch *et al.* 2004).

Procrustes superimposition minimizes the differences between landmark configurations so that they best fit each other, in a sense like the mythological

Procrustes did with his guests and the bed. In fact, statistically, Procrustes superimposition is less about superimposing than about getting *shape variables* by removing *nuisance parameters*, following Goodall's (1991) perturbation model. Estimates of shape variation must be independent of the effects of variation in parameters unrelated to shape variation (nuisance parameters) even though a mean shape may be expressed relatively to some particular coordinate system. The parameters describing the shapes of two equivalent landmark configurations are estimated by a Procrustes superimposition with a least-squares oriented approach involving three steps (Rohlf & Slice 1990; Mitteroecker 2007; Figure 2.1):

(1) *Translation*: to centre each landmark configuration at the origin by subtracting the coordinates of its centroid from the corresponding coordinates of each landmark. The centroid is the coordinate-wise average of the landmarks of one shape, and the landmark coordinates now reflect their deviation from the centroid.

(2) *Scaling*: to scale the landmark configurations to the same centroid size (the square root of the summed squared deviations of the coordinates from their common centroid). Centroid size is a measure of scale for landmark configurations, which has been shown to be approximately uncorrelated with shape for small isotropic landmark variation (Bookstein 1991b; Dryden & Mardia 1998). As a convention, and because computation becomes easier, centroid size is set to one for all landmark configurations (unit centroid size).

(3) *Rotation*: one of the two translated and scaled landmark configurations is rotated until the sum of the squared Euclidean distances between the equivalent landmarks is minimized (*i.e.*, to minimize the partial Procrustes distance).

For more than two landmark configurations, this algorithm has been extended and is known as generalized least-squares (GLS) Procrustes superimposition, also called *generalized Procrustes analysis* (GPA, Rohlf & Slice 1990). GPA uses as a criterion to minimize differences between configurations, the summed squared distances between corresponding landmarks (the Procrustes distances). In more than two configurations, the rotation step becomes an iterative algorithm. First, the translated and scaled landmark configurations are rotated to one of these configurations (usually the first one). The ensuing coordinates are averaged and all configurations are then rotated to fit this initial consensus. The resulting coordinates are averaged again to yield a new consensus configuration to fit to. The algorithm is repeated until convergence is reached, usually after a few iterations. The resulting average is the shape whose sum of squared distances to the other shapes is minimal and is thus the maximum likelihood

estimate of the mean for certain statistical models (Dryden & Mardia 1998; Mitteroecker 2007).

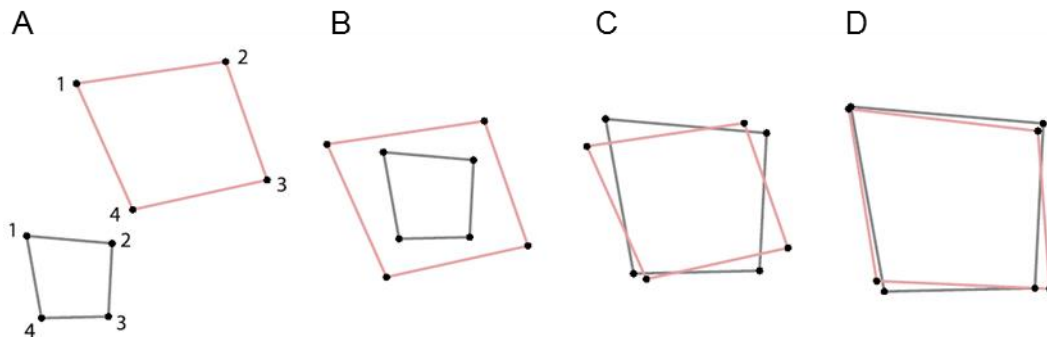


Figure 2.1. Procrustes superimposition: the three steps. A, two raw configurations of landmarks. B, translation of the two configurations onto each other, centred at the centroid. C, scale the translated landmark configurations to the same centroid size. D, rotation of the translated and scaled configurations to minimize the sum of the squared distances between equivalent landmarks. Adapted from Mitteroecker & Gunz (2009).

The coordinates of the resulting translated, scaled and rotated landmarks are called *Procrustes shape coordinates* and their individual differences from the average shape are often termed Procrustes residuals (Mitteroecker 2007). The average shape (the consensus configuration) is the shape whose sum of squared distances to the other shapes is minimal and is thus the maximum likelihood estimate of the mean for certain statistical models (Dryden & Mardia 1998; Mitteroecker & Gunz 2009). Scaling the specimens to unit centroid size (called a partial Procrustes fit) may resemble several other standard approaches to size correction, but Procrustes scaling (a better, full Procrustes fit) is not the actual least-squares solution. A least-squared solution can be achieved by scaling. Dryden and Mardia (1998) refer to it as partial Procrustes fitting. A full Procrustes fit (Rohlf 1999) would be a smaller sum of squared deviations among the landmark configurations, achieved by constraining the size of a configuration to $\cos \theta$, where θ is the angle, in radians, between the vector of shape coordinates of that specimen (single column vector with kp elements) and the vector of the mean shape. Most applications of this method use only partial Procrustes fitting (Mitteroecker 2007).

The scaling step removes all information on the overall size. As mentioned before, in many biological studies it is desirable to include size in the analysis. This is

achieved by augmenting the Procrustes shape coordinates by the natural logarithm of centroid size into the analysis (Mitteroecker *et al.* 2004; Mitteroecker, Gunz, & Bookstein 2005). Such an analysis is said to be carried out in *form space*, rather than in *shape space* (Mitteroecker & Gunz 2009).

When two or more configurations are to be mapped on one another, the use of the interpolation function called thin-plate spline is an established practice and is explained in the next subsection.

2.3.4. The Thin-plate Spline

In morphometrics, *thin-plate spline* (TPS) interpolation (Bookstein 1989, 1991b) is used to compute a mapping function from one template landmark configuration to a target configuration, very much in the sense of D'Arcy Thompson's (1917) transformation grids (Mitteroecker 2007). This mapping function can also be applied to points other than the template configuration, like the nodes of a regular square grid (in the template figure space). The parameters characterizing the mapping from one form to another can then be visualized by the "deformation" that results from applying the mapping to this regular grid. The transformation grids indicate relative stretchings and contractions of the space of the landmark configuration, rather than the physical mapping of particles between two objects. Transformation grids are simply a visual aid to assessing shape differences.

The TPS interpolation function from a template configuration to a target configuration is usually applied to the vertices of a regular grid, so that the shape differences between the two geometries can be read from the transformation of this grid (Mitteroecker & Gunz 2009). When the actual shape differences are subtle, the transformation can be extrapolated by an arbitrary factor to ease the interpretation of the grid. In the course of computation, the TPS function is applied to each coordinate axis separately and so can be used for both two-dimensional (2D) and three-dimensional (3D) data. Though less effective for visualizing 3D shape differences, the mapping function of the transformation grid can be applied to any points in the vicinity of the template landmarks and the algorithm can be used effectively to transform a 3D model of the template specimen (Bookstein 1989, 1991b; Mitteroecker & Gunz 2009). Nevertheless, a sequence of warped surfaces can provide a useful alternative to

transformation grids for describing 3D shape and form differences (Mitteroecker & Gunz 2009).

The TPS function can also be applied to the pixels of an image or to the voxels of volumetric data derived from CT or MRI scans (Mitteroecker & Gunz 2009). However, when warping the pixel locations from the template to the target space according to the two landmark configurations, pixels may overlap in the target image or positions in the image may be empty. To avoid such fragmented images, the TPS algorithm is often used instead to unwarped an image (Mitteroecker & Gunz 2009). The pixel positions of the target image are warped to the template, identifying the pixels that correspond across the two images. The grey values or the colour values of the target pixels are then substituted by the corresponding values in the template image; the resulting unwarped image is a continuous image with no gaps or holes (Mitteroecker & Gunz 2009).

A mention of the concept of bending energy is pertinent. Bending energy is a measure of shape differences between two landmark configurations, which does not depend on the registration of the configurations. But bending energy is not a metric measure of distance rather it is just the non-affine part of the transformation and hence is usually not used for statistical analysis. Its main current use is in controlling the sliding of semi-landmarks (Bookstein, Gunz, & Mitteroecker 2005). The TPS formalism can also be applied to decompose shape transformations into a range of geometrically independent components (partial warps) with different geometric scale and hence different bending energy (Bookstein 1989, 1991b). A decomposition of the mean form (principal warps) can be used as an orthogonal basis to span tangent space, but is of limited biological relevance (Rohlf 1998; Monteiro 2000).

Geometric morphometrics has been used (with some degree of criticism; Weber, Bookstein, & Strait 2011; see also O'Higgins *et al.* 2012) to complement the biomechanically focused method of finite elements analysis, which is discussed next.

2.4. Finite Element Analysis

Computer-based approaches to the study of functional morphology have become more common and complementary to traditional comparative anatomy and experimentation (Kupczik 2008). Finite element analysis (FEA) is a technique that reconstructs stress, strain, and deformation in material structures and has its origin in mathematical and engineering problems (reviewed by Rayfield 2007). FEA became prominent as an analytical technique still within the field of engineering (Zienkiewicz 1971), where it is used to predict structural performance of mechanical systems, but it spread to areas outside it such as orthopaedic medicine (Huiskes & Chao 1983) and has since been applied to vertebrate musculo-skeletal biomechanics to model deformation and the stress-strain regimen in existing biological structures (Kupczik 2008). It allows the study of vertebrate functional morphology in a non-invasive way and where traditional experimental approaches are not feasible (Kupczik 2008). Reviews on the use of this modelling technique to study biological systems can be found in Richmond *et al.* (2005); Ross (2005); Rayfield (2007); or Panagiotopoulou (2009).

FEA is often used to study stresses and strains in extant (*e.g.* Pierce, Angielczyk, & Rayfield 2008, 2009; Cox *et al.* 2011, 2012) and fossil animals (*e.g.* Rayfield *et al.* 2001; Grine *et al.* 2010) and, more rarely, in artificial constructs such as hypothesised representations of ancestral conditions (Ross 2005). FEA can also add to the study of patterns of growth and development, and to investigations of adaptive hypotheses concerning skeletal form using an iterative adaptive approach in which loading and removing elements can generate close-to-reality shapes from amorphous blocks (Preuschoft & Witzel 2004a; b; Witzel & Preuschoft 2005). Ross (2005) states that improvements in model building techniques will make possible increased applications of FEA to study the functional effects of variation in morphology through ontogenetic or phylogenetic transformations. The question arises as to whether FEA is actually producing answers that reflect reality; what are the sources or error that can be introduced in each step of the method?

Constructing and analysing a finite element model from 3D digital data can be divided into four major steps: pre-processing, solution, post-processing and validation (Kupczik 2008). Richmond *et al.* (2005) actually consider only three steps, combining validation and post-processing (interpretation). A schematic simplification of the process is provided in Figure 2.2.

CT scans

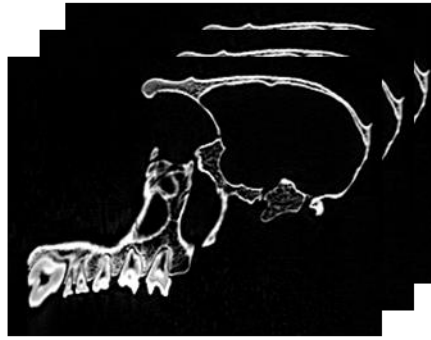


Image segmentation

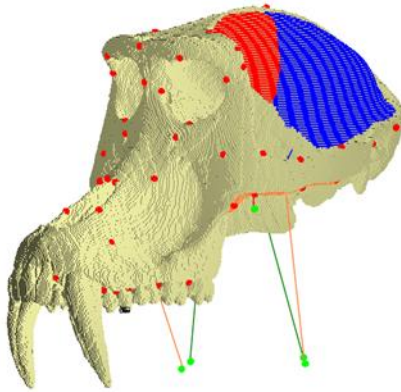
Material properties

Boundary conditions



Pre-processing

Finished model



Nodal displacement computation

Strains calculation

Scaling



Solution and Post-processing

Strains and Deformations

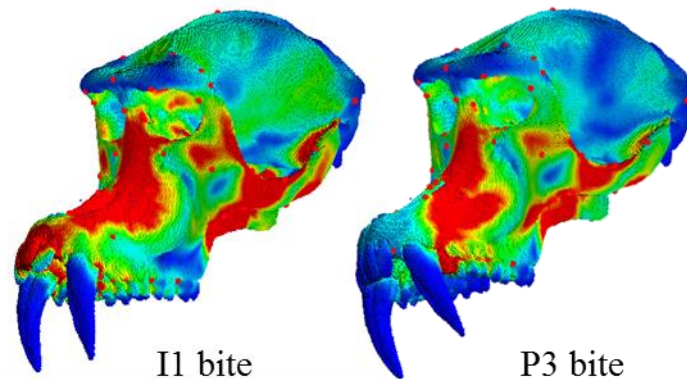


Figure 2.2. A schematic simplification of steps in finite element analysis (FEA). See text for more details.

2.4.1. Pre-processing: Finite Element Model Building

The pre-processing step starts with acquiring image data that will then be converted into a finite element mesh. Some authors (Richmond 1998; Rayfield 2004; Richmond *et al.* 2005) previously claimed that for most questions at hand 2D analyses are adequate, but since the advances in engineering computing of the early 2000s, the use of 3D became feasible and is now common. Laser scans of structures can be transformed into wireframe models (Richmond *et al.* 2005), but omit internal architecture. Most used today are 3D imaging techniques such as computerized tomography (CT) (Kupczik 2008). The result of CT scanning an object is a series of image slices which together form a virtual 3D representation of the object surface and interior (Hsieh 2009). The process of extracting the object from the digital image slices and assigning its parts to discrete labels is called *segmentation* (Kupczik 2008). Procedures and algorithms for segmentation include semi-automatic approaches, but finding appropriate thresholding algorithms to demarcate the bone from surrounding material reliably throughout a structure where bone varies in thickness and density (Fajardo, Ryan, & Kappelman 2002) is complex and error prone (Richmond *et al.* 2005) and so is most often done manually.

When image segmentation has been completed, a (2D or 3D) model can be generated and converted into a finite element mesh consisting of *finite elements* which are commonly tetrahedrons or voxels. Finite elements are no more than geometrically simple domains interconnected at their vertices, together making up a bigger, geometrically complex domain (the whole model). Element vertices are called *nodes* and are a coordinate location in Cartesian space where degrees of freedom, *i.e.*, displacements, are defined; displacements are determined in response to the load (Richmond *et al.* 2005; see solution step below). When the finite elements are voxels, each voxel can be directly and conveniently converted into a cubic finite element (Kupczik 2008).

Mathematically, FEA aims to find approximate solutions for partial differential equations (Fagan 1992; Bhatti 2005). After the model is discretized (*i.e.*, subdivided into finite elements), the equations governing each element are calculated and assembled in a system that describes the behaviour of the body as a whole (Fagan 1992). This system generally takes the form $\mathbf{A}u = f$, where \mathbf{A} is a square matrix of stiffness, u is the vector of (unknown) nodal displacements, and f is the vector of applied nodal forces (Fagan 1992).

Building finite element models can be extremely time-consuming. The process has yet to be optimized and accelerated in order for it be possible to build the large number of models required to investigate the actual effects of variation in form on variation in function (Ross 2005). A high number of elements and nodes make the model computationally expensive, an issue that is less and less problematic as computational power increases. It nevertheless can be successfully overcome by modelling only half of the structure (assuming symmetry) or by using a coarser mesh with fine elements only near regions of geometric complexity; or by using a 2D model when it suffices (Richmond *et al.* 2005). In any case, material properties and boundary conditions of a model have to be put in place requiring some time to estimate.

2.4.2. Pre-processing: Material Properties and Boundary Conditions

After the finite element mesh is created, the mechanical properties of the elements (materials) of the objects involved must be specified. Two of the most common are stiffness (Young's modulus of elasticity, see also Subsection 1.2.3) and Poisson's ratio (Currey 2002; Kupczik 2008). The magnitude and orientation per element of these properties, as well as their spatial variation within the model has significant implications for the results of an FEA (Kupczik 2008). Elastic property data for the cortical bone of the human, macaque and baboon skull determined by mechanical testing can be found in Peterson and Dechow (2003) and in Wang *et al.* (2006). In voxel models, elastic property data can also be derived from the density values of CT scans, using the scaling relationships between CT numbers, bone density and elasticity (Marinescu *et al.* 2005).

The elastic or Young's modulus (E) is defined as

$$E = \sigma/\epsilon \quad (2.1)$$

where σ denotes stress and ϵ strain, measured in simple extension or compression (Richmond *et al.* 2005). It is, thus, a measure of stiffness. Poisson's ratio is the lateral strain divided by axial strain, representing how much the sides of a material will contract as it is tensed to maintain volume (Richmond *et al.* 2005).

Apart from assigning material properties, it is necessary to define some boundary conditions (Bhatti 2005). There are two types of boundary conditions: the kinematic or essential boundary conditions that prevent rigid movement of the model, and the natural or non-essential boundary conditions that include the forces applied to the model (Richmond *et al.* 2005). The first type includes the displacement constraints required to anchor the model in space (Kupczik 2008). The second type includes the force estimates that are going to load the model. These estimates are derived from experimental data and estimated using physiological cross-sectional areas (PCSA) of the muscles through dissection (discussed further in Chapter 5). They take into account the muscle activity pattern of the individual muscles in living animals (Ross *et al.* 2005; Kupczik 2008). The forces applied to the model (loads; Subsection 1.2.3) are vectors with points of application, magnitudes and directions (Richmond *et al.* 2005). The locations of the loads (*e.g.* muscle forces) may be either approximations based on knowledge of the anatomical region, or more precisely from images or dissections (Richmond *et al.* 2005). In the case of muscle direction, it can be approximated by a line drawn from the origin of the entire muscle to its insertion (Ross *et al.* 2005). As for magnitude of muscle force, it can be approximated using muscle PCSA as an estimate of maximum potential muscle force (Ross *et al.* 2005). Force estimates are available for the masticatory muscles of macaques (Strait *et al.* 2005, 2007; Ross *et al.* 2005).

Since there is no available bite and joint reaction force data for most papionins (also required boundary conditions), a common approach is to constrain the teeth and jaw joint to fix the cranium in the same position, thus mimicking the reaction forces in the direction of the load (Strait *et al.* 2005; Ross *et al.* 2005; Kupczik *et al.* 2007). Alternatively, multibody dynamics analysis (MDA) can be used to estimate bite and joint reaction forces and facilitate experimentation with muscle architecture and activity patterns (Curtis *et al.* 2008).

2.4.3. Solution and Post-processing

After setting the material properties and the boundary conditions, the model has to be solved. This is usually done in a high-performance workstation with multiple processors and a fast graphics interface (Kupczik 2008). Solving a model means that

node displacements are computed, and from them, the resulting strains and stresses are calculated (Richmond *et al.* 2005; Kupczik 2008).

The elastic modulus (Young's modulus E; see also Subsection 1.2.3) determines the nodal displacements resulting from the nodal forces (Richmond *et al.* 2005). As seen before, stress and strain are related through E for a given elastic property (Equation 2.1). In most biomechanical models, stresses or strains (as well as deformations) resulting from an FEA are the data of interest (Richmond *et al.* 2005).

When the model is solved, the post-processing step takes place and the results can be presented and visualized in the form of scaled strain contour plots or animated deformations (Kupczik 2008; Figure 2.2). The results should obviously be interpreted in the context of the question asked (Richmond *et al.* 2005).

2.4.4. Validation and Sensitivity

Validation is a critical step in FEA without which researchers would not be able to assess how much the model actually represents the real biological specimen (Richmond *et al.* 2005). Researchers need to be able to tackle both the precision and accuracy (*sensu* Richmond *et al.* 2005) of the model. Precision can be assessed through a convergence test in which the model is repeatedly calculated with increasingly finer meshes until the displacement magnitude of a chosen test area converges towards a precise solution of that model; accuracy can be improved by including data from experimental work into the model, seeking to minimize discrepancies between the model and *in vivo* results (Richmond *et al.* 2005). Ultimately, it is the researcher who has to decide how accurate is accurate enough (Richmond *et al.* 2005).

Independent experiments are critical to modelling a mechanical problem in a realistic manner, the best means of validation inevitably being the direct measurements of strain, as in *in vivo* gauge experiments (Rubin & Lanyon 1982; Hylander & Johnson 1992; Ross 2001; Richmond *et al.* 2005). Strain gauges have to be glued on the bone surface and not only offer limited data about the surface strain distribution (Gröning *et al.* 2009), but also raise issues of *in vivo* animal welfare or *ex vivo* specimen integrity (for example, irreplaceable museum specimens should not be damaged). One other way of measuring strain that is becoming popular is laser speckle interferometry, which is a non-contact system for measuring displacements from which principal strains can be

calculated (Kessler *et al.* 2006; Yang *et al.* 2007; Gröning *et al.* 2009; Panagiotopoulou *et al.* 2012). Results from any FEA can only be interpreted when matched to the actual biological variation (Kupczik 2008). Potentially, the best validation includes *in vitro* as well as *in vivo* experimentation (Richmond *et al.* 2005).

However, independent empirical data must be available to test the reliability of a model (Richmond *et al.* 2005; Strait *et al.* 2005, 2007; Marinescu *et al.* 2005; Ross *et al.* 2005; Kupczik *et al.* 2007). Fortunately, some published data on *in vivo* strain magnitude and orientation are becoming increasingly available and can be used to validate models (*e.g.* Marinescu *et al.* 2005).

Essential for the understanding of consequences of error in the input parameters of a finite element model (especially in the absence of available experimental data for validation) is a sensitivity analysis (Kupczik 2008). It should test for the effects of changes of the applied loads, variations of the material properties of differences in the structure and size of the model on the modelling results, among other things (Strait *et al.* 2005; Ross *et al.* 2005; Kupczik *et al.* 2007; Curtis *et al.* 2008). Many FEA-based studies have focused on the sensitivity of the method to different variables (Panagiotopoulou, Kupczik, & Cobb 2011; Gröning *et al.* 2011; Parr *et al.* 2012).

FEA allows the study of deformation by expressing it in terms of stress and strain at each node comprising the model. Recently, a link between FEA and geometric morphometrics has been attempted, using landmark configurations to read and compare global deformations from FEA (O'Higgins *et al.* 2011). Strain is one way of assessing changes in size and shape but landmark-based methods are another. Analysis of size and shape-changing deformations under biting loads using geometric morphometrics are complementary to strain-based assessments of deformation in that they relate to large scale (global) deformations, while strains describe deformations at each node, using strain contour plots as the only indication of global deformations (O'Higgins *et al.* 2011, 2012). A brief review and description of the landmark-based deformation analysis is given next and used extensively in Chapters 6 and 7 of this thesis.

2.5. Landmark-based Deformations Analysis

Landmark-based analysis of deformations is a novel methodology developed recently and with only a few published examples of its use (O'Higgins *et al.* 2011; Gröning *et al.* 2011; Cox *et al.* 2011; Parr *et al.* 2012). It combines FEA and geometric morphometrics in a way that allows visualisation of global deformations from FEA and comparison among models, providing a quantitative method to compare the behaviour of different finite element models. It is anticipated that, with development, it will open the door to inter- and intra-population FEA studies.

The concept of engineering or size and shape-changing deformations (large scale, global deformations) describes deformations as the change in shape (or size) of an object due to an applied force (Truesdell & Noll 2004; O'Higgins *et al.* 2011). It opposes the continuum mechanics concept of deformation which means the transformation of a rigid body from a reference configuration to a new configuration even without change in shape (Truesdell & Noll 2004). Throughout this thesis the single word *deformation* will always mean size and shape-changing deformation.

2.5.1. Landmark Displacement in Finite Element Analysis

Visualizing and analysing deformations relies on the ability of a finite element model to predict them (see Section 2.4). A set of GMM landmarks is chosen as described in Section 2.3. Each landmark is placed on the surface of the model cranium, in a position that has to be equivalent among all the specimens in the comparative study (see Subsection 2.3.1). The Cartesian coordinates of each landmark change as the cranium deforms, each one of them being displaced to different XYZ coordinates. This causes the landmark configuration to change in size and shape. Whereas the pure displacement of each landmark is not directly interpretable in terms of changes in size and shape because translations and rotations intrude, the global landmark configuration is. When these changes are compared, differences in deformation reflect differences in mechanical performance within that same model. In comparing FEA results following different loadings of the same model specimen, the full configurations of landmarks after translation and rotation can be put through a full geometric morphometric analysis to assess deformations at the scale of the landmark configuration as a whole, which is

usually large (global). This contrasts with strains which describe deformations in each element one by one.

This geometric morphometric approach can potentially be extended to allow the comparison of several finite element models. When resulting landmark configurations of several models are analysed, differences in deformation reflect differences in mechanical performance among them. However, there are several difficulties in directly comparing changes in size and shape between different models. In fact these difficulties are in part a consequence of the difference in size and shape of models even before any load is applied to them. The very question of differences in deformation becomes less sensible as the differences among models increase. Conversely, when size and shape differences between models are few (and disappear altogether between identical models) comparing their deformation is unequivocal when they are loaded in the same way. This means that the issue of similarity of deformation can only be approached approximately, but with increasing security as unloaded forms converge on a single form. Additionally, size and shape differences among the various unloaded models tend to dominate the analysis, because they are very large compared to the differences in size and shape among the different loadcases of each model. In consequence, differences in size and shape among unloaded models must be discounted prior to analysis of differences due to deformation. This is achieved by first carrying out a GPA with all loaded and unloaded specimens to produce shape variables. Next, the residual size-and-shape variables due to loading are computed by subtracting the landmark configurations of the unloaded from the loaded state for each specimen.

$$\text{residuals} = \text{loaded } (x, y, z) - \text{unloaded } (x, y, z) \quad (2.2)$$

Subsequent analyses use the residuals to compare deformations, and visualise them by drawing them on the mean of all the unloaded specimens, which is achieved by adding it to the residuals. This effectively eliminates the differences in size and shape among the unloaded models (in a purely isometric and non-mechanical sense), leaving only differences in deformation.

2.5.2. Scaling to Bite Force

In comparative studies of relative deformation after simulated biting loads, in order to ensure that the observed differences in deformation among models can be interpreted as differences in skeletal response to the same bite force among specimens, rather than as an artefact of differences in applied force, some equivalent loading has to be decided upon. One possibility is to consider equivalence in terms of applied muscle forces; another is in terms of bite force (Fitton *et al.* in prep.). Since deformation scales linearly and with a slope of 1 with force, this latter is achieved by first measuring the predicted bite force and, knowing the desired bite force, scaling the deformations (changes in size and shape of the landmark configuration) accordingly. In this thesis the equivalent loading is a bite force of 100N, to which value all the calculated bite forces (see Section 7.2 for further details) and landmark configuration deformations are scaled.

The scaling to the same bite force step is computed on the residuals and only after this should the mean unloaded configurations be added to the (now scaled) residuals. It is processed firstly by computing the residuals from the original unloaded specimens, using Equation 2.2. Then, each residual is multiplied by a scaling factor, using the formula:

$$\text{residual} \times (\text{same bite force} / \text{calculated bite force}) \quad (2.3)$$

where the same bite force is the desired bite force to scale the deformations to (100N in this thesis, see Section 7.2), and the calculated bite force should be computed from a finite element model after loading on a particular tooth. The scaled value is then added to the original unloaded data and a full shape GPA is performed. After that, the residuals from the Procrustes registered landmark coordinates are computed. Then the mean of all original unloaded specimens is calculated and added to the residuals.

Finally, size differences among configuration due to loading are restored by using, for each loadcase, the ratios of their centroid sizes to their unloaded centroid size to proportionately scale the configurations relative to each other:

$$(\text{mean} + \text{residual}) \times (\text{mean unloaded CS} \times [\text{loaded CS}/\text{unloaded CS}]) \quad (2.4)$$

to each coordinate value, where CS denoted the natural logarithm of the centroid size of each configuration after the full GPA. The mean original configuration must also be

multiplied by the mean centroid size of the original, unloaded configuration so that it can be plotted together with the loaded configurations. Changes in size and shape among and within models due to loading are then assessed using principal component analysis (PCA).

2.5.3. Visualizing Deformation

The results of subsequent size-and-shape analysis can be visualized using warped surface visualizations. Transformation grids computed using TPSs between the reference and target load cases (although issues have been raised about this, see Subection 2.3.4) can be used to aid in the interpretation of the deformation differences along the axes or between points on the principal component plot, such as in every geometric morphometric analysis. As with landmark configuration among specimens, geometric morphometrics facilitates the assessment of variations in form (size and shape) among load cases using multivariate methods (Bookstein 1991b; O'Higgins 1997; Dryden & Mardia 1998; Rohlf 2000; Slice 2007; Milne & O'Higgins 2012; O'Higgins & Milne 2013). The Procrustes size and shape distances between the loadings indicate the magnitudes of the differences in form among unloaded and loaded models. PCA is carried out with size-and-shape variables resulting from translation and rotation of the unloaded and loaded landmark configurations.

Apart from the so far reviewed methods, some other multivariate statistics must be discussed in this chapter before closing. These include ordination methods (such as principal components analysis), correlation methods (two-block partial least squares analysis) and significance tests.

2.6. Multivariate Statistical Analysis

In addressing complex problems such as the comparison of shape (and form), a multivariate approach is fundamental for testing and visualizing hypotheses. Here, the pertinent statistical methods used in later chapters of this thesis are outlined.

2.6.1. Principal Components Analysis

Principal components analysis (PCA, Pearson 1901) is a method for reducing a large set of variables to few dimensions (*principal components*) that represent most of the variation in the data. PCA is computed by an eigendecomposition of the sample covariance matrix (an excellent explanation of matrix algebra can be found in Carroll, Green, & Chaturvedi 1997) and is a rigid rotation of the data preserving the distances among the specimens (Mitteroecker & Gunz 2009). Principal component scores are the projections of (sizes and) shapes onto the space spanned by the eigenvectors. The space has the same dimensions as the original distances, but ordered according to variance. They can be plotted as 2D or 3D graphs and allow one to assess group differences, growth trends, outliers, *etc.*, in data based on the shape and form variables only (without incorporating prior information, *e.g.* such as group affiliation) (Mitteroecker & Gunz 2009). The eigenvectors, or principal components, can be visualized as actual deformations by working backwards from the loadings of coordinates on these components.

Principal components are statistical artefacts, rather than biological entities, largely depending on the composition of the sample, they do not represent biologically meaningful factors (Mitteroecker & Gunz 2009). In morphometrics there is one known exception: the first principal component of a single species or population sometimes represents allometry, the shape variation induced by overall size variation (Klingenberg 1998). This happens only if allometric variation is the dominant factor in the data, such as in ontogenetic studies. Multivariate regression is preferred to estimate allometry otherwise (Mitteroecker & Gunz 2009).

2.6.2. Partial Least Squares Analysis

Partial least squares (PLS) is a method to assess relationships among two (or more) blocks of variables measured on the same entities (Wold 1966). It can be used to examine the relationship between two blocks of size-and-shape variables, one block of size-and-shape and another of non-shape variables, and, of course, two blocks of non-shape variables (Zelditch *et al.* 2004; Mitteroecker & Gunz 2009). Blocks of size-and-shape variables can be related to each other, such as in morphological integration (*e.g.*

Monteiro, Bonato, & Dos Reis 2005); or to biomechanical variables, such as deformations or bite force (*e.g.* Cox *et al.* 2011); or to ecological and behavioural factors, such as geographical variation or dietary categories (*e.g.* Meloro & O'Higgins 2011). An important feature of PLS is that the data must be partitioned *a priori* into blocks before the analysis begins (Zelditch *et al.* 2004).

Specifically, two-block PLS analysis of covariation yields linear combinations that optimally (in a least squares sense) describe the covariances among the sets of variables and so provide a low-dimensional basis to assess the association between different blocks of variables. The method employs a mathematical technique called singular value decomposition (SVD), related to an eigendecomposition used to extract principal components from the variance-covariance matrix (Rohlf & Corti 2000) and partial warps from the bending-energy matrix (Bookstein 1989, 1991b). Because PLS uses SVD, the vectors generated by PLS are called singular axes (Zelditch *et al.* 2004). When size-and-shape variables are concerned, the results of a PLS can be visualized as shape deformations (singular warps) (Mitteroecker & Gunz 2009).

2.6.3. Statistical Significance Tests

A mention of statistical significance tests is required here. Many geometric morphometric analyses are based on randomization tests, such as permutation tests or bootstrap tests (Mitteroecker & Gunz 2009), rather than parametric methods to assess the statistical significance level of a given hypothesis. Most parametric tests require more cases than variables and a specific (usually a normal) distribution of the variables, whereas randomization tests are free from these restrictions as long as the cases are sampled independently. Furthermore, test statistics can be designed even for complex hypotheses and compared with their permutation distribution (Mitteroecker & Gunz 2009). Geometric morphometric analyses in Chapters 3 and 4 utilize randomization tests embedded in the software, as well as a *t*-test to test if the slope of the regression is different from 1. Chapter 8 uses the RV-coefficient (Escoufier 1973; Robert & Escoufier 1976), which is equivalent to a permutation test using the sum of squared covariances or the sum of squared singular values (from a PLS) as the test statistic. Analyses in Chapters 6 and 7 are not suitable for significance testings due to low sample size.

2.7. Summary

In summary, the methods used throughout this thesis to study the evolution of the papionin cranial form and its potential biomechanical adaptation to feeding are quantitative genetic analysis, geometric morphometric analysis, finite element analysis, the novel landmark-based deformations analysis and multivariate statistical analysis. Quantitative genetics studies the correlation and the variance-covariance matrix among multivariate traits. Geometric morphometrics is the statistical analysis of form (shape and size) based on Cartesian landmark coordinates and associated to the statistical theory of shape. Finite element analysis is an analytical technique used to predict structural performance of mechanical systems, including the vertebrate musculo-skeletal system, in a non-invasive way. Landmark-based deformation analysis combines the previous two methods in a way that allows visualisation of size and shape-changing deformations from finite element analysis and comparison among models, providing a quantitative method to compare the behaviour of different finite element models in terms of deformations. Multivariate statistical methods are essential for testing and visualizing hypotheses about complex problems, such as the comparison of form. The material used are simulated data (in part of the quantitative genetic analysis), 3D computerized tomography scans of dry crania (used in model building for FEA), and 3D landmark data chiefly taken from 3D computerized tomography scans.

The remaining chapters of this thesis regard the testing of hypotheses concerning papionin cranial evolution and mechanical adaptation as outlined in Section 1.1. The immediate Chapters 3 and 4 deal with a test on the evolutionary divergence of papionin crania by the action of a neutral microevolutionary force (random genetic drift).

Chapter 3. Simulating Type I Error Rates for Testing Random Genetic Drift with Phenotypic Covariance Matrices

Published research paper (see Appendix C) with reference:

Prôa, M., O'Higgins, P. & Monteiro, L.R. (2013) Type I error rates for testing genetic drift with phenotypic covariance matrices: a simulation study. *Evolution*, **67**(1), 185–195. DOI: 10.1111/j.1558-5646.2012.01746.x

3.1. Introduction

Understanding the evolution of cranial form and its mechanical adaptation to the function of feeding first requires an understanding of the evolutionary processes acting on it. There are two main types of evolutionary processes: neutral processes (the most important of which is random genetic drift), and adaptive processes, including natural selection. When no adaptive processes are acting on a form, then that form is evolving neutrally, *i.e.*, it is not directed towards a greater degree of adaptation. If random genetic drift was the single driver of the evolution of papionin cranial form, responsible for the divergence of cranial form among the papionins, then it follows that differences in cranial form among the papionins cannot be interpreted as adaptations to any particular function. On the other hand, if random genetic drift can be excluded as a single evolutionary driver of evolution, then differences found in papionin cranial form likely have a more adaptive interpretation (such as the biomechanical demands of different dietary strategies). Thus, it is important that before finite element analysis is used to assess functional adaptation in the cranium, random genetic drift is excluded as an explanation of these differences.

When testing for evolutionary processes, quantitative genetic methods are the best approach (see Subsection 2.1). Quantitative genetics provides inferences of evolutionary processes via the study of evolutionary divergence patterns and their

relationship to intra-population adult variation (Lande 1979; Ackermann & Cheverud 2002, 2004; Marroig & Cheverud 2004; Monteiro & Gomes-jr 2005; Perez & Monteiro 2009). The connection between neutral microevolutionary processes and macroevolutionary patterns is centred around the additive genetic variance-covariance matrix (\mathbf{G}) (Lande 1980b; Arnold *et al.* 2001; Jones *et al.* 2003; Bégin & Roff 2004; see also Subsection 1.2.1), which is thought to determine both the response to selection and the pattern of neutral divergence, at least among populations over a small time scale (Lande 1980b; Felsenstein 1988; Zeng 1988).

The expected pattern of phenotypic divergence among populations caused by random genetic drift in correlated traits can be used as a null hypothesis to test for neutral evolution (Lande 1979, 1980b). Put simply, the quantitative genetic approach relies on showing that the pattern of morphological divergence observed among sampled species means differs from that within species. This assumes that drift will follow the “line of least resistance” (Schluter 1996; Marroig & Cheverud 2005) and occur in ways that simply replicate within taxon variation. If variation among taxa follows a different pattern to that within, it is more likely that these interspecific differences have been acquired through a more active evolutionary process such as natural selection. The aim of this chapter is to assess the extent to which such quantitative genetic models are robust in the face of violations of their underlying assumptions as a preliminary to applying these methods to assess the likelihood that drift alone underlies differences in cranial form among papionins, in the next chapter. This assessment of whether or not random genetic drift underlies differences among papionins is, in turn, an essential preliminary to comparative biomechanical simulations of masticatory system functioning since the interpretation of these assumes that the differences observed are not neutral.

The sampling distribution of the change in trait means in one generation ($\Delta\bar{\mathbf{z}}$) has a mean of 0 and variance-covariance matrix \mathbf{G}/N_e , the genetic covariance matrix in a population divided by the effective population size (Lande 1979). If the average phenotype of a population a is represented by a column vector $\bar{\mathbf{z}}_a$ of polygenic traits with additive genetic and environmental components following multivariate normal distributions (Lande 1980b), the probability distribution Φ of after t generations will be

$$\Phi(\bar{\mathbf{z}}_a, t) \sim N[\bar{\mathbf{z}}_0, \mathbf{G}(t/N_e)] \quad (3.1)$$

which is a normal distribution with a mean equal to that of the initial population and variance-covariance matrix $\mathbf{G}(t/N_e)$ (Lande 1979). If a number of populations are evolving independently (*i.e.* without gene flow), the expected among-population phenotypic variance-covariance matrix (\mathbf{B}) is a function of the genetic covariance matrix (\mathbf{G}), effective population size (N_e) and the number of generations (t):

$$\mathbf{B} = \mathbf{G}(t/N_e) \quad (3.2)$$

As a result, the comparison of among-population (\mathbf{B} phenotypic) and within-group (\mathbf{G} genetic) variance-covariance matrices can be used as a means to determine whether genetic drift as a null model explains the pattern of divergence observed (Lofsvold 1986, 1988; Roff, Mousseau, & Howard 1999; Ackermann & Cheverud 2002; Bégin & Roff 2004).

Because phenotypic covariances are much easier to estimate than their genetic counterparts, replacing average \mathbf{G} with the pooled phenotypic within-group covariance matrix (\mathbf{W}), provided that the phenotypic covariance matrices for diverging populations remain similar, has been a widely used approach to study the evolutionary mechanisms of divergence (Ackermann & Cheverud 2002, 2004; Marroig & Cheverud 2004; Perez & Monteiro 2009). Cheverud (1988) investigated the relationship between genetic and phenotypic correlation matrices using data taken from the literature and concluded that phenotypic correlations were reasonable estimates (and generally proportional, though perhaps not in a strict mathematical sense) of the respective genetic correlations. A second conclusion from these data was that phenotypic covariances \mathbf{W} estimated with large samples might approach \mathbf{G} more accurately than genetic covariances estimated from small effective sample sizes, at least for morphometric data (Cheverud 1988; Revell *et al.* 2010). A number of meta analyses from literature reviews and empirical results have to some degree corroborated Cheverud's findings (Roff 1995, 1996; Koots & Gibson 1996; Waitt & Levin 1998; Roff *et al.* 1999). Nonetheless, this approach has been criticized on several grounds (Willis, Coyne, & Kirkpatrick 1991), but mostly because \mathbf{W} is not mathematically proportional (*i.e.* having a constant ratio) to average \mathbf{G} . Apart from the issue of similarity and proportionality between matrices, more specific consideration of the actual consequences of using \mathbf{W} as a surrogate of average \mathbf{G} in empirical studies (Bégin & Roff 2004; Klingenberg, Debat, & Roff 2010) should prove fruitful and one such aspect, the impact in terms of type I error rates, is the focus of the present study.

Quantitative genetic theory predicts phenotypic covariances within a single population (**P**) to be the sum of the genetic covariation (**G**) and the environmental covariances (**E**), $\mathbf{P} = \mathbf{G} + \mathbf{E}$ (Falconer & Mackay 1996), as seen in Section 1.2.1. A part-whole correlation is expected between phenotypic and genetic covariances; therefore phenotypic covariances can be considered an estimate of genetic covariances with added error due to environmental covariances, even if not mathematically proportional.

Most of the discussion on the surrogacy of average **G** by **W** revolves around the similarities and differences between phenotypic and genetic covariances in single populations or from literature reviews, and the differences in empirical comparative results obtained when using one kind of estimate or the other. The latter are rare, due to the difficulty in estimating genetic parameters for a large number of species at the same time (Bégin & Roff 2004). Considering that Lande's (1979, 1980) model expects the among-population covariance matrix **B** to be proportional to the average **G** when genetic drift is the sole evolutionary mechanism, for the purpose of evolutionary divergence tests of neutral evolution, the relevant discussion is not whether **G** and **P** are exactly proportional in single populations, but whether using the phenotypic pooled within-group covariance matrix **W** instead of the average **G** will add enough error (caused by the environmental covariances) to lead into erroneous conclusions. The tests that have been used in the comparison of among-species phenotypic covariances and genetic covariances (Lofsvold 1988; Ackermann & Cheverud 2002, 2004) do not test for exact proportionality between **B** and average **G**, but for similarity in different matrix features, such as the correlation of principal components and the distribution of eigenvalues. The expectation of proportionality rests on a number of assumptions (Lande 1979) that are probably violated in most natural populations (Lofsvold 1988), *e.g.* through the lack of large effective population sizes (Lofsvold 1988), or because of differences in the starting times of lineages (Revell 2007). Furthermore, error in the estimation of the average **G** might lead to unpredictable deviations from the expectation. Lofsvold (1988) has suggested that the acceptance of genetic drift as a null hypothesis will be more robust to the breaking of the model's assumptions than the rejection (so type I error rates are of more concern than the power), and in real studies it might be hard to determine the actual cause of rejection, natural selection being one of the possible explanations. One might expect that a consequence of using pooled within-group phenotypic instead of genetic covariances would be to increase the probability of rejecting (type I error rate) a true null hypothesis of genetic drift.

In this study, the consequences of using pooled within-group phenotypic instead of average genetic covariance matrices in the Ackermann and Cheverud (2002) test of genetic drift (referred to as the AC test from here on) in terms of type I error rates are examined using a simulation of phenotypic evolution in diverging populations. The most relevant parameters are identified and a number of recommendations are discussed.

3.2. Material and Methods

The material used is both real shape data retrieved from the literature (see Subsection 3.2.1) and simulated data. The methods are simulations run on programmed code (Appendix B). The simulations were performed using the quantitative genetic theory from Lande (1979, 1980). Starting from an ancestral population with genetic covariance matrix \mathbf{G} and mean vector $\bar{\mathbf{z}}_0$, a number (15 or 30) of descendant population mean vectors $\bar{\mathbf{z}}_a$ were generated using the t -fold convolution in Equation 3.1 for a range of t/N_e ratios (0.000001 to 100 in increments of 1 in log10 scale). This approach is equivalent to a random walk in multivariate space where each descendant population is evolving at a rate equivalent to \mathbf{G}/N_e . Instead of generating the intermediate phenotypes for each step (generation) of the random walk, the convolution allows for a direct generation of the end points with the same results and in a computationally efficient way.

The descendant populations from the ancestral distribution $N[\bar{\mathbf{z}}_0, \mathbf{G}]$ were sampled n times (sample sizes 10 to 100, in increments of 10) according to the multivariate normal distribution $N[\bar{\mathbf{z}}_a, \mathbf{P}]$, for each population. The first step in the simulations required an ancestral genetic variance-covariance matrix (\mathbf{G}) to generate species means and the second step required a phenotypic within-population variance-covariance matrix (\mathbf{P}) to generate individual specimens for each population. The same \mathbf{P} was used for all populations (the pooled within-group phenotypic covariance matrix \mathbf{W} is an estimate of the original \mathbf{P}). Different simulation models were used, either generating random \mathbf{G} and \mathbf{P} matrices as starting parameters (fully stochastic), or using predetermined matrices obtained from real data sets. The fully stochastic sets of simulations required the generation of random positive definite covariance matrices

(where all eigenvalues are > 0) that could be used as parameters in the generation of random multivariate normal numbers representing individuals sampled, as described below.

Throughout the chapter, correlations of lower triangular covariance matrices excluding diagonals (variances) are used as one measure of structural similarity (alongside Common Principal Components – CPC, Phillips & Arnold 1999). Note that permutations of the matrix elements were not used for testing significance of correlations. This procedure is not indicated for testing similarity in covariance matrices if variables have differences in scale (Cheverud & Marroig 2007), but was the most appropriate choice for these simulations. This is because the algorithm for the generation of random positive definite matrices (see details below) yielded matrices where covariances were small relative to variances. As a result, even when two covariance matrices were independently generated, they presented high positive matrix correlations when the diagonal was included (or when using comparison methods such as random skewers), because the variances and covariances would systematically form two groups of values in the matrix scatterplot. Only when diagonals were excluded, was the expected correlation for independent matrices 0. This particular structure in the random matrices (high variances, small covariances) is a consequence of generating positive definite matrices, because matrices with high covariances relative to variances are likely to be non-positive definite. Therefore, the most accurate description of matrix similarities in our simulations was derived from matrix correlations, using the lower triangular elements, excluding the diagonals. This is equivalent to comparing correlation matrices derived from the covariance matrix, as the information regarding variances is disregarded. In real data sets there would be no justification to exclude the variances from the structural comparisons, as differences in scale of variances and covariances are a relevant part of the structure.

3.2.1. Simulation Model 1

As a first set of simulations, real matrices rather than randomly generated ones are used. The matrices for the main simulations were obtained from a honey bee (*Apis mellifera*) wing shape data set with 16 shape variables (partial warps), modified (used only landmarks 11-20) from Monteiro *et al.* (2002), and a gastropod shell shape data set

(*Physa heterostropha*) with 14 shape variables (DeWitt 1996, 1998). The average heritability of bee wing variables (calculated as $\mathbf{1}(\mathbf{I}\mathbf{o}\mathbf{G})(\mathbf{I}\mathbf{o}\mathbf{P})^{-1} \mathbf{1} m^{-1}$, where $\mathbf{1}$ is a row vector of ones, \mathbf{I} is the identity matrix, \mathbf{o} is a Hadamard (element-wise) product, and m is the number of variables) was 0.217, and the effective sample size, given that 21 bee colonies were used was 4.6. The effective sample size was calculated as the product of heritability and the number of families, as described in Cheverud (1988). For the shell shape data set, the average heritability was 0.607, and the effective sample size was 11.5 (19 families were used). These two data sets present important differences in the structural similarity of \mathbf{G} and \mathbf{P} . For the bee wing data, the matrix correlation between \mathbf{G} and \mathbf{P} was 0.804, whereas for the shell data set the correlation was 0.442. Although the average heritability was smaller for the bee wing data, their genetic and phenotypic matrices were more similar than in the shell data set. This is not unexpected, as these average heritabilities do not measure matrix similarity, only the relative magnitudes of the genetic and phenotypic variances. A comparison of these genetic and phenotypic covariance matrices via CPC indicated that the bee data set matrices shared the full set of principal components (full CPC model supported by the jump-up approach) and the shell data set matrices shared no principal components (Unrelated model supported).

3.2.2. Simulation Model 2

In this model, \mathbf{P} and \mathbf{G} were exactly proportional and differed only by a scalar multiplication. \mathbf{G} was defined first as a random positive definite covariance matrix using the eigenvector method from Marsaglia and Olkin (1984) and Joe (2006). The eigenvector method first generates random eigenvalues ($\lambda_1, \dots, \lambda_m$) from a uniform distribution (the diagonal matrix \mathbf{L}). A lower bound of eigenvalues was set to 1 and an eigenvalue ratio (between upper and lower bound) set to 10. The algorithm then generates a random orthogonal matrix of eigenvectors \mathbf{Q} (via QR-decomposition) and constructs the genetic covariance matrix \mathbf{G} as $\mathbf{Q}\mathbf{L}\mathbf{Q}^T$. The phenotypic covariance matrix was defined by the scalar multiplication $\mathbf{P} = k\mathbf{G}$, where k is a uniform random number from 1 to 10. This approach generates a random uniform distribution of covariance matrices in the space of positive definite covariance matrices (Joe 2006). In this set of simulations, as in all other fully stochastic models, \mathbf{G} and \mathbf{P} had 15 dimensions.

3.2.3. Simulation Model 3

In this model, **G** and **P** are defined as independent random positive definite covariance matrices using the uniform correlation matrix method (Joe 2006), where a random correlation matrix (**R**) is first generated from a uniform distribution of partial correlation coefficients. The variances are generated separately as a diagonal matrix $\mathbf{S} = \text{diag}(\sigma_1^2, \dots, \sigma_m^2)$ with elements obtained from a uniform distribution ranging from 1 to 10. The random covariance matrices are constructed as **SRS**. **G** and **P** were independently derived in this model, with the restriction that the variances in **P** are always larger than the respective variances in **G**. To achieve this, the variances (diagonal) of **P** were random multiples of the respective variances in **G**. This procedure ensures that the variances of **P** were always larger, but **P** and **G** were independent. A series of 1000 simulations using this model yielded a distribution of **G** and **P** matrix correlations with a 95% confidence interval (using 2.5 and 97.5 quantiles) of -0.194 to 0.201 , and a median of 0.0004 . A further structural comparison of model 3 matrices was performed by CPC of 100 simulated **G P** pairs. Comparisons were done among estimated covariance matrices after generating 300 random observations from a multivariate normal distribution with a mean vector of zeros and random **G** and **P** (defined as above) as parametric covariance matrices. Because the model fitting in CPC depends on sample sizes, a standard $n = 300$ was maintained for all other comparisons as well. The results indicated the Unrelated model (no shared principal components) in all comparisons. Although the covariance structure is independently generated, all matrices generated by this method have variances on a much larger scale than the covariances. Therefore, there is some structural similarity because all matrices have clearly two groups of elements (covariances and variances), and the variances are always much larger than the covariances. This model is not biologically reasonable because **G** and **P** independence is unlikely (even if not proportional) due to a part-whole relationship. The model is included as a control, as the opposite to the mathematical proportionality of simulation model 2, allowing for a check that the simulations behaved as expected at extremes of **G** and **P** similarity and independence.

3.2.4. Simulation Model 4

Simulation model 4 was designed to generate correlated **G** and **P** matrices, but without a common principal component structure. In order to achieve this, the quantitative genetic relation $\mathbf{P} = \mathbf{G} + \mathbf{E}$ was used. In these models, **G** and **E** were defined first and independently. **P** was then defined as a random matrix with expected value **G** and a random perturbation **E** (Marsaglia & Olkin 1983). **E** and **G** were generated by the uniform correlation matrix method described in simulation model 3, where **G** has a range of variances between 1 and $\sigma_{\max G}^2$ (with a maximum of 10), and **E** has a range of variances between 0 and $\sigma_{\max E}^2$, where $\sigma_{\max G}^2$ and $\sigma_{\max E}^2$ are the function parameters determining the upper limits of the range of variances in **G** and **E**, respectively. The expected value of the average heritability of the variables in the simulations is the ratio $(\sigma_{\max G}^2 - 1)/([\sigma_{\max G}^2 - 1] + \sigma_{\max E}^2)$. This method generated correlated **P** and **G**, but without a common PC structure. This pattern is ensured because the variables with larger variances in **E** will be generally different than the variables with larger variances in **G** so that **P** is less likely to inherit principal components from **G** (H. Joe, pers. comm.). Of course, as the variances in **E** become smaller than variances in **G** ($\sigma_{\max E}^2 \ll \sigma_{\max G}^2$), common principal components between **P** and **G** appear. The distribution of matrix correlations from 1000 model 4 simulations (using $\sigma_{\max G}^2 = 10$ and $\sigma_{\max E}^2 = 9$ for a similar range of variances) presented a 95% CI of 0.560 to 0.897, and a median of 0.776. A CPC analysis of 100 model 4 simulations of **G** and **P** was performed to check for common eigenstructure. The simulations showed strong support for the Unrelated model (no common principal components) in 65% of the cases, using the jump-up approach. The remaining simulations supported 1 (26%) or 2 (9%) common principal components. In simulation model 4, the perturbation of expected value **G** by **E** included random rotations of its eigenstructure, even if matrix correlations were high.

3.2.5. Simulation Model 5

In simulation model 5, \mathbf{G} was defined as a random positive definite covariance matrix using the eigenvector method from Marsaglia and Olkin (1984) and Joe (2006), but where $\sigma_{\max\mathbf{G}}^2$ is the max/min eigenvalue ratio (this parameter will have a different interpretation than in model 4, but the average heritabilities expected are exactly the same in models 4 and 5). \mathbf{P} was defined as the sum $\mathbf{G}+\mathbf{E}$, where \mathbf{E} was generated by the uniform correlation method, with a variance range of 0 to $\sigma_{\max\mathbf{E}}^2$. In this model, \mathbf{P} readily inherits the principal component structure of \mathbf{G} , even when $\sigma_{\max\mathbf{E}}^2 \sim \sigma_{\max\mathbf{G}}^2$. The matrix correlation in these simulated matrices (with $\sigma_{\max\mathbf{G}}^2 = 10$, and $\sigma_{\max\mathbf{E}}^2 = 9$) were smaller than in model 4 (matrix correlation distribution 95% CI = 0.061 to 0.462, median = 0.274), but the CPC analysis shows strong support for a shared latent structure, where 13% of the simulations supported the Unrelated model (0 CPCs), and 60% of the simulations supported models with 3 or more common PCs. The perturbation caused by \mathbf{E} generates random differences between \mathbf{P} and \mathbf{G} , but not a random rotation of the eigenstructure of \mathbf{G} (when $\sigma_{\max\mathbf{G}}^2 > \sigma_{\max\mathbf{E}}^2$). This pattern is caused by a lambda ratio ($\sigma_{\max\mathbf{G}}^2$) of 10 or larger, which will produce \mathbf{G} matrices with sharp elliptical contours (noticeable principal components), ensuring that the principal component structure of \mathbf{G} is inherited by \mathbf{P} , even when $\sigma_{\max\mathbf{G}}^2 \sim \sigma_{\max\mathbf{E}}^2$ (H. Joe, pers. comm.).

An illustrative bivariate example of the typical main differences between simulation models 4 and 5 is depicted in Figure 3.1. For each model and t/N_e , simulations are shown with four populations descending from an ancestor (0,0) with a random genetic covariance matrix (shown as dashed lines in Figure 3.1) and a random phenotypic matrix. The same phenotypic covariance matrices were used to generate 30 observations in each population and these are depicted as distinct clusters around each descendant. In simulation model 4, the matrix \mathbf{P} is a random rotation of \mathbf{G} , whereas in simulation model 5, the main axes of \mathbf{G} are preserved in \mathbf{P} .

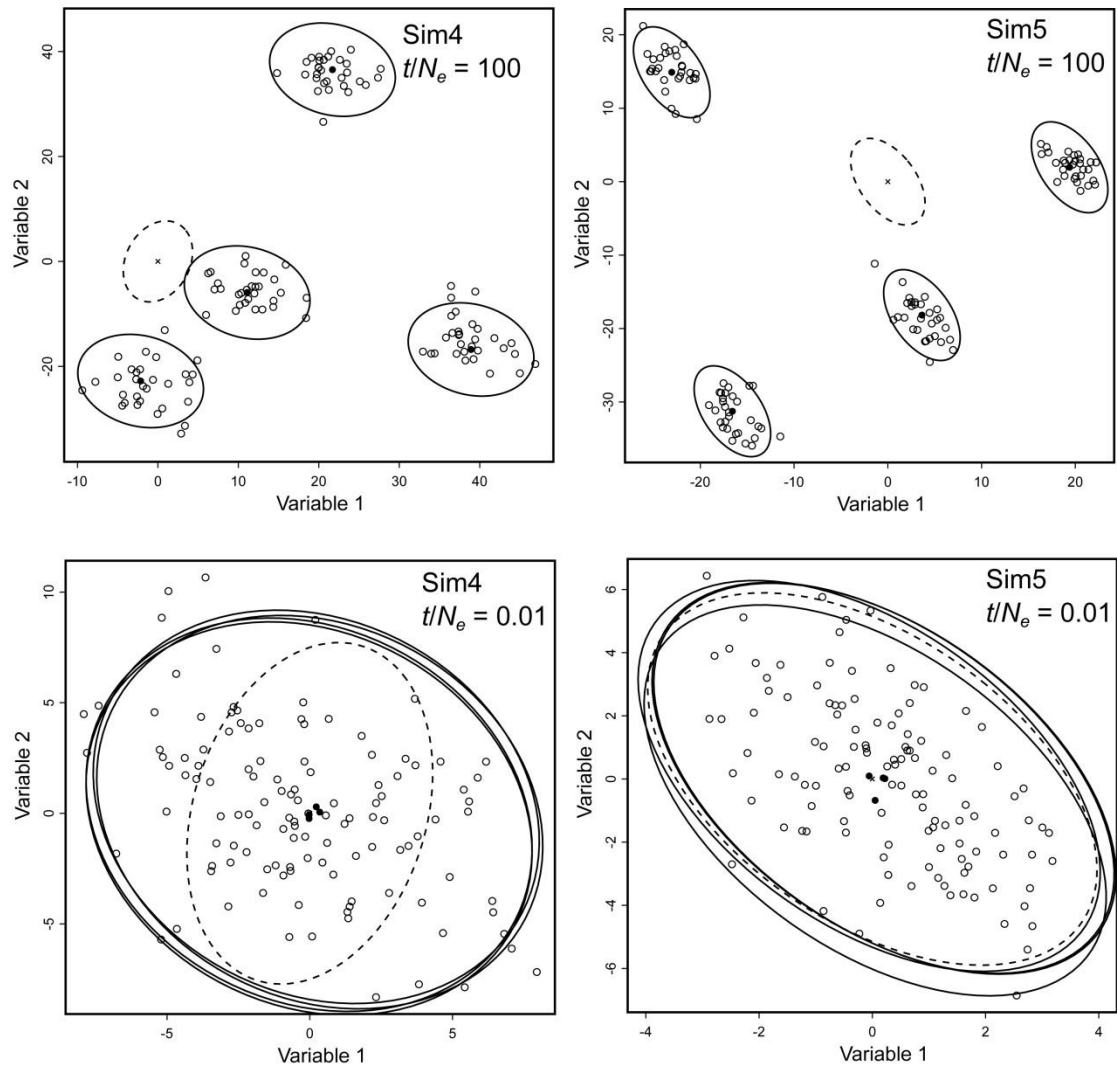


Figure 3.1. Simulation of genetic drift in four populations. The means of each population were evolved from an ancestral multivariate normal distribution with mean = $(0,0)$ and covariance matrix = $\mathbf{G}(t/N_e)$. Each population was randomly sampled 30 times using the respective average and covariance matrix \mathbf{P} . Left panels correspond to simulation model 4, where \mathbf{P} and \mathbf{G} are correlated, but do not share principal components. Right panels correspond to simulation model 5, where \mathbf{P} and \mathbf{G} share principal components but have low correlation. The ancestral genetic covariance matrix is depicted as a dashed ellipse. The population phenotypic covariance matrices are depicted as solid ellipses. Filled circles correspond to population means and open circles correspond to individual observations.

3.2.6. Genetic Drift Test

Genetic drift as a neutral model for phenotypic divergence was tested by comparing the among-population covariance matrix (\mathbf{B}) and the within-population phenotypic covariance matrix (\mathbf{W} , as a surrogate of the average \mathbf{G}) for the simulated data using the method of Ackermann and Cheverud (2002, 2004). This involved extracting the eigenvectors (\mathbf{M}) and eigenvalues (\mathbf{m}) of \mathbf{W} , and projecting each population phenotypic vector of means $\bar{\mathbf{z}}$ on \mathbf{M} , $\mathbf{Y} = \bar{\mathbf{z}}\mathbf{M}$. The vector of means for each population was the one estimated from the simulated samples, not the parametric means generated from the ancestral \mathbf{G} and ancestral vector of means. Finally, the variances for each column of \mathbf{Y} were calculated and a regression of the variances of \mathbf{Y} on \mathbf{m} performed following

$$\ln(\mathbf{Y}_i) = \ln(t/N_e) + \beta \ln(\mathbf{m}_i). \quad (3.3)$$

Testing with a t -test whether the slope of the regression (β) is different from 1 indicates whether the pattern is compatible with genetic drift. The null hypothesis of genetic drift is rejected if the slope deviates significantly from 1 (Ackermann & Cheverud 2002, 2004).

For each combination of parameters (ancestral \mathbf{G} , \mathbf{P} , t/N_e ratio, sample size, number of descendant populations, $\sigma_{\max E}^2/\sigma_{\max G}^2$) in different models, 1000 data sets were simulated to estimate type I error rates. In the simulated data sets, the only mechanism producing phenotypic divergence among the descendant populations was genetic drift. When using a significance level of $\alpha = 0.05$, a true null hypothesis is expected to have a 5% chance of being rejected (a type I error). If the use of phenotypic covariances as proxies for genetic ones in the genetic drift test does increase the type I error rates, it is expected that, using a significance level of 5%, the null model of genetic drift will be rejected in more than 5% of the simulated samples.

All the simulations and analyses were run in the R environment (R Development Core Team 2013) using functions from the packages MASS (Venables & Ripley 2002), clusterGeneration (Qiu & Joe 2009), and vegan (Oksanen *et al.* 2007). The R code (commented) used for the simulations is available in Appendix B.

3.3. Results

For the simulation using the bee wing shape data (genetic and phenotypic covariance matrices) as starting parameters, the type I error rate decreased with increasing sample sizes for small t/N_e ratios (between 0.01 and 0.000001) irrespective of the number of populations (15, 30) used (Figures 3.2A, 3.3A). The error rate increased for larger sample sizes when $t/N_e \geq 0.1$. The correlation between **G** and **W** remained stable over simulations for all t/N_e , with a median matrix correlation of 0.788, and a 95% confidence interval (based on 0.025 and 0.975 quantiles) from 0.741 to 0.830. The matrix correlation for the ancestral (original) **P** and **G** was 0.804.

For the simulation using the shell shape data as starting parameters, the type I error rates remain at acceptable levels for sample sizes above 20 in t/N_e ratios equal to or below 0.001, and both numbers of populations (15, 30) (Figures 3.2B, 3.3B). For the simulation with $t/N_e = 0.01$, the error rates increase with sample size. This is a slightly worse result than in the simulations with bee wing parameters, because in the latter, the simulation with $t/N_e = 0.01$ yielded acceptable error rates (Figure 3.2A and B). The correlation between average **G** and **W** also remained stable over simulations using the shell data set for all t/N_e , with a median matrix correlation of 0.441, and a 95% confidence interval (based on 0.025 and 0.975 quantiles) from 0.405 to 0.479. The matrix correlation for the ancestral (original) **P** and **G** was 0.442.

In the simulation model 2, where **G** and **P** differed only by a random constant (Figure 3.2C), the resulting pattern showed slight fluctuations around the expected type I error rate (0.05) for any value of t/N_e . This result was observed for sample sizes above 40 individuals per population regardless of the number of populations (15 or 30 – Figures 3.2C, 3.3C).

The simulation model 3, where **P** and **G** were generated independently (Figure 3.2D, 3.3D), presented acceptable type I error rates only for t/N_e ratios equal to or below 0.00001, regardless of the number of populations. The simulations with $t/N_e > 0.001$ all presented type I error rates above 0.8 and are not shown in the Figure. Because in this model, **G** and **P** have independent covariances, the test would be expected to show significant deviations from the unity slope for any combination of parameters. This suggests that the power of the test must be small for such values of t/N_e .

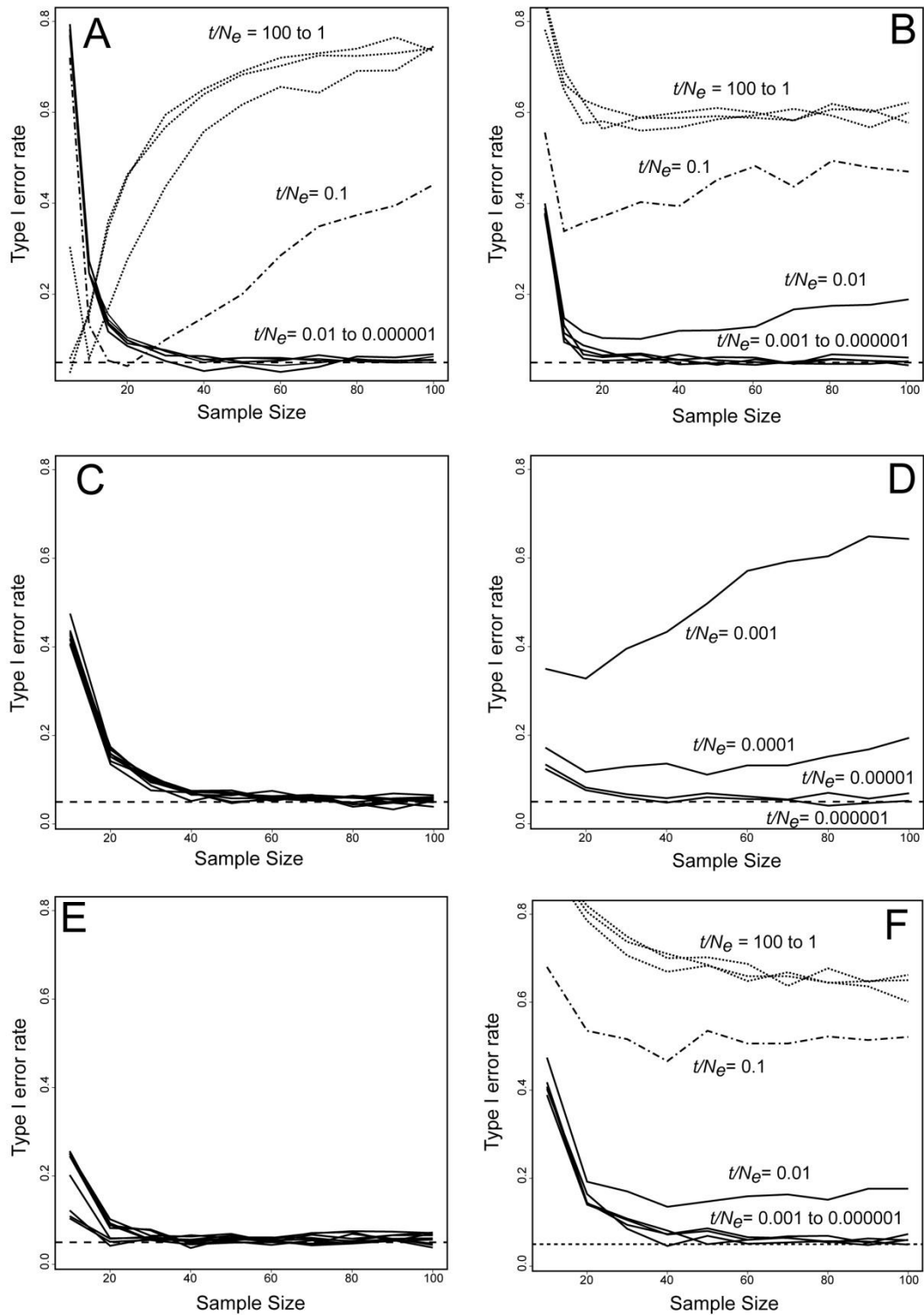


Figure 3.2. Type I error rates for the simulated analyses with varying sample sizes and t/N_e ratios (drift intensities). The legends and line types indicate the value of t/N_e used (only when differences among lines are noticeable). The dashed horizontal straight line indicates the expected type I error rate of 0.05. All simulations in this Figure were performed with 15 populations. A) Error rates for the bee wing data set. B) Error rates for the shell data set. C) Stochastic simulations (model 2) where \mathbf{G} was random and \mathbf{P} was exactly proportional to it $\mathbf{P} = k\mathbf{G}$ (multiplication by a random scalar k drawn from

a uniform distribution between 1 and 10). D) Stochastic simulation (model 3) where both \mathbf{G} and \mathbf{P} were random and completely independent. E) Stochastic simulation (model 4) where \mathbf{G} and \mathbf{P} were correlated ($\mathbf{P} = \mathbf{G} + \mathbf{E}$), but did not share a common latent structure (\mathbf{G} and \mathbf{E} with the same range of variances). F) Stochastic simulation (model 5) where \mathbf{G} and \mathbf{P} were correlated and shared a common latent structure (\mathbf{G} and \mathbf{E} with the same range of variances). See text for model details.

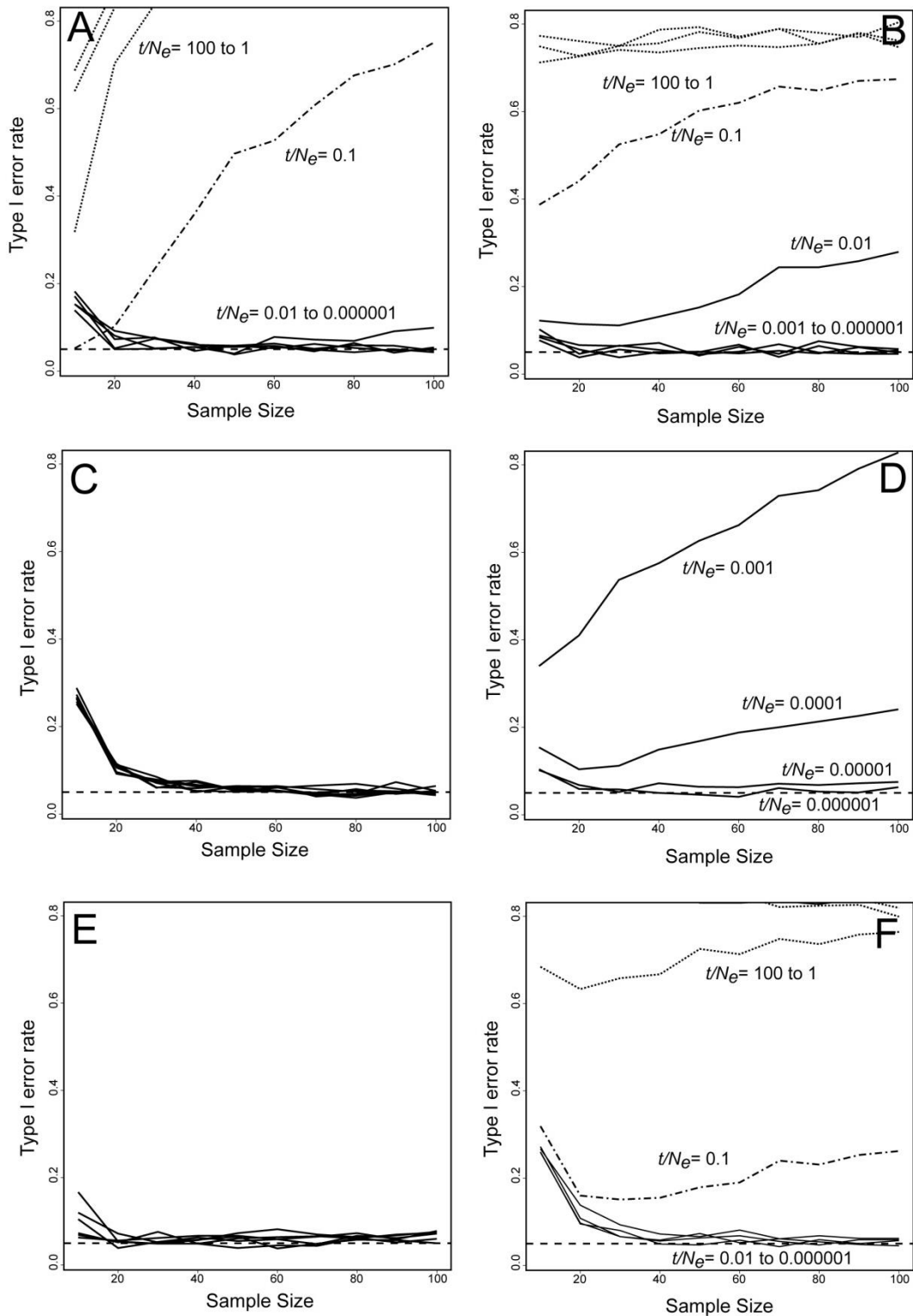


Figure 3.3. Type I error rates for the simulated analyses with varying sample sizes and t/N_e ratios (drift intensities). The legends and line types indicate the value of t/N_e used. The dashed horizontal straight line indicates the expected type I error rate of 0.05. All simulations in this Figure were performed with 30 populations. A) Error rates for the bee wing data set. B) Error rates for the shell data set. C) Stochastic simulations (model 2) where \mathbf{G} was random and \mathbf{P} was exactly proportional to it $\mathbf{P} = k\mathbf{G}$ (multiplication by

a random scalar k drawn from a uniform distribution between 1 and 10). D) Stochastic simulation (model 3) where both \mathbf{G} and \mathbf{P} were random and completely independent. E) Stochastic simulation (model 4) where \mathbf{G} and \mathbf{P} were correlated ($\mathbf{P} = \mathbf{G} + \mathbf{E}$), but did not share a common latent structure (\mathbf{G} and \mathbf{E} with the same range of variances). F) Stochastic simulation (model 5) where \mathbf{G} and \mathbf{P} were correlated and shared a common latent structure (\mathbf{G} and \mathbf{E} with the same range of variances).

Simulation models 4 and 5 were designed to generate **G** and **P** correlated matrices, where $\mathbf{P} = \mathbf{G} + \mathbf{E}$. In simulation model 4, the random matrix **E** adds variation to the genetic covariances and variances, including a random rotation of the eigenstructure when **P** is calculated, even if the range of variances in **E** ($\sigma_{\max E}^2$) is the same or a bit smaller than the range of variances in **G** ($\sigma_{\max G}^2$). In simulation model 5, the **E** matrix only causes differences in the principal components of **G** and **P** when $\sigma_{\max E}^2 > \sigma_{\max G}^2$. The first set of analyses was performed using the same range of variances in **G** and **E** for both models. The simulation model 4 presented acceptable error rates for sample sizes larger than 20 regardless of t/N_e ratio and number of populations. The simulation model 5 presented acceptable type I error rates only for t/N_e ratios equal to or below 0.001, regardless of the number of populations (Figures 3.2E and F; 3.3E and F).

Exploring the simulations with a larger range of parameters, it was found that the ratio of upper limits of environmental and genetic variance ranges ($\sigma_{\max E}^2/\sigma_{\max G}^2$) also influences the type I error rates of the test. One unexpected result was that in simulation model 4, as $\sigma_{\max E}^2$ gets smaller than $\sigma_{\max G}^2$, the type I error rates increase. Simulations were again performed with fixed sample sizes (100), number of groups (15) and t/N_e (10) to assess the influence of $\sigma_{\max E}^2/\sigma_{\max G}^2$ on the slope of the AC test (Figure 3.4). In the right panel of Figure 3.4, using simulation model 5 (where **P** readily inherits the eigenvectors of **G**), as the value of $\sigma_{\max E}^2/\sigma_{\max G}^2$ gets smaller, the slope of the test converges to 1, as expected under genetic drift. On the other hand, in the simulation model 4 (left panel of Figure 3.4), the expected value of the slope under simulation of drift is 1 only when $\sigma_{\max E}^2 \sim \sigma_{\max G}^2$. As the ratio of variance ranges get smaller, the expected slope converges to ~ 1.3 , and this pattern explains why the type I error rates increase when $\sigma_{\max E}^2$ gets smaller than $\sigma_{\max G}^2$. The simulations using the real matrices (model 1) and the same parameters described above had expected slopes of 1.3 (bees) and 0.8 (*Physa* shells). Slopes larger than 1 might be obtained when the variance among population averages projected on the first eigenvectors of **W** is larger than the corresponding eigenvalues, whereas slopes smaller than 1 are the result of less among population variation than predicted by the eigenvalues of the first PCs of **W**.

Considering that, for simulation model 5, smaller variance range ratios lead to the expected slope under genetic drift, the combination of simulation parameters that would lead to acceptable type I error rates on the AC test were explored (Table 3.1). When the ratio $\sigma_{\max E}^2/\sigma_{\max G}^2$ is decreased, the correlations between **P** and **G** increase, as

well as the number of common principal components. If $\sigma_{\max E}^2$ is around 20% of $\sigma_{\max G}^2$, the matrix correlations observed are not particularly high, as compared to real \mathbf{P} and \mathbf{G} matrices estimated with large sample sizes, but they do share a common eigenstructure, and for any value of t/N_e , the type I error rates approach acceptable values. Performing the same simulations with more variables ($m = 30$), the same results are obtained with larger within-population sample sizes ($n > 100$) (results not shown). It is evident from these results that the combination of parameters yielding acceptable type I error rates is sensitive to the models under which the starting matrices were generated.

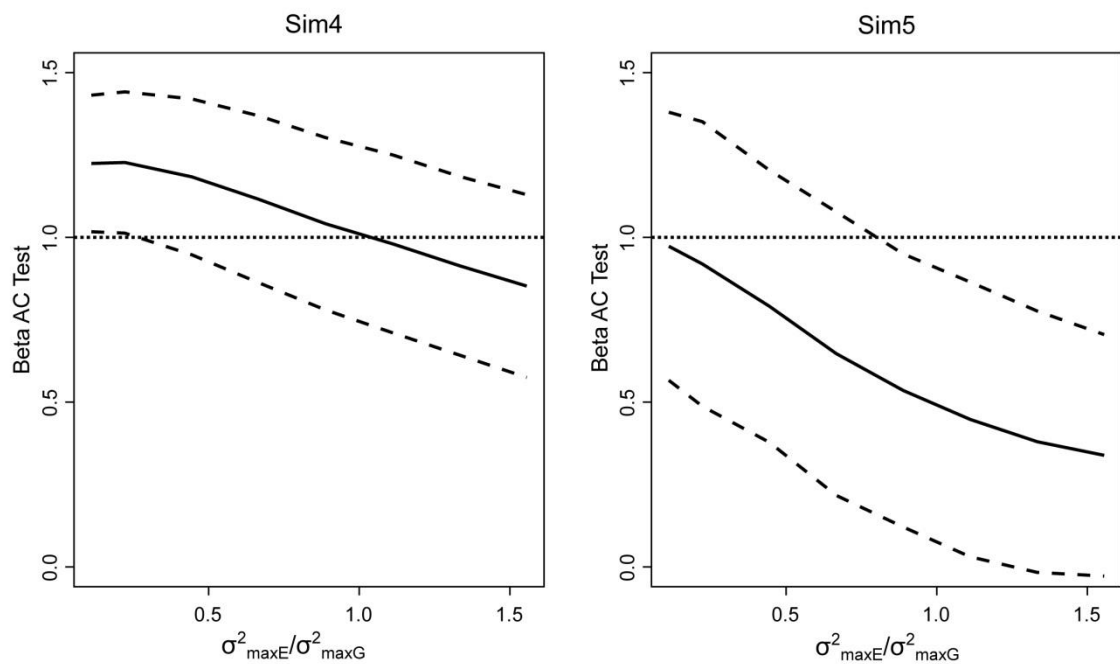


Figure 3.4. Slopes (β) of the Ackermann and Cheverud test in relation to the ratio of upper bounds of environmental ($\sigma_{\max E}^2$) and genetic ($\sigma_{\max G}^2$) variances in the simulations for models 4 (Sim4) and 5 (Sim5), using $t/N_e = 10$, 15 dimensions in \mathbf{G} , 15 populations, and 100 observations per population. Genetic variances ranged between 1 and $\sigma_{\max G}^2 = 10$ and the environmental variances ranged between 0 and $\sigma_{\max E}^2 = 1$ to 15. The solid lines show the expected (mean) value for the slope over 1000 simulations, whereas the dashed lines indicate the upper and lower limits of 95% confidence intervals. The dotted line indicates the unity slope, which is the theoretical expectation under genetic drift.

Table 3.1. Type I error rates for the genetic drift test using simulation model 5 (1000 repetitions), with 15 variables, 15 groups and 50 individuals per group ($\alpha = 0.05$), with varying t/N_e . $\sigma_{\max E}^2/\sigma_{\max G}^2$ is the ratio of the upper bounds of variances in the environmental and genetic matrices (see text), CI- h^2 is the 95% confidence interval for the average heritability in each set of simulations, CI-MatCor is the 95% confidence interval for $\mathbf{G P}$ matrix correlations in each set of simulations, fCPC is the percentage of significant full CPC models for \mathbf{G} and \mathbf{P} in 100 simulations, CICPCs is the 95% confidence interval (percentiles) for the number of common principal components for \mathbf{G} and \mathbf{P} in 100 simulations.

$\sigma_{\max E}^2/\sigma_{\max G}^2$	GP Matrix comparisons				t/N_e			
	CI- h^2	CI-MatCor	fCPC	CICPCs	100	10	1	0.1
0.1	0.86-0.94	0.808-0.970	100	14	0.058	0.062	0.056	0.048
0.2	0.76-0.88	0.543-0.891	100	14	0.048	0.057	0.058	0.043
0.3	0.70-0.84	0.385-0.812	79	7-14	0.097	0.084	0.102	0.077
0.4	0.64-0.80	0.277-0.729	67	4-14	0.139	0.159	0.188	0.132

3.4. Discussion

Testing diversification by genetic drift is a useful starting point in the study of evolutionary variation (Lynch 1990; Ackermann & Cheverud 2004; Weaver, Roseman, & Stringer 2007; Perez & Monteiro 2009). Cheverud's (1988) suggestion that genetic covariance matrices could be safely replaced by phenotypic matrices for evolutionary inferences was greeted with scepticism, and "Cheverud's conjecture" (Roff 1995) has been tested and discussed in a number of papers (*e.g.* Roff 1995, 1996; Koots & Gibson 1996; Waitt & Levin 1998; Roff *et al.* 1999; Bégin & Roff 2004; Hadfield *et al.* 2007; Kruuk, Slate, & Wilson 2008), usually by comparing the similarity of genetic and phenotypic covariances, seldom by checking the influence of matrix differences in the results of tests. Thus, the evidence gathered has been equivocal and the most relevant studies (large reviews of data) indicate a general agreement with Cheverud (1988), but also recommend caution in the interpretations of results because matrix comparisons among isolated populations using genetic or phenotypic covariances might differ in important ways (Roff *et al.* 1999; Bégin & Roff 2004).

The results of this study indicate that the type I error of Ackermann and Cheverud's (2002, 2004) test of proportionality between **G** and **W** is influenced mainly by the structural similarity between the ancestral **G** and **P**, the ratio of variance ranges (approximated by the average heritability), and the ratio of time and effective population size t/N_e . If the parametric genetic and phenotypic covariance matrices are exactly proportional, as in the simulation model 2, the type I error rates are acceptable for any t/N_e ratio (as expected). On the other extreme (simulation model 3), where **G** and **P** were generated with an unrealistic minimum of structural similarity, the type I error rate is unacceptable for most values of t/N_e .

The simulations showed that, even if the ancestral **G** and **P** are not proportional, but do share a large number of principal components, have a average heritability around 0.5 and matrix correlation above 0.7 over all variables (as in our simulation model 5), acceptable type I error rates will be obtained for any t/N_e ratio. When **G** and **P** do not share principal components but are highly correlated ($r > 0.7$) and have average heritabilities approaching 0.5, the type I error rates should be acceptable for any t/N_e ratio (as in simulation model 4). Average heritabilities different from 0.5 will bias the expectation of the slope in the AC test due to concentration of variation among projections of population averages in the first eigenvectors of **W**. In these cases, type I error rates will still be acceptable for $t/N_e < 0.01$.

The combination of parameters laid out is not an unrealistic expectation. The literature indicates that considerable agreement between genetic and phenotypic correlations is often found and that the correlations between **G** and **P** are usually above 0.6 for morphological data when effective sample sizes are large (Cheverud 1988; Roff 1996; Koots & Gibson 1996; Waitt & Levin 1998; Bégin & Roff 2004; Kruuk *et al.* 2008; de Oliveira, Porto, & Marroig 2009).

In a study where only phenotypic data are available, it might be complicated or impossible to determine whether the relationship between the ancestral **G** and **P** fits into the assumptions outlined above. These parameter values can, nevertheless, be used as guidelines for comparisons among populations as indirect evidence of ancestral **G** and **P** similarity (de Oliveira *et al.* 2009), or one might use the Monte Carlo simulation approach described below to estimate a confidence interval for the slope of the AC test under drift.

The example data sets used here (simulation model 1) seem to behave in a similar way to simulation model 4 for extremes of low and high $\sigma_{\max E}^2/\sigma_{\max G}^2$. The expected slope for the simulations using the bee matrices was 1.3, the similarity of **G**

and **P** was high and they did share principal components, but the average heritability was low (it should have been higher than 0.6 to fit the model 4 more closely). On the other hand, the simulations with shell matrices had an expected slope of 0.8, **G** and **P** similarity was low, they did not share principal components, but the average heritability was high (should have been lower than 0.3). Such results would be observed if model 4 was changed to calculate $\mathbf{P} = k(\mathbf{G} + \mathbf{E})$, so that the average heritability would be decreased or increased by the scalar k without influence in the correlation or shared structure between **P** and **G**. These results suggest that **G** and **P** are related in complex ways which can hardly be reduced to scalar comparisons without considerable loss of information. If some information about **G** and **P** is available, this simulation approach to estimate the expected slope of the AC test might be used and this expectation in the test of the real data might be taken (instead of the theoretical unity slope). For example, in the bee wing analyses, a slope of 1.3 could have been used as parameter in the t -test of the AC tests and the type I error rates would be acceptable for any value of t/N_e . Alternatively, the 95% confidence interval for the expected AC test slope under genetic drift simulations ranged from 1.1 to 1.5, and an observed slope could be compared with this interval for evidence of departure from the neutral expectation. When genetic data are not available, it might be possible to use the between-population covariance matrix (**B**), estimated from phylogenetic independent contrasts if possible (Revell 2007) and the within-population phenotypic covariance matrix **W** as proxies for the ancestral **G** and **P**, respectively, in the simulations to estimate the expected slope under drift. A simulation function provided in Appendix B (simulationAC-slope.R) calculates a mean estimate and a 95% confidence interval for AC test slopes under genetic drift for any ancestral **G** and **P**. Observed slopes can be compared to the confidence interval or the mean estimate can replace the parameter slope = 1 in the ordinary t -test.

Within-population sample sizes influence the type I error rates, but they need to be considered in conjunction with the number of populations and the dimensionality of the matrices. For the fully stochastic simulations here performed, all matrices had 15 dimensions and most acceptable type I errors were observed for within-population samples larger than 40. The number of populations used had a slight but negligible effect.

It is possible that sampling error in the estimation of **G** might lead to a similar pattern of type I errors as when average **G** is replaced by **W**, because the parametric and estimated **G** matrices are not likely to be exactly proportional as well. It is not clear whether sampling error in the estimation of **G** is comparable to the environmental

covariance matrix **E**, but a part of Cheverud's conjecture was that **W** could be a more reliable estimate of the parametric **G** than a genetic matrix estimated from a small effective sample size (Cheverud 1988), and phenotypic correlation estimates are often within the confidence intervals of genetic correlations (Roff 1996; Koots & Gibson 1996). The instability of covariance matrix and factor estimation for small sample sizes is well known in multivariate statistics (MacCallum *et al.* 1999; Krzanowski 2000), and genetic covariance matrices can be particularly demanding with respect to samples sizes (Cheverud 1988). Patterns caused by sampling error in the estimation of genetic covariance matrices, such as biases on eigenvalues are well known (Meyer & Kirkpatrick 2010) and a considerably large statistical literature is devoted to such topics. As long as the sampling error can be considered independent from the parametric **G**, the simulation function provided in Appendix B can be adjusted to address specific concerns regarding the error in the estimation of **G**.

In some of the simulations, particularly model 1 (with predetermined matrices) and the fully stochastic simulation where **G** and **P** were random and completely independent (model 2), a trend was observed where for higher values of t/N_e , the type I error rates increase with within-population sample size (see Figures 3.2A, B and D). This counterintuitive result was also observed in simulation model 4, when $\sigma_{\max E}^2$ is smaller than $\sigma_{\max G}^2$ (Figure 3.5). Considering that, depending on this ratio, the differences between **G** and **P** caused the expected value of the slope of the AC test to be larger than 1 (as shown in Figure 3.4 due to more variation among populations than predicted by the eigenvalues of **W**), the type I error rates increase with sample sizes because the confidence intervals become narrower (there is an expected increase in power) and a larger percentage of simulated tests will show significant results. The type I error converges to a value that depends on the magnitude of deviation of the expected AC test slope from 1 and the size of the confidence interval. For smaller t/N_e ratios, there is a reduction in the contribution of the **G** matrix to among-population variation (it will be proportional to $t/N_e \mathbf{G}$). Because the simulations calculate among group variation using averages estimated from the n observations generated by **P** at each population (and not the parametric means generated by **G**), when t/N_e decreases, most among-population variation is generated and predicted by **W**, and the expected slope of the AC test is 1. This also explains the effect in reverse, when $\sigma_{\max E}^2 > \sigma_{\max G}^2$, causing among population variation to be smaller than the eigenvalues of **W** and the expected slope of the AC test to be < 1 (Figure 3.4).

In the next chapter, the genetic drift test proposed by Ackermann and Cheverud (2002, 2004) is applied to a papionin sample of cranial landmarks to understand whether as neutral pattern of divergence is likely, or whether papionin cranial form is more likely to have evolved due to non-random processes such as natural selection.

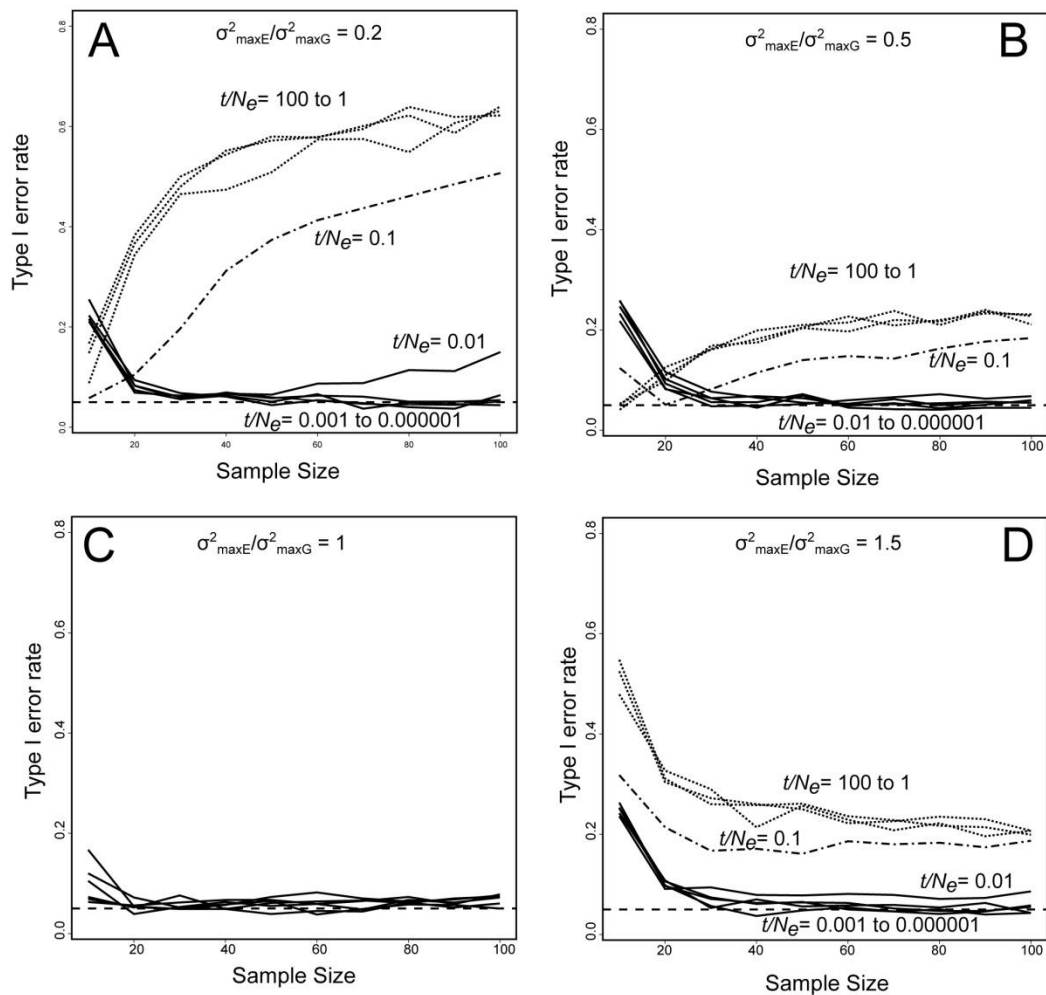


Figure 3.5. Type I error rates for the simulated analyses under model 4 with varying $\sigma^2_{\max E}/\sigma^2_{\max G}$, sample sizes and t/N_e ratios (drift intensities). The legends and line types indicate the value of t/N_e used when differences are meaningful. The dashed horizontal straight line indicates the expected type I error rate of 0.05. All simulations in this Figure were performed with 15 populations. The value of $\sigma^2_{\max E}/\sigma^2_{\max G}$ for each set is indicated on the top of each panel.

Chapter 4. Testing the Role of Random Genetic Drift in the Evolutionary Divergence of Papionin Crania

4.1. Introduction

It follows from the previous chapter that the parameters influencing the type I error of Ackermann and Cheverud's (2002, 2004) test of proportionality between the among-population covariance matrix (**B**) and the phenotypic within-group variance-covariance matrix (**W**) are the structural similarity between the ancestral additive genetic variance-covariance matrix (**G**) and the ancestral phenotypic covariance matrix within a single population (**P**), the ratio of variance ranges (approximated by the average heritability), and the ratio of time and effective population size t/N_e . If the parametric **G** and **P** are exactly proportional (Section 3.2.2, simulation model 2), the type I error rates are acceptable for any t/N_e ratio (as expected). If **G** and **P** are not exactly proportional (Section 3.2.3, simulation model 3), the type I error rate is unacceptable for a range of values of t/N_e .

This procedure can thus be used as a null hypothesis to test for neutral evolution in the pattern of divergence of papionin cranial form. Papionins are variable in terms of cranial form and each form is argued to have evolved for a different function, while constrained by their close phylogenetic relationships (see Subsections 1.3.1 and 1.3.5). For example, the genus *Cercocebus* has adaptations such as a shortened face that increases bite force (Singleton 2004), but its sister genus *Mandrillus* does not (Fleagle & McGraw 1999). Bearing the molecular phylogeny in mind (Figure 1.3), the question arises as to why sister genera have evolved different cranial forms. Since feeding is a fundamental animal behaviour, form variation in an adaptive radiation tends to exhibit itself as trophic adaptation (Schluter 2000). Indeed, in numerous primates dietary differentiation has been associated with morphological adaptation (Ravosa 1990; Daegling 1992; Singleton 2005; Taylor 2006). Ecological differences between, for example again, *Cercocebus* and *Mandrillus* would suggest some adaptation of each genus to different environments, and so natural selection would have acted to produce a short face in one case and a long face in the other (see Subsection 1.3.5).

It is not always easy to know for certain whether a particular trait evolved as an adaptation to a function, and criticisms against a strict “adaptationist programme” arose in the 1970s (Gould & Lewontin 1979). That criticism led to a view that natural selection could not be nearly as pervasive as previously thought (Gould & Lewontin 1979; Alberch 1983; Wake & Larson 1987; Goodwin 1994; reviewed by Schwenk & Wagner 2004). More than that, many authors argue that intrinsic constraints on the production of variation are at least as important as natural selection in shaping patterns of phenotypic diversity (reviewed by Gould 2002, and Schwenk & Wagner 2004). Testing diversification by random genetic drift is a useful starting point in the study of evolutionary variation (Lynch 1990; Ackermann & Cheverud 2004; Weaver *et al.* 2007; Perez & Monteiro 2009) and indeed some papionins are already considered a good example of random genetic drift: the species attributed to the genus *Macaca* show considerable variation in face size, all of it verified to be natural variation within the group (O’Higgins & Collard 2002). On the whole, the recency of the papionin radiation (see Section 1.3) impairs the clear demarcation of subgroups since they have not had a long, independent evolution (Jablonski 2002), particularly within the *Papio*, *Theropithecus* and *Lophocebus* branch (Harris 2000; Singleton 2002; Tosi *et al.* 2003). This makes testing for the neutral evolution of their cranial form even more relevant prior to making interpretations about cranial adaptation.

Although molecular sequence data for some papionin monkey species is available (*e.g.* Zinner *et al.* 2012), neither is there a large enough number of species sequenced for a comparative analysis, nor is the genotype-phenotype matching established (studies on the relationship between genotype and phenotype in papionins are scarce and include Willmore *et al.* 2009a; b). One of the few possible ways to study phenotype divergence, thus, is by using the **W** matrix instead of the **G** matrix (see Chapter 3 and Subsection 4.2.2), following Cheverud’s (1988) suggestion that genetic covariance matrices can be safely replaced by phenotypic matrices for evolutionary inferences. The evidence gathered has been equivocal and the most relevant studies (which are mostly large reviews of data; Roff 1995; Waitt & Levin 1998; Reusch & Blanckenhorn 1998; Dochtermann 2011) indicate a general agreement with Cheverud (1988), but also recommend caution in the interpretations of results.

The aim of this study was to test the hypothesis that the cranial form of each papionin genus (represented by the 7 species used throughout this thesis and outlined in Section 1.3) has diverged from the common ancestor by random genetic drift, *i.e.*, to assess whether random genetic drift alone could explain the observed cranial differences

in form among the papionin tribe by applying a quantitative genetic model (Ackermann & Cheverud 2002, 2004) and using a well-established papionin molecular phylogeny (Disotell 1994; Harris 2000) as a basis for interpretation of results. Based on that phylogeny, it is more likely, for example, that the differences in cranial form between the sister genera *Cercocebus* and *Mandrillus* have not arisen by the action of random genetic drift alone, and the same for the group including *Papio*, *Lophocebus* and *Theropithecus*.

4.2. Material and Methods

The R functions used in Chapter 3 (Appendix B) are utilised here, using actual **P** matrices for data much as in Simulation Model 1 (Section 3.2.1). The **P** matrices were extracted from landmark data of real papionin crania not previously studied, rather than simulated data or previously analysed real data sets as was the case in Chapter 3.

4.2.1. Sample Data Set

The data comprise 46 three-dimensional landmarks (see Subsection 2.3.1) digitized on the left side of a sample of 181 adult male crania belonging to 6 genera and 7 species within the Tribe Papionini, namely 15 *Cercocebus torquatus*, 20 *Lophocebus albigena*, 39 *Macaca fascicularis*, 20 *Mandrillus sphinx*, 40 *Papio anubis*, 30 *Papio hamadryas*, and 17 *Theropithecus gelada*.

Table 4.1 and Figure 4.1 present the actual landmarks descriptively and topographically; they were first described (on a different group of primates) in the literature (Cardini, Jansson, & Elton 2007; Cardini & Elton 2008). This landmark dataset was retrieved from a complete and comprehensive Old World monkey dataset presently unpublished and collected by Dr Andrea Cardini; it is used here with his kind permission.

Table 4.1. Landmarks used for the random genetic drift test, adapted from Cardini, Jansson, & Elton (2007). They were placed on the midline and left side only.

Number	Description
1	Prosthion: antero-inferior point on projection of pre-maxilla between central incisors
2	Equivalent to prosthion but between central and lateral incisors
3	Posterior-most point of lateral incisor alveolus
4	Anterior-most point of canine alveolus
5	Mesial P3: most mesial point on P3 alveolus, projected onto alveolar margin
6–9	Contact points between adjacent pre-molars/molars, labially onto alveolar margin
10	Posterior midpoint onto alveolar margin of M3
11–14	Contact points between adjacent pre-molars/molars, lingually onto alveolar margin
15	Greater palatine foramen
16	Point of maximum curvature on the posterior edge of the palatine
17	Tip of posterior nasal spine
18	Meeting point between the basisphenoid, basioccipital and petrous temporal bone
19	Most medial point on the petrous part of temporal bone
20	Most medial point of the foramen lacerum
21	Meeting point of petrous temporal bone, alisphenoid and base of zygomatic process
22–23	Anterior and posterior tip of the external auditory meatus
24	Stylomastoid foramen
25	Distal extremity of jugular foramen
26	Carotid foramen
27	Medial extremity of jugular foramen
28	Basion: anterior-most point of foramen magnum
29	Anterior extremity of occipital condyle along margin of foramen magnum
30	Hypoglossal canal
31	Centre of condylar fossa
32	Posterior extremity of occipital condyle along margin of foramen magnum
33	Opisthion: posterior-most point of foramen magnum
34	Inion: most posterior point of the cranium
35	Most lateral meeting point of mastoid part of temporal bone and supraoccipital
36	Nasospinale: inferior-most midline point of piriform aperture
37	Point corresponding to largest width of piriform aperture
38	Meeting point of nasal and pre-maxilla on margin of piriform aperture
39	Rhinion: most anterior midline point on nasals
40	Nasion: midline point on fronto-nasal suture
41	Glabella: most projecting midline point of frontals at the level of supra-orbital ridges
42	Supra-orbital notch
43	Antero-superior point of zygomaticomaxillary suture taken at orbit rim
44	Centre of optic foramen
45	Superior point of zygomaticotemporal suture on lateral face of zygomatic arch
46	Antero-inferior point of zygomaticomaxillary suture

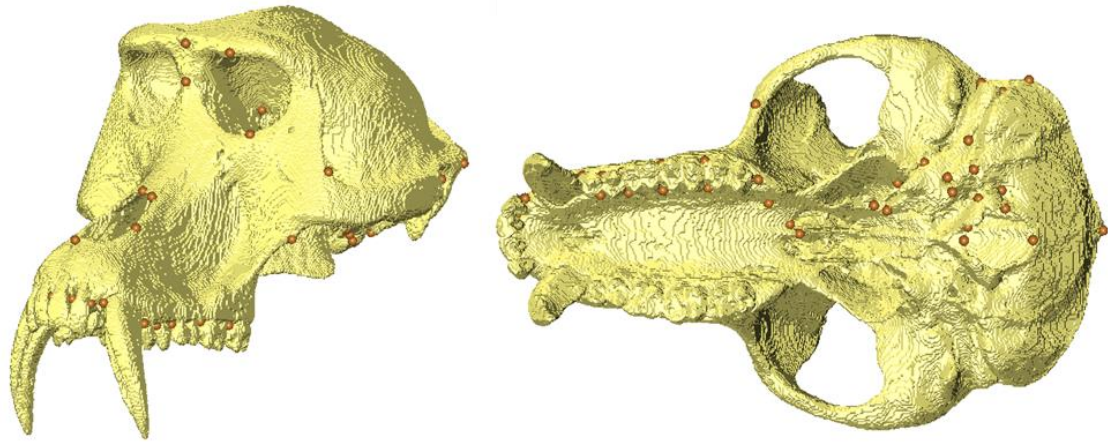


Figure 4.1. Set of 46 landmarks on the midline and left side showed on the surface of a male *Theropithecus gelada* cranium. See Table 4.1 for description of landmarks.

4.2.2. Genetic Drift Test

To study whether or not the observed differences could be explained by random genetic drift, the within- and among-group variance-covariance matrices were compared. Exactly as in Chapter 3, following the claim (Cheverud 1988) that, in contemporary populations, the \mathbf{W} matrix is often proportional to the \mathbf{G} matrix, one can substitute the latter by the former (Lande 1979; Felsenstein 1988). If the populations under study have diversified by random (neutral) processes alone, the pattern of among-group phenotypic variation is expected to be proportional to the within-group phenotypic variation.

As described in Chapter 3 (Subsection 3.2.6), random genetic drift as a neutral model for phenotypic divergence was tested by comparing \mathbf{B} and \mathbf{W} (as a surrogate of the average \mathbf{G}) using the method of Ackermann & Cheverud (2002, 2004). This involved an eigendecomposition of \mathbf{W} to extract its eigenvectors (\mathbf{M}) and eigenvalues (\mathbf{m}), and projecting each population phenotypic vector of means $\bar{\mathbf{z}}$ on \mathbf{M} , $\mathbf{Y} = \bar{\mathbf{z}}\mathbf{M}$. The vector of means for each population was the one estimated from the landmark data set, not the parametric means generated from the ancestral \mathbf{G} and ancestral vector of means. The variances for each column of \mathbf{Y} were then calculated and a regression of the variances of \mathbf{Y} on the eigenvalues \mathbf{m} was performed (Equation 3.3).

Testing with a t -test whether the slope of the regression (β) is different from 1 indicates whether the pattern is compatible with random genetic drift. The null

hypothesis of random genetic drift is rejected if the slope deviates significantly from 1 (Ackermann & Cheverud 2002, 2004).

When using a significance level of $\alpha = 0.05$, it is expected that a true null hypothesis has a 5% chance of being rejected (a type I error). If the use of phenotypic covariances as proxies for genetic ones in the genetic drift test does increase the type I error rates, it is expected to find that, using a significance level of 5%, the null model of genetic drift is rejected in more than 5% of the simulated samples. Lofsvold (1988) has suggested that the acceptance of random genetic drift as a null hypothesis is more robust to the breaking of model assumptions than its rejection (so type I error rates are of more concern than the power), and in real data studies it might be hard to determine the actual cause of random genetic drift rejection, natural selection being one of the possible explanations.

Like in Ackermann and Cheverud (2002, 2004), a papionin phylogenetic tree (Disotell *et al.* 1992; Disotell 1994; Harris 2000) is used here as a basis for the analyses and for the interpretation of results. In total, 6 analyses were performed: an analysis with the whole sample (all genera), another with all genera except *Macaca*, which is the most different genus and can be said to be the outgroup of this phylogenetic tree; another analysis for the sister taxa *Cercocebus* and *Mandrillus*, another for the *Papio*, *Lophocebus* and *Theropithecus* group, which is an unresolved polytomy; another with *Lophocebus* and *Theropithecus*, which is one of the possibilities to resolve the polytomy, and finally an analysis with only the two species of the genus *Papio*, *P. anubis* and *P. hamadryas*. Grouping *Lophocebus* with *Theropithecus* was decided here as opposed to grouping any one of these taxa with *Papio* because the *Papio*, *Lophocebus* and *Theropithecus* polytomy prevents a fully resolved consensus molecular phylogeny for papionins. An analysis grouping two species of *Papio* and another genus would be biased in terms of number of species per genus, and thus this arrangement seems to be acceptable for this analysis (see also Section 4.1; Harris 2000).

All the analyses were run in the R environment (R Development Core Team 2013) using functions from the packages MASS (Venables & Ripley 2002), clusterGeneration (Qiu & Joe 2009), and vegan (Oksanen *et al.* 2007). The R code used to run the analyses is presented in Appendix B.

4.3. Results

In Figure 4.2 a modified version (fully resolved) of the consensus phylogeny (Figure 1.3) of papionins is shown. The values of the slope test and the p-value of significance are shown on tree nodes. Each corresponds to the analysis computed on all the species to the right of that node. An image of the form of each papionin cranium is also shown, as well as species names.

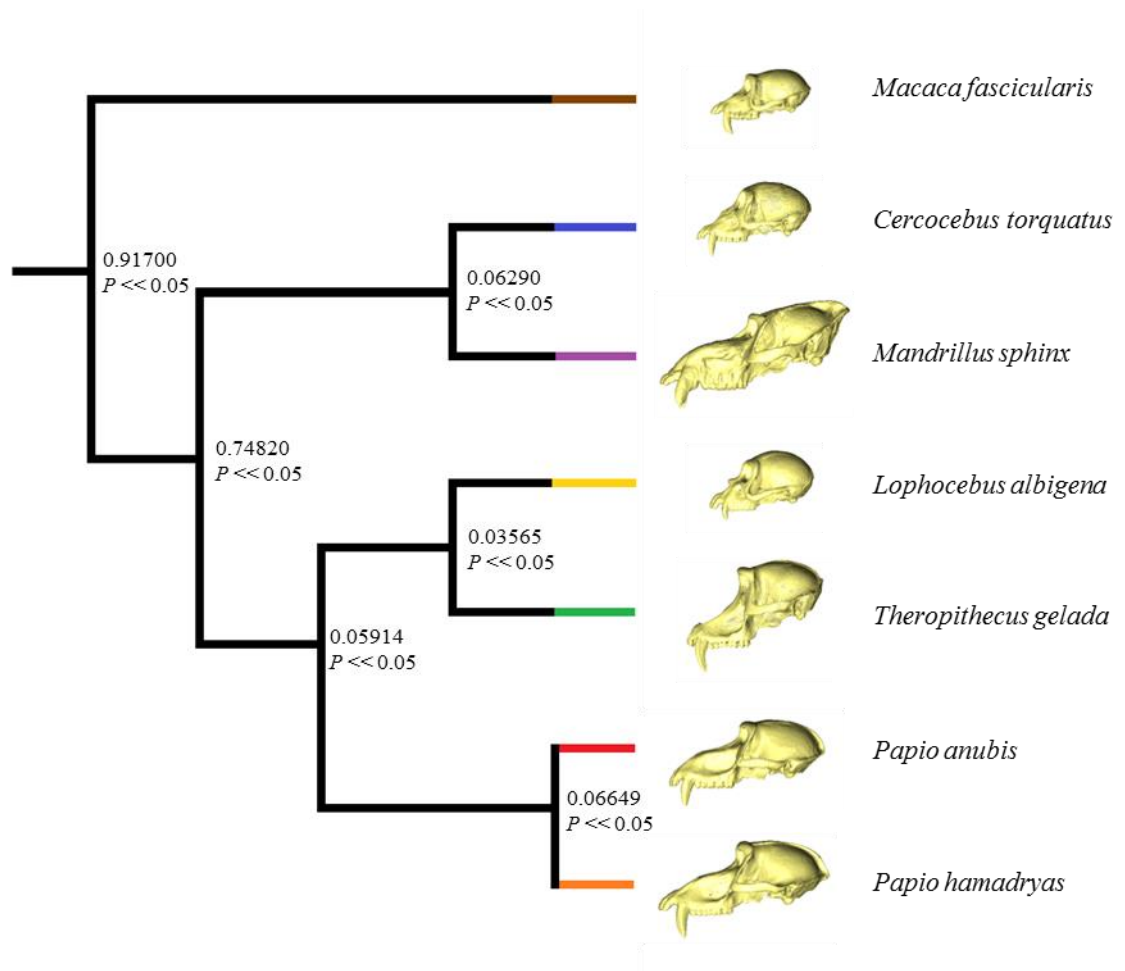


Figure 4.2. Phylogenetic tree showing the 6 analyses performed. Slope and p-values shown on tree nodes, each corresponding to one analysis with all the species to the right of the node. The values are significant for an α of 0.05, meaning that the results are not consistent with a species divergence driven by random genetic drift alone.

The test on the null hypothesis of divergence by random genetic drift alone is significant for every analysis. The slope between among- and within-group genotypic variance-covariance matrices differs significantly from one in every analysis, even though the test results in a slope of 0.917 for the analysis on the whole sample. The hypothesis is therefore rejected in every analysis, even in the analysis that includes only the two species of *Papio* which are very close both phylogenetically and in terms of cranial form.

4.4. Discussion

A test on the null hypothesis of the divergence of papionins by random genetic drift alone was carried out supported by an established molecular phylogeny. From the results it can be concluded that random genetic drift was most likely not the single microevolutionary process acting on the form of the papionin cranium. Non-random processes are therefore likely to have acted, driving the form of the cranium as a response to environmental pressures, such as geography, climate, competition, predators, and especially diet. But interpreting these results directly as biological is ill advised. First, as demonstrated in Chapter 3, the sample size required to increase the power of the test enough to make such interpretations is not met by the sample size available for this study. A sample size of hundreds of specimens would fit the assumptions of the model better. Second, this study included only male specimens and if the analyses were repeated including females (and females can differ extensively from males in terms of cranial morphology), the slope deviation from 1 may or may not be significant in all the analyses.

Thirdly, the landmarks describing the shape of the cranium might not be the most appropriate to capture the geometry of the actual evolving morphology. The use of midline and left side landmarks only might have had an effect on the analysis, and the full set of cranial landmarks (including the right side, paired landmarks) might result in a different outcome. The right side landmarks were not collected originally in order to increase the efficiency of an otherwise time-consuming task, but they can be easily produced by reflecting the left side landmarks on the midline, creating a symmetric landmark set (Klingenberg, Barluenga, & Meyer 2002). Of course, the real crania are

not symmetric, but statistically the error introduced in the shape analysis by symmetrizing or averaging the paired landmarks is small when compared, for example, with errors in landmark collection or superimposition (Zelditch *et al.* 2004). This means that adding right side landmarks (either by collecting them or by reflecting the left side ones) would add new information to the analysis only if asymmetry was significant, which is not the case in papionins.

Yet, the test was proved to be robust in falsifying the underlying assumptions (Prôa, O'Higgins, & Monteiro 2013; see also Chapter 3), and the results indicate that the form of the cranium of papionin species, within the Tribe Papionini, has not diverged solely at random from a common ancestor. Even the two very closely related *Papio* species (that even interbreed between them; Jolly *et al.* 1997) failed to meet the assumptions of the random genetic drift model, and appear to be sufficiently different in terms of cranial form (as described by this landmark set) to each have specific adaptations. Since one important function of the cranial anatomy is feeding and intra-oral food processing, hypotheses can be constructed with regard to the role diet might have had in the adaptive evolution of papionin cranial form and finite element models can be used to test those assumptions.

The following chapters are concerned with the process of building finite element models for finite element analysis (FEA), with sensitivity analyses to test the effect of several model-building issues on the results of the FEA analyses, and with testing biomechanical hypothesis of papionin cranial adaptation to different diets. The very last analytical chapter of this thesis attempts to directly relate the biomechanical parameters as resulting from FEA with diet and cranial form in papionins.

Chapter 5. Building Three-dimensional Models of Papionin Crania for Finite Element Analysis

5.1. Introduction

It was shown in the previous chapter that random genetic drift was most likely not the single microevolutionary process acting on the form of the papionin cranium. Non-random processes must therefore have been acting on the cranium, driving its evolution as a response to environmental pressures, such as geography, climate, competition, predators, or diet. To test hypotheses of how diet could have played a role in the evolution of the papionin cranium, virtual biomechanical models are believed to be a good tool to use (Chalk *et al.* 2011). The extent to which such modelling is informative with regard to diet will also be a focus of this and subsequent chapters.

The cranium is a highly complex structure that encloses and protects the brain and the sensory organs of vision, hearing, smell and taste. It also supports the structures that allow food intake and processing (De Iuliis & Pulerà 2011). Because of its complexity, it is difficult to measure, visualize, and describe (Hildebrand & Goslow 2001) and is best visualized in three dimensions (3D). Historically, an intuitive way to create 3D pictures is to use stereopairs of images, which are images of the same specimen taken from slightly different angles and printed side-by-side; the user then stares at a point in between and allows the eyes to focus beyond the page (Hildebrand & Goslow 2001). However, a technique to create 3D images of objects extensively used today is *modelling* (not to be confused with bone modelling, Subsection 1.2.4).

Modelling consists of building a 3D model from a series of slices of the object, usually in a virtual environment (Hildebrand & Goslow 2001). Models are built to simulate real situations: models are expected “to increase knowledge and insight about reality, and to estimate or predict variables of interest” (Nigg & Herzog 2006). Models are considered the best solution particularly when studying biomechanical parameters of the cranium of papionins: valuable (and often unique) museum specimens that cannot be replaced, such as those so often used in such studies, are best tampered with inside the computational space, rather than in a real biomechanics laboratory. The damage to,

or destruction of specimens would also render the reproducibility of experiments impossible. With the advent of X-ray computerized tomography (CT) and increments of computer power, visualization of the cranium in 3D is not only possible, but desirable, since it allows for simulation analyses that would be destructive if done on the actual specimen (Hildebrand & Goslow 2001).

Building 3D models for finite element analysis (FEA), virtual as they may be, is not a trivial problem and has to be handled cautiously, especially due to their eventual interpretation in the light of biological reality. When aiming to interpret results as reflecting biology, attention should always be paid to the model building step, because simple geometric abstractions of real biological structures limit the potential of the model to be interpreted and may not be a valid representation of the behaviour of the real structure (Richmond *et al.* 2005). As George E. P. Box famously said, “all models are wrong, but some are useful” (Box & Draper 1987, p. 424). Biological structures like bone can react biologically (*e.g.* bone resorption or bone formation; see Subsection 1.2.4) or mechanically (*e.g.* deformation), or both, to external forces (Nigg & Herzog 2006).

In building 3D models of bone structures, the material properties of the various types of bone must be taken into account. Yet, several papers (Gong, Arnold, & Cohn 1964; Turner *et al.* 1999; Bumrerraj & Katz 2001) indicate that, for the cranium, cortical bone and trabecular bone have, in fact, the same material properties (or rather, the Young’s modulus of trabecular bone falls within the range of that of cortical bone), and thus need not be considered separately.

Likewise, the boundary conditions of the model (see Subsection 2.4.2) must be set. In the case of models of the cranium, the muscles and muscle forces acting on the living organisms have to be modelled accordingly, as well as the constraints the cranium has to endure. According to Antón (1996, 1999), the architecture of a muscle and the bone morphology supporting it are well correlated. The masticatory musculature of a young *Macaca mulatta* (Schwartz & Huelke 1963), and that of an adult *Papio* sp. (Swindler & Wood 1973) are the only such anatomy described for papionins in the literature. These two descriptions were used in this thesis as a conservative model to extrapolate the masticatory muscle anatomy of the other papionin species. This was considered reasonable due to lack of actual specimens to dissect, and due to the phylogenetic similarity among the species used. Indeed, Swindler and Wood (1973), who describe the anatomy of genera so phylogenetically distant (even if within the order

Primates) as *Pan*, *Papio* and *Homo*, found that the masticatory musculature of these species to be roughly the same (the same set of muscles), with minor differences.

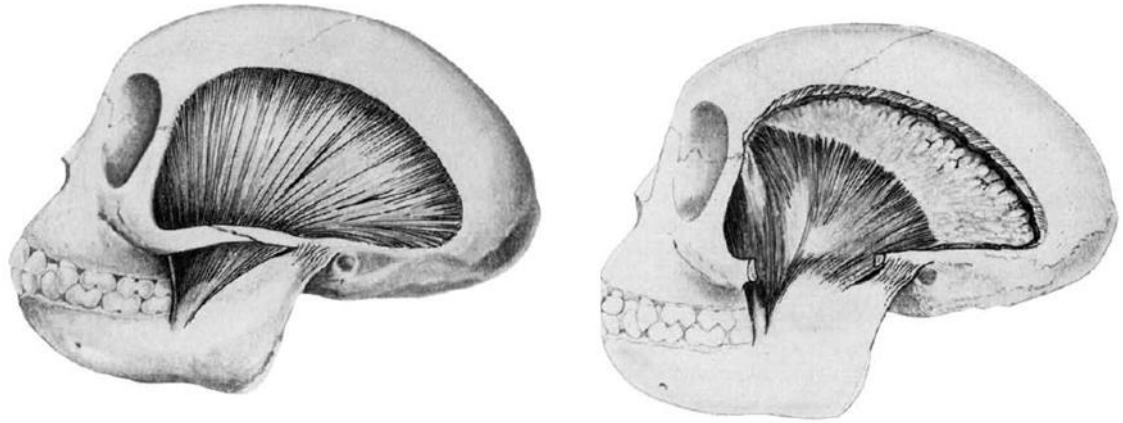


Figure 5.1. Origin and insertion of the temporal muscle in a specimen of *Macaca mulatta*. Adapted from Schwartz & Huelke 1963.

Regarding the anatomy of the temporal muscle (Figure 5.1 in a young *Macaca* specimen), Swindler and Wood (1973) found that in *Papio* adult males it reaches the midline, attaching to a sagittal crest particularly along the posterior surface of the parietal bone. This muscle seems to be divisible into superficial and deep portions both in *Papio* (Swindler & Wood 1973) and in *Macaca* (Schwartz & Huelke 1963). As for the anatomy of the masseter muscle of these primates, it is not different from that described in general terms in Chapter 1 (Subsection 1.3.6) and can be seen in Figure 5.2 in a *Macaca* specimen. The *Macaca* medial pterygoid muscle (Figure 5.3) is a paired quadrilateral muscle situated between the medial surface of the mandibular ramus and the lateral pharyngeal wall; it originates from the pterygoid fossa, between the medial and lateral pterygoid plates, filling its entire depth (Schwartz & Huelke 1963). Some fibres arise from the inferior portion of the lateral surface of the lateral pterygoid plate, and the immediately adjacent area of the palatine and maxillary bones (this is hardly surprising since in other mammals, for instance, canids, this muscle originates on the lateral surface of the pterygoid plate, rather than on its medial surface; Ström *et al.* 1988; Evans & de Lahunta 2010). Fibres insert on to the medial surface of the gonial angle of the mandible beneath the mandibular foramen and onto the base of the mandible at the angle (Schwartz & Huelke 1963). The lateral pterygoid muscle is the smallest of the group, and, in being principally a jaw opening muscle, it only stabilizes

the mandible (Osborn 1995; Shi *et al.* 2012). It had little effect on a previously built masticatory model of a *Macaca fascicularis* in the laboratory (L. Fitton pers. comm.), and so was not included in the models built in the present thesis.

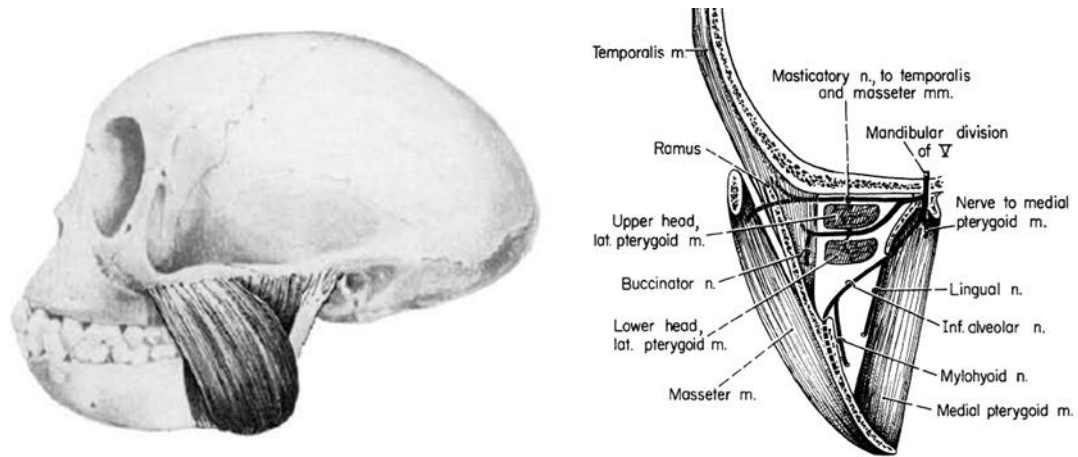


Figure 5.2. Left panel: Origin and insertion of the masseter muscle in a specimen of *Macaca mulatta*; right panel: Coronal section at the ramus of the mandible illustrating the relative positions of temporal, masseter and medial pterygoid muscles. Adapted from Schwartz & Huelke 1963.

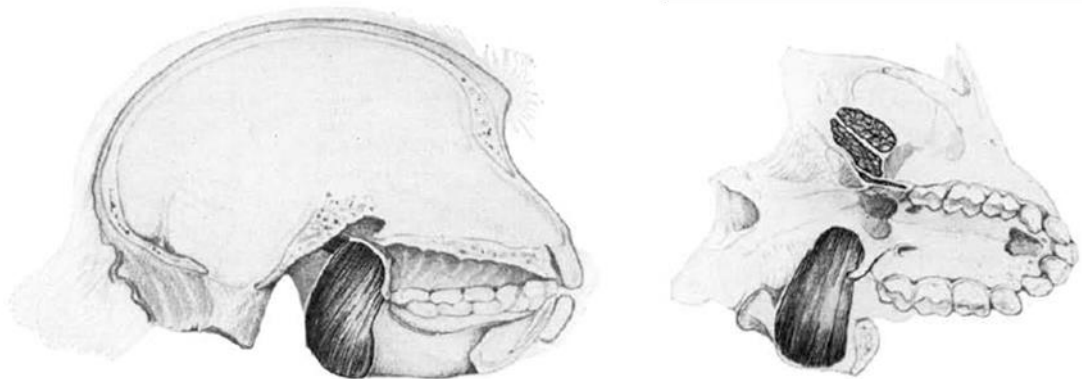


Figure 5.3. Origin and insertion of the medial pterygoid muscle in a specimen of *Macaca mulatta*. Adapted from Schwartz & Huelke 1963.

The main objective of this chapter is to describe the building of virtual 3D models of papionin crania for FEA (pre-processing step; see Subsections 2.4.1 and 2.4.2), starting with a review of image segmentation techniques, moving on to the necessary boundary conditions. A second objective of this chapter is to describe the

model solution step of FEA (see Subsection 2.4.3) where maximum bite force is computed and landmark displacement happens. Both these types of data are an integral part of subsequent FEA (post-processing step; see Subsection 2.4.4) and analysis of deformations, including its visualization.

5.2. Building 3D Models of Papionin Crania

This section describes the material (sample specimens) and methods (image segmentation and boundary conditions) used to build the models used for FEA in this and subsequent chapters of this thesis. Example figures from one of the models (a model of a male *Theropithecus gelada*) are provided. All models are built using the same protocol described here, making model building error consistent among them. Errors and sensitivity analyses of the effects that model building decisions have on FEA results are discussed in Chapter 6.

5.2.1. Sample Specimens

The data used to build the models were CT scans of 9 different papionin individuals, 7 adult males and 2 adult females. Dry crania of representatives of each species (*Cercocebus torquatus*, *Lophocebus albigena*, *Macaca fascicularis*, *Mandrillus sphinx*, *Papio anubis*, *Papio hamadryas* and *Theropithecus gelada*) were obtained for CT scanning from various museums (Table 5.1). Dry crania coming from animals shot in the wild were given preference, but this was not always possible. All genera of the Tribe Papionini are represented with the exception of the recently attributed genus *Rungwecebus* (Jones *et al.* 2005; Davenport *et al.* 2006), which was left out due to its as yet *incertae sedis* status in papionin taxonomy and phylogeny (see Subsection 1.3.1) and lack of available crania. Species were chosen to represent varying diets among the group (including the extreme specialist genus *Theropithecus*).

Table 5.1. Dry crania specimens used to build models.

Species	Age Sex	Specimen	Repository	Provenance
<i>Cercocebus torquatus</i>	adult male	C13.21	University of Liverpool	Unknown
<i>Lophocebus albigena</i>	adult male	RCS A 81.441	RCS Hunterian Museum	Batouri District, French Camerouns
<i>Macaca fascicularis</i>	adult male	Mac 17	The Hull York Medical School	Unknown
<i>Mandrillus sphinx</i>	adult male	0173.dc3	University of Liverpool	Unknown
<i>Papio anubis</i>	adult female	RCS A 92.28	RCS Hunterian Museum	Mount Meru East, Tanganika Territories
<i>Papio anubis</i>	adult male	RCS A 92.25	RCS Hunterian Museum	Mount Meru East, Tanganika Territories
<i>Papio hamadryas</i>	adult male	LEEDM.C. 1982.320.4144	Leeds Museum Discovery Centre	Unknown
<i>Theropithecus gelada</i>	adult female	0177.dc3	University of Liverpool	Unknown
<i>Theropithecus gelada</i>	adult male	PRICT 446, ID 9030	Digital Morphology Museum KUPRI	Unknown

5.2.2. Image Segmentation

One of the first steps of building a model from a CT image stack is *image segmentation* (see also Subsection 2.4.1). The process of segmentation consists simply of extracting the material of interest (in this case bone) out of the void (or other surrounding background and tissues) where it is embedded in a CT image (Hsieh 2009). However, distinguishing between the material of interest and the background is not trivial: although finding the exact threshold between the two can be done using objective methods, some subjective decisions have to be taken, commonly making the final segmented model effectively a combination of threshold and manual segmentation. Ideally, the model should be as anatomically accurate as possible, representing a

minimal amount of simplification (Nigg & Herzog 2006). In CT imaging, the threshold between two tissues is most reliably estimated as being located exactly half way between two CT number levels. This level is known as half maximum height (HMH, Spoor & Zonneveld 1995) and equals the mean of the two CT number levels at either side of the threshold. HMH is calculated by setting the window width of the segmentation editor at the CT scanner maximum, usually 4095HU (Hounsfield units, unit of grey-scale values on the Hounsfield scale of radiodensity, where radiodensity of air is -1000HU and that of distilled water is 0HU; radiodensity of bone will be several thousands; Hsieh 2009), meaning a window width ranging from -1024HU to 3071HU (Spoor & Zonneveld 1995). All the CT scans here were segmented using this exact grey-scale window range, but HMH was decided against, since preliminary investigations (not shown) resulted in ambiguous and highly variable segmentation, not only between different regions of the cranium (as Fajardo *et al.* 2002 pointed out), but also within the same region. An iterative approach to thresholding is also possible, but is most effective in high-resolution CT scans (Ryan & van Rietbergen 2005) unlike the ones available for this study (Table 5.2). Thus the images here were segmented using an initial automated threshold using the built-in function in the segmentation software Avizo and finished with extensive manual segmentation.

Table 5.2. Computerized tomography (CT) image resolution.

Species	Specimen	Resolution		
		x	y	z
<i>C. torquatus</i>	C13.21	0.151	0.151	0.151
<i>L. albigena</i>	RCS A 81.441	0.309	0.309	0.700
<i>M. fascicularis</i>	Mac 17	0.099	0.099	0.099
<i>M. sphinx</i>	0173.dc3	0.143	0.143	0.143
<i>P. anubis</i> (f)	RCS A 92.28	0.320	0.320	0.700
<i>P. anubis</i> (m)	RCS A 92.25	0.400	0.400	0.699
<i>P. hamadryas</i>	LEEDM.C.1982.320.4144	0.436	0.436	0.699
<i>T. gelada</i> (f)	0177.dc3	0.488	0.488	0.625
<i>T. gelada</i> (m)	PRICT 446, ID 9030	0.300	0.300	0.300

Resolution in millimeters (mm).

The stack of all slices of a CT scan can be regarded as a data volume, which can be used to create a 3D volume model of the scanned object. Each element of the model (voxel) will have dimensions $l_p^2 \times l_t$, where l_p^2 are the dimensions of the square pixel, and l_t is the slice thickness (Hsieh 2009). For a comparative study with different models, all models should be downsampled to the same voxel size to eliminate false differences in size among models due to the number of voxels constituting each model; this is not a scaling of the models, but rather ensures that a proportionately different amount of voxels is used to build differently sized specimens. For consistency, all the models here were downsampled from their varying original resolutions (Table 5.2) to a common voxel size of $0.428 \times 0.428 \times 0.428$ mm. Differences in CT scanner resolution create difficulties in segmenting accurately the trabecular bone and the comparative nature of this study raised issues about the accurate modelling of the internal architecture of the trabecular bone. As such the question arises as to whether or not trabecular bone need be represented at all as being different from cortical bone within the models. However, the effects of differences in segmentation of trabeculae relative to the error introduced by modelling bone as a solid material with no trabecular spaces is yet unknown. Thus, a sensitivity analysis to assess the relative impacts of these different approaches in terms of local strains and global deformations is described in Chapter 6.

All image processing was carried out using Avizo, an image processing software (Visualisation Sciences Group, USA). Once the image processing was finished, a model was generated using non-commercial, custom built software *vox2vec.exe* to produce a finite element mesh consisting of eight-noded cubic elements. It is these meshes that were imported into the software VOX-FE, an FEA pre- and post-processing voxel-based software tool that uses direct voxel conversion (Fagan *et al.* 2007; Liu *et al.* 2012).

5.2.3. Boundary Conditions

Almost all papionins species are endangered, and the difficulty and the enormity of the task of obtaining wild papionin cadavers prevented the determination of muscle attachments and orientation from dissected material as would have been desirable. Thus, muscle information was retrieved from the literature (Schwartz & Huelke 1963; Swindler & Wood 1973; Antón 1999, 2000; Diogo & Abdala 2010). *In vivo*, the estimation of muscle force is normally achieved by calculating the physiological cross-

sectional area (PCSA, Alexander & Vernon 1975; see also Subsection 2.4.2) of the muscle, the area of a plane perpendicular to the line of action of the muscle (line between the origin and the insertion of the muscle) at the mid-point (midway on that line). In the case where no real muscle information is available, the anatomical cross-sectional area (ACSA) is often used instead (Demes & Creel 1988; Antón 1999; Christiansen & Adolfssen 2005; Ellis *et al.* 2008). ACSA is based on bony proxies, assuming that muscles are intimately related to the bones where they originate and insert (Antón 1996, 1999), and that it is possible to estimate the muscle area even when only bone information is available. Understandably, it is a widely used protocol in fossil studies (Demes & Creel 1988; O’Higgins *et al.* 2011). Maximum muscle force is then calculated using the formula: $F_{\max} = ACSA \times k$, where k is the specific tension constant (37 N/cm^2 , Weijs & Hillen 1985).

For the studies in this thesis, muscle attachments, PCSA and orientations (ascertained via dissection) and also muscle activation (loading predicted via multibody dynamic analysis, MDA) are available for the *Macaca fascicularis* model (Kupczik *et al.* 2007; Liu *et al.* 2012; Fitton *et al.* 2012) but for none of the others. Since the impact of varying muscle loadings in the biomechanical response of a finite element model cranium was shown to be much less than that of varying bite location (for controlled bite force magnitude; Fitton *et al.* 2012), a decision to use ACSA in all models was taken, including *Macaca* for consistency when comparing among models.

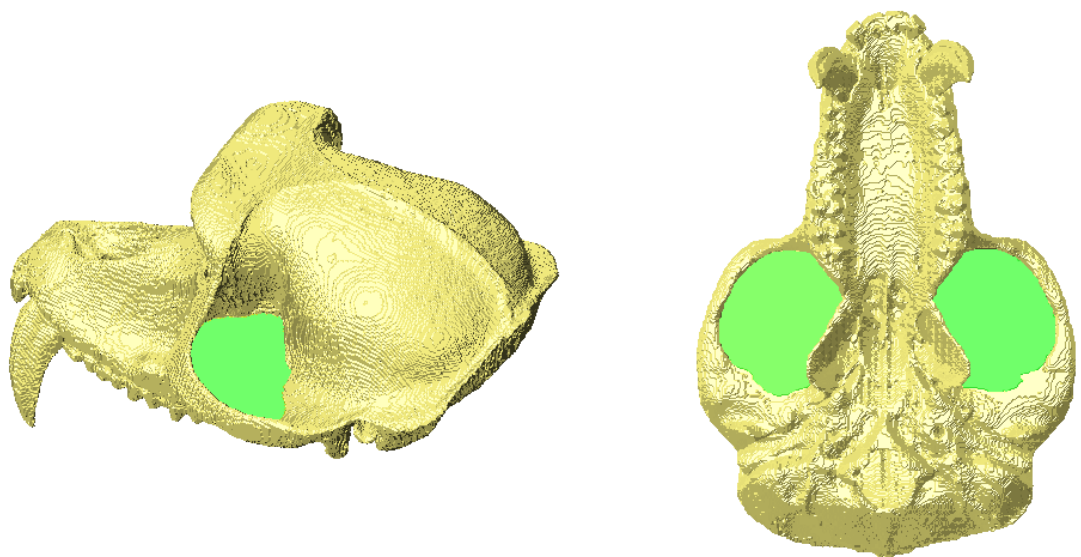


Figure 5.4. Anatomical cross sectional area (ACSA) of the temporal muscle in a male Theropithecus gelada. Area shown in green. Areas on both sides are calculated and then averaged.

Figure 5.4 shows the ACSA of the temporal muscle in an example model. Having the occlusal plane as reference, the ACSA of the temporal muscle is calculated by first measuring the number of voxels of the temporal fossa through the zygomatic arch; since the area is in pixels and the standard pixel area is $0.25 \text{ mm} \times 0.25 \text{ mm} = 0.0625 \text{ mm}^2$, the area in cm^2 is calculated by multiplying the number of voxels (volume) by the standard pixel area. That area is then divided between anterior and posterior muscle according to the number of nodes selected for each muscle (based mostly on Schwartz & Huelke 1963 and Swindler & Wood 1973) on the FEA model. The division of the temporal muscle into anterior and posterior was devised because the division in superficial and deep proved difficult to model in VOX-FE. The anterior/posterior division, on either side, is not clear even in wet samples and was initially done by inferring the direction in which the muscle fibres would pull, infero-superiorly by the anterior, or inferoanterior-superoposterior by the posterior. Yet, the separation between anterior and posterior fibres is approximate and was finally inferred from comparison with accounts of the musculature of *Macaca*, available in the literature (Schwartz & Huelke 1963; Swindler & Wood 1973) and from dissections in our research group.

The ACSA of the masseter muscle is here calculated by taking the length of the muscle scar on the zygomatic arch to approximate the length of the muscle, and the Euclidean distance from a midpoint on the mandibular ramus to the zygomatic arch, perpendicular to the ramus, on the occlusal plane, to approximate its width. Since the masseter is mostly a rectangular muscle (Rogers 1992), this gives an estimate of the real area. Figure 5.5 shows the estimation of the ACSA of the masseter muscle in an example model. As for the ACSA of the medial pterygoid muscle, it is estimated by defining a region on the internal aspect of the gonial angle of the mandible delimited by the muscle scar (Antón 2000). Even though this is not the ideal location to measure ACSA, measuring closer to the midpoint of the muscle proved impossible with the available data. Figure 5.6 shows the estimation of the ACSA of the medial pterygoid muscle. The lateral pterygoid is excluded from the models; the division of the masseter muscle into superficial and deep masseter (see Subsection 1.3.6) is also not included. These decisions are here taken on the basis of the difficulty of estimating the relative anatomical position (and consequently the ACSA) of these muscles in a virtual model and, in the case of the lateral pterygoid, to the realisation that this muscle contributes more to the stability of the mandible than to the production of bite force during mastication (Osborn 1995; Shi *et al.* 2012). Estimated ACSA values and calculated muscle force for each muscle are presented in Tables 5.3 and 5.4.

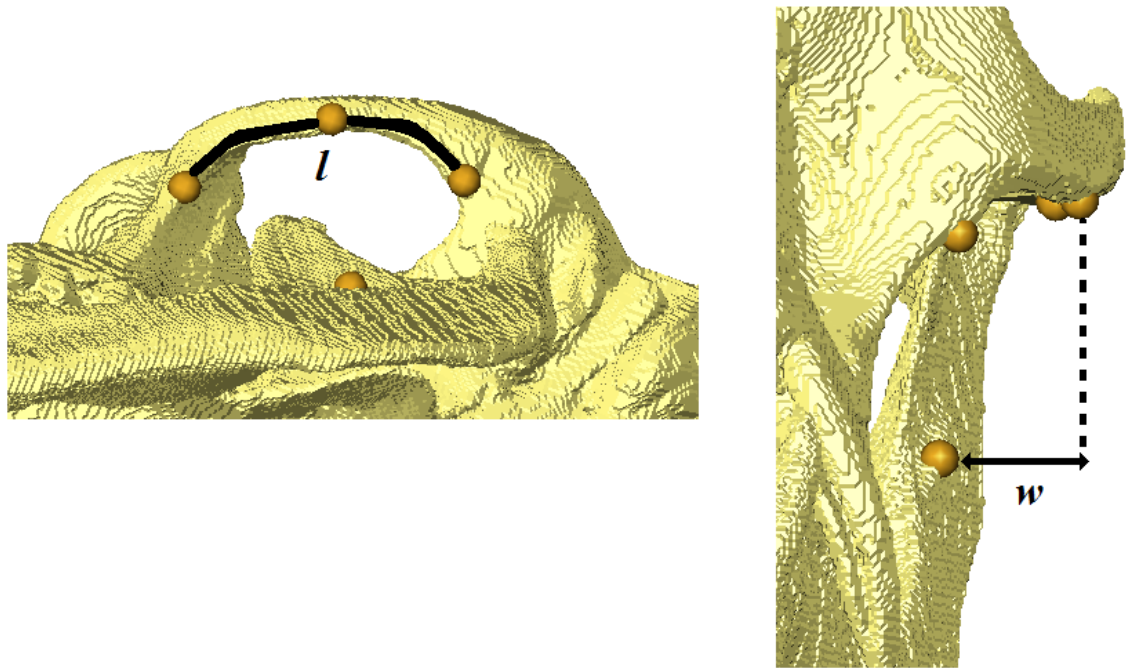


Figure 5.5. Estimation of the anatomical cross sectional area (ACSA) of the masseter muscle in a male *Theropithecus gelada*. The area is calculated by considering the rectangle as the simplest geometric shape capturing most of the masseter area. The length of the muscle scar on the zygomatic arch (l) and the distance from mid-ramus to the furthest zygomatic point (w) are used as area parameters. Areas on both sides are calculated and then averaged. Landmarks are shown as guidelines only.

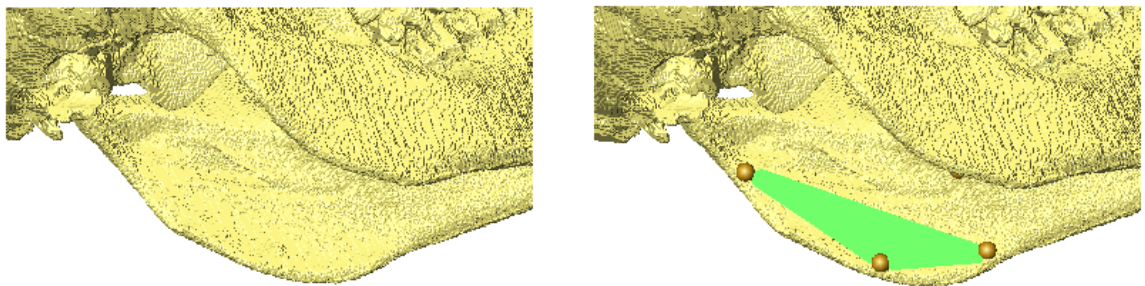


Figure 5.6. Estimation of the anatomical cross sectional area (ACSA) of the medial pterygoid muscle in a male *Theropithecus gelada*. Area shown in green. The furthest extent of the muscle scar on the inside of the mandible was delimited with landmarks. The triangle was deemed the simplest geometric shape capturing most of the bony scar area. Areas on both sides are calculated and then averaged.

Table 5.3. Estimated muscle anatomical cross-sectional area (ACSA) and muscle forces.

Species	Temporal		Masseter		Medial Pterygoid	
	ACSA	Force	ACSA	Force	ACSA	Force
<i>C. torquatus</i>	8.49	314.29	5.39	199.40	2.46	90.85
<i>L. albigena</i>	7.97	295.03	3.66	132.76	1.84	67.99
<i>M. fascicularis</i>	5.93	219.45	5.31	196.59	1.35	50.07
<i>M. sphinx</i>	11.93	441.58	11.62	430.10	3.44	127.24
<i>P. anubis</i> (f)	7.71	285.28	4.75	175.73	2.16	79.80
<i>P. anubis</i> (m)	12.10	447.73	9.99	369.99	3.09	114.48
<i>P. hamadryas</i>	15.37	568.66	11.21	414.92	2.25	83.24
<i>T. gelada</i> (f)	5.75	212.64	5.72	211.78	2.19	81.05
<i>T. gelada</i> (m)	12.32	455.77	8.44	312.29	3.04	112.41

ACSA in squared centimetres (cm²); force in Newtons (N).

Table 5.4. Estimated anterior and posterior temporal parameters, modelled as percentage contributions of anterior and posterior temporal muscle.

Species	Anterior Temporal			Posterior Temporal		
	% Tem.	ACSA	Force	% Tem.	ACSA	Force
<i>C. torquatus</i>	36.53	3.10	114.80	63.47	5.39	199.49
<i>L. albigena</i>	27.95	2.23	82.61	72.05	5.74	212.43
<i>M. fascicularis</i>	33.38	1.98	73.27	66.62	3.95	146.18
<i>M. sphinx</i>	27.69	3.43	126.87	72.31	8.51	314.71
<i>P. anubis</i> (f)	24.76	1.91	70.64	75.24	5.80	214.65
<i>P. anubis</i> (m)	24.01	2.91	107.50	75.99	9.20	340.24
<i>P. hamadryas</i>	21.12	3.25	120.28	78.88	12.12	448.53
<i>T. gelada</i> (f)	31.20	1.79	66.34	68.80	3.95	146.31
<i>T. gelada</i> (m)	29.31	3.29	121.65	70.69	9.03	334.13

ACSA in squared centimetres (cm²); force in newtons (N).

All finite element models were constrained at the working (left) side tooth in the infero-superior (vertical) direction and at the glenoid fossae for anchoring (the average number of nodes constrained was 120; but see Chapter 6 for a sensitivity analysis on the jaw joint constraint). Bites on all teeth except the canine were simulated. The canine

was chosen not to enter the analyses because it is highly sexually dimorphic, which makes equivalent loading between sexes difficult, and also because it seems to play little role in feeding in this particular group of animals (Fleagle 1999). The vertical constraint placed in each left side tooth (cusps only) simulated the bite, whose force is the reaction force to this constraint (see further below Subsection 5.3.1 for more details). The load applied in each loading regimen was the sum of the maximum muscle force magnitudes estimated by ACSA, averaged from each side. They were designed to reflect the maximum bite force the specimens under study could produce. The orientation of the muscles was estimated by landmarking the further most insertion point of each masticatory muscle on the mandible in closed position, and later using that single landmark as a guideline to direct the force of the respective muscle in VOX-FE. Figure 5.7 shows a fully built FEA model before solution.

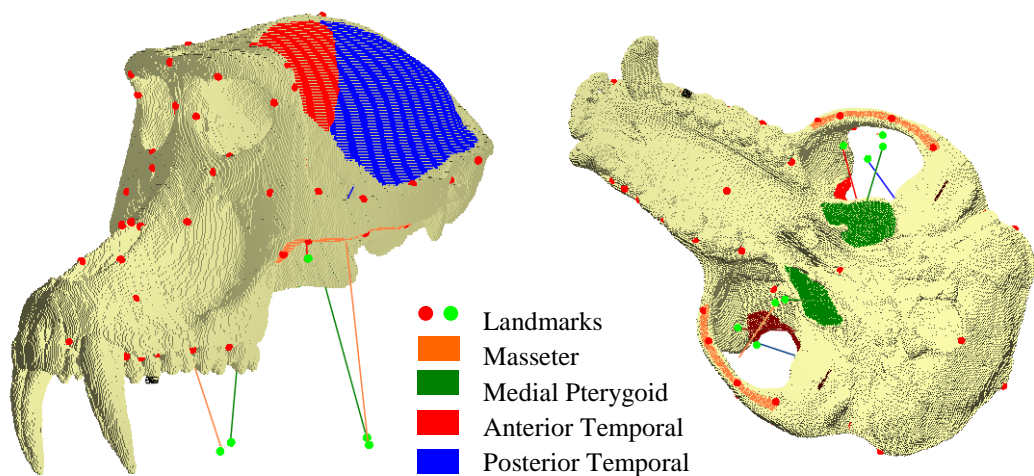


Figure 5.7. Example of a fully built FEA model before solution (male Theropithecus gelada), with a P4 bite, and shown at three quarters and inferior view. Blue, posterior temporal muscle; red, anterior temporal muscle; orange, masseter muscle; and green, medial pterygoid muscle. The vectors of force are shown in the same colour as the muscles whose force they represent. The green landmarks represent muscle insertion points on the mandible and were used as guidelines for muscle force vectors. The red landmarks are chosen to assess global deformations after FEA. Notice the black box representing the nodes constrained at the left P4, simulating a bite on that tooth. Anchoring constraints placed at the glenoid fossae are shown in brown. All other specimens and simulated bites were built the same way.

The Young's modulus of bone in the primate cranium varies among anatomical locations, ranging from 12.5 GPa in the posterior part of the zygomatic arch to 20.8 GPa in the anterior zygomatic region (Strait *et al.* 2005 studying a *Macaca fascicularis* model). The average of Young's modulus values from all cranial regions is 17.3 GPa (Strait *et al.* 2005; see also Ethier & Simmons 2007 and Kupczik *et al.* 2007), which is the value used in all studies in this thesis. All materials were modelled as linear elastic and isotropic with a Poisson's ratio of 0.28, again an average of values from all cranial regions (Strait *et al.* 2005). Due to the large number of elements, the solution of each model was performed using a Dell™ high-performance cluster (HPC) with 45 cores (Dell Inc., Round Rock, Texas, USA) available in the Hull York Medical School, York. The solver software (Liu *et al.* 2012) is a Linux-based, non-commercial, and custom built *PARA_BMU*, which is a modified iterative solver, similar to that reported by van Rietbergen *et al.* (1996).

The next section describes how bite force and landmark displacement data are calculated after FEA solution. Resulting bite force values and the visualization of landmark-based deformation of the 9 built models are discussed. An example of the strains and deformations is shown, but these are given greater centrality in Chapters 6 and 7 in relation to specific tests of hypotheses.

5.3. Model solution: bite force and landmarks

Apart from allowing for the visualization of strain distributions and strain magnitudes, results output from an FEA include calculated maximum bite force and landmark data (when selected landmarks are included in the analysis). This section describes how maximum bite force was calculated and how landmark displacement data was used after FEA solution to study deformations on the 9 models of papionin crania. Maximum bite force results are presented in Table 5.5 (*a, b*), and deformations (Figure 5.8) are visualized as a comparative principal components plot of deformations with surface warpings and transformation grids (Figure 5.9). These data are of great importance in the landmark-based analysis of deformations (see Section 2.5) used in subsequent chapters.

Table 5.5a. Bite forces and jaw joint reaction forces, as computed from FEA.

Bite	Forces	<i>C. torquatus</i>	<i>L. albigena</i>	<i>M. fascicularis</i>	<i>M. sphinx</i>	<i>P. hamadryas</i>
I1	bite force	237.18	178.40	197.64	316.00	278.34
	reaction force	776.50	658.84	550.10	1414.75	1070.98
I2	bite force	249.44	185.45	209.24	322.71	285.95
	reaction force	764.60	652.27	538.56	1408.26	1063.51
P3	bite force	329.94	258.16	283.80	473.67	384.60
	reaction force	686.28	584.29	464.49	1262.00	966.56
P4	bite force	357.72	283.99	309.55	518.52	415.77
	reaction force	659.41	560.46	438.95	1218.69	935.98
M1	bite force	400.25	316.26	342.01	580.73	466.27
	reaction force	618.46	531.01	406.78	1159.26	886.23
M2	bite force	467.81	373.91	419.53	674.32	543.48
	reaction force	553.86	479.09	330.30	1069.64	811.11
M3	bite force	566.78	458.03	522.36	764.48	650.46
	reaction force	460.72	406.31	229.64	877.13	707.10

Forces in Newtons (N).

Table 5.5b. Bite forces and jaw joint reaction forces (continued).

Bite	Forces	<i>P. anubis</i> (m)	<i>T. gelada</i> (m)	<i>P. anubis</i> (f)	<i>T. gelada</i> (f)
I1	bite force	292.69	366.62	186.77	216.02
	reaction force	1260.72	1193.85	696.84	635.31
I2	bite force	299.89	372.83	192.77	223.14
	reaction force	1253.89	1187.91	691.25	628.17
P3	bite force	387.70	478.17	236.77	262.46
	reaction force	1170.45	1088.21	650.49	589.06
P4	bite force	422.23	508.83	257.84	281.35
	reaction force	1137.78	1059.35	631.13	570.27
M1	bite force	467.48	570.46	293.19	317.61
	reaction force	1095.19	1001.75	598.88	534.22
M2	bite force	542.33	681.20	350.41	378.97
	reaction force	1025.21	899.62	547.44	473.12
M3	bite force	648.80	846.49	434.37	481.58
	reaction force	735.94	751.64	474.64	371.56

Forces in Newtons (N).

5.3.1. Maximum Bite Force

Maximum bite force is calculated in VOX-FE simply by summing the reaction forces at each node constrained in the vertical direction at the tooth (the bite location), after a muscle load case. A different bite force is thus calculated per tooth, and each load case also results in reaction forces at the glenoid fossae (Table 5.5*a, b*). Maximum bite forces from each FEA are used in the analysis of deformations (described below in Subsection 5.3.2) and later, in Chapter 8, to assess the relationship with diet.

In general, larger sized specimens have a higher absolute maximum bite force, due to absolutely larger muscles (measured by ACSA; Tables 5.3 and 5.4) producing absolute higher muscle forces. The male *T. gelada* and *M. sphinx* have the highest maximum bite force values, while the smaller *L. albigena* and the female *P. anubis* have comparatively smaller bite forces. In every specimen the highest maximum bite force among all teeth is achieved by the third molar (M3), with maximum bite force decreasing disto-mesially along the dental row from M3 to I1. This is a straightforward consequence of lever-arm mechanics and so is related to the length of the rostrum. The jaw joint reaction forces at the glenoid fossae show, as expected, the inverse of the bite force: a decrease from I1 to M3. Absolute maximum bite force is used in later chapters to scale the deformations of each model to the same bite force at each tooth (100N; see also Section 7.2) as a preliminary to PCA (Figure 5.9; Chapters 6 and 7). It is also used as a biomechanical parameter in itself in relation to investigation of the mechanical correlates of diet (Chapter 8).

5.3.2. Landmarks and Visualizing Deformations

To compare global deformations predicted by FEA among a sample, a common set of 70 anatomically equivalent 3D landmarks (Table 5.6) is placed on each cranium (Figures 5.7 and 5.8). Landmarks were chosen based on the cranial shape literature and on previous models of the papionin crania. The landmark configuration was designed to capture the shape of the cranium including a good description of the face. The Cartesian coordinates of each landmark change as the cranium deforms in FEA. This causes the landmark configuration to change in size and shape, creating a new landmark configuration which can be compared to the original, undeformed landmark

configuration. When resulting landmark configurations of several models are analysed, differences in deformations reflect differences in mechanical performance. The analysis of deformations is fully described in Section 2.5.

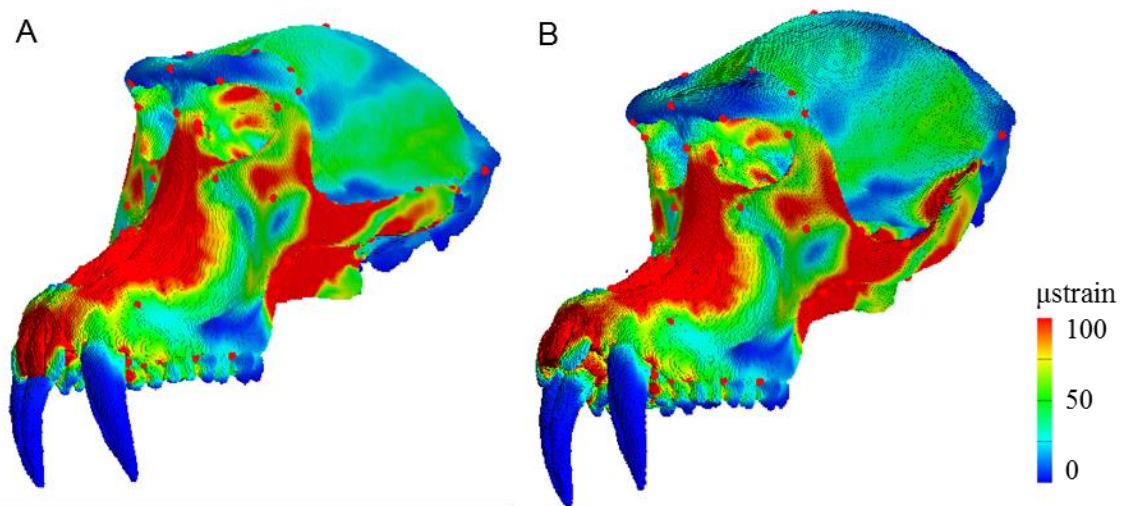


Figure 5.8. Results of a finite element analysis. A, von Mises' strain contour plot resulting from a simulated bite on the first incisor (I1), in a model of a male Theropithecus gelada; the strain magnitudes have been scaled to 100N bite force. B, global deformations (displacements $\times 50$) of the model after the I1 bite, where the form of the landmark configuration can be seen to change as the cranium deforms.

Figure 5.8 depicts an example of the results expected from FEA, including a strain contour plot and a visualization of deformations after loading on an example model, with landmarks to be used in assessing that global deformation quantitatively. In Figure 5.9 a principal components plot is presented that shows size and shape changes (here read as global deformations) among the 9 finite element models, with transformation grids for visualization of change. Transformation grids are simply a visual aid to assessing shape differences and do not represent actual physical movement (see Subsection 2.3.4). With the landmark set chosen, the first principal component axis (PC1) describes mostly antero-posterior bending, while the second axis (PC2) is mostly describing deformation of the zygomatic arches, due to the pull of the masseter muscle; the third (PC3) and fourth (PC4) axes describe torsion of the face (not shown). These four principal components account for 90% of the total variance in the sample.

Table 5.6. Landmarks for deformations analyses used in subsequent chapters.

Number	Description
1	Central point between incisors at alveolar margin
2	Premaxillary suture at inferior margin of nasal aperture
3	Tip of nasal bones in midline
4	Naso-frontal suture in the midline
5	Upper margin of supra-orbital rim in the midline
6	Bregma
7	External occipital protuberance
8	Basilar
9	Midline of transverse palatine suture
10 / 38	Uppermost central point on orbital aperture
11 / 39	Most lateral part of nasal aperture
12 / 40	Inferior border of alveolar margin between I2 and C
13 / 41	Inferior border of alveolar margin between C and P3
14 / 42	Inferior border of alveolar margin between P3 and P4
15 / 43	Inferior border of alveolar margin between P4 and M1
16 / 44	Inferior border of alveolar margin between M1 and M2
17 / 45	Inferior border of alveolar margin between M2 and M3
18 / 46	Inferior border of alveolar margin behind M3
19 / 47	Superior apex of the inferior orbital fissure
20 / 48	Porion
21 / 49	Zygomatico-maxillary suture on the inferior orbital margin
22 / 50	Zygomatico-frontal suture on the lateral orbital margin
23 / 51	Fronto-lacrimal suture on the medial orbital margin
24 / 52	Nearest point to maxillary-premaxillary suture on the nasal aperture
25 / 53	Zygomatico-maxillary suture at root of zygomatic arch
26 / 54	Superior root of zygomatic arch
27 / 55	Inferior root of zygomatic arch
28 / 56	Infra-orbital foramen
29 / 57	Most supero-lateral point on the supra-orbital rim
30 / 58	Most lateral point on zygomatico-frontal suture on the orbital rim
31 / 59	Most anterior point along the temporal line
32 / 60	Zygomatico-temporal suture on the superior border of the zygomatic arch
33 / 61	Superior root of the zygomatic arch between the suture and porion
34 / 62	Most lateral point behind the porion, on the temporal line
35 / 63	Point directly inferior to the zygomatico-temporal suture, on the superior border
36 / 64	Posterior root of zygomatic arch inferior border, anterior to glenoid
37	Posterior border of foramen magnum in the midline
65 / 68	Central nasal region
66 / 69	Central zygoma region
67 / 70	Central maxillary region, above premolars

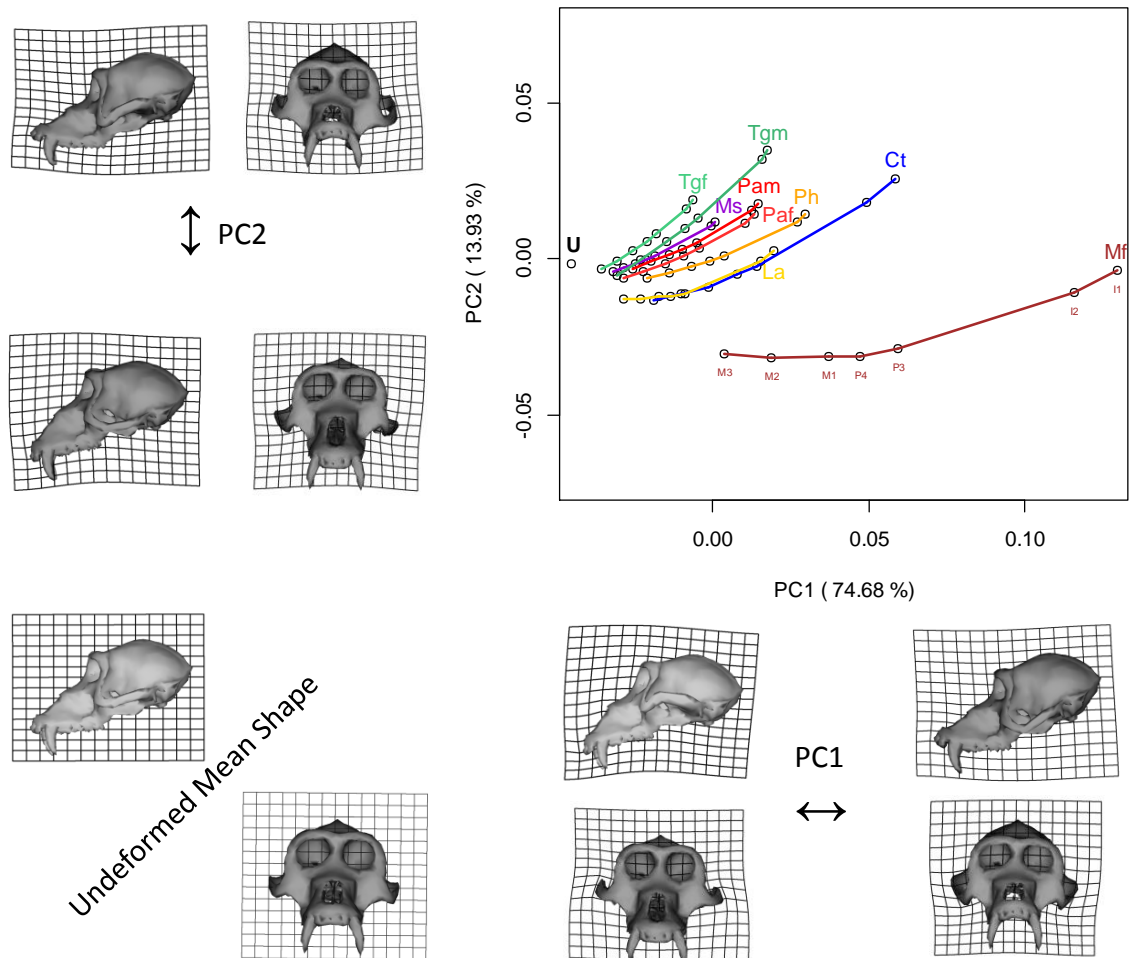


Figure 5.9. PCA showing cranial deformations after bites along the left dental row (I1 to M3) scaled to 100N force, in 9 finite element models, along the first two principal components, PC1 and PC2 (the proportion of total variance explained by PC1 and PC2 is also shown). Ct, blue: *Cercocebus torquatus*. La, yellow: *Lophocebus albigena*. Mf, brown: *Macaca fascicularis*. Ms, violet: *Mandrillus sphinx*. Pam, red: male *Papio anubis*. Paf, light red: female *Papio anubis*. Ph, orange: *Papio hamadryas*. Tgm, green: male *Theropithecus gelada*. Tgf, light green: female *Theropithecus gelada*. The shape changes associated to each principal component are visualized using a mean specimen surface and a transformation grid; here, shape changes correspond to global deformations after load.

The deformations depicted in the Figure 5.9 show the undeformed (original, unloaded) mean of all specimens, and a trajectory of deformed states ranging from the M3 bite (least deformed) to I1 (most deformed) along PC1, for every specimen. The main differences among specimens are found in the “length” of the deformation along PC1 (extent of antero-posterior bending) and PC2 (zygomatic arch deformation) and in their directions through size and shape space. This Figure 5.9 introduces the methodology while specific hypothesis-testing comparisons between two or more specimens will follow in Chapter 7.

5.4. Discussion

This chapter describes the steps taken in the process of building 9 finite element models of papionin crania, as well as the FEA results that will be used in subsequent chapters. It outlines the sample specimens, reviews image segmentation techniques and boundary conditions of the models, and how maximum bite force and landmarks are utilised after the model solution step of FEA. This chapter serves as a preliminary approach to subsequent chapters that use the models, bite force and landmark data for analyses of deformations. These are complementary to strain-based assessments of deformations in that they relate to global (large scale) deformations while strains describe deformations locally at each node (O’Higgins *et al.* 2011, 2012).

It is apparent that building 3D models from CT scans is not a trivial task. Issues immediately arise with respect to the resolution of available scans (Table 5.1): there are differences in scanner specifications and even in the type of scanning (micro CT or medical CT). This produces CT stacks with resolutions that render comparisons between two or more specimens not straightforward. Ideally, a sample of specimens to test particular hypotheses would be scanned at the same resolution and in the same scanner device. This is not always possible due to the rarity of some specimens, museum loan rules (many place constraints on transport and removal of specimens from their premises) and availability of an adequate CT scanner.

Differences in image resolution results in differences in image segmentation, because it becomes difficult to distinguish presence from absence of bone in certain anatomical regions, for example, the trabecular bone of the basicranium or the sphenoid

region. Thus, some compromises are necessary to build models that are comparable from different CT scans. One such compromise might be reached by filling in all the spaces in the trabecular bone of every cranium, regardless of their CT resolution, and attributing to this filling material the properties of cortical bone. A sensitivity test on the behaviour of a finite element model using this approach is attempted in Chapter 6.

Specific issues in building these particular 9 papionin models include the segmentation of teeth. The set of studies in this thesis includes a large scale FEA comparison (the largest ever attempted to date), and considering that models should be built with increasing complexity, teeth and other cranial features were not, at present, modelled with material properties of their own (they were attributed the material properties of cortical bone). This is the first study of a wide range of different species models ever done and there is a large amount of data to compare before complexity must be added.

Another of the major immediate problems that arise when building 3D biomechanical models is the accuracy of the muscle forces estimated. Estimation from bony proxy ACSA provides maximum muscle forces that can be widely different from *in vivo* measured maximum muscle forces (L. Fitton, pers. comm.). Moreover, they raise questions of usefulness of the parameter maximum muscle force as a proxy for the extreme ability of an animal. It is thought that most animals use their muscles to their fullest extent but very rarely during their lifetime. Thus, it would be perhaps more useful to use an estimated average muscle force for single individuals or populations, but no method has yet proved to be effective in making that estimation.

Maximum bite force estimation, following muscle force estimation, diverges in the same way as the latter from *in vivo* measured bite force (Hylander 1986 in *Macaca*), but remains correct within the environment of the respective model, *i.e.*, when comparing bite forces at different teeth in the same animal. Another way of calculating maximum bite force is using lever-arm mechanics, whose results (not shown) are similar to the FEA calculations, but perhaps more prone to user error due to the many manual measurements that need to be taken, while in a computerized method forces are computed to an accuracy of several decimal places.

Studying cranial deformations using landmarks in FEA is a novel methodology made possible by bringing together the resources of geometric morphometrics and FEA. The more common statistical analysis of shape is here extended to include size and shape, which serves as an adjunct to the more established approach to deformations using local strains and coloured contour plots (see also Subsection 2.4.4 and Section

2.5). Proper use of the method and discussion of its results are given in Chapters 6 and 7. Here only an example of the PCA of deformations was shown together with visualisations of cranial shape changes described by principal components (Figure 5.9). Most variation in deformations occurs in anterior-posterior and zygomatic arch bending, both being described by the first two principal components. These differences among the papionin specimens in deformations due to biting are later (Chapter 8) related to cranial form, ecological factors (diet) and other biomechanical variables (maximum bite force) to study their importance in the evolution of papionin cranial form and the extent to which the use of FEA can provide insight into it.

The next chapter presents sensitivity analyses that are essential before moving on to the biological hypothesis-testing analyses found in Chapter 7.

Chapter 6. Testing the Effects of Model Building Decisions on the Results of Finite Element Analysis

6.1. Introduction

The previous chapter described how the three-dimensional (3D) models used in this thesis were built for finite element analysis (FEA). Building any model, 3D or otherwise, is a non-trivial matter and there are many potential model building decisions that should be taken into account when interpreting results. It is desirable to validate a finite element model (see Subsection 2.4.4) by comparing model results with data collected from *in vivo* (strain gauges, *e.g.* Hylander & Bays 1979), *in vitro* (MDA, *e.g.* Curtis *et al.* 2008) and bone strain experiments (Chalk *et al.* 2011), and by incorporating some of these into the model (*e.g.* Fitton *et al.* 2012), but such validation is not always possible. In this study, with the exception of the *Macaca* model, it was not possible to obtain crania that could be subjected to laboratory testing (due mostly to museum loans policies; see also Subsections 2.4.4 and Section 5.1). Furthermore, given the constraints imposed by CT scanning, the original data for each model differ considerably in resolution and grey scale (see Table 5.2), rendering the production of comparable anatomically detailed models difficult. Thus it was necessary to adopt a standard approach to model building that limited anatomical accuracy in all models to the quality obtained in the least good CT scan. This meant that details of cortical thicknesses and internal architecture could not be reproduced with any accuracy. Thus, models were simplified; the internal architecture and variations in cortical thickness were not represented. This inevitably means that the models behave differently than if detailed anatomical representations were in place and are unlikely to yield strains and deformations that match the actual strains and deformations arising from physical loading of the cranium *in vivo*.

Over the last ten years, there have been several studies that have related finite element model performance to the measured performance of physical crania and mandibles (Rayfield *et al.* 2001; Marinescu *et al.* 2005; McHenry *et al.* 2006; Pierce *et al.* 2008, 2009; Dumont *et al.* 2011; O'Higgins *et al.* 2011; Tseng *et al.* 2011; Cox *et al.*

2011, 2012). These have demonstrated repeatedly that models perform reliably, at least in terms of relative strains among anatomical regions when cortical thicknesses are close to actual thicknesses and trabecular bone is modelled as a bulk material with low Young's modulus.

In this thesis, model building is further simplified for the reasons outlined above, and so it becomes important to know how such simplifications impact on model performance. To these ends, sensitivity analyses are performed. As mentioned in Chapter 2 (Subsection 2.4.4), a sensitivity analysis should test the effects of changes in the applied loads, variations of the material properties of differences in the structure and size of the model on the modelling results, among other things (Strait *et al.* 2005; Ross *et al.* 2005; Kupczik *et al.* 2007; Curtis *et al.* 2008). The aim is to understand the consequences of model building decisions in order to allow proper interpretation of results. Many FEA-based studies have focused on the sensitivity of the method to different variables (Sellers & Crompton 2004; Ross *et al.* 2005; Panagiotopoulou *et al.* 2011; Gröning *et al.* 2011; Cox *et al.* 2011; Parr *et al.* 2012; Fitton *et al.* 2012).

Ultimately, it is the researcher who has to decide how sensitive a model has to be to different model building decisions in order for FEA results to be interpretable biologically (Richmond *et al.* 2005). As such, all the FEA studies in this thesis were carried out under the assumption that, whatever errors might be introduced, if they are consistent among all models, then the model performances should be comparable for the type of questions that are of interest here. This is the reason why, as explained in the previous chapter, all of the 9 models were built using the very same protocol. Yet, some sensitivity tests were considered necessary and are described in this chapter.

As noted above, here it was necessary to simplify model building to account for significant differences in raw data (CT images). Among the difficulties caused by these differences are inevitable errors in representing varying cortical thicknesses and internal bone architecture. Beyond this, issues arise with regard to how best to constrain and load models. Thus, in this chapter three major model building decisions are assessed in sensitivity analyses:

- (1) First, constraints imposed by CT scanning differences in the cortical thicknesses and internal architecture from one specimen to another, which cannot be reliably represented (Parr *et al.* 2012). Thus, models of the same specimen could conceivably show significant differences in strains and deformations depending on whether trabecular bone is segmented in great detail or represented as a solid material with spaces filled. While the issue of how to represent trabeculae and other internal

aspects of bone anatomy is important in this context it is of special importance, for example, for fossil analyses because internal architecture is often filled with amorphous matter during the fossilization process, rendering subsequent detailed reconstruction impossible. It is also relevant to note that anatomical exactitude would require imaging and computer processing power beyond what is currently available.

(2) Second, when simulating the forces applied to a cranium in 3D space it is necessary to anchor the cranium to prevent it from moving freely in space as if pushed or pulled, not loaded (Kupczik 2008). Since there is no available bite and joint reaction force data for most papionins, a common approach is to constrain the teeth and jaw joint to fix the cranium, thus mimicking the reaction forces (Strait *et al.* 2005; Ross *et al.* 2005; Kupczik *et al.* 2007). Whereas biting is simulated by a single tooth constraint, here applied vertically to mimic a downwardly directed bite, the most sensible way of constraining the jaw joint is less evident and can be done by anchoring both sides of the jaw joint or only one, leaving the other one free to deform with the whole cranium. It is expected that, in the second case, part of the muscle force exerted should be expended in creating a rotatory movement around the fully constrained fulcrum, and thus preventing the model from deforming properly.

(3) Finally, input muscle force has been considered to have a major effect in biomechanical models (Sellers & Crompton 2004; Ross *et al.* 2005; Tseng *et al.* 2011; Fitton *et al.* 2012). Particularly the force applied by the masseter and temporal muscles appears to have the greatest effect on the tooth (bite) reaction force estimated with FEA (Sellers & Crompton 2004). Papionins in the wild never bite with the same force every time and almost never use the maximum force the muscles can achieve, which means that to accurately estimate strains and deformations it is important to accurately estimate applied masticatory muscle forces at a particular instant during feeding (Ross *et al.* 2005). But this is not possible in most cases, due to the difficulty in measuring muscle forces even in *in vivo* experimental conditions (which, in any case, can never reproduce exactly the natural conditions the animal experiences in the wild). Sensitivity analyses are therefore undertaken here to assess the effect of variant muscle forces on the behaviour of a finite element model. It is expected that, for any muscle, a higher force should result in higher strains and higher deformations, and lower forces in lower strains and deformations.

The objectives of this chapter are, then, to explore the effect of 3D model building decisions on the local strains and global deformations arising from FEA. The hypotheses being tested can be phrased as null hypotheses: (1) a change in the internal

structure of the model does not have a major effect on strains and deformations arising from FEA; (2) a change in jaw joint anchoring constraint does not have a major effect on strains and deformations arising from FEA; and (3) changes in muscle force magnitudes do not have a major effect on strains and deformations arising from FEA.

6.2. Material and Methods

The material used here is a dry cranium of a male *Theropithecus gelada* (see Table 5.1). The analyses are performed only in the male *Theropithecus* model because they are very time consuming, and all the other models, built in the same way, are assumed to behave in the same manner. The cranium was CT scanned (Table 5.2) and a 3D model was built for FEA according to every step described in Chapter 5 (Section 5.2), from CT image segmentation to boundary conditions, finite element solution and post-processing. The results are presented in (1) the form of scaled contour plots, with corresponding strain values at each landmark location reported in table format in Appendix D, and (2) principal components plots of deformations (as described in Subsections 2.5.3 and 5.3.2).

All the different models and load cases were submitted to FEA simulating bites along the left-side dental row, as described in Chapter 5 (Subsection 5.2.3). The deformations of each cranium resulting from each bite are compared using landmark-based geometric morphometrics, as described in Section 2.5. Principal components plots of deformations include all other species models to provide an indication of the magnitude of the model building decision effect in relation to the magnitude of differences among models.

6.2.1. Differences in Internal Architecture

To test the effect of varying the internal architecture of a model on the results of FEA, the *Theropithecus* model cranium had its internal architecture built in two ways: (1) all hollow spaces in the trabecular bone filled in with bulk material and given the

material properties of cortical bone (*filled model*); and (2) all hollow spaces in the trabecular bone left intact and the trabeculae carefully segmented (*unfilled model*), within the limits of CT scan resolution, as shown in Figure 6.1. Major anatomical features, such as the external auditory meatus, were left unfilled in both models. Due to the complexity of the task, teeth were neither fully segmented nor fully filled in any of the models: they were segmented using an automated threshold function in the segmentation software, and were given the material properties of cortical bone. It is to be expected that the unfilled model presents higher strains and deforms more than the filled model due to the absolute quantity of “bone” (number of voxels in the model, higher in the filled model).

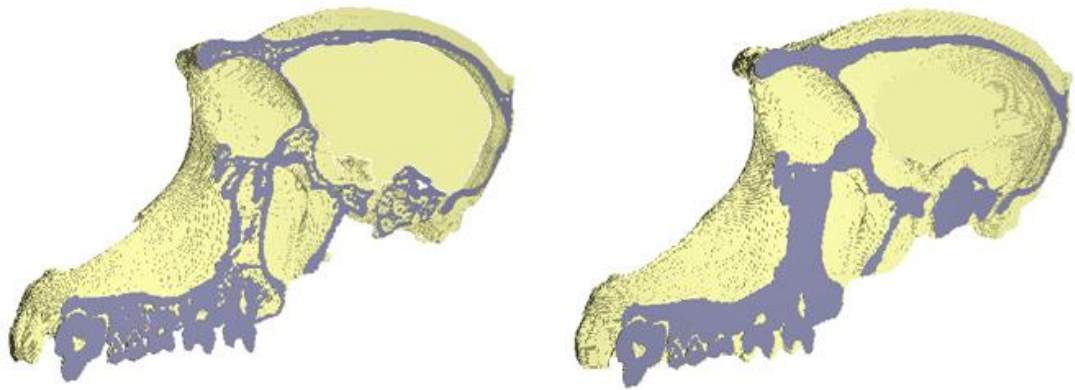


Figure 6.1. Cross-section through two differently built models of male Theropithecus gelada to show the two ways the internal architecture was modelled: on the left, the fully segmented internal architecture model (unfilled model), where all the hollow spaces in the trabecular bone can be seen; on the right, the hollow spaces in the trabecular bone filled and given the material properties of cortical bone (filled model).

6.2.2. Differences in Jaw Joint Constraint

To test the effect of varying jaw joint constraints of a model on FEA results, the *Theropithecus* model had the jaw joint constrained in two ways: (1) in all three axes of the 3D space (effectively fully anchoring the joint in that position), or (2) only in the axis of the reaction force, parallel to the vertical bite (thus allowing the model to move

freely in the other two axes). However, for FEA, full anchoring is required in at least one side of the jaw joint (to prevent the model from continuously moving in space, rather than deform) and thus the balancing (right) side of the jaw joint was constrained in all three axes; the working (left) side was thus constrained in the vertical axis only. The filled *Theropithecus* model used in the previous sensitivity analysis is used here fully constrained for comparison. Full anchoring is also used in the crania of other species with which the results of this experiment will be compared.

6.2.3. Differences in Estimated Muscle Force

Since muscle force magnitudes vary among different muscles and within the same muscle across several specimens (Table 6.1), it was necessary to assess the effects of estimated muscle forces on FEA results. To this end, the filled *Theropithecus* model is loaded in two ways that are rather extreme in their deviation from biological reality: (1) all muscle forces set to 300N (Load Case 1 in Table 6.1); and (2) all muscle forces set to 300N except for masseter muscle on both sides of the cranium, which was set to 150N (Load Case 2 in Table 6.1). Masseter force rather than the forces of other muscles was varied because estimation of its magnitude is considered one of the major sources of error in finite element models (Sellers & Crompton 2004; Fitton *et al.* 2012). Both load cases are compared to the model built with ACSA-estimated muscle forces.

Table 6.1. Muscle force magnitudes of different load cases of the same model.

Muscle	Force Magnitude		
	ACSA	Load Case 1	Load Case 2
Anterior Temporal	121.646	300.000	300.000
Posterior Temporal	334.126	300.000	300.000
Masseter	312.287	300.000	150.000
Medial Pterygoid	112.408	300.000	300.000

Forces in Newtons (N).

6.3. Results

Results are here presented as strain contour plots resulting from the VOX-FE software (see Subsection 5.2.2) and as principal components plots of deformations. For the scaling step of the landmark-based deformations analysis (see Subsections 2.5.2 and 5.3.2) the bite force calculated at each bite point in each model is required and is presented in Table 6.2 (also refer to Table 5.5*b* for the filled model bite force). Tables of strain values at landmark locations are provided in Appendix D.

Table 6.2. Bite forces and jaw joint reaction forces of the models in this chapter.

Bite	Forces	<i>Filled</i>	<i>Unfilled</i>	<i>Jaw Joint</i>	<i>Load Case 1</i>	<i>Load Case 2</i>
I1	bite force	366.62	366.59	374.37	506.33	426.30
	reaction force	1193.85	1193.86	1186.50	1657.83	1474.64
I2	bite force	372.83	372.77	380.96	514.85	433.50
	reaction force	1187.91	1187.99	1180.14	1649.52	1467.83
P3	bite force	478.17	478.10	488.24	660.39	556.04
	reaction force	1088.21	1088.25	1078.75	1508.72	1352.07
P4	bite force	508.83	508.77	519.74	702.79	591.74
	reaction force	1059.35	1059.41	1049.15	1467.89	1318.58
M1	bite force	570.46	571.29	582.33	790.15	665.32
	reaction force	1001.75	1000.98	990.90	1384.07	1249.98
M2	bite force	681.20	682.26	695.03	944.46	795.32
	reaction force	899.62	898.65	887.04	1237.23	1130.28
M3	bite force	846.49	843.24	863.64	1167.40	983.24
	reaction force	751.64	754.50	736.85	1028.80	961.96

Forces in Newtons (N).

6.3.1. Differences in Internal Architecture

Strain contour plots in the first sensitivity analysis (Figure 6.2, first and second column from the left) show little overall difference in strain distribution between the filled and the unfilled models. The major differences seen in strains are among different bites of the same model, not between models with variant internal architecture. In fact, the bite force generated by both models is almost exactly the same (Table 6.2). There are, however, differences in magnitudes of strains in localized regions of the cranium, such as the orbit and the zygomatic arch, with higher strains in the unfilled model for all bites (strain values in Tables D.1 to D.7 in Appendix D; see also Table 5.6 and Figure 5.7 for landmark location). The PCA of deformations (Figure 6.3) shows both models, filled and unfilled, clustering close together for all bite points along the dental row, and away from models of all the other papionin species. The magnitude of deformation is higher in the unfilled model for every bite load (the point representing each load case is further from the unloaded model than the filled, albeit slightly), as expected, but the trajectory of deformation is similar between both models. The first two principal components explain 87.52% of the total variance in the papionin sample.

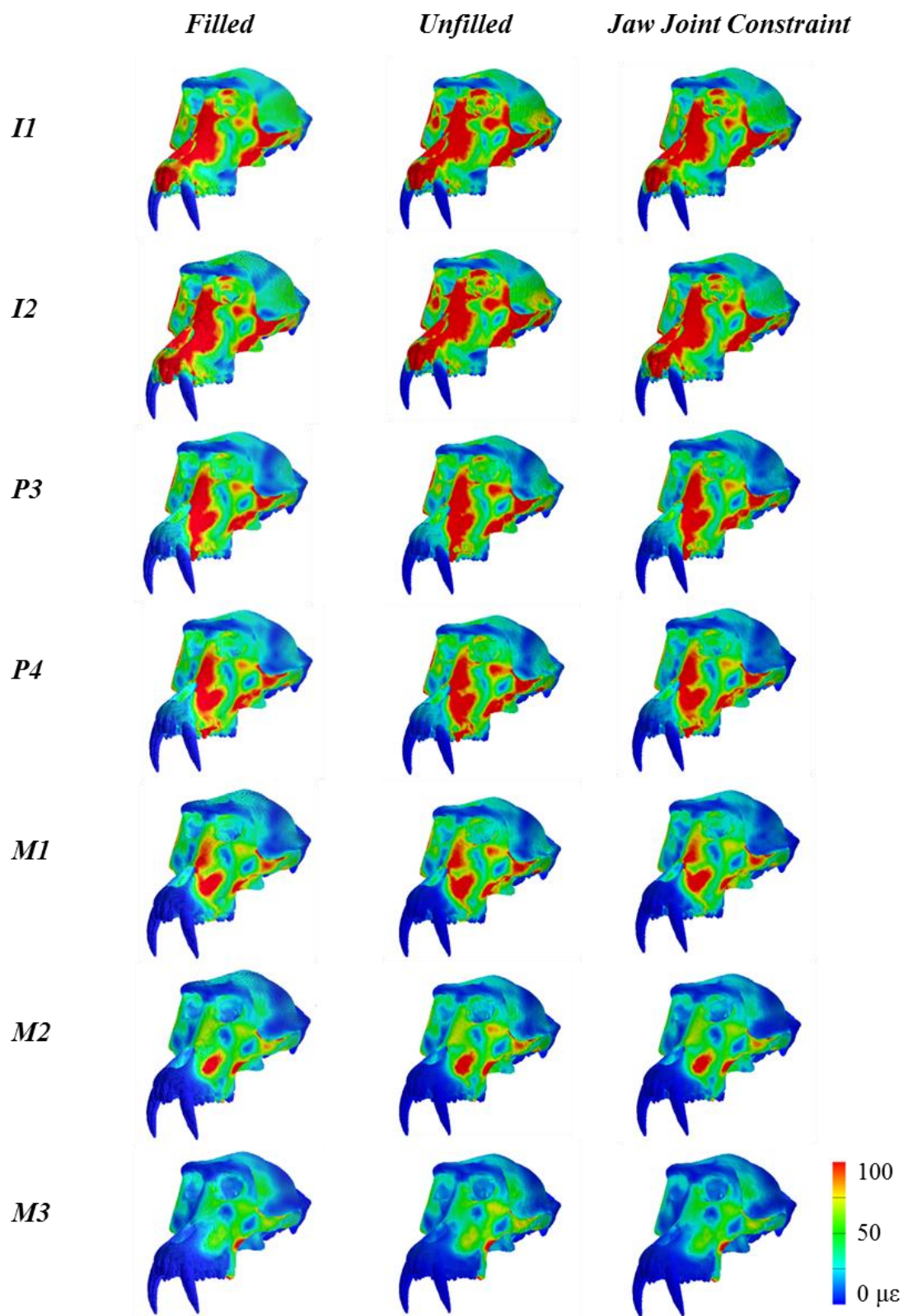


Figure 6.2. Von Mises' strain contour plots of the male *Theropithecus gelada*: filled, unfilled, and modified jaw joint constraint (see text for details). Each row represents a bite on one left tooth, first incisor (I1), second incisor (I2), first premolar (P3), second premolar (P4), first molar (M1), second molar (M2), and third molar (M3). Values in microstrain (μstrain). All bites scaled to 100N.

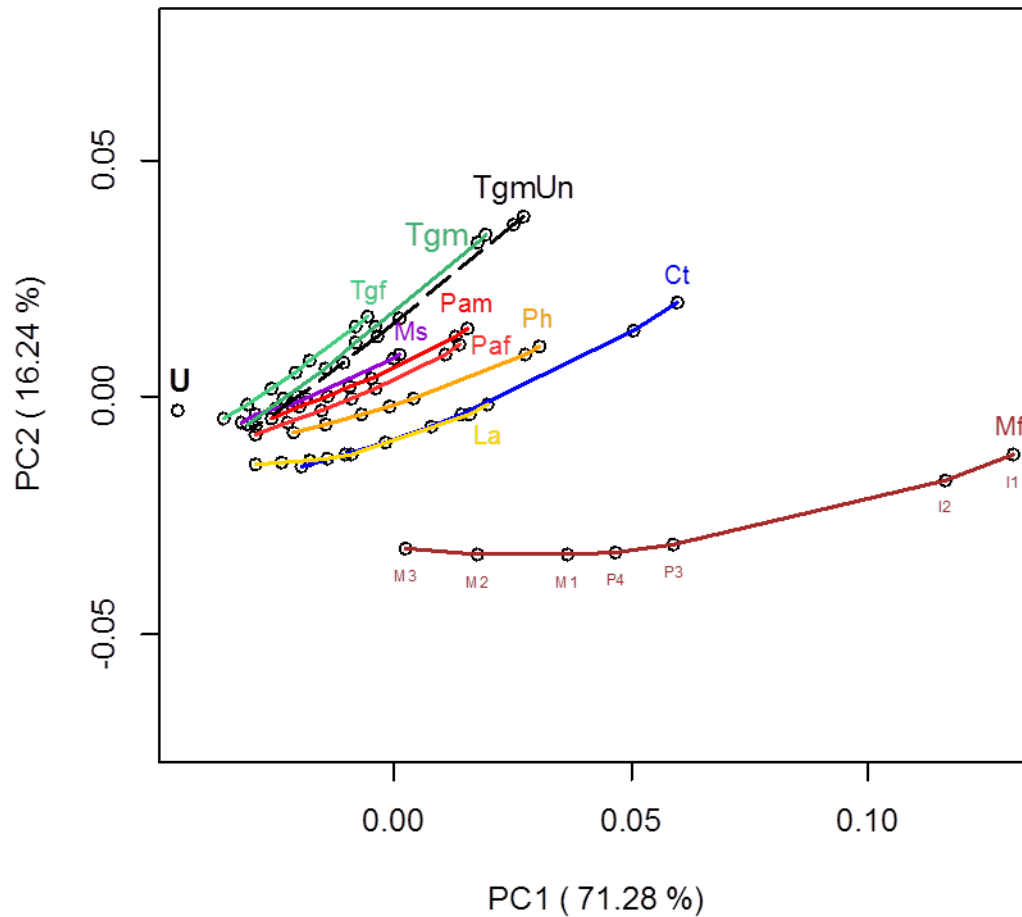


Figure 6.3. PCA of deformations with the two models of *Theropithecus gelada* with different internal architecture, filled and unfilled, among other species models. Lines denote the deformations arising from bites in a single specimen at different points along the left dental row, first incisor (I1), second incisor (I2), first premolar (P3), second premolar (P4), first molar (M1), second molar (M2), and third molar (M3). Ct, blue: *Cercocebus torquatus*. La, yellow: *Lophocebus albigena*. Mf, brown: *Macaca fascicularis*. Ms, violet: *Mandrillus sphinx*. Pam, red: male *Papio anubis*. Paf, light red: female *Papio anubis*. Ph, orange: *Papio hamadryas*. Tgf, light green: female *Theropithecus gelada*. Tgm, green: male *Theropithecus gelada* (filled model). TgmUn, black dashed: male *Theropithecus gelada* (unfilled model). The isolated point marked U represents the undeformed mean of all models.

6.3.2. Differences in Jaw Joint Constraint

The same lack of difference arises in the second sensitivity analysis, where strain contour plots show almost identical strain maps between the models (Figure 6.2, first and third columns from left). Major differences in strain distribution remain among different bites of the same model and not between the differently constrained models. In fact, for any one bite, the bite force generated by either model is very similar (Table 6.2). Magnitudes of strains show even less difference between models than in the first sensitivity analysis, and are localized mainly to the zygomatic region for each tooth bite (strain values in Tables D.1 to D.7 in Appendix D; see also Table 5.6 and Figure 5.7 for landmark location). The PCA of deformations (Figure 6.5) shows that the model with modified constraints behaves very similarly to the model with full constraints for all bites along the dental row. It is however displaced in PC2 (noted in Figure 5.9 to relate mainly to zygomatic arch deformation), indicating a similar trajectory of deformations but with a consistent difference. The trajectory of deformations and the magnitudes of strains remain very similar between both models. The first two principal components explain almost 90% (87.01%) of the total variance in the papionin sample. In Figure 6.4A the displacements (here meaning deformation plus rigid body motion; see the difference between continuum mechanics deformation and engineering deformation in Section 5.2) of the fully constrained model are shown. Deformations are evident and dominate the visualisation. In contrast, in Figure 6.4B, the displacements of the model that is constrained only in one axis in the balancing side of the jaw, for every bite, are dominated by a rotatory motion, which is much greater in magnitude than the actual deformations.

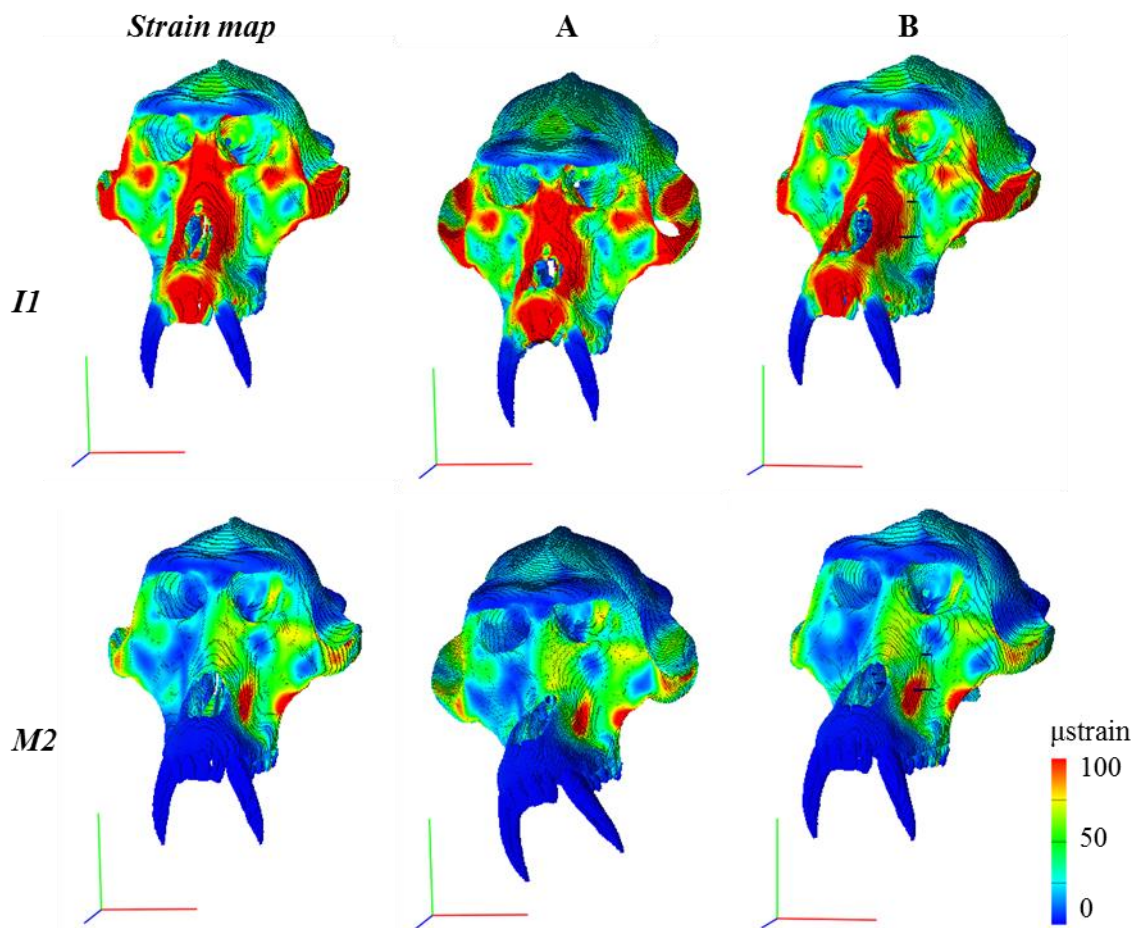


Figure 6.4. Displacement (deformation plus rigid body motions) when the model is (A) constrained in all three axes in both sides of the jaw joint, and (B) constrained in the working side only in the vertical axis (the balancing side was kept constrained in all three axes for anchoring purposes), multiplied by a scalar of 50 for visualization, during bite loads in the first incisor (I1) and second molar (M2). In (A), deformations of the face and zygomatic arches dominate the visualization, whereas in (B) rotation rather than deformation dominates the visualization, i.e., the model rotates around the fully constrained balancing side axis. Values in microstrain (μstrain). All bites scaled to 100N.

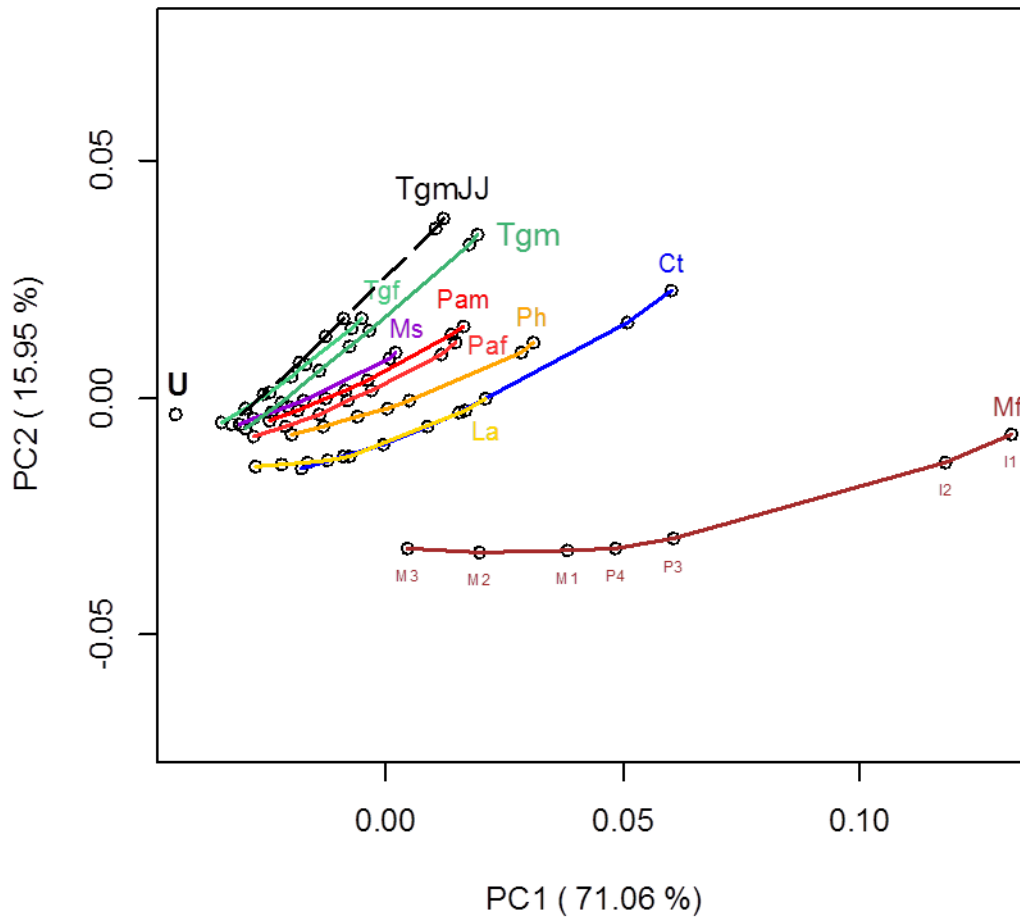


Figure 6.5. PCA of deformations with the two models of *Theropithecus gelada* with different jaw joint constraints, among other species models. Lines denote the deformations arising from bites in a single specimen at different points along the left dental row, first incisor (I1), second incisor (I2), first premolar (P3), second premolar (P4), first molar (M1), second molar (M2), and third molar (M3). Ct, blue: *Cercocebus torquatus*. La, yellow: *Lophocebus albigena*. Mf, brown: *Macaca fascicularis*. Ms, violet: *Mandrillus sphinx*. Pam, red: male *Papio anubis*. Paf, light red: female *Papio anubis*. Ph, orange: *Papio hamadryas*. Tgf, light green: female *Theropithecus gelada*. Tgm, green: male *Theropithecus gelada*, model constrained in all three axes in both sides of the jaw joint. TgmJJ, black dashed: male *Theropithecus gelada*, model constrained in the working side only in the vertical axis (the balancing side was kept constrained in all three axes for anchoring purposes). The isolated point marked U represents the undeformed mean of all models.

6.3.3. Differences in Estimated Muscle Force

The results of the sensitivity analysis on the effects of varying muscle force showed the biggest differences when compared to the other two analyses. Strain contour plots (Figure 6.6) show no difference in strain distributions between load cases yet substantial differences in strain magnitudes across the cranium, with greater differences again in the zygomatic region. The major strain distribution differences, in any case, are found among different bites, not between varied muscle load cases. Major strain magnitude differences between the ACSA load case and the other two load cases are in the midline and in the zygomatic region, for each bite (strain values in Tables D.8 to D.14 in Appendix D; see also Table 5.6 and Figure 5.7 for landmark location). Deformations, as shown in the PCA (Figure 6.7), also diverge from the standard ACSA load case in this specimen, indicating differences both in trajectory and in magnitude of deformations. As expected, higher maximum muscle forces lead to larger deformation (longer trajectories). Additionally, the dislocation of the two experimental load cases trajectories from the standard ACSA-loaded trajectory suggests that the models also deform differently. The two experimental load case trajectories nevertheless cluster closer to the male *Theropithecus* model with ACSA-estimated muscle forces, and so the differences are still quite small when compared to the differences in trajectories among all species models. The first two principal components explain again almost 90% (87.35%) of the total variance in the papionin sample, yet with relatively more variance explained by the second principal component than by the first principal component, compared to the previous analyses. This is likely because the experimental load cases are principally displaced in the second principal component, related to zygomatic bending (see Figure 5.9). The magnitude of muscle force seems to bear a greater effect in the behaviour of the finite element model than the other two model building decisions here examined.

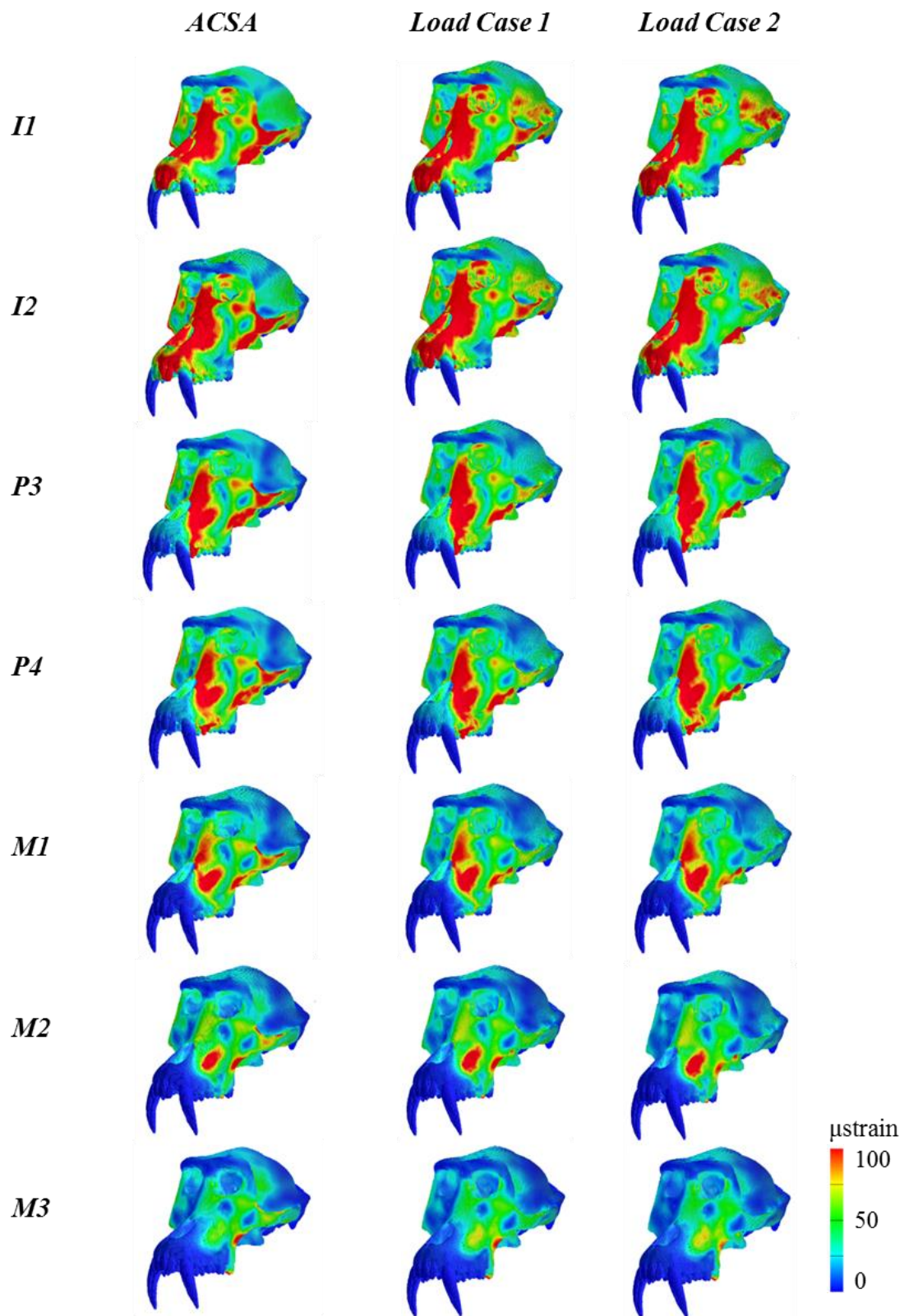


Figure 6.6. Von Mises' strain contour plots of the male Theropithecus gelada model with ACSA muscle forces and two other load cases as seen in Table 6.1. Each row represents a bite in each left tooth, first incisor (I1), second incisor (I2), first premolar (P3), second premolar (P4), first molar (M1), second molar (M2), and third molar (M3). Values in microstrain (μstrain). All bites scaled to 100N.

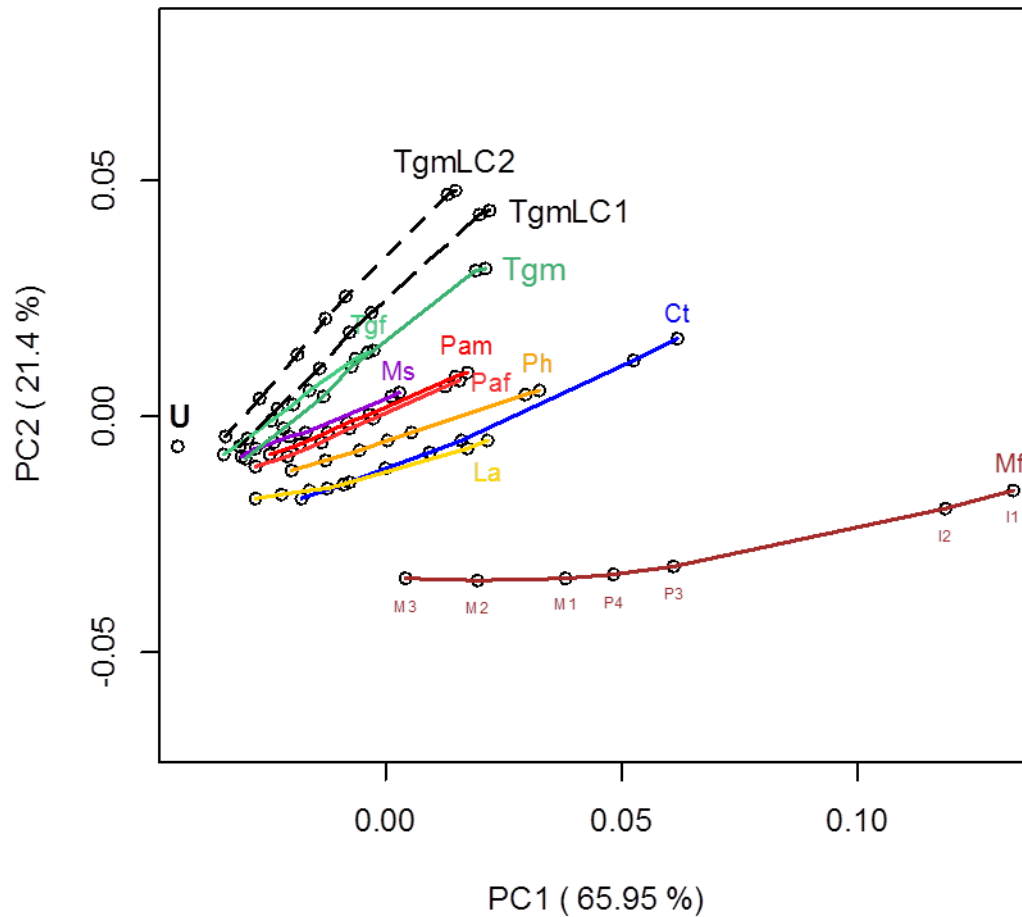


Figure 6.7. PCA of deformations with the *Theropithecus gelada* model loaded with different muscle load cases (Table 6.1) and showed among other species models. Lines denote the deformations arising from bites in a single specimen at different points along the left dental row, first incisor (I1), second incisor (I2), first premolar (P3), second premolar (P4), first molar (M1), second molar (M2), and third molar (M3). Ct, blue: *Cercocebus torquatus*. La, yellow: *Lophocebus albigena*. Mf, brown: *Macaca fascicularis*. Ms, violet: *Mandrillus sphinx*. Pam, red: male *Papio anubis*. Paf, light red: female *Papio anubis*. Ph, orange: *Papio hamadryas*. Tgf, light green: female *Theropithecus gelada*. Tgm, green: male *Theropithecus gelada*, ACSA-estimated muscle force. TgmLC1, black dashed: male *Theropithecus gelada*, Load Case 1 (see Table 6.1). TgmLC2, black dashed: male *Theropithecus gelada*, Load Case 2 (see Table 6.1). The isolated point marked U represents the undeformed mean of all models.

6.4. Discussion

This chapter explores the effect of three model building decisions on local strains and global deformations resulting from FEA. The assessments focused on the effects of varying internal architecture, jaw joint anchoring constraints, and muscle force magnitudes. None of these was expected to have a major effect on the strains and deformations arising from FEA for comparing among species, and that expectation was generally met, although muscle force magnitude had the greatest effect.

On the whole, different decisions to building the male *Theropithecus gelada* model had effects that were small and so results were within an acceptable range for comparative biomechanical performance with FEA. *A priori*, the results would be considered acceptable if the different models would all fall in the same region of the PCA plot (in terms of deformations); conversely, the results would be unacceptable if different models of the same cranium would fall in different regions of the plot, preventing the comparison between species. Ideally, for an even better understanding of those effects these sensitivity analyses should be expanded to other models (including models of the same animal species) and, if possible, significance statistics should be attempted. This, however, would be a much larger study than the one presented here and even here it was the extremely time-consuming nature of model building and sensitivity analyses that forced the application of these analyses to only one model, with the assumption that all other models perform similarly. There is no reason to expect that the behaviour of other models will be very different to this one and massive effort in model building and analysis would be required to apply sensitivity analyses to all models considered in a comparative study. Such study awaits advances in model building and computational power to facilitate the analysis of large samples.

In the first analysis, the trajectory of deformations remains the same and only the magnitude of deformations appears to have changed. Thus, shape transformations described by the first two principal components remain the same as in Figure 5.9, with mostly antero-posterior bending in PC1, and mostly zygomatic arch deformation in PC2. The same magnitude difference can be seen in the strain contour plots. These magnitude differences are likely due to stiffening of the cranium in the filled model (deforms less). The differences probably fall within the range of variation of the species *Theropithecus gelada*, and had models of other *Theropithecus* specimens been included in the analysis this realization would have been no doubt clearer. Thus, varying the internal architecture of a model appears to have little effect on the results of the FEA.

This is particularly interesting because it endorses the filling of hollow spaces in trabecular bone when CT scans resolution is low, and also grants confidence in using a bulk filled model of a fossil when the internal architecture has been lost in the fossilization process.

The major difference when constraining the working side jaw joint only in one of the three axes is that the model now rotates around the fully constrained region (the balancing side jaw joint). Since this rotatory motion tends to dominate the analysis, anchoring of only one of the jaw joint sides and leaving the other one free is not a satisfactory approach to studying deformations. The strain contour plots (Figure 6.4) return the same distribution of strains across the cranium as the fully anchored model (Figure 6.2, right column), even when scaled to 100N bite force; but there is a difference (small as it may be) in magnitude of strain (Tables D.1 to D.7), reflecting the lower deformations that are overshadowed by the dominant rotation. The rotation is undesirable for the deformations-related questions addressed here, thus the model with full, three axes anchoring on both sides of the jaw joint is used in subsequent chapters.

Among the three examined model building decisions, the one that has the greatest effect on the behaviour of the model is without a doubt the magnitude of the input muscle forces. This finding is corroborated by published findings (Sellers & Crompton 2004; Ross *et al.* 2005; Tseng *et al.* 2011; Fitton *et al.* 2012). As was expected, a higher force resulted in higher strains and higher deformations. Changing the masseter force appears to have a major effect, but more studies are needed in order to establish whether it has greater effect on FEA results than other muscles. Since, although desirable, accuracy of forces can never be fully achieved, the ability to interpret results biologically in a large sample comparative study has to rely on consistency of approach to muscle loading across all models to be compared. Thus, analyses in subsequent chapters use the ACSA-estimated muscle forces, which is a consistent and previously applied (Demes & Creel 1988; Antón 1999; Christiansen & Adolfssen 2005; Ellis *et al.* 2008) procedure.

In conclusion, considering the results of the sensitivity analyses, filled models (as mentioned before, chosen over unfilled models because of the differences in segmentation from different CT resolution quality), with jaw joint constraints in three axes in both working and balancing sides (to avoid unwanted model rotatory motion), and muscle forces estimated from ACSA as described in Chapter 5 (Subsection 5.2.3) can be expected to perform reasonably in relation to reality and so can be used to test

biologically relevant biomechanical hypotheses of papionin adaptation to diet in Chapter 7, in a comparative approach.

Chapter 7. Comparative Studies of Cranial Biomechanical Performance under Biting Loads among Papionins

7.1. Introduction

It was established in the previous chapter that the effect of model building decisions such as the effect of varying internal architecture, jaw joint constraints or even muscle force, are within an acceptable range for comparisons of relative biomechanical performance of finite element models of the cranium, if applied consistently to the whole sample (Chapter 5). Thus papionin cranial models built and loaded in the same ways can reasonably be used to test hypotheses of comparative biomechanical performance during biting loads. The aim of this chapter is to test for differences in local strains and global deformations that might be attributed to differences in papionin diet and feeding habits, in various comparative scenarios. Potential relationships, *e.g.* between diet and performance that emerge in this chapter are formally tested in the next.

Diets are varied within the Tribe Papionini, even though they are closely phylogenetically related, with some species having been observed eating hard foods (durophagous: *Cercocebus torquatus*, *Lophocebus albigena*, and *Mandrillus sphinx*), and others almost exclusively tough foods (graminivorous: *Theropithecus gelada*), while some others can be considered generalists (omnivorous: *Papio* spp. and *Macaca fascicularis*), eating mainly fruits and brittle foods (see Table 1.1, Subsection 1.3.3). Differences in the form of the cranium in each species might thus be interpreted as the consequence of biomechanical adaptation to feeding on the particular diets of each species (Subsection 1.4.3).

Since the forms of (male) crania among papionins have most likely not evolved by random genetic drift alone (see Chapter 4), diet will be assessed here as a possible selective agent driving the evolution of cranial form. Each of these different diets is hypothesised as having an effect on the biomechanics of cranial form, with different repetitive masticatory habits having driven the definition of the cranial anatomies of the different species. Five comparative scenarios are here analysed:

(1) A comparison between the three durophagous genera. The hard-food eating genera share adaptations that are expected to strengthen the cranium, minimizing strains and deformations (Subsection 1.4.3). *Cercocebus* and its sister taxon, *Mandrillus*, although differing hugely in size and cranial shape, both exhibit cranio-mandibular traits that can be interpreted as suited to crack open hard seeds and nuts (Fleagle & McGraw 1999), and thus are expected to perform similarly in terms of strains and deformations under biting loads. If so, this may reflect constraints placed on the evolution of cranial anatomy by the need to crack hard foods, although Astaras *et al.* (2008) found no evidence of dietary specialization in the genus *Mandrillus* for hard decaying seeds on the forest floor. In fact, *Mandrillus*, while observed to eat hard foods, is known to eat more soft pulp fruits than the other two durophagous genera (Lahm 1986) and its larger size and snout length is thought to be highly related not to dietary biomechanical requirements but to sexual and social behaviour. The presence of paranasal ridges on the male *Mandrillus* and the shelf-like superior temporal lines overlying the origins of the temporal muscle (Groves 2001) may cause a stiffening of the cranium, possibly with an effect on its biomechanical performance. Conversely, the genus *Lophocebus*, not a sister taxon of the other two but also reported to eat hard foods, lacks several hard-food eating anatomical features that are present in *Cercocebus* (Fleagle & McGraw 2002; see Subsection 1.4.3), but shares the same short snout, raising questions of convergent adaptation. *Lophocebus* is thus expected to perform similarly to *Cercocebus* on the grounds of form similarity but perhaps deform more for the same bite force, since it does not appear to have the anatomical adaptations to high bite force that *Cercocebus* has (Fleagle & McGraw 2002). The three species of papionins considered durophagous (*C. torquatus*, *L. albigena*, and *M. sphinx*) are thus expected to perform similarly in terms of strains and deformations due to having similar diets and despite differences in cranial anatomy or phylogenetic relationships.

(2) A comparison between long-faced omnivorous and long-faced specialized graminivorous species. These long-faced papionins (*Papio anubis*, *Papio hamadryas* and *Theropithecus gelada*) share a recent common ancestor and their distribution territories border one another (indeed, they are known to interbreed, Jolly *et al.* 1997; see also Subsections 1.3.1 and 1.3.2), but they eat diets that impose very different biomechanical constraints on the cranium (see Subsection 1.4.3). The more omnivorous *Papio* spp. have teeth that are not specialized, with postcanine teeth moderately broad with low cusps and basins (Hildebrand & Goslow 2001) and a long snout (Groves 2001), while the exclusively graminivorous genus *Theropithecus* has adaptations to

repetitive feeding on leaves or grass (Hylander 1979a, 1992; Bouvier 1986b; Jablonski 1993). *Theropithecus* exhibits larger, high-crowned postcanine teeth with accessory cusps and a somewhat shorter but deep face (when compared with other long-faced papionins; Groves 2001), but also a relatively longer masseter lever arm and higher jaw joint (Jolly 1970; Jablonski 1993; Ravosa 1996). *Theropithecus* needs to produce large amounts of effort over time to masticate its tough and fibrous foods (Fitton 2007), contrary to other long-faced papionins, and the model is thus expected to deform rather singularly compared to the other papionins. It should be noted that *P. anubis* supplements its diet with meat and other animal matter (Melnick & Pearl 1987), which are tough and soft foods (Lucas 2004), but does so only in an opportunistic manner with perhaps little effect on cranial adaptation. The expectation here is the following: crania of omnivorous species, *P. anubis* and *P. hamadryas*, are expected to perform similarly in terms of strains and deformations, while the cranium of graminivorous *T. gelada* is expected to perform singularly, differently from the two *Papio*.

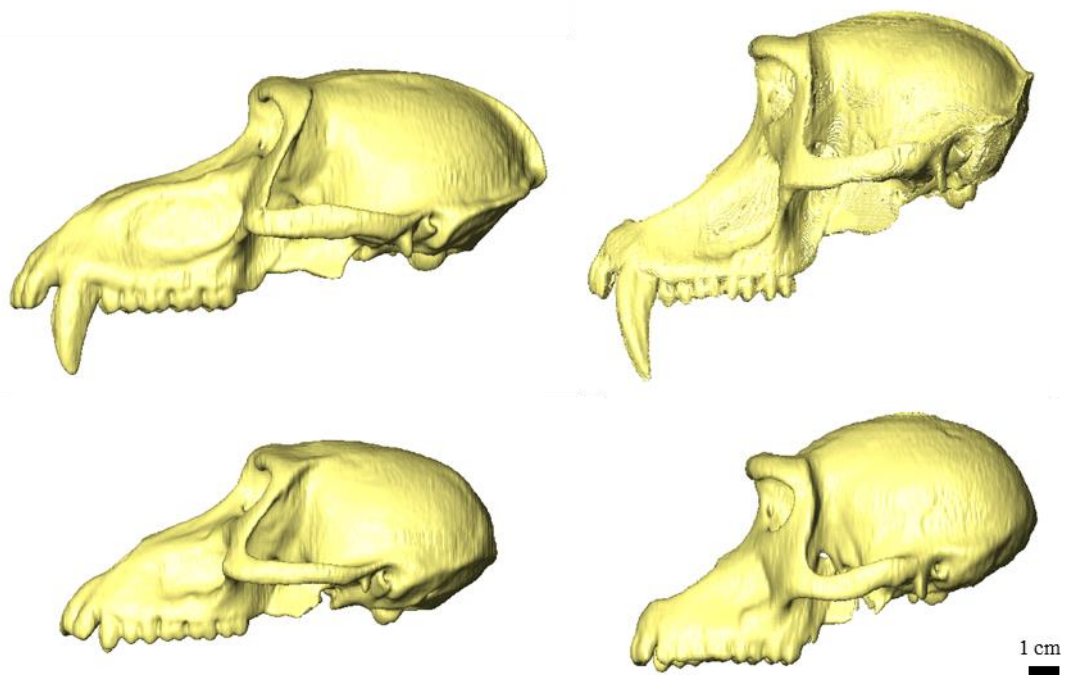


Figure 7.1. The crania of male and female of two species of long-faced papionins. Above left a male *Papio anubis*, below left a female *Papio anubis*; above right a male *Theropithecus gelada*, below right a female *Theropithecus gelada*.

(3) A comparison of cranial biomechanical performance between sexes. In the two species *Papio anubis* and *Theropithecus gelada*, males and females eat the same foods (see Subsection 1.3.3), yet differences in cranial form between the sexes in those species are striking (Figure 7.1). Females tend to be smaller in size and have shorter snouts and much shorter canines. However, since they have the same diet, it is expected that adaptation to that same diet must have occurred in both sexes, despite differences in form. Many cranial features are interpreted in the literature as being sexually dimorphic, which implies that diet had a less important effect on the evolution of cranial form than sexual selection. Conversely, if differences in cranial biomechanical performance between sexes are smaller than differences between species with different diets, this could be interpreted as a strong signal for diet as a major driver of cranial form. The expectation here is the following: female and male crania of the same species that eat the same diet are expected to perform similarly under biting loads in terms of strains and deformations (despite differences in cranial form between sexes) and differently from other species.

(4) A comparison between the species with extreme dietary specializations: durophagous and graminivorous. The durophagous genus *Cercocebus* is here used rather than *Lophocebus* or *Mandrillus* not only because it is widely described as an example of a hard foods eater (Fleagle & McGraw 1999; Shah 2003), but also because it is described as actually having clear cranial anatomical features interpreted as adaptations to feeding on hard foods (Hylander 1975; Kay 1981; Fleagle & McGraw 2002; Singleton 2004), while morphological descriptions in the literature about the other two are less clear. Those adaptations are relatively large upper second premolars (P4) that resemble the first molar in size to increase surface area to crush seeds (Fleagle & McGraw 2002), and a shortened face that increases bite force (Singleton 2004). The graminivorous genus *Theropithecus* has adaptations to repetitive feeding on leaves or grass (Hylander 1979a, 1992; Bouvier 1986b; Jablonski 1993). As mentioned before, it has larger, high-crowned postcanine teeth with accessory cusps and a somewhat shorter but deep face (when compared with other long-faced papionins; Groves 2001), but also relatively longer masseter lever arms and higher jaw joints (Jolly 1970; Jablonski 1993; Ravosa 1996). *Theropithecus* need to produce large amounts of effort to masticate their tough and fibrous foods (Fitton 2007) and the model is thus expected to deform quite differently to the durophagous extreme. The durophagous *Cercocebus* is thus expected to perform relatively more efficiently (minimizing strains) at the premolars in relation to the graminivorous *Theropithecus*, which uses the postcanine teeth as a grinding stone,

and is thus expected to perform relatively more efficiently at molar bites both in terms of strains and deformations.

(5) A comparison between the omnivorous phylogenetic outgroup *Macaca* and all other papionins. The omnivorous *Macaca* is the phylogenetic outgroup within the papionins and retains ancestral traits that might impact on cranial performance. The existence of a maxillary sinus in the genus *Macaca* alone among all papionins (Ankel-Simons 2007) is expected to have an effect on strains and deformations of the cranium because it introduces a void into the face (the *Macaca* model is the smallest and has the lowest skeletal volume of them all, see Table 7.1, thus making it likely to deform more). The ability to eat hard foods, for example, might not be present in this genus due to that anatomical feature. In terms of diet alone, though, the omnivorous *Macaca fascicularis* species would be expected to fall out closer to the two *Papio* spp. which have a similar omnivorous diet, and not as an outgroup. Inter-generically (and inter-specifically), the major trend in anatomical cranial difference among papionins relates to the length of the rostrum: the genera *Papio*, *Mandrillus* and *Theropithecus* have long faces, while the face of *Cercocebus* and *Lophocebus* is shorter; *Macaca* is generally considered to have a moderately elongated face (Singleton 2004; Ankel-Simons 2007). The expectation here is that the cranium of *Macaca fascicularis* performs differently from all other papionins due to a strong phylogenetic signal (less derived morphology), or closer to other omnivores if diet is a signal stronger than phylogeny.

It is generally expected that, regardless of the species, strains and deformations are higher when biting on the incisors, progressively decreasing when the load arm length decreases along the dental row, reaching lower values when biting on the molars. As such, long-faced papionins are expected to deform relatively more on the antero-posterior direction than short-faced papionins, for the same bite force.

The objectives of this chapter are thus to test for differences in cranial biomechanical performance (local strains and global deformations) that could be attributed to differences in diet and feeding habits in papionins. The expectations described above are formulated as null hypotheses to be tested: (1) there are no differences in cranial biomechanical performance among the durophagous genera, despite differences in cranial form or phylogenetic relationships; (2) there are no differences in cranial performance between long-faced omnivorous and graminivorous papionins; (3) there are no differences in cranial performance between the sexes in *P. anubis* and *T. gelada*; (4) there are no differences in cranial performance between a durophagous species and a graminivorous species; and (5) there are no differences in

cranial performance between the omnivorous outgroup *Macaca* and the other species. The overall expectation is that specialized feeders will perform differently than generalists; that male-female differences will be smaller than inter-specific differences; and that phylogeny is the dominant signal reflected in cranial biomechanical performance within papionins.

Table 7.1. Cranium and rostrum lengths of the models. The length of the cranium is defined as the distance from the central point between incisors at alveolar margin to the external occipital protuberance; the length of rostrum is defined as the distance from the central point between incisors at alveolar margin to the alveolare. Also shown are model volumes expressed in number of nodes per model.

Species	Cranium length (cm)	Rostrum length (cm)	Volume (nodes)
<i>C. torquatus</i>	13.6	6.2	1136507
<i>L. albigena</i>	12.6	5.6	1148144
<i>M. fascicularis</i>	11.8	5.3	804159
<i>M. sphinx</i>	23.3	11.1	4850691
<i>P. anubis</i> (f)	15.4	6.7	1752113
<i>P. anubis</i> (m)	19.5	8.8	2738941
<i>P. hamadryas</i>	19.9	8.9	3203614
<i>T. gelada</i> (f)	15.3	6.4	2190709
<i>T. gelada</i> (m)	17.5	7.9	1992109

7.2. Material and Methods

The material used here comprises dry crania of 7 male and 2 female individual specimens corresponding to 7 species and 6 genera of papionins (Table 5.1). The crania were scanned (Table 5.2) and three-dimensional (3D) models were built for finite element analysis (FEA) according to every step described in Chapter 5, from computerized tomographic (CT) image segmentation to boundary conditions, finite element solution and post-processing. Internal bony architecture was not represented in the model; instead regions of trabecular bone were filled and allocated the material

properties of cortical bone, due to discrepancies in CT resolution among the models, as discussed in Chapter 5 (Subsection 5.2.2) and analysed in Chapter 6 (Subsection 6.3.1). The muscle forces were estimated from anatomical cross-sectional area (ACSA; Tables 5.3 and 5.4). The sensitivity analysis (Subsection 6.3.3) showed that model building decisions in input muscle forces were unlikely to have a large impact in the interpretation of FEA results if there is consistency of muscle loading across all models to be compared (see Subsection 6.4). Bites were simulated on all teeth on the left side except the canine. The results are presented (1) in the form of scaled contour plots, with corresponding strain values at each landmark location (Appendix E), and (2) as PCA of deformations under biting loads (see Subsections 2.5.3 and 5.3.2).

To make the models comparable, the strains and deformations were scaled (Subsection 2.5.2) to the expected magnitudes arising from a bite force of 100N on each tooth. Since the relationship between force and strain is linear with a slope of 1 (O'Higgins & Milne 2013), scaling is straightforward and 100N is physiologically realistic (see Subsection 2.5.2). A bite of 100N was chosen because the estimated maximum muscle force is heavily dependent on muscle ACSA, yet a muscle of larger size does not mean that the animal applies the maximum force all the time while feeding. In fact, a bite force of 100N seems to be in the range of frequent bite forces for papionins based on the type of foods they eat and the average force necessary to process most of them (Lucas 2004). So given the measured bite force in FEA it is straightforward to scale strains and residuals to any value by ratio.

On the other hand, a large muscle can mean not only that the animal is capable of generating a higher bite force, but also that the animal uses that muscle continuously (a large muscle reduces muscle fatigue from overuse by allowing sequential recruitment of muscle fibres; *e.g.* Biewener 2005), meaning perhaps an evolutionary adaptation to that action.

7.3. Results

Results are presented as strain contour plots resulting from the FEA software (see Section 5.2) and as principal component plots of deformations under biting loads. Tables of strain magnitudes at landmark locations are provided in Appendix E.

7.3.1. Among Durophagous Genera

Strain contour plots of the comparative test among durophagous genera can be seen in Figure 7.2. Major differences in strain distribution are present among different bites of the same model but not among different models. For all genera, von Mises' strains (an index gained from the combinations of principal strains at any given point) are always higher along the zygomatic arch compared with the rest of the cranium for all bites, in all three models. There are marked differences in the distribution of strains between *Mandrillus* and the other genera, with low strains along the paranasal ridges, an anatomical feature unique to that genus. The strains in *Cercocebus* and *Lophocebus*, though similar in distribution, are somewhat greater in the *Cercocebus* than in the slightly smaller *Lophocebus*, contrary to what would be expected. In all three models, strains are greater when biting on the incisors along the maxilla, nasal and zygomatic bones, progressively decreasing as the load arm length decreases along the dental row, reaching the lowest values at molar bites. Values of maximum and minimum principal strains for the chosen landmarks and differences in strain between models at landmark locations are listed in Tables E.1 to E.7 (Appendix E). Strain differences between models are largest between *Cercocebus* and the other two models, *Lophocebus* and *Mandrillus*, particularly in the midline (when biting with the incisors), the inferior region of the orbit (for all bites) and the zygomatic region (for all bites).

A principal components plot of large scale deformations is shown in Figure 7.3. The largest deformations are achieved by the I1 bite in *Cercocebus*, with *Lophocebus* performing closer to *Cercocebus*, differences between the two being in magnitude of deformation rather than in trajectory of deformation. It is apparent that deformations are smaller in *Mandrillus* than in the other two genera for all bites, as would be expected from size differences, but the trajectory of deformations appears to be quite similar to the other two genera, with differences being mostly in magnitude of deformations. The

first two principal components explain 93.03% of the total variance in this sample. To facilitate interpretation of Figure 7.3, Figure 7.4 presents a visualization of differences in deformations due to two bites (I1 and M3) between two specimens. Deformation differences between the least deforming *Mandrillus* and *Cercocebus* during I1 biting are increased antero-posterior bending in *Cercocebus*. Comparing an M3 bite between *Mandrillus* and *Lophocebus* shows in *Lophocebus* increased torsion of the face and greater relative superior deformation of the maxilla in the region of M3.

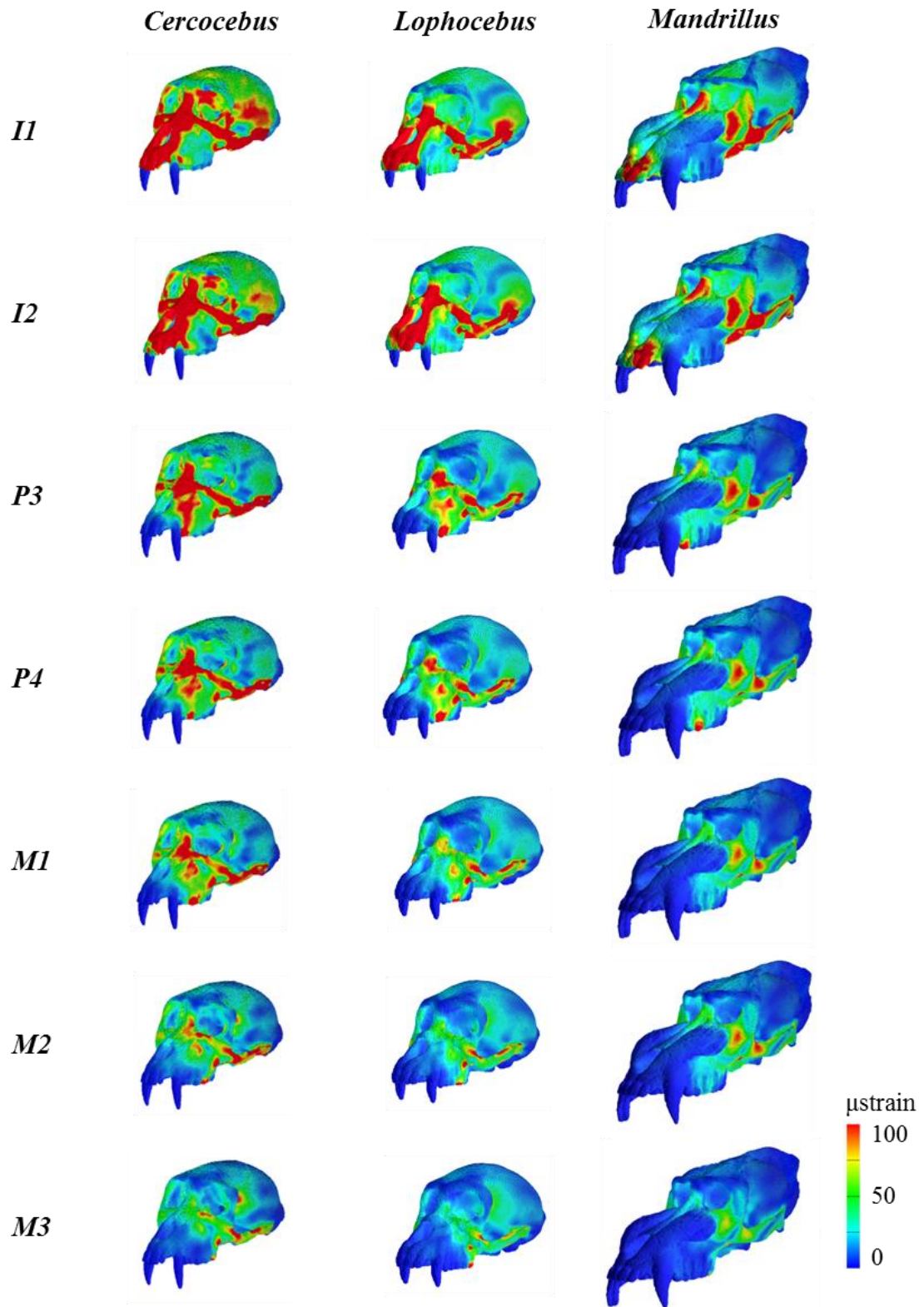


Figure 7.2. Von Mises' strain contour plots of three cranial models of durophagous genera: *Cercocebus*, *Lophocebus* and *Mandrillus*. Each row represents a bite on a particular left tooth; first incisor (*I1*), second incisor (*I2*), first premolar (*P3*), second premolar (*P4*), first molar (*M1*), second molar (*M2*), and third molar (*M3*); each column represents a different species model. Values in microstrain (μ strain). All bites scaled to 100N.

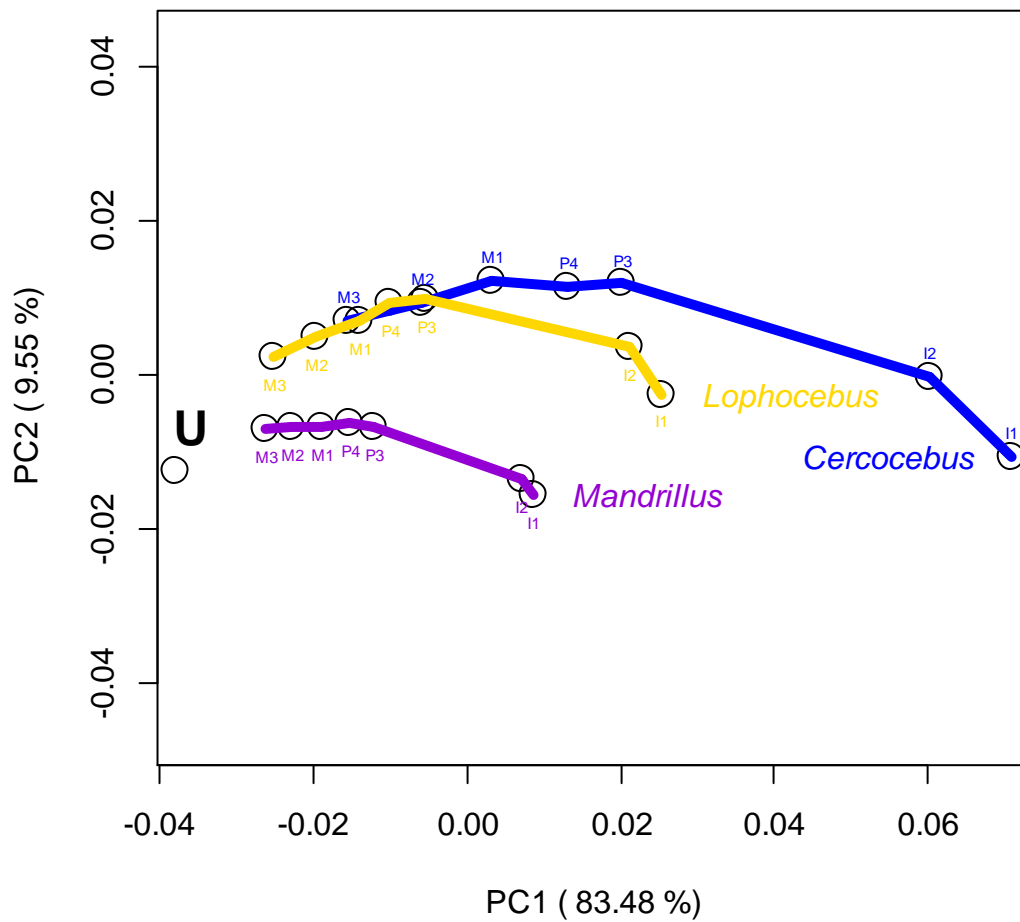


Figure 7.3. Cranial deformations among durophagous genera visualized using PCA of size-and-shape variables. Lines denote the deformations arising from bites in a single specimen at different points along the left dental row, first incisor (I1), second incisor (I2), first premolar (P3), second premolar (P4), first molar (M1), second molar (M2), and third molar (M3). Yellow, *Lophocebus*; Blue, *Cercocebus*; Violet, *Mandrillus*. The isolated point marked U represents the undeformed mean of the three models.

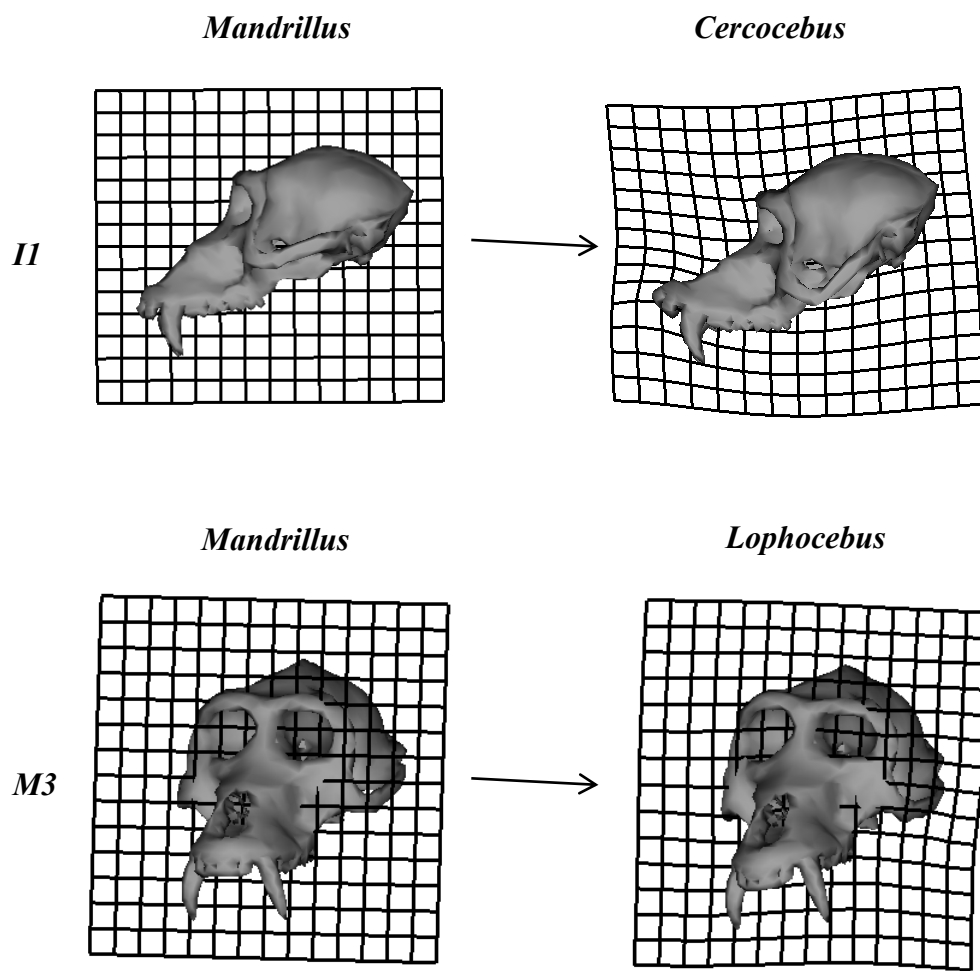


Figure 7.4. Visualization of differences in deformations due to two bites (*II* and *M3*) between specimen pairs. Deformations magnified $\times 1000$ for *II* bite, $\times 3000$ for *M3* bite.

7.3.2. Omnivorous versus Graminivorous

Figure 7.5 presents von Mises' strain contour plots for the comparative analysis between long-faced omnivorous and graminivorous species. Major differences in strain distribution are present among different bites of the same model and not among different models. As with the previous models, von Mises' strains are always higher along the zygomatic arch compared with the rest of the cranium for all bites, in all three models. The major differences in von Mises' strain distributions are between *Theropithecus* and the two *Papio* spp. *Theropithecus* shows higher strains along the nasal and maxillary region than do the *Papio* spp., particularly for the more mesial bite points; conversely, the two *Papio* show higher strains in the zygomatic region, inferior to the orbit. Lower strains are present in the zygomatic arch during P4 and molar bites in *Theropithecus*, compared to both *Papio*. Strains show higher values when biting on the incisors, progressively decreasing when the load arm length decreases along the dental row, reaching the lowest values during molar bites. Values of maximum and minimum principal strains for the chosen landmarks and strain differences between models at those landmark locations are listed in Tables E.8 to E.14 (Appendix E). Smaller strain differences can be seen between both *Papio* models, each of them differing from *Theropithecus* in the zygomatic region for all bites. Differences between *P. anubis* and *P. hamadryas* are also greater in the zygomatic region, particularly during premolar bites.

A principal components plot of deformations is shown in Figure 7.6. The two *Papio* spp. deform almost exactly the same, with *P. hamadryas* deforming only slightly more than *P. anubis* for all bites. *Theropithecus* deforms differently than the *Papio* spp., following a different deformation trajectory along PC2 (mostly zygomatic arch deformation and some frontal bending; see Section 5.3) and showing differences, such as deforming much less in M3 biting and deforming virtually the same at I1 and I2 bites, in relation to the undeformed mean. The first two principal components explain 86.52% of the total variance in the papionin sample. Figure 7.7 presents a visualization of deformations due to two bites (I1 and M3) between the omnivorous *P. hamadryas* and the graminivorous *T. gelada*. The differences in deformation between them in both bites relate to torsion of the face and relative displacement of the zygomatic arch. There is a greater degree of deformation in the anterior face in *T. gelada* during I1 bite, while the zygomatic arch shows much less relatively inferior displacement. Similarly during M3 bite the zygomatic arch appears much stiffer, displacing relatively much less

inferiorly (appearing as relative superior displacement in the visualisation). Again there is more torsion in *T. gelada*, but more concentrated in the mid-face region. Visualisations of differences in both bites show a relative inferior displacement of the maxilla as a whole in *T. gelada*, reflecting greater relative upward displacement for both bites in *P. hamadryas*; a less stiff maxilla in the latter. Thus relative to *P. hamadryas*, *T. gelada* appears to manifest a stiffer zygomatic arch and maxilla in relation to vertical displacements, while being more prone to torsion. While only M3 and incisor biting have been visualised, the displacements of bites on PC2 (more negative) in *T. gelada* relative to *P. hamadryas* are consistent and so the differences in deformation that arise along the dental row grade smoothly between these bites.

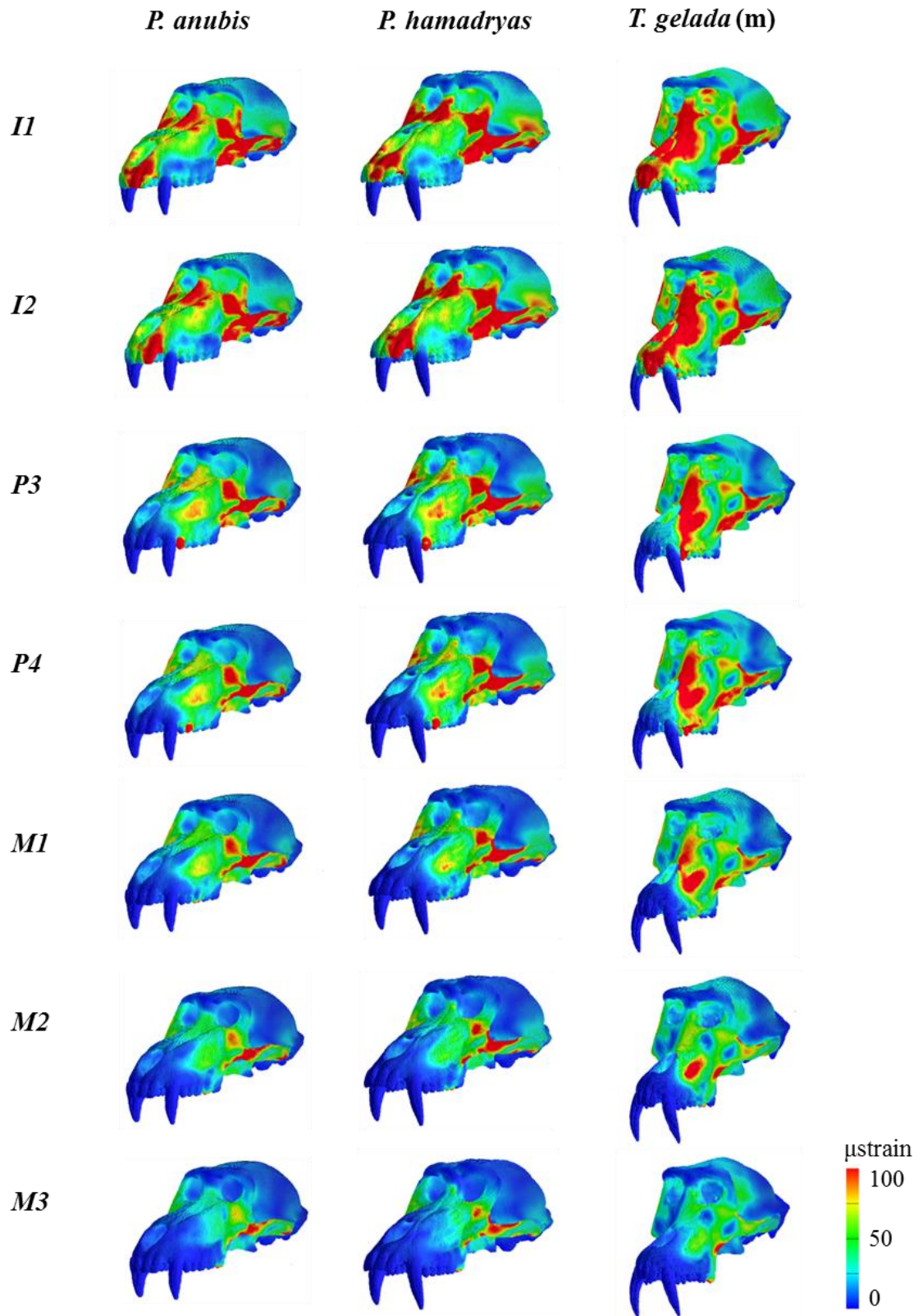


Figure 7.5. Von Mises' strain contour plot of omnivorous (*P. anubis*, *P. hamadryas*) and graminivorous species (*T. gelada*). Each row represents a bite on a particular left tooth; first incisor (*I1*), second incisor (*I2*), first premolar (*P3*), second premolar (*P4*), first molar (*M1*), second molar (*M2*), and third molar (*M3*); each column represents a different species model. Values in microstrain (μstrain). All bites scaled to 100N.

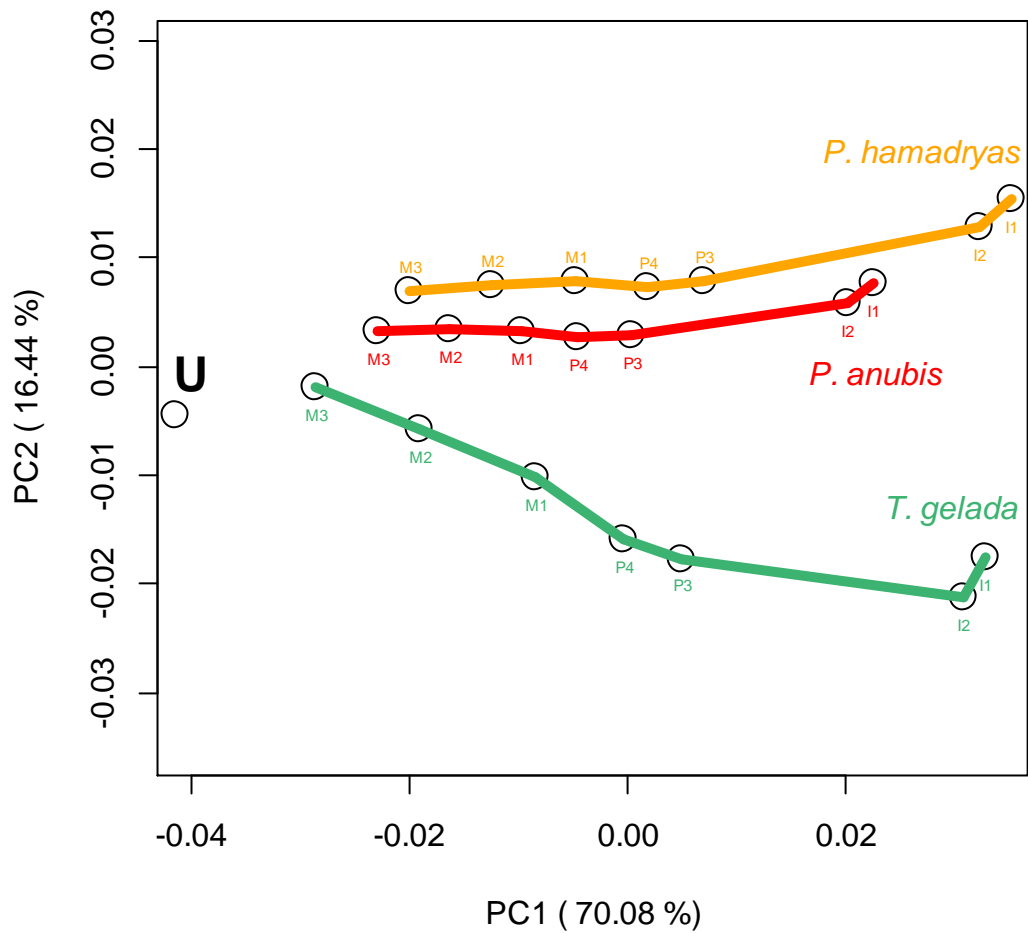


Figure 7.6. Cranial deformations between omnivorous (*P. anubis*, *P. hamadryas*) and graminivorous species (*T. gelada*) visualized using PCA of size-and-shape variables. Lines denote the deformations arising from bites in a single specimen at different points along the left dental row, first incisor (I1), second incisor (I2), first premolar (P3), second premolar (P4), first molar (M1), second molar (M2), and third molar (M3). Light blue, male *Papio anubis*; Blue, male *Papio hamadryas*; Green, male *Theropithecus gelada*. The isolated point marked U represents the undeformed mean of the three models.

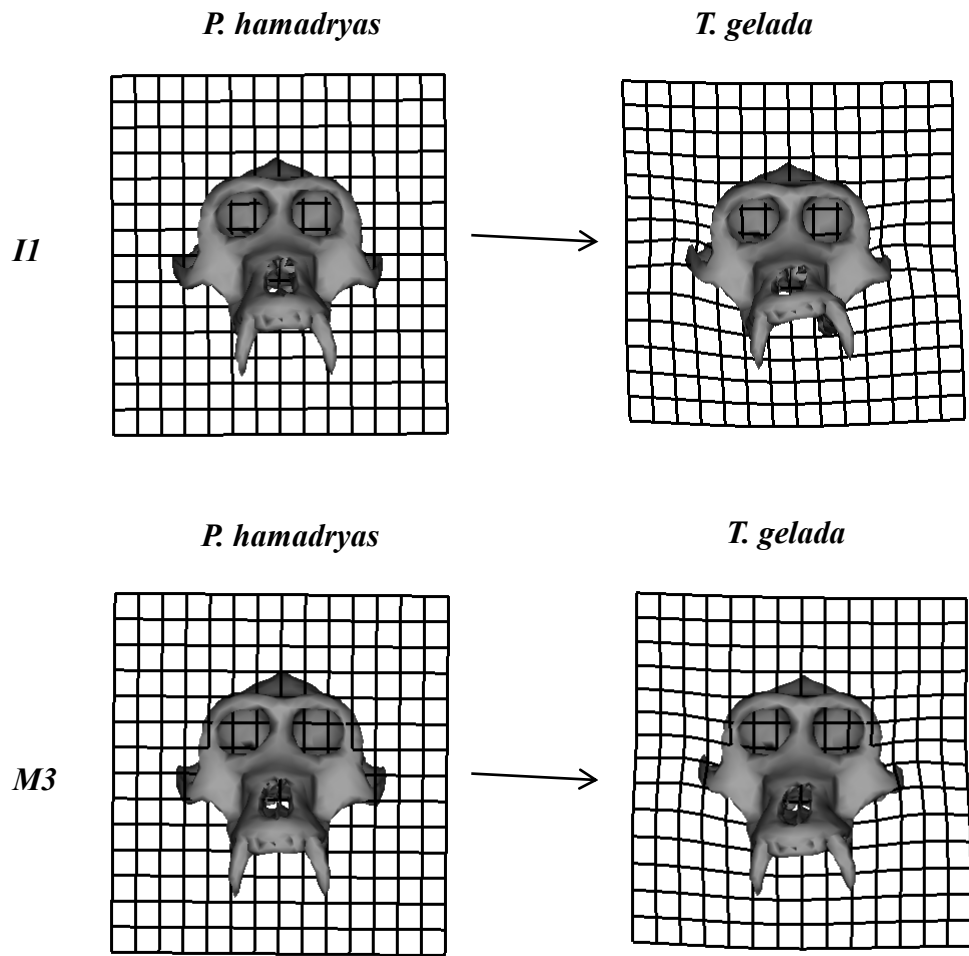


Figure 7.7. Visualization of differences in deformations due to two bites (*I1* and *M3*) between specimen pairs. Deformations magnified $\times 1000$.

7.3.3. Male *versus* Female

Strain contour plots for the comparisons between male and female are shown in Figure 7.8. Again, major differences in strain distribution are among different bites of the same model and then to a lesser extent among models. Von Mises' strains are always higher along the zygomatic arch compared with the rest of the cranium for all bites, in all four models. It is clear that larger differences are seen between species than between male and female of the same species. The female *P. anubis* shows the same pattern as the male with little difference in strains: higher strain in the nasal region during incisor bites, and lower strain in the zygomatic arch overall. The female *Theropithecus* differs more from the male, with strains lower than the male, particularly in P4 and molar bite. As expected, in all four models strains show higher values when biting on the incisors with higher strain along the maxilla, nasal and zygomatic bones, progressively decreasing when the load arm length decreases along the dental row, reaching lower values at molar bites. Values of maximum and minimum principal strains for the chosen landmarks and strain differences between models at those landmark locations are listed in Tables E.15 to E.21 (Appendix E). Differences can be seen between male and female of each species, but differences between male and female *Theropithecus* are much larger than between male and female *P. anubis* for all bites. Differences between *P. anubis* male and female are smaller during premolar and molar bites. As in the previous analysis, the anatomical region where large differences can be seen is the zygomatic in both species.

A principal components plot of deformations is shown in Figure 7.9. Deformations described by PC1 and PC2, approximate those in the visualisations of Figure 7.7. Note that male and female of each species fall with each other, and away from the other species. *P. anubis* male and female deform almost identically, with the female deforming only slightly less than the male for all bites. Differences between male and female *Theropithecus* are more marked, with the female deforming far less than the male particularly during incisor bites; the trajectory followed, though, is the same, with differences being mainly in magnitude of deformation. The first two principal components explain 82.16% of the total variance in the papionin sample.

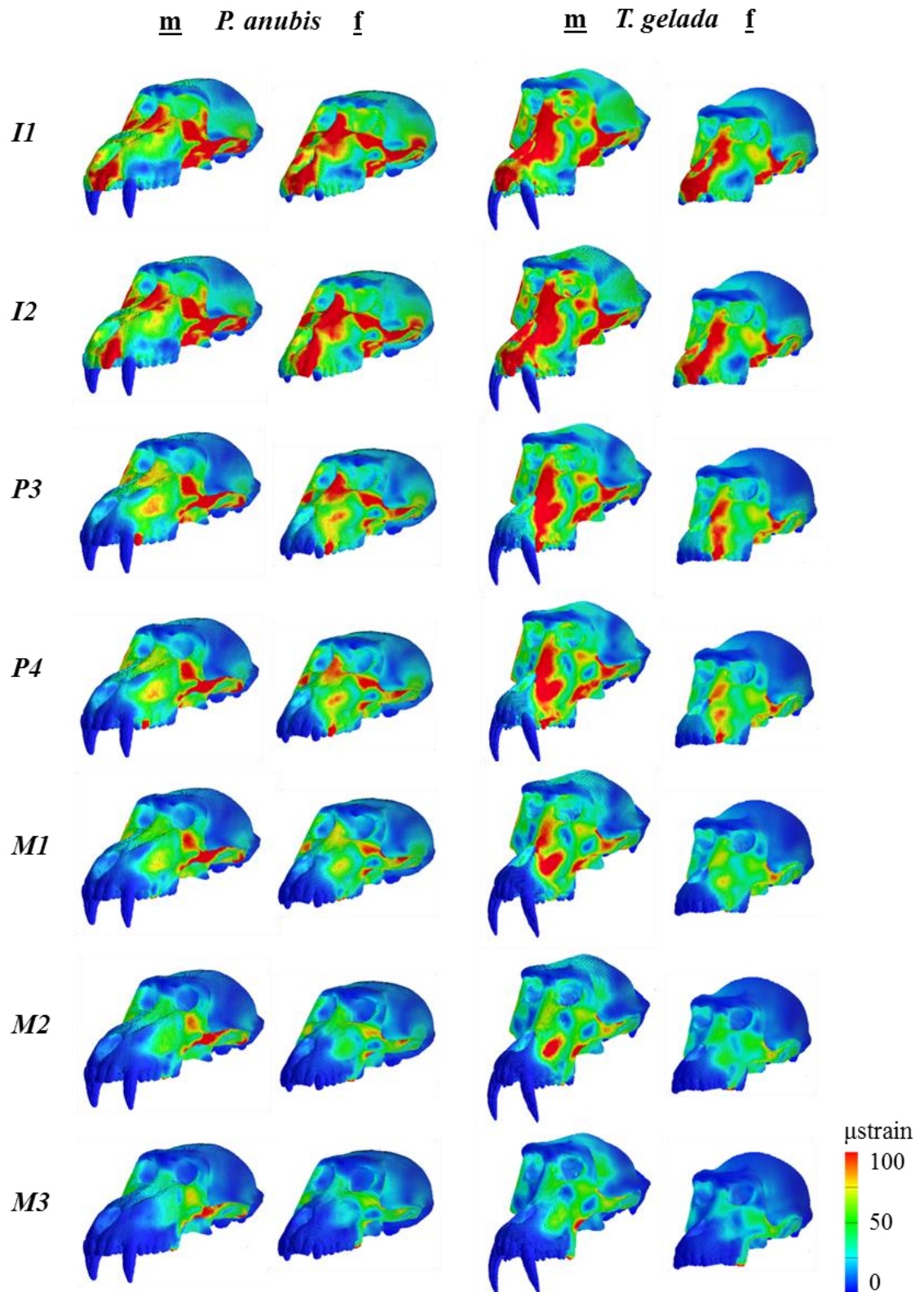


Figure 7.8. Von Mises' strain contour plots of models representing male (*m*) and female (*f*) of the species *P. anubis* and *T. gelada*. Each row represents a bite on a particular left tooth; first incisor (*I1*), second incisor (*I2*), first premolar (*P3*), second premolar (*P4*), first molar (*M1*), second molar (*M2*), and third molar (*M3*); each column represents a different species model. Values in microstrain (μ strain). All bites scaled to 100N.

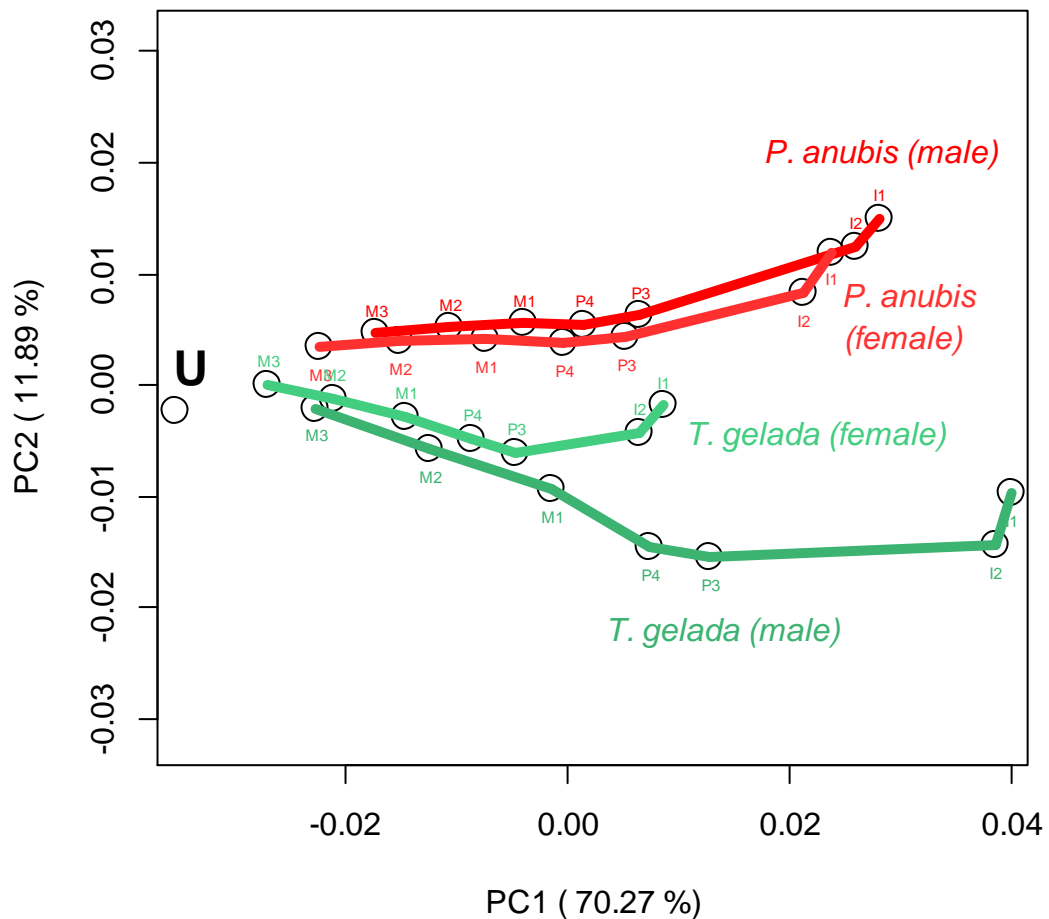


Figure 7.9. Cranial deformations between male and female in two papionin species (*P. anubis* and *T. gelada*) visualized using PCA of size-and-shape variables. Lines denote the deformations arising from bites in a single specimen at different points along the left dental row, first incisor (I1), second incisor (I2), first premolar (P3), second premolar (P4), first molar (M1), second molar (M2), and third molar (M3). Red, *Papio anubis* (male and female); Green, *Theropithecus gelada* (male and female). The isolated point marked U represents the undeformed mean of the four models.

7.3.4. Durophagous versus Graminivorous

Strain contour plots from the comparative analysis between a durophagous species and an exclusively graminivorous species are presented in Figure 7.10. Once again, major differences in strain distribution are among different bites of the same model and not among different models. The two models used in this analysis are the same ones described for the previous analyses (*Cercocebus*, Subsection 7.2.1; male *Theropithecus*, Subsection 7.2.2 and 7.2.3). As described above, von Mises' strains are always higher along the zygomatic arch compared with the rest of the cranium for all bites, in both models. There are marked differences in von Mises' strain distributions between both models. Whereas both exhibit high strains along the nasal and maxillary regions in I1 and I2 bite, those strains almost disappear in *Cercocebus* at premolar and molar bites. *Cercocebus* also exhibits somewhat higher strain in the zygomatic region inferior to the orbit when compared with *Theropithecus*. In general, the striking differences between these two models appear to be at premolar bites, where strains in *Cercocebus* are much less than in *Theropithecus*. Again as expected, in both models strains show higher values when biting on the incisors with higher strain along the maxilla, nasal and zygomatic bones, progressively decreasing when the load arm length decreases along the dental row, reaching lower values at molar bites. Values of maximum and minimum principal strains for the chosen landmark locations and strain differences between models at those landmark locations are listed in Tables E.22 to E.29 (Appendix E). Larger differences can be seen along the midline, the maxilla and the zygomatic region in both models.

A principal components plot of deformations is shown in Figure 7.11. *Cercocebus* and *Theropithecus* follow different deformation trajectories. *Cercocebus* deforms almost entirely along PC1, with greater deformation in I1 bite. *Theropithecus* deforms in both PC1 and PC2 (these two PCs comprise 90.39% of the total variation) with M3 bite making the cranium deform less than *Cercocebus*. Since PC2 is associated with deformations of the zygomatic arch, this structure appears to deform differently in *Theropithecus* relative to *Cercocebus*. *Cercocebus* is smaller than *Theropithecus* (Table 7.1) so it would be expected to deform more, but it is interesting to note that this is not true except for incisor bites. Figure 7.12 presents a visualization of deformations due to two bites (I1 and M3) between two specimens. The difference in deformation between *Theropithecus* and *Cercocebus* during I1 biting is an increase in antero-posterior bending and zygomatic arch deflection in *Cercocebus* relative to *Theropithecus*. M3 bite

shows in *Cercocebus* relative to *Theropithecus* mostly increased deflection of the zygomatic arch and increased relative vertical deformation of the maxilla.

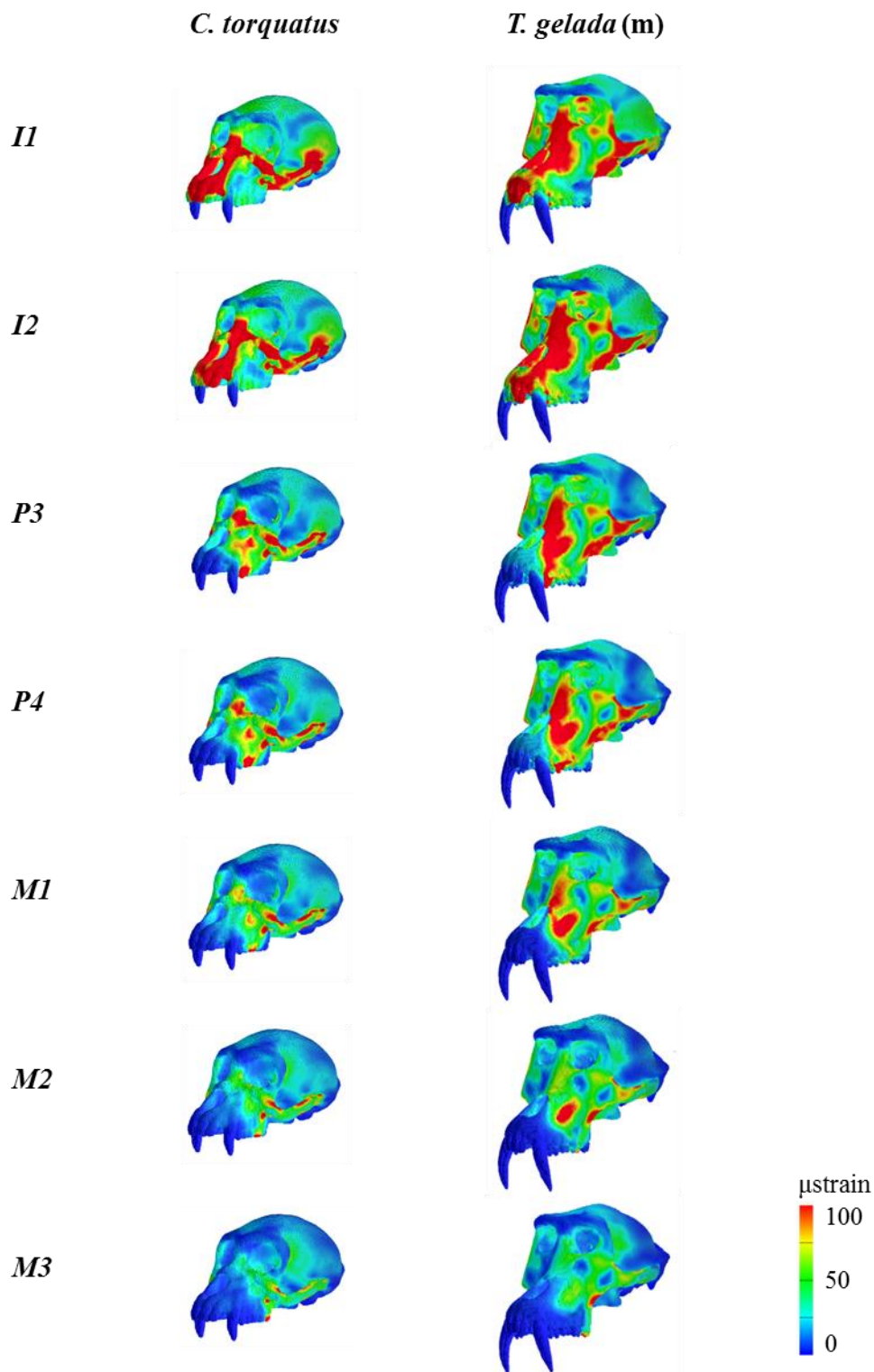


Figure 7.10. Von Mises' strain contour plot of the durophagous species *Cercocebus torquatus* and the graminivorous species *Theropithecus gelada* (male). Each row represents a bite on a particular left tooth; first incisor (I1), second incisor (I2), first premolar (P3), second premolar (P4), first molar (M1), second molar (M2), and third molar (M3); each column represents a different species model. Values in microstrain (μ strain). All bites scaled to 100N.

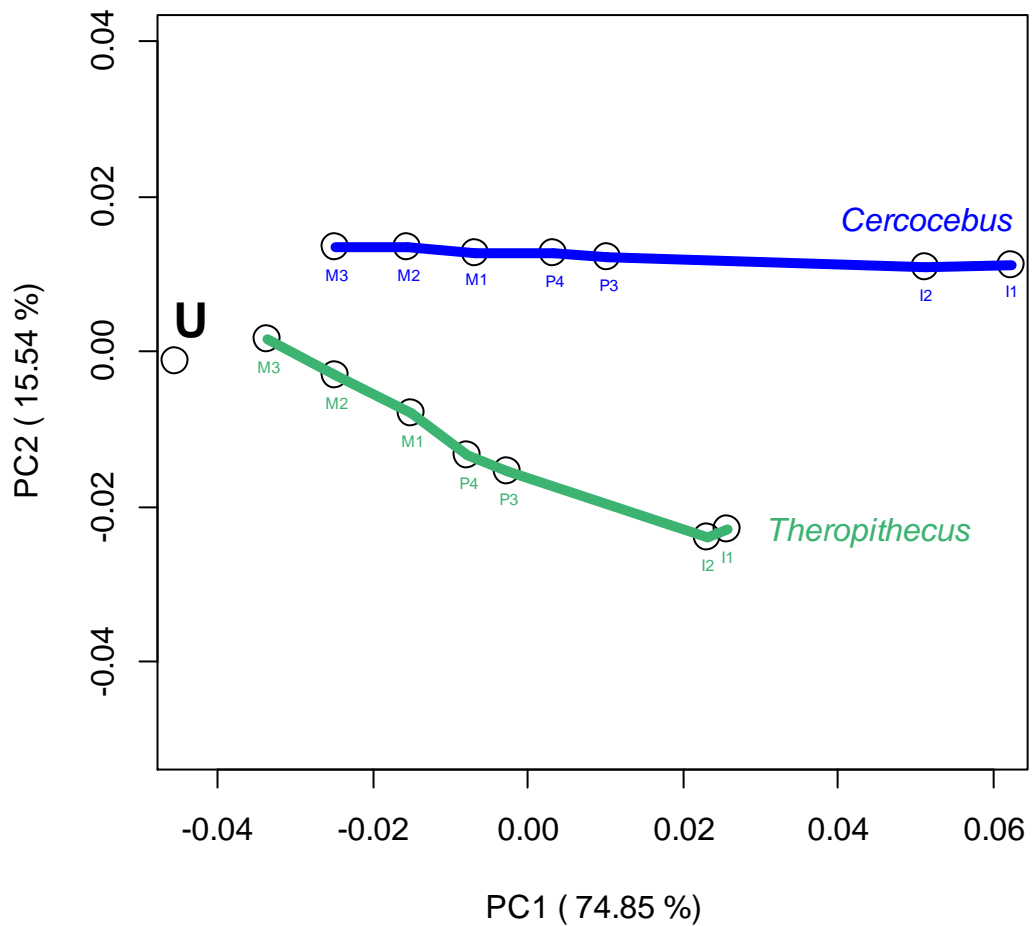


Figure 7.11. Cranial deformations between the durophagous species *Cercocebus torquatus* and the graminivorous species *Theropithecus gelada* (male) visualized using PCA of size-and-shape variables. Lines denote the deformations arising from bites in a single specimen at different points along the left dental row, first incisor (I1), second incisor (I2), first premolar (P3), second premolar (P4), first molar (M1), second molar (M2), and third molar (M3). The green lines denote the deformation across the left dental row of the male *Theropithecus* model and the blue lines represent the same on the *Cercocebus* model. The isolated point marked U represents the undeformed mean of the two models.

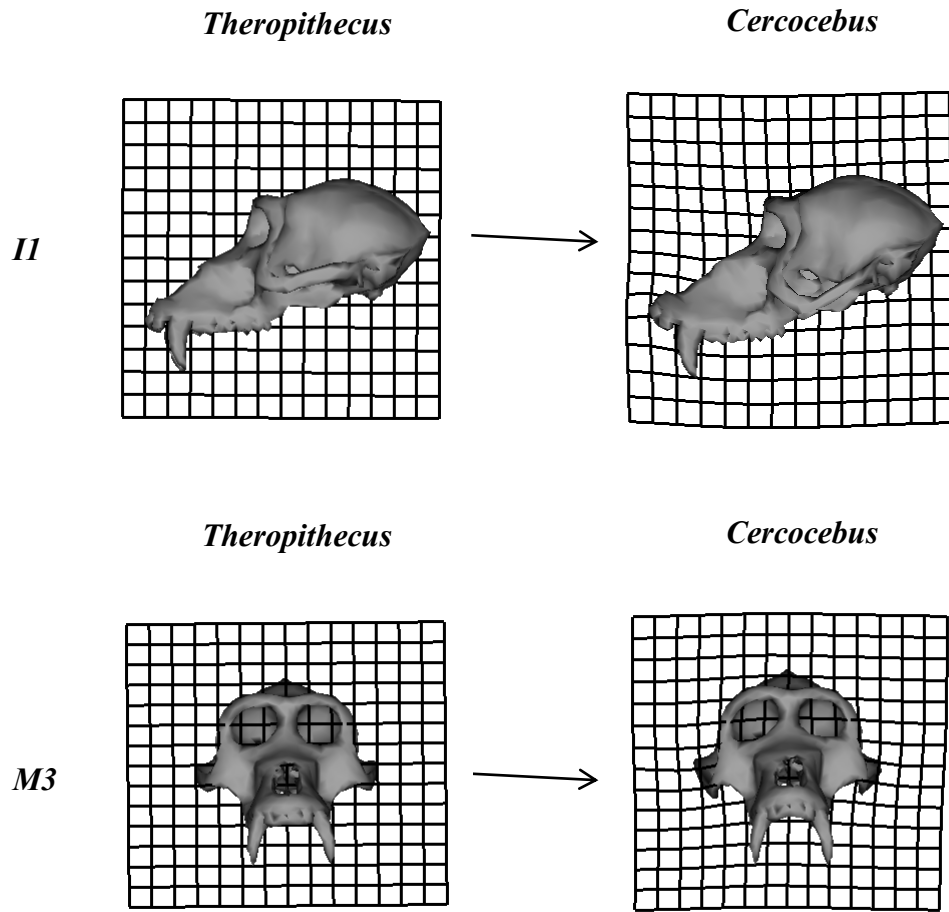


Figure 7.12. Visualization of differences in deformations due to two bites (I1 and M3) between specimen pairs. Deformations magnified $\times 1000$ for I1 bite, $\times 2000$ for M3 bite.

7.3.5. All Models

The last comparison concerns all the models used up to here plus a model of the outgroup genus *Macaca*. The strain contour plot of the *Macaca* model can be seen in Figure 7.13, far right column, among strain contour plots for all other models. Not differently from the others, *Macaca* shows von Mises' strains higher along the zygomatic arch compared with the rest of the cranium for all bites. However, strains are higher over the face compared to the other models, particularly during incisor bites, and these remain high in the zygomatic arch during all bites along the dental row. Also the cranial vault shows much higher strains than those exhibited by any other model. In *Macaca* as in all other models, strains show the same higher values when biting on the incisors progressively decreasing when the load arm length decreases along the dental row, reaching lower values at molar bites. Values of maximum and minimum principal strains for the chosen landmark locations in *Macaca* are listed in Tables E.22 to E.29 (Appendix E).

A principal components plot of deformations is shown in Figure 7.14. The *Macaca* model is clearly different from the other models. It follows a similar curved trajectory, albeit displaced towards the negative pole of PC2 but it is longer, indicating a greater degree of deformation. The magnitudes of the large scale deformations are much greater than any other model for all bites. These results are in line with the strain contour plots, where *Macaca* is the most different from other models. Deformations appear to reflect the phylogeny of the group only in the clear demarcation of *Macaca* from the rest of the group. From a phylogenetic point of view, whereas *Lophocebus*, the *Papio* models and *Theropithecus* can conceivably be interpreted as clustering together, the sister taxa *Cercocebus* and *Mandrillus* are located in very different regions on the plot, with *Cercocebus* falling out with the similarly durophagous and short-faced *Lophocebus*, and *Mandrillus* falling out with the long-faced species. The first two principal components explain almost 90% (88.61%) of the total variance in the whole papionin sample. Visualizations of deformations along PC1 and PC2 can be found in Figure 5.9.

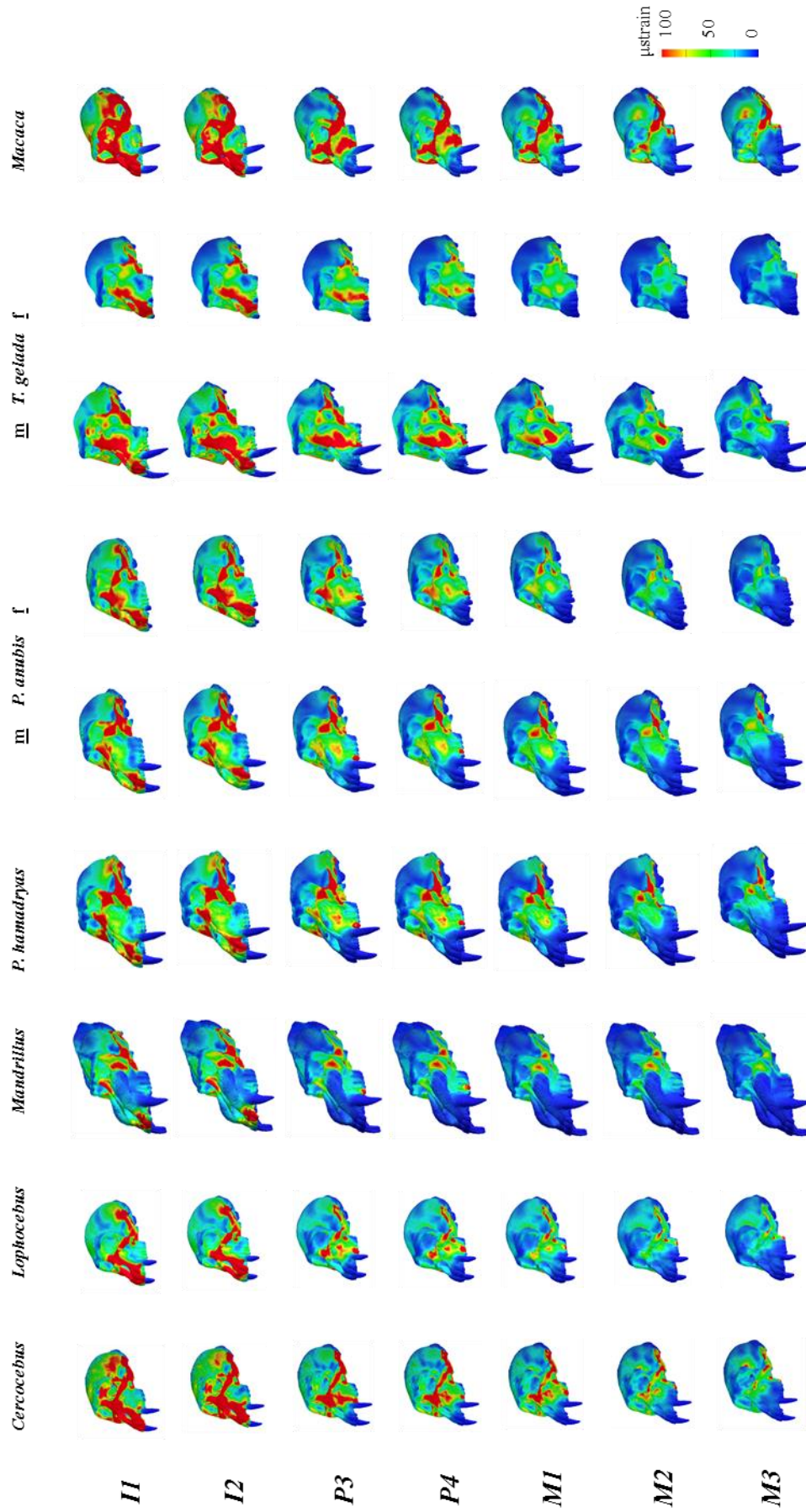


Figure 7.13. Summary of Von Mises' strain contour plots of all models, including de outgroup Macaca. Each row represents a bite on a particular left tooth; first incisor (I1), second incisor (I2), first premolar (P3), second premolar (P4), first molar (M1), second molar (M2), and third molar (M3); each column represents a different species model. Values in microstrain (μstrain). All bites scaled to 100N.

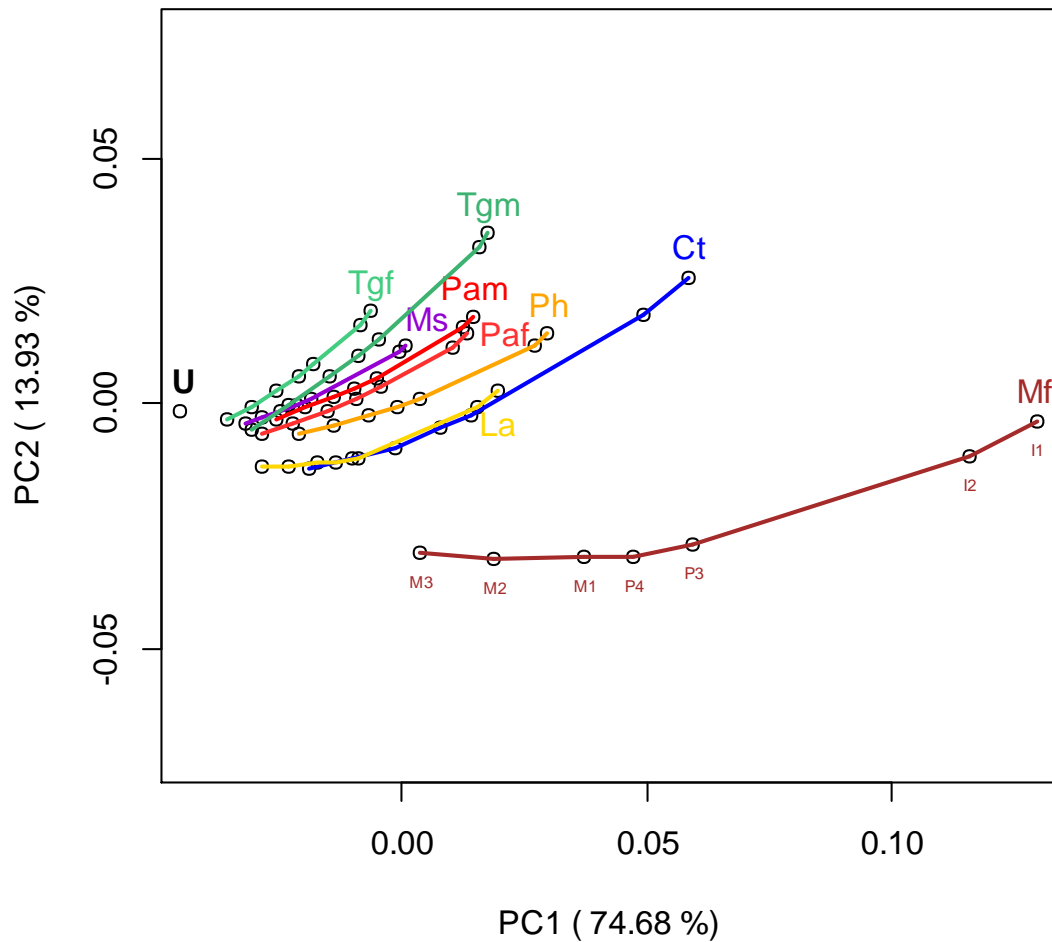


Figure 7.14. Cranial deformations of the whole sample visualized using PCA of size-and-shape variables. Lines denote the deformations arising from bites in a single specimen at different points along the left dental row, first incisor (I1), second incisor (I2), first premolar (P3), second premolar (P4), first molar (M1), second molar (M2), and third molar (M3). Ct, blue: *Cercocebus torquatus*. La, yellow: *Lophocebus albigena*. Mf, brown: *Macaca fascicularis*. Ms, violet: *Mandrillus sphinx*. Pam, red: male *Papio anubis*. Paf, light red: female *Papio anubis*. Ph, orange: *Papio hamadryas*. Tgm, green: male *Theropithecus gelada*. Tgf, light green: female *Theropithecus gelada*. The isolated point marked U represents the undeformed mean of all models.

7.4. Discussion

This chapter aimed to test for differences in biomechanical performance (local strains and global deformations) of the papionin cranium that could be attributed to differences in diet of papionin species, testing five comparative scenarios. The overall expectations were that the cranium of specialized feeders performs differently to generalists during biting loads; that male-female differences were smaller than inter-specific differences in biomechanical performance; and that phylogeny was reflected in the biomechanical performance within this group. In general, these expectations were met, even though phylogeny is not strongly reflected in the performance of the cranium.

In all models, as expected from lever-arm mechanics due to the length of the snout, the incisor load made the cranium deformed more, while strain and deformation decreased progressively when the lever arm length decreased along the dental row, reaching lower values when biting on M3. This is the general aspect of a single model with varying tooth bite loads, deforming in a trajectory along PC1 (antero-posterior bending). Along PC2, trajectories with different direction reflected differences in deformation generally regarding deformation of the zygomatic arch (Figure 5.9). Nevertheless, generally long-faced specimens did not deform more than short-faced ones, but that could be attributed to size since the short-faced species are also smaller in size than long-faced ones (Table 7.1).

In the first comparative scenario, the three cranial models belonging to durophagous genera performed quite similarly, as expected. The model of *Mandrillus* showed lower strains and deformed less than *Lophocebus* and *Cercocebus* (Figure 7.3), but the distribution of strains and the trajectory of deformations was mostly the same with differences only in the magnitude. This can be explained by the overall robustness of the *Mandrillus* cranium and also by its anatomical peculiarities such as paranasal ridges (which showed much lower strains for all bites) and enlarged sagittal crest that stiffen the cranium preventing it from deforming greatly. It can also be explained simply by differences in size between *Mandrillus* and the other species since the *Mandrillus* cranium model is of much greater size than the smaller *Cercocebus* or *Lophocebus* (Table 7.1), it was thus expected to show less strains and deformations than them (where there is no change in shape, doubling the size halves the strains, O'Higgins & Milne 2013). Both similar-sized, short-faced, durophagous species presented similar strains and, in the PCA of deformations, clustered together and away from *Mandrillus*, suggesting some degree of convergence between the two. Yet *Cercocebus* seemed to

have higher strains and deform at a higher magnitude than the slightly smaller *Lophocebus*, and showed the greatest degree of deformations of all three durophagous species. This might be due to model building issues, such as technical issues in CT scanning, or even to the idiosyncratic nature of these two particular individuals (thus, reinforcing the need to increase the intra-specific sample size), and not to specific (generic) adaptation to diet. However, if borne out by studies of more specimens belonging to this species (genus), it would imply that, despite hard object feeding in *Cercocebus*, its cranium presents less resistance to biting loads.

The second scenario returned striking differences both in strains and deformations between the two *Papio* spp. and *Theropithecus* (Figures 7.5 and 7.6). The formal null hypothesis of no differences between omnivorous and graminivorous species was rejected. As expected, the two omnivorous *Papio* spp. exhibited similar strains and deformations, while the graminivorous *Theropithecus* performed rather differently from them. It is interesting to notice the similar deformations in both incisor bites of the male *Theropithecus* which showed little difference between them in relation to the unloaded mean (at least along PC1), reflecting a relatively shorter (less prognathic) snout, perhaps a reflection of the species feeding habits (exclusive use of the postcanine teeth for food processing).

In the third scenario, an immediate realization was that male and female of each species clustered unmistakably together and away from other species, for both strains and deformations. Even though the magnitude of strains and deformations between male and female *Theropithecus* was very different, the trajectory of deformations was largely the same, with the male showing perhaps larger deformations along PC1 (antero-posterior bending, Figure 5.9). The male *Theropithecus* retained similar deformation in I1 and I2 bites as already mentioned, but this did not happen in the female model, which cannot be explained by differences in diet. On the other hand, although there were some differences in strains, large scale deformation differences between male and female *P. anubis* were very small, which means that resistance to load appears to be conserved in this species, even though they vary in cranial form. The differences in incisor bite performance among sexes of *T. gelada* may reflect reduced dietary constraints on the anterior dentition and facial skeleton, since the postcanine dentition plays a relatively more dominant role in food processing in this species than is the case in *P. anubis*. The increased deformation seen in the males is probably due to increased prognathism, which is adaptive for social display and the use of canine weaponry. The male *T. gelada*,

unlike *P. anubis*, does not require extensive adaptations to increase cranial mechanical resistance to load during incisor biting due to its molar dominated graminivorous diet.

In the fourth scenario, there were clear differences in the biomechanical performance between crania from the two dietary extremes. The trajectory of deformations was completely different and lower deformations in postcanine bite in *Theropithecus* might be an indication of the use of these teeth in repetitive tough-food consumption. The fact that the zygomatic arch appears to deform more in *Cercocebus* can perhaps be explained by the more frequent and repetitive loading experienced in the graminivorous *Theropithecus*, which requires a stouter, stiffer zygomatic arch. Deformation differences at bites with I1 and I2 in *Theropithecus* were small, compared with the same bites in *Cercocebus*, suggesting differences in anterior dental loading patterns. The hypothesized expectation that the durophagous *Cercocebus* would perform relatively more efficiently (minimizing strains) at premolar bites in relation to the graminivorous *Theropithecus* is accepted (Tables E.24 and E.25), and so is the hypothesis that *Theropithecus* was expected to perform relatively more efficiently at the molar bites, both in terms of local strains and large scale deformations (Figure 7.10; Tables E.26, E.27 and E.28).

In the analysis of all taxa including the omnivorous phylogenetic outgroup *Macaca*, the durophagous *Mandrillus* was expected to deform less than generalists because of its diet and because it is the largest in size (Table 7.1). It did deform less than all the others (except *Theropithecus*), but the other two durophagous species actually deformed much more. This might be because these are the smaller and shorter-faced species, for which a bite force of 100N is higher than the average bite force they perform in the wild. The same could be said for *Macaca*, even though the distance in terms of deformation from the other models was too large to be due to such a simple explanation. Was there an apparent size effect? It seems possible in that smaller species had more negative scores on PC2 and larger curves along PC1. This will be returned to in Chapter 8. But perhaps the most striking result of these analyses is that *Macaca* fell out away from the rest of the group (Figure 7.14). The interpretation of this might be that *Macaca* is the phylogenetic outgroup within the Tribe Papionini, thus retaining ancestral traits that might be important mechanically and sharing less derived characters with the other papionins than they do among themselves. The presence of the hollow sinus may have had an effect on the cranial stiffness, since it considerably lightens the internal structure of the cranium, diminishing its resistance to load and making it deform more than would be expected for a short-faced papionin. Indeed, even the short-

faceted durophages *Lophocebus* and *Cercocebus* deformed less than the relatively short-faced generalist *Macaca*. It would be imaginable that the cranium of *Macaca* would be less adapted to feeding, for example, on hard foods and, thus, have not have cranial form selected for that particular feeding strategy. This leads to a possible scenario for the divergence of papionins from a *Macaca*-like ancestor (Benefit & McCrossin 2002; see also Subsection 1.3.1): that the maxillary sinus was lost and the face stiffened in the common ancestor of all papionins excluding *Macaca* in response to a shift in diet towards durophagy. Later evolution related to social systems and adaptation to diverse diets underpinned further diversification of the group. This is speculation consistent with the findings and requires further testing.

Despite this discussion, interpreting FEA results, whether in terms of strains or deformations, as biologically meaningful propositions is not trivial. An initial difficulty in making interpretations about the evolution of the papionin cranium from these results rests upon the small sample size used in these analyses. Robust biological extrapolations from the results of any test to the evolution and ecology of populations have to be supported by statistical significance drawn on a sample size large enough to reflect the behaviour of a group of animals, and reduce the chances of the test picking up individual (or small sample size) biases in the population under study. Further FEAs and analyses of deformations should then deal with expanded sample sizes (larger than a single model per species), and significance statistics should be applied. This should then show whether or not inter-specific differences are real and significantly different from intra-specific patterns.

Nevertheless, the results of this chapter point towards the possibility that different diets can be interpreted from differences in strains and deformations. How these differences in biomechanical performance actually relate to diet is a problem tackled in the next chapter.

Chapter 8. The Association between Diet, Cranial Form, Maximum Bite Force, and Cranial Deformations in Papionins

8.1. Introduction

In Chapter 7, comparative scenarios for interpreting differences in cranial strains and deformations under biting loads in relation to differences in diet of papionin species were assessed. This was a largely qualitative approach which yielded some potentially interesting insights. In this chapter, the associations among diet, cranial form, and performance during biting simulations (large scale cranial deformations and maximum bite force) are further assessed using statistical techniques to quantify the degree of each apparent association and its significance. These analyses are largely exploratory, utilising novel methods and approaches, as much to assess if they are informative as to understand how form and function interact. Thus, the analyses presented here represent a starting point, a preliminary investigation, rather than a complete survey which would be well beyond the scope of this thesis.

As discussed before (Chapter 5), biomechanical performance parameters that derive from finite element analysis (FEA) include estimates of maximum bite force. It was demonstrated that different papionin species undergo different cranial deformations under biting load (see Figures 5.9 and 7.14). Maximum bite force also differs among the sampled species (see Table 5.5*a* and *b*), and is commonly used to study biomechanical performance in both extant and fossil species (Oyen & Tsay 1991; Sellers & Crompton 2004; Christiansen & Adolfssen 2005; Wroe, McHenry, & Thomason 2005; Christiansen & Wroe 2007; Nogueira, Peracchi, & Monteiro 2009; Sakamoto, Lloyd, & Benton 2010). However, the relationship between those performance parameters and other biologically interesting variables such as form and diet remains unclear after these comparisons. Diet is certainly one of the most apparent selective agents in the life of an animal (Herring 1993; Schluter 2000), with many studies based on the hypothesis that cranial form is influenced by the functioning of the masticatory system, and that it is adapted to food acquisition and intra-oral processing (*e.g.* Hylander *et al.* 1991*a*;

Jablonski 1993; Taylor 2002; Lieberman *et al.* 2004; Nogueira *et al.* 2005; Dumont *et al.* 2011; Hogg *et al.* 2011; Terhune 2011). Since the species under scrutiny in this thesis are known to have different diets (Subsection 1.3.3), it is hypothesised that diet is associated with maximum bite force and deformations. Indeed, this assumption is already often used in palaeontological analyses, where biomechanical tests are performed in fossils and the results interpreted in terms of ecological behaviour, including the type of diet consumed (*e.g.* Strait *et al.* 2009). But no attempt has been made to compare such performance parameters among extant organisms with known diets, in order to understand if and how they reflect on diet. A statistical association would be of paramount importance when inferring diet from fossils, but also in comparative analysis of other extant species. If cranial deformations or maximum bite force are strongly associated with diet, then it is conceivable that a simple biomechanical analysis could infer diet of, for example, fossil hominins, by analogy with the papionins, as Jolly (2001) posits.

The objectives of this chapter are to test whether or not differences in cranial form, in maximum bite force and in cranial deformations under biting simulations among papionin species are associated with differences in diet among species. Also, it aims to assess if and how cranial form is associated with both maximum bite force and deformations. The null hypotheses are: (1) there is no association (and no significant correlation) between diet and cranial form; (2) there is no association (and no significant correlation) between diet and maximum bite force; and (3) there is no association (and no significant correlation) between diet and cranial deformations under biting. Additionally, the following null hypotheses relate to the association between cranial form and the two biomechanical parameters: (4) there is no association (and no significant correlation) between cranial form and maximum bite force; and (5) there is no association (and no significant correlation) between cranial form and cranial deformations under biting.

8.2. Material and Methods

Crania from 7 species of papionin monkeys were modelled using CT data, as described in Chapter 5. They were the same models used in Chapter 7, including the 2

female papionin models. As in the previous chapters, papionins were chosen as a system because they comprise a group of primates with well-established phylogeny, large variations in cranial form and well known ecologies and diets (Subsection 1.3.3). FEA was used to simulate bites at different teeth, as was described in Chapter 5. Cranial form and cranial deformations were assessed using 70 landmarks distributed over the cranium (see Subsection 5.3.2). Geometric morphometric size and shape analyses were used to characterise global deformations produced during 100N bites (see Sections 2.5 and 7.2). Maximum bite forces were computed from FEA during bites (Table 5.5*a* and *b*).

The associations between blocks of data were assessed by two-block partial least squares (PLS, Rohlf & Corti 2000; see Subsection 2.6.2), a multivariate analysis of association. The blocks of data analysed with PLS are multivariate matrices extracted from maximum bite force at each tooth, large scale deformations, diet and form. Maximum bite force values were used directly in an $m \times n$ matrix where m denotes the specimens (9) and n the bites (7). Further, to reduce the number of dimensions of the deformations, each set of 7 deformations arising from different biting loads per model was condensed into a single point describing the shape of the trajectory of deformations using an approach similar to two-state multivariate change analysis (Chun *et al.* 2007; Adams & Collyer 2007, 2009; Collyer & Adams 2007). This was achieved by taking all 9 principal components scores from the previous whole-sample analysis (Subsection 7.3.6) and reordering them into an $m \times p$ matrix where m denotes the specimens (9) and p the number of principal components for each bite ($n \times p$). Then, a principal component analysis (PCA; Subsection 2.3.3) was computed; the resulting 9 principal component score vectors that describe differences in the form and location of biting performance trajectories (from Figure 7.12) were used as a block of data for the PLS analyses. Additionally, the scatter of trajectories is examined for correlation with size, using cranial length (Table 7.1) as a measure of size, with an RV-coefficient.

Broad qualitative dietary categories such as attributed in Table 1.1 were not used here, but instead a quantitative proportion of each food category consumed per species based on the literature was calculated and used (Table 8.1). When performing the analyses, food category percentage was expressed as a proportion with 1 being 100 (by dividing each value by 100). Finally, a matrix of landmark coordinates (m specimens \times k shape coordinates) after a full GPA was used as descriptor of cranial form.

The significance of the association between blocks was tested using permutation tests for the null hypothesis of complete independence between the two blocks of data. Significance levels are calculated for the singular value associated with each pair of

PLS axes, and also for the correlation between the scores for each pair of PLS axes. Since PLS extracts axes of maximum covariation between two blocks of data, cranial form variation and cranial deformations variation can be visualised at the extremes of these axes. Other multivariate data (maximum bite force and diet) can be interpreted with the loadings, where a high loading is an important factor in the covariation. The RV-coefficient (Escoufier 1973; Robert & Escoufier 1976; Claude 2008) was also used as a means to test that association. The RV-coefficient takes values between 0 and 1 and assesses the extent of covariation between two blocks of variables (see also Subsection 2.6.2). PLS and correlation analyses were performed in the data analysis packages PAST, version 2.17 (Hammer, Harper, & Ryan 2001; Hammer & Harper 2006) and MorphoJ (Klingenberg 2011). PLS plots and RV-coefficients were drawn and calculated using R functions (R Development Core Team 2013).

Table 8.1. Proportion of each food category consumed per species shown in percentage (%) of total diet. Taken from the literature (see Subsection 1.3.3).

Species	Food Categories					
	fruits	leaves	flowers	roots	animals	other
<i>C. torquatus</i>	86.0	10.0	1.0	0.0	2.0	1.0
<i>L. albigena</i>	65.4	4.5	3.3	0.0	25.3	1.5
<i>M. fascicularis</i>	66.7	17.2	8.9	0.0	4.1	3.1
<i>M. sphinx</i>	81.1	5.7	0.8	1.0	4.9	6.5
<i>P. anubis</i>	54.9	32.0	7.5	1.7	2.7	1.2
<i>P. hamadryas</i>	45.0	28.0	22.0	2.0	0.0	3.0
<i>T. gelada</i>	6.9	91.8	0.8	0.5	0.0	0.0

8.3. Results

Results are presented as tables of singular values and correlations, and as PLS plots with visualizations of transformations along the axes. Figure 8.1 presents the scatter plot (PCA) of the 9 principal component score vectors that describe differences in the form and location of biting performance trajectories (*i.e.*, summarises curves as

single points in a new PCA based on PCs1-9 of the analysis in Figure 7.14). The RV-coefficient of those 9 principal components scores and size (cranial length) is 0.31832, with a P-value of 0.09969 (not significant for 0.05). This indicates that size alone does not explain the differences in large scale deformations arising from biting among these species.

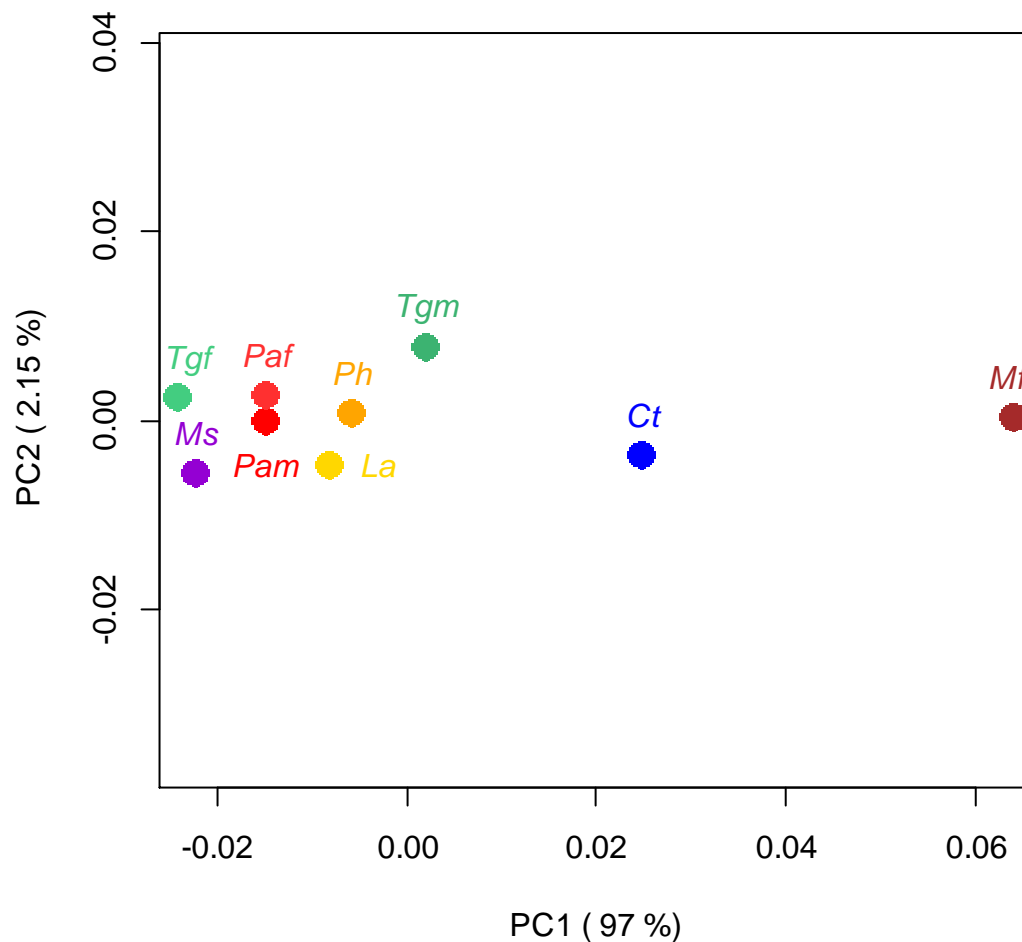


Figure 8.1. Scatter plot of the 9 principal component score vectors that describe cranial deformations of the whole sample visualized using a PCA. Points denote differences in the form and location of biting performance trajectories for each species in the analysis of Figure 7.14. Ct, blue: *Cercocebus torquatus*. La, yellow: *Lophocebus albigena*. Mf, brown: *Macaca fascicularis*. Ms, violet: *Mandrillus sphinx*. Pam, red: male *Papio anubis*. Paf, light red: female *Papio anubis*. Ph, orange: *Papio hamadryas*. Tgm, green: male *Theropithecus gelada*. Tgf, light green: female *Theropithecus gelada*.

8.3.1. Diet *versus* Cranial Form

Table 8.2 presents the singular values and pairwise correlations of PLS scores between cranial form and diet. The only significant singular axis is PLS1 (describing 98.213% of the total covariance). The RV-coefficient for the whole PLS is 0.4484597 ($p = 0.06117582$), not significant for a significance level of 0.05. Figure 8.2 presents a plot of the first singular axis (PLS1) from the PLS of cranial form and diet. This association is highly significant (Table 8.2; $p = 0.0057$). Loadings for the dietary categories and a depiction of change in cranial form along PLS1 for this block of data are also shown. The positive extreme of PLS1 for cranial form shows an enlarged cranium with elongated snout corresponding to a diet high in leaves, *versus* a small cranium with shorter snout corresponding to a diet high in fruit. Three groups can be seen in the plot: the two models of *Theropithecus*, male and female, that stand out as the most different in both cranial form and diet along PLS1; the long-faced, frugivorous/omnivorous *Papio* species; and the short-faced, mostly frugivorous species plus *Mandrillus*. It is interesting to note that the sister taxa *Cercocebus* (short-faced) and *Mandrillus* (long-faced), that have similar diet (frugivory/durophagy) yet are very different in terms of cranial form, actually cluster together. However, the plot does not show a patterning of relationships between species that might be expected from the phylogenetic relationship between them. Sister taxa, such as *Theropithecus*, *Lophocebus* and *Papio* cluster far from one another, while the outgroup *Macaca* does not stand out as different from other short-faced species.

Table 8.2. Singular values with P-values, percentage of total covariance explained by each axis, and pairwise correlations of PLS scores between cranial form and diet with P-values. Significant P-values ($\alpha = 0.05$) are shown in italics and marked with *. For the whole analysis $RV = 0.4484597$, $p = 0.06117582$.

	Singular value	P-value (perm.)	% total covar.	Correlation	P-value (perm.)
PLS1	0.02953201	0.0737	98.213	0.93694	<i>0.0057*</i>
PLS2	0.00321861	0.8418	1.167	0.51995	0.9178
PLS3	0.00221859	0.5635	0.554	0.90410	0.0460
PLS4	0.00072518	0.1827	0.059	0.60112	0.7175
PLS5	0.00024752	0.1035	0.007	0.67828	0.6247

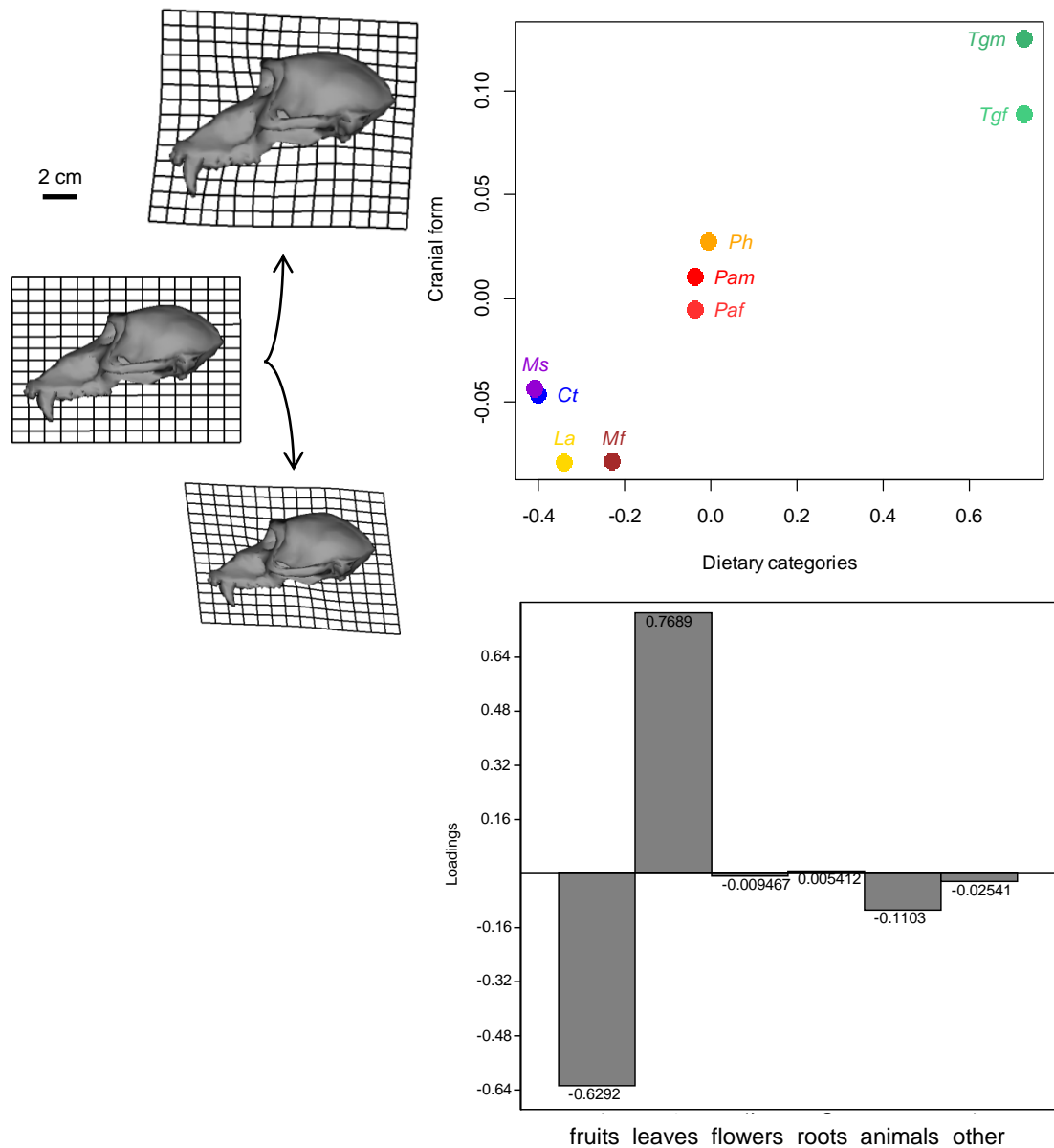


Figure 8.2. PLS analysis of cranial form and dietary categories. Loadings for the dietary categories and a depiction of change in cranial form along PLS1 are also shown. *Ct*, blue: *Cercocebus torquatus*. *La*, yellow: *Lophocebus albigena*. *Mf*, brown: *Macaca fascicularis*. *Ms*, violet: *Mandrillus sphinx*. *Pam*, red: male *Papio anubis*. *Paf*, light red: female *Papio anubis*. *Ph*, orange: *Papio hamadryas*. *Tgm*, green: male *Theropithecus gelada*. *Tgf*, light green: female *Theropithecus gelada*.

8.3.2. Diet *versus* Maximum Bite Force

Table 8.3 presents the singular values and pairwise correlations of PLS scores between maximum bite force and diet. No significant correlation is found for any PLS axis. The low association between maximum bite force and diet is further evidenced by the RV-coefficient for the PLS which is 0.03417624 ($p = 0.7269898$), not significant for a significance level of 0.05. Figure 8.3 presents a plot of the first singular axis (PLS1) from the PLS of maximum bite force and diet, which is not significant (Table 8.3). Loadings for both blocks of data are also shown. The extremes of variation are fruit eaters, biting with the incisors and leaf eaters biting with the molars. The plot shows no clear groupings, apart from perhaps the two male *Papio* that have the similar (but not the same) diet. The distancing of male and female models in both *Papio anubis* and *Theropithecus* is also apparent. Interesting to note is the frugivorous/durophagous *Mandrillus* showing the same extreme bite force as the graminivorous *Theropithecus* male, while the female *Theropithecus* shows maximum bite forces of the level of the frugivorous short-faced species.

Table 8.3. Singular values with *P*-values, percentage of total covariance explained by each axis, and pairwise correlations of PLS scores between maximum bite force and diet with *P*-values. Significant *P*-values ($\alpha = 0.05$) are shown in italics and marked with *. For the whole analysis $RV = 0.03417624$, $p = 0.7269898$.

	Singular value	P-value (perm.)	% total covar.	Correlation	P-value (perm.)
PLS1	21.94906594	0.6924	97.870	0.21189	0.8219
PLS2	3.23280249	0.1609	2.123	0.17927	0.8683
PLS3	0.17912346	0.9150	0.007	0.19889	0.7080
PLS4	0.04078020	0.7414	0.000	0.21114	0.6581
PLS5	0.01359169	0.4312	0.000	0.09545	0.9639

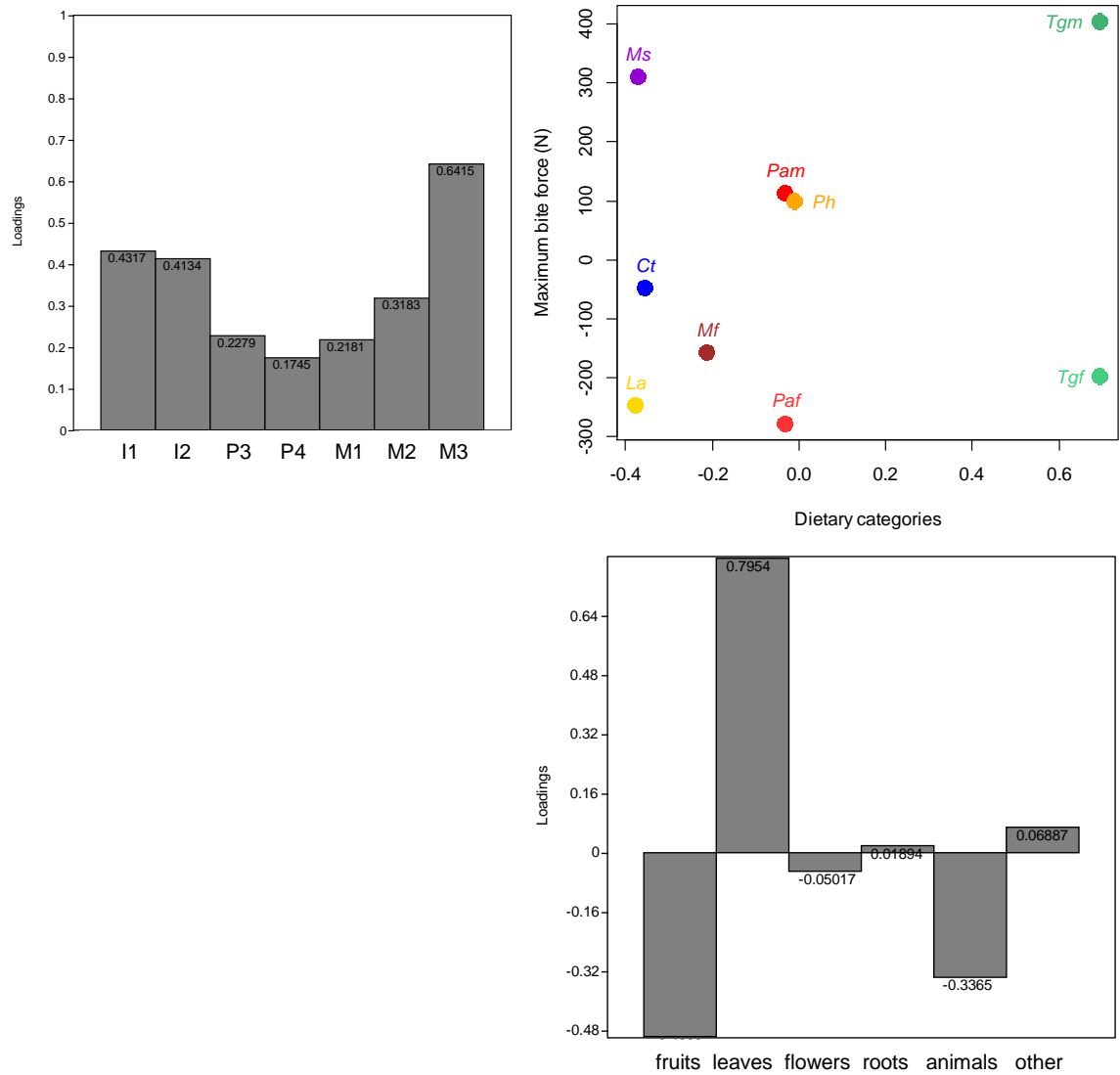


Figure 8.3. PLS analysis of maximum bite force and diet. Loadings for both blocks of variables are also shown. *Ct*, blue: *Cercocebus torquatus*. *La*, yellow: *Lophocebus albigena*. *Mf*, brown: *Macaca fascicularis*. *Ms*, violet: *Mandrillus sphinx*. *Pam*, red: male *Papio anubis*. *Paf*, light red: female *Papio anubis*. *Ph*, orange: *Papio hamadryas*. *Tgm*, green: male *Theropithecus gelada*. *Tgf*, light green: female *Theropithecus gelada*.

8.3.3. Diet *versus* Cranial Deformations

Table 8.4 presents the singular values and pairwise correlations of PLS scores between cranial deformations and diet. The correlation for the first PLS axis (describing 98.865% of the total covariance) is not significant. Only PLS3 shows significant correlation, but it describes only a minute percentage of the total covariance. The RV-coefficient of the PLS is 0.1662508 ($p = 0.3444324$), not significant for a significance level of 0.05. Figure 8.4 presents a plot of the first singular axis (PLS1) from the PLS of cranial deformations and diet. These are not significantly correlated (Table 8.4). Loadings for the dietary categories and a visualization of the extremes of deformation along PLS1 are also shown. The inset transformation grids visualising these differences are enlarged and shown in Figure 8.5. Fruits and leaves are the extremes of PLS1 for the first block of data, while the extremes of PLS1 for the second block are higher deformation *versus* lower deformation, particularly in the zygomatic arch (Figure 8.5; see also Figure 5.9). Standing out in the plot is the *Macaca* model, with higher deformations and a frugivorous diet. All the other specimens deform much less than *Macaca*, regardless of their diet. They cluster in three groups, mainly due to differences in diet on PLS1 of that block of data: male and female *Theropithecus*, graminivorous, deforming the least; the three *Papio* specimens, omnivorous; and the short-faced species plus *Mandrillus*, all frugivorous/durophagous species. Apart from the *Papio* species, sister taxa do not cluster together, not even *Cercocebus* and *Mandrillus* that do so when cranial form is considered (Figure 8.2).

Table 8.4. Singular values with P-values, percentage of total covariance explained by each axis, and pairwise correlations of PLS scores between cranial deformations and diet with P-values. Significant P-values ($\alpha = 0.05$) are shown in italics and marked with *. For the whole analysis $RV = 0.1662508$, $p = 0.3444324$.

	Singular value	P-value (perm.)	% total covar.	Correlation	P-value (perm.)
PLS1	0.01323222	0.3244	98.865	0.43616	0.3926
PLS2	0.00132619	0.4500	0.993	0.48512	0.2784
PLS3	0.00049557	0.1933	0.139	0.76557	<i>0.0330*</i>
PLS4	0.00007009	0.5124	0.003	0.32480	0.5116
PLS5	0.00001625	0.5767	0.000	0.30704	0.4951

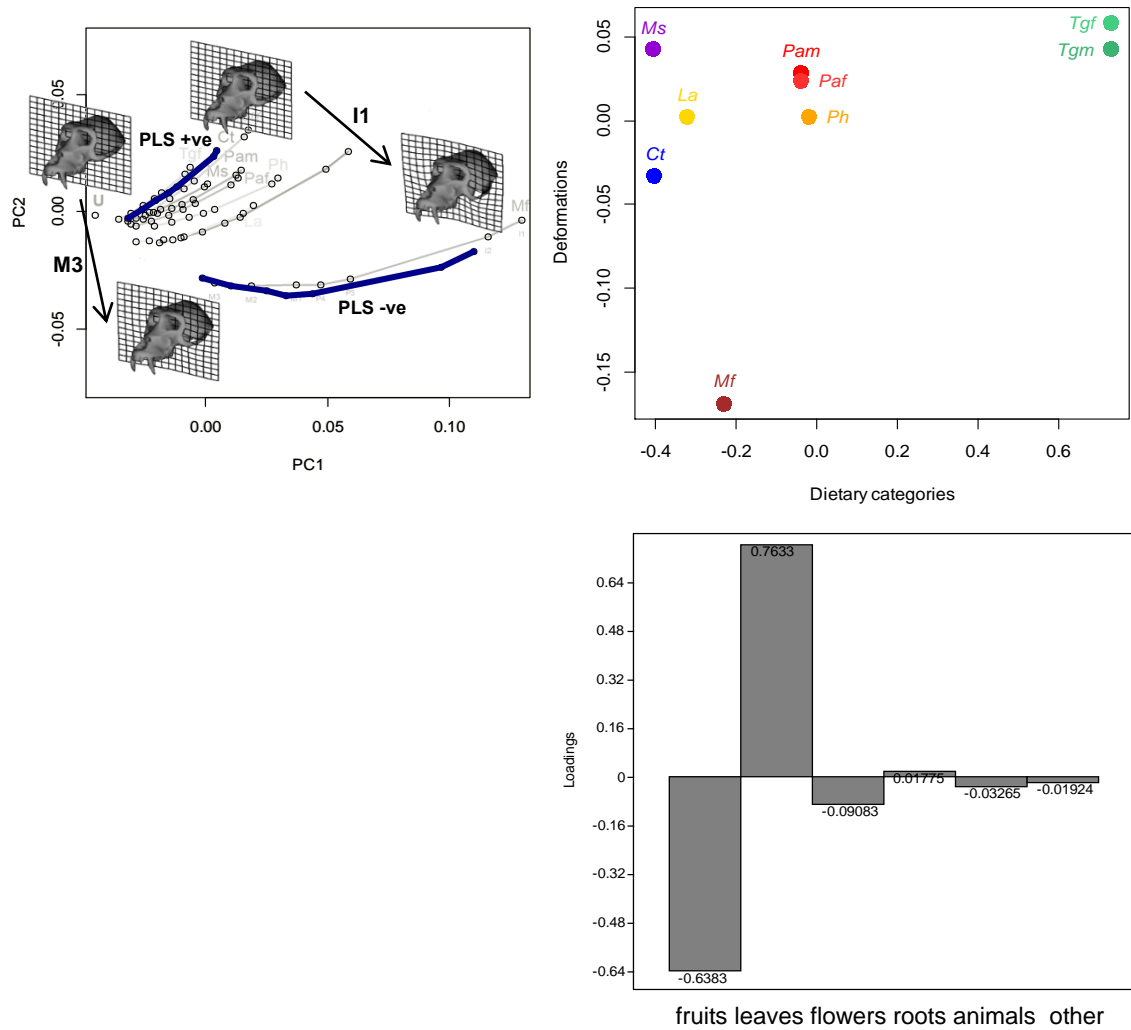


Figure 8.4. PLS analysis of cranial deformations and diet. Loadings for the dietary categories and a visualization of the extremes of deformation along PLS1 (I1 and M3 bites) are also shown. Ct, blue: *Cercocebus torquatus*. La, yellow: *Lophocebus albigena*. Mf, brown: *Macaca fascicularis*. Ms, violet: *Mandrillus sphinx*. Pam, red: male *Papio anubis*. Paf, light red: female *Papio anubis*. Ph, orange: *Papio hamadryas*. Tgm, green: male *Theropithecus gelada*. Tgf, light green: female *Theropithecus gelada*.

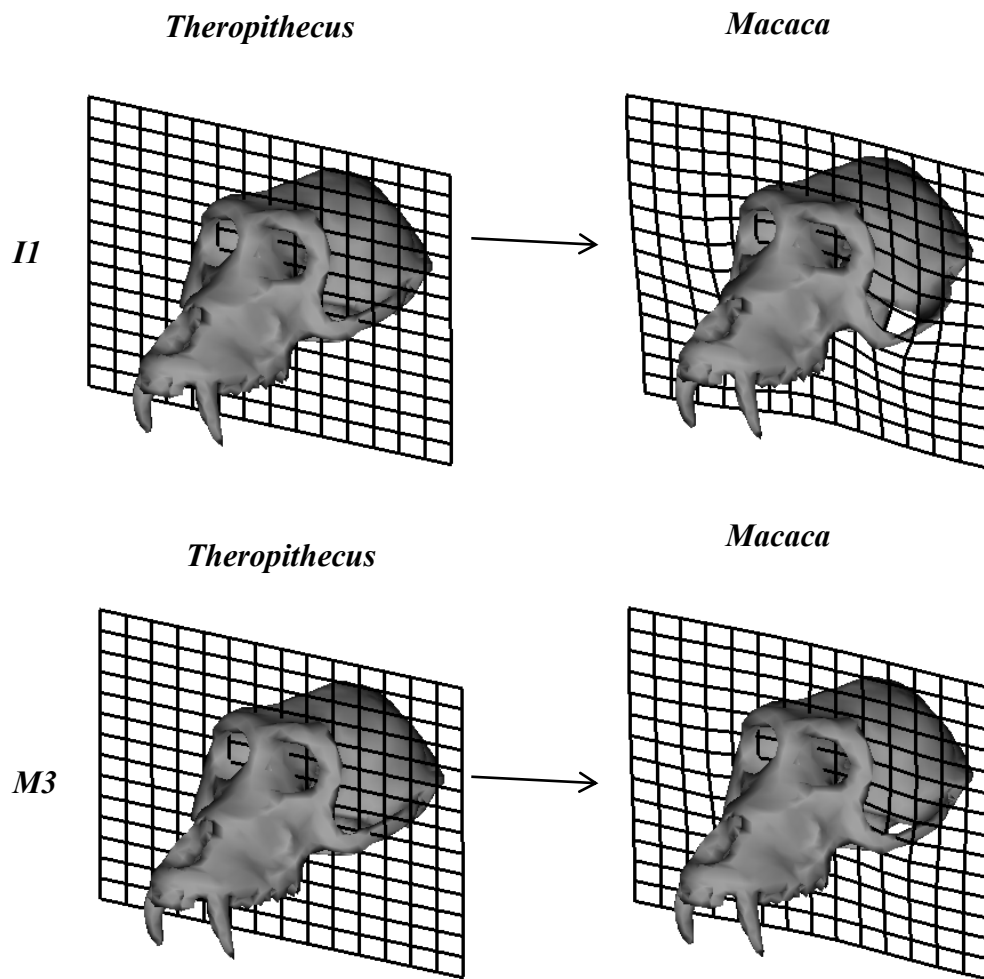


Figure 8.5. Visualization of deformations between the two extremes of deformation along PLS1. Deformation of the zygomatic arch is dominant during I1 bite, while an M3 bite makes it deform much less. Deformations magnified $\times 1000$.

8.3.4. Cranial Form *versus* Maximum Bite Force

Table 8.5 presents the singular values and pairwise correlations of PLS scores between maximum bite force and cranial form. Although the correlation for PLS2, PLS4 and PLS5 is significant, together those PLS axes describe less than 1% of the covariance between the two blocks, while the non-significant PLS1 describes 99.186%. The RV-coefficient of the PLS is 0.4547798 ($p = 0.05497457$), not quite significant for a significance level of 0.05. Figure 8.6 presents a plot of the first singular axis (PLS1) from the PLS of maximum bite force and cranial form. Loadings for the maximum bite force (from these loadings more negative scores on PLS1 from the block of bite force data indicate greater bite force) and a depiction of change in cranial form along PLS1 are also shown. The long-faced *Mandrillus* and male *Theropithecus* are at one extreme and the short-faced species are at the other. The male *Papio anubis* and *Papio hamadryas* cluster in the middle. *Mandrillus* and male *Theropithecus* have higher maximum bite forces than all other specimens, including the females of both *Papio anubis* and *Theropithecus* that cluster closer to the short-faced species with low maximum bite forces.

Table 8.5. Singular values with *P*-values, percentage of total covariance explained by each axis, and pairwise correlations of PLS scores between maximum bite force and cranial form with *P*-values. Significant *P*-values ($\alpha = 0.05$) are shown in italics and marked with *. For the whole analysis $RV = 0.4547798$, $p = 0.05497457$.

	Singular value	P-value (perm.)	% total covar.	Correlation	P-value (perm.)
PLS1	18.37787939	0.0683	99.186	0.75565	0.1979
PLS2	1.57494327	0.0744	0.728	0.95695	<i>0.0005*</i>
PLS3	0.53250333	0.2799	0.083	0.72826	0.3300
PLS4	0.07479704	0.9289	0.002	0.89223	<i>0.0317*</i>
PLS5	0.04365700	0.7424	0.001	0.95208	<i>0.0039*</i>
PLS6	0.02120313	0.9977	0.000	0.88924	0.1636
PLS7	0.00713779	0.7517	0.000	0.80546	0.3734

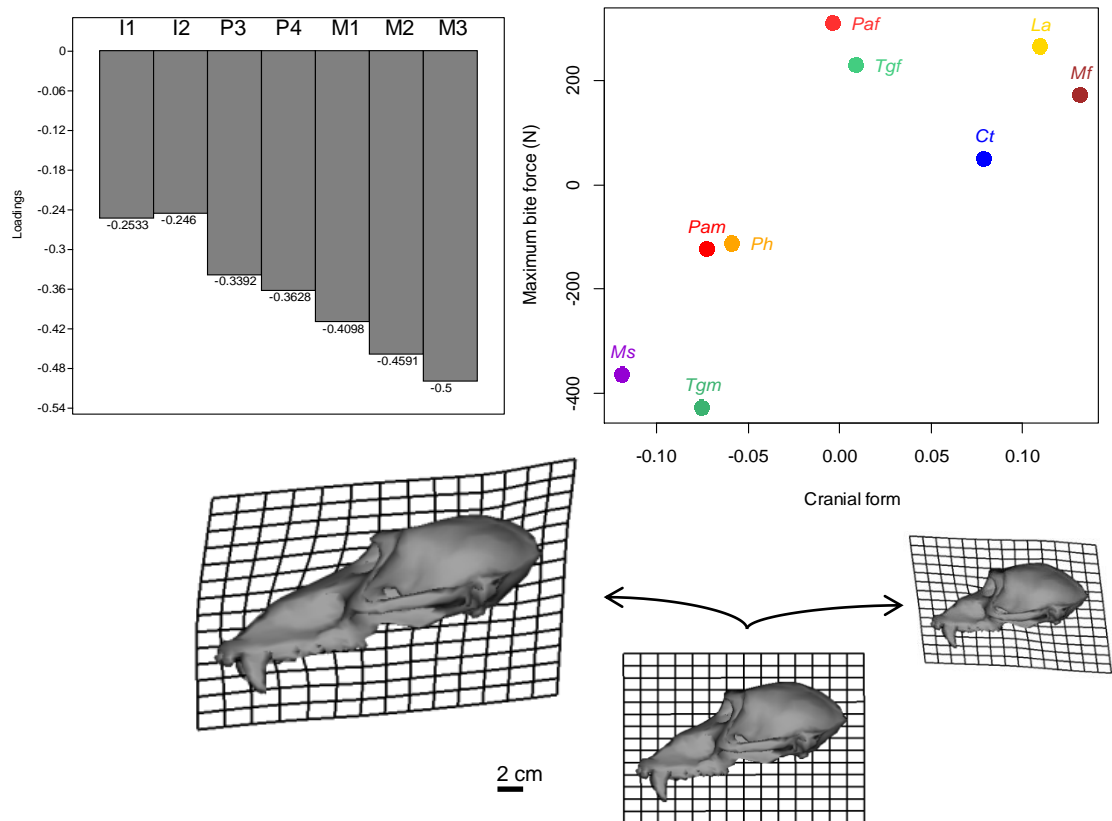


Figure 8.6. PLS analysis of maximum bite force and cranial form. Loadings for the maximum bite force and a depiction of change in cranial form along PLS1 are also shown. *Ct*, blue: *Cercocebus torquatus*. *La*, yellow: *Lophocebus albigena*. *Mf*, brown: *Macaca fascicularis*. *Ms*, violet: *Mandrillus sphinx*. *Pam*, red: male *Papio anubis*. *Paf*, light red: female *Papio anubis*. *Ph*, orange: *Papio hamadryas*. *Tgm*, green: male *Theropithecus gelada*. *Tgf*, light green: female *Theropithecus gelada*.

8.3.5. Cranial Form *versus* Cranial Deformations

Table 8.6 presents the singular values and pairwise correlations of PLS scores between cranial deformations and cranial form. No significant correlation is found for any PLS axis considered alone. However, the RV-coefficient for the whole PLS is 0.5047034 ($p = 0.0207365$), significant for a significance level of 0.05. Figure 8.7 presents a plot of the first singular axis (PLS1) from the PLS of cranial deformations and cranial form. The principal component plot of deformations (Figure 7.11) and a depiction of change in cranial form along PLS1 are also shown. The two extremes of PLS1 for cranial form show a long face corresponding to lower deformations, *versus* a short face corresponding to higher deformations. *Macaca* stands out as the most distant from the others both in cranial form and deformations. Nevertheless, the two blocks of data show a good association between them, with *Macaca* and *Mandrillus* as extremes of the covariation. In essence, large crania with long faces deform less.

Table 8.6. Singular values with P-values, percentage of total covariance explained by each axis, and pairwise correlations of PLS scores between cranial deformations and cranial form with P-values. Significant P-values ($\alpha = 0.05$) are shown in italics marked with *. For the whole analysis $RV = 0.5047034$, $p = 0.0207365$.

	Singular value	P-value (perm.)	% total covar.	Correlation	P-value (perm.)
PLS1	0.00521006	<i>0.0217*</i>	97.120	0.78451	0.1261
PLS2	0.00084623	0.4557	2.562	0.65764	0.4352
PLS3	0.00024851	0.7028	0.221	0.68888	0.3835
PLS4	0.00013482	0.7507	0.065	0.86108	0.0993
PLS5	0.00008688	0.4021	0.027	0.62277	0.8418
PLS6	0.00002813	0.7086	0.003	0.81502	0.2488
PLS7	0.00002015	0.2564	0.001	0.87718	0.1431
PLS8	0.00000788	0.9433	0.000	0.86831	0.2248

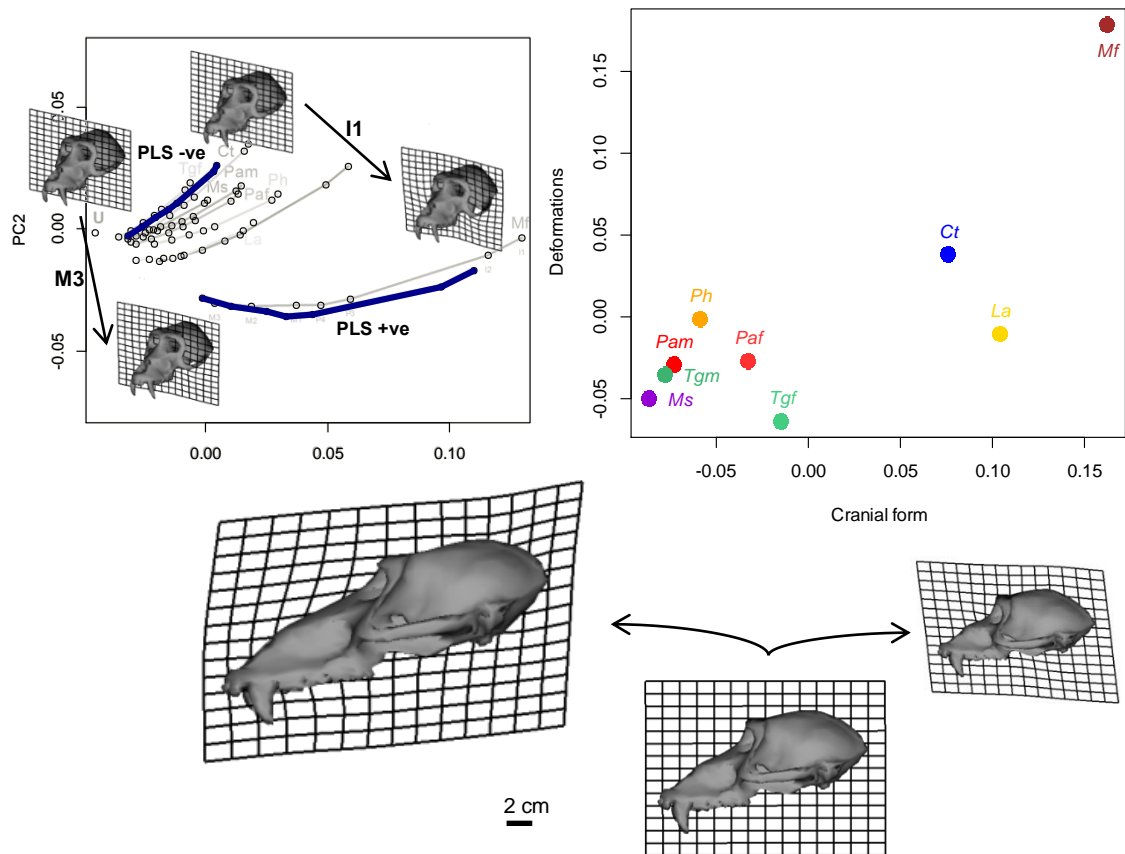


Figure 8.7. PLS analysis of cranial deformations and cranial form. A visualization of the extremes of deformation along PLS1 (I1 and M3 bites) and a depiction of change in cranial form along PLS1 are also shown. Ct, blue: *Cercocebus torquatus*. La, yellow: *Lophocebus albigena*. Mf, brown: *Macaca fascicularis*. Ms, violet: *Mandrillus sphinx*. Pam, red: male *Papio anubis*. Paf, light red: female *Papio anubis*. Ph, orange: *Papio hamadryas*. Tgm, green: male *Theropithecus gelada*. Tgf, light green: female *Theropithecus gelada*.

8.4. Discussion

This chapter tests the association among cranial form, diet, and biomechanical parameters resulting from FEA (maximum bite force and deformations under biting load), in a sample of papionin species with known diets. Results show that the best overall association (RV) is between cranial form and cranial deformations under biting, whereas the association between diet and cranial form is weaker overall but significant for the first axis of covariation (explaining 98.213% of the total covariance). The biomechanical parameters appear to be less clearly associated with diet.

The strong association (significant RV) between cranial deformations and cranial form is expected, since the relationship between function and form is universally recognized (Wolff 1991; Liem *et al.* 2001; Benton 2005; Boyd & Nigg 2006; see also Section 1.2). The strong association (significant correlation) between cranial form and diet in the first singular axis is not unexpected again because form is generally perceived as corresponding to function and masticatory function necessary to process a particular diet was expected to relate to cranial form. The striking result here is that cranial form has such an unequivocal relation to diet, although the result was not significant overall when measured by the RV-coefficient. This is probably due to small sample size. Inequivocal is that the PLSs indicate a much greater association between diet and cranial form than between diet and any of the biomechanical performance parameters. Maximum bite force and deformations under biting show a non-significant correlation with diet. Again this result might be due to the exiguous sample size used here, a problem which comes from the time-consuming nature of building finite element models (Chapter 5). It does however suggest that in studies that aim to predict diet from the cranium (such as with fossil material), form described by a set of landmarks would be a better predictor of diet than any biomechanical parameter calculated from that cranium.

The association between cranial deformations and diet, despite not being significant, point to *Macaca* (the phylogenetic outgroup) as being distinct from all other species. Although feeding on an omnivorous diet similar to *Papio* spp., *Macaca* deforms at a greater magnitude than any other papionin, possibly as a consequence of retaining ancestral traits (such as the maxillary sinus) that have an effect on the biomechanical behaviour of the cranium. A future analysis where *Macaca* is removed from the sample will perhaps show a less weak association between diet and deformations.

What became clear with these results is that these associations do not match the expected groupings if phylogeny was the only driver of cranial form and biomechanical performance. Contrary to Losos (2011) finding that the shape of the head in lizards primarily reflects phylogeny, regardless of what they eat, for example, none of the papionin analysis showed any phylogenetic signal and more readily presented differences in anatomy (length of face, robustness) than the phylogenetic relationship among species. In the analyses including maximum bite force, even males and females of the same species clustered separately, meaning that biomechanical performance in these animals is related less to phylogenetic constraints than to anatomical differences between them. A test on the association (and correlation) between biomechanical parameters and phylogeny can be performed in future when a larger sample size is available (both in number of species and in number of individuals per species) in order to better clarify the role of phylogeny on cranial biomechanical performance.

Moreover, it cannot be excluded that the dietary proportions as they were calculated might have biased the analyses towards a weak association between biomechanical parameters and dietary categories (although they appear sufficient to show a clear association with cranial form). The information about dietary categories was taken from literature describing reports of sightings in the wild which are often incomplete or even contradictory (see review in Subsection 1.3.3). Repeating the PLS analyses with an improved dietary categories matrix might shed some light on the perceived weak association between deformations and diet, even though cranial form so clearly associates with it.

Problems with estimating performance parameters from FEA, including model building issues and large scale deformation analysis, cannot be ruled out either. As seen in Chapter 6, differences in internal architecture modelling and anchoring constraints are likely to have little effect on the results of an FEA, but estimating muscle forces from ACSA can result in substantial differences in finite model performance, leading to biases in the PLS analysis. Model building problems were thoroughly discussed in Chapters 5 and 6.

In conclusion, the association between cranial form and cranial deformations is strong. However, the maximum bite force and cranial deformations under biting, as resulting from FEA, appear to associate with diet less well than does cranial form defined by a set of landmarks. Further work is therefore needed before ecological and behavioural interpretations from FEA can be made. Future studies will ideally require an extended sample and a better characterised diet.

Chapter 9. Conclusion

9.1. Summary of Key Findings

The overall, broad aim of this thesis is to move towards a greater understanding of the evolution of cranial form and its biomechanical adaptation to the function of feeding, using the papionin cranium as a system. It starts by testing the hypothesis of cranial form divergence by random genetic drift alone; if rejected, the form of each papionin cranium should reflect adaptation to the particular biomechanical demands of different dietary strategies. To study that adaptation, after model building and sensitivity analyses, hypotheses about the biomechanical performance of the cranium are then formulated in terms of the diet of each papionin species, and tested using 3D finite element models and geometric morphometrics. Lastly, the hypothesis that cranial form, maximum bite force and cranial deformations under biting load are associated with one another is also tested using multivariate statistics.

A review of principal aspects required for the understanding of the evolution of form and function of the papionin cranium was undertaken in Chapter 1. In Chapter 2, an overview of methods used in the thesis was provided. After that, the actual research questions concerning the evolution of papionin cranial form and feeding adaptations (as well as the necessary tests on the methods used) were addressed.

From Chapter 3, type I error rates in comparing genetic and phenotypic matrices are kept within acceptable ranges if particular conditions are observed. In summary (Chapter 3), replacing **G** with **W** when testing the null hypothesis of divergence by genetic drift is not likely to increase the type I error rates of the AC test, unless the ancestral **G** and **W** are structurally dissimilar (mathematical proportionality is not a required condition), the t/N_e ratio is large and sample sizes are small (< 40 per group). A Monte Carlo simulation approach might be used to estimate the expected slope of the AC test under drift, taking into account the structural differences between **G** and **P**. A number of other methods have been proposed to compare among-population and within population covariance matrices (Lofsvold 1988; Bégin & Roff 2001; Revell *et al.* 2007). Not all of these alternative methods will have increased type I error rates when average

G is replaced by **W**. Type II errors are also a possibility, as genetic drift is the alternative hypothesis in some tests (Revell *et al.* 2007). The simulation function provided as an appendix (Appendix B) can be modified to account for other methods of matrix comparison. Alternatively, model-based approaches (Butler & King 2004) should provide reliable and possibly more informative tests of evolutionary processes and scenarios. The simulation approaches, particularly the more sophisticated individual-based models (Revell 2007) should prove useful in further analyses, comparing methods and testing evolutionary quantitative genetics models.

In Chapter 4, a test on the null hypothesis of the divergence of papionin cranial forms by random genetic drift alone, supported by an established molecular phylogeny, concluded that random genetic drift was most likely not the single microevolutionary process acting on the form of the papionin cranium. Non-random processes are therefore likely to have acted, driving the form of the cranium as a response to environmental pressures including diet. The test is proved to be robust in falsifying the underlying assumptions (Prôa, O'Higgins, & Monteiro 2013; see also Chapter 3), and the results indicate that the form of the cranium of papionin species, within the Tribe Papionini, has not diverged solely neutrally from a common ancestor, with diet being possibly a selective agent driving the evolution of papionin cranial form. Interpreting these results directly as biological, though, is ill advised due to the small sample size used. Likewise this particular set of landmarks may be inaccurately describing the cranium and another, more comprehensive set, might reflect better the evolution of the papionin cranium. The inclusion of female specimens would also add to the accuracy of the analysis.

After discarding the hypothesis that the papionin cranium evolved by random genetic drift alone, biomechanical models were built to test evolutionary adaptation to diet. Chapter 5 described the steps taken in the process of building 3D finite element models of papionin crania used in subsequent chapters. It reviewed image segmentation techniques and boundary conditions of the models, described how bite force and landmarks are utilised after the model solution step of FEA, and discussed problems encountered in collecting or estimating the input parameters for such models. Low resolution of available scans, leading to difficulties in image segmentation, was dealt with by using filled, less complex models. The models were fully anchored at both sides of the jaw joint to avoid unwanted rigid body motion. Muscle forces were estimated from bony proxies and applied consistently among models. Nevertheless, to test the feasibility of these models building decisions, sensitivity analyses were undertaken.

In Chapter 6, three tests on the effect that model building decisions might have on FEA results concluded that varying the internal architecture has a minimal effect; that incomplete anchoring in the jaw joint reduces deformations by creating a rotation movement around the single fully constrained fulcrum; and that muscle force input has a large effect on FEA results, but nevertheless deformations differences among models are bigger than differences among load cases of the same model thus making a reasonable comparison among models viable.

That established, the models were used in Chapter 7 to perform comparative analyses of strains and deformations between species, testing hypotheses of dietary differences among papionins. In all models incisor bite results in higher strains and deformations of the cranium, decreasing progressively when the load arm length decreases along the dental row, reaching lower values when biting on M3. The durophagous *Mandrillus* deforms less than *Lophocebus* and *Cercocebus*, other durophagous species, which can be explained by the larger size and overall robustness of *Mandrillus* and also by its paranasal ridges and enlarged sagittal crest that stiffen the cranium. Durophagous *Lophocebus* and *Cercocebus* deform similarly, with only differences in magnitude of deformations. These differences suggest that *Cercocebus* is less able to resist biting forces than *Lophocebus* despite being of slightly greater size (cranial length; although note it has very similar skeletal volume to *Lophocebus*; Table 7.1). There are clear differences between the two omnivorous *Papio* spp. and the graminivorous *Theropithecus*. Male and female crania of the same species tend to perform similarly to each other and differently from other species. There are also clear differences in strains and deformations between the two dietary extremes, durophagous and graminivorous, each with particular adaptations in the cranium that can be seen in the biomechanical performance of the cranium. The cranium of the omnivorous outgroup of papionins, *Macaca*, performs differently from all other species, which can be interpreted as being due to its retaining of ancestral traits that are important mechanically, such as the maxillary sinus.

Lastly, Chapter 8 attempted the understanding of the association between diet and cranial form, maximum bite force and cranial deformations under biting load, and between cranial form and the two biomechanical performance parameters. Results show that the statistically significant association is between cranial form and cranial deformations, with a strong correlation between diet and cranial form along the first singular axis of a PLS analysis. Bite force and deformations show a much less clear association with diet but point to *Macaca* and *Theropithecus* as being distinct from all

other species, a pattern that does not match the expected groupings if phylogeny were the only driver of cranial form and biomechanical performance.

9.2. Implications for Future Research

Future research on the evolution of the papionin cranium and its adaptation to diet and feeding habits should address both biological and methodological questions. Quantitative genetic models (like the model used here in Chapters 3 and 4) are a commonly used approach to study the effect of microevolutionary processes (such as natural selection or random genetic drift) on macroevolutionary patterns (such as cranial form evolution) (*e.g.* Perez & Monteiro 2009). For biomechanical studies it has been suggested that complex models (like finite element models) should be used instead of simple geometric models of the cranium when testing hypotheses of about craniofacial biomechanics and diet (Chalk *et al.* 2011).

In evolutionary studies, the approach taken in Chapter 4 of working under the assumption of neutral evolution is a good starting point, but future research in species evolution (divergence) by means of natural selection, using landmark, biomechanical or other data, are perhaps better tackled under the quantitative genetic framework known as the Hansen model (Hansen 1997; Butler & King 2004) or using an individual-based model (Revell 2007), rather than under a purely neutral model of divergence by random genetic drift. Moreover, combining these form and function studies with phylogenetic comparative methods is starting to be a more utilized approach (Monteiro 2013), and might provide a more complete approach to future studies of form and function under an evolutionary approach.

In terms of the technical use of FEA in further studies that focus on comparing species, they would benefit enormously from preliminary studies of intra-specific variation. A comparison between models of specimens of the same species would enlighten greatly their comparative biomechanical behaviour, particularly from an evolutionary point of view. The differences found among specimens of the same species might be similar to the differences found among specimens of different species, thus blurring the interpretation of FEA results altogether. This said, ongoing related work in humans by close colleagues shows considerable similarity of strain contour maps within

humans (M. V. Toro-Ibacache, pers. comm.). As suggested already in Chapters 7 and 8, repeating these FEAs and deformations analyses with an enlarged sample size would greatly increase the ability to make more robust interpretations, particularly when those interpretations are evolutionary.

Furthermore, in building finite element models gathering data from real specimens, such as bite force from *in vivo* experiments and real muscle PCSA, is a further step to increase the complexity and accuracy of these finite element models and so, the robustness of the analysis of deformations under loading. Increasing the complexity of the 3D models which could involve segmenting teeth (Benazzi *et al.* 2012), periodontal ligament (Panagiotopoulou *et al.* 2011; Gröning *et al.* 2011), lateral pterygoid muscle (Osborn 1995; Sellers & Crompton 2004), including the temporal fascia (Curtis *et al.* 2011), and even including the mandible (Marinescu *et al.* 2005; Wroe *et al.* 2010) is definitely a path to follow. In future research, rescanning the specimens in the same CT scanner (microCT scanner preferentially) to bypass differences in CT resolution would also be a sensible course of action.

Questions about size need also be taken into account in further analyses of deformations, for example, an analysis of the relationship between deformations and size by performing a regression of the principal component scores of deformations against centroid size. If it is found that there is a significant relationship between deformations and size, further analyses related to scaling can then be considered. Scaling can be done in several ways, one of them is scaling of muscle forces to the same bite forces, but muscle forces could be scaled according to cranium length (to the square of cranium length, because as length increases, muscle cross-sectional area increases by the square). This is all about what aspects of performance are of interest and these will vary from study to study, questions and analyses should be focused on the questions under study. Some consideration needs to be given in future work to what different scalings mean in terms of performance comparisons, what is being compared and whether this is appropriate to the biological question at hand.

Future developments could also include looking in detail at particular regions, such as the zygomatic arch. Deformation of the zygomatic arch seems to dominate the analysis of deformations under this modelling approach, but that might not be the case when the temporal fascia is taken into account in model building to counterbalance the force of the masseter muscle during biting (Curtis *et al.* 2011). Thus, removing from the analysis the raw landmarks placed on the zygomatic arches shows a rather different picture of cranial deformations among these animals (Figure 9.1). Also focusing more

on the subtle changes in the face that are more likely related to diet is desirable, such as specific bites or degree of prognathism (which is related to gape, Fitton 2007), rather than considering the whole cranium.

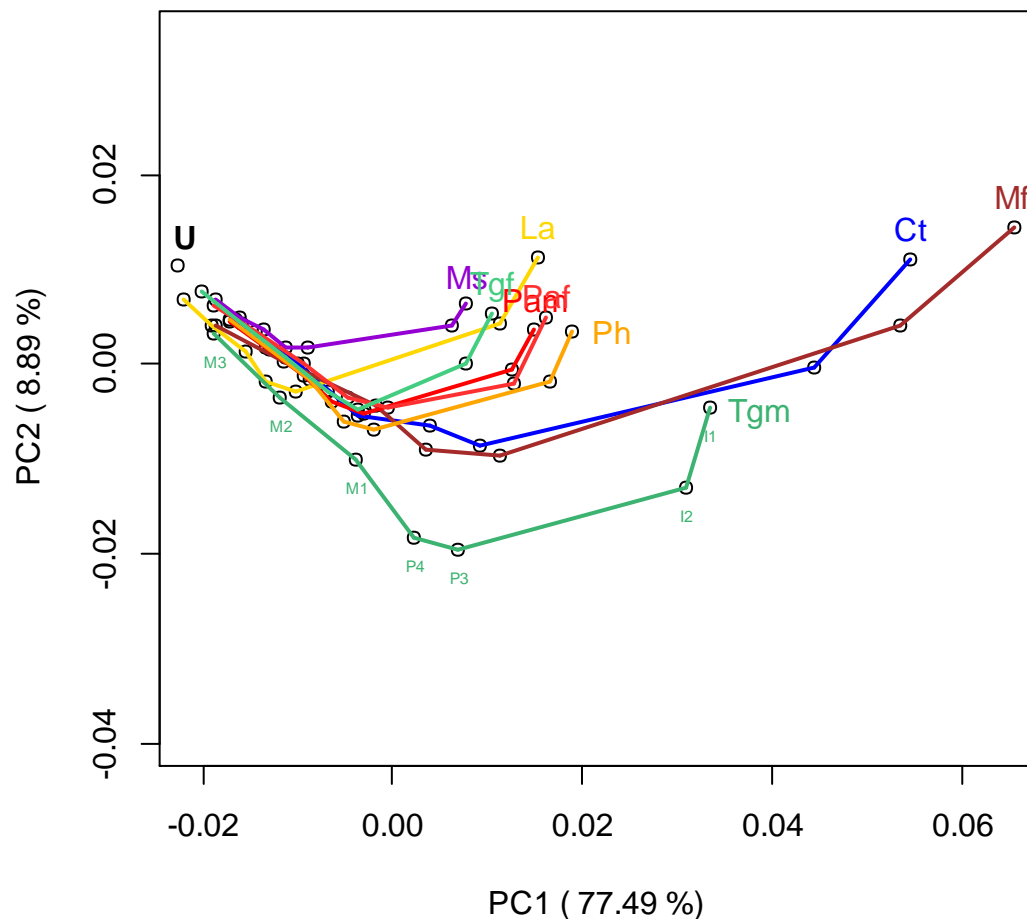


Figure 9.1. Cranial deformations excluding landmarks on the zygomatic arch of the whole sample visualized using a preliminary PCA of size-and-shape variables. Lines denote the deformations arising from bites in a single specimen at different points along the left dental row, first incisor (I1), second incisor (I2), first premolar (P3), second premolar (P4), first molar (M1), second molar (M2), and third molar (M3). Ct, blue: *Cercocebus torquatus*. La, yellow: *Lophocebus albigena*. Mf, brown: *Macaca fascicularis*. Ms, violet: *Mandrillus sphinx*. Pam, red: male *Papio anubis*. Paf, light red: female *Papio anubis*. Ph, orange: *Papio hamadryas*. Tgm, green: male *Theropithecus gelada*. Tgf, light green: female *Theropithecus gelada*. The isolated point marked U represents the undeformed mean of all models.

Results in Chapter 7 showed that the cranium of *Macaca* appears to be less adapted to feeding on hard foods and, thus, have not have cranial form selected for that particular feeding strategy. Further testing is thus possible under the scenario of divergence of the papionins (excluding *Macaca*) from a *Macaca*-like ancestor towards a more durophagous diet, with the loss of maxillary sinus and the face stiffening in response to that shift in diet. Later evolution related to social systems and adaptation to diverse diets may have then underpinned the diversification of the group into the extant species (genera).

Apparent from the results of Chapter 8 is the usefulness of using form to predict ecological context, especially diet. Form appears to be more useful than biomechanical, functional parameters in this regard. With a sufficiently large sample, analyses of form seem to be a direct and clear method to make behavioural inferences rather than “functional signals,” at least when the “functional signal” arises from FEA. Biomechanical adaptation occurs as a consequence of changes in form, and form is driven by several and diverse factors. Thus, skeletal form is perceived as a compromise between mechanics and other influences (Ruff *et al.* 2006). It is clear from the results of this thesis that further work is needed before ecological and behavioural interpretations from FEA can be made with any reliability. The findings of Chapter 7 provide tantalising clues as to how FEA might be informative about diet, thus detailed comparisons of particular species and focal areas of deformation do seem to yield important information about diet. Consequently, other than an extended sample size, future FEA studies of this kind will require a more detailed approach to modelling crania, and the scaling considerations mentioned above, as well as better characterised dietary categories as well.

Nevertheless, the application of FEA and analysis of global deformations to fossils is a promising avenue that requires much more development. In fossils, often form is the only biological trait preserved and inferences of dietary behaviour directly from form are very common (*e.g.* Kay 1981; Strait *et al.* 2007; and even Grine *et al.* 2012). The reliability of those inferences, though, are unknown at present and the only way to make them is by analogy with the form of extant organisms with known diets. Assumptions on which functional interpretations of fossils from FEA are based had not been tested with extant species until this thesis. Only through a more thorough understanding of the mechanical demands that different diets place on the masticatory system of extant species, and of the behavioural strategies that extant species employ to mitigate those demands, can inferences be made regarding fossil species. “The logical

and statistical basis for inference about trait function in fossils is the relationship between form and function in living taxa” (Ross *et al.* 2002). The trait is studied in extant taxa to determine its function and then hypothesised to have the same function in the fossil taxon (Ross *et al.* 2002). FEA provides an alternative method to study structure-function relationships in fossil animals, even in the absence of living analogues (Ross 2005). However, more studies are needed to establish how skeletal performance in resisting loads from specific tasks (*e.g.* biting) relates to ecological parameters. The results of this thesis are certainly a precedent and a starting point for these types of studies, but indicate that much work is yet to be done in order to understand how inferences can be made from FEA.

Literature Cited

- Ackermann, R.R. & Cheverud, J.M. (2002) Discerning evolutionary processes in patterns of tamarin (genus *Saguinus*) craniofacial variation. *American Journal of Physical Anthropology*, **117**, 260–271.
- Ackermann, R.R. & Cheverud, J.M. (2004) Detecting genetic drift versus selection in human evolution. *Proceedings of the National Academy of Sciences of the United States of America*, **101**, 17946–17951.
- Adams, D.C. & Collyer, M.L. (2007) Analysis of character divergence along environmental gradients and other covariates. *Evolution*, **61**, 510–515.
- Adams, D.C. & Collyer, M.L. (2009) A general framework for the analysis of phenotypic trajectories in evolutionary studies. *Evolution*, **63**, 1143–1154.
- Adams, D.C., Rohlf, F.J. & Slice, D. (2004) Geometric morphometrics: Ten years of progress following the “revolution.” *Italian Journal of Zoology*, **71**, 5–16.
- Alberch, P. (1983) Morphological variation in the neotropical salamander genus *Bolitoglossa*. *Evolution*, **37**, 906–919.
- Aldrich-Blake, F.P., Bunn, T.K., Dunbar, R.I. & Headley, P.M. (1971) Observations on baboons, *Papio anubis*, in an arid region in Ethiopia. *Folia Primatologica*, **15**, 1–35.
- Alexander, R.M. (2005) Mechanics of animal movement. *Current Biology*, **15**, R616–R619.
- Alexander, R.M. (2006) Dinosaur biomechanics. *Proceedings of the Royal Society B Biological Sciences*, **273**, 1849–1855.
- Alexander, R.M. & Vernon, A. (1975) The dimensions of knee and ankle muscles and the forces they exert. *Journal of Human Movement Studies*, **1**, 115–123.
- Alfaro, M.E., Bolnick, D.I. & Wainwright, P.C. (2004) Evolutionary consequences of redundant design in labrid fishes. *Integrative and Comparative Biology*, **44**, 514.
- Alfaro, M.E., Bolnick, D.I. & Wainwright, P.C. (2005) Evolutionary consequences of many-to-one mapping of jaw morphology to mechanics in labrid fishes. *The American Naturalist*, **165**, E140–E154.
- Ankel-Simons, F. (2007) *Primate Anatomy: An Introduction*, 3rd ed. Academic Press, Burlington, MA.

- Antón, S.C. (1996) Tendon-associated bone features of the masticatory system in Neandertals. *Journal of Human Evolution*, **31**, 391–408.
- Antón, S.C. (1999) Macaque masseter muscle: internal architecture, fiber length and cross-sectional area. *International Journal of Primatology*, **20**, 441–462.
- Antón, S.C. (2000) Macaque pterygoid muscles: Internal architecture, fiber length, and cross-sectional area. *International Journal of Primatology*, **21**, 131–156.
- Arnold, S.J. (1983) Morphology, performance and fitness. *American Zoologist*, **23**, 347–361.
- Arnold, S.J., Bürger, R., Hohenlohe, P.A., Ajie, B.C. & Jones, A.G. (2008) Understanding the evolution and stability of the G-matrix. *Evolution*, **62**, 2451–2461.
- Arnold, S.J., Pfrender, M.E. & Jones, A.G. (2001) The adaptive landscape as a conceptual bridge between micro- and macroevolution. *Genetica*, **112-113**, 9–32.
- Ashley-Ross, M.A. & Gillis, G.B. (2002) A brief history of vertebrate functional morphology. *Integrative and Comparative Biology*, **42**, 183–189.
- Astaras, C., Krause, S., Mattner, L., Rehse, C. & Waltert, M. (2011) Associations between the drill (*Mandrillus leucophaeus*) and sympatric monkeys in Korup National Park, Cameroon. *American Journal of Primatology*, **73**, 127–134.
- Astaras, C., Mühlenberg, M. & Waltert, M. (2008) Note on drill (*Mandrillus leucophaeus*) ecology and conservation status in Korup National Park, Southwest Cameroon. *American Journal of Primatology*, **70**, 306–310.
- Baker, G., Jones, L.H. & Wardrop, I.D. (1959) Cause of wear in sheeps' teeth. *Nature*, **184**, 1583–1584.
- Barton, R.A., Byrne, R.W. & Whiten, A. (1996) Ecology, feeding competition and social structure in baboons. *Behavioral Ecology and Sociobiology*, **38**, 321–329.
- Barton, R.A. & Whiten, A. (1993) Feeding competition among female olive baboons, *Papio anubis*. *Animal Behaviour*, **46**, 777–789.
- Beer, F.P., Johnston, E.R. & DeWolf, J.T. (1992) *Mechanics of Materials*. McGraw-Hill, New York, NY.
- Bégin, M. & Roff, D.A. (2001) An analysis of G matrix variation in two closely related cricket species, *Gryllus firmus* and *G. pennsylvanicus*. *Journal of Evolutionary Biology*, **14**, 1–13.
- Bégin, M. & Roff, D.A. (2004) From micro- to macroevolution through quantitative genetic variation: positive evidence from field crickets. *Evolution*, **58**, 2287–2304.

- Bemben, D.A., Buchanan, T.D., Bemben, M.G. & Knehans, A.W. (2004) Influence of type of mechanical loading, menstrual status, and training season on bone density in young women athletes. *The Journal of Strength & Conditioning Research*, **18**, 220–226.
- Benazzi, S., Kullmer, O., Grosse, I.R. & Weber, G.W. (2012) Brief communication: comparing loading scenarios in lower first molar supporting bone structure using 3D finite element analysis. *American Journal of Physical Anthropology*, **147**, 128–134.
- Benefit, B.R. & McCrossin, M.L. (2002) The Victoriapithecidae, Cercopithecoidea. *The Primate Fossil Record* (ed W.C. Hartwig), pp. 241–253. Cambridge University Press, Cambridge.
- Benton, M.J. (2005) *Vertebrate Palaeontology*, 3rd ed. Blackwell Publishing, Malden, MA.
- Berenstain, L. (1986) Responses of long-tailed macaques to drought and fire in eastern Borneo: A preliminary report. *Biotropica*, **18**, 257–262.
- Bhatti, M.A. (2005) *Fundamental Finite Element Analysis and Applications: With Mathematica and Matlab Computations*. John Wiley & Sons, Hoboken, NJ.
- Biewener, A.A. (2005) Biomechanical consequences of scaling. *Journal of Experimental Biology*, **208**, 1665–1676.
- Bock, W.J. & von Wahlert, G. (1965) Adaptation and the form-function complex. *Evolution*, **19**, 269–299.
- Bookstein, F.L. (1989) Principal warps: Thin-plate splines and the decomposition of deformations. *IEEE Transactions on Pattern Analysis and Machine Intelligence*, **11**, 567–585.
- Bookstein, F.L. (1991a) *Morphometric Tools for Landmark Data: Geometry and Biology* (ed FL Bookstein). Cambridge University Press, Cambridge.
- Bookstein, F.L. (1991b) Thin-plate splines and the atlas problem for biomedical images. *Information Processing in Medical Imaging* (eds A.C.F. Colchester & D.J. Hawkes), pp. 326–342. Springer Verlag, Berlin.
- Bookstein, F.L. (1997) Semilandmarks in three dimensions. *Modern Morphometrics in Physical Anthropology* (ed D.E. Slice), pp. 73–98. Kluwer Academic/Plenum Publishers, New York, NY.
- Bookstein, F. (1998) Singularities as features of deformation grids. *Medical Image Computing and Computer-Assisted* (ed W.M. Wells), pp. 788–797. Springer Verlag, Berlin.

- Bookstein, F.L., Gunz, P. & Mitteroecker, P. (2005) Semilandmarks in three dimensions. *Modern Morphometrics in Physical Anthropology* (ed D.E. Slice), pp. 73–98. Kluwer Academic/Plenum Publisher, New York, NY.
- Bouvier, M. (1986a) Biomechanical scaling of mandibular dimensions in New World Monkeys. *International Journal of Primatology*, **7**, 551–567.
- Bouvier, M. (1986b) A biomechanical analysis of mandibular scaling in old world monkeys. *American Journal of Physical Anthropology*, **69**, 473–482.
- Bouvier, M. & Hylander, W.L. (1981) Effect of bone strain on cortical bone structure in macaques (*Macaca mulatta*). *Journal of Morphology*, **167**, 1–12.
- Box, G.E.P. & Draper, N.R. (1987) *Empirical Model-Building and Response Surfaces*. John Wiley & Sons, New York, NY.
- Boyd, S.K. & Nigg, B.M. (2006) Bone. *Biomechanics of the Musculo-skeletal System*, 3rd ed (eds B.M. Nigg & W. Herzog), pp. 65–94. John Wiley & Sons, Chichester.
- Bright, J.A. (2012) The importance of craniofacial sutures in biomechanical finite element models of the domestic pig. *PLoS ONE*, **7**, e31769.
- Bromage, T.G. (1986) *A Comparative Scanning Electron Microscope Study of Facial Growth and Remodeling in Early Hominids*. Unpublished PhD thesis. University of Toronto.
- Bromage, T.G. & Boyde, A. (2008) Bone growth remodeling of the early human face. *Essentials of Facial Growth* (eds D.H. Enlow & M. Hans), pp. 319–342. W B Saunders Co., New York, NY.
- Bucinell, R.B., Daegling, D.J., McGraw, W.S. & Rapoff, A.J. (2010) Full-field characterization of wishboning strain in the colobine mandibular symphysis. *The Anatomical Record (Hoboken, N.J. : 2007)*, **293**, 549–556.
- Buckland-Wright, J.C. (1978) Bone structure and the patterns of force transmission in the cat skull (*Felis catus*). *Journal of Morphology*, **155**, 35–61.
- Bull, J.J., Heineman, R.H. & Wilke, C.O. (2011) The phenotype-fitness map in experimental evolution of phages. *PLoS ONE*, **6**, e27796.
- Bumrerraj, S. & Katz, J.L. (2001) Scanning acoustic microscopy study of human cortical and trabecular bone. *Annals of Biomedical Engineering*, **29**, 1034–1042.
- Burr, D.B., Milgrom, C., Fyhrie, D., Forwood, M., Nyska, M., Finestone, A., Hoshaw, S., Saiag, E. & Simkin, A. (1996) In-vivo measurement of human tibial strains during vigorous activity. *Bone*, **18**, 405–410.
- Butler, M.A. & King, A.A. (2004) Phylogenetic comparative analysis: A modeling approach for adaptive evolution. *The American Naturalist*, **164**, 683–695.

- Cachel, S. (2006) *Primate and Human Evolution*. Cambridge University Press, Cambridge.
- Cardini, A. & Elton, S. (2008) Does the skull carry a phylogenetic signal? Evolution and modularity in the guenons. *Biological Journal of the Linnean Society*, **93**, 813–834.
- Cardini, A., Jansson, A.-U. & Elton, S. (2007) A geometric morphometric approach to the study of ecogeographical and clinal variation in vervet monkeys. *Journal of Biogeography*, **34**, 1663–1678.
- Carroll, J.D., Green, P.E. & Chaturvedi, A. (1997) *Mathematical Tools for Applied Multivariate Analysis*. Academic Press, San Diego, CA.
- Chalk, J., Richmond, B.G., Ross, C.F., Strait, D.S., Wright, B.W., Spencer, M.A., Wang, Q. & Dechow, P.C. (2011) A finite element analysis of masticatory stress hypotheses. *American Journal of Physical Anthropology*, **145**, 1–10.
- Cheverud, J.M. (1982) Relationships among ontogenetic, static, and evolutionary allometry. *American Journal of Physical Anthropology*, **59**, 139–149.
- Cheverud, J.M. (1988) A comparison of genetic and phenotypic correlations. *Evolution*, **42**, 958–968.
- Cheverud, J.M. & Marroig, G. (2007) Comparing covariance matrices: Random skewers method compared to the common principal components model. *American Journal of Physical Anthropology*, **30**, 461–469.
- Christiansen, P. & Adolfssen, J.S. (2005) Bite forces, canine strength and skull allometry in carnivores (Mammalia, Carnivora). *Journal of Zoology*, **266**, 133–151.
- Christiansen, P. & Wroe, S. (2007) Bite forces and evolutionary adaptations to feeding ecology in Carnivores. *Ecology*, **88**, 347–358.
- Chun, Y.J., Collyer, M.L., Moloney, K.A. & Nason, J.D. (2007) Phenotypic plasticity of native vs. invasive purple loosestrife: A two-state multivariate approach. *Ecology*, **88**, 1499–1512.
- Claude, J. (2008) *Morphometrics with R* (eds R Gentleman, K Hornik, and G Parmigiani). Springer, Berlin.
- Collyer, M.L. & Adams, D.C. (2007) Analysis of two-state multivariate phenotypic change in ecological studies. *Ecology*, **88**, 683–692.
- Conner, J.K. & Hartl, D.L. (2004) *A Primer of Ecological Genetics*. Sinauer Associates, Sunderland, MA.

- Corlett, R.T. & Lucas, P.W. (1990) Alternative seed-handling strategies in primates: seed-spitting by long-tailed macaques (*Macaca fascicularis*). *Oecologia Berl*, **82**, 166–171.
- Cowgill, L.W., Eleazer, C.D., Auerbach, B.M., Temple, D.H. & Okazaki, K. (2012) Developmental variation in ecogeographic body proportions. *American Journal of Physical Anthropology*, **148**, 557–570.
- Cowlshaw, G. (1997) Trade-offs between foraging and predation risk determine habitat use in a desert baboon population. *Animal Behaviour*, **53**, 667–686.
- Cox, P.G., Fagan, M.J., Rayfield, E.J. & Jeffery, N. (2011) Finite element modelling of squirrel, guinea pig and rat skulls: Using geometric morphometrics to assess sensitivity. *Journal of Anatomy*, **219**, 696–709.
- Cox, P.G., Rayfield, E.J., Fagan, M.J., Herrel, A., Pataky, T.C. & Jeffery, N. (2012) Functional evolution of the feeding system in rodents (ed A Goswami). *PLoS ONE*, **7**, e36299.
- Currey, J.D. (2002) *Bones: Structure and Mechanics*. Princeton University Press, Princeton, NJ.
- Curtis, N., Kupczik, K., O'higgins, P., Moazen, M. & Fagan, M. (2008) Predicting skull loading: Applying multibody dynamics analysis to a macaque skull. *The Anatomical Record*, **291**, 491–501.
- Curtis, N., Witzel, U., Fitton, L.C., O'Higgins, P. & Fagan, M. (2011) The mechanical significance of the temporal fasciae in *Macaca fascicularis*: An investigation using finite element analysis. *The Anatomical Record*, **294**, 1178–1190.
- Cypher, B.L., Murdoch, J.D. & Ralls, K. (2004) Two observations of tree climbing by the San Joaquin kit fox. *The Southwestern Naturalist*, **49**, 522–523.
- Daegling, D.J. (1992) Mandibular morphology and diet in the genus *Cebus*. *International Journal of Primatology*, **13**, 545–570.
- Daegling, D.J., Granatosky, M.C., McGraw, W.S. & Rapoff, A.J. (2011) Reduced stiffness of alveolar bone in the colobine mandible. *American Journal of Physical Anthropology*, **144**, 421–431.
- Dalsky, G.P., Stocke, K.S., Ehsani, A.A., Slatopolsky, E., Lee, W.C. & Birge, S.J. (1988) Weight-bearing exercise training and lumbar bone mineral content in postmenopausal women. *Annals of Internal Medicine*, **108**, 824–828.
- Darwin, C. (1859) *On the Origin of the Species*. John Murray, London.
- Davenport, T.R.B., Stanley, W.T., Sargis, E.J., De Luca, D.W., Mpunga, N.E., Machaga, S.J. & Olson, L.E. (2006) A new genus of African monkey,

- Rungwecebus*: Morphology, ecology, and molecular phylogenetics. *Science*, **312**, 1378–1381.
- Dechow, P.C. & Carlson, D.S. (1990) Occlusal force and craniofacial biomechanics during growth in rhesus monkeys. *American Journal of Physical Anthropology*, **83**, 219–237.
- Delson, E. (1975) Evolutionary history of the Cercopithecidae. *Contributions to Primatology*, **5**, 167–217.
- Delson, E. (1993) The fossils from Africa and India and the taxonomy of the genus. *Theropithecus: The Rise and Fall of a Primate Genus* (ed N. Jablonski), pp. 157–190. Cambridge University Press, Cambridge.
- Demes, B. & Creel, N. (1988) Bite force, diet, and cranial morphology of fossil hominids. *Journal of Human Evolution*, **17**, 657–670.
- DeWitt, T.J. (1996) *Functional Tradeoffs and Phenotypic Plasticity in the Freshwater Snail Physa*. Binghamton University, Vestal, NY.
- DeWitt, T.J. (1998) Costs and limits of phenotypic plasticity: Tests with predator-induced morphology and life history in a freshwater snail. *Journal of Evolutionary Biology*, **11**, 465–480.
- Dial, K.P., Goslow Jr., G.E. & Jenkins Jr., F.A. (1991) The functional anatomy of the shoulder in the European starling (*Sturnus vulgaris*). *Journal of Morphology*, **207**, 327–344.
- Diogo, R. & Abdala, V. (2010) *Muscles of Vertebrates: Comparative Anatomy, Evolution, Homologies and Development*. Science Publishers, Enfield, NH.
- Disotell, T.R. (1994) Generic level relationships of the Papionini (Cercopithecoidea). *American Journal of Physical Anthropology*, **94**, 47–57.
- Disotell, T.R. (1996) The phylogeny of Old World monkeys. *Evolutionary Anthropology: Issues, News, and Reviews*, **5**, 18–24.
- Disotell, T.R., Honeycutt, R.L. & Ruvolo, M. (1992) Mitochondrial DNA phylogeny of the Old-World monkey tribe Papionini. *Molecular Biology and Evolution*, **9**, 1–13.
- Dochtermann, N.A. (2011) Testing cheverud's conjecture for behavioral correlations and behavioral syndromes. *Evolution*, **65**, 1814–1820.
- Dominy, N.J., Grubb, P.J., Jackson, R. V, Lucas, P.W., Metcalfe, D.J., Svenning, J.-C. & Turner, I.M. (2008) In tropical lowland rain forests monocots have tougher leaves than dicots, and include a new kind of tough leaf. *Annals of Botany*, **101**, 1363–1377.

- Dryden, I.L. (1989) *The Statistical Analysis of Shape Data*. Unpublished PhD thesis. University of Leeds.
- Dryden, I.L. & Mardia, K. V. (1998) *Statistical Shape Analysis*. John Wiley & Sons, Chichester.
- Dullemeijer, P. (1980) Functional morphology and evolutionary biology. *Acta Biotheoretica*, **29**, 151–250.
- Dumont, E.R. (1997) Cranial shape in fruit, nectar, and exudate feeders: Implications for interpreting the fossil record. *American Journal of Physical Anthropology*, **102**, 187–202.
- Dumont, E.R., Davis, J.L., Grosse, I.R. & Burrows, A.M. (2011) Finite element analysis of performance in the skulls of marmosets and tamarins. *Journal of Anatomy*, **218**, 151–162.
- Dunbar, R.I. & Dunbar, E.P. (1974a) Ecological relations and niche separation between sympatric terrestrial primates in Ethiopia. *Folia Primatologica*, **21**, 36–60.
- Dunbar, R.I. & Dunbar, E.P. (1974b) On hybridization between *Theropithecus gelada* and *Papio anubis* in the wild. *Journal of Human Evolution*, **3**, 187–192.
- Dunn, J. (2011) *A Comparison of the Subspecific Divergence of Two Sympatric African Monkeys, Papio Hamadryas & Chlorocebus Aethiops: Morphology, Environment, Diet & Phylogeny*. Unpublished PhD thesis. The University of Hull and The University of York.
- Dunn, G.F., Hack, G.D., Robinson, W.L. & Koritzer, R.T. (1996) Anatomical observation of a craniomandibular muscle originating from the skull base: The sphenomandibularis. *Cranio - The Journal of Craniomandibular Practice*, **14**, 97–103; discussion 104–105.
- Ellis, J.L., Thomason, J.J., Kebreab, E. & France, J. (2008) Calibration of estimated biting forces in domestic canids: Comparison of post-mortem and in vivo measurements. *Journal of Anatomy*, **212**, 769–780.
- Endo, B. (1966) Experimental studies on the mechanical significance of the form of the human facial skeleton. *Japanese Faculty of Sciences University of Tokyo Section 5*, **3**, 1–106.
- Endo, B. (1970) Analysis of stresses around the orbits due to masseter and temporalis muscles respectively. *Journal of the Anthropological Society of Nippon*, **78**, 569–573.
- Escoufier, Y. (1973) La dépendance de deux aléas vectoriels critères et visualisation. *Revue de statistique appliquée*, **21**, 5–16.

- Ethier, C.R. & Simmons, C.A. (2007) *Introductory Biomechanics: From Cells to Organisms*. Cambridge University Press, Cambridge.
- Evans, H.E. & de Lahunta, A. (2010) *Guide to the Dissection of the Dog*, 7th ed. Saunders Elsevier, St Louis, MO.
- Fagan, M.J. (1992) *Finite Element Analysis*. Pearson Prentice Hall, Harlow.
- Fagan, M.J., Curtis, N., Dobson, C.A., Kupczik, K., Moazen, M., Page, L., Phillips, R. & O'Higgins, P. (2007) Voxel-based finite element analysis—working directly with microCT scan data. *Journal of Morphology*, **268**, 1071.
- Fajardo, R.J., Ryan, T.M. & Kappelman, J. (2002) Assessing the accuracy of high-resolution X-ray computed tomography of primate trabecular bone by comparisons with histological sections. *American Journal of Physical Anthropology*, **118**, 1–10.
- Falconer, D.S. & Mackay, T.F.C. (1996) *Introduction to Quantitative Genetics*, 4th ed. Pearson Prentice Hall, Harlow.
- Faulkner, J.A. (2003) Terminology for contractions of muscles during shortening, while isometric, and during lengthening. *Journal of Applied Physiology*, **95**, 455–459.
- Felsenstein, J. (1985) Confidence limits on phylogenies: an approach using the bootstrap. *Evolution*, **39**, 783–791.
- Felsenstein, J. (1988) Phylogenies and quantitative characters. *Annual Review of Ecology and Systematics*, **19**, 445–471.
- Fernandez-Duque, E. (2011) Rensch's rule, Bergmann's effect and adult sexual dimorphism in wild monogamous owl monkeys (*Aotus azarai*) of Argentina. *American Journal of Physical Anthropology*, **146**, 38–48.
- Fisher, R.A. (1918) The correlation between relatives on the supposition of Mendelian inheritance. *Transactions of the Royal Society of Edinburgh*, **52**, 399–433.
- Fitton, L.C. (2007) *Form-Function Complex of the Primate Masticatory Apparatus. An Investigation into the Form-Function Complex of the Cercopithecinae Masticatory Apparatus Using Computer Modelling*. Unpublished PhD thesis. University of Liverpool.
- Fitton, L.C., Shi, J.F., Fagan, M.J. & O'Higgins, P. (2012) Masticatory loadings and cranial deformation in *Macaca fascicularis*: A finite element analysis sensitivity study. *Journal of Anatomy*, **221**, 55–68.
- Fitton L.C., Shi J.F., Fagan M.J. & O'Higgins P. Skull mechanics and masticatory function in two Cercopithecine species *Cercocebus torquatus* and *Macaca fascicularis*. In preparation.

- Fleagle, J.G. (1999) *Primate Adaptation and Evolution*, 2nd ed. Elsevier Academic Press, San Diego, CA.
- Fleagle, J.G. & McGraw, W.S. (1999) Skeletal and dental morphology supports diphyletic origin of baboons and mandrills. *Proceedings of the National Academy of Sciences of the United States of America*, **96**, 1157–61.
- Fleagle, J.G. & McGraw, W.S. (2002) Skeletal and dental morphology of African papionins: Unmasking a cryptic clade. *Journal of Human Evolution*, **42**, 267–92.
- Foley, R.A. (1993) African terrestrial primates: The comparative evolutionary biology of *Theropithecus* and the Hominidae. *Theropithecus: The Rise and Fall of a Primate Genus* (ed N.G. Jablonski), pp. 245–270. Cambridge University Press, Cambridge.
- Forwood, M.R. & Burr, D.B. (1993) Physical activity and bone mass: Exercises in futility? *Bone and Mineral*, **21**, 89–112.
- Friedlander, A.L., Genant, H.K., Sadowsky, S., Byl, N.N. & Glüer, C.C. (1995) A two-year program of aerobics and weight training enhances bone mineral density of young women. *Journal of Bone and Mineral Research*, **10**, 574–585.
- Frost, H.M. (1964) *The Laws of Bone Structure*. C.C. Thomas, Springfield, IL.
- Frost, H.M. (1987) Bone “mass” and the “mechanostat”: A proposal. *The Anatomical Record*, **219**, 1–9.
- Frost, S.R., Marcus, L.F., Bookstein, F.L., Reddy, D.P. & Delson, E. (2003) Cranial allometry, phylogeography, and systematics of large-bodied papionins (primates: Cercopithecinae) inferred from geometric morphometric analysis of landmark data. *The Anatomical Record Part A: Discoveries in Molecular, Cellular, and Evolutionary Biology*, **275**, 1048–1072.
- Futuyma, D. (2009) *Evolution*. Sinauer Associates, Sunderland, MA.
- Galilei, G. (1638) *Discorsi e Dimonstrazioni Matematiche, Intorno à Due Nuoue Scienze*. Lodewijk Elzevir, Leiden.
- Gartlan, J.S. & Struhsaker, T.T. (1972) Polyspecific associations and niche separation of rain-forest anthropoids in Cameroon, West Africa. *Journal of Zoology*, **168**, 221–266.
- Gilbert, C.C. (2007) Craniomandibular morphology supporting the diphyletic origin of mangabeys and a new genus of the *Cercocebus/Mandrillus* clade, *Procercocebus*. *Journal of Human Evolution*, **53**, 69–102.
- Gilbert, C. (2008) *African Papionin Phylogenetic History and Plio-Pleistocene Biogeography*. Unpublished PhD thesis. Stony Brook University.

- Gillespie, J.H. (2004) *Population Genetics: A Concise Guide*. The Johns Hopkins University Press, Baltimore, MD.
- Gong, J.K., Arnold, J.S. & Cohn, S.H. (1964) Composition of trabecular and cortical bone. *The Anatomical Record*, **149**, 325–331.
- Goodall, C. (1991) Procrustes methods in the statistical analysis of shape. *Journal of the Royal Statistical Society Series B Methodological*, **53**, 285–339.
- Goodman, M., Porter, C.A., Czelusniak, J., Page, S.L., Schneider, H., Shoshani, J., Gunnell, G. & Groves, C.P. (1998) Toward a phylogenetic classification of Primates based on DNA evidence complemented by fossil evidence. *Molecular Phylogenetics and Evolution*, **9**, 585–598.
- Goodwin, B. (1994) *How the Leopard Changed Its Spots : The Evolution of Complexity*. Princeton University Press, Princeton, NJ.
- Gould, S.J. (1966) Allometry and size in ontogeny and phylogeny. *Biological Reviews*, **41**, 587–640.
- Gould, S.J. (2002) *The Structure of Evolutionary Theory*. Belknap Press of Harvard University Press, Cambridge, MA.
- Gould, S.J. & Lewontin, R.C. (1979) The spandrels of San Marco and the Panglossian paradigm: A critique of the adaptationist programme. *Proceedings of the Royal Society B Biological Sciences*, **205**, 581–98.
- Greaves, W.S. (1985) The mammalian postorbital bar as a torsion-resisting helical strut. *Journal of Zoology Series A*, **207**, 125–136.
- Greaves, W.S. (1995) Functional predictions from theoretical models of the skull and jaws in reptiles and mammals. *Functional Morphology in Vertebrate Paleontology* (ed J.J. Thomason), pp. 99–115. Press Syndicate of the University of Cambridge, Cambridge.
- Greaves, W.S. (2009) The jaw lever system in ungulates: a new model. *Journal of Zoology*, **184**, 271–285.
- Greene, H.W. (1986) Natural history and evolutionary biology. *Predator-prey relationships: perspectives and approaches from the study of lower vertebrates* (eds M.E. Feder & G. V. Lauder), pp. 99–108. University of Chicago Press, Chicago, IL.
- Grine, F.E., Judex, S., Daegling, D.J., Ozcivici, E., Ungar, P.S., Teaford, M.F., Sponheimer, M., Scott, J., Scott, R.S. & Walker, A. (2010) Craniofacial biomechanics and functional and dietary inferences in hominin paleontology. *Journal of Human Evolution*, **58**, 293–308.

- Grine, F.E., Sponheimer, M., Ungar, P.S., Lee-Thorp, J. & Teaford, M.F. (2012) Dental microwear and stable isotopes inform the paleoecology of extinct hominins. *American Journal of Physical Anthropology*, **148**, 285–317.
- Griswold, C.K., Logsdon, B. & Gomulkiewicz, R. (2007) Neutral evolution of multiple quantitative characters: A genealogical approach. *Genetics*, **176**, 455–66.
- Gröning, F., Fagan, M.J. & O’Higgins, P. (2011) The effects of the periodontal ligament on mandibular stiffness: A study combining finite element analysis and geometric morphometrics. *Journal of Biomechanics*, **44**, 1304–1312.
- Gröning, F., Liu, J., Fagan, M.J. & O’Higgins, P. (2009) Validating a voxel-based finite element model of a human mandible using digital speckle pattern interferometry. *Journal of Biomechanics*, **42**, 1224–1229.
- Groves, C.P. (1978) Phylogenetic and population systematics of the mangabeys (Primates: Cercopithecoidea). *Primates*, **19**, 1–34.
- Groves, C.P. (1989) *A Theory of Human and Primate Evolution*. Oxford University Press, Oxford.
- Groves, C. (2001) *Primate Taxonomy (Smithsonian Series in Comparative Evolutionary Biology)*. Smithsonian Books, Washington, DC.
- Gumert, M.D., Kluck, M. & Malaivijitnond, S. (2009) The physical characteristics and usage patterns of stone axe and pounding hammers used by long-tailed macaques in the Andaman Sea region of Thailand. *American Journal of Primatology*, **71**, 594–608.
- Hadfield, J.D., Nutall, A., Osorio, D. & Owens, I.P.F. (2007) Testing the phenotypic gambit: Phenotypic, genetic and environmental correlations of colour. *Journal of Evolutionary Biology*, **20**, 549–557.
- Haldane, J.B.S. (1932) *The Causes of Evolution*. Longmans, Green & Co., London.
- Hall, B.K. (1994) *Homology: The Hierarchical Basis of Comparative Biology* (ed BK Hall). Academic Press, San Diego, CA.
- Ham, R. (1994) *Behaviour and Ecology of Grey-Cheeked Mangabeys (Cercocebus Albigena) in the Lopé Reserve, Gabon*. University of Stirling.
- Hammer, Ø. & Harper, D.A.T. (2006) *Paleontological Data Analysis*. Wiley-Blackwell, Malden, MA.
- Hammer, Ø., Harper, D.A.T. & Ryan, P.D. (2001) PAST: Paleontological statistics software package for education and data analysis. *Palaeontologia Electronica*, **4**, 9pp.

- Hansen, T. (1997) Stabilizing selection and the comparative analysis of adaptation. *Evolution*, **51**, 1341–1351.
- Harding, R.S. (1976) Ranging patterns of a troop of baboons (*Papio anubis*) in Kenya. *Folia Primatologica*, **25**, 143–185.
- Harris, E.E. (2000) Molecular systematics of the Old World monkey tribe Papionini: Analysis of the total available genetic sequences. *Journal of Human Evolution*, **38**, 235–256.
- Harris, E.E. & Disotell, T.R. (1998) Nuclear gene trees and the phylogenetic relationships of the mangabeys (Primates: Papionini). *Molecular Biology and Evolution*, **15**, 892.
- Harrison, M.J.S. (1988) The mandrill in Gabon’s rain forest—ecology, distribution and status. *Oryx*, **22**, 218–228.
- Harvey, P.H. & Pagel, M.D. (1991) *The Comparative Method in Evolutionary Biology*. Oxford University Press, Oxford.
- Hatze, H. (1974) The meaning of the term “biomechanics”. *Journal of Biomechanics*, **7**, 189–190.
- Hayes, V.J., Freedman, L. & Oxnard, C.E. (1990) The taxonomy of savannah baboons: An odontomorphometric analysis. *American Journal of Primatology*, **22**, 171–190.
- Herring, S.W. (1993) Functional morphology of mammalian mastication. *American Zoologist*, **33**, 289–299.
- Herring, S.W. (2008) Mechanical influences on suture development and patency. *Frontiers of Oral Biology*, **12**, 41–56.
- Herring, S.W. & Teng, S. (2000) Strain in the braincase and its sutures during function. *American Journal of Physical Anthropology*, **112**, 575–593.
- Herring, S.W., Teng, S., Huang, X., Mucci, R.J. & Freeman, J. (1996) Patterns of bone strain in the zygomatic arch. *The Anatomical Record*, **246**, 446–457.
- Hertz, P.E., Huey, R.B. & Garland, T. (1988) Time budgets, thermoregulation, and maximal locomotor performance: Are reptiles olympians or boy scouts? *American Zoologist*, **28**, 927–938.
- Herzog, W. (2006) Muscle. *Biomechanics of the Musculo-skeletal System*, 3rd ed (eds B.M. Nigg & W. Herzog), pp. 169–225. John Wiley & Sons, Chichester.
- Hildebrand, M. & Goslow, G. (2001) *Analysis of Vertebrate Structure*, 5th ed. John Wiley & Sons, New York, NY.
- Hill, R.A. & Dunbar, R.I.M. (2002) Climatic determinants of diet and foraging behaviour in baboons. *Evolutionary Ecology*, **16**, 579–593.

- Hillson, S. (1992) *Mammal Bones & Teeth: An Introductory Guide to Methods of Identification*. The Institute of Archaeology, University College London, London.
- Hogg, R.T., Ravosa, M.J., Ryan, T.M. & Vinyard, C.J. (2011) The functional morphology of the anterior masticatory apparatus in tree-gouging marmosets (Cebidae, Primates). *Journal of Morphology*, **272**, 833–849.
- Horn, A.D. (1987) The socioecology of the black mangabey (*Cercocebus aterrimus*) near Lake Tumba, Zaire. *American Journal of Primatology*, **12**, 165–180.
- Hoshino, J. (1985) Feeding ecology of mandrills (*Mandrillus sphinx*) in campo animal reserve, Cameroon. *Primates*, **26**, 248–273.
- Hsieh, J. (2009) *Computed Tomography: Principles, Design, Artifacts, and Recent Advances*, 2nd ed. SPIE Press, Bellingham, WA.
- Huiskes, R. & Chao, E.Y. (1983) A survey of finite element analysis in orthopedic biomechanics: The first decade. *Journal of Biomechanics*, **16**, 385–409.
- Hutchinson, J.R. (2012) On the inference of function from structure using biomechanical modelling and simulation of extinct organisms. *Biology Letters*, **8**, 115–118.
- Hylander, W.L. (1975) Incisor size and diet in anthropoids with special reference to Cercopithecidae. *Science*, **189**, 1095–1098.
- Hylander, W.L. (1977) In vivo bone strain in the mandible of *Galago crassicaudatus*. *American Journal of Physical Anthropology*, **46**, 309–26.
- Hylander, W.L. (1979a) The functional significance of primate mandibular form. *Journal of Morphology*, **160**, 223–240.
- Hylander, W.L. (1979b) Experimental analysis of temporomandibular joint reaction force in macaques. *American Journal of Physical Anthropology*, **51**, 433–456.
- Hylander, W.L. (1979c) Mandibular function in *Galago crassicaudatus* and *Macaca fascicularis*: An in vivo approach to stress analysis of the mandible. *Journal of Morphology*, **159**, 253–296.
- Hylander, W.L. (1984) Stress and strain in the mandibular symphysis of primates: A test of competing hypotheses. *American Journal of Physical Anthropology*, **64**, 1–46.
- Hylander, W.L. (1985) Mandibular function and biomechanical stress and scaling. *American Zoologist*, **25**, 315–330.
- Hylander, W.L. (1986) In-vivo bone strain as an indicator of masticatory bite force in *Macaca fascicularis*. *Archives of Oral Biology*, **31**, 149–157.

- Hylander, W.L. (1992) Functional anatomy. *The Temporomandibular Joint. A Biological Basis for Clinical Practice* (eds B.G. Sarnat & D.M. Laskin), pp. 60–92. Saunders, Philadelphia, PA.
- Hylander, W.L. & Bays, R. (1979) An in vivo strain-gauge analysis of the squamosal-dentary joint reaction force during mastication and incisal biting in *Macaca mulatta* and *Macaca fascicularis*. *Archives of Oral Biology*, **24**, 689–697.
- Hylander, W.L. & Johnson, K.R. (1992) Strain gradients in the craniofacial region of primates. *The Biological Mechanisms of Tooth Movement and Craniofacial Adaptation*. (ed Z. Davidovitch), pp. 559–569. Ohio State University, Columbus, OH.
- Hylander, W.L. & Johnson, K.R. (1994) Jaw muscle function and wishboning of the mandible during mastication in macaques and baboons. *American Journal of Physical Anthropology*, **94**, 523–547.
- Hylander, W.L., Johnson, K.R. & Crompton, A.W. (1987) Loading patterns and jaw movements during mastication in *Macaca fascicularis*: A bone-strain, electromyographic, and cineradiographic analysis. *American Journal of Physical Anthropology*, **72**, 287–314.
- Hylander, W.L., Johnson, K.R. & Crompton, A.W. (1992) Muscle force recruitment and biomechanical modeling: An analysis of masseter muscle function during mastication in *Macaca fascicularis*. *American Journal of Physical Anthropology*, **88**, 365–387.
- Hylander, W.L., Picq, P.G. & Johnson, K.R. (1991a) Masticatory-stress hypotheses and the supraorbital region of primates. *American Journal of Physical Anthropology*, **86**, 1–36.
- Hylander, W.L., Picq, P.G. & Johnson, K.R. (1991b) Function of the supraorbital region of primates. *Archives of Oral Biology*, **36**, 273–281.
- Hylander, W.L. & Ravosa, M.J. (1992) An analysis of the supraorbital region of Primates: A morphometric and experimental approach. *Structure, Function and Evolution of Teeth* (eds P. Smith & E. Tchernov), pp. 223–255. Freund Publishing House, London and Tel Aviv.
- Hylander, W.L., Ravosa, M.J., Ross, C.F. & Johnson, K.R. (1998) Mandibular corpus strain in primates: Further evidence for a functional link between symphyseal fusion and jaw-adductor muscle force. *American Journal of Physical Anthropology*, **107**, 257–271.

- Irschick, D.J. & Garland, T. (2001) Integrating function and ecology in studies of adaptation: Investigations of locomotor capacity as a model system. *Annual Review of Ecology and Systematics*, **32**, 367–396.
- Irschick, D.J. & Losos, J.B. (1998) A comparative analysis of the ecological significance of maximal locomotor performance in Caribbean *Anolis* lizards. *Evolution*, **52**, 219–226.
- IUCN. (2011) The IUCN Red List of Threatened Species. Version 2011.2, <http://www.iucnredlist.org/>
- De Iuliis, G. & Pulerà, D. (2011) *The Dissection of Vertebrates: A Laboratory Manual*, 2nd ed. Academic Press, Burlington, MA.
- Iwamoto, T. (1979) Ecological and sociological studies of gelada baboons. Feeding ecology. *Contributions to Primatology*, **16**, 279–330.
- Iwamoto, T. & Dunbar, R.I.M. (1983) Thermoregulation, Habitat Quality and the Behavioural Ecology of Gelada Baboons. *The Journal of Animal Ecology*, **52**, 357–366.
- Jablonski, N.G. (1993) Evolution of the masticatory apparatus in *Theropithecus*. *Theropithecus: The Rise and Fall of a Primate Genus* (ed N.G. Jablonski), pp. 299–329. Cambridge University Press, Cambridge.
- Jablonski, N.G. (2002) Fossil Old World monkeys: The late Neogene radiation. *The Primate Fossil Record* (ed W.C. Hartwig), pp. 255–299. Cambridge University Press, Cambridge.
- Jaslow, C.R. (1990) Mechanical properties of cranial sutures. *Journal of Biomechanics*, **23**, 313–321.
- Joe, H. (2006) Generating random correlation matrices based on partial correlations. *Journal of Multivariate Analysis*, **97**, 2177–2189.
- Jolly, C.J. (1966) Introduction to the Cercopithecoidea, with notes on their use as laboratory animals. *Symposia of the Zoological Society of London*, **17**, 427–457.
- Jolly, C.J. (1970) The seed-eaters : A new model of hominid differentiation based on a baboon analogy. *Man*, **5**, 5–26.
- Jolly, C.J. (2001) A proper study for mankind: Analogies from the Papionin monkeys and their implications for human evolution. *Yearbook of Physical Anthropology*, **44**, 177–204.
- Jolly, C.J., Woolley-Barker, T., Beyene, S., Disotell, T.R. & Phillips-Conroy, J.E. (1997) Intergeneric hybrid baboons. *International Journal of Primatology*, **18**, 597–627.

- Jones, A.G., Arnold, S.J. & Bürger, R. (2003) Stability of the G-matrix in a population experiencing pleiotropic mutation, stabilizing selection, and genetic drift. *Evolution*, **57**, 1747–1760.
- Jones, T., Ehardt, C.L., Butynski, T.M., Davenport, T.R.B., Mpunga, N.E., Machaga, S.J. & De Luca, D.W. (2005) The highland mangabey *Lophocebus kipunji*: A new species of African monkey. *Science*, **308**, 1161–1164.
- Jones, C. & Sabater Pi, J. (1968) Comparative ecology of *Cercocebus albigena* (Gray) and *Cercocebus torquatus* (Kerr) in Rio Muni, West Africa. *Folia Primatologica*, **9**, 99–113.
- De Jong, W.C., Korfage, J. a M. & Langenbach, G.E.J. (2011) The role of masticatory muscles in the continuous loading of the mandible. *Journal of Anatomy*, **218**, 625–36.
- Kawai, M. & Iwamoto, T. (1979) Ecological and sociological studies of gelada baboons. Nomadism and activities. *Contributions to Primatology*, **16**, 251–278.
- Kay, R.F. (1978) Molar structure and diet in Cercopithecidae. *Development, Function and Evolution of Teeth* (eds P.M. Butler & K.A. Joysey), pp. 309–339. Academic Press, San Diego, CA.
- Kay, R.F. (1981) The nut-crackers – a new theory of the adaptations of the Ramapithecinae. *American Journal of Physical Anthropology*, **55**, 141–151.
- Kay, R.F. (1984) On the use of anatomical features to infer foraging behavior in extinct primates. *Adaptations for Foraging in Nonhuman Primates* (eds P.S. Rodman & J.G.H. Cant), pp. 21–53. Columbia University Press, New York, NY.
- Kay, R.F. & Hylander, W.L. (1978) The dental structure of mammalian folivores with special reference to primates and phalangeroids (Marsupialia). *The Biology of Arboreal Folivores* (ed G.G. Montgomery), pp. 173–191. Smithsonian Institution Press, Washington, DC.
- Kendall, D.G.D.G. (1984) Shape manifolds, procrustean metrics, and complex projective spaces. *Bulletin of the London Mathematical Society*, **16**, 81–121.
- Kerr, A.A. (2010) *Introductory Biomechanics*. Churchill Livingstone, Edinburgh.
- Kessler, O., Lacatusu, E., Sommers, M.B., Mayr, E. & Bottlang, M. (2006) Malrotation in total knee arthroplasty: Effect on tibial cortex strain captured by laser-based strain acquisition. *Clinical Biomechanics*, **21**, 603–609.
- Klingenberg, C.P. (1998) Heterochrony and allometry: The analysis of evolutionary change in ontogeny. *Biological Reviews*, **73**, 79–123.

- Klingenberg, C.P. (2011) MorphoJ: An integrated software package for geometric morphometrics. *Molecular Ecology Resources*, **11**, 353–357.
- Klingenberg, C.P., Barluenga, M. & Meyer, A. (2002) Shape analysis of symmetric structures: Quantifying variation among individuals and asymmetry. *Evolution*, **56**, 1909–1920.
- Klingenberg, C.P., Debat, V. & Roff, D.A. (2010) Quantitative genetics of shape in cricket wings: Developmental integration in a functional structure. *Evolution*, **64**, 1–49.
- Koots, K.R. & Gibson, J.P. (1996) Realized sampling variances of estimates of genetic parameters and the difference between genetic and phenotypic correlations. *Genetics*, **143**, 1409–1416.
- Kruuk, L.E.B.B., Slate, J. & Wilson, A.J. (2008) New answers for old questions: The evolutionary quantitative genetics of wild animal populations. *Annual Review of Ecology, Evolution, and Systematics*, **39**, 525–548.
- Krzanowski, W. (2000) *Principles of Multivariate Analysis: A User's Perspective*. Oxford University Press, Oxford.
- Kupczik, K. (2008) Virtual biomechanics: Basic concepts and technical aspects of finite element analysis in vertebrate morphology. *Journal of Anthropological Sciences*, **86**, 193–198.
- Kupczik, K., Dobson, C.A., Fagan, M.J., Crompton, R.H., Oxnard, C.E., O'Higgins, P. & O'Higgins, P. (2007) Assessing mechanical function of the zygomatic region in macaques: Validation and sensitivity testing of finite element models. *Journal of Anatomy*, **210**, 41–53.
- Lahm, S.A. (1986) Diet and habitat preference of *Mandrillus sphinx* in Gabon: Implications of foraging strategy. *American Journal of Primatology*, **11**, 9–26.
- Lambert, J.E., Chapman, C.A., Wrangham, R.W. & Conklin-Brittain, N. Lou. (2004) Hardness of cercopithecine foods: Implications for the critical function of enamel thickness in exploiting fallback foods. *American Journal of Physical Anthropology*, **125**, 363–368.
- Lande, R. (1979) Quantitative genetic analysis of multivariate evolution, applied to brain: Body size allometry. *Evolution*, **33**, 402.
- Lande, R. (1980a) The genetic covariance between characters maintained by pleiotropic mutations. *Genetics*, **94**, 203–215.
- Lande, R. (1980b) Genetic variation and phenotypic evolution during allopatric speciation. *The American Naturalist*, **116**, 463–479.

- Lande, R. & Arnold, S.J. (1983) The measurement of selection on correlated characters. *Evolution*, **37**, 1210–1226.
- Lane, N.E., Bloch, D.A., Jones, H.H., Marshall, W.H., Wood, P.D. & Fries, J.F. (1986) Long-distance running, bone density, and osteoarthritis. *Jama The Journal Of The American Medical Association*, **255**, 1147–1151.
- Lane, N.E., Kaneps, A.J., Stover, S.M., Modin, G. & Kimmel, D.B. (1996) Bone mineral density and turnover following forelimb immobilization and recovery in young adult dogs. *Calcified Tissue International*, **59**, 401–406.
- Lauder, G.V. (1995) On the inference of function from structure. *Functional Morphology in Vertebrate Paleontology* (ed J.J. Thomason), pp. 1–18. Cambridge University Press, Cambridge.
- Leakey, M. (1985) Early Miocene Cercopithecids from Buluk, Northern Kenya. *Folia Primatologica*, **44**, 1–14.
- Leigh, S.R. (2006) Cranial ontogeny of *Papio* baboons (*Papio hamadryas*). *American Journal of Physical Anthropology*, **130**, 71–84.
- Lieberman, D.E. (1996) How and why humans grow thin skulls: Experimental evidence for systemic cortical robusticity. *American Journal of Physical Anthropology*, **101**, 217–236.
- Lieberman, D.E., Krovitz, G.E., Yates, F.W., Devlin, M. & St Claire, M. (2004) Effects of food processing on masticatory strain and craniofacial growth in a retrognathic face. *Journal of Human Evolution*, **46**, 655–677.
- Liem, K., Bemis, W., Walker, W.F. & Grande, L. (2001) *Functional Anatomy of the Vertebrates: An Evolutionary Perspective*, 3rd ed. Brooks/Cole, Cengage Learning, Belmont, CA.
- Ligon, J.D. (1992) The role of phylogenetic history in the evolution of contemporary avian mating and parental care systems (ed DM Power). *Current Ornithology*, **10**, 1–46.
- Liu, J., Shi, J., Fitton, L.C., Phillips, R., Higgins, P.O., Fagan, M.J. & O’Higgins, P. (2012) The application of muscle wrapping to voxel-based finite element models of skeletal structures. *Biomechanics and Modeling in Mechanobiology*, **11**, 35–47.
- Lofsvold, D. (1986) Quantitative genetics of morphological differentiation in *Peromyscus*. I. Tests of the homogeneity of genetic covariance structure among species and subspecies. *Evolution*, **40**, 559–573.
- Lofsvold, D. (1988) Quantitative genetics of morphological differentiation in *Peromyscus*. II. Analysis of selection and drift. *Evolution*, **42**, 54–67.

- Losos, J.B. (2011) Convergence, adaptation, and constraint. *Evolution*, **65**, 1827–1840.
- Lucas, P.W. (2004) *Dental Functional Morphology: How Teeth Work*. Cambridge University Press, Cambridge.
- Lucas, P.W. & Teaford, M.F. (1994) Functional morphology of colobine teeth. *Colobine Monkeys: Their Ecology Behaviour and Evolution* (eds G. Davies & J. Oates), pp. 173–203. Cambridge University Press, Cambridge.
- Luschei, E.S. & Goodwin, G.M. (1974) Patterns of mandibular movement and jaw muscle activity during mastication in the monkey. *Journal of Neurophysiology*, **37**, 954–966.
- Lynch, M. (1990) The rate of morphological evolution in mammals from the standpoint of the neutral expectation. *The American Naturalist*, **136**, 727–741.
- Lynch, M. & Walsh, B. (1998) *Genetics and Analysis of Quantitative Traits*. Sinauer Associates, Sunderland, MA.
- MacCallum, R.C., Widaman, K.F., Zhang, S. & Hong, S. (1999) Sample size in factor analysis. *Psychological Methods*, **4**, 84–99.
- MacLean, P.D. (1990) *The Triune Brain in Evolution: Role in Paleocerebral Functions*. Plenum Press, New York, NY.
- Marinescu, R., Daegling, D.J. & Rapoff, A.J. (2005) Finite-element modeling of the anthropoid mandible: the effects of altered boundary conditions. *The Anatomical Record Part A: Discoveries in Molecular, Cellular, and Evolutionary Biology*, **283**, 300–309.
- Marroig, G. & Cheverud, J.M. (2004) Did natural selection or genetic drift produce the cranial diversification of neotropical monkeys? *The American Naturalist*, **163**, 417–428.
- Marroig, G. & Cheverud, J.M. (2005) Size as a line of least evolutionary resistance: Diet and adaptive morphological radiation in New World monkeys. *Evolution*, **59**, 1128–1142.
- Marsaglia, G. & Olkin, I. (1983) Generating correlation matrices. *SIAM Journal on Scientific and Statistical Computing*, **5**, 470.
- Marshall, A.J., Boyko, C.M., Feilen, K.L., Boyko, R.H. & Leighton, M. (2009) Defining fallback foods and assessing their importance in primate ecology and evolution. *American Journal of Physical Anthropology*, **140**, 603–614.
- Marshall, A.J. & Wrangham, R.W. (2007) Evolutionary Consequences of Fallback Foods. *International Journal of Primatology*, **28**, 1219–1235.

- McHenry, C.R., Clausen, P.D., Daniel, W.J.T., Meers, M.B. & Pendharkar, A. (2006) Biomechanics of the rostrum in crocodylians: a comparative analysis using finite-element modeling. *The Anatomical Record Part A: Discoveries in Molecular, Cellular, and Evolutionary Biology*, **288**, 827–849.
- McKittrick, M.C. (1993) Phylogenetic constraint in evolutionary theory: Has it any explanatory power? *Annual Review of Ecology and Systematics*, **24**, 307–330.
- McNamara, J.A. (1974) An electromyographic study of mastication in the rhesus monkey (*Macaca mulatta*). *Archives of Oral Biology*, **19**, 821–823.
- van der Meijden, A., Kleinteich, T. & Coelho, P. (2012) Packing a pinch: Functional implications of chela shapes in scorpions using finite element analysis. *Journal of Anatomy*, **220**, 423–34.
- Melnick, D.J. & Pearl, M.C. (1987) Cercopithecines in multimale groups: Genetic diversity and population structure. *Primate Societies* (eds B.B. Smuts, D.L. Cheney, R.M. Seyfarth, R.W. Wrangham & T.T. Struhsaker), pp. 121–134. University of Chicago Press, Chicago, IL.
- Meloro, C. & O’Higgins, P. (2011) Ecological adaptations of mandibular form in fissiped carnivora. *Journal of Mammalian Evolution*, **18**, 185–200.
- Mendel, G. (1866) Versuche über Pflanzenhybriden. *Verhandlungen des naturforschenden Vereins Brünn*, **4**, 3–47.
- Meyer, K. & Kirkpatrick, M. (2010) Better estimates of genetic covariance matrices by “bending” using penalized maximum likelihood. *Genetics*, **185**, 1097–1110.
- Michel, B.A., Lane, N.E., Bloch, D.A., Jones, H.H. & Fries, J.F. (1991) Effect of changes in weight-bearing exercise on lumbar bone mass after age fifty. *Annals of Medicine*, **23**, 397–401.
- Miller, E.R. (1999) Faunal correlation of Wadi Moghara, Egypt: Implications for the age of *Prohylobates tandyi*. *Journal of Human Evolution*, **36**, 519–533.
- Milne, N. & O’Higgins, P. (2012) Scaling of form and function in the xenarthran femur: A 100-fold increase in body mass is mitigated by repositioning of the third trochanter. *Proceedings of the Royal Society B Biological Sciences*, **279**, 3449–3456.
- Mitani, M. (1989) *Cercocebus torquatus*: Adaptive feeding and ranging behaviors related to seasonal fluctuations of food resources in the tropical rain forest of south-western Cameroon. *Primates*, **30**, 307–323.

- Mitani, M. (1991) Niche overlap and polyspecific associations among sympatric cercopithecids in the campo animal reserve, Southwestern Cameroon. *Primates*, **32**, 137–151.
- Mitteroecker, P. (2007) *Evolutionary and Developmental Morphometrics of the Hominoid Cranium*. Unpublished PhD thesis. Universität Wien, Vienna.
- Mitteroecker, P. & Gunz, P. (2009) Advances in geometric morphometrics. *Evolutionary Biology*, **36**, 235–247.
- Mitteroecker, P., Gunz, P., Bernhard, M., Schaefer, K. & Bookstein, F.L. (2004) Comparison of cranial ontogenetic trajectories among great apes and humans. *Journal of Human Evolution*, **46**, 679–697.
- Mitteroecker, P., Gunz, P. & Bookstein, F.L. (2005) Heterochrony and geometric morphometrics: A comparison of cranial growth in *Pan paniscus* versus *Pan troglodytes*. *Evolution & Development*, **7**, 244–258.
- Monteiro, L.R. (2000) Why morphometrics is special: The problem with using partial warps as characters for phylogenetic inference. *Systematic Biology*, **49**, 796–800.
- Monteiro, L.R. (2013) Morphometrics and the comparative method: Studying the evolution of biological shape. *Hystrix, the Italian Journal of Mammalogy*, **24**, 12.
- Monteiro, L.R., Bonato, V. & dos Reis, S.F. (2005) Evolutionary integration and morphological diversification in complex morphological structures: Mandible shape divergence in spiny rats (Rodentia, Echimyidae). *Evolution & Development*, **7**, 429–439.
- Monteiro, L.R., Diniz-Filho, J.A.F., dos Reis, S.F. & Araújo, E.D. (2002) Geometric estimates of heritability in biological shape. *Evolution*, **56**, 563–572.
- Monteiro, L.R. & Gomes-jr, J.L. (2005) Morphological divergence rate tests for natural selection: Uncertainty of parameter estimation and robustness of results. *Genetics and Molecular Biology*, **28**, 345–355.
- Morales, J.C. & Melnick, D.J. (1998) Phylogenetic relationships of the macaques (Cercopithecidae: *Macaca*), as revealed by high resolution restriction site mapping of mitochondrial ribosomal genes. *Journal of Human Evolution*, **34**, 1–23.
- Morris, F.L., Naughton, G.A., Gibbs, J.L., Carlson, J.S. & Wark, J.D. (1997) Prospective ten-month exercise intervention in premenarcheal girls: Positive effects on bone and lean mass. *Journal of Bone and Mineral Research*, **12**, 1453–1462.

- Myatt, J.P., Crompton, R.H., Payne-Davis, R.C., Vereecke, E.E., Isler, K., Savage, R., D'Août, K., Günther, M.M. & Thorpe, S.K. (2012) Functional adaptations in the forelimb muscles of non-human great apes. *Journal of Anatomy*, **220**, 13–28.
- Nigg, B.M. & Herzog, W. (2006) *Biomechanics of the Musculo-Skeletal System*, 3rd ed. Wiley, Chichester.
- Nogueira, M.R., Monteiro, L.R., Peracchi, A.L. & de Araújo, A.F.B. (2005) Ecomorphological analysis of the masticatory apparatus in the seed-eating bats, genus *Chiroderma* (Chiroptera: Phyllostomidae). *Journal of Zoology*, **266**, 355–364.
- Nogueira, M.R., Peracchi, A.L. & Monteiro, L.R. (2009) Morphological correlates of bite force and diet in the skull and mandible of phyllostomid bats. *Functional Ecology*, **23**, 715–723.
- Nordström, A., Karlsson, C., Nyquist, F., Olsson, T., Nordström, P. & Karlsson, M. (2005) Bone loss and fracture risk after reduced physical activity. *Journal of Bone and Mineral Research*, **20**, 202–207.
- Norris, J. (1988) Diet and feeding behavior of semi-free ranging mandrills in an enclosed gabonais forest. *Primates*, **29**, 449–463.
- O'Higgins, P. (1997) Methodological issues in the description of forms. *Fourier descriptors and their applications in Biology* (ed P.E. Lestrel), pp. 74–105. Cambridge University Press, Cambridge.
- O'Higgins, P. (2000) Advances in approaches to the study of morphological variation in the hominid fossil record: Biology, landmarks and geometry. *Journal of Anatomy*, **197**, 103–120.
- O'Higgins, P., Cobb, S.N., Fitton, L.C., Gröning, F., Phillips, R., Liu, J. & Fagan, M.J. (2011) Combining geometric morphometrics and functional simulation: An emerging toolkit for virtual functional analyses. *Journal of Anatomy*, **218**, 3–15.
- O'Higgins, P. & Collard, M. (2002) Sexual dimorphism and facial growth in papionin monkeys. *Journal of Zoology*, **257**, 255–272.
- O'Higgins, P., Fitton, L.C., Phillips, R., Shi, J., Liu, J., Gröning, F., Cobb, S.N. & Fagan, M.J. (2012) Virtual functional morphology: Novel approaches to the study of craniofacial form and function. *Evolutionary Biology*, 1–15.
- O'Higgins, P. & Milne, N. (2013) Applying geometric morphometrics to compare changes in size and shape arising from finite elements analyses. *Hystrix, the Italian Journal of Mammalogy*, **24**, 7.

- Oksanen, J., Blanchet, F.G., Kindt, R., Legendre, P., O'Hara, R.B., Simpson, G.L., Solymos, P., Stevens, M.H.H. & Wagner, H. (2007) vegan: Community Ecology Package. *R package version, 1*, R package version 1.17–9.
- de Oliveira, F.B., Porto, A. & Marroig, G. (2009) Covariance structure in the skull of Catarrhini: A case of pattern stasis and magnitude evolution. *Journal of Human Evolution*, **56**, 417–430.
- Osborn, J.W. (1987) Relationship between the mandibular condyle and the occlusal plane during hominid evolution: Some of its effects on jaw mechanics. *American Journal of Physical Anthropology*, **73**, 193–207.
- Osborn, J.W. (1995) Biomechanical implications of lateral pterygoid contribution to biting and jaw opening in humans. *Archives of Oral Biology*, **40**, 1099–1108.
- Owen, R. (1848) *The Archetype and Homologies of the Vertebrate Skeleton*. Richard and John E. Taylor, London.
- Oxnard, C. & O'Higgins, P. (2009) Biology clearly needs morphometrics. Does morphometrics need biology? *Biological Theory*, **4**, 84–97.
- Oyen, O.J. & Russell, M.D. (1982) Histogenesis of the craniofacial skeleton and models of facial growth. *The Effect of Surgical Intervention on Craniofacial Growth* (eds J.A. McNamara, D.S. Carlson & K.A. Ribbens), pp. 361–372. University of Michigan, Ann Arbor, MI.
- Oyen, O.J. & Tsay, T.P. (1991) A biomechanical analysis of craniofacial form and bite force. *American Journal of Orthodontics and Dentofacial Orthopedics*, **99**, 298–309.
- Oyen, O.J., Walker, A.C. & Rice, R.W. (1979) Craniofacial growth in olive baboons (*Papio cynocephalus anubis*): Browridge formation. *Growth*, **43**, 174–187.
- Panagiotopoulou, O. (2009) Finite element analysis (FEA): Applying an engineering method to functional morphology in anthropology and human biology. *Annals of Human Biology*, **36**, 609–623.
- Panagiotopoulou, O., Kupczik, K. & Cobb, S.N. (2011) The mechanical function of the periodontal ligament in the macaque mandible: A validation and sensitivity study using finite element analysis. *Journal of Anatomy*, **218**, 75–86.
- Panagiotopoulou, O., Wilshin, S.D., Rayfield, E.J., Shefelbine, S.J. & Hutchinson, J.R. (2012) What makes an accurate and reliable subject-specific finite element model? A case study of an elephant femur. *Journal of the Royal Society, Interface*, **9**, 351–361.

- Parr, W.C.H., Wroe, S., Chamoli, U., Richards, H.S., McCurry, M.R., Clausen, P.D. & McHenry, C. (2012) Toward integration of geometric morphometrics and computational biomechanics: New methods for 3D virtual reconstruction and quantitative analysis of Finite Element Models. *Journal of Theoretical Biology*, **301C**, 1–14.
- Patel, P.K., Widera, G.E.O., Harris, G.F., Hospital, S. & Avenue, O.P. (2002) Determination of physiological cross-section area of patient-specific masticatory muscles with three-dimensional medical imaging analysis. *Methodology*, 2538–2539.
- Pearson, K. (1901) On lines and planes of closest fit to systems of points in space. *Philosophical Magazine Series 6*, **2**, 559–572.
- Perez, S.I. & Monteiro, L.R. (2009) Nonrandom factors in modern human morphological diversification: A study of craniofacial variation in southern South American populations. *Evolution*, **63**, 978–993.
- Peterson, J. & Dechow, P.C.P.C. (2003) Material properties of the human cranial vault and zygoma. *The Anatomical Record Part A: Discoveries in Molecular, Cellular, and Evolutionary Biology*, **274**, 785–797.
- Phillips, P.C. & Arnold, S.J. (1999) Hierarchical comparison of genetic variance-covariance matrices. I. Using the Flury hierarchy. *Evolution*, **53**, 1506–1515.
- Pierce, S.E., Angielczyk, K.D. & Rayfield, E.J. (2008) Patterns of morphospace occupation and mechanical performance in extant crocodylian skulls: A combined geometric morphometric and finite element modeling approach. *Journal of Morphology*, **269**, 840–864.
- Pierce, S.E., Angielczyk, K.D. & Rayfield, E.J. (2009) Shape and mechanics in thalattosuchian (Crocodylomorpha) skulls: Implications for feeding behaviour and niche partitioning. *Journal of Anatomy*, **215**, 555–576.
- Pirie, P.L. (1978) Allometric scaling in the postcanine dentition with reference to primate diets. *Primates*, **19**, 583–591.
- Poulsen, J.R., Clark, C.J. & Smith, T.B. (2001) Seasonal variation in the feeding ecology of the grey-cheeked mangabey (*Lophocebus albigena*) in Cameroon. *American Journal of Primatology*, **54**, 91–105.
- Prendergast, P.J. & Taylor, D. (1994) Prediction of bone adaptation using damage accumulation. *Journal of Biomechanics*, **27**, 1067–1076.

- Preuschoft, H., Demes, B., Meier, M. & Baer, H.F. (1986) The biomechanical principles of the upper jaw of long-snouted vertebrates. *Zeitschrift für Morphologie und Anthropologie*, **76**, 1–24.
- Preuschoft, H. & Witzel, U. (2004a) A biomechanical approach to craniofacial shape in primates, using FESA. *Annals of Anatomy Anatomischer Anzeiger*, **186**, 397–404.
- Preuschoft, H. & Witzel, U. (2004b) Functional structure of the skull in hominoidea. *Folia Primatologica*, **75**, 219–252.
- Prôa, M., O’Higgins, P. & Monteiro, L.R. (2013) Type I error rates for testing genetic drift with phenotypic covariance matrices: A simulation study. *Evolution*, **67**, 185–195.
- Qiu, W. & Joe, H. (2009) clusterGeneration: Random cluster generation (with specified degree of separation). *R package version*, R package version 1.2.7.
- R Development Core Team. (2013) R: A Language and Environment for Statistical Computing, <http://www.r-project.org>
- Rafferty, K.L., Herring, S.W. & Marshall, C.D. (2003) Biomechanics of the rostrum and the role of facial sutures. *Journal of Morphology*, **257**, 33–44.
- Ravosa, M.J. (1988) Allometry of the mandibular corpus and symphysis in prostomian primates. *American Zoologist*, **28**, 910.
- Ravosa, M.J. (1990) Functional assessment of subfamily variation in maxillomandibular morphology among Old World monkeys. *American Journal of Physical Anthropology*, **82**, 199–212.
- Ravosa, M.J. (1991a) The ontogeny of cranial sexual dimorphism in two old world monkeys: *Macaca fascicularis* (Cercopithecinae) and *Nasalis larvatus* (Colobinae). *International Journal of Primatology*, **12**, 403–426.
- Ravosa, M.J. (1991b) Interspecific perspective on mechanical and nonmechanical models of primate circumorbital morphology. *American Journal of Physical Anthropology*, **85**, 95–112.
- Ravosa, M.J. (1991c) Interspecific perspective on mechanical and nonmechanical models of primate circumorbital morphology. *American Journal of Physical Anthropology*, **86**, 369–396.
- Ravosa, M.J. (1996) Jaw morphology and function in living and fossil Old World monkeys. *International Journal of Primatology*, **17**, 909–932.
- Ravosa, M.J. & Profant, L.P. (2000) Evolutionary morphology of the skull in Old World monkeys. *Old World Monkeys* (eds P.F. Whitehead & C.J. Jolly), pp. 237–268. Cambridge University Press, Cambridge.

- Rayfield, E.J. (2004) Cranial mechanics and feeding in *Tyrannosaurus rex*. *Proceedings of the Royal Society B Biological Sciences*, **271**, 1451–1459.
- Rayfield, E.J. (2007) Finite element analysis and understanding the biomechanics and evolution of living and fossil organisms. *Annual Review of Earth and Planetary Sciences*, **35**, 541–576.
- Rayfield, E.J., Norman, D.B., Horner, C.C., Horner, J.R., Smith, P.M., Thomason, J.J., Upchurch, P. & Ray, E.J. (2001) Cranial design and function in a large theropod dinosaur. *Nature*, **409**, 1033–1037.
- Reeve, H.K. & Sherman, P.W. (1993) Adaptation and the goals of evolutionary research. *The Quarterly Review of Biology*, **68**, 1–32.
- Reusch, T. & Blanckenhorn, W.U. (1998) Quantitative genetics of the dung fly *Sepsis cynipsea*: Cheverud's conjecture revisited. *Heredity*, **81**, 111–119.
- Revell, L.J. (2007) Testing the genetic constraint hypothesis in a phylogenetic context: a simulation study. *Evolution*, **61**, 2720–7.
- Revell, L.J., Harmon, L.J., Langerhans, R.B. & Kolbe, J.J. (2007) A phylogenetic approach to determining the importance of constraint on phenotypic evolution in the neotropical lizard *Anolis cristatellus*. *Evolutionary Ecology Research*, **9**, 261–282.
- Revell, L.J., Mahler, D.L., Sweeney, J.R., Sobotka, M., Fancher, V.E. & Losos, J.B. (2010) Nonlinear selection and the evolution of variances and covariances for continuous characters in an anole. *Journal of Evolutionary Biology*, **23**, 407–421.
- Richmond, B.G. (1998) *Ontogeny and Biomechanics of Phalangeal Form in Primates*. State University of New York, Stony Brook, NY.
- Richmond, B.G., Wright, B.W., Grosse, I., Dechow, P.C., Ross, C.F., Spencer, M.A. & Strait, D.S. (2005) Finite element analysis in functional morphology. *The Anatomical Record Part A: Discoveries in Molecular, Cellular, and Evolutionary Biology*, **283**, 259–274.
- Ridley, M. (2004) *Evolution*. Blackwell Publishing, Malden, MA.
- van Rietbergen, B., Weinans, H., Huiskes, R. & Polman, B.J.W. (1996) Computational strategies for iterative solutions of large FEM applications employing voxel data. *International Journal for Numerical Methods in Engineering*, **39**, 2743–2767.
- Robert, P. & Escoufier, Y. (1976) A unifying tool for linear multivariate statistical methods: The RV-coefficient. *Applied Statistics*, **25**, 257–265.
- Roff, D.A. (1995) The estimation of genetic correlations from phenotypic correlations: a test of Cheverud's conjecture. *Heredity*, **74**, 481–490.

- Roff, D.A. (1996) The evolution of genetic correlations: an analysis of patterns. *Evolution*, **50**, 1392–1403.
- Roff, D.A. (1997) *Evolutionary Quantitative Genetics*. Chapman & Hall, New York, NY.
- Roff, D. (2002) Comparing G matrices: A MANOVA approach. *Evolution*, **56**, 1286–1291.
- Roff, D., Mousseau, T. & Howard, D. (1999) Variation in genetic architecture of calling song among populations of *Allonemobius socius*, *A. fasciatus*, and a hybrid population: Drift or selection? *Evolution*, **53**, 216–224.
- Rogers, A. (1992) *Textbook of Anatomy*. Churchill Livingstone, Edinburgh.
- Rogers, M.E., Abernethy, K.A., Fontaine, B., Wickings, E.J., White, L.J.T. & Tutin, C.E.G. (1996) Ten days in the life of a mandrill horde in the Lopé Reserve, Gabon. *American Journal of Primatology*, **40**, 297–313.
- Rohlf, F.J. (1998) On applications of geometric morphometrics to studies of ontogeny and phylogeny. *Systematic Biology*, **47**, 147–158; discussion 159–167.
- Rohlf, F.J. (1999) Shape statistics: Procrustes superimpositions and tangent spaces. *Journal of Classification*, **16**, 197–223.
- Rohlf, F.J. (2000) Statistical power comparisons among alternative morphometric methods. *American Journal of Physical Anthropology*, **111**, 463–478.
- Rohlf, F.J. & Corti, M. (2000) Use of two-block partial least-squares to study covariation in shape. *Systematic Biology*, **49**, 740–753.
- Rohlf, F.J. & Marcus, L.F. (1993) A revolution morphometrics. *Trends in Ecology & Evolution*, **8**, 129–132.
- Rohlf, F.J. & Slice, D. (1990) Extensions of the Procrustes method for the optimal superimposition of landmarks. *Systematic Zoology*, **39**, 40–59.
- Ross, C.F. (2001) In vivo function of the craniofacial haft: The interorbital “pillar”. *American Journal of Physical Anthropology*, **116**, 108–139.
- Ross, C.F. (2005) Finite element analysis in vertebrate biomechanics. *The Anatomical Record Part A: Discoveries in Molecular, Cellular, and Evolutionary Biology*, **283**, 253–258.
- Ross, C.F. (2008) Does the primate face torque? *Primate Craniofacial Function and Biology* (eds C. Vinyard, M.J. Ravosa & C. Wall), Springer, Boston, MA.
- Ross, C.F., Lockwood, C., Fleagle, J. & Jungers, W. (2002) Adaptation and behavior in the primate fossil record. *Reconstructing Behavior in the Primate Fossil Record*

- (eds J.M. Plavcan, R.F. Kay, W.L. Jungers & C.P. Van Schaik), pp. 1–43. Kluwer Academic / Plenum Publishers, New York, NY.
- Ross, C.F., Patel, B.A., Slice, D.E., Strait, D.S., Dechow, P.C., Richmond, B.G. & Spencer, M.A. (2005) Modeling masticatory muscle force in finite element analysis: Sensitivity analysis using principal coordinates analysis. *The Anatomical Record Part A: Discoveries in Molecular, Cellular, and Evolutionary Biology*, **283**, 288–99.
- Rowe, N. (1996) *The Pictorial Guide to the Living Primates*. Pogonias Press, Charlestown, RI.
- Rubin, C.T. (1984) Skeletal strain and the functional significance of bone architecture. *Calcified Tissue International*, **36 Suppl 1**, S11–18.
- Rubin, C.T. & Lanyon, L.E. (1982) Limb mechanics as a function of speed and gait: A study of functional strains in the radius and tibia of horse and dog. *Journal of Experimental Biology*, **101**, 187–211.
- Rubin, C.T. & Lanyon, L.E. (1984) Dynamic strain similarity in vertebrates; an alternative to allometric limb bone scaling. *Journal of Theoretical Biology*, **107**, 321–327.
- Ruff, C.B. (2008) Biomechanical analyses of archaeological human skeletons. *Biological Anthropology of the Human Skeleton*, 2nd ed (eds M.A. Katzenberg & S.R. Saunders), pp. 183–206. John Wiley & Sons, Hoboken, NJ.
- Ruff, C., Holt, B. & Trinkaus, E. (2006) Who’s afraid of the big bad Wolff?: “Wolff’s law” and bone functional adaptation. *American Journal of Physical Anthropology*, **129**, 484–498.
- Russell, M.D. (1982) Tooth eruption and browridge formation. *American Journal of Physical Anthropology*, **58**, 59–65.
- Russell, M.D. (1985) The supraorbital torus: “A most remarkable peculiarity.” *Current Anthropology*, **26**, 337–360.
- Ryan, T.M. & van Rietbergen, B. (2005) Mechanical significance of femoral head trabecular bone structure in *Loris* and *Galago* evaluated using micromechanical finite element models. *American Journal of Physical Anthropology*, **126**, 82–96.
- Sakamoto, M., Lloyd, G.T. & Benton, M.J. (2010) Phylogenetically structured variance in felid bite force: The role of phylogeny in the evolution of biting performance. *Journal of Evolutionary Biology*, **23**, 463–78.
- Schlichting, C.D. & Pigliucci, M. (1998) *Phenotypic Evolution: A Reaction Norm Perspective*. Sinauer Associates, Sunderland, MA.

- Schluter, D. (1996) Adaptive radiation along genetic lines of least resistance. *Evolution*, **50**, 1766.
- Schluter, D. (2000) *The Ecology of Adaptive Radiation*. Oxford University Press, Oxford.
- Schreier, A.L. (2010) Feeding ecology, food availability and ranging patterns of wild hamadryas baboons at Filoha. *Folia Primatologica*, **81**, 129–145.
- Schwartz, D.J. & Huelke, D.F. (1963) Morphology of the head and neck of the macaque monkey: The muscles of mastication and the mandibular division of the trigeminal nerve. *Journal of Dental Research*, **42**, 1222–1233.
- Schwenk, K. & Wagner, G.P. (2004) The relativism of constraints on phenotypic evolution. *Phenotypic Integration: Studying the Ecology and Evolution of Complex Phenotypes* (eds M. Pigliucci & K. Preston), pp. 390–408. Oxford University Press, Oxford.
- Sellers, W.I. & Crompton, R.H. (2004) Using sensitivity analysis to validate the predictions of a biomechanical model of bite forces. *Annals of Anatomy Anatomischer Anzeiger*, **186**, 89–95.
- Shah, N.F. (2003) *Foraging Strategies in Two Sympatric Mangabey Species (Cercocebus Agilis and Lophocebus Albigena)*. Unpublished PhD thesis. Stony Brook University, Stony Brook, NY.
- Shi, J., Curtis, N., Fitton, L.C., O'Higgins, P. & Fagan, M.J. (2012) Developing a musculoskeletal model of the primate skull: Predicting muscle activations, bite force, and joint reaction forces using multibody dynamics analysis and advanced optimisation methods. *Journal of Theoretical Biology*, **310**, 21–30.
- Shrive, N.G. (2006) Strain Measurement. *Biomechanics of the Musculo-skeletal System*, 3rd ed (eds B.M. Nigg & W. Herzog), pp. 392–408. John Wiley & Sons, Chichester.
- Singleton, M. (2002) Patterns of cranial shape variation in the Papionini (Primates: Cercopithecinae). *Journal of Human Evolution*, **42**, 547–578.
- Singleton, M. (2004) Geometric morphometric analysis of functional divergence in mangabey facial form. *Journal of Anthropological Sciences*, **82**, 29–45.
- Singleton, M. (2005) Functional shape variation in the cercopithecine masticatory complex. *Modern Morphometrics in Physical Anthropology* (ed D.E. Slice), pp. 319–348. Kluwer Academic / Plenum Publishers, New York, NY.
- Slice, D.E. (2005) *Modern Morphometrics in Physical Anthropology* (ed DE Slice). Springer.

- Slice, D.E. (2007) Geometric Morphometrics. *Annual Review of Anthropology*, **36**, 261–281.
- Smith, R.J. (1978) Mandibular biomechanics and temporomandibular joint function in primates. *American Journal of Physical Anthropology*, **49**, 341–349.
- Snell, R. (1995) *Clinical Anatomy for Medical Students*, 5th ed. Lippincott Williams & Wilkins, Philadelphia, PA.
- Spoor, F. & Zonneveld, F. (1995) Morphometry of the primate bony labyrinth: A new method based on high-resolution computed tomography. *Journal of Anatomy*, **186**, 271–86.
- Stammbach, E. (1987) Desert, forest and montane baboons: Multilevel-societies. *Primate Societies* (eds B.B. Smuts, D.L. Cheney, R.M. Seyfarth, R.W. Wrangham & T.T. Struhsaker), pp. 112–120. University of Chicago Press.
- Steiper, M.E., Young, N.M. & Sukarna, T.Y. (2004) Genomic data support the hominoid slowdown and an Early Oligocene estimate for the hominoid–cercopithecoid divergence. *Proceedings of the National Academy of Sciences of the United States of America*, **101**, 17021–17026.
- Stevens, N.J., Seiffert, E.R., O'Connor, P.M., Roberts, E.M., Schmitz, M.D., Krause, C., Gorscak, E., Ngasala, S., Hieronymus, T.L. & Temu, J. (2013) Palaeontological evidence for an Oligocene divergence between Old World monkeys and apes. *Nature*, **advance on**.
- Stewart, C.B. & Disotell, T.R. (1998) Primate evolution - in and out of Africa. *Current Biology*, **8**, R582–8.
- Stewart, A.-M.E., Gordon, C.H., Wich, S.A., Schroor, P. & Meijaard, E. (2008) Fishing in *Macaca fascicularis*: A rarely observed innovative behavior. *International Journal of Primatology*, **29**, 543–548.
- Strait, D.S., Richmond, B.G., Spencer, M.A., Ross, C.F., Dechow, P.C. & Wood, B.A. (2007) Masticatory biomechanics and its relevance to early hominid phylogeny: An examination of palatal thickness using finite-element analysis. *Journal of Human Evolution*, **52**, 585–599.
- Strait, D.S., Wang, Q., Dechow, P.C., Ross, C.F., Richmond, B.G., Spencer, M.A. & Patel, B.A. (2005) Modeling elastic properties in finite-element analysis: How much precision is needed to produce an accurate model? *The Anatomical Record Part A: Discoveries in Molecular, Cellular, and Evolutionary Biology*, **283**, 275–287.

- Strait, D.S., Weber, G.W., Neubauer, S., Chalk, J., Richmond, B.G., Lucas, P.W., Spencer, M.A., Schrein, C., Dechow, P.C., Ross, C.F., Grosse, I.R., Wright, B.W., Constantino, P., Wood, B.A., Lawn, B., Hylander, W.L., Wang, Q., Byron, C., Slice, D.E. & Smith, A.L. (2009) The feeding biomechanics and dietary ecology of *Australopithecus africanus*. *Proceedings of the National Academy of Sciences of the United States of America*, **106**, 2124–9.
- Ström, D., Holm, S., Clemensson, E., Haraldson, T. & Carlsson, G.E. (1988) Gross anatomy of the craniomandibular joint and masticatory muscles of the dog. *Archives of Oral Biology*, **33**, 597–604.
- Swartz, S.M. (1993) The biomechanics of primate limbs. *Postcranial Adaptation in Nonhuman Primates* (ed D.L. Gebo), pp. 5–42. Northern Illinois University Press, De Kalb, IL.
- Swedell, L. (2002) Ranging behavior, group size and behavioral flexibility in Ethiopian hamadryas baboons (*Papio hamadryas hamadryas*). *Folia Primatologica*, **73**, 95–103.
- Swindler, D.R. (2002) *Primate Dentition: An Introduction to the Teeth of Non-Human Primates*. Cambridge University Press, Cambridge.
- Swindler, D.R. & Wood, C. (1973) *An Atlas of Primate Gross Anatomy: Baboon, Chimpanzee, and Man*. University of Washington Press, Seattle, WA.
- Szalay, F.S. & Delson, E. (1979) *Evolutionary History of the Primates*. Academic Press, New York, NY.
- Taylor, A.B. (2002) Masticatory form and function in the African apes. *American Journal of Physical Anthropology*, **117**, 133–156.
- Taylor, A.B. (2006) Diet and mandibular morphology in African apes. *International Journal of Primatology*, **27**, 181–201.
- Taylor, A.B. & Vinyard, C.J. (2004) Comparative analysis of masseter fiber architecture in tree-gouging (*Callithrix jacchus*) and nongouging (*Saguinus oedipus*) callitrichids. *Journal of Morphology*, **261**, 276–285.
- Terhune, C.E. (2011) Dietary correlates of temporomandibular joint morphology in New World primates. *Journal of Human Evolution*, **61**, 583–596.
- Thompson, D.W. (1917) *On Growth and Form*. Cambridge University Press, Cambridge.
- Thompson, D.W. (1942) *On Growth and Form*. Cambridge University Press, Cambridge.

- Thorington, R.W. & Groves, C.P. (1970) An annotated classification of the Cercopithecoidea. *Old World Monkeys: Evolution, Systematics and Behavior*. (eds J.R. Napier & P.H. Napier), pp. 629–647. Academic Press, New York, NY.
- Tosi, A.J., Disotell, T.R., Morales, J.C. & Melnick, D.J. (2003) Cercopithecine Y-chromosome data provide a test of competing morphological evolutionary hypotheses. *Molecular Phylogenetics and Evolution*, **27**, 510–521.
- Tosi, A.J., Morales, J.C. & Melnick, D.J. (2000) Comparison of Y chromosome and mtDNA phylogenies leads to unique inferences of macaque evolutionary history. *Molecular Phylogenetics and Evolution*, **17**, 133–144.
- Truesdell, C. & Noll, W. (2004) *The Non-Linear Field Theories of Mechanics* (ed S Flugge). Springer Verlag, Berlin.
- Tseng, Z.J., McNitt-Gray, J.L., Flashner, H., Wang, X. & Enciso, R. (2011) Model sensitivity and use of the comparative finite element method in mammalian jaw mechanics: mandible performance in the gray wolf. *PloS ONE*, **6**, e19171.
- Turner, C.H., Rho, J., Takano, Y., Tsui, T.Y. & Pharr, G.M. (1999) The elastic properties of trabecular and cortical bone tissues are similar: Results from two microscopic measurement techniques. *Journal of Biomechanics*, **32**, 437–441.
- Türp, J.C., Cowley, T. & Stohler, C.S. (1997) Media hype: Musculus sphenomandibularis. *Acta Anatomica*, **158**, 150–154.
- Tutin, C.E., Ham, R.M., White, L.J. & Harrison, M.J. (1997) The primate community of the Lopé Reserve, Gabon: Diets, responses to fruit scarcity, and effects on biomass. *American Journal of Primatology*, **42**, 1–24.
- Tuukkanen, J., Peng, Z. & Väänänen, H.K. (1994) Effect of running exercise on the bone loss induced by orchidectomy in the rat. *Calcified Tissue International*, **55**, 33–37.
- Ungar, P.S. (1995) Fruit preferences of four sympatric primate species at Ketambe, northern Sumatra, Indonesia. *International Journal of Primatology*, **16**, 221–245.
- Ungar, P.S. (2010) *Mammal Teeth: Origin, Evolution, and Diversity*. The Johns Hopkins University Press, Baltimore, MD.
- Vanhooydonck, B., Herrel, A., Van Damme, R. & Irschick, D.J. (2006) The quick and the fast: the evolution of acceleration capacity in *Anolis* lizards. *Evolution: International Journal of Organic Evolution*, **60**, 2137–2147.
- Vaughan, T.A., Ryan, J.M. & Czaplewski, N.J. (2010) *Mammalogy*, 5th ed. Jones & Bartlett Publishers, Burlington, MA.

- Venables, W.N. & Ripley, B.D. (2002) *Modern Applied Statistics with S*, 4th ed (eds J Chambers, W Eddy, W Härdle, S Sheather, and L Tierney). Springer.
- Wainwright, P.C. (2007) Functional Versus Morphological Diversity in Macroevolution. *Annual Review of Ecology, Evolution, and Systematics*, **38**, 381–401.
- Waite, D.E. & Levin, D.A. (1998) Genetic and phenotypic correlations in plants: A botanical test of Cheverud's conjecture. *Heredity*, **80**, 310–319.
- Wake, D.B. & Larson, A. (1987) Multidimensional analysis of an evolving lineage. *Science*, **238**, 42–8.
- Wang, Q., Strait, D.S. & Dechow, P.C. (2006) A comparison of cortical elastic properties in the craniofacial skeletons of three primate species and its relevance to the study of human evolution. *Journal of Human Evolution*, **51**, 375–82.
- Weaver, T.D., Roseman, C.C. & Stringer, C.B. (2007) Were neandertal and modern human cranial differences produced by natural selection or genetic drift? *Journal of Human Evolution*, **53**, 135–145.
- Weber, G.W., Bookstein, F.L. & Strait, D.S. (2011) Virtual anthropology meets biomechanics. *Journal of Biomechanics*, **44**, 1429–1432.
- Weijjs, W. & Hillen, B. (1985) Physiological cross-section of the human jaw muscles. *Acta Anatomica*, **121**, 31–35.
- White, T.D., Black, M.T. & Folkens, P.A. (2012) *Human Osteology*, 3rd ed. Academic Press, Burlington, MA.
- Whiten, A., Byrne, R.W., Barton, R.A., Waterman, P.G. & Henzi, S.P. (1991) Dietary and foraging strategies of baboons [and Discussion]. *Philosophical Transactions of the Royal Society of London. Series B, Biological sciences*, **334**, 187–195; discussion 195–197.
- Wieczkowski, J. (2009) Brief communication: Puncture and crushing resistance scores of Tana river mangabey (*Cercocebus galeritus*) diet items. *American Journal of Physical Anthropology*, **140**, 572–577.
- Williams, G. (1996) *Adaptation and Natural Selection*. Princeton University Press, Princeton, NJ.
- Williams, S.H., Wright, B.W. & Truong, V.A.N.D.E.N. (2005) Mechanical properties of foods used in experimental studies of primate masticatory function. *October*, **346**, 329–346.
- Willis, J.H., Coyne, J.A. & Kirkpatrick, M. (1991) Can one predict the evolution of quantitative characters without genetics? *Evolution*, **45**, 441–444.

- Willmore, K.E., Roseman, C.C., Rogers, J., Cheverud, J.M. & Richtsmeier, J.T. (2009a) Comparison of mandibular phenotypic and genetic integration between baboon and mouse. *Evolutionary Biology*, **36**, 19–36.
- Willmore, K.E., Roseman, C.C., Rogers, J., Richtsmeier, J.T. & Cheverud, J.M. (2009b) Genetic variation in baboon craniofacial sexual dimorphism. *Evolution*, **63**, 799–806.
- Witzel, U. & Preuschoft, H. (2005) Finite-element model construction for the virtual synthesis of the skulls in vertebrates: Case study of *Diplodocus*. *The Anatomical Record Part A: Discoveries in Molecular, Cellular, and Evolutionary Biology*, **283**, 391–401.
- Wold, H. (1966) Estimation of principal components and related models by iterative least squares. *Multivariate Analysis* (ed P. Krishnaiah), pp. 391–420. Academic Press, New York, NY.
- Wolff, J. (1892) *Das Gesetz Der Transformation Der Knochen*. August Hirschwald, Berlin.
- Wolff, R.G. (1991) *Functional Chordate Anatomy*. D. C. Heath and Co., Lexington, MA.
- Wright, S. (1921a) Systems of mating. I. The biometric relations between parent and offspring. *Genetics*, **6**, 111–123.
- Wright, S. (1921b) Systems of mating. II. The effects of inbreeding on the genetic composition of a population. *Genetics*, **6**, 124–143.
- Wright, S. (1921c) Systems of mating. III. Assortative mating based on somatic resemblance. *Genetics*, **6**, 144–161.
- Wright, S. (1921d) Systems of mating. IV. The effects of selection. *Genetics*, **6**, 162–166.
- Wright, S. (1921e) Systems of mating. V. General considerations. *Genetics*, **6**, 167–178.
- Wright, S. (1922) Coefficients of inbreeding and relationship. *The American Naturalist*, 330–338.
- Wright, B., Ulibarri, L., O'Brien, J., Sadler, B., Prodhan, R., Covert, H. & Nadler, T. (2008) It is tough out there: Variation in the toughness of ingested leaves and feeding behavior among four Colobinae in Vietnam. *International Journal of Primatology*, **29**, 1455–1466.
- Wroe, S. (2010) Cranial mechanics of mammalian carnivores: Recent advances using a finite element approach. *Carnivoran Evolution: New Views on Phylogeny, Form,*

- and Function* (eds A. Goswami & A. Friscia), pp. 466–485. Cambridge University Press, Cambridge.
- Wroe, S., Ferrara, T.L., McHenry, C.R., Curnoe, D. & Chamoli, U. (2010) The craniomandibular mechanics of being human. *Proceedings of the Royal Society B Biological Sciences*, **277**, 3579.
- Wroe, S., McHenry, C. & Thomason, J. (2005) Bite club: Comparative bite force in big biting mammals and the prediction of predatory behaviour in fossil taxa. *Proceedings of the Royal Society B Biological Sciences*, **272**, 619–625.
- Yamashita, N. (1998) Functional dental correlates of food properties in five Malagasy lemur species. *American Journal of Physical Anthropology*, **106**, 169–188.
- Yang, L., Zhang, P., Liu, S., Samala, P.R., Su, M. & Yokota, H. (2007) Measurement of strain distributions in mouse femora with 3D-digital speckle pattern interferometry. *Optics and Lasers in Engineering*, **45**, 843–851.
- Yeager, C.P. (1996) Feeding ecology of the long-tailed macaque (*Macaca fascicularis*) in Kalimantan Tengah, Indonesia. *International Journal of Primatology*, **17**, 51–62.
- Young, R.L., Sweeney, M.J. & Badyaev, A. V. (2010) Morphological diversity and ecological similarity: Versatility of muscular and skeletal morphologies enables ecological convergence in shrews. *Functional Ecology*, **24**, 556–565.
- Zelditch, M.L., Swiderski, D.L., Sheets, H.D. & Fink, W.L. (2004) *Geometric Morphometrics for Biologists: A Primer*. Academic Press, San Diego, CA.
- Zeng, Z. (1988) Long-term correlated response, interpopulation covariation, and interspecific allometry. *Evolution*, **42**, 363–374.
- Zernicke, R.F., Judex, S. & Lorincz, C. (2006) Adaptation of biological materials to exercise, disuse, and aging. *Biomechanics of the Musculo-skeletal System*, 3rd ed (eds B.M. Nigg & W. Herzog), pp. 226–243. John Wiley & Sons, Chichester.
- Zienkiewicz, O.C. (1971) *The Finite Element Method in Engineering Science*. McGraw-Hill Inc., New York, NY.
- Zinner, D., Wertheimer, J., Liedigk, R., Groeneveld, L.F. & Roos, C. (2012) Baboon phylogeny as inferred from complete mitochondrial genomes. *American Journal of Physical Anthropology*, **150**, 133–140.

Appendix A. Complete Taxonomy of Papionins

The taxonomic nomenclature presented here follows Groves (2001) and Vaughan *et al.* (2010). This table includes extant species only.

Domain Eukarya (Whittaker & Margulis, 1978)

Kingdom Animalia (Linnaeus, 1758)

Superphylum Deuterostomia (Grobber, 1908)

Phylum Chordata (Bateson, 1885)

Class Mammalia (Linnaeus, 1758)

Subclass Theria (Parker & Haswell, 1897)

Infraclass Eutheria (Huxley, 1880)

Order Primates (Linnaeus, 1758)

Suborder Anthropeidea (Mivart, 1864)

Infraorder Catarrhini (É. Geoffroy, 1812)

Superfamily Cercopithecoidea (Gray, 1821)

Family Cercopithecidae (Gray, 1821)

Subfamily Cercopithecinae (Gray, 1821)

Tribe Papionini (Burnett, 1828)

Genus *Macaca* (Lacépède, 1799)

Species *Macaca sylvanus* (Linnaeus, 1758)

Species *Macaca silenus* (Linnaeus, 1758)

Species *Macaca nemestrina* (Linnaeus, 1766)

Species *Macaca leonina* (Blyth, 1863)

Species *Macaca pagensis* (Miller, 1903)

Species *Macaca siberu* (Fuentes & Olson, 1995)

Species *Macaca maura* (F. Cuvier, 1823)

Species *Macaca ochreata* (Ogilby, 1840)

Species *Macaca tonkeana* (Meyer, 1899)

Species *Macaca hecki* (Matschie, 1901)

Species *Macaca nigrescens* (Temminck, 1849)

Species *Macaca nigra* (Desmarest, 1822)

Species *Macaca fascicularis** (Raffles, 1821)

Species *Macaca arctoides* (I. Geoffroy, 1831)

→

- Species *Macaca mulatta* (Zimmermann, 1780)
 Species *Macaca cyclopis* (Swinhoe, 1862)
 Species *Macaca fuscata* (Blyth, 1875)
 Species *Macaca sinica* (Linnaeus, 1771)
 Species *Macaca radiata* (É. Geoffroy, 1812)
 Species *Macaca assamensis* (M' Clelland, 1840)
 Species *Macaca thibetana* (Milne-Edwards, 1870)
 Species *Macaca munzala* (Sinha *et al.*, 2005)
 Species *Macaca brunnescens* (Matschi, 1901)
 Genus *Cercocebus* (É. Geoffroy, 1812)
 Species *Cercocebus atys* (Audebert, 1797)
 Species *Cercocebus torquatus** (Kerr, 1792)
 Species *Cercocebus agilis* (Milne-Edwards, 1886)
 Species *Cercocebus chrysogaster* (Lydekker, 1900)
 Species *Cercocebus galeritus* (Peters, 1879)
 Species *Cercocebus sanjei* (Mittermeier, 1986)
 Genus *Papio* (Erxleben, 1777)
 Species *Papio hamadryas** (Linnaeus, 1758)
 Species *Papio papio* (Desmarest, 1820)
 Species *Papio anubis** (Lesson, 1827)
 Species *Papio cynocephalus* (Linnaeus, 1766)
 Species *Papio ursinus* (Kerr, 1792)
 Genus *Lophocebus* (Palmer, 1903)
 Species *Lophocebus albigena** (Gray, 1850)
 Species *Lophocebus aterrimus* (Oudemans, 1890)
 Species *Lophocebus opdenboschi* (Schouteden, 1944)
 Genus *Mandrillus* (Ritgen, 1824)
 Species *Mandrillus sphinx** (Linnaeus, 1758)
 Species *Mandrillus leucophaeus* (F. Cuvier, 1807)
 Genus *Theropithecus* (I. Geoffroy, 1843)
 Species *Theropithecus gelada** (Rüppell, 1835)
 Genus *Rungwecebus* (Davenport *et al.*, 2006)
 Species *Rungwecebus kipunji* (Jones *et al.*, 2005)

* Species used in this thesis

Appendix B. R Functions used in Chapters 3 and 4

For the analyses presented in Chapters 3 and 4 two R functions were written. The first, with file name `simulationAC-typeIerror.R`, performs completely stochastic simulations and calculates the type I error rate of the Ackermann and Cheverud (AC) random genetic drift test. The second, with file name `simulationAC-slope.R`, performs completely stochastic simulations and calculates the expected slope of the AC random genetic drift test for pre-determined **G** and **P** matrices or simulations.

Function to perform completely stochastic simulations and calculate the type I error rate of the AC test.

```
#Function parameters:
#method = choose "sim1", "sim2", "sim3", "sim4", "sim5",
according to description in the text (Chapter 3)
#m = genetic covariance matrix dimension
#tNe = number of generations (t) divided by effective
population size (Ne)
#pop = number of populations
#n = sample size for each population
#sim.n = number of simulations

simulateGP<-function(method,m,tNe,pop,n,sim.n,
                     G="NULL",P="NULL"){

#Define an empty variable to contain the results
prob <- vector()

require(MASS)
require(clusterGeneration)
for (i in 1:sim.n){
  if (method=="sim1"){
    if (G=="NULL"){
      stop("you need to provide a valid G matrix!\n")}
    if (P=="NULL"){
      stop("you need to provide a valid P matrix!\n")}
  }

#Predetermined G and P will be used
if (method=="sim2"){

#G is defined as a random positive definite matrix, and P = xG,
only different by a random constant of proportionality.
G<-genPositiveDefMat(dim=m,lambdaLow=1,ratioLambda=10)$Sigma
P<-runif(1,min=1,max=10)*G
}
if (method=="sim3"){

#G and P matrices are defined randomly and independently from
each other, with the constraint that the variances in P are
always larger than the respective variances in G.
```

```

G<-genPositiveDefMat(
  dim=m, covMethod="unifcorrmat", rangeVar=c(1,10))$Sigma
R<-genPositiveDefMat(
  dim=m, covMethod="unifcorrmat", rangeVar=c(1,1))$Sigma
var<-runif(m, 2, 9)*diag(G)
P<-diag(sqrt(var))%*%R%*%diag(sqrt(var))
}
if (method=="sim4"){

#G and E matrices are defined randomly and independently from
each other, whereas P = G+E. P and G do not share a common PC
structure but are related
G<-genPositiveDefMat(~
  dim=m, covMethod="unifcorrmat", rangeVar=c(1,10))$Sigma
P<-G+genPositiveDefMat(
  dim=m, covMethod="unifcorrmat", rangeVar=c(1,15))$Sigma
}
if (method=="sim5"){

#G and E matrices are defined randomly and independently from
each other, whereas P = G+E. P and G share a common PC structure
G<-genPositiveDefMat(
  dim=m, lambdaLow=1, ratioLambda=10)$Sigma
P<-G+genPositiveDefMat(
  dim=m, covMethod="unifcorrmat", rangeVar=c(1,5))$Sigma
}

#Generate samples from pop populations with n obs each. the
ancestral vector is composed of m zeros.
M<-mvrnorm(pop, rep(0, ncol(G)), tNe*G)
group<-factor(rep(seq(1:pop), each=n))
data <- matrix(0, pop*n, ncol(P))
for (j in 1:(n*pop)){
  data[j,]<-mvrnorm(1, M[group[j],], P)
}

#Calculate matrix of mean vectors from simulations
zmeans<-matrix(
  unlist(by(data, group, colMeans)), nrow=pop, ncol=ncol(G),
  byrow=T)

#Calculate within-group phenotypic covariance and extract
eigenvalues
eigW<-eigen(
  cov(data-zmeans[rep(1:nrow(zmeans), each=n),]))

#Project mean vectors for the 15 pops on within group
eigenvectors
zm.proj<-zmeans%*%eigW$vector

#Calculate among-group variance
v<-diag(cov(zm.proj))

#Perform the AC test with t-test for unity slope
model<-summary(lm(log(v)~log(eigW$values)))
prob[i]<-pt(abs((model$coefficients[2,1]-
1)/model$coefficients[2,2]),
  df=model$df[2], lower.tail=F)*2
}
tIe<-mean(prob<0.05)
return(tIe)
}

```

Function to perform completely stochastic simulations and calculate expected slope of AC-test for specific G and P matrices or simulations.

```

#Function parameters:
#method = choose "sim1", "sim2", "sim3", "sim4", "sim5",
according to description in the text (Chapter 3)
#m = genetic covariance matrix dimension
#tNe = number of generations (t) divided by effective
population size (Ne)
#pop = number of populations
#n = sample size for each population
#sim.n = number of simulations
#smax = maximum variance in environmental matrix (min is always
0), genetic variances always between 1 and 10.

simulateGPBeta<-function(method,m,tNe,pop,n,sim.n, G="NULL",
P="NULL", smax){

#define an empty variable to contain the results
beta <- vector()

require(MASS)
require(clusterGeneration)
for (i in 1:sim.n){
  if (method=="sim1"){
    if (G=="NULL"){
      stop("you need to provide a valid G matrix!\n")
    }
    if (P=="NULL"){
      stop("you need to provide a valid P matrix!\n")
    }
  }
}

#Predetermined G and P will be used
if (method=="sim2"){

#G is defined as a random positive definite matrix, and P = xG,
only different by a random constant of proportionality.
  G<-genPositiveDefMat(dim=m,lambdaLow=1,ratioLambda=10)$Sigma
  P<-runif(1,min=1,max=10)*G
}
if (method=="sim3"){

#G and P matrices are defined randomly and independently from
each other, with the constraint that the variances in P are
always larger than the respective variances in G.
  G<-genPositiveDefMat(
    dim=m,covMethod="unifcorrmat",rangeVar=c(1,10))$Sigma
  R<-genPositiveDefMat(
    dim=m,covMethod="unifcorrmat",rangeVar=c(1,1))$Sigma
  var<-runif(m,2,9)*diag(G)
  P<-diag(sqrt(var))%*%R%*%diag(sqrt(var))
}
if (method=="sim4"){

#G and E matrices are defined randomly and independently from
each other, whereas P = G+E. P and G do not share a common PC
structure but are related
  G<-genPositiveDefMat(
    dim=m,covMethod="unifcorrmat",rangeVar=c(1,10))$Sigma
  P<-G+genPositiveDefMat(
    dim=m,covMethod="unifcorrmat",rangeVar=c(0,smax))$Sigma
}
}

```

```

if (method=="sim5"){

#G and E matrices are defined randomly and independently from
each other, whereas P = G+E. P and G share a common PC structure
  G<-genPositiveDefMat(
    dim=m,lambdaLow=1,ratioLambda=10)$Sigma
  P<-G+genPositiveDefMat(
    dim=m,covMethod="unifcorrmat",rangeVar=c(0,smax))$Sigma
}

#Generate samples from pop populations with n obs each. the
ancestral vector is composed of m zeros.
M<-mvrnorm(pop,rep(0,ncol(G)),tNe*G)
group<-factor(rep(seq(1:pop),each=n))
data <- matrix(0,pop*n,ncol(P))
for (j in 1:(n*pop)){data[j,]<-mvrnorm(1,M[group[j],],P)}

#Calculate matrix of mean vectors from simulations
zmeans<-matrix(
  unlist(by(data,group,colMeans)),nrow=pop,ncol=ncol(G),
  byrow=T)

#Calculate within-group phenotypic covariance and extract
eigenvalues
eigW<-eigen(
  cov(data-zmeans[rep(1:nrow(zmeans),each=n),]))

#Project mean vectors for the 15 pops on within group
eigenvectors
zm.proj<-zmeans%*%eigW$eigenvectors

#Calculate among-group variance
v<-diag(cov(zm.proj))

#Calculate slope of the AC test
model<-summary(lm(log(v)~log(eigW$values)))
beta[i]<-model$coefficients[2,1]
}

#Calculate 95% confidence limits
UL<-mean(beta)+1.96*sd(beta)
LL<-mean(beta)-1.96*sd(beta)
return(c(mean(beta),UL,LL))
}

```

Appendix C. Published Research Paper

A modified version of Chapter 3 of this thesis has been published as a research paper in the peer-review journal *Evolution* (accepted for publication in July 2012, published online in August 2012, published in print in January 2013) with the title “Type I error rates for testing genetic drift with phenotypic covariance matrices: a simulation study,” and citation reference:

Prôa, M., O’Higgins, P. & Monteiro, L.R. (2013) Type I error rates for testing genetic drift with phenotypic covariance matrices: a simulation study. *Evolution*, **67**(1), 185–195. DOI: 10.1111/j.1558-5646.2012.01746.x

The author of this thesis contributed with designing the simulations, writing the R functions (Appendix B), performing analyses, and writing the paper. A copy of the paper is shown here as image files.



TYPE I ERROR RATES FOR TESTING GENETIC DRIFT WITH PHENOTYPIC COVARIANCE MATRICES: A SIMULATION STUDY

Miguel Prôa,^{1,2} Paul O'Higgins,¹ and Leandro R. Monteiro^{1,3}

¹Centre for Anatomical and Human Sciences, The Hull York Medical School, The University of York, Heslington, York, YO10 5DD, United Kingdom

²E-mail: miguel.proa@hym.s.ac.uk

³Laboratório de Ciências Ambientais, Universidade Estadual do Norte Fluminense, Av. Alberto Lamego 2000, cep 28013-620, Campos dos Goytacazes, RJ, Brazil

Received November 22, 2010

Accepted July 3, 2012

Studies of evolutionary divergence using quantitative genetic methods are centered on the additive genetic variance–covariance matrix (G) of correlated traits. However, estimating G properly requires large samples and complicated experimental designs. Multivariate tests for neutral evolution commonly replace average G by the pooled phenotypic within-group variance–covariance matrix (W) for evolutionary inferences, but this approach has been criticized due to the lack of exact proportionality between genetic and phenotypic matrices. In this study, we examined the consequence, in terms of type I error rates, of replacing average G by W in a test of neutral evolution that measures the regression slope between among-population variances and within-population eigenvalues (the Ackermann and Cheverud [AC] test) using a simulation approach to generate random observations under genetic drift. Our results indicate that the type I error rates for the genetic drift test are acceptable when using W instead of average G when the matrix correlation between the ancestral G and P is higher than 0.6, the average character heritability is above 0.7, and the matrices share principal components. For less-similar G and P matrices, the type I error rates would still be acceptable if the ratio between the number of generations since divergence and the effective population size (t/N_e) is smaller than 0.01 (large populations that diverged recently). When G is not known in real data, a simulation approach to estimate expected slopes for the AC test under genetic drift is discussed.

KEY WORDS: Cheverud's conjecture, divergence rates, G-matrix, genetic drift test, multivariate evolution.

Quantitative genetic methods provide inferences of evolutionary processes via the study of evolutionary divergence patterns and their relationship to intrapopulation adult variation (Lande 1979; Ackermann and Cheverud 2002, 2004; Marroig and Cheverud 2004; Monteiro and Gomes-Jr 2005; Perez and Monteiro 2009). The connection between neutral microevolutionary processes and macroevolutionary patterns is centered around the additive genetic variance–covariance matrix (G) (Lande 1980; Arnold et al. 2001; Jones et al. 2003; Bégin and Roff 2004), which is thought to determine both the response to selection and the pattern of neutral

divergence, at least among populations over a small time scale (Lande 1980; Felsenstein 1988; Zeng 1988).

The expected pattern of phenotypic divergence among populations caused by random genetic drift in correlated traits can be used as a null hypothesis to test for neutral evolution (Lande 1979, 1980). The sampling distribution of the change in trait means in one generation ($\Delta\bar{z}$) has a mean of 0 and variance–covariance matrix G/N_e , the genetic covariance matrix in a population divided by the effective population size (Lande 1979). If the average phenotype of a population a is represented by a column vector \bar{z}_a of

polygenic traits with additive genetic and environmental components following multivariate normal distributions (Lande 1980), the probability distribution Φ after t generations will be

$$\Phi(\bar{z}_a, t) \sim N[\bar{z}_0, G(t/N_e)], \quad (1)$$

which is a normal distribution with a mean equal to that of the initial population and variance-covariance matrix $\mathbf{G}(t/N_e)$ (Lande 1979). If a number of populations are evolving independently (i.e., without gene flow), the expected among-population phenotypic variance-covariance matrix (\mathbf{B}) is a function of the genetic covariance matrix (\mathbf{G}), effective population size (N_e), and the number of generations (t):

$$\mathbf{B} = \mathbf{G}(t/N_e). \quad (2)$$

As a result, the comparison of among-population (\mathbf{B} phenotypic) and within-group (\mathbf{G} genetic) variance-covariance matrices can be used as a means to determine whether genetic drift as a null model explains the pattern of divergence observed (Lofsvold 1986, 1988; Roff et al. 1999; Ackermann and Cheverud 2002; Bégin and Roff 2004).

Because phenotypic covariances are much easier to estimate than their genetic counterparts, replacing average \mathbf{G} with the pooled phenotypic within-group covariance matrix (\mathbf{W}), provided that the phenotypic covariance matrices for diverging populations remain similar, has been a widely used approach to study the evolutionary mechanisms of divergence (Ackermann and Cheverud 2002, 2004; Marroig and Cheverud 2004; Perez and Monteiro 2009). Cheverud (1988) investigated the relationship between genetic and phenotypic correlation matrices using data taken from the literature and concluded that phenotypic correlations were reasonable estimates (and generally proportional, although perhaps not in a strict mathematical sense) of the respective genetic correlations. A second conclusion from these data was that phenotypic covariances \mathbf{W} estimated with large samples might approach \mathbf{G} more accurately than genetic covariances estimated from small effective sample sizes, at least for morphometric data (Cheverud 1988; Revell et al. 2010). A number of meta-analyses from literature reviews and empirical results have to some degree corroborated Cheverud's findings (Roff 1995; 1996; Koots and Gibson 1996; Roff et al. 1999; Waitt and Levin 1998). Nonetheless, this approach has been criticized on several grounds (Willis et al. 1991), but mostly because \mathbf{W} is not mathematically proportional (i.e., having a constant ratio) to average \mathbf{G} . Apart from the issue of similarity and proportionality between matrices, more specific consideration of the actual consequences of using \mathbf{W} as a surrogate of average \mathbf{G} in empirical studies (Bégin and Roff 2004; Klingenberg et al. 2010) should prove fruitful and one such aspect, the impact in terms of type I error rates, is the focus of the present study.

Quantitative genetic theory predicts phenotypic covariances within a single population (\mathbf{P}) to be the sum of the genetic covariance (\mathbf{G}) and the environmental covariances (\mathbf{E}), $\mathbf{P} = \mathbf{G} + \mathbf{E}$ (Falconer and Mackay 1996). A part-whole correlation is expected between phenotypic and genetic covariances; therefore, phenotypic covariances can be considered an estimate of genetic covariances with added error due to environmental covariances, even if not mathematically proportional.

Most of the discussion on the surrogacy of average \mathbf{G} by \mathbf{W} revolves around the similarities and differences between phenotypic and genetic covariances in single populations or from literature reviews, and the differences in empirical comparative results obtained when using one kind of estimate or the other. The latter are rare, due to the difficulty in estimating genetic parameters for a large number of species at the same time (Bégin and Roff 2004). Considering that Lande's (1979, 1980) model expects the among-population covariance matrix \mathbf{B} to be proportional to the average \mathbf{G} when genetic drift is the sole evolutionary mechanism, for the purpose of evolutionary divergence tests of neutral evolution, the relevant discussion is not whether \mathbf{G} and \mathbf{P} are exactly proportional in single populations, but whether using the phenotypic pooled within-group covariance matrix \mathbf{W} instead of the average \mathbf{G} will add enough error (caused by the environmental covariances) to lead into erroneous conclusions. The tests that have been used in the comparison of among-species phenotypic covariances and genetic covariances (Lofsvold 1988; Ackermann and Cheverud 2002, 2004) do not test for exact proportionality between \mathbf{B} and average \mathbf{G} , but for similarity in different matrix features, such as the correlation of principal components and the distribution of eigenvalues. The expectation of proportionality rests on a number of assumptions (Lande 1979) that are probably violated in most natural populations (Lofsvold 1988), for example, through the lack of large effective population sizes (Lofsvold 1988), or because of differences in the starting times of lineages (Revell 2007). Furthermore, error in the estimation of the average \mathbf{G} might lead to unpredictable deviations from the expectation. Lofsvold (1988) has suggested that the acceptance of genetic drift as a null hypothesis will be more robust to the breaking of the model's assumptions than the rejection (so type I error rates are of more concern than the power), and in real studies it might be hard to determine the actual cause of rejection, natural selection being one of the possible explanations. One might expect that a consequence of using pooled within-group phenotypic instead of genetic covariances would be to increase the probability of rejecting (type I error rate) a true null hypothesis of genetic drift.

In this study, we examined the consequences of using pooled within-group phenotypic instead of average genetic covariance matrices in the Ackermann and Cheverud (2002) test of genetic drift (referred to as the AC test from here on) in terms of type I error rates using a simulation of phenotypic evolution in

diverging populations. We identified the most relevant parameters and discuss a number of recommendations.

Material and Methods

SIMULATION MODELS: GENERAL DESCRIPTION

The simulations were performed using the quantitative genetic theory from Lande (1979, 1980). Starting from an ancestral population with genetic covariance matrix \mathbf{G} and mean vector \bar{z}_0 , a number (15 or 30) of descendant population mean vectors \bar{z}_a were generated using the t -fold convolution in equation (1) for a range of t/N_e ratios (0.00001–100 in increments of 1 in \log_{10} scale). This approach is equivalent to a random walk in multivariate space where each descendant population is evolving at a rate equivalent to \mathbf{G}/N_e . Instead of generating the intermediate phenotypes for each step (generation) of the random walk, the convolution allows for a direct generation of the end points with the same results and in a computationally efficient way.

The descendant populations from the ancestral distribution $N[\bar{z}_0, \mathbf{G}]$ were sampled n times (sample sizes 10–100, in increments of 10) according to the multivariate normal distribution $N[\bar{z}_a, \mathbf{P}]$, for each population. The first step in the simulations required an ancestral genetic variance–covariance matrix (\mathbf{G}) to generate species means and the second step required a phenotypic within-population variance–covariance matrix (\mathbf{P}) to generate individual specimens for each population. The same \mathbf{P} was used for all populations (the pooled within-group phenotypic covariance matrix \mathbf{W} is an estimate of the original \mathbf{P}). Different simulation models were used, either generating random \mathbf{G} and \mathbf{P} matrices as starting parameters (fully stochastic), or using predetermined matrices obtained from real datasets. The fully stochastic sets of simulations required the generation of random positive definite covariance matrices (where all eigenvalues are >0) that could be used as parameters in the generation of random multivariate normal numbers representing individuals sampled, as described below.

Throughout the paper, we used correlations of lower triangular covariance matrices excluding diagonals (variances) as one measure of structural similarity (alongside Common Principal Components—CPCs, Phillips and Arnold 1999). Note that permutations of the matrix elements were not used for testing significance of correlations. This procedure is not indicated for testing similarity in covariance matrices if variables have differences in scale (Cheverud and Marroig 2007), but was the most appropriate choice in our simulations. This is because the algorithm for the generation of random positive definite matrices (see details below) yielded matrices where covariances were small relative to variances. As a result, even when two covariance matrices were independently generated, they presented high positive matrix correlations when the diagonal was included (or when using

comparison methods such as random skewers), because the variances and covariances would systematically form two groups of values in the matrix scatterplot. Only when diagonals were excluded, was the expected correlation for independent matrices 0. This particular structure in the random matrices (high variances, small covariances) is a consequence of generating positive definite matrices, because matrices with high covariances relative to variances are likely to be nonpositive definite. Therefore, the most accurate description of matrix similarities in our simulations was derived from matrix correlations, using the lower triangular elements, excluding the diagonals. This is equivalent to comparing correlation matrices derived from the covariance matrix, as the information regarding variances is disregarded. In real datasets, there would be no justification to exclude the variances from the structural comparisons, as differences in scale of variances and covariances are a relevant part of the structure.

SIMULATION MODEL 1

In this set of simulations, we used real matrices rather than randomly generated ones. The matrices for the main simulations were obtained from a honey bee (*Apis mellifera*) wing shape dataset with 16 shape variables (partial warps), modified (used only landmarks 11–20) from Monteiro et al. (2002), and a gastropod shell shape dataset (*Physa heterostropha*) with 14 shape variables (DeWitt 1996, 1998). The average heritability of bee wing variables (calculated as $\mathbf{I}(\mathbf{I}\mathbf{G})(\mathbf{I}\mathbf{P})^{-1} \mathbf{I} m^{-1}$, where \mathbf{I} is a row vector of ones, \mathbf{I} is the identity matrix, \circ is a Hadamard [element-wise] product, and m is the number of variables) was 0.217, and the effective sample size, given that 21 bee colonies were used, was 4.6. The effective sample size was calculated as the product of heritability and the number of families, as described in Cheverud (1988). For the shell shape dataset, the average heritability was 0.607, and the effective sample size was 11.5 (19 families were used). These two datasets present important differences in the structural similarity of \mathbf{G} and \mathbf{P} . For the bee wing data, the matrix correlation between \mathbf{G} and \mathbf{P} was 0.804, whereas for the shell dataset the correlation was 0.442. Although the average heritability was smaller for the bee wing data, their genetic and phenotypic matrices were more similar than in the shell dataset. This is not unexpected, as these average heritabilities do not measure matrix similarity, only the relative magnitudes of the genetic and phenotypic variances. A comparison of these genetic and phenotypic covariance matrices via CPC indicated that the bee dataset matrices shared the full set of principal components (full CPC model supported by the jump-up approach) and the shell dataset matrices shared no principal components (Unrelated model supported).

SIMULATION MODEL 2

In this model, \mathbf{P} and \mathbf{G} were exactly proportional and differed only by a scalar multiplication. \mathbf{G} was defined first as a

random positive definite covariance matrix using the eigenvector method from Marsaglia and Olkin (1984) and Joe (2006). The eigenvector method first generates random eigenvalues ($\lambda_1, \dots, \lambda_m$) from a uniform distribution (the diagonal matrix \mathbf{L}). A lower bound of eigenvalues was set to 1 and an eigenvalue ratio (between upper and lower bound) set to 10. The algorithm then generates a random orthogonal matrix of eigenvectors \mathbf{Q} (via QR-decomposition) and constructs the genetic covariance matrix \mathbf{G} as \mathbf{QLQ}^T . The phenotypic covariance matrix was defined by the scalar multiplication $\mathbf{P} = k\mathbf{G}$, where k is a uniform random number from 1 to 10. This approach generates a random uniform distribution of covariance matrices in the space of positive definite covariance matrices (Joe 2006). In this set of simulations, as in all other fully stochastic models, \mathbf{G} and \mathbf{P} had 15 dimensions.

SIMULATION MODEL 3

In this model, \mathbf{G} and \mathbf{P} are defined as independent random positive definite covariance matrices using the uniform correlation matrix method (Joe, 2006), where a random correlation matrix (\mathbf{R}) is first generated from a uniform distribution of partial correlation coefficients. The variances are generated separately as a diagonal matrix $\mathbf{S} = \text{diag}(\sigma_1^2, \dots, \sigma_m^2)$ with elements obtained from a uniform distribution ranging from 1 to 10. The random covariance matrices are constructed as **SRS**. \mathbf{G} and \mathbf{P} were independently derived in this model, with the restriction that the variances in \mathbf{P} are always larger than the respective variances in \mathbf{G} . To achieve this, the variances (diagonal) of \mathbf{P} were random multiples of the respective variances in \mathbf{G} . This procedure ensures that the variances of \mathbf{P} were always larger, but \mathbf{P} and \mathbf{G} were independent. A series of 1000 simulations using this model yielded a distribution of \mathbf{G} and \mathbf{P} matrix correlations with a 95% confidence interval (CI) (using 2.5 and 97.5 quantiles) of -0.194 to 0.201 , and a median of 0.0004 . A further structural comparison of model 3 matrices was performed by CPC of 100 simulated \mathbf{G} \mathbf{P} pairs. We compared estimated covariance matrices after generating 300 random observations from a multivariate normal distribution with a mean vector of zeros and random \mathbf{G} and \mathbf{P} (defined as above) as parametric covariance matrices. Because the model fitting in CPC depends on sample sizes, we have maintained a standard $n = 300$ for all other comparisons as well. The results indicated the Unrelated model (no shared principal components) in all comparisons. Although the covariance structure is independently generated, all matrices generated by this method have variances on a much larger scale than the covariances. Therefore, there is some structural similarity because all matrices have clearly two groups of elements (covariances and variances), and the variances are always much larger than the covariances. This model is not biologically reasonable because \mathbf{G} and \mathbf{P} independence is unlikely (even if not proportional) due to a part-whole relationship. The model is included as a control, as the opposite to the mathemat-

ical proportionality of simulation model 2, allowing for a check that the simulations behaved as expected at extremes of \mathbf{G} and \mathbf{P} similarity and independence.

SIMULATION MODEL 4

Simulation model 4 was designed to generate correlated \mathbf{G} and \mathbf{P} matrices, but without a CPC structure. To achieve this, we have used the quantitative genetic relation $\mathbf{P} = \mathbf{G} + \mathbf{E}$. In these models, \mathbf{G} and \mathbf{E} were defined first and independently. \mathbf{P} was then defined as a random matrix with expected value \mathbf{G} and a random perturbation \mathbf{E} (Marsaglia and Olkin 1984). \mathbf{E} and \mathbf{G} were generated by the uniform correlation matrix method described in simulation model 3, where \mathbf{G} has a range of variances between 1 and $\sigma_{\max\mathbf{G}}^2$ (we used a maximum of 10), and \mathbf{E} has a range of variances between 0 and $\sigma_{\max\mathbf{E}}^2$, where $\sigma_{\max\mathbf{G}}^2$ and $\sigma_{\max\mathbf{E}}^2$ are the function parameters determining the upper limits of the range of variances in \mathbf{G} and \mathbf{E} , respectively. The expected value of the average heritability of the variables in the simulations is the ratio $(\sigma_{\max\mathbf{G}}^2 - 1)/([\sigma_{\max\mathbf{G}}^2 - 1] + \sigma_{\max\mathbf{E}}^2)$. This method generated correlated \mathbf{P} and \mathbf{G} , but without a common PC structure. This pattern is ensured because the variables with larger variances in \mathbf{E} will be generally different than the variables with larger variances in \mathbf{G} so that \mathbf{P} is less likely to inherit principal components from \mathbf{G} (H. Joe, pers. comm.). Of course, as the variances in \mathbf{E} become smaller than variances in \mathbf{G} ($\sigma_{\max\mathbf{E}}^2 \ll \sigma_{\max\mathbf{G}}^2$), CPCs between \mathbf{P} and \mathbf{G} appear. The distribution of matrix correlations from 1000 model 4 simulations (using $\sigma_{\max\mathbf{G}}^2 = 10$ and $\sigma_{\max\mathbf{E}}^2 = 9$ for a similar range of variances) presented a 95% CI of 0.560 – 0.897 , and a median of 0.776 . To check for common eigenstructure, we performed a CPC analysis of 100 model 4 simulations of \mathbf{G} and \mathbf{P} . The simulations showed strong support for the Unrelated model (no CPCs) in 65% of the cases, using the jump-up approach. The remaining simulations supported 1 (26%) or 2 (9%) CPCs. In simulation model 4, the perturbation of expected value \mathbf{G} by \mathbf{E} included random rotations of its eigenstructure, even if matrix correlations were high.

SIMULATION MODEL 5

In simulation model 5, \mathbf{G} was defined as a random positive definite covariance matrix using the eigenvector method from Marsaglia and Olkin (1984) and Joe (2006), but where $\sigma_{\max\mathbf{G}}^2$ is the max/min eigenvalue ratio (this parameter will have a different interpretation than in model 4, but the average heritabilities expected are exactly the same in models 4 and 5). \mathbf{P} was defined as the sum $\mathbf{G} + \mathbf{E}$, where \mathbf{E} was generated by the uniform correlation method, with a variance range of 0 to $\sigma_{\max\mathbf{E}}^2$. In this model, \mathbf{P} readily inherits the principal component structure of \mathbf{G} , even when $\sigma_{\max\mathbf{E}}^2 \sim \sigma_{\max\mathbf{G}}^2$. The matrix correlation in these simulated matrices (with $\sigma_{\max\mathbf{G}}^2 = 10$, and $\sigma_{\max\mathbf{E}}^2 = 9$) was smaller than in model 4 (matrix correlation distribution 95% CI = 0.061 – 0.462 , median = 0.274), but the

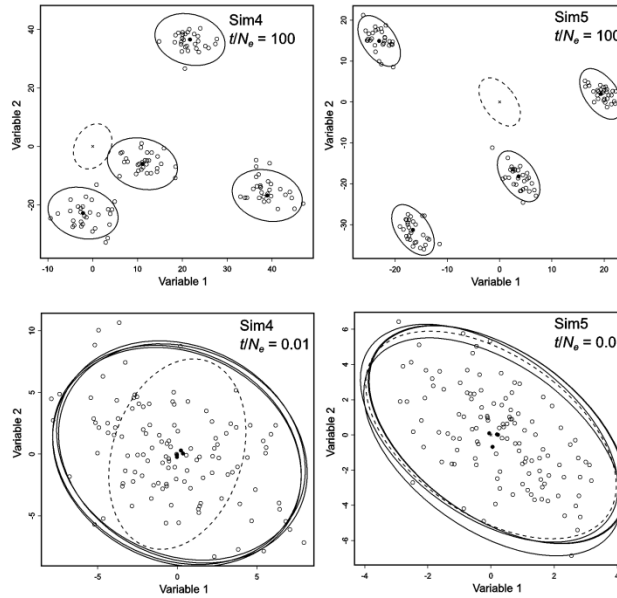


Figure 1. Simulation of genetic drift in four populations. The means of each population were evolved from an ancestral multivariate normal distribution with mean = (0,0) and covariance matrix = $G(t/N_e)$. Each population was randomly sampled 30 times using the respective average and covariance matrix P . Left panels correspond to simulation model 4, where P and G are correlated, but do not share principal components. Right panels correspond to simulation model 5, where P and G share principal components but have low correlation. The ancestral genetic covariance matrix is depicted as a dashed ellipse. The population phenotypic covariance matrices are depicted as solid ellipses. Filled circles correspond to population means and open circles correspond to individual observations.

CPC analysis shows strong support for a shared latent structure, where 13% of the simulations supported the Unrelated model (0 CPCs), and 60% of the simulations supported models with 3 or more common PCs. The perturbation caused by E generates random differences between P and G , but not a random rotation of the eigenstructure of G (when $\sigma^2_{\max G} > \sigma^2_{\max E}$). This pattern is caused by a lambda ratio ($\sigma^2_{\max G}$) of 10 or larger, which will produce G matrices with sharp elliptical contours (noticeable principal components), ensuring that the principal component structure of G is inherited by P , even when $\sigma^2_{\max G} \sim \sigma^2_{\max E}$ (H. Joe, pers. comm.).

An illustrative bivariate example of the typical main differences between simulation models 4 and 5 is depicted in Figure 1. We simulated for each model and t/N_e , four populations descending from an ancestor (0,0) with a random genetic covariance matrix (shown as dashed lines in Fig. 1) and a random phenotypic matrix. The same phenotypic covariance matrices were used to generate 30 observations in each population and these are depicted as distinct clusters around each descendant. In simulation model

4, the matrix P is a random rotation of G , whereas in simulation model 5, the main axes of G are preserved in P .

GENETIC DRIFT TEST

Genetic drift as a neutral model for phenotypic divergence was tested by comparing the among-population covariance matrix (B) and the within-population phenotypic covariance matrix (W , as a surrogate of the average G) for the simulated data using the method of Ackermann and Cheverud (2002, 2004). This involved extracting the eigenvectors (M) and eigenvalues (m) of W , and projecting each population phenotypic vector of means \bar{z} on M , $Y = \bar{z}M$. The vector of means for each population was the one estimated from the simulated samples, not the parametric means generated from the ancestral G and ancestral vector of means. Finally, we calculated the variances for each column of Y and performed a regression of the variances of Y on m

$$\ln(Y_i) = \ln(t/N_e) + \beta \ln(m_i) \tag{3}$$

Testing with a t -test whether the slope of the regression (β) is different from 1 indicates whether the pattern is compatible with genetic drift. The null hypothesis of genetic drift is rejected if the slope deviates significantly from 1 (Ackermann and Cheverud 2002).

For each combination of parameters (ancestral \mathbf{G} , \mathbf{P} , t/N_e ratio, sample size, number of descendant populations, $\sigma_{\max E}^2/\sigma_{\max G}^2$) in different models, we simulated 1000 datasets to estimate type I error rates. In the simulated datasets, the only mechanism producing phenotypic divergence among the descendant populations was genetic drift. When using a significance level of $\alpha = 0.05$, we expect that a true null hypothesis has a 5% chance of being rejected (a type I error). If the use of phenotypic covariances as proxies for genetic ones in the genetic drift test does increase the type I error rates, we expect to find that, using a significance level of 5%, the null model of genetic drift will be rejected in more than 5% of the simulated samples.

All the simulations and analyses were run in the R environment (R Development Core Team, 2010) using functions from the packages MASS (Venables and Ripley 2002), clusterGeneration (Qiu and Joe 2009), and vegan (Oksanen et al. 2010). The R code (commented) used for the simulations is available as Supporting information.

Results

For the simulation using the bee wing shape data (genetic and phenotypic covariance matrices) as starting parameters, the type I error rate decreased with increasing sample sizes for small t/N_e ratios (between 0.01 and 0.000001) irrespective of the number of populations (15, 30) used (Figs. 2A, S1A). The error rate increased for larger sample sizes when $t/N_e \geq 0.1$. The correlation between \mathbf{G} and \mathbf{W} remained stable over simulations for all t/N_e , with a median matrix correlation of 0.788, and a 95% CI (based on 0.025 and 0.975 quantiles) from 0.741 to 0.830. The matrix correlation for the ancestral (original) \mathbf{P} and \mathbf{G} was 0.804.

For the simulation using the shell shape data as starting parameters, the type I error rates remain at acceptable levels for sample sizes above 20 in t/N_e ratios equal to or below 0.001, and both numbers of populations (15, 30) (Figs. 2B, S1B). For the simulation with $t/N_e = 0.01$, the error rates increase with sample size. This is a slightly worse result than in the simulations with bee wing parameters, because in the latter, the simulation with $t/N_e = 0.01$ yielded acceptable error rates (Fig. 2A, B). The correlation between average \mathbf{G} and \mathbf{W} also remained stable over simulations using the shell dataset for all t/N_e , with a median matrix correlation of 0.441, and a 95% CI (based on 0.025 and 0.975 quantiles) from 0.405 to 0.479. The matrix correlation for the ancestral (original) \mathbf{P} and \mathbf{G} was 0.442.

In the simulation model 2, where \mathbf{G} and \mathbf{P} differed only by a random constant (Fig. 2C), the resulting pattern showed slight fluctuations around the expected type I error rate (0.05) for any value of t/N_e . This result was observed for sample sizes above 40 individuals per population regardless of the number of populations (15 or 30; Figs. 2C, S1C).

The simulation model 3, where \mathbf{P} and \mathbf{G} were generated independently (Figs. 2D, S1D), presented acceptable type I error rates only for t/N_e ratios equal to or below 0.00001, regardless of the number of populations. The simulations with $t/N_e > 0.001$ all presented type I error rates above 0.8 and are not shown in the Figure. Because in this model \mathbf{G} and \mathbf{P} have independent covariances, the test would be expected to show significant deviations from the unity slope for any combination of parameters. This suggests that the power of the test must be small for such values of t/N_e .

Simulation models 4 and 5 were designed to generate \mathbf{G} and \mathbf{P} correlated matrices, where $\mathbf{P} = \mathbf{G} + \mathbf{E}$. In simulation model 4, the random matrix \mathbf{E} adds variation to the genetic covariances and variances, including a random rotation of the eigenstructure when \mathbf{P} is calculated, even if the range of variances in \mathbf{E} ($\sigma_{\max E}^2$) is the same or a bit smaller than the range of variances in \mathbf{G} ($\sigma_{\max G}^2$). In simulation model 5, the \mathbf{E} matrix only causes differences in the principal components of \mathbf{G} and \mathbf{P} when $\sigma_{\max E}^2 > \sigma_{\max G}^2$. The first set of analyses was performed using the same range of variances in \mathbf{G} and \mathbf{E} for both models. The simulation model 4 presented acceptable error rates for sample sizes larger than 20 regardless of t/N_e ratio and number of populations. The simulation model 5 presented acceptable type I error rates only for t/N_e ratios equal to or below 0.001, regardless of the number of populations (Figs. 2E, F, S1E, S1F).

Exploring the simulations with a larger range of parameters, we found that the ratio of upper limits of environmental and genetic variance ranges ($\sigma_{\max E}^2/\sigma_{\max G}^2$) also influences the type I error rates of the test. One unexpected result was that in simulation model 4, as $\sigma_{\max E}^2$ gets smaller than $\sigma_{\max G}^2$, the type I error rates increase. We performed the simulations again, with fixed sample sizes (100), number of groups (15), and t/N_e (10) to assess the influence of $\sigma_{\max E}^2/\sigma_{\max G}^2$ on the slope of the AC test (Fig. 3). In the right panel of Figure 3, using simulation model 5 (where \mathbf{P} readily inherits the eigenvectors of \mathbf{G}), as the value of $\sigma_{\max E}^2/\sigma_{\max G}^2$ gets smaller, the slope of the test converges to 1, as expected under genetic drift. On the other hand, in the simulation model 4 (left panel of Fig. 3), the expected value of the slope under simulation of drift is 1 only when $\sigma_{\max E}^2 \sim \sigma_{\max G}^2$. As the ratio of variance ranges get smaller, the expected slope converges to approximately 1.3, and this pattern explains why the type I error rates increase when $\sigma_{\max E}^2$ gets smaller than $\sigma_{\max G}^2$. The simulations using the real matrices (model 1) and the same parameters described above had expected slopes of 1.3 (bees) and 0.8 (*Physa* shells).

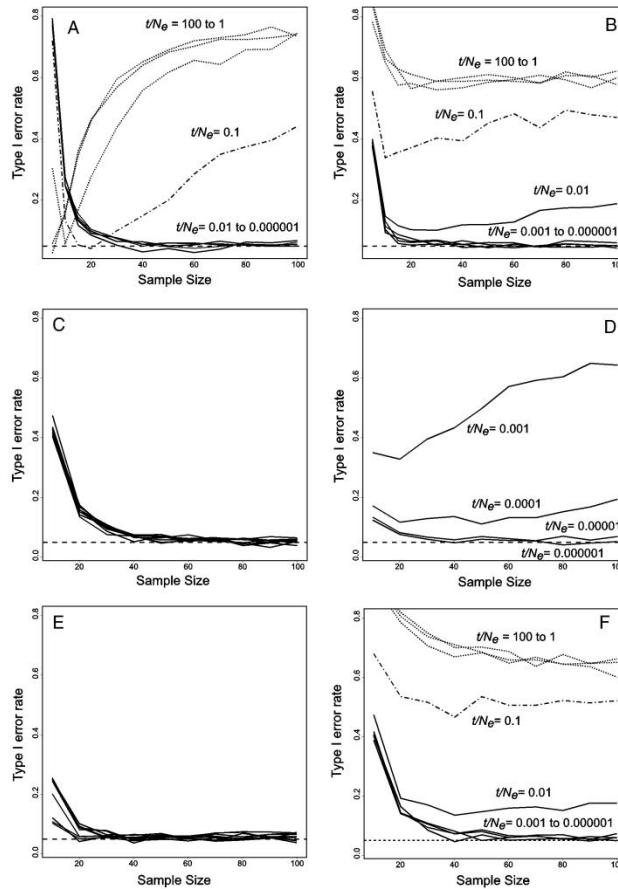


Figure 2. Type I error rates for the simulated analyses with varying sample sizes and t/N_e ratios (drift intensities). The legends and line types indicate the value of t/N_e used (only when differences among lines are noticeable). The dashed horizontal straight line indicates the expected type I error rate of 0.05. All simulations in this figure were performed with 15 populations. (A) Error rates for the bee wing dataset. (B) Error rates for the shell dataset. (C) Stochastic simulations (model 2) where G was random and P was exactly proportional to it $P = kG$ (multiplication by a random scalar k drawn from a uniform distribution between 1 and 10). (D) Stochastic simulation (model 3) where both G and P were random and completely independent. (E) Stochastic simulation (model 4) where G and P were correlated ($P = G + E$), but did not share a common latent structure (G and E with the same range of variances). (F) Stochastic simulation (model 5) where G and P were correlated and shared a common latent structure (G and E with the same range of variances). See text for model details.

Slopes larger than 1 might be obtained when the variance among population averages projected on the first eigenvectors of W is larger than the corresponding eigenvalues, whereas slopes smaller than 1 are the result of less among-population variation than predicted by the eigenvalues of the first PCs of W .

Considering that, for simulation model 5, smaller variance range ratios lead to the expected slope under genetic drift, we explored the combination of simulation parameters that would lead to acceptable type I error rates on the AC test (Table 1). When we decrease the $\sigma_{\max E}^2 / \sigma_{\max G}^2$ ratio, the correlations

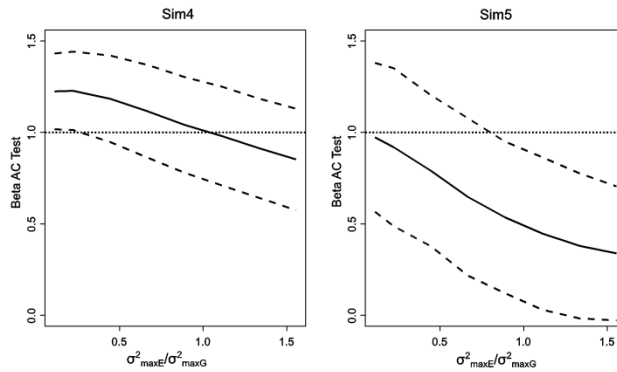


Figure 3. Slopes (β) of the Ackermann and Cheverud test in relation to the ratio of upper bounds of environmental ($\sigma^2_{\max E}$) and genetic ($\sigma^2_{\max G}$) variances in the simulations for models 4 (Sim4) and 5 (Sim5), using $t/N_e = 10$, 15 dimensions in \mathbf{G} , 15 populations, and 100 observations per population. Genetic variances ranged between 1 and $\sigma^2_{\max G} = 10$ and the environmental variances ranged between 0 and $\sigma^2_{\max E} = 1-15$. The solid lines show the expected (mean) value for the slope over 1000 simulations, whereas the dashed lines indicate the upper and lower limits of 95% CIs. The dotted line indicates the unity slope, which is the theoretical expectation under genetic drift.

Table 1. Type I error rates for the genetic drift test using simulation model 5 (1000 repetitions), with 15 variables, 15 groups, and 50 individuals per group ($\alpha = 0.05$), with varying t/N_e . $\sigma^2_{\max E}/\sigma^2_{\max G}$ is the ratio of the upper bounds of variances in the environmental and genetic matrices (see text), $CI-h^2$ is the 95% CI for the average heritability in each set of simulations, $CI-MatCor$ is the 95% CI for \mathbf{G} matrix correlations in each set of simulations, $fCPC$ is the percentage of significant full CPC models for \mathbf{G} and \mathbf{P} in 100 simulations, $CICPCs$ are the 95% CI (percentiles) for the number of common principal components for \mathbf{G} and \mathbf{P} in 100 simulations.

GP matrix comparisons					t/N_e			
$\sigma^2_{\max E}/\sigma^2_{\max G}$	$CI-h^2$	$CI-MatCor$	$fCPC$	$CICPCs$	100	10	1	0.1
0.1	0.86 – 0.94	0.808 – 0.970	100	14	0.058	0.062	0.056	0.048
0.2	0.76 – 0.88	0.543 – 0.891	100	14	0.048	0.057	0.058	0.043
0.3	0.70 – 0.84	0.385 – 0.812	79	7–14	0.097	0.084	0.102	0.077
0.4	0.64 – 0.80	0.277 – 0.729	67	4–14	0.139	0.159	0.188	0.132

between \mathbf{P} and \mathbf{G} increase, as well as the number of CPCs. If $\sigma^2_{\max E}$ is around 20% of $\sigma^2_{\max G}$, the matrix correlations observed are not particularly high, as compared to real \mathbf{P} and \mathbf{G} matrices estimated with large sample sizes, but they do share a common eigenstructure, and for any value of t/N_e , the type I error rates approach acceptable values. Performing the same simulations with more variables ($m = 30$), the same results are obtained with larger within-population sample sizes ($n > 100$) (results not shown). It is evident from these results that the combination of parameters yielding acceptable type I error rates is sensitive to the models under which the starting matrices were generated.

Discussion

Testing diversification by genetic drift is a useful starting point in the study of evolutionary variation (Lynch 1990; Ackermann and

Cheverud 2004; Weaver et al. 2007; Perez and Monteiro 2009). Cheverud’s (1988) suggestion that genetic covariance matrices could be safely replaced by phenotypic matrices for evolutionary inferences was greeted with scepticism, and “Cheverud’s conjecture” (Roff 1995) has been tested and discussed in a number of papers (e.g., Roff 1995, 1996; Koots and Gibson, 1996; Waitt and Levin 1998; Roff et al. 1999; Bégin and Roff 2004; Hadfield et al. 2006; Kruuk et al. 2007), usually by comparing the similarity of genetic and phenotypic covariances, seldom by checking the influence of matrix differences in the results of tests. Thus, the evidence gathered has been equivocal and the most relevant studies (large reviews of data) indicate a general agreement with Cheverud (1988), but also recommend caution in the interpretations of results because matrix comparisons among isolated populations using genetic or phenotypic covariances might

differ in important ways (Roff et al. 1999; Bégin and Roff 2004).

Our results indicate that the type I error of Ackermann and Cheverud's (2002, 2004) test of proportionality between **B** and **W** is influenced mainly by the structural similarity between the ancestral **G** and **P**, the ratio of variance ranges (approximated by the average heritability), and the ratio of time and effective population size t/N_e . If the parametric genetic and phenotypic covariance matrices are exactly proportional, as in the simulation model 2, the type I error rates are acceptable for any t/N_e ratio (as expected). On the other extreme (simulation model 3), where **G** and **P** were generated with an unrealistic minimum of structural similarity, the type I error rate is unacceptable for most values of t/N_e .

The simulations showed that even if the ancestral **G** and **P** are not proportional but do share a large number of principal components, have an average heritability around 0.5, and matrix correlation above 0.7 over all variables (as in our simulation model 5), acceptable type I error rates will be obtained for any t/N_e ratio. When **G** and **P** do not share principal components but are highly correlated ($r > 0.7$) and have average heritabilities approaching 0.5, the type I error rates should be acceptable for any t/N_e ratio (as in our simulation model 4). Average heritabilities different from 0.5 will bias the expectation of the slope in the AC test due to concentration of variation among projections of population averages in the first eigenvectors of **W**. In these cases, type I error rates will still be acceptable for $t/N_e < 0.01$.

The combination of parameters laid out is not an unrealistic expectation. The literature indicates that considerable agreement between genetic and phenotypic correlations is often found and that the correlations between **G** and **P** are usually above 0.6 for morphological data when effective sample sizes are large (Cheverud 1988; Koots and Gibson, 1996; Roff 1996; Waitt and Levin 1998; Bégin and Roff 2004; Kruuk et al. 2007; de Oliveira et al. 2009).

In a study where only phenotypic data are available, it might be complicated or impossible to determine whether the relationship between the ancestral **G** and **P** fits into the assumptions outlined above. These parameter values can, nevertheless, be used as guidelines for comparisons among populations as indirect evidence of ancestral **G** and **P** similarity (de Oliveira et al. 2009), or one might use the Monte Carlo simulation approach described below to estimate a CI for the slope of the AC test under drift.

Our example datasets (simulation model 1) seem to behave in a similar way to simulation model 4 for extremes of low and high $\sigma_{\max E}^2/\sigma_{\max G}^2$. The expected slope for the simulations using the bee matrices was 1.3, the similarity of **G** and **P** was high, they did share principal components, but the average heritability was low (it should have been higher than 0.6 to fit the model 4 more closely). On the other hand, the simulations with shell matrices had an expected slope of 0.8, **G** and **P** similarity was

low, they did not share principal components, but the average heritability was high (should have been lower than 0.3). Such results would be observed if model 4 was changed to calculate $\mathbf{P} = k(\mathbf{G} + \mathbf{E})$, so that the average heritability would be decreased or increased by the scalar k without influence in the correlation or shared structure between **P** and **G**. These results suggest that **G** and **P** are related in complex ways, which can hardly be reduced to scalar comparisons without considerable loss of information. If some information about **G** and **P** is available, one might use this simulation approach to estimate the expected slope of the AC test and use this expectation in the test of the real data (instead of the theoretical unity slope). For example, in the bee wing analyses, we could have used a slope of 1.3 as parameter in the t -test of the AC tests and the type I error rates would be acceptable for any value of t/N_e . Alternatively, the 95% CI for the expected AC test slope under genetic drift simulations ranged from 1.1 to 1.5, and an observed slope could be compared with this interval for evidence of departure from the neutral expectation. When genetic data are not available, it might be possible to use the between-population covariance matrix (**B**), estimated from phylogenetic independent contrasts if possible (Revell 2007) and the within-population phenotypic covariance matrix **W** as proxies for the ancestral **G** and **P**, respectively, in the simulations to estimate the expected slope under drift. A simulation function provided as Supporting information (simulationAC-slope.R) will calculate a mean estimate and a 95% CI for AC test slopes under genetic drift for any ancestral **G** and **P**. Observed slopes can be compared to the CI or the mean estimate can replace the parameter slope = 1 in the ordinary t -test.

Within-population sample sizes influence the type I error rates, but they need to be considered in conjunction with the number of populations and the dimensionality of the matrices. For our fully stochastic simulations, all matrices had 15 dimensions and most acceptable type I errors were observed for within-population samples larger than 40. The number of populations used had a slight but negligible effect.

It is possible that sampling error in the estimation of **G** might lead to a similar pattern of type I errors as when average **G** is replaced by **W**, because the parametric and estimated **G** matrices are not likely to be exactly proportional as well. It is not clear whether sampling error in the estimation of **G** is comparable to the environmental covariance matrix **E**, but a part of Cheverud's conjecture was that **W** could be a more reliable estimate of the parametric **G** than a genetic matrix estimated from a small effective sample size (Cheverud 1988), and phenotypic correlation estimates are often within the CIs of genetic correlations (Koots and Gibson 1996; Roff 1996). The instability of covariance matrix and factor estimation for small sample sizes is well known in multivariate statistics (MacCallum et al. 1999; Krzanowski 2000), and genetic covariance matrices can be particularly demanding with respect to

samples sizes (Cheverud 1988). Patterns caused by sampling error in the estimation of genetic covariance matrices, such as biases on eigenvalues, are well known (Meyer and Kirkpatrick 2010) and a considerably large statistical literature is devoted to such topics. As long as the sampling error can be considered independent from the parametric \mathbf{G} , the simulation function provided as Supporting information can be adjusted to address specific concerns regarding the error in the estimation of \mathbf{G} .

In some of the simulations, particularly model 1 (with pre-determined matrices) and the fully stochastic simulation where \mathbf{G} and \mathbf{P} where random and completely independent (model 2), a trend was observed where for higher values of t/N_e , the type I error rates increase with within-population sample size (see Fig. 2A, B, D). This counterintuitive result was also observed in simulation model 4, when $\sigma_{\max E}^2$ is smaller than $\sigma_{\max G}^2$ (Fig. S2). Considering that, depending on this ratio, the differences between \mathbf{G} and \mathbf{P} caused the expected value of the slope of the AC test to be larger than 1 (as shown in Fig. 3 due to more variation among populations than predicted by the eigenvalues of \mathbf{W}), the type I error rates increase with sample sizes because the CIs become narrower (there is an expected increase in power) and a larger percentage of simulated tests will show significant results. The type I error converges to a value that depends on the magnitude of deviation of the expected AC test slope from 1 and the size of the CI. For smaller t/N_e ratios, there is a reduction in the contribution of the \mathbf{G} matrix to among-population variation (it will be proportional to $t/N_e \mathbf{G}$). Because the simulations calculate among-group variation using averages estimated from the n observations generated by \mathbf{P} at each population (and not the parametric means generated by \mathbf{G}), when t/N_e decreases, most among-population variation is generated and predicted by \mathbf{W} , and the expected slope of the AC test is 1. This also explains the effect in reverse, when $\sigma_{\max E}^2 > \sigma_{\max G}^2$, causing among-population variation to be smaller than the eigenvalues of \mathbf{W} and the expected slope of the AC test to be < 1 (Fig. 3).

In summary, replacing \mathbf{G} with \mathbf{W} when testing the null hypothesis of divergence by genetic drift is not likely to increase the type I error rates of the AC test, unless the ancestral \mathbf{G} and \mathbf{W} are structurally dissimilar (mathematical proportionality is not a required condition), the t/N_e ratio is large, and sample sizes are small (< 40 per group). A Monte Carlo simulation approach might be used to estimate the expected slope of the AC test under drift, taking into account the structural differences between \mathbf{G} and \mathbf{P} . A number of other methods have been proposed, which were used to compare among-population and within-population covariance matrices (Lofsvold 1988; Bégin and Roff 2001; Revell et al. 2007). Not all of these alternative methods will have their type I error rates increased when average \mathbf{G} is replaced by \mathbf{W} . Type II errors are also a possibility, as genetic drift is the alternative hypothesis in some tests (Revell et al. 2007). The simulation

function provided as Supporting information can be modified to account for other methods of matrix comparison. Alternatively, model-based approaches (Butler and King 2004) should provide reliable and possibly more informative tests of evolutionary processes and scenarios. The simulation approaches, particularly the more sophisticated individual-based models (Revell 2007), should prove useful in further analyses, comparing methods and testing evolutionary quantitative genetics models.

ACKNOWLEDGMENTS

The authors would like to thank T. DeWitt for allowing the use of the *Physa* shape data as simulation parameters. Previous versions of the manuscript were greatly improved by comments from G. Marroig and anonymous reviewers. MP was funded by the Fundação para a Ciência e a Tecnologia (Portugal), through the Ph.D. Programme in Computational Biology, Instituto Gulbenkian de Ciência (Portugal). LRM is funded by the Conselho Nacional de Desenvolvimento Científico e Tecnológico (CNPq, Brazil) and the Fundação de Amparo à Pesquisa do Estado do Rio de Janeiro (FAPERJ). The authors declare no conflict of interest.

LITERATURE CITED

- Ackermann, R. R., and J. M. Cheverud. 2002. Discerning evolutionary processes in patterns of tamarin (genus *Saguinus*) craniofacial variation. *Am. J. Phys. Anthropol.* 117:260–271.
- . 2004. Detecting genetic drift versus selection in human evolution. *Proc. Natl. Acad. Sci. USA* 101:17946–17951.
- Arnold, S. J., M. E. Pfrender, and A. G. Jones. 2001. The adaptive landscape as a conceptual bridge between micro- and macro-evolution. *Genetica* 112–113:9–32.
- Bégin, M., and D. A. Roff. 2001. An analysis of \mathbf{G} matrix variation in two closely related cricket species, *Gryllus firmus* and *G. pennsylvanicus*. *J. Evol. Biol.* 14:1–13.
- . 2004. From micro- to macroevolution through quantitative genetic variation: positive evidence from field crickets. *Evolution* 58:2287–2304.
- Butler, M. A., and A. A. King. 2004. Phylogenetic comparative analysis: a modeling approach for adaptive evolution. *Am. Nat.* 164:683–695.
- Cheverud, J. 1988. A comparison of genetic and phenotypic correlations. *Evolution* 42:958–968.
- Cheverud, J., and G. Marroig. 2007. Comparing covariance matrices: random skewers method compared to the common principal components model. *Genet. Mol. Biol.* 30:461–469.
- de Oliveira, F. B., A. Porto, and G. Marroig. 2009. Covariance structure in the skull of Catarrhini: a case of pattern stasis and magnitude evolution. *J. Hum. Evol.* 56:417–430.
- DeWitt, T. J. 1996. Functional tradeoffs and phenotypic plasticity in the freshwater snail *Physa*. Ph.D. diss., Binghamton University, Binghamton, New York.
- . 1998. Costs and limits of phenotypic plasticity: tests with predator-induced morphology and life history in a freshwater snail. *J. Evol. Biol.* 11:465–480.
- Falconer, D. S., and T. F. C. Mackay. 1996. Introduction to quantitative genetics. 4th ed. Pearson Prentice Hall, Harlow, U. K.
- Felsenstein, J. 1988. Phylogenies and quantitative characters. *Annu. Rev. Ecol. Syst.* 19:445–471.
- Hadfield, J. D., A. Nutall, D. Osorio, and I. P. F. Owens. 2006. Testing the phenotypic gambit: phenotypic, genetic and environmental correlations of colour. *J. Evol. Biol.* 20:549–557.

- Joe, H. 2006. Generating random correlation matrices based on partial correlations. *J. Multivariate Anal.* 97:2177–2189.
- Jones, A. G., S. J. Arnold, and R. Bürger. 2003. Stability of the **G**-matrix in a population experiencing pleiotropic mutation, stabilizing selection, and genetic drift. *Evolution* 57:1747–1760.
- Klingenberg, C. P., V. Debat, and D. A. Roff. 2010. Quantitative genetics of shape in cricket wings: developmental integration in a functional structure. *Evolution* 64:2935–2951.
- Koots, K. R., and J. P. Gibson. 1996. Realized sampling variances of estimates of genetic parameters and the difference between genetic and phenotypic correlations. *Genetics* 143:1409–1416.
- Kruuk, L. E. B., J. Slate, and A. J. Wilson. 2007. New answers for old questions: the evolutionary quantitative genetics of wild animal populations. *Annu. Rev. Ecol. Evol. Syst.* 39:525–548.
- Krzyszowski, W. J. 2000. Principles of multivariate analysis: a user's perspective. 2nd ed. Oxford Univ. Press, Oxford, U. K.
- Lande, R. 1979. Quantitative genetic analysis of multivariate evolution, applied to brain:body size allometry. *Evolution* 33:402–416.
- . 1980. Genetic variation and phenotypic evolution during allopatric speciation. *Am. Nat.* 116:463–479.
- Lofsvold, D. 1986. Quantitative genetics of morphological differentiation in *Peromyscus*. I. Tests of homogeneity of genetic covariance structure among species and subspecies. *Evolution* 40:559–573.
- . 1988. Quantitative genetics of morphological differentiation in *Peromyscus*. II. Analysis of selection and drift. *Evolution* 42:54–67.
- Lynch, M. 1990. The rate of morphological evolution in mammals from the standpoint of the neutral expectation. *Am. Nat.* 136:727–741.
- MacCallum, R. C., K. F. Widaman, S. Zhang, and S. Hong. 1999. Sample size in factor analysis. *Psychol. Methods* 4:84–99.
- Marroig, G., and J. M. Cheverud. 2004. Did natural selection or genetic drift produce the cranial diversification of neotropical monkeys? *Am. Nat.* 163:417–428.
- Marsaglia, G., and I. Olkin. 1984. Generating correlation matrices. *SIAM J. Sci. Statist. Comput.* 5:470–475.
- Meyer, K., and M. Kirkpatrick. 2010. Better estimates of genetic covariance matrices by “bending” using penalized maximum likelihood. *Genetics* 185:1097–1110.
- Monteiro, L. R., and J. L. Gomes, Jr. 2005. Morphological divergence rate tests for natural selection: uncertainty of parameter estimation and robustness of results. *Genet. Mol. Biol.* 28:345–355.
- Monteiro, L. R., J. A. F. Diniz-Filho, S. F. dos Reis, and E. D. Araújo. 2002. Geometric estimates of heritability in biological shape. *Evolution* 56:563–572.
- Oksanen, J., F. G. Blanchet, R. Kindt, P. Legendre, R. B. O'Hara, G. L. Simpson, P. Solymos, M. H. H. Stevens, and H. Wagner. 2010. *vegan*: Community Ecology Package. R package version 1.17–4. Available at <http://CRAN.R-project.org/package=vegan>. Accessed April 30, 2010.
- Perez, S. I., and L. R. Monteiro. 2009. Nonrandom factors in modern human morphological diversification: a study of craniofacial variation in southern south american populations. *Evolution* 63:978–993.
- Phillips, P., and S. J. Arnold. 1999. Hierarchical comparison of genetic variance-covariance matrices I. Using the Flury hierarchy. *Evolution* 53:1506–1515.
- Qiu, W., and H. Joe. 2009. *clusterGeneration*: random cluster generation (with specified degree of separation). R package version 1.2.7. Available at <http://CRAN.R-project.org/package=clusterGeneration>. Accessed September 18, 2011.
- R Development Core Team. 2010. *R: a language and environment for statistical computing*. R Foundation for Statistical Computing. Vienna, Austria. Available at <http://www.R-project.org>. Accessed April 30, 2010.
- Revell, L. J. 2007. Testing the genetic constraint hypothesis in a phylogenetic context: a simulation study. *Evolution* 61:2720–2727.
- Revell, L. J., L. J. Harmon, R. B. Langerhans, and J. J. Kolbe. 2007. A phylogenetic approach to determining the importance of constraint on phenotypic evolution in the neotropical lizard *Anolis cristatellus*. *Evol. Ecol. Res.* 9:261–282.
- Revell, L. J., D. L. Mahler, J. R. Sweeney, M. Sobotka, V. E. Fancher, and J. B. Losos. 2010. Nonlinear selection and the evolution of variances and covariances for continuous characters in an anole. *J. Evol. Biol.* 23:407–421.
- Roff, D. 1995. The estimation of genetic correlations from phenotypic correlations: a test of Cheverud's conjecture. *Heredity* 74:481–490.
- . 1996. The evolution of genetic correlations: an analysis of patterns. *Evolution* 50:1392–1403.
- Roff, D., T. Mousseau, and D. Howard. 1999. Variation in genetic architecture of calling song among populations of *Allonemobius socius*, *A. fasciatus*, and a hybrid population: drift or selection? *Evolution* 53:216–224.
- Venables, W. N., and B. D. Ripley. 2002. *Modern applied statistics with S*. 4th ed. Springer, New York.
- Waitt, D. E., and D. A. Levin. 1998. Genetic and phenotypic correlations in plants: a botanical test of Cheverud's conjecture. *Heredity* 80:310–319.
- Weaver, T. D., C. C. Roseman, and C. B. Stringer. 2007. Were neandertal and modern human cranial differences produced by natural selection or genetic drift? *J. Hum. Evol.* 53:135–145.
- Willis, J. H., J. A. Coyne, and M. Kirkpatrick. 1991. Can one predict the evolution of quantitative characters without genetics? *Evolution* 45:441–444.
- Zeng, Z. B. 1988. Long-term correlated response, interpopulation covariation, and interspecific allometry. *Evolution* 42:363–374.

Associate Editor: G. Marroig

Supporting Information

The following supplementary material is available for this article:

Figure S1. Type I error rates for the simulated analyses with varying sample sizes and t/N_e ratios (drift intensities).

Figure S2. Type I error rates for the simulated analyses under model 4 with varying $\sigma_{2\max E}/\sigma_{2\max G}$, sample sizes, and t/N_e ratios (drift intensities).

Supporting Information may be found in the online version of this article.

Please note: Wiley-Blackwell is not responsible for the content or functionality of any supporting information supplied by the authors. Any queries (other than missing material) should be directed to the corresponding author for the article.

Appendix D. Strain values from Chapter 6

Strain values as output from FEAs performed in Chapter 6 are here presented in table form. Maximum (ϵ_1) and minimum (ϵ_3) principal strain values at the location of 70 landmarks are displayed in microstrain (μstrain). Each table represents a simulated bite with one tooth along the dental row, from first incisor (I1) to third molar (M3), to the exclusion of the canine. Also displayed are strain differences ($\Delta\epsilon_1$ and $\Delta\epsilon_3$) at landmark locations between models or load cases (see Chapter 6 for details). The placing of these strain tables here rather than in the chapter proper is due to the vastness of space they require, which is easier to manage in an appendix.

Table D.1. Maximum ($\epsilon 1$) and minimum ($\epsilon 3$) principal strain values at the location of 70 landmarks during first incisor (I1) bite load for the filled, unfilled and jaw joint constraint sensitivity tests (see text for more details), and strain differences ($\Delta \epsilon 1$ and $\Delta \epsilon 3$) at landmark locations between models. Strain values are in microstrain (μ strain).

I1 bite landmark	Filled		Unfilled		Jaw Joint		Filled-Unfilled		Filled-JawJoint	
	$\epsilon 1$	$\epsilon 3$	$\epsilon 1$	$\epsilon 3$	$\epsilon 1$	$\epsilon 3$	$\Delta \epsilon 1$	$\Delta \epsilon 3$	$\Delta \epsilon 1$	$\Delta \epsilon 3$
1	646.29	-552.11	654.99	-560.54	657.09	-563.60	-8.70	8.43	-10.80	11.48
2	208.52	-109.23	279.06	-125.97	211.68	-110.72	-70.55	16.74	-3.16	1.49
3	266.00	-96.64	291.42	-105.16	272.74	-99.34	-25.42	8.51	-6.74	2.70
4	52.97	-235.65	65.46	-291.28	57.97	-258.11	-12.50	55.64	-5.01	22.46
5	59.08	-18.98	69.12	-22.18	58.74	-18.83	-10.04	3.21	0.35	-0.15
6	32.80	-99.76	40.46	-121.28	32.90	-100.16	-7.66	21.52	-0.10	0.40
7	2.14	-0.85	3.69	-1.47	7.17	-2.78	-1.56	0.62	-5.03	1.93
8	217.62	-70.22	224.43	-78.78	267.82	-103.34	-6.82	8.56	-50.20	33.12
9	153.01	-324.59	165.78	-289.06	157.21	-331.74	-12.77	-35.52	-4.20	7.16
10	19.85	-14.72	24.51	-17.42	18.69	-14.60	-4.66	2.71	1.16	-0.12
11	167.55	-489.47	172.24	-503.44	171.80	-502.15	-4.69	13.97	-4.25	12.68
12	265.55	-158.28	365.44	-259.08	272.09	-162.30	-99.90	100.79	-6.55	4.02
13	23.13	-51.89	24.08	-53.61	23.83	-53.41	-0.96	1.71	-0.70	1.52
14	222.93	-117.64	229.51	-121.22	228.11	-120.41	-6.57	3.58	-5.18	2.77
15	149.83	-97.46	154.39	-100.61	153.18	-99.72	-4.56	3.15	-3.35	2.26
16	110.40	-53.01	119.98	-56.58	114.38	-54.64	-9.58	3.57	-3.98	1.63
17	102.17	-42.26	108.67	-44.75	104.54	-43.17	-6.50	2.49	-2.37	0.91
18	161.90	-62.75	282.21	-100.52	163.35	-63.29	-120.31	37.77	-1.45	0.54
19	44.85	-94.33	56.59	-57.76	47.98	-141.66	-11.74	-36.57	-3.12	47.33
20	0.79	-0.14	0.75	-0.47	0.77	-0.69	0.03	0.33	0.01	0.54
21	295.63	-88.27	344.48	-104.24	267.85	-79.83	-48.85	15.96	27.78	-8.44
22	224.28	-101.30	266.46	-115.68	232.77	-104.18	-42.18	14.37	-8.49	2.88
23	115.10	-377.12	121.57	-399.06	119.18	-391.68	-6.47	21.94	-4.07	14.56
24	125.98	-386.48	129.48	-395.56	131.41	-402.92	-3.50	9.07	-5.43	16.43
25	260.30	-265.86	256.93	-264.11	261.76	-262.91	3.37	-1.75	-1.46	-2.95
26	476.56	-203.76	500.14	-213.97	439.93	-190.59	-23.59	10.21	36.62	-13.16
27	220.30	-391.01	223.10	-395.03	220.03	-387.45	-2.81	4.02	0.26	-3.55
28	342.56	-76.96	332.47	-80.29	304.75	-69.43	10.09	3.33	37.80	-7.54
29	37.35	-107.10	40.40	-115.58	37.83	-108.58	-3.05	8.48	-0.49	1.48
30	39.68	-103.24	44.14	-114.01	40.83	-105.72	-4.46	10.77	-1.15	2.48
31	44.71	-18.17	57.96	-25.88	53.84	-20.34	-13.25	7.71	-9.13	2.17
32	183.21	-647.35	188.56	-668.10	180.86	-638.99	-5.34	20.75	2.36	-8.36
33	126.14	-42.46	120.35	-45.30	161.09	-52.40	5.79	2.85	-34.96	9.94
34	6.72	-17.70	44.50	-34.86	1.77	-3.96	-37.77	17.16	4.96	-13.74
35	427.56	-134.12	426.25	-131.66	424.23	-133.89	1.31	-2.46	3.32	-0.23
36	161.31	-74.62	143.16	-49.69	175.22	-94.56	18.15	-24.93	-13.91	19.94
37	13.83	-38.93	17.20	-42.92	142.41	-62.77	-3.37	4.00	-128.58	23.84
38	26.76	-8.52	33.33	-10.15	27.92	-8.57	-6.57	1.63	-1.17	0.05
39	143.87	-501.44	145.88	-508.37	146.49	-510.91	-2.01	6.92	-2.62	9.47
40	227.23	-59.49	252.94	-63.12	231.26	-60.59	-25.71	3.63	-4.03	1.10
41	127.80	-49.22	120.43	-51.84	131.48	-50.00	7.36	2.62	-3.69	0.78
42	128.08	-58.33	137.97	-62.69	130.08	-59.31	-9.89	4.36	-1.99	0.98
43	400.62	-97.65	410.08	-100.64	405.78	-98.91	-9.46	2.99	-5.17	1.26
44	333.28	-85.83	339.43	-87.65	338.06	-86.77	-6.15	1.82	-4.78	0.94
45	144.40	-47.59	153.31	-50.27	146.89	-48.23	-8.90	2.68	-2.49	0.64
46	89.11	-42.87	148.83	-55.73	89.77	-43.25	-59.73	12.85	-0.67	0.37
47	146.58	-36.38	163.88	-50.34	118.18	-33.92	-17.30	13.96	28.39	-2.47
48	5.16	-13.32	9.62	-23.94	18.27	-41.06	-4.46	10.62	-13.11	27.74
49	341.26	-108.51	385.85	-125.08	271.51	-85.67	-44.59	16.57	69.75	-22.84
50	254.82	-89.60	295.55	-103.50	224.60	-79.17	-40.73	13.90	30.22	-10.43
51	124.96	-385.14	133.82	-412.38	129.87	-399.59	-8.85	27.23	-4.91	14.45
52	211.00	-230.27	240.92	-244.34	214.23	-236.14	-29.92	14.07	-3.24	5.87
53	270.84	-455.38	267.93	-445.45	278.10	-479.15	2.91	-9.93	-7.26	23.76
54	465.01	-225.92	499.61	-240.46	361.81	-196.25	-34.60	14.54	103.19	-29.67
55	114.54	-222.35	119.42	-243.57	108.08	-194.72	-4.88	21.23	6.46	-27.63
56	149.94	-96.57	189.01	-87.98	102.48	-92.18	-39.07	-8.59	47.46	-4.39
57	38.23	-124.15	41.47	-133.02	37.68	-122.31	-3.24	8.87	0.55	-1.84
58	53.52	-111.50	59.54	-120.44	51.63	-108.16	-6.02	8.94	1.90	-3.34
59	25.74	-8.83	36.42	-12.02	19.48	-6.74	-10.68	3.19	6.26	-2.09
60	150.67	-462.22	163.84	-495.70	123.55	-384.17	-13.17	33.47	27.13	-78.05
61	103.40	-52.50	102.67	-86.41	223.68	-72.23	0.73	33.91	-120.28	19.73
62	4.22	-11.43	16.23	-37.24	14.73	-6.08	-12.01	25.81	-10.51	-5.35
63	350.48	-188.64	348.23	-184.26	298.96	-162.89	2.26	-4.37	51.52	-25.75
64	282.42	-107.88	282.76	-98.49	322.36	-207.27	-0.33	-9.39	-39.94	99.40
65	209.70	-573.74	229.43	-614.36	211.70	-579.91	-19.73	40.61	-1.99	6.17
66	248.95	-158.21	251.03	-167.15	215.03	-147.72	-2.08	8.94	33.93	-10.48
67	46.07	-178.52	52.48	-196.50	47.98	-184.11	-6.41	17.98	-1.91	5.59
68	184.64	-562.04	190.88	-583.78	194.22	-582.55	-6.24	21.74	-9.58	20.51
69	225.95	-133.85	229.04	-145.56	154.62	-81.82	-3.09	11.71	71.32	-52.02
70	53.91	-117.58	57.25	-118.10	53.99	-119.64	-3.34	0.53	-0.08	2.07

Table D.2. Maximum ($\epsilon 1$) and minimum ($\epsilon 3$) principal strain values at the location of 70 landmarks during second incisor (I2) bite load for the filled, unfilled and jaw joint constraint sensitivity tests (see text for more details), and strain differences ($\Delta \epsilon 1$ and $\Delta \epsilon 3$) at landmark locations between models. Strain values are in microstrain (μ strain).

I2 bite landmark	Filled		Unfilled		Jaw Joint		Filled-Unfilled		Filled-JawJoint	
	$\epsilon 1$	$\epsilon 3$	$\epsilon 1$	$\epsilon 3$	$\epsilon 1$	$\epsilon 3$	$\Delta \epsilon 1$	$\Delta \epsilon 3$	$\Delta \epsilon 1$	$\Delta \epsilon 3$
1	147.64	-397.31	164.47	-420.39	149.93	-404.84	-16.83	23.08	-2.28	7.53
2	273.62	-211.46	359.01	-253.61	277.83	-214.71	-85.39	42.15	-4.22	3.25
3	272.14	-100.94	297.25	-109.45	279.25	-103.76	-25.11	8.51	-7.11	2.82
4	51.87	-231.54	64.20	-286.33	56.93	-253.87	-12.33	54.79	-5.06	22.33
5	59.19	-19.01	69.23	-22.24	58.65	-18.85	-10.04	3.24	0.54	-0.15
6	33.28	-101.32	40.99	-123.03	33.45	-101.96	-7.71	21.71	-0.17	0.64
7	2.17	-0.88	3.72	-1.49	7.29	-2.85	-1.55	0.62	-5.12	1.98
8	218.27	-71.04	224.66	-80.09	269.70	-106.01	-6.39	9.05	-51.43	34.97
9	160.63	-337.63	174.15	-304.27	165.54	-345.73	-13.52	-33.35	-4.91	8.10
10	23.75	-15.70	28.28	-18.31	22.74	-15.51	-4.53	2.62	1.00	-0.19
11	184.50	-547.32	191.31	-568.05	189.26	-561.58	-6.81	20.73	-4.76	14.26
12	797.07	-523.21	950.41	-713.88	815.45	-534.72	-153.34	190.68	-18.38	11.52
13	12.79	-33.16	14.01	-36.49	13.27	-34.33	-1.22	3.34	-0.48	1.18
14	222.47	-122.54	232.15	-126.46	227.76	-125.43	-9.67	3.93	-5.29	2.90
15	160.55	-105.55	167.32	-109.96	163.73	-107.72	-6.77	4.42	-3.18	2.17
16	51.77	-35.72	61.03	-39.32	54.40	-36.89	-9.27	3.60	-2.64	1.17
17	96.08	-42.40	100.70	-43.72	98.31	-43.28	-4.63	1.32	-2.23	0.87
18	196.05	-76.23	334.91	-119.59	198.42	-77.06	-138.86	43.36	-2.37	0.83
19	47.63	-113.45	53.38	-70.13	52.11	-162.81	-5.75	-43.32	-4.47	49.36
20	0.73	-0.14	0.73	-0.42	0.73	-0.70	0.00	0.28	0.00	0.56
21	310.33	-92.77	364.12	-110.33	283.63	-84.64	-53.79	17.56	26.71	-8.13
22	181.80	-90.14	222.05	-103.53	190.12	-92.95	-40.26	13.39	-8.32	2.80
23	118.82	-388.54	125.60	-411.02	123.03	-403.68	-6.78	22.48	-4.20	15.15
24	188.81	-581.47	195.46	-601.95	195.75	-602.41	-6.65	20.47	-6.94	20.93
25	264.10	-272.91	261.01	-271.20	265.74	-270.34	3.09	-1.71	-1.64	-2.57
26	501.67	-212.33	527.54	-223.28	468.02	-200.37	-25.87	10.94	33.65	-11.96
27	223.50	-405.38	226.01	-409.87	223.70	-403.89	-2.50	4.49	-0.20	-1.49
28	367.77	-81.13	364.10	-87.11	330.35	-73.71	3.66	5.98	37.42	-7.42
29	36.86	-105.85	39.88	-114.24	37.38	-107.46	-3.02	8.39	-0.52	1.61
30	38.30	-98.67	42.77	-109.71	39.37	-101.19	-4.46	11.04	-1.07	2.52
31	25.01	-12.70	35.06	-19.08	32.83	-13.78	-10.05	6.38	-7.82	1.09
32	184.39	-651.78	189.00	-669.89	182.46	-644.84	-4.61	18.11	1.93	-6.95
33	101.60	-36.78	95.26	-41.71	131.35	-44.29	6.34	4.92	-29.76	7.50
34	6.72	-17.69	43.29	-34.83	1.52	-3.60	-36.57	17.14	5.20	-14.10
35	426.10	-131.93	422.38	-128.61	424.07	-132.26	3.72	-3.32	2.04	0.33
36	155.48	-64.63	137.14	-39.44	167.27	-83.30	18.34	-25.19	-11.80	18.67
37	13.97	-38.42	17.72	-42.64	143.26	-63.02	-3.75	4.22	-129.29	24.60
38	22.44	-8.30	29.12	-9.75	23.26	-8.11	-6.68	1.46	-0.81	-0.19
39	116.57	-407.60	116.07	-405.76	118.77	-415.52	0.51	-1.84	-2.20	7.92
40	241.29	-72.36	255.66	-79.72	246.34	-73.85	-14.37	7.35	-5.05	1.49
41	268.20	-41.23	260.19	-43.07	275.02	-41.94	8.01	1.83	-6.82	0.71
42	123.71	-61.47	132.40	-63.77	125.73	-62.70	-8.69	2.30	-2.02	1.22
43	349.71	-87.06	354.24	-87.57	354.27	-88.27	-4.54	0.51	-4.56	1.21
44	409.61	-97.19	413.02	-97.99	416.36	-98.50	-3.41	0.79	-6.75	1.31
45	152.04	-48.15	162.09	-51.31	154.85	-48.80	-10.05	3.16	-2.81	0.66
46	62.40	-30.01	110.29	-40.92	62.61	-30.19	-47.89	10.92	-0.21	0.19
47	169.13	-40.76	189.61	-55.39	138.77	-36.37	-20.48	14.63	30.36	-4.39
48	5.49	-14.19	10.05	-25.12	18.56	-41.82	-4.57	10.93	-13.07	27.63
49	331.08	-105.17	370.60	-120.02	261.38	-82.33	-39.53	14.85	69.69	-22.84
50	276.13	-96.76	319.67	-111.83	246.43	-86.30	-43.54	15.07	29.71	-10.46
51	121.60	-372.06	130.73	-399.22	126.54	-386.42	-9.14	27.16	-4.95	14.36
52	250.05	-147.65	285.85	-159.57	253.40	-151.42	-35.80	11.92	-3.35	3.77
53	264.36	-432.23	261.11	-421.39	271.71	-455.46	3.25	-10.84	-7.36	23.23
54	444.13	-224.23	477.37	-238.90	342.71	-195.98	-33.25	14.66	101.42	-28.25
55	111.18	-216.52	115.79	-237.41	104.86	-189.84	-4.61	20.88	6.32	-26.68
56	138.81	-78.82	174.61	-72.80	89.84	-72.15	-35.80	-6.02	48.97	-6.67
57	37.99	-123.68	41.24	-132.56	37.47	-121.88	-3.25	8.88	0.53	-1.79
58	54.70	-115.08	60.71	-123.64	52.86	-111.88	-6.01	8.56	1.84	-3.20
59	45.59	-15.10	57.87	-19.15	39.16	-12.96	-12.27	4.05	6.43	-2.14
60	145.71	-445.86	159.00	-479.77	118.80	-368.47	-13.28	33.90	26.91	-77.39
61	117.51	-52.86	115.41	-84.18	240.54	-75.73	2.11	31.32	-123.02	22.86
62	4.10	-11.17	16.16	-37.03	14.97	-6.17	-12.05	25.87	-10.87	-5.00
63	345.79	-186.96	344.76	-183.01	294.15	-160.95	1.03	-3.95	51.63	-26.01
64	285.14	-112.32	285.24	-101.16	326.11	-214.88	-0.10	-11.17	-40.98	102.56
65	223.38	-612.74	245.92	-659.43	225.75	-620.01	-22.53	46.69	-2.37	7.27
66	274.91	-193.37	279.04	-202.31	242.48	-184.86	-4.13	8.94	32.43	-8.51
67	131.93	-285.57	134.16	-313.42	133.65	-293.91	-2.23	27.85	-1.71	8.33
68	159.67	-486.77	162.81	-500.82	168.85	-506.23	-3.14	14.06	-9.19	19.47
69	205.31	-107.54	206.27	-118.03	135.29	-56.91	-0.96	10.49	70.03	-50.63
70	63.28	-156.18	63.59	-158.92	68.76	-161.46	-0.31	2.74	-5.48	5.28

Table D.3. Maximum ($\epsilon 1$) and minimum ($\epsilon 3$) principal strain values at the location of 70 landmarks during first premolar (P3) bite load for the filled, unfilled and jaw joint constraint sensitivity tests (see text for more details), and strain differences ($\Delta \epsilon 1$ and $\Delta \epsilon 3$) at landmark locations between models. Strain values are in microstrain (μ strain).

P3 bite landmark	Filled		Unfilled		Jaw Joint		Filled-Unfilled		Filled-JawJoint	
	$\epsilon 1$	$\epsilon 3$	$\epsilon 1$	$\epsilon 3$	$\epsilon 1$	$\epsilon 3$	$\Delta \epsilon 1$	$\Delta \epsilon 3$	$\Delta \epsilon 1$	$\Delta \epsilon 3$
1	24.92	-37.60	28.83	-43.92	24.82	-37.61	-3.90	6.33	0.10	0.02
2	73.76	-147.59	89.76	-167.26	73.71	-149.61	-15.99	19.67	0.05	2.02
3	232.67	-90.58	249.11	-96.45	238.73	-93.08	-16.44	5.87	-6.07	2.50
4	44.21	-197.99	54.96	-245.41	48.71	-218.95	-10.75	47.42	-4.51	20.96
5	55.72	-18.02	66.01	-21.46	55.11	-17.78	-10.29	3.44	0.61	-0.25
6	35.72	-109.04	43.72	-131.68	35.99	-110.01	-8.00	22.64	-0.26	0.97
7	3.38	-1.38	4.86	-1.97	8.50	-3.41	-1.47	0.59	-5.12	2.03
8	199.47	-68.40	206.89	-78.34	253.35	-110.63	-7.42	9.93	-53.88	42.23
9	190.23	-351.20	203.02	-334.26	196.82	-360.78	-12.79	-16.94	-6.59	9.58
10	34.46	-19.52	38.61	-21.92	33.40	-19.25	-4.15	2.39	1.06	-0.27
11	73.16	-209.72	77.27	-221.25	75.42	-216.54	-4.11	11.53	-2.25	6.82
12	48.73	-44.97	81.36	-75.02	50.06	-45.60	-32.62	30.05	-1.32	0.63
13	246.69	-658.09	249.78	-669.31	252.03	-672.43	-3.09	11.22	-5.34	14.34
14	423.89	-966.92	419.92	-954.40	433.29	-987.67	3.98	-12.52	-9.40	20.74
15	322.15	-459.34	326.21	-462.29	327.83	-468.11	-4.06	2.95	-5.68	8.77
16	66.61	-244.02	65.39	-244.08	67.48	-247.51	1.22	0.05	-0.87	3.49
17	54.81	-71.97	53.68	-73.50	55.85	-73.05	1.14	1.53	-1.04	1.08
18	236.48	-92.54	380.48	-136.79	239.46	-93.72	-144.00	44.26	-2.98	1.18
19	62.25	-140.55	68.35	-98.25	61.02	-186.91	-6.10	-42.30	1.22	46.36
20	0.55	-0.16	0.68	-0.28	0.45	-0.48	-0.12	0.12	0.10	0.32
21	359.58	-108.33	421.91	-128.34	333.90	-100.60	-62.33	20.02	25.68	-7.73
22	87.29	-70.59	117.99	-78.01	93.08	-72.08	-30.70	7.42	-5.78	1.49
23	123.35	-403.06	130.72	-425.96	127.57	-418.01	-7.37	22.91	-4.23	14.95
24	262.76	-801.91	272.35	-832.38	271.13	-826.97	-9.59	30.46	-8.37	25.06
25	277.64	-289.48	276.19	-287.80	279.53	-287.71	1.46	-1.68	-1.88	-1.77
26	576.89	-238.89	611.51	-252.81	545.46	-227.49	-34.63	13.92	31.43	-11.41
27	231.35	-448.01	233.21	-455.52	231.95	-448.01	-1.85	7.51	-0.59	0.00
28	411.10	-86.08	426.34	-97.84	374.00	-78.89	-15.24	11.76	37.09	-7.19
29	34.31	-98.78	36.96	-106.05	34.76	-100.10	-2.65	7.27	-0.45	1.32
30	32.62	-80.10	36.61	-90.63	33.65	-82.19	-3.99	10.54	-1.03	2.10
31	12.33	-34.70	11.30	-30.46	10.67	-26.84	1.02	-4.24	1.66	-7.86
32	185.44	-656.35	187.76	-666.04	183.52	-649.19	-2.33	9.69	1.91	-7.16
33	47.79	-37.95	48.54	-57.94	65.30	-34.65	-0.76	19.99	-17.51	-3.30
34	6.13	-15.91	35.93	-31.60	0.78	-1.79	-29.81	15.69	5.35	-14.11
35	414.50	-125.60	401.85	-119.25	413.13	-127.24	12.65	-6.34	1.37	1.65
36	143.07	-38.22	125.44	-12.15	150.74	-55.46	17.63	-26.07	-7.67	17.25
37	13.88	-29.89	18.95	-35.05	152.25	-64.35	-5.08	5.15	-138.37	34.46
38	12.59	-11.06	17.95	-10.87	12.57	-10.21	-5.36	-0.19	0.02	-0.85
39	37.21	-128.30	34.58	-118.69	37.65	-130.17	2.63	-9.61	-0.44	1.87
40	81.12	-21.51	91.86	-24.76	82.85	-21.85	-10.74	3.25	-1.73	0.34
41	236.85	-75.35	221.93	-67.08	242.86	-77.79	14.92	-8.27	-6.01	2.44
42	50.53	-38.78	52.12	-37.22	51.19	-39.58	-1.59	-1.56	-0.67	0.80
43	108.15	-36.04	105.21	-32.99	108.33	-37.08	2.93	-3.05	-0.19	1.04
44	289.04	-61.07	279.28	-59.04	293.00	-61.49	9.76	-2.02	-3.96	0.43
45	99.21	-28.92	103.72	-30.53	100.96	-29.17	-4.51	1.61	-1.76	0.25
46	12.46	-5.99	35.14	-12.61	11.56	-5.64	-22.68	6.62	0.89	-0.35
47	192.07	-45.16	215.91	-57.46	159.95	-37.36	-23.85	12.31	32.12	-7.80
48	5.84	-15.11	10.56	-26.60	18.74	-42.26	-4.73	11.49	-12.90	27.15
49	280.86	-89.48	309.01	-99.82	210.46	-66.43	-28.14	10.34	70.40	-23.06
50	309.20	-108.51	357.99	-125.88	280.42	-98.27	-48.79	17.38	28.78	-10.23
51	99.35	-292.82	108.97	-318.11	103.72	-305.13	-9.63	25.29	-4.37	12.31
52	311.10	-117.41	335.11	-126.43	314.94	-118.60	-24.01	9.02	-3.84	1.19
53	259.98	-415.41	257.05	-406.08	268.11	-439.41	2.93	-9.32	-8.13	24.00
54	425.95	-222.53	458.73	-237.32	328.01	-195.85	-32.78	14.79	97.94	-26.68
55	109.00	-206.69	113.54	-226.85	103.18	-181.11	-4.54	20.16	5.81	-25.58
56	110.90	-44.72	141.06	-49.15	58.26	-30.35	-30.16	4.43	52.64	-14.37
57	33.85	-110.51	36.91	-118.84	33.24	-108.44	-3.06	8.33	0.61	-2.07
58	52.18	-114.38	57.73	-122.24	50.35	-111.18	-5.55	7.86	1.84	-3.20
59	91.93	-30.13	107.96	-35.57	86.58	-28.35	-16.03	5.44	5.35	-1.78
60	135.23	-409.95	148.31	-443.36	108.91	-334.15	-13.08	33.41	26.32	-75.81
61	139.67	-54.32	135.18	-82.08	264.40	-83.93	4.48	27.76	-124.73	29.60
62	3.35	-9.14	14.13	-32.18	17.05	-7.00	-10.78	23.03	-13.70	-2.14
63	329.22	-180.21	328.32	-176.26	277.57	-153.85	0.90	-3.95	51.66	-26.37
64	288.86	-119.34	288.38	-105.43	331.25	-225.63	0.49	-13.91	-42.39	106.29
65	170.98	-530.47	188.95	-573.94	172.04	-535.67	-17.97	43.47	-1.06	5.20
66	333.81	-289.24	342.67	-297.99	304.24	-284.15	-8.86	8.75	29.57	-5.09
67	360.85	-539.38	370.87	-585.77	368.35	-554.09	-10.01	46.39	-7.50	14.71
68	90.40	-271.88	89.33	-272.29	98.10	-286.40	1.07	0.40	-7.69	14.52
69	169.17	-73.68	165.84	-82.34	101.91	-30.00	3.32	8.67	67.26	-43.67
70	136.65	-157.82	141.19	-158.89	143.89	-163.23	-4.54	1.08	-7.24	5.41

Table D.4. Maximum ($\epsilon 1$) and minimum ($\epsilon 3$) principal strain values at the location of 70 landmarks during second premolar (P4) bite load for the filled, unfilled and jaw joint constraint sensitivity tests (see text for more details), and strain differences ($\Delta \epsilon 1$ and $\Delta \epsilon 3$) at landmark locations between models. Strain values are in microstrain (μ strain).

P4 bite landmark	Filled		Unfilled		Jaw Joint		Filled-Unfilled		Filled-JawJoint	
	$\epsilon 1$	$\epsilon 3$	$\epsilon 1$	$\epsilon 3$	$\epsilon 1$	$\epsilon 3$	$\Delta \epsilon 1$	$\Delta \epsilon 3$	$\Delta \epsilon 1$	$\Delta \epsilon 3$
1	18.07	-31.83	21.07	-37.22	17.83	-31.97	-3.00	5.39	0.24	0.13
2	55.65	-136.71	66.30	-156.48	55.54	-138.74	-10.65	19.77	0.11	2.03
3	216.65	-85.15	230.94	-90.34	222.56	-87.64	-14.29	5.19	-5.91	2.49
4	42.09	-188.24	52.32	-233.24	46.62	-208.78	-10.23	45.01	-4.53	20.54
5	54.81	-17.79	65.41	-21.39	54.10	-17.54	-10.60	3.60	0.70	-0.25
6	36.39	-111.16	44.45	-134.01	36.72	-112.33	-8.06	22.86	-0.34	1.17
7	3.72	-1.52	5.17	-2.10	8.89	-3.59	-1.45	0.58	-5.17	2.07
8	194.83	-68.22	203.06	-78.41	249.35	-112.66	-8.24	10.19	-54.52	44.44
9	197.41	-335.68	209.47	-324.60	204.38	-345.42	-12.06	-11.08	-6.97	9.73
10	37.57	-20.79	41.68	-23.14	36.49	-20.59	-4.12	2.35	1.08	-0.20
11	58.11	-142.49	61.82	-151.86	60.12	-147.90	-3.71	9.37	-2.01	5.41
12	42.27	-38.65	69.78	-63.48	43.27	-39.25	-27.51	24.83	-1.01	0.60
13	50.70	-116.72	55.29	-130.90	51.94	-119.59	-4.59	14.18	-1.24	2.87
14	291.26	-399.59	300.93	-398.23	298.38	-409.04	-9.67	-1.36	-7.12	9.46
15	308.18	-1197.92	301.44	-1186.90	315.08	-1223.94	6.74	-11.01	-6.90	26.03
16	104.33	-373.43	103.66	-375.57	106.13	-379.78	0.67	2.14	-1.79	6.35
17	63.47	-109.82	63.76	-113.96	64.60	-111.86	-0.29	4.15	-1.13	2.04
18	245.34	-96.23	389.80	-140.80	248.67	-97.52	-144.45	44.57	-3.33	1.29
19	68.10	-145.97	74.90	-106.65	64.77	-190.08	-6.80	-39.32	3.34	44.11
20	0.54	-0.18	0.67	-0.24	0.38	-0.41	-0.12	0.06	0.16	0.23
21	372.26	-112.39	435.99	-132.74	347.38	-104.80	-63.73	20.36	24.88	-7.59
22	66.87	-70.85	92.23	-74.79	72.02	-71.77	-25.36	3.94	-5.15	0.93
23	124.28	-406.41	131.56	-428.63	128.38	-421.59	-7.28	22.22	-4.10	15.18
24	261.73	-797.17	271.11	-826.96	270.16	-822.47	-9.38	29.80	-8.44	25.30
25	281.55	-293.63	280.44	-291.93	283.63	-292.06	1.11	-1.70	-2.08	-1.57
26	597.43	-246.28	634.62	-261.09	568.80	-235.91	-37.20	14.81	28.62	-10.37
27	233.50	-459.44	235.35	-468.00	234.44	-461.38	-1.85	8.56	-0.93	1.93
28	418.43	-86.45	439.94	-99.73	381.97	-79.25	-21.51	13.29	36.46	-7.20
29	33.54	-96.60	36.06	-103.49	33.98	-97.92	-2.52	6.89	-0.44	1.32
30	31.09	-74.71	34.88	-84.88	32.13	-76.78	-3.79	10.17	-1.04	2.07
31	15.41	-47.62	14.37	-44.58	13.54	-39.47	1.05	-3.03	1.87	-8.15
32	185.68	-657.42	187.44	-664.96	184.13	-651.61	-1.76	7.55	1.55	-5.81
33	41.59	-46.47	46.05	-72.21	51.66	-38.58	-4.46	25.74	-10.08	-7.89
34	6.00	-15.43	33.98	-30.76	0.92	-1.73	-27.98	15.33	5.08	-13.70
35	411.54	-124.46	396.59	-117.38	411.15	-126.76	14.95	-7.08	0.39	2.30
36	140.54	-31.50	123.40	-5.22	146.95	-47.74	17.14	-26.28	-6.41	16.24
37	14.29	-27.88	19.68	-33.38	154.48	-64.56	-5.39	5.50	-140.18	36.67
38	11.26	-13.05	15.89	-12.08	10.97	-12.02	-4.64	-0.96	0.28	-1.02
39	29.63	-100.66	27.05	-90.97	30.06	-102.07	2.58	-9.69	-0.43	1.41
40	72.51	-18.52	84.07	-21.40	74.21	-18.94	-11.56	2.88	-1.71	0.42
41	214.57	-74.14	201.39	-67.01	219.90	-76.56	13.18	-7.12	-5.33	2.42
42	40.67	-34.95	41.36	-33.13	41.13	-35.74	-0.69	-1.82	-0.45	0.79
43	79.00	-37.28	75.05	-33.44	79.11	-38.79	3.95	-3.84	-0.10	1.52
44	249.43	-51.05	239.63	-49.07	252.60	-51.48	9.80	-1.98	-3.18	0.43
45	87.11	-24.78	90.60	-26.11	88.71	-25.01	-3.49	1.33	-1.59	0.23
46	6.78	-3.35	25.71	-9.14	5.83	-2.98	-18.93	5.79	0.94	-0.37
47	192.07	-46.19	215.81	-58.16	158.90	-37.22	-23.74	11.97	33.17	-8.97
48	5.89	-15.27	10.65	-26.88	18.74	-42.28	-4.76	11.60	-12.85	27.01
49	264.98	-84.50	291.35	-94.08	194.63	-61.44	-26.37	9.58	70.35	-23.06
50	314.57	-110.61	364.20	-128.37	286.10	-100.52	-49.63	17.75	28.47	-10.10
51	92.35	-267.72	102.21	-292.62	96.52	-279.53	-9.86	24.90	-4.18	11.81
52	307.64	-117.14	328.52	-125.17	311.52	-118.35	-20.88	8.03	-3.88	1.21
53	260.30	-415.96	257.65	-407.59	268.63	-440.40	2.65	-8.37	-8.33	24.44
54	424.37	-222.13	457.30	-236.94	327.30	-195.59	-32.93	14.81	97.07	-26.54
55	109.01	-204.56	113.61	-224.63	103.35	-179.15	-4.60	20.07	5.66	-25.40
56	105.05	-39.74	134.41	-46.44	51.94	-23.54	-29.36	6.70	53.10	-16.20
57	32.41	-105.91	35.44	-114.17	31.80	-103.77	-3.02	8.25	0.61	-2.14
58	51.08	-113.38	56.51	-121.18	49.23	-110.22	-5.43	7.80	1.85	-3.16
59	102.68	-33.64	119.26	-39.26	97.54	-31.98	-16.58	5.62	5.14	-1.65
60	132.71	-401.15	145.73	-434.40	106.57	-325.82	-13.02	33.25	26.15	-75.33
61	144.14	-54.70	139.15	-81.76	268.73	-85.53	4.98	27.07	-124.59	30.83
62	3.15	-8.60	13.59	-30.87	17.62	-7.23	-10.43	22.27	-14.47	-1.37
63	324.54	-178.23	323.53	-174.22	272.85	-151.78	1.01	-4.01	51.69	-26.45
64	289.55	-120.80	288.92	-106.36	332.13	-227.56	0.63	-14.44	-42.58	106.76
65	145.21	-479.42	160.71	-521.05	145.81	-483.92	-15.50	41.63	-0.60	4.50
66	348.71	-318.42	358.88	-327.32	320.50	-315.18	-10.17	8.91	28.21	-3.24
67	295.75	-509.72	305.76	-553.39	302.36	-524.13	-10.01	43.67	-6.61	14.41
68	82.76	-243.30	81.65	-242.34	90.27	-257.32	1.11	-0.96	-7.51	14.01
69	162.16	-68.57	158.10	-77.04	95.57	-28.73	4.06	8.47	66.59	-39.85
70	141.48	-155.76	147.08	-157.73	148.89	-161.14	-5.61	1.97	-7.41	5.38

Table D.5. Maximum ($\epsilon 1$) and minimum ($\epsilon 3$) principal strain values at the location of 70 landmarks during first molar (M1) bite load for the filled, unfilled and jaw joint constraint sensitivity tests (see text for more details), and strain differences ($\Delta \epsilon 1$ and $\Delta \epsilon 3$) at landmark locations between models. Strain values are in microstrain (μ strain).

M1 bite landmark	Filled		Unfilled		Jaw Joint		Filled-Unfilled		Filled-JawJoint	
	$\epsilon 1$	$\epsilon 3$	$\epsilon 1$	$\epsilon 3$	$\epsilon 1$	$\epsilon 3$	$\Delta \epsilon 1$	$\Delta \epsilon 3$	$\Delta \epsilon 1$	$\Delta \epsilon 3$
1	3.30	-9.60	3.51	-11.09	2.92	-9.38	-0.22	1.49	0.38	-0.22
2	11.12	-30.54	21.29	-32.79	10.44	-31.30	-10.16	2.26	0.68	0.76
3	186.56	-72.97	197.62	-76.98	191.64	-75.13	-11.07	4.01	-5.08	2.16
4	37.92	-168.81	47.21	-209.65	42.32	-189.06	-9.29	40.84	-4.39	20.25
5	52.95	-17.22	63.56	-20.83	52.30	-16.97	-10.62	3.61	0.65	-0.25
6	37.36	-114.16	45.56	-137.41	37.65	-115.13	-8.20	23.25	-0.29	0.98
7	4.46	-1.81	5.89	-2.38	9.48	-3.78	-1.43	0.57	-5.02	1.97
8	181.47	-65.45	191.25	-75.80	236.42	-112.27	-9.78	10.35	-54.95	46.82
9	188.66	-303.31	196.59	-295.41	195.80	-312.49	-7.93	-7.90	-7.13	9.18
10	39.79	-22.06	43.82	-24.41	38.80	-21.88	-4.03	2.35	0.99	-0.17
11	48.75	-26.86	52.32	-27.96	48.78	-27.69	-3.56	1.10	-0.03	0.83
12	2.34	-4.48	1.76	-6.20	2.77	-4.46	0.58	1.72	-0.43	-0.02
13	21.30	-41.49	22.21	-46.65	21.12	-42.50	-0.92	5.17	0.17	1.01
14	98.45	-60.77	101.49	-54.35	100.21	-62.03	-3.03	-6.42	-1.76	1.26
15	132.15	-79.95	142.44	-78.08	136.53	-84.98	-10.29	-1.87	-4.39	5.03
16	65.29	-247.18	62.58	-239.99	66.47	-252.52	2.70	-7.19	-1.19	5.34
17	53.59	-107.81	53.81	-111.49	54.87	-110.44	-0.23	3.68	-1.28	2.63
18	187.22	-72.89	287.65	-103.96	189.77	-73.92	-100.43	31.07	-2.56	1.02
19	78.87	-155.23	84.48	-114.13	72.94	-197.46	-5.61	-41.11	5.93	42.22
20	0.54	-0.19	0.67	-0.23	0.37	-0.30	-0.13	0.05	0.17	0.11
21	402.15	-121.96	466.42	-142.29	377.03	-114.36	-64.26	20.33	25.12	-7.60
22	62.62	-72.79	85.71	-75.11	66.69	-73.50	-23.09	2.33	-4.07	0.72
23	122.86	-402.91	130.06	-424.61	126.85	-417.71	-7.20	21.70	-4.00	14.80
24	198.83	-604.91	201.32	-613.26	206.29	-627.20	-2.49	8.35	-7.46	22.29
25	282.14	-290.67	281.57	-289.34	284.16	-289.09	0.57	-1.33	-2.02	-1.59
26	606.46	-249.77	646.28	-265.50	575.40	-238.54	-39.82	15.73	31.06	-11.23
27	234.15	-465.30	236.26	-475.34	234.58	-465.49	-2.11	10.04	-0.43	0.19
28	428.07	-86.71	450.69	-99.71	391.19	-79.63	-22.62	12.99	36.88	-7.08
29	33.22	-95.65	35.50	-101.82	33.60	-96.75	-2.28	6.17	-0.38	1.09
30	29.31	-68.18	32.70	-77.53	30.37	-70.01	-3.39	9.35	-1.05	1.84
31	15.48	-48.64	13.96	-45.05	13.67	-40.78	1.51	-3.59	1.80	-7.86
32	185.35	-656.37	187.00	-663.43	183.75	-649.96	-1.65	7.06	1.61	-6.41
33	40.16	-51.94	46.24	-81.51	49.03	-40.43	-6.07	29.57	-8.87	-11.51
34	5.65	-14.24	30.63	-28.48	1.52	-1.66	-24.99	14.24	4.13	-12.58
35	407.86	-123.33	391.71	-115.82	407.44	-125.66	16.14	-7.51	0.41	2.33
36	139.60	-28.83	122.56	-1.96	145.92	-45.59	17.03	-26.87	-6.33	16.76
37	14.77	-23.60	20.32	-29.21	159.06	-65.21	-5.55	5.61	-144.29	41.61
38	9.99	-14.34	13.79	-12.84	9.65	-13.26	-3.81	-1.50	0.33	-1.08
39	21.93	-73.66	19.83	-65.81	22.15	-74.30	2.10	-7.85	-0.22	0.64
40	19.51	-8.24	22.17	-8.92	20.57	-9.26	-2.66	0.68	-1.06	1.02
41	111.86	-39.29	98.23	-32.18	116.00	-41.33	13.63	-7.11	-4.14	2.04
42	19.06	-20.21	18.06	-17.69	19.23	-20.87	1.00	-2.51	-0.17	0.66
43	35.68	-27.43	31.12	-22.15	35.65	-29.70	4.56	-5.28	0.03	2.28
44	140.04	-27.32	128.78	-25.30	141.40	-27.24	11.27	-2.02	-1.36	-0.08
45	59.34	-16.32	59.98	-16.71	60.41	-16.48	-0.64	0.38	-1.07	0.15
46	9.62	-4.79	28.01	-10.07	8.63	-4.38	-18.39	5.28	0.99	-0.42
47	175.23	-42.16	197.67	-53.03	142.90	-32.77	-22.44	10.87	32.33	-9.39
48	5.64	-14.61	10.35	-26.13	18.45	-41.41	-4.71	11.52	-12.81	26.79
49	247.86	-79.38	275.66	-89.06	177.16	-56.18	-27.80	9.68	70.69	-23.19
50	305.14	-107.55	354.28	-125.24	276.69	-97.46	-49.14	17.69	28.45	-10.09
51	80.44	-226.45	90.42	-250.28	84.46	-237.60	-9.99	23.84	-4.02	11.16
52	247.26	-93.30	259.47	-97.73	250.14	-94.25	-12.21	4.43	-2.88	0.95
53	267.10	-439.85	265.19	-433.92	275.77	-465.98	1.91	-5.93	-8.67	26.13
54	442.85	-222.80	477.38	-237.54	345.10	-194.95	-34.52	14.74	97.75	-27.85
55	112.95	-206.98	117.91	-227.35	107.50	-180.99	-4.95	20.37	5.45	-25.98
56	103.47	-41.06	133.12	-47.65	51.16	-26.37	-29.65	6.59	52.31	-14.69
57	29.97	-97.80	32.87	-105.67	29.32	-95.51	-2.90	7.87	0.65	-2.28
58	47.91	-108.29	53.11	-116.31	46.06	-105.03	-5.19	8.02	1.86	-3.26
59	104.34	-34.13	121.09	-39.78	99.34	-32.43	-16.76	5.65	5.00	-1.70
60	133.15	-401.87	145.88	-434.35	107.20	-326.89	-12.73	32.47	25.94	-74.99
61	135.66	-53.23	130.34	-80.84	258.65	-82.05	5.32	27.61	-122.99	28.82
62	2.89	-7.71	12.34	-27.92	18.61	-7.65	-9.45	20.21	-15.73	-0.07
63	320.15	-176.01	317.68	-171.50	268.90	-149.93	2.46	-4.50	51.25	-26.08
64	287.45	-116.74	286.70	-102.45	329.49	-222.60	0.75	-14.29	-42.05	105.86
65	134.05	-395.60	148.02	-435.66	137.35	-398.48	-13.97	40.06	-3.30	2.88
66	347.03	-319.17	359.12	-330.30	318.57	-315.26	-12.09	11.14	28.47	-3.90
67	165.55	-296.48	164.23	-317.84	169.47	-307.39	1.32	21.36	-3.92	10.91
68	82.94	-241.86	83.81	-244.73	90.26	-255.23	-0.88	2.87	-7.32	13.37
69	169.16	-83.08	166.32	-92.86	99.32	-33.47	2.84	9.78	69.84	-49.61
70	98.25	-99.35	103.20	-99.12	105.10	-103.84	-4.95	-0.23	-6.85	4.50

Table D.6. Maximum ($\epsilon 1$) and minimum ($\epsilon 3$) principal strain values at the location of 70 landmarks during second molar (M2) bite load for the filled, unfilled and jaw joint constraint sensitivity tests (see text for more details), and strain differences ($\Delta \epsilon 1$ and $\Delta \epsilon 3$) at landmark locations between models. Strain values are in microstrain (μ strain).

M2 bite landmark	Filled		Unfilled		Jaw Joint		Filled-Unfilled		Filled-JawJoint	
	$\epsilon 1$	$\epsilon 3$	$\epsilon 1$	$\epsilon 3$	$\epsilon 1$	$\epsilon 3$	$\Delta \epsilon 1$	$\Delta \epsilon 3$	$\Delta \epsilon 1$	$\Delta \epsilon 3$
1	3.44	-5.75	5.16	-7.71	4.24	-6.37	-1.72	1.96	-0.80	0.61
2	12.34	-18.20	19.75	-24.19	13.93	-20.49	-7.41	6.00	-1.59	2.30
3	124.32	-49.41	129.83	-51.59	128.23	-51.15	-5.50	2.18	-3.91	1.74
4	32.13	-133.82	38.76	-166.07	35.14	-151.96	-6.63	32.25	-3.01	18.14
5	50.56	-16.69	61.82	-20.66	49.79	-16.39	-11.26	3.97	0.77	-0.30
6	39.46	-120.79	47.85	-144.66	39.94	-122.37	-8.40	23.87	-0.48	1.58
7	5.73	-2.33	7.08	-2.87	11.03	-4.47	-1.35	0.53	-5.30	2.14
8	166.41	-66.17	181.37	-78.41	221.64	-118.45	-14.96	12.24	-55.23	52.28
9	151.09	-209.28	155.99	-206.40	157.86	-217.25	-4.90	-2.89	-6.77	7.96
10	48.59	-25.97	52.58	-28.21	47.69	-25.74	-3.99	2.25	0.90	-0.22
11	54.71	-23.63	59.28	-25.32	53.93	-23.49	-4.58	1.69	0.77	-0.14
12	4.15	-3.67	10.38	-11.44	4.52	-3.63	-6.23	7.77	-0.37	-0.05
13	6.60	-20.02	7.14	-22.40	6.89	-20.63	-0.54	2.38	-0.29	0.61
14	25.31	-14.57	27.22	-11.78	26.80	-15.54	-1.91	-2.79	-1.50	0.97
15	58.67	-36.61	63.46	-36.42	61.63	-39.10	-4.79	-0.20	-2.96	2.49
16	14.50	-12.23	36.05	-21.83	18.07	-13.28	-21.55	9.59	-3.57	1.05
17	73.74	-175.11	76.75	-184.47	75.63	-179.26	-3.01	9.36	-1.89	4.15
18	97.91	-37.51	133.17	-50.22	99.19	-37.93	-35.25	12.71	-1.28	0.42
19	100.78	-184.85	99.94	-146.07	90.64	-222.09	0.84	-38.77	10.14	37.24
20	0.60	-0.27	0.66	-0.18	0.38	-0.31	-0.06	-0.09	0.22	0.04
21	459.14	-140.20	525.02	-160.68	436.41	-133.32	-65.87	20.48	22.73	-6.88
22	39.24	-101.47	45.14	-94.04	41.00	-99.59	-5.90	-7.43	-1.76	-1.88
23	122.01	-402.31	128.26	-420.32	126.02	-416.98	-6.25	18.02	-4.01	14.68
24	147.68	-446.27	147.40	-445.74	153.98	-464.89	0.28	-0.52	-6.30	18.62
25	286.50	-292.73	286.46	-292.03	288.85	-291.63	0.04	-0.70	-2.35	-1.10
26	654.20	-267.31	702.81	-286.14	629.34	-258.23	-48.61	18.83	24.86	-9.08
27	239.17	-489.67	242.08	-503.59	240.63	-493.96	-2.91	13.92	-1.46	4.29
28	469.36	-91.82	507.65	-108.38	434.63	-85.15	-38.29	16.56	34.72	-6.67
29	31.43	-90.58	33.05	-94.95	31.83	-91.71	-1.62	4.36	-0.40	1.13
30	25.41	-51.45	27.65	-58.70	26.33	-53.15	-2.24	7.25	-0.92	1.70
31	25.63	-79.02	24.45	-80.80	23.87	-71.14	1.18	1.78	1.76	-7.88
32	186.76	-661.68	187.73	-666.14	185.55	-656.63	-0.97	4.46	1.21	-5.05
33	42.15	-87.58	54.44	-129.85	40.96	-71.44	-12.29	42.27	1.20	-16.14
34	5.42	-12.57	24.24	-25.17	4.40	-3.01	-18.83	12.60	1.02	-9.57
35	404.80	-122.44	385.51	-113.96	405.89	-126.00	19.28	-8.48	-1.09	3.56
36	134.90	-13.45	119.63	-14.74	138.89	-27.68	15.27	-28.19	-3.99	14.23
37	17.78	-18.32	23.26	-23.92	166.31	-65.16	-5.48	5.60	-148.53	46.84
38	9.52	-21.72	11.36	-18.40	9.04	-20.69	-1.84	-3.32	0.48	-1.03
39	11.72	-35.26	10.33	-27.82	12.00	-35.44	1.39	-7.44	-0.28	0.18
40	8.68	-12.19	10.31	-13.93	9.52	-13.39	-1.63	1.74	-0.84	1.20
41	56.00	-23.20	45.17	-18.30	58.70	-24.73	10.82	-4.90	-2.70	1.53
42	6.85	-11.47	5.21	-9.28	7.12	-12.14	1.64	-2.19	-0.27	0.67
43	13.49	-29.08	9.81	-25.03	14.29	-32.39	3.68	-4.05	-0.80	3.30
44	51.00	-8.70	39.40	-6.98	50.83	-8.57	11.60	-1.72	0.17	-0.13
45	31.97	-7.99	30.17	-7.69	32.71	-8.16	1.80	-0.30	-0.74	0.17
46	6.70	-3.63	20.26	-7.35	5.84	-3.28	-13.56	3.72	0.86	-0.35
47	166.20	-43.97	187.07	-54.37	132.48	-32.72	-20.87	10.41	33.72	-11.25
48	5.56	-14.42	10.30	-26.12	18.23	-40.80	-4.73	11.69	-12.67	26.38
49	208.75	-67.25	236.35	-76.43	137.83	-44.02	-27.60	9.17	70.92	-23.24
50	307.39	-109.12	356.05	-126.80	279.49	-99.32	-48.67	17.68	27.90	-9.80
51	59.01	-143.90	70.17	-166.80	62.48	-153.01	-11.16	22.90	-3.47	9.11
52	191.13	-72.15	195.62	-73.72	192.64	-72.65	-4.49	1.57	-1.51	0.51
53	273.08	-460.25	272.25	-458.10	282.30	-488.67	0.82	-2.15	-9.22	28.41
54	454.95	-222.74	490.65	-237.37	358.96	-194.23	-35.71	14.63	95.99	-28.51
55	116.46	-206.04	121.71	-226.57	111.64	-180.15	-5.24	20.53	4.82	-25.89
56	94.76	-36.32	123.78	-45.44	42.39	-21.07	-29.02	9.12	52.37	-15.25
57	25.40	-82.87	28.11	-90.20	24.65	-80.29	-2.71	7.33	0.76	-2.58
58	43.81	-102.92	48.53	-110.69	41.95	-99.66	-4.72	7.77	1.87	-3.26
59	125.16	-40.85	142.17	-46.57	120.76	-39.39	-17.01	5.72	4.40	-1.46
60	129.00	-386.82	141.38	-418.32	103.52	-312.94	-12.38	31.50	25.48	-73.88
61	137.08	-52.73	130.65	-79.41	258.18	-82.07	6.43	26.68	-121.09	29.34
62	2.44	-6.15	10.41	-23.35	20.50	-8.41	-7.97	17.20	-18.06	2.26
63	308.44	-170.71	304.75	-165.78	257.41	-144.87	3.68	-4.93	51.03	-25.84
64	287.04	-116.32	285.94	-101.08	328.90	-221.99	1.11	-15.24	-41.86	105.67
65	157.91	-232.07	184.68	-270.20	162.99	-233.03	-26.77	38.13	-5.08	0.96
66	378.86	-381.79	399.22	-401.72	352.99	-381.68	-20.36	19.93	25.87	-0.12
67	60.25	-186.83	57.31	-196.75	61.71	-194.71	2.94	9.92	-1.47	7.88
68	73.98	-201.72	76.18	-204.37	81.29	-214.65	-2.20	2.65	-7.31	12.93
69	163.40	-86.20	160.94	-97.16	92.95	-35.75	2.45	10.95	70.45	-50.45
70	91.52	-68.62	98.79	-68.08	97.99	-72.33	-7.28	-0.54	-6.48	3.71

Table D.7. Maximum ($\epsilon 1$) and minimum ($\epsilon 3$) principal strain values at the location of 70 landmarks during third molar (M3) bite load for the filled, unfilled and jaw joint constraint sensitivity tests (see text for more details), and strain differences ($\Delta \epsilon 1$ and $\Delta \epsilon 3$) at landmark locations between models. Strain values are in microstrain (μ strain).

M3 bite landmark	Filled		Unfilled		Jaw Joint		Filled-Unfilled		Filled-JawJoint	
	$\epsilon 1$	$\epsilon 3$	$\epsilon 1$	$\epsilon 3$	$\epsilon 1$	$\epsilon 3$	$\Delta \epsilon 1$	$\Delta \epsilon 3$	$\Delta \epsilon 1$	$\Delta \epsilon 3$
1	11.68	-11.03	17.12	-15.06	12.52	-11.93	-5.44	4.02	-0.85	0.89
2	35.16	-30.62	55.59	-42.85	37.13	-32.99	-20.42	12.23	-1.97	2.36
3	43.75	-19.27	45.69	-20.49	46.11	-20.36	-1.94	1.22	-2.36	1.08
4	39.85	-91.84	48.38	-113.83	39.90	-105.95	-8.53	21.98	-0.05	14.11
5	47.12	-16.06	58.90	-20.41	46.40	-15.74	-11.78	4.34	0.72	-0.33
6	42.49	-130.32	51.12	-154.93	43.17	-132.48	-8.63	24.61	-0.68	2.16
7	7.70	-3.13	8.88	-3.60	13.26	-5.30	-1.18	0.46	-5.56	2.16
8	152.90	-74.63	178.21	-92.09	205.38	-131.24	-25.31	17.47	-52.48	56.61
9	58.65	-115.08	62.79	-109.89	63.07	-121.11	-4.15	-5.19	-4.42	6.03
10	59.70	-31.02	63.65	-33.08	58.97	-30.88	-3.94	2.06	0.73	-0.14
11	16.56	-7.27	25.16	-10.60	15.55	-6.80	-8.60	3.33	1.01	-0.48
12	9.89	-5.43	21.83	-17.59	10.36	-5.48	-11.94	12.15	-0.47	0.05
13	2.06	-5.84	1.69	-4.72	2.41	-6.45	0.37	-1.12	-0.35	0.62
14	17.18	-10.76	23.90	-15.21	18.15	-11.37	-6.72	4.45	-0.98	0.62
15	20.86	-17.22	20.32	-15.68	22.59	-18.83	0.54	-1.54	-1.72	1.62
16	29.74	-9.82	33.85	-12.87	32.32	-10.56	-4.11	3.06	-2.58	0.74
17	17.59	-21.43	14.39	-14.02	17.47	-20.67	3.20	-7.42	0.12	-0.77
18	109.64	-157.89	130.65	-327.45	111.57	-162.11	-21.01	169.56	-1.93	4.22
19	126.07	-215.64	111.28	-185.42	110.58	-248.02	14.79	-30.22	15.49	32.38
20	0.70	-0.44	0.67	-0.30	0.46	-0.39	0.03	-0.14	0.24	-0.04
21	545.72	-167.93	609.37	-187.18	525.61	-161.93	-63.65	19.25	20.11	-6.00
22	45.66	-170.57	45.68	-169.08	45.35	-167.20	-0.01	-1.49	0.31	-3.37
23	118.73	-395.60	122.90	-406.75	122.50	-409.92	-4.17	11.15	-3.78	14.32
24	75.16	-221.31	72.37	-212.71	79.86	-234.95	2.80	-8.61	-4.69	13.64
25	284.74	-287.28	283.40	-286.21	287.12	-285.98	1.34	-1.07	-2.38	-1.31
26	710.93	-288.56	770.51	-311.29	691.18	-281.39	-59.58	22.74	19.75	-7.17
27	244.29	-511.53	248.20	-528.45	246.54	-519.37	-3.91	16.92	-2.25	7.84
28	542.86	-115.59	596.54	-125.55	510.57	-111.18	-53.69	9.96	32.28	-4.42
29	29.42	-84.66	29.84	-86.11	29.86	-85.62	-0.43	1.45	-0.44	0.96
30	24.15	-31.88	23.98	-35.16	25.26	-33.31	0.17	3.27	-1.11	1.42
31	38.89	-114.16	40.82	-123.42	37.39	-106.64	-1.93	9.26	1.49	-7.52
32	190.02	-673.49	191.38	-679.26	189.20	-670.29	-1.36	5.77	0.82	-3.21
33	53.91	-137.63	71.54	-193.27	50.81	-124.03	-17.63	55.64	3.10	-13.60
34	5.77	-10.54	15.74	-20.83	8.67	-4.91	-9.97	10.29	-2.90	-5.63
35	408.88	-123.67	390.80	-115.56	411.92	-128.61	18.08	-8.10	-3.04	4.94
36	130.86	2.98	119.62	3.65	132.74	-6.84	11.25	-0.67	-1.88	9.82
37	25.63	-13.70	28.95	-17.70	177.00	-65.05	-3.32	4.00	-151.37	51.35
38	11.33	-32.97	11.46	-27.99	10.98	-32.37	-0.13	-4.98	0.35	-0.60
39	14.14	-8.60	20.97	-9.76	15.20	-8.96	-6.83	1.16	-1.06	0.36
40	4.28	-17.33	4.83	-20.60	4.63	-18.62	-0.55	3.27	-0.35	1.29
41	10.75	-8.91	3.83	-9.24	12.28	-10.05	6.92	0.33	-1.53	1.15
42	3.88	-7.82	4.22	-9.71	4.38	-8.66	-0.34	1.89	-0.50	0.84
43	5.83	-22.11	7.12	-23.45	6.63	-25.53	-1.29	1.34	-0.80	3.42
44	6.53	-19.92	8.96	-34.15	7.45	-22.81	-2.43	14.24	-0.92	2.89
45	8.79	-3.39	7.41	-5.32	9.44	-4.09	1.39	1.93	-0.65	0.70
46	6.74	-3.75	17.39	-6.56	5.86	-3.44	-10.64	2.81	0.88	-0.32
47	162.99	-46.34	179.44	-56.43	129.21	-35.09	-16.46	10.09	33.77	-11.25
48	5.37	-13.96	10.12	-25.86	17.84	-39.72	-4.75	11.89	-12.47	25.76
49	163.65	-53.30	195.15	-63.28	92.55	-30.01	-31.50	9.98	71.09	-23.29
50	309.54	-110.85	354.96	-127.50	282.65	-101.49	-45.42	16.65	26.89	-9.37
51	50.78	-53.18	61.31	-73.54	52.54	-58.77	-10.54	20.36	-1.76	5.59
52	104.32	-37.73	105.82	-38.37	104.53	-37.98	-1.50	0.64	-0.21	0.24
53	280.32	-485.70	280.96	-489.06	290.21	-516.70	-0.64	3.36	-9.88	31.00
54	474.93	-223.54	512.54	-238.10	381.57	-194.44	-37.60	14.55	93.36	-29.10
55	121.57	-207.84	127.18	-228.78	117.73	-183.08	-5.61	20.94	3.84	-24.76
56	84.98	-33.34	116.13	-45.13	34.16	-20.06	-31.15	11.79	50.82	-13.28
57	19.66	-63.84	22.16	-70.48	18.78	-60.95	-2.50	6.65	0.88	-2.88
58	39.27	-96.79	43.27	-103.83	37.53	-93.68	-4.00	7.04	1.74	-3.11
59	150.10	-48.84	165.84	-54.09	146.38	-47.64	-15.73	5.25	3.72	-1.20
60	125.03	-372.07	137.01	-402.59	100.24	-300.02	-11.98	30.52	24.78	-72.04
61	135.15	-51.58	127.50	-77.47	253.26	-80.56	7.65	25.89	-118.11	28.98
62	2.27	-4.38	7.61	-16.82	23.27	-9.54	-5.35	12.44	-21.00	5.16
63	295.52	-164.79	290.46	-159.40	245.15	-139.35	5.06	-5.39	50.37	-25.44
64	285.65	-113.88	284.10	-97.61	327.03	-218.83	1.55	-16.27	-41.37	104.94
65	188.12	-70.84	224.25	-105.02	196.68	-71.13	-36.13	34.18	-8.56	0.29
66	417.75	-453.07	454.08	-493.24	394.51	-456.38	-36.32	40.17	23.25	3.31
67	28.80	-100.55	29.57	-106.27	30.52	-105.71	-0.77	5.72	-1.72	5.16
68	59.37	-144.47	64.29	-151.32	66.55	-156.56	-4.92	6.85	-7.18	12.10
69	162.43	-96.74	162.33	-110.29	91.42	-46.09	0.10	13.54	71.01	-50.65
70	76.10	-32.37	84.20	-30.43	82.21	-35.16	-8.10	-1.94	-6.11	2.79

Table D.8. Maximum ($\epsilon 1$) and minimum ($\epsilon 3$) principal strain values at the location of 70 landmarks during first incisor (II) bite load for the varying muscle force load cases sensitivity tests (see text for more details), and strain differences ($\Delta \epsilon 1$ and $\Delta \epsilon 3$) at landmark locations between models. Strain values are in microstrain (μ strain).

II bite landmark	ACSA		Load Case 1		Load Case 2		ACSA-LoadCase1		ACSA-LoadCase2	
	$\epsilon 1$	$\epsilon 3$	$\epsilon 1$	$\epsilon 3$	$\epsilon 1$	$\epsilon 3$	$\Delta \epsilon 1$	$\Delta \epsilon 3$	$\Delta \epsilon 1$	$\Delta \epsilon 3$
1	646.29	-552.11	904.02	-774.40	761.32	-652.19	-257.73	222.29	-115.03	100.08
2	208.52	-109.23	380.22	-174.43	316.58	-147.04	-171.71	65.20	-108.06	37.81
3	266.00	-96.64	413.23	-148.98	354.15	-127.57	-147.23	52.34	-88.15	30.93
4	52.97	-235.65	95.38	-424.58	81.65	-363.76	-42.41	188.93	-28.68	128.11
5	59.08	-18.98	99.55	-31.96	80.41	-25.84	-40.46	12.98	-21.33	6.86
6	32.80	-99.76	41.71	-125.45	42.44	-127.31	-8.91	25.68	-9.64	27.55
7	2.14	-0.85	0.93	-2.31	0.83	-2.09	1.21	1.46	1.30	1.24
8	217.62	-70.22	368.08	-129.23	336.70	-119.67	-150.46	59.01	-119.08	49.45
9	153.01	-324.59	235.15	-332.17	198.98	-232.13	-82.14	7.58	-45.97	-92.45
10	19.85	-14.72	37.71	-23.33	34.61	-19.41	-17.86	8.61	-14.75	4.70
11	167.55	-489.47	239.09	-699.25	202.02	-591.04	-71.55	209.78	-34.47	101.56
12	265.55	-158.28	503.32	-356.78	422.70	-299.40	-237.78	198.50	-157.16	141.12
13	23.13	-51.89	35.51	-74.61	31.39	-63.21	-12.38	22.71	-8.26	11.31
14	222.93	-117.64	314.86	-168.25	263.87	-142.42	-91.92	50.61	-40.94	24.78
15	149.83	-97.46	209.91	-138.98	174.84	-117.29	-60.08	41.51	-25.01	19.82
16	110.40	-53.01	167.32	-77.16	141.95	-64.38	-56.91	24.15	-31.54	11.37
17	102.17	-42.26	145.70	-59.90	120.43	-49.47	-43.54	17.65	-18.26	7.21
18	161.90	-62.75	365.80	-130.49	294.25	-105.07	-203.90	67.74	-132.34	42.32
19	44.85	-94.33	88.90	-110.18	87.44	-111.28	-44.05	15.85	-42.58	16.95
20	0.79	-0.14	0.89	-0.54	0.80	-0.29	-0.11	0.40	-0.02	0.14
21	295.63	-88.27	347.19	-104.78	210.92	-63.48	-51.55	16.51	84.71	-24.79
22	224.28	-101.30	201.21	-102.97	66.00	-54.18	23.07	1.67	158.28	-47.12
23	115.10	-377.12	172.79	-567.72	149.58	-492.05	-57.69	190.60	-34.48	114.93
24	125.98	-386.48	183.72	-561.61	157.63	-482.06	-57.73	175.13	-31.65	95.57
25	260.30	-265.86	235.53	-261.81	107.83	-143.75	24.77	-4.05	152.47	-122.11
26	476.56	-203.76	409.90	-178.83	166.67	-74.78	66.66	-24.93	309.89	-128.98
27	220.30	-391.01	218.51	-337.69	132.94	-151.34	1.79	-53.32	87.35	-239.66
28	342.56	-76.96	298.73	-70.57	145.49	-32.86	43.83	-6.39	197.07	-44.11
29	37.35	-107.10	54.10	-156.14	43.46	-126.12	-16.75	49.04	-6.12	19.02
30	39.68	-103.24	57.50	-154.25	45.03	-124.56	-17.82	51.01	-5.35	21.32
31	44.71	-18.17	43.69	-33.56	22.51	-36.62	1.02	15.38	22.20	18.45
32	183.21	-647.35	187.97	-662.71	104.47	-363.31	-4.76	15.36	78.74	-284.03
33	126.14	-42.46	182.81	-59.40	126.29	-40.07	-56.68	16.95	-0.16	-2.39
34	6.72	-17.70	68.97	-52.96	65.47	-50.13	-62.24	35.26	-58.74	32.43
35	427.56	-134.12	453.07	-147.13	279.10	-102.39	-25.51	13.02	148.46	-31.72
36	161.31	-74.62	143.91	-59.88	67.85	-24.27	17.41	-14.74	93.46	-50.35
37	13.83	-38.93	33.35	-101.11	32.00	-96.76	-19.52	62.19	-18.16	57.84
38	26.76	-8.52	48.71	-13.89	42.96	-11.99	-21.95	5.37	-16.20	3.47
39	143.87	-501.44	201.29	-701.32	169.11	-589.13	-57.42	199.88	-25.24	87.69
40	227.23	-59.49	348.61	-87.26	292.92	-73.48	-121.38	27.77	-65.70	13.99
41	127.80	-49.22	170.07	-70.91	145.56	-59.29	-42.27	21.69	-17.76	10.07
42	128.08	-58.33	189.22	-85.61	158.41	-71.53	-61.14	27.28	-30.33	13.20
43	400.62	-97.65	552.47	-135.27	456.30	-111.56	-151.85	37.62	-55.69	13.91
44	333.28	-85.83	472.33	-119.72	399.75	-100.01	-139.05	33.88	-66.48	14.18
45	144.40	-47.59	209.46	-68.59	175.18	-57.38	-65.05	21.00	-30.78	9.79
46	89.11	-42.87	185.65	-69.51	145.05	-54.31	-96.54	26.64	-55.94	11.44
47	146.58	-36.38	176.89	-64.10	124.06	-46.34	-30.31	27.71	22.51	9.95
48	5.16	-13.32	12.24	-30.31	9.90	-24.00	-7.08	16.99	-4.74	10.68
49	341.26	-108.51	405.40	-131.95	257.21	-84.52	-64.14	23.44	84.05	-23.99
50	254.82	-89.60	301.73	-106.12	183.33	-64.31	-46.91	16.51	71.49	-25.29
51	124.96	-385.14	190.65	-583.75	166.27	-504.89	-65.69	198.60	-41.31	119.75
52	211.00	-230.27	340.51	-348.52	291.26	-299.29	-129.51	118.25	-80.27	69.02
53	270.84	-455.38	245.31	-382.70	123.41	-162.57	25.53	-72.69	147.43	-292.81
54	465.01	-225.92	397.69	-223.35	146.74	-114.74	67.32	-2.57	318.26	-111.18
55	114.54	-222.35	98.94	-226.14	76.61	-126.37	15.61	3.79	37.93	-95.97
56	149.94	-96.57	176.71	-97.95	90.78	-73.66	-26.78	1.37	59.15	-22.91
57	38.23	-124.15	55.50	-177.85	45.09	-143.87	-17.27	53.70	-6.86	19.72
58	53.52	-111.50	76.16	-165.18	59.48	-137.34	-22.63	53.68	-5.96	25.84
59	25.74	-8.83	18.90	-14.58	15.76	-34.41	6.84	5.75	9.98	25.58
60	150.67	-462.22	153.70	-469.53	81.06	-254.28	-3.03	7.30	69.61	-207.95
61	103.40	-52.50	135.66	-80.67	87.27	-42.42	-32.26	28.17	16.13	-10.09
62	4.22	-11.43	26.36	-61.45	24.67	-57.48	-22.14	50.02	-20.45	46.05
63	350.48	-188.64	358.15	-188.94	213.25	-113.38	-7.67	0.30	137.23	-75.26
64	282.42	-107.88	277.60	-102.12	139.67	-51.32	4.83	-5.75	142.76	-56.56
65	209.70	-573.74	320.89	-860.16	271.97	-730.51	-111.19	286.41	-62.26	156.76
66	248.95	-158.21	293.76	-169.74	220.15	-109.06	-44.81	11.54	28.80	-49.14
67	46.07	-178.52	76.57	-271.91	67.49	-230.02	-30.50	93.38	-21.42	51.50
68	184.64	-562.04	268.80	-821.91	229.12	-701.33	-84.16	259.87	-44.48	139.29
69	225.95	-133.85	257.57	-133.79	185.53	-78.64	-31.62	-0.05	40.42	-55.21
70	53.91	-117.58	83.03	-165.85	72.40	-142.02	-29.12	48.27	-18.49	24.45

Table D.9. Maximum (ϵ_1) and minimum (ϵ_3) principal strain values at the location of 70 landmarks during second incisor (I2) bite load for the varying muscle force load cases sensitivity tests (see text for more details), and strain differences ($\Delta\epsilon_1$ and $\Delta\epsilon_3$) at landmark locations between models. Strain values are in microstrain (μstrain).

I2 bite landmark	ACSA		Load Case 1		Load Case 2		ACSA-LoadCase1		ACSA-LoadCase2	
	ϵ_1	ϵ_3	ϵ_1	ϵ_3	ϵ_1	ϵ_3	$\Delta\epsilon_1$	$\Delta\epsilon_3$	$\Delta\epsilon_1$	$\Delta\epsilon_3$
1	147.64	-397.31	227.14	-580.67	191.36	-489.37	-79.50	183.37	-43.72	92.07
2	273.62	-211.46	493.04	-353.31	413.07	-299.22	-219.42	141.86	-139.45	87.76
3	272.14	-100.94	421.29	-154.89	360.91	-132.52	-149.15	53.94	-88.77	31.58
4	51.87	-231.54	93.65	-417.79	80.21	-358.05	-41.77	186.25	-28.33	126.51
5	59.19	-19.01	99.72	-32.09	80.57	-25.95	-40.53	13.08	-21.38	6.94
6	33.28	-101.32	42.46	-127.89	43.06	-129.37	-9.18	26.57	-9.78	28.05
7	2.17	-0.88	0.88	-2.26	0.81	-2.05	1.29	1.38	1.36	1.17
8	218.27	-71.04	368.14	-130.95	336.74	-121.14	-149.87	59.91	-118.47	50.10
9	160.63	-337.63	247.44	-353.91	210.02	-251.12	-86.81	16.29	-49.39	-86.51
10	23.75	-15.70	43.39	-25.08	39.63	-21.18	-19.64	9.39	-15.88	5.48
11	184.50	-547.32	265.46	-788.57	224.21	-666.25	-80.96	241.26	-39.71	118.93
12	797.07	-523.21	1311.83	-984.93	1103.57	-828.43	-514.76	461.72	-306.49	305.22
13	12.79	-33.16	20.40	-50.42	18.12	-42.56	-7.61	17.26	-5.33	9.40
14	222.47	-122.54	318.11	-175.18	266.40	-148.03	-95.64	52.65	-43.92	25.49
15	160.55	-105.55	226.11	-150.79	187.38	-126.48	-65.56	45.25	-26.83	20.94
16	51.77	-35.72	85.75	-53.27	73.27	-44.27	-33.98	17.55	-21.50	8.54
17	96.08	-42.40	134.58	-58.28	111.04	-48.01	-38.50	15.88	-14.96	5.60
18	196.05	-76.23	438.71	-156.84	355.64	-127.26	-242.66	80.61	-159.59	51.03
19	47.63	-113.45	86.78	-130.65	85.64	-129.39	-39.15	17.19	-38.01	15.94
20	0.73	-0.14	0.82	-0.47	0.75	-0.25	-0.09	0.33	-0.02	0.11
21	310.33	-92.77	374.34	-113.21	233.74	-70.59	-64.01	20.45	76.59	-22.17
22	181.80	-90.14	144.75	-91.15	38.06	-64.56	37.05	1.00	143.74	-25.58
23	118.82	-388.54	178.35	-584.25	154.25	-506.01	-59.53	195.72	-35.43	117.48
24	188.81	-581.47	274.92	-846.95	234.43	-722.34	-86.11	265.48	-45.62	140.87
25	264.10	-272.91	241.32	-271.00	112.94	-150.39	22.78	-1.91	151.15	-122.52
26	501.67	-212.33	447.47	-191.41	198.12	-85.17	54.20	-20.93	303.55	-127.16
27	223.50	-405.38	220.31	-355.43	129.42	-161.39	3.19	-49.95	94.09	-243.99
28	367.77	-81.13	343.33	-80.39	184.92	-41.85	24.43	-0.74	182.85	-39.27
29	36.86	-105.85	53.38	-154.31	42.85	-124.55	-16.52	48.46	-6.00	18.70
30	38.30	-98.67	55.52	-148.22	43.27	-119.39	-17.22	49.55	-4.97	20.72
31	25.01	-12.70	25.23	-36.58	21.30	-53.53	-0.22	23.88	3.71	40.83
32	184.39	-651.78	188.60	-665.08	105.00	-365.22	-4.22	13.30	79.38	-286.57
33	101.60	-36.78	143.75	-49.15	92.19	-29.66	-42.16	12.37	9.41	-7.13
34	6.72	-17.69	67.24	-52.86	63.99	-50.03	-60.52	35.17	-57.28	32.34
35	426.10	-131.93	446.05	-140.73	271.22	-94.65	-19.94	8.80	154.88	-37.28
36	155.48	-64.63	135.42	-45.67	64.02	-12.62	20.06	-18.96	91.46	-52.00
37	13.97	-38.42	33.10	-100.26	31.76	-96.03	-19.14	61.84	-17.79	57.61
38	22.44	-8.30	42.28	-12.64	37.20	-10.55	-19.84	4.34	-14.76	2.26
39	116.57	-407.60	160.07	-559.54	134.39	-469.70	-43.49	151.94	-17.81	62.10
40	241.29	-72.36	353.23	-110.26	297.30	-92.91	-111.94	37.90	-56.01	20.54
41	268.20	-41.23	364.47	-58.79	309.79	-49.06	-96.27	17.56	-41.59	7.83
42	123.71	-61.47	181.88	-88.59	152.45	-74.88	-58.17	27.12	-28.74	13.41
43	349.71	-87.06	476.29	-118.55	392.81	-98.32	-126.58	31.49	-43.10	11.26
44	409.61	-97.19	574.98	-134.63	486.68	-112.90	-165.37	37.44	-77.07	15.71
45	152.04	-48.15	221.76	-70.05	185.59	-58.60	-69.71	21.91	-33.55	10.45
46	62.40	-30.01	132.37	-49.06	100.20	-37.09	-69.97	19.05	-37.80	7.09
47	169.13	-40.76	212.06	-71.25	151.36	-52.18	-42.93	30.49	17.78	11.42
48	5.49	-14.19	12.83	-31.93	10.40	-25.37	-7.34	17.74	-4.92	11.18
49	331.08	-105.17	384.40	-124.94	239.57	-78.61	-53.32	19.77	91.51	-26.56
50	276.13	-96.76	334.72	-116.85	210.90	-72.94	-58.59	20.09	65.23	-23.82
51	121.60	-372.06	186.45	-565.58	162.78	-489.57	-64.85	193.52	-41.18	117.52
52	250.05	-147.65	400.49	-229.06	340.73	-197.64	-150.44	81.42	-90.68	50.00
53	264.36	-432.23	235.67	-351.65	117.61	-142.85	28.69	-80.58	146.75	-289.38
54	444.13	-224.23	369.68	-223.53	128.95	-120.14	74.45	-0.70	315.18	-104.09
55	111.18	-216.52	96.89	-221.75	84.67	-125.46	14.29	5.23	26.51	-91.07
56	138.81	-78.82	156.10	-74.41	71.80	-51.78	-17.29	-4.41	67.00	-27.04
57	37.99	-123.68	55.19	-177.22	44.81	-143.31	-17.20	53.54	-6.82	19.64
58	54.70	-115.08	77.87	-169.71	61.00	-141.24	-23.18	54.64	-6.30	26.16
59	45.59	-15.10	39.94	-14.63	16.38	-17.03	5.66	-0.47	29.22	1.93
60	145.71	-445.86	147.14	-447.79	75.56	-236.25	-1.42	1.93	70.15	-209.62
61	117.51	-52.86	157.51	-81.97	107.55	-45.46	-40.00	29.11	9.96	-7.40
62	4.10	-11.17	26.27	-61.21	24.60	-57.31	-22.17	50.04	-20.50	46.15
63	345.79	-186.96	354.01	-187.73	210.52	-113.25	-8.23	0.77	135.27	-73.71
64	285.14	-112.32	281.39	-107.69	142.55	-54.57	3.75	-4.63	142.59	-57.75
65	223.38	-612.74	343.68	-922.49	291.15	-782.96	-120.30	309.75	-67.76	170.22
66	274.91	-193.37	330.31	-216.18	248.73	-145.90	-55.40	22.80	26.18	-47.47
67	131.93	-285.57	174.72	-434.65	140.37	-367.70	-42.78	149.08	-8.43	82.12
68	159.67	-486.77	229.99	-707.46	196.45	-605.14	-70.32	220.70	-36.78	118.38
69	205.31	-107.54	229.53	-99.17	166.44	-54.02	-24.21	-8.37	38.88	-53.53
70	63.28	-156.18	81.98	-224.17	65.72	-192.11	-18.69	67.99	-2.44	35.92

Table D.10. Maximum (ϵ_1) and minimum (ϵ_3) principal strain values at the location of 70 landmarks during first premolar (P3) bite load for the varying muscle force load cases sensitivity tests (see text for more details), and strain differences ($\Delta\epsilon_1$ and $\Delta\epsilon_3$) at landmark locations between models. Strain values are in microstrain (μstrain).

P3 bite landmark	ACSA		Load Case 1		Load Case 2		ACSA-LoadCase1		ACSA-LoadCase2	
	ϵ_1	ϵ_3	ϵ_1	ϵ_3	ϵ_1	ϵ_3	$\Delta\epsilon_1$	$\Delta\epsilon_3$	$\Delta\epsilon_1$	$\Delta\epsilon_3$
1	24.92	-37.60	40.13	-61.51	33.91	-52.29	-15.21	23.92	-8.99	14.69
2	73.76	-147.59	124.17	-236.93	104.51	-203.16	-50.41	89.34	-30.75	55.57
3	232.67	-90.58	354.70	-136.85	304.80	-117.29	-122.03	46.27	-72.13	26.71
4	44.21	-197.99	80.84	-361.33	69.49	-310.75	-36.63	163.34	-25.28	112.76
5	55.72	-18.02	95.27	-31.04	76.89	-25.13	-39.56	13.01	-21.17	7.10
6	35.72	-109.04	46.25	-139.90	46.26	-139.46	-10.53	30.86	-10.53	30.43
7	3.38	-1.38	0.54	-0.85	0.47	-0.83	2.84	-0.53	2.91	-0.55
8	199.47	-68.40	341.91	-127.77	314.52	-118.34	-142.44	59.36	-115.05	49.94
9	190.23	-351.20	291.35	-399.20	250.65	-292.74	-101.12	48.00	-60.42	-58.47
10	34.46	-19.52	58.26	-30.77	52.45	-26.32	-23.79	11.25	-17.98	6.80
11	73.16	-209.72	108.00	-309.54	91.65	-262.87	-34.83	99.82	-18.49	53.15
12	48.73	-44.97	113.72	-105.16	96.53	-89.44	-64.99	60.19	-47.79	44.47
13	246.69	-658.09	344.03	-920.93	289.19	-773.57	-97.34	262.84	-42.50	115.48
14	423.89	-966.92	578.46	-1318.09	485.93	-1109.59	-154.57	351.17	-62.04	142.67
15	322.15	-459.34	444.17	-636.02	369.89	-533.76	-122.02	176.68	-47.74	74.42
16	66.61	-244.02	91.30	-335.54	77.41	-281.34	-24.68	91.51	-10.79	37.31
17	54.81	-71.97	72.14	-101.78	59.85	-85.89	-17.33	29.81	-5.04	13.92
18	236.48	-92.54	501.61	-180.62	408.56	-147.28	-265.13	88.08	-172.08	54.74
19	62.25	-140.55	107.74	-170.78	103.39	-164.43	-45.49	30.23	-41.14	23.88
20	0.55	-0.16	0.64	-0.29	0.57	-0.19	-0.09	0.12	-0.02	0.03
21	359.58	-108.33	454.10	-138.07	300.90	-91.48	-94.51	29.74	58.68	-16.85
22	87.29	-70.59	50.31	-106.31	44.64	-163.66	36.98	35.72	42.66	93.07
23	123.35	-403.06	185.40	-604.94	160.14	-523.44	-62.05	201.88	-36.80	120.39
24	262.76	-801.91	380.92	-1164.80	323.56	-989.72	-118.16	362.89	-60.80	187.81
25	277.64	-289.48	261.91	-291.62	129.38	-164.03	15.73	2.14	148.26	-125.45
26	576.89	-238.89	563.35	-232.09	296.21	-119.92	13.54	-6.81	280.67	-118.97
27	231.35	-448.01	223.28	-410.04	117.81	-193.98	8.07	-37.97	113.55	-254.03
28	411.10	-86.08	432.90	-95.89	265.50	-59.53	-21.81	9.81	145.60	-26.55
29	34.31	-98.78	49.36	-142.95	39.47	-115.02	-15.05	44.17	-5.16	16.23
30	32.62	-80.10	46.74	-121.60	35.67	-96.77	-14.12	41.50	-3.05	16.68
31	12.33	-34.70	28.81	-90.52	33.37	-110.22	-16.48	55.82	-21.04	75.52
32	185.44	-656.35	186.73	-659.51	103.39	-360.22	-1.29	3.16	82.05	-296.12
33	47.79	-37.95	53.02	-45.19	21.26	-30.80	-5.24	7.23	26.53	-7.15
34	6.13	-15.91	56.83	-48.17	55.16	-46.00	-50.71	32.26	-49.03	30.09
35	414.50	-125.60	413.67	-122.51	239.20	-72.73	0.83	-3.09	175.30	-52.87
36	143.07	-38.22	120.87	-7.97	60.66	-8.54	22.20	-30.25	82.41	-29.67
37	13.88	-29.89	29.39	-86.32	28.26	-84.08	-15.52	56.43	-14.38	54.19
38	12.59	-11.06	24.31	-11.34	20.47	-7.62	-11.71	0.28	-7.88	-3.44
39	37.21	-128.30	47.49	-163.10	39.59	-135.97	-10.28	34.80	-2.38	7.68
40	81.12	-21.51	127.59	-34.37	107.73	-28.99	-46.47	12.86	-26.61	7.47
41	236.85	-75.35	311.83	-96.16	265.48	-82.93	-74.99	20.82	-28.63	7.59
42	50.53	-38.78	71.90	-52.85	60.39	-45.34	-21.37	14.07	-9.87	6.56
43	108.15	-36.04	138.68	-48.94	112.93	-43.83	-30.53	12.90	-4.79	7.79
44	289.04	-61.07	391.55	-81.39	333.03	-68.43	-102.51	20.32	-43.99	7.36
45	99.21	-28.92	141.48	-41.38	118.17	-34.44	-42.28	12.45	-18.97	5.52
46	12.46	-5.99	28.63	-10.17	12.88	-4.65	-16.17	4.18	-0.42	-1.34
47	192.07	-45.16	252.55	-76.89	187.80	-58.45	-60.48	31.73	4.27	13.29
48	5.84	-15.11	13.54	-33.98	10.99	-27.07	-7.70	18.87	-5.15	11.96
49	280.86	-89.48	299.65	-96.95	168.64	-55.13	-18.79	7.47	112.22	-34.35
50	309.20	-108.51	387.19	-135.91	255.05	-89.66	-77.99	27.40	54.15	-18.84
51	99.35	-292.82	156.47	-453.59	137.73	-395.39	-57.13	160.76	-38.38	102.57
52	311.10	-117.41	462.31	-173.25	389.63	-145.33	-151.21	55.84	-78.53	27.92
53	259.98	-415.41	227.72	-329.06	103.25	-124.31	32.26	-86.35	156.74	-291.10
54	425.95	-222.53	346.62	-223.77	115.99	-126.14	79.33	1.24	309.96	-96.40
55	109.00	-206.69	92.69	-209.52	83.40	-117.66	16.30	2.83	25.60	-89.03
56	110.90	-44.72	111.10	-35.75	34.35	-14.50	-0.20	-8.97	76.55	-30.22
57	33.85	-110.51	49.19	-158.29	39.76	-127.41	-15.33	47.79	-5.91	16.90
58	52.18	-114.38	74.57	-168.64	58.93	-141.09	-22.39	54.26	-6.74	26.71
59	91.93	-30.13	105.58	-35.14	58.92	-19.88	-13.66	5.01	33.00	-10.25
60	135.23	-409.95	132.61	-397.81	63.49	-194.80	2.63	-12.15	71.75	-215.15
61	139.67	-54.32	190.59	-85.00	137.99	-50.91	-50.92	30.68	1.68	-3.41
62	3.35	-9.14	23.47	-54.56	22.24	-51.73	-20.12	45.42	-18.89	42.58
63	329.22	-180.21	332.62	-179.34	194.25	-108.08	-3.40	-0.87	134.98	-72.13
64	288.86	-119.34	286.62	-117.27	147.02	-62.63	2.24	-2.06	141.84	-56.71
65	170.98	-530.47	265.03	-805.30	224.94	-684.97	-94.05	274.82	-53.96	154.49
66	333.81	-289.24	414.40	-344.55	316.15	-250.72	-80.59	55.31	17.66	-38.52
67	360.85	-539.38	506.75	-815.98	422.93	-691.80	-145.90	276.60	-62.07	152.41
68	90.40	-271.88	128.52	-392.83	111.02	-340.93	-38.12	120.94	-20.61	69.05
69	169.17	-73.68	178.74	-54.91	133.30	-40.69	-9.57	-18.76	35.87	-32.99
70	136.65	-157.82	189.21	-224.44	155.87	-192.43	-52.56	66.62	-19.22	34.61

Table D.11. Maximum ($\epsilon 1$) and minimum ($\epsilon 3$) principal strain values at the location of 70 landmarks during second premolar (P4) bite load for the varying muscle force load cases sensitivity tests (see text for more details), and strain differences ($\Delta \epsilon 1$ and $\Delta \epsilon 3$) at landmark locations between models. Strain values are in microstrain (μ strain).

P4 bite landmark	ACSA		Load Case 1		Load Case 2		ACSA-LoadCase1		ACSA-LoadCase2	
	$\epsilon 1$	$\epsilon 3$	$\epsilon 1$	$\epsilon 3$	$\epsilon 1$	$\epsilon 3$	$\Delta \epsilon 1$	$\Delta \epsilon 3$	$\Delta \epsilon 1$	$\Delta \epsilon 3$
1	18.07	-31.83	29.40	-52.27	24.88	-44.51	-11.33	20.43	-6.81	12.68
2	55.65	-136.71	92.27	-222.47	77.98	-191.29	-36.61	85.76	-22.33	54.58
3	216.65	-85.15	329.56	-128.40	283.64	-110.17	-112.91	43.24	-67.00	25.02
4	42.09	-188.24	77.15	-344.46	66.38	-296.60	-35.06	156.22	-24.29	108.36
5	54.81	-17.79	94.48	-30.95	76.23	-25.07	-39.67	13.16	-21.42	7.28
6	36.39	-111.16	47.26	-143.10	47.10	-142.15	-10.87	31.94	-10.72	31.00
7	3.72	-1.52	0.60	-0.57	0.50	-0.57	3.11	-0.95	3.22	-0.95
8	194.83	-68.22	335.78	-127.47	309.21	-117.96	-140.96	59.25	-114.38	49.74
9	197.41	-335.68	301.35	-386.92	260.04	-283.31	-103.94	51.23	-62.63	-52.38
10	37.57	-20.79	62.62	-32.59	56.17	-27.92	-25.06	11.80	-18.61	7.13
11	58.11	-142.49	86.59	-213.60	73.59	-182.06	-28.47	71.11	-15.48	39.57
12	42.27	-38.65	97.71	-89.19	83.10	-76.04	-55.44	50.54	-40.84	37.39
13	50.70	-116.72	75.81	-178.54	63.48	-148.88	-25.11	61.82	-12.78	32.16
14	291.26	-399.59	413.76	-551.11	347.62	-465.21	-122.50	151.53	-56.37	65.62
15	308.18	-1197.92	418.03	-1638.34	352.90	-1378.77	-109.84	440.42	-44.72	180.85
16	104.33	-373.43	144.18	-517.21	121.94	-434.29	-39.85	143.77	-17.60	60.85
17	63.47	-109.82	87.23	-158.66	73.12	-134.26	-23.76	48.84	-9.65	24.45
18	245.34	-96.23	514.51	-186.15	419.45	-151.93	-269.17	89.92	-174.10	55.70
19	68.10	-145.97	116.62	-182.10	110.91	-174.15	-48.52	36.12	-42.80	28.17
20	0.54	-0.18	0.62	-0.24	0.56	-0.19	-0.07	0.07	-0.02	0.01
21	372.26	-112.39	473.57	-144.15	317.30	-96.58	-101.32	31.76	54.96	-15.81
22	66.87	-70.85	45.50	-133.13	54.37	-199.30	21.37	62.28	12.51	128.46
23	124.28	-406.41	186.57	-608.65	161.11	-526.55	-62.29	202.24	-36.83	120.15
24	261.73	-797.17	379.22	-1157.40	322.11	-983.45	-117.49	360.23	-60.38	186.28
25	281.55	-293.63	267.65	-296.86	133.89	-167.72	13.90	3.23	147.66	-125.92
26	597.43	-246.28	595.28	-243.57	323.32	-129.79	2.15	-2.71	274.10	-116.48
27	233.50	-459.44	224.99	-425.67	116.92	-204.79	8.51	-33.77	116.58	-254.65
28	418.43	-86.45	452.80	-98.74	283.35	-65.08	-34.37	12.29	135.08	-21.37
29	33.54	-96.60	48.11	-139.38	38.41	-112.02	-14.57	42.78	-4.87	15.42
30	31.09	-74.71	44.22	-113.49	33.43	-89.84	-13.13	38.79	-2.34	15.14
31	15.41	-47.62	33.65	-110.60	37.64	-127.50	-18.24	62.98	-22.23	79.88
32	185.68	-657.42	186.20	-657.98	102.94	-358.92	-0.52	0.56	82.74	-298.49
33	41.59	-46.47	44.82	-60.24	23.60	-52.40	-3.23	13.78	17.98	5.93
34	6.00	-15.43	54.07	-46.92	52.80	-44.92	-48.06	31.48	-46.80	29.48
35	411.54	-124.46	405.41	-118.73	231.07	-67.77	6.13	-5.73	180.47	-56.69
36	140.54	-31.50	118.80	1.40	61.96	-17.53	21.74	-32.89	78.59	-13.97
37	14.29	-27.88	28.80	-82.84	27.56	-81.09	-14.51	54.95	-13.26	53.20
38	11.26	-13.05	20.66	-12.17	16.76	-7.62	-9.40	-0.88	-5.50	-5.42
39	29.63	-100.66	37.07	-124.77	30.83	-103.72	-7.44	24.11	-1.20	3.06
40	72.51	-18.52	116.93	-29.73	98.86	-25.11	-44.43	11.21	-26.35	6.59
41	214.57	-74.14	283.53	-96.12	241.65	-82.92	-68.96	21.98	-27.07	8.78
42	40.67	-34.95	57.24	-47.40	48.19	-40.89	-16.56	12.45	-7.52	5.94
43	79.00	-37.28	100.13	-52.73	82.60	-49.09	-21.13	15.45	-3.59	11.81
44	249.43	-51.05	337.02	-67.72	287.26	-56.96	-87.59	16.67	-37.83	5.91
45	87.11	-24.78	123.44	-35.26	103.04	-29.28	-36.33	10.48	-15.93	4.50
46	6.78	-3.35	15.60	-5.53	2.12	-1.26	-8.82	2.18	4.66	-2.09
47	192.07	-46.19	254.20	-79.52	190.27	-61.74	-62.13	33.33	1.81	15.55
48	5.89	-15.27	13.66	-34.35	11.09	-27.39	-7.77	19.08	-5.20	12.11
49	264.98	-84.50	275.33	-89.01	148.35	-48.56	-10.35	4.51	116.62	-35.95
50	314.57	-110.61	395.72	-139.39	262.35	-92.72	-81.15	28.77	52.23	-17.89
51	92.35	-267.72	147.12	-418.33	129.91	-365.75	-54.78	150.61	-37.56	98.02
52	307.64	-117.14	452.33	-171.46	380.69	-143.76	-144.69	54.32	-73.05	26.62
53	260.30	-415.96	228.03	-330.01	100.88	-122.95	32.27	-85.95	159.42	-293.01
54	424.37	-222.13	344.83	-223.34	114.86	-126.14	79.54	1.21	309.51	-95.99
55	109.01	-204.56	91.74	-206.31	81.10	-115.22	17.27	1.76	27.91	-89.34
56	105.05	-39.74	103.34	-32.07	31.56	-13.01	1.70	-7.67	73.49	-26.73
57	32.41	-105.91	47.16	-151.82	38.06	-121.97	-14.75	45.91	-5.64	16.06
58	51.08	-113.38	73.12	-167.40	57.95	-140.32	-22.04	54.02	-6.87	26.94
59	102.68	-33.64	120.90	-40.16	71.38	-23.92	-18.22	6.52	31.30	-9.71
60	132.71	-401.15	129.07	-385.45	60.54	-184.45	3.64	-15.69	72.18	-216.70
61	144.14	-54.70	197.07	-85.64	143.96	-52.05	-52.93	30.94	0.18	-2.65
62	3.15	-8.60	22.72	-52.78	21.61	-50.23	-19.57	44.17	-18.45	41.62
63	324.54	-178.23	326.28	-176.70	189.32	-106.29	-1.74	-1.53	135.23	-71.94
64	289.55	-120.80	287.59	-119.36	147.94	-64.65	1.97	-1.44	141.61	-56.15
65	145.21	-479.42	225.99	-732.53	192.08	-623.99	-80.78	253.11	-46.87	144.57
66	348.71	-318.42	435.95	-384.25	333.66	-283.51	-87.24	65.83	15.05	-34.91
67	295.75	-509.72	418.26	-772.70	349.26	-656.19	-122.52	262.98	-53.51	146.47
68	82.76	-243.30	117.93	-351.60	102.12	-306.32	-35.17	108.30	-19.36	63.01
69	162.16	-68.57	168.73	-48.30	127.01	-39.69	-6.57	-20.27	35.15	-28.88
70	141.48	-155.76	197.36	-222.82	162.69	-191.04	-55.88	67.07	-21.21	35.28

Table D.12. Maximum ($\epsilon 1$) and minimum ($\epsilon 3$) principal strain values at the location of 70 landmarks during first molar (M1) bite load for the varying muscle force load cases sensitivity tests (see text for more details), and strain differences ($\Delta\epsilon 1$ and $\Delta\epsilon 3$) at landmark locations between models. Strain values are in microstrain (μstrain).

M1 bite landmark	ACSA		Load Case 1		Load Case 2		ACSA-LoadCase1		ACSA-LoadCase2	
	$\epsilon 1$	$\epsilon 3$	$\epsilon 1$	$\epsilon 3$	$\epsilon 1$	$\epsilon 3$	$\Delta\epsilon 1$	$\Delta\epsilon 3$	$\Delta\epsilon 1$	$\Delta\epsilon 3$
1	3.30	-9.60	4.95	-15.78	4.26	-13.69	-1.66	6.18	-0.96	4.09
2	11.12	-30.54	28.76	-49.17	23.96	-44.14	-17.63	18.63	-12.84	13.60
3	186.56	-72.97	282.99	-109.70	244.45	-94.42	-96.43	36.74	-57.89	21.46
4	37.92	-168.81	69.92	-311.39	60.32	-268.79	-32.00	142.58	-22.39	99.98
5	52.95	-17.22	91.87	-30.16	74.03	-24.41	-38.92	12.94	-21.08	7.19
6	37.36	-114.16	48.80	-147.83	48.40	-146.15	-11.45	33.68	-11.04	32.00
7	4.46	-1.81	1.01	-0.38	0.74	-0.26	3.44	-1.43	3.72	-1.55
8	181.47	-65.45	317.90	-123.15	293.84	-114.09	-136.43	57.70	-112.37	48.64
9	188.66	-303.31	284.84	-347.50	247.41	-251.55	-96.18	44.19	-58.75	-51.75
10	39.79	-22.06	65.54	-34.30	58.54	-29.28	-25.75	12.24	-18.75	7.22
11	48.75	-26.86	71.53	-38.75	59.55	-32.70	-22.78	11.89	-10.80	5.84
12	2.34	-4.48	2.90	-9.48	2.80	-8.59	-0.56	5.00	-0.45	4.12
13	21.30	-41.49	29.22	-60.61	23.81	-48.80	-7.92	19.12	-2.52	7.31
14	98.45	-60.77	139.03	-75.93	117.06	-65.23	-40.58	15.16	-18.61	4.46
15	132.15	-79.95	198.25	-106.53	168.04	-91.50	-66.10	26.58	-35.89	11.55
16	65.29	-247.18	85.45	-323.07	72.32	-269.41	-20.17	75.89	-7.04	22.23
17	53.59	-107.81	74.07	-155.78	61.96	-131.18	-20.48	47.96	-8.37	23.37
18	187.22	-72.89	371.41	-134.54	297.82	-108.05	-184.20	61.65	-110.61	35.16
19	78.87	-155.23	129.28	-191.47	121.50	-182.20	-50.41	36.24	-42.63	26.97
20	0.54	-0.19	0.63	-0.22	0.54	-0.17	-0.09	0.04	-0.01	-0.01
21	402.15	-121.96	516.14	-157.50	353.19	-107.82	-113.99	35.54	48.96	-14.14
22	62.62	-72.79	45.96	-143.29	57.20	-209.73	16.66	70.51	5.42	136.94
23	122.86	-402.91	184.45	-603.02	159.30	-521.74	-61.59	200.11	-36.44	118.83
24	198.83	-604.91	281.71	-858.68	239.53	-730.40	-82.88	253.77	-40.70	125.49
25	282.14	-290.67	268.94	-292.90	134.49	-163.82	13.21	2.23	147.66	-126.85
26	606.46	-249.77	611.52	-249.73	336.79	-134.94	-5.06	-0.04	269.68	-114.84
27	234.15	-465.30	225.32	-434.64	115.70	-210.72	8.83	-30.66	118.45	-254.58
28	428.07	-86.71	469.10	-98.92	298.20	-71.38	-41.03	12.21	129.87	-15.33
29	33.22	-95.65	47.33	-137.02	37.77	-110.08	-14.11	41.36	-4.56	14.43
30	29.31	-68.18	41.02	-103.09	30.67	-81.01	-11.71	34.91	-1.35	12.83
31	15.48	-48.64	33.23	-111.20	37.28	-127.89	-17.75	62.56	-21.81	79.25
32	185.35	-656.37	185.53	-655.82	102.36	-357.08	-0.18	-0.55	82.99	-299.29
33	40.16	-51.94	43.96	-72.11	26.82	-65.91	-3.80	20.16	13.34	13.97
34	5.65	-14.24	49.29	-43.63	48.74	-42.11	-43.65	29.40	-43.10	27.87
35	407.86	-123.33	398.38	-116.22	224.86	-65.14	9.47	-7.11	183.00	-58.19
36	139.60	-28.83	118.02	5.78	63.03	-21.65	21.58	-34.61	76.57	-7.18
37	14.77	-23.60	27.08	-74.76	25.80	-74.17	-12.31	51.15	-11.03	50.56
38	9.99	-14.34	17.05	-12.56	13.20	-7.38	-7.07	-1.78	-3.21	-6.96
39	21.93	-73.66	27.02	-89.79	22.39	-74.41	-5.09	16.14	-0.46	0.75
40	19.51	-8.24	30.67	-12.92	25.91	-11.31	-11.16	4.68	-6.40	3.07
41	111.86	-39.29	139.65	-47.59	120.03	-41.89	-27.79	8.30	-8.18	2.60
42	19.06	-20.21	25.07	-26.16	21.26	-23.16	-6.02	5.96	-2.21	2.95
43	35.68	-27.43	42.62	-40.61	36.62	-41.21	-6.94	13.18	-0.94	13.78
44	140.04	-27.32	182.58	-34.53	157.18	-28.99	-42.54	7.21	-17.14	1.67
45	59.34	-16.32	80.83	-22.12	67.16	-18.19	-21.49	5.80	-7.82	1.87
46	9.62	-4.79	18.90	-6.53	5.00	-1.72	-9.28	1.74	4.62	-3.08
47	175.23	-42.16	232.01	-74.37	174.81	-59.45	-56.78	32.21	0.42	17.29
48	5.64	-14.61	13.24	-33.32	10.73	-26.51	-7.60	18.71	-5.09	11.89
49	247.86	-79.38	253.33	-81.90	129.86	-42.50	-5.47	2.52	118.00	-36.88
50	305.14	-107.55	381.82	-135.10	250.67	-89.24	-76.69	27.55	54.47	-18.32
51	80.44	-226.45	130.62	-359.10	116.06	-315.94	-50.18	132.65	-35.63	89.50
52	247.26	-93.30	356.18	-133.30	299.57	-111.56	-108.91	40.00	-52.30	18.26
53	267.10	-439.85	238.14	-363.14	105.93	-140.19	28.96	-76.72	161.17	-299.66
54	442.85	-222.80	369.66	-221.30	128.34	-117.54	73.19	-1.50	314.51	-105.26
55	112.95	-206.98	93.40	-204.55	67.03	-110.93	19.56	-2.43	45.92	-96.04
56	103.47	-41.06	99.73	-33.34	24.59	-11.45	3.74	-7.72	78.88	-29.61
57	29.97	-97.80	43.55	-139.93	35.04	-111.98	-13.58	42.13	-5.07	14.19
58	47.91	-108.29	68.83	-161.11	54.79	-135.51	-20.92	52.82	-6.88	27.22
59	104.34	-34.13	123.22	-40.80	72.96	-24.29	-18.88	6.67	31.38	-9.84
60	133.15	-401.87	129.20	-385.12	60.65	-183.92	3.94	-16.76	72.50	-217.96
61	135.66	-53.23	183.08	-82.62	131.31	-48.66	-47.42	29.38	4.35	-4.57
62	2.89	-7.71	20.97	-48.63	20.13	-46.73	-18.08	40.92	-17.24	39.01
63	320.15	-176.01	317.88	-172.55	182.03	-102.37	2.27	-3.46	138.11	-73.64
64	287.45	-116.74	284.23	-113.14	144.96	-59.12	3.21	-3.60	142.48	-57.62
65	134.05	-395.60	208.64	-613.85	178.92	-524.86	-74.59	218.25	-44.87	129.26
66	347.03	-319.17	436.22	-388.35	333.52	-286.39	-89.19	69.18	13.51	-32.77
67	165.55	-296.48	220.99	-443.87	183.21	-378.10	-55.44	147.40	-17.66	81.62
68	82.94	-241.86	121.04	-355.10	104.83	-309.64	-38.10	113.24	-21.89	67.78
69	169.16	-83.08	174.82	-65.02	124.75	-36.18	-5.66	-18.06	44.41	-46.91
70	98.25	-99.35	135.85	-140.71	110.34	-121.32	-37.60	41.36	-12.09	21.97

Table D.13. Maximum ($\epsilon 1$) and minimum ($\epsilon 3$) principal strain values at the location of 70 landmarks during second molar (M2) bite load for the varying muscle force load cases sensitivity tests (see text for more details), and strain differences ($\Delta\epsilon 1$ and $\Delta\epsilon 3$) at landmark locations between models. Strain values are in microstrain (μstrain).

M2 bite landmark	ACSA		Load Case 1		Load Case 2		ACSA-LoadCase1		ACSA-LoadCase2	
	$\epsilon 1$	$\epsilon 3$	$\epsilon 1$	$\epsilon 3$	$\epsilon 1$	$\epsilon 3$	$\Delta\epsilon 1$	$\Delta\epsilon 3$	$\Delta\epsilon 1$	$\Delta\epsilon 3$
1	3.44	-5.75	6.84	-10.68	5.49	-9.01	-3.40	4.93	-2.05	3.26
2	12.34	-18.20	25.08	-34.91	19.66	-30.60	-12.74	16.72	-7.32	12.41
3	124.32	-49.41	188.66	-74.36	164.92	-64.61	-64.34	24.94	-40.60	15.20
4	32.13	-133.82	57.25	-250.12	49.66	-217.21	-25.12	116.30	-17.53	83.39
5	50.56	-16.69	89.48	-29.92	72.07	-24.26	-38.93	13.23	-21.51	7.57
6	39.46	-120.79	52.00	-157.93	51.09	-154.65	-12.54	37.14	-11.64	33.86
7	5.73	-2.33	2.55	-1.04	2.00	-0.82	3.18	-1.29	3.73	-1.51
8	166.41	-66.17	299.34	-123.61	277.00	-113.47	-132.93	57.45	-110.59	47.30
9	151.09	-209.28	230.02	-225.77	203.80	-151.58	-78.93	16.49	-52.72	-57.70
10	48.59	-25.97	77.85	-39.77	68.97	-33.96	-29.26	13.80	-20.39	8.00
11	54.71	-23.63	79.42	-34.12	65.52	-28.28	-24.72	10.49	-10.82	4.65
12	4.15	-3.67	13.65	-15.40	10.95	-12.61	-9.50	11.72	-6.79	8.94
13	6.60	-20.02	9.05	-27.68	7.18	-21.44	-2.45	7.66	-0.58	1.43
14	25.31	-14.57	36.91	-18.02	30.82	-16.48	-11.60	3.45	-5.51	1.91
15	58.67	-36.61	87.85	-54.30	74.54	-48.41	-29.18	17.69	-15.87	11.80
16	14.50	-12.23	44.87	-27.17	35.87	-21.54	-30.37	14.94	-21.38	9.31
17	73.74	-175.11	105.59	-254.48	88.39	-213.44	-31.85	79.37	-14.65	38.33
18	97.91	-37.51	153.11	-58.43	113.34	-43.64	-55.20	20.92	-15.43	6.13
19	100.78	-184.85	150.70	-235.21	139.48	-219.16	-49.92	50.36	-38.70	34.32
20	0.60	-0.27	0.62	-0.14	0.60	-0.17	-0.02	-0.12	0.00	-0.09
21	459.14	-140.20	597.82	-183.09	422.30	-129.45	-138.67	42.89	36.84	-10.75
22	39.24	-101.47	64.20	-242.79	85.04	-305.43	-24.96	141.32	-45.80	203.96
23	122.01	-402.31	181.90	-596.94	157.14	-516.59	-59.89	194.63	-35.13	114.28
24	147.68	-446.27	206.56	-625.26	176.33	-534.08	-58.88	178.99	-28.65	87.81
25	286.50	-292.73	275.43	-296.14	139.63	-165.95	11.07	3.41	146.86	-126.78
26	654.20	-267.31	689.91	-278.49	403.08	-159.54	-35.71	11.18	251.12	-107.77
27	239.17	-489.67	231.96	-471.72	119.17	-239.52	7.21	-17.95	120.00	-250.15
28	469.36	-91.82	552.10	-117.22	371.65	-100.98	-82.74	25.40	97.71	9.15
29	31.43	-90.58	43.92	-127.41	34.91	-102.04	-12.50	36.82	-3.48	11.46
30	25.41	-51.45	33.39	-76.27	23.72	-57.91	-7.97	24.82	1.69	6.46
31	25.63	-79.02	46.44	-159.98	49.39	-168.91	-20.81	80.95	-23.76	89.88
32	186.76	-661.68	186.50	-659.58	103.17	-360.16	0.26	-2.09	83.59	-301.52
33	42.15	-87.58	55.91	-139.63	45.98	-131.10	-13.76	52.05	-3.83	43.52
34	5.42	-12.57	39.98	-38.62	40.71	-37.70	-34.57	26.04	-35.30	25.13
35	404.80	-122.44	388.21	-111.84	214.15	-58.44	16.59	-10.60	190.65	-64.00
36	134.90	-13.45	116.65	4.16	74.88	-45.32	18.25	-17.61	60.02	31.87
37	17.78	-18.32	25.34	-61.97	23.68	-63.00	-7.55	43.65	-5.90	44.68
38	9.52	-21.72	12.50	-19.08	8.13	-11.62	-2.98	-2.65	1.39	-10.10
39	11.72	-35.26	13.85	-37.22	11.40	-30.15	-2.13	1.96	0.33	-5.11
40	8.68	-12.19	14.69	-20.16	12.73	-17.61	-6.01	7.97	-4.05	5.42
41	56.00	-23.20	66.00	-28.36	58.23	-25.87	-10.00	5.17	-2.23	2.67
42	6.85	-11.47	8.22	-15.20	7.63	-14.37	-1.37	3.73	-0.77	2.89
43	13.49	-29.08	18.26	-49.12	18.43	-50.66	-4.77	20.04	-4.93	21.57
44	51.00	-8.70	60.57	-9.55	55.67	-8.25	-9.57	0.85	-4.67	-0.45
45	31.97	-7.99	40.05	-9.85	33.09	-8.15	-8.08	1.85	-1.11	0.16
46	6.70	-3.63	8.77	-3.23	2.40	-5.24	-2.07	-0.40	4.31	1.61
47	166.20	-43.97	223.80	-82.33	171.88	-71.14	-57.60	38.36	-5.68	27.17
48	5.56	-14.42	13.15	-33.28	10.65	-26.47	-7.59	18.85	-5.09	12.04
49	208.75	-67.25	199.08	-64.36	84.52	-27.93	9.67	-2.90	124.23	-39.33
50	307.39	-109.12	384.42	-137.40	253.45	-91.38	-77.03	28.28	53.94	-17.74
51	59.01	-143.90	102.15	-242.80	92.00	-217.89	-43.14	98.90	-32.99	73.98
52	191.13	-72.15	264.94	-99.66	221.73	-83.22	-73.81	27.52	-30.60	11.07
53	273.08	-460.25	247.35	-393.73	111.10	-158.02	25.73	-66.52	161.98	-302.23
54	454.95	-222.74	386.39	-219.42	138.37	-112.22	68.55	-3.32	316.58	-110.52
55	116.46	-206.04	95.57	-198.41	54.11	-103.67	20.89	-7.64	62.35	-102.37
56	94.76	-36.32	86.78	-30.12	14.30	-8.25	7.98	-6.20	80.46	-28.07
57	25.40	-82.87	36.95	-118.48	29.53	-93.96	-11.54	35.61	-4.12	11.09
58	43.81	-102.92	63.42	-154.31	51.10	-130.76	-19.61	51.39	-7.29	27.84
59	125.16	-40.85	151.97	-50.07	96.66	-31.95	-26.81	9.22	28.50	-8.90
60	129.00	-386.82	123.04	-362.90	55.51	-165.17	5.96	-23.92	73.49	-221.65
61	137.08	-52.73	184.11	-81.36	132.50	-48.09	-47.03	28.63	4.58	-4.64
62	2.44	-6.15	18.27	-42.26	17.86	-41.36	-15.83	36.11	-15.42	35.21
63	308.44	-170.71	300.39	-164.65	167.97	-96.16	8.05	-6.05	140.47	-74.54
64	287.04	-116.32	283.42	-112.22	144.35	-58.66	3.63	-4.11	142.70	-57.67
65	157.91	-232.07	259.88	-385.12	222.84	-333.01	-101.96	153.05	-64.92	100.94
66	378.86	-381.79	490.37	-485.58	377.96	-366.93	-111.51	103.79	0.89	-14.86
67	60.25	-186.83	77.35	-275.36	66.53	-235.68	-17.10	88.53	-6.29	48.85
68	73.98	-201.72	110.45	-298.83	95.90	-261.99	-36.47	97.11	-21.92	60.26
69	163.40	-86.20	164.56	-68.27	113.38	-31.93	-1.17	-17.94	50.02	-54.28
70	91.52	-68.62	129.29	-97.13	104.92	-84.58	-37.77	28.50	-13.40	15.95

Table D.14. Maximum ($\epsilon 1$) and minimum ($\epsilon 3$) principal strain values at the location of 70 landmarks during third molar (M3) bite load for the varying muscle force load cases sensitivity tests (see text for more details), and strain differences ($\Delta \epsilon 1$ and $\Delta \epsilon 3$) at landmark locations between models. Strain values are in microstrain (μ strain).

M3 bite landmark	ACSA		Load Case 1		Load Case 2		ACSA-LoadCase1		ACSA-LoadCase2	
	$\epsilon 1$	$\epsilon 3$	$\epsilon 1$	$\epsilon 3$	$\epsilon 1$	$\epsilon 3$	$\Delta \epsilon 1$	$\Delta \epsilon 3$	$\Delta \epsilon 1$	$\Delta \epsilon 3$
1	11.68	-11.03	23.16	-20.69	19.14	-17.39	-11.48	9.66	-7.46	6.35
2	35.16	-30.62	72.98	-59.89	58.95	-51.10	-37.82	29.27	-23.79	20.47
3	43.75	-19.27	71.29	-30.53	65.50	-27.32	-27.53	11.26	-21.74	8.05
4	39.85	-91.84	67.08	-174.72	57.59	-153.24	-27.23	82.88	-17.74	61.40
5	47.12	-16.06	85.39	-29.54	68.68	-24.01	-38.27	13.48	-21.56	7.94
6	42.49	-130.32	56.54	-172.16	54.92	-166.65	-14.05	41.84	-12.43	36.33
7	7.70	-3.13	5.01	-2.05	4.07	-1.67	2.70	-1.08	3.63	-1.46
8	152.90	-74.63	285.90	-133.20	263.00	-118.44	-133.01	58.57	-110.10	43.82
9	58.65	-115.08	97.26	-89.15	90.81	-35.52	-38.61	-25.93	-32.16	-79.56
10	59.70	-31.02	93.27	-46.65	82.03	-39.84	-33.57	15.63	-22.33	8.82
11	16.56	-7.27	31.34	-13.42	24.74	-10.72	-14.78	6.15	-8.19	3.45
12	9.89	-5.43	29.02	-23.31	23.67	-18.98	-19.13	17.88	-13.78	13.55
13	2.06	-5.84	3.18	-6.12	4.17	-5.55	-1.12	0.28	-2.11	-0.28
14	17.18	-10.76	31.19	-22.03	25.15	-19.23	-14.02	11.28	-7.97	8.47
15	20.86	-17.22	26.79	-23.53	22.28	-21.43	-5.93	6.31	-1.42	4.21
16	29.74	-9.82	46.35	-16.17	39.12	-12.79	-16.61	6.36	-9.38	2.98
17	17.59	-21.43	22.17	-25.91	20.14	-25.20	-4.58	4.48	-2.55	3.76
18	109.64	-157.89	193.84	-486.20	169.24	-425.61	-84.21	328.31	-49.61	267.72
19	126.07	-215.64	165.77	-288.40	151.91	-263.89	-39.70	72.76	-25.84	48.25
20	0.70	-0.44	0.65	-0.25	0.67	-0.23	0.05	-0.19	0.03	-0.20
21	545.72	-167.93	714.96	-219.83	521.24	-160.43	-169.24	51.91	24.48	-7.50
22	45.66	-170.57	101.91	-382.22	121.35	-427.72	-56.24	211.65	-75.69	257.16
23	118.73	-395.60	174.46	-578.10	150.84	-500.59	-55.73	182.49	-32.12	104.98
24	75.16	-221.31	103.15	-304.01	89.36	-263.87	-27.99	82.70	-14.19	42.56
25	284.74	-287.28	271.37	-288.47	136.65	-160.13	13.38	1.19	148.09	-127.15
26	710.93	-288.56	783.92	-313.61	482.86	-189.61	-73.00	25.05	228.07	-98.95
27	244.29	-511.53	240.04	-505.56	125.50	-267.47	4.25	-5.97	118.79	-244.06
28	542.86	-115.59	680.25	-166.74	483.33	-148.79	-137.40	51.14	59.53	33.20
29	29.42	-84.66	39.48	-115.09	31.17	-91.73	-10.06	30.43	-1.75	7.07
30	24.15	-31.88	27.17	-42.54	17.71	-28.69	-3.02	10.65	6.43	-3.19
31	38.89	-114.16	68.32	-218.04	67.73	-217.80	-29.43	103.88	-28.84	103.64
32	190.02	-673.49	191.84	-677.83	107.70	-375.49	-1.82	4.34	82.32	-298.00
33	53.91	-137.63	81.85	-229.50	71.13	-210.22	-27.94	91.86	-17.22	72.58
34	5.77	-10.54	27.04	-31.45	29.25	-31.09	-21.27	20.91	-23.48	20.55
35	408.88	-123.67	394.67	-113.18	218.52	-58.21	14.21	-10.49	190.36	-65.45
36	130.86	2.98	123.30	-31.08	99.80	-76.42	7.56	34.06	31.07	79.40
37	25.63	-13.70	22.62	-42.84	20.40	-46.05	3.00	29.14	5.23	32.35
38	11.33	-32.97	12.67	-32.34	8.45	-22.95	-1.34	-0.63	2.88	-10.02
39	14.14	-8.60	30.00	-13.44	26.41	-11.43	-15.85	4.83	-12.27	2.83
40	4.28	-17.33	6.95	-29.36	6.20	-25.47	-2.68	12.03	-1.93	8.13
41	10.75	-8.91	7.19	-13.82	7.82	-13.05	3.56	4.91	2.93	4.14
42	3.88	-7.82	6.88	-14.85	6.62	-13.61	-3.00	7.04	-2.74	5.79
43	5.83	-22.11	11.61	-44.64	11.46	-46.17	-5.78	22.53	-5.62	24.06
44	6.53	-19.92	12.78	-43.98	11.99	-35.77	-6.25	24.06	-5.46	15.85
45	8.79	-3.39	10.52	-9.66	9.00	-9.47	-1.72	6.27	-0.21	6.08
46	6.74	-3.75	5.50	-3.17	3.32	-8.65	1.50	-0.58	3.42	4.90
47	162.99	-46.34	219.48	-91.47	171.85	-84.34	-56.50	45.13	-8.86	38.00
48	5.37	-13.96	12.92	-32.93	10.44	-26.15	-7.55	18.97	-5.07	12.19
49	163.65	-53.30	141.99	-46.03	37.01	-13.08	21.65	-7.27	126.63	-40.22
50	309.54	-110.85	383.64	-138.55	254.25	-92.58	-74.10	27.70	55.29	-18.27
51	50.78	-53.18	86.61	-110.61	76.55	-104.13	-35.83	57.43	-25.77	50.95
52	104.32	-37.73	136.85	-49.90	111.39	-40.82	-32.53	12.17	-7.07	3.09
53	280.32	-485.70	259.05	-434.33	119.99	-187.18	21.27	-51.37	160.33	-298.52
54	474.93	-223.54	414.26	-218.34	157.12	-107.14	60.67	-5.21	317.81	-116.41
55	121.57	-207.84	100.80	-193.98	43.25	-96.04	20.77	-13.86	78.31	-111.80
56	84.98	-33.34	75.28	-29.85	6.87	-8.74	9.70	-3.49	78.10	-24.60
57	19.66	-63.84	28.70	-91.20	22.67	-71.07	-9.05	27.36	-3.01	7.23
58	39.27	-96.79	57.52	-146.32	47.42	-125.55	-18.25	49.53	-8.15	28.77
59	150.10	-48.84	184.40	-60.38	123.73	-40.59	-34.30	11.54	26.37	-8.25
60	125.03	-372.07	116.99	-340.91	50.39	-146.26	8.04	-31.16	74.64	-225.81
61	135.15	-51.58	179.82	-78.79	129.10	-46.22	-44.67	27.21	6.05	-5.36
62	2.27	-4.38	14.38	-33.15	14.58	-33.68	-12.12	28.77	-12.32	29.30
63	295.52	-164.79	281.02	-155.81	152.43	-89.25	14.50	-8.98	143.09	-75.54
64	285.65	-113.88	281.01	-108.06	142.39	-55.51	4.64	-5.82	143.26	-58.38
65	188.12	-70.84	312.50	-155.32	266.10	-138.24	-124.38	84.48	-77.98	67.40
66	417.75	-453.07	565.35	-611.11	440.53	-472.13	-147.60	158.04	-22.78	19.06
67	28.80	-100.55	44.48	-148.24	40.29	-127.11	-15.68	47.69	-11.49	26.56
68	59.37	-144.47	93.75	-223.03	81.77	-197.08	-34.38	78.56	-22.40	52.61
69	162.43	-96.74	162.62	-82.50	106.52	-36.42	-0.19	-14.24	55.91	-60.33
70	76.10	-32.37	109.32	-43.10	88.13	-38.37	-33.22	10.73	-12.03	6.01

Appendix E. Strain values from Chapter 7

Strain values as output from FEAs performed in Chapter 7 are here presented in table form. Maximum (ϵ_1) and minimum (ϵ_3) principal strain values at the location of 70 landmarks are displayed in microstrain (μstrain). Each table represents a simulated bite with one tooth along the dental row, from first incisor (I1) to third molar (M3), to the exception of the canine tooth. Also displayed are strain differences ($\Delta\epsilon_1$ and $\Delta\epsilon_3$) at landmark locations between models for each analysis (see Chapter 7 for details). The placing of these strain tables in an appendix rather than in the chapter proper is due to the vastness of space they require, which is easier to manage here.

Table E.1. Maximum ($\epsilon 1$) and minimum ($\epsilon 3$) principal strain values at the location of 70 landmarks during first incisor (I1) bite load for the 3 models of durophagous species, and strain differences ($\Delta\epsilon 1$ and $\Delta\epsilon 3$) at landmark locations between models. Strain values are in microstrain (μ strain).

I1 bite landmark	Cerrocoebus		Lophoebus		Mandrillus		Cerrocoebus-Lophoebus		Cerrocoebus-Mandrillus		Lophoebus-Mandrillus	
	$\epsilon 1$	$\epsilon 3$	$\epsilon 1$	$\epsilon 3$	$\epsilon 1$	$\epsilon 3$	$\Delta\epsilon 1$	$\Delta\epsilon 3$	$\Delta\epsilon 1$	$\Delta\epsilon 3$	$\Delta\epsilon 1$	$\Delta\epsilon 3$
1	511.69	-672.17	194.02	-321.04	153.22	-234.08	317.67	-351.13	358.47	-438.10	40.80	-86.96
2	628.19	-376.16	400.12	-102.73	149.43	-111.74	228.07	-273.43	478.76	-264.42	250.69	9.01
3	980.40	-272.94	44.30	-21.16	32.70	-17.70	936.10	-251.78	947.70	-255.24	11.60	-3.46
4	151.60	-399.15	42.26	-123.09	97.98	-325.00	109.34	-276.06	53.63	-74.15	-55.72	201.91
5	22.71	-43.94	17.63	-15.99	30.52	-11.55	5.08	-27.95	-7.81	-32.39	-12.89	-4.44
6	49.58	-17.26	32.93	-42.79	19.07	-47.52	16.66	25.53	30.52	30.26	13.86	4.73
7	2.15	-1.05	22.10	-8.11	5.39	-20.08	-19.96	7.07	-3.24	19.04	16.71	11.97
8	59.50	-46.18	56.39	-11.01	260.36	-47.64	3.11	-35.17	-200.86	1.45	-203.97	36.62
9	158.86	-249.21	72.62	-164.71	53.42	-154.11	86.23	-84.50	105.43	-95.10	19.20	-10.60
10	61.43	-27.62	24.52	-10.21	103.78	-32.04	36.90	-17.42	-42.36	4.42	-79.26	21.84
11	178.19	-629.68	117.99	-360.20	53.67	-194.11	60.20	-269.48	124.53	-435.58	64.33	-166.09
12	307.09	-162.59	254.66	-112.75	123.68	-41.57	52.43	-49.84	183.41	-121.02	130.98	-71.18
13	275.53	-83.70	90.42	-32.02	114.02	-33.10	185.10	-51.68	161.51	-50.60	-23.59	1.07
14	134.68	-48.31	70.04	-39.87	137.14	-44.26	64.64	-8.44	-2.46	-4.05	-67.10	4.39
15	222.70	-79.11	43.04	-29.32	46.49	-25.53	179.67	-49.79	176.22	-53.58	-3.45	-3.79
16	68.05	-23.21	77.68	-22.36	54.57	-14.11	-9.63	-0.85	13.49	-9.10	23.12	-8.25
17	43.65	-19.81	30.92	-19.07	36.02	-9.75	12.73	-0.74	7.63	-10.06	-5.09	-9.32
18	154.64	-44.07	84.12	-34.13	186.63	-55.96	70.52	-9.94	-31.99	11.89	-102.51	21.83
19	147.25	-64.01	46.14	-37.74	94.34	-36.34	101.11	-26.27	52.91	-27.67	-48.20	-1.41
20	87.70	-72.09	70.55	-150.10	25.34	-78.68	17.15	78.00	62.36	6.58	45.21	-71.42
21	434.19	-145.77	111.60	-39.09	171.35	-57.47	322.59	-106.67	262.84	-88.30	-59.75	18.38
22	121.87	-84.47	25.73	-27.81	71.97	-205.36	96.13	-56.66	49.90	120.89	-46.23	177.55
23	97.39	-342.43	37.04	-155.24	65.55	-201.23	60.35	-187.19	31.83	-141.20	-28.51	45.98
24	268.26	-336.33	115.71	-175.02	186.25	-85.07	152.55	-161.30	82.01	-251.26	-70.54	-89.96
25	64.20	-32.69	90.78	-314.63	190.83	-297.63	-26.58	281.94	-126.63	264.93	-100.05	-17.01
26	931.55	-272.48	675.29	-221.62	566.62	-282.49	256.26	-50.87	364.93	10.01	108.67	60.88
27	235.65	-426.34	188.77	-241.59	305.64	-335.19	46.88	-184.75	-69.99	-91.15	-116.87	93.60
28	193.54	-65.28	180.06	-86.86	50.45	-153.96	13.48	21.57	143.08	88.68	129.60	67.10
29	43.04	-93.35	17.93	-47.28	12.20	-9.79	25.11	-46.07	30.84	-83.56	5.73	-37.49
30	29.75	-68.35	24.12	-55.26	93.35	-28.12	5.63	-13.10	-63.59	-40.23	-69.23	-27.13
31	113.49	-55.90	30.69	-11.53	19.50	-70.86	82.81	-44.37	93.99	14.96	11.19	59.33
32	124.63	-365.61	100.19	-291.29	134.64	-363.62	24.44	-74.31	-10.01	-1.99	-34.45	72.33
33	380.03	-134.90	187.51	-69.80	204.15	-76.20	192.52	-65.10	175.88	-58.70	-16.64	6.39
34	9.47	-25.92	12.36	-18.51	3.25	-7.35	-2.88	-7.41	6.23	-18.57	9.11	-11.16
35	192.17	-197.38	247.37	-54.89	318.58	-73.48	-55.20	-142.49	-126.41	-123.90	-71.21	18.58
36	291.88	-611.14	163.44	-467.56	187.69	-403.02	128.43	-143.58	104.18	-208.12	-24.25	-64.53
37	1.79	-1.03	46.76	-13.16	12.15	-3.65	-44.97	12.13	-10.36	2.63	34.62	-9.51
38	15.03	-11.97	3.76	-12.25	73.16	-20.28	11.27	0.28	-58.13	8.31	-69.40	8.03
39	170.42	-501.43	112.62	-428.58	43.83	-146.33	57.80	-72.85	126.59	-355.10	68.79	-282.25
40	578.06	-181.77	247.66	-75.63	104.15	-39.35	330.40	-106.14	473.91	-142.42	143.51	-36.28
41	275.97	-128.02	57.87	-25.55	206.57	-40.95	218.10	-102.46	69.40	-87.07	-148.70	15.39
42	194.16	-63.31	64.46	-27.59	245.64	-52.40	129.70	-35.72	-51.47	-10.91	-181.18	24.81
43	171.66	-55.58	84.68	-29.66	97.93	-24.70	86.98	-25.92	73.73	-30.88	-13.25	-4.97
44	123.32	-30.65	59.61	-23.66	51.03	-13.13	63.71	-6.99	72.29	-17.53	8.57	-10.53
45	49.89	-41.71	50.46	-30.85	33.18	-6.25	-0.58	-10.86	16.71	-35.46	17.29	-24.60
46	98.13	-58.39	141.33	-41.50	90.71	-28.29	-43.21	-16.89	7.42	-30.10	50.62	-13.21
47	122.90	-114.71	76.60	-27.03	73.94	-29.83	46.30	-87.69	48.96	-84.89	2.66	2.80
48	68.09	-171.89	51.80	-166.13	24.69	-79.80	16.30	-5.77	43.40	-92.10	27.11	-86.33
49	393.05	-125.02	305.31	-63.27	130.23	-38.69	87.75	-61.75	262.82	-86.33	175.08	-24.58
50	124.36	-93.91	33.10	-24.44	30.17	-99.22	91.26	-69.47	94.19	5.31	2.93	74.78
51	102.75	-349.71	49.63	-159.39	80.15	-286.78	53.12	-190.32	22.60	-62.93	-30.52	127.39
52	1203.18	-286.31	95.97	-54.30	222.05	-67.92	1107.22	-232.01	981.14	-218.39	-126.08	13.62
53	108.02	-70.59	163.85	-753.68	36.03	-32.58	-55.83	683.09	72.00	-38.02	127.82	-721.10
54	815.71	-357.81	605.77	-161.76	1070.75	-249.36	209.94	-196.05	-255.04	-108.45	-464.98	87.60
55	225.86	-520.69	144.84	-442.61	231.17	-417.13	81.02	-78.08	-5.31	-103.56	-86.33	-25.48
56	87.20	-120.58	164.39	-159.97	33.80	-80.64	-77.19	39.39	53.40	-39.93	130.60	-79.33
57	58.60	-137.25	23.15	-52.33	18.00	-17.61	35.45	-84.92	40.60	-119.63	5.15	-34.71
58	43.15	-66.56	17.11	-42.32	32.05	-13.72	26.04	-24.24	11.11	-52.84	-14.93	-28.60
59	121.87	-46.01	60.42	-16.62	12.00	-25.45	61.45	-29.39	109.87	-20.56	48.42	8.83
60	172.82	-522.74	105.64	-312.28	106.64	-357.58	67.19	-210.46	66.19	-165.16	-1.00	45.31
61	494.29	-158.98	208.24	-76.41	103.42	-48.81	286.05	-82.56	390.87	-110.17	104.82	-27.60
62	8.01	-21.52	13.07	-15.50	0.92	-0.91	-5.07	-6.02	7.09	-20.61	12.16	-14.59
63	681.47	-227.83	313.90	-102.83	103.65	-24.90	367.57	-125.00	577.82	-202.93	210.25	-77.93
64	352.98	-862.32	168.82	-526.73	123.78	-241.91	184.17	-335.59	229.20	-620.41	45.04	-284.81
65	94.21	-171.60	93.00	-115.49	14.07	-34.20	1.21	-56.11	80.14	-137.40	78.93	-81.29
66	314.26	-163.75	137.97	-64.55	353.47	-174.31	176.29	-99.20	-39.21	10.56	-215.50	109.76
67	35.05	-66.91	9.65	-19.28	19.17	-12.10	25.40	-47.63	15.87	-54.80	-9.53	-7.17
68	129.36	-120.16	137.27	-185.82	11.80	-25.71	-7.91	65.66	117.56	-94.45	125.47	-160.11
69	446.75	-201.70	208.10	-101.26	260.95	-92.71	238.64	-100.44	185.80	-108.99	-52.85	-8.55
70	26.13	-59.38	31.24	-25.25	10.79	-5.22	-5.11	-34.12	15.34	-54.16	20.45	-20.04

Table E.2. Maximum ($\epsilon 1$) and minimum ($\epsilon 3$) principal strain values at the location of 70 landmarks during second incisor (I2) bite load for the 3 models of durophagous species, and strain differences ($\Delta\epsilon 1$ and $\Delta\epsilon 3$) at landmark locations between models. Strain values are in microstrain (μstrain).

I2 bite landmark	Cerrocebus		Lophocebus		Mandrillus		Cerrocebus-Lophocebus		Cerrocebus-Mandrillus		Lophocebus-Mandrillus	
	$\epsilon 1$	$\epsilon 3$	$\epsilon 1$	$\epsilon 3$	$\epsilon 1$	$\epsilon 3$	$\Delta\epsilon 1$	$\Delta\epsilon 3$	$\Delta\epsilon 1$	$\Delta\epsilon 3$	$\Delta\epsilon 1$	$\Delta\epsilon 3$
1	192.44	-348.01	177.61	-266.08	83.87	-139.61	14.83	-81.93	108.57	-208.40	93.74	-126.47
2	561.70	-327.76	335.74	-129.86	177.98	-169.11	225.96	-197.90	383.72	-158.66	157.76	39.25
3	889.70	-245.11	46.74	-21.96	31.52	-17.11	842.96	-223.14	858.18	-228.00	15.22	-4.85
4	149.96	-398.13	45.16	-125.84	97.11	-322.73	104.80	-272.28	52.85	-75.39	-51.94	196.89
5	21.63	-42.32	18.23	-15.98	31.55	-11.63	3.40	-26.33	-9.92	-30.69	-13.32	-4.35
6	47.99	-19.03	33.22	-42.88	19.18	-47.83	14.78	23.85	28.82	28.80	14.04	4.95
7	1.66	-0.81	22.29	-8.18	5.40	-20.08	-20.63	7.37	-3.74	19.27	16.90	11.90
8	52.14	-44.88	57.94	-11.10	261.20	-47.60	-5.80	-33.78	-209.06	2.72	-203.26	36.50
9	166.13	-256.02	77.24	-164.83	54.32	-161.33	88.89	-91.19	111.81	-94.69	22.92	-3.50
10	80.53	-30.02	43.50	-17.15	105.93	-32.17	37.02	-12.87	-25.40	2.15	-62.42	15.02
11	181.46	-640.56	119.40	-382.53	57.32	-200.83	62.06	-258.03	124.14	-439.72	62.08	-181.70
12	483.26	-369.87	340.44	-219.10	137.31	-62.83	142.81	-150.77	345.95	-307.04	203.14	-156.27
13	365.72	-109.36	127.37	-56.42	138.44	-39.70	238.35	-52.94	227.28	-69.66	-11.07	-16.72
14	171.06	-60.09	88.89	-44.78	147.04	-48.72	82.17	-15.32	24.02	-11.37	-58.15	3.94
15	237.59	-88.69	39.24	-21.66	50.12	-29.67	198.35	-67.03	187.46	-59.02	-10.89	8.01
16	48.04	-16.80	58.47	-16.63	52.57	-13.32	-10.43	-0.17	-4.53	-3.48	5.90	-3.32
17	33.85	-14.92	32.58	-19.15	37.71	-10.18	1.27	4.23	-3.86	-4.73	-5.14	-8.97
18	194.63	-46.29	98.58	-40.74	197.13	-59.42	96.05	-5.56	-2.50	13.13	-98.55	18.68
19	109.40	-45.70	28.95	-29.08	82.90	-27.85	80.45	-16.62	26.50	-17.85	-53.95	-1.23
20	82.10	-66.63	69.51	-144.04	23.25	-72.25	12.59	77.41	58.85	5.62	46.26	-71.79
21	463.14	-155.28	120.23	-41.72	190.69	-64.12	342.91	-113.56	272.45	-91.16	-70.46	22.40
22	74.72	-89.70	18.30	-49.07	79.48	-224.29	56.42	-40.63	-4.75	134.59	-61.17	175.22
23	105.33	-365.46	35.74	-163.72	64.83	-195.35	69.59	-201.74	40.50	-170.10	-29.09	31.63
24	251.66	-373.83	100.90	-188.19	157.60	-82.65	150.76	-185.64	94.06	-291.19	-56.70	-105.55
25	61.55	-36.01	93.93	-318.69	192.04	-314.02	-32.38	282.69	-130.49	278.01	-98.11	-4.68
26	945.72	-277.22	676.64	-222.12	580.20	-281.16	269.08	-55.10	365.52	3.94	96.44	59.04
27	225.75	-426.33	182.63	-237.00	306.95	-340.40	43.12	-189.33	-81.20	-85.94	-124.32	103.40
28	212.14	-67.56	189.39	-94.00	52.80	-164.34	22.75	26.44	159.35	96.79	136.60	70.35
29	41.12	-87.41	19.19	-50.59	11.55	-8.75	21.94	-36.82	29.57	-78.66	7.63	-41.84
30	25.17	-49.49	18.58	-42.41	94.10	-28.40	6.59	-7.08	-68.93	-21.09	-75.52	-14.01
31	93.68	-55.95	13.15	-7.24	30.90	-106.54	80.54	-48.70	62.79	50.60	-17.75	99.30
32	114.44	-340.64	97.15	-282.59	135.62	-366.35	17.29	-58.06	-21.18	25.70	-38.47	83.76
33	349.74	-129.48	173.71	-67.95	193.35	-73.03	176.03	-61.53	156.39	-56.45	-19.63	5.08
34	8.03	-22.67	11.37	-17.26	2.98	-6.72	-3.34	-5.41	5.06	-15.94	8.40	-10.53
35	194.79	-210.87	240.87	-54.02	317.60	-72.79	-46.09	-156.85	-122.82	-138.08	-76.73	18.77
36	281.26	-577.87	158.17	-445.68	183.41	-392.80	123.09	-132.19	97.84	-185.07	-25.25	-52.88
37	2.15	-1.44	47.67	-13.49	12.34	-3.75	-45.52	12.05	-10.19	2.31	35.32	-9.74
38	9.59	-16.95	7.42	-24.52	70.23	-19.78	2.17	7.57	-60.64	2.83	-62.81	-4.74
39	122.20	-354.75	87.00	-328.03	33.83	-112.57	35.20	-26.72	88.37	-242.18	53.17	-215.46
40	377.49	-111.89	185.48	-56.88	74.34	-30.93	192.01	-55.00	303.16	-80.96	111.14	-25.96
41	166.88	-89.25	41.52	-23.64	162.70	-32.72	125.35	-65.61	4.18	-56.53	-121.18	9.08
42	146.86	-66.12	50.22	-25.66	214.60	-45.81	96.64	-40.46	-67.74	-20.31	-164.38	20.15
43	134.34	-42.86	76.57	-30.47	88.36	-21.63	57.77	-12.40	45.98	-21.23	-11.79	-8.83
44	108.25	-26.94	51.10	-21.64	47.70	-12.34	57.15	-5.30	60.55	-14.61	3.40	-9.30
45	37.26	-32.79	38.72	-24.91	29.83	-5.62	-1.46	-7.88	7.43	-27.17	8.88	-19.28
46	73.67	-50.37	112.51	-32.59	80.60	-25.00	-38.84	-17.78	-6.93	-25.37	31.91	-7.59
47	150.38	-112.54	96.56	-32.14	74.32	-36.42	53.82	-80.40	76.06	-76.11	22.24	4.28
48	68.80	-176.67	52.60	-171.65	25.54	-84.39	16.20	-5.02	43.26	-92.28	27.05	-87.25
49	353.31	-112.19	271.97	-56.80	96.16	-29.61	81.34	-55.39	257.15	-82.58	175.81	-27.19
50	172.57	-85.65	58.89	-24.87	26.91	-81.18	113.68	-60.79	145.65	-4.47	31.98	56.31
51	98.28	-314.94	48.10	-138.52	85.12	-292.71	50.17	-176.42	13.16	-22.23	-37.01	154.19
52	1259.53	-281.32	105.71	-56.38	230.44	-69.55	1153.81	-224.94	1029.09	-211.77	-124.73	13.17
53	107.46	-66.98	153.07	-705.73	45.02	-27.06	-45.62	638.74	62.44	-39.93	108.06	-678.67
54	801.35	-354.05	600.87	-160.96	1062.90	-254.86	200.47	-193.10	-261.55	-99.19	-462.03	93.91
55	220.46	-505.30	144.34	-445.07	229.91	-406.71	76.11	-60.22	-9.45	-98.58	-85.56	-38.36
56	79.00	-96.92	141.62	-127.65	33.68	-73.78	-62.62	30.73	45.32	-23.14	107.94	-53.87
57	57.24	-135.92	20.78	-47.00	19.42	-19.14	36.46	-88.92	37.82	-116.78	1.37	-27.86
58	45.08	-76.07	20.04	-51.00	30.22	-13.14	25.04	-25.07	14.86	-62.93	-10.18	-37.86
59	139.49	-53.46	78.60	-21.90	11.37	-16.95	60.88	-31.56	128.12	-36.51	67.24	-4.95
60	177.48	-537.28	107.84	-318.77	105.78	-354.50	69.65	-218.51	71.70	-182.78	2.06	35.73
61	509.64	-163.26	221.10	-79.62	110.94	-49.27	288.54	-83.64	398.71	-114.00	110.17	-30.36
62	8.23	-22.21	13.70	-16.33	0.97	-0.93	-5.47	-5.87	7.26	-21.28	12.73	-15.40
63	688.99	-230.35	318.12	-103.96	103.73	-24.84	370.86	-126.40	585.25	-205.51	214.39	-79.11
64	361.94	-885.14	173.59	-546.05	126.92	-251.25	188.34	-339.09	235.02	-633.90	46.67	-294.81
65	70.65	-184.75	77.31	-107.71	13.90	-32.98	-6.65	-77.04	56.75	-151.77	63.40	-74.73
66	313.41	-161.65	136.75	-65.63	378.00	-192.60	176.66	-96.02	-64.59	30.95	-241.26	126.97
67	50.51	-111.26	21.23	-46.70	26.78	-11.60	29.28	-64.55	23.73	-99.65	-5.55	-35.10
68	155.95	-111.43	148.83	-161.38	11.35	-23.67	7.12	49.95	144.60	-87.76	137.48	-137.71
69	433.24	-200.85	209.02	-99.75	247.35	-84.97	224.22	-101.09	185.89	-115.87	-38.33	-14.78
70	61.60	-60.31	50.63	-26.86	9.60	-4.64	10.97	-33.45	51.99	-55.67	41.02	-22.22

Table E.3. Maximum ($\epsilon 1$) and minimum ($\epsilon 3$) principal strain values at the location of 70 landmarks during first premolar (P3) bite load for the 3 models of durophagous species, and strain differences ($\Delta \epsilon 1$ and $\Delta \epsilon 3$) at landmark locations between models. Strain values are in microstrain (μ strain).

P3 bite landmark	Cercopithecus		Lophocebus		Mandrillus		Cercopithecus-Lophocebus		Cercopithecus-Mandrillus		Lophocebus-Mandrillus	
	$\epsilon 1$	$\epsilon 3$	$\epsilon 1$	$\epsilon 3$	$\epsilon 1$	$\epsilon 3$	$\Delta \epsilon 1$	$\Delta \epsilon 3$	$\Delta \epsilon 1$	$\Delta \epsilon 3$	$\Delta \epsilon 1$	$\Delta \epsilon 3$
1	6.17	-7.74	14.59	-13.57	4.51	-5.68	-8.42	5.83	1.66	-2.06	10.08	-7.89
2	141.43	-32.20	40.30	-12.37	16.72	-8.68	101.13	-19.83	124.72	-23.52	23.59	-3.69
3	563.54	-154.45	36.16	-17.30	15.46	-9.10	527.39	-137.16	548.09	-145.35	20.70	-8.19
4	129.72	-353.13	47.42	-117.17	83.51	-286.35	82.31	-235.96	46.21	-66.78	-36.09	169.19
5	15.08	-33.89	19.98	-13.52	39.87	-12.99	-4.90	-20.37	-24.78	-20.90	-19.88	-0.53
6	48.53	-25.93	34.12	-43.00	19.82	-49.63	14.41	17.07	28.71	23.70	14.30	6.64
7	0.41	-0.48	24.39	-8.91	5.38	-20.04	-23.98	8.43	-4.97	19.57	19.01	11.14
8	50.23	-36.12	57.53	-10.85	246.15	-45.15	-7.30	-25.26	-195.92	9.04	-188.61	34.30
9	167.44	-241.04	85.18	-137.63	52.21	-158.34	82.27	-103.41	115.24	-82.70	32.97	20.71
10	117.24	-44.24	81.32	-30.82	114.92	-33.30	35.92	-13.42	2.32	-10.93	-33.60	2.48
11	81.52	-96.94	53.69	-41.12	39.35	-12.03	27.83	-55.82	42.17	-84.91	14.34	-29.09
12	49.97	-42.04	5.82	-12.00	11.83	-17.00	44.16	-30.04	38.15	-25.04	-6.01	5.00
13	130.81	-317.42	111.11	-203.34	87.02	-296.02	19.70	-114.09	43.80	-21.40	24.10	92.69
14	111.72	-49.47	232.41	-578.77	157.90	-261.44	-120.69	529.30	-46.17	211.97	74.52	-317.33
15	148.01	-124.74	111.07	-124.57	53.82	-100.81	36.93	-0.17	94.19	-23.94	57.26	-23.76
16	74.99	-86.43	55.37	-144.97	31.51	-74.07	19.62	58.54	43.48	-12.35	23.86	-70.89
17	11.05	-29.71	3.75	-4.73	11.91	-4.41	7.30	-24.97	-0.86	-25.29	-8.16	-0.32
18	194.79	-45.04	79.67	-33.33	160.35	-49.18	115.12	-11.70	34.45	4.15	-80.67	15.85
19	34.43	-24.85	14.38	-37.95	59.02	-34.31	20.05	13.10	-24.59	9.46	-44.64	-3.64
20	66.00	-54.35	66.52	-127.96	11.09	-34.71	-0.52	73.61	54.91	-19.65	55.43	-93.25
21	494.25	-165.15	125.73	-42.07	271.88	-92.86	368.53	-123.09	222.37	-72.29	-146.15	50.80
22	53.50	-169.92	44.06	-142.32	111.91	-305.92	9.44	-27.60	-58.41	135.99	-67.84	163.60
23	100.99	-345.32	29.15	-143.25	57.49	-161.89	71.84	-202.08	43.50	-183.43	-28.35	18.64
24	161.36	-273.41	53.22	-148.58	85.29	-45.36	108.14	-124.83	76.07	-228.05	-32.07	-103.22
25	63.57	-48.63	104.78	-325.92	192.00	-382.31	-41.20	277.29	-128.42	333.67	-87.22	56.39
26	996.95	-294.11	716.21	-235.46	647.13	-285.19	280.74	-58.65	349.82	-8.92	69.08	49.73
27	210.95	-444.13	171.48	-228.15	299.72	-356.76	39.47	-215.98	-88.77	-87.37	-128.24	128.61
28	271.92	-91.38	195.34	-90.13	50.77	-153.07	76.57	-1.25	221.15	61.70	144.58	62.94
29	33.29	-66.12	18.35	-48.05	8.43	-3.61	14.94	-18.06	24.86	-62.51	9.92	-44.44
30	24.08	-15.34	7.57	-6.90	99.42	-30.20	16.51	-8.43	-75.34	14.86	-91.85	23.29
31	58.05	-61.93	11.67	-34.47	73.03	-240.16	46.38	-27.46	-14.98	178.24	-61.36	205.69
32	93.25	-286.89	90.55	-263.68	138.26	-373.81	2.70	-23.20	-45.00	86.92	-47.71	110.12
33	276.50	-120.16	133.14	-66.02	147.73	-60.40	143.36	-54.14	128.76	-59.76	-14.59	-5.62
34	4.29	-12.53	8.15	-13.17	1.47	-2.87	-3.86	0.64	2.82	-9.66	6.68	-10.30
35	201.55	-244.09	220.12	-51.18	310.23	-69.31	-18.56	-192.91	-108.68	-174.78	-90.11	18.13
36	258.12	-505.89	145.29	-391.77	165.57	-351.45	112.83	-114.12	92.55	-154.45	-20.28	-40.33
37	3.60	-2.65	52.46	-14.91	12.74	-4.05	-48.86	12.26	-9.14	1.40	39.73	-10.86
38	10.80	-29.67	11.87	-40.59	59.31	-20.68	-1.07	10.92	-48.51	-8.99	-47.45	-19.91
39	35.56	-101.81	26.20	-90.80	9.26	-26.98	9.36	-11.01	26.29	-74.83	16.93	-63.82
40	27.95	-15.28	30.26	-9.01	6.27	-5.26	-2.31	-6.26	21.68	-10.01	23.99	-3.75
41	37.88	-24.46	9.94	-7.79	56.22	-11.01	27.95	-16.67	-18.33	-13.45	-46.28	3.22
42	49.39	-24.12	14.58	-7.76	105.90	-22.54	34.80	-16.36	-56.51	-1.59	-91.32	14.78
43	50.08	-15.99	25.28	-9.27	46.08	-12.02	24.80	-6.72	4.00	-3.98	-20.80	2.74
44	38.86	-8.78	16.86	-8.25	26.18	-6.67	22.00	-0.52	12.68	-2.11	-9.32	-1.58
45	11.39	-20.49	12.93	-14.09	14.76	-2.48	-1.54	-6.40	-3.37	-18.01	-1.83	-11.61
46	44.84	-36.53	65.10	-18.97	50.36	-15.21	-20.26	-17.56	-5.52	-21.32	14.74	-3.75
47	139.41	-76.35	106.17	-36.23	75.43	-54.81	33.24	-40.12	63.98	-21.55	30.74	18.57
48	65.31	-178.93	52.72	-174.96	25.46	-86.76	12.59	-3.97	39.85	-92.17	27.26	-88.20
49	281.96	-89.16	202.92	-43.14	22.47	-14.33	79.05	-46.02	259.50	-74.82	180.45	-28.81
50	238.03	-88.88	102.60	-34.39	33.03	-39.08	135.44	-54.49	205.00	-49.80	69.56	4.69
51	88.49	-243.38	48.97	-99.69	95.74	-277.87	39.52	-143.70	-7.25	34.49	-46.77	178.18
52	918.22	-193.90	75.88	-32.84	90.73	-27.02	842.34	-161.06	827.48	-166.87	-14.86	-5.82
53	108.57	-69.51	153.75	-700.26	56.47	-22.91	-45.18	630.74	52.10	-46.60	97.28	-677.35
54	807.32	-358.85	602.35	-161.93	1063.83	-269.08	204.97	-196.92	-256.51	-89.78	-461.48	107.15
55	223.37	-512.29	145.73	-451.01	212.73	-382.49	77.64	-61.28	10.63	-129.80	-67.01	-68.52
56	86.32	-54.08	93.51	-57.68	28.34	-51.69	-7.19	3.60	57.98	-2.39	65.17	-5.99
57	51.77	-125.41	18.72	-40.37	22.11	-23.08	33.05	-85.03	29.65	-102.33	-3.39	-17.29
58	45.89	-82.98	24.45	-63.53	23.50	-10.72	21.44	-19.45	22.39	-72.26	0.95	-52.81
59	148.69	-57.68	107.32	-28.84	33.55	-10.64	41.36	-28.84	115.14	-47.03	73.78	-18.20
60	179.80	-545.45	111.38	-329.37	102.45	-342.90	68.42	-216.09	77.35	-202.55	8.93	13.53
61	508.89	-162.90	232.19	-82.63	127.35	-50.68	276.70	-80.27	381.54	-112.22	104.84	-31.95
62	7.31	-19.79	13.54	-16.32	0.90	-0.70	-6.23	-3.47	6.41	-19.09	12.64	-15.62
63	671.82	-224.66	319.79	-104.38	100.92	-23.78	352.03	-120.28	570.90	-200.89	218.86	-80.61
64	367.36	-897.26	179.43	-570.39	135.20	-276.48	187.93	-326.87	232.16	-620.78	44.23	-293.91
65	112.50	-155.05	52.20	-41.46	23.07	-9.13	60.30	-113.60	89.43	-145.92	29.13	-32.33
66	302.93	-151.58	136.16	-63.80	478.46	-265.95	166.77	-87.78	-175.53	114.36	-342.30	202.15
67	211.27	-320.96	114.95	-213.14	84.26	-111.64	96.32	-107.82	127.01	-209.33	30.69	-101.51
68	104.95	-61.60	82.80	-69.56	7.84	-12.07	22.15	7.96	97.10	-49.52	74.96	-57.48
69	398.40	-192.19	206.28	-96.34	218.39	-71.25	192.12	-95.85	180.01	-120.93	-12.11	-25.08
70	26.42	-12.17	25.13	-8.89	8.51	-3.44	1.29	-3.28	17.91	-8.73	16.62	-5.45

Table E.4. Maximum ($\epsilon 1$) and minimum ($\epsilon 3$) principal strain values at the location of 70 landmarks during second premolar (P4) bite load for the 3 models of durophagous species, and strain differences ($\Delta \epsilon 1$ and $\Delta \epsilon 3$) at landmark locations between models. Strain values are in microstrain (μ strain).

P4 bite landmark	Cerrocebus		Lophocebus		Mandrillus		Cerrocebus-Lophocebus		Cerrocebus-Mandrillus		Lophocebus-Mandrillus	
	$\epsilon 1$	$\epsilon 3$	$\epsilon 1$	$\epsilon 3$	$\epsilon 1$	$\epsilon 3$	$\Delta \epsilon 1$	$\Delta \epsilon 3$	$\Delta \epsilon 1$	$\Delta \epsilon 3$	$\Delta \epsilon 1$	$\Delta \epsilon 3$
1	7.63	-6.83	8.43	-7.69	3.95	-4.84	-0.80	0.86	3.68	-1.99	4.48	-2.85
2	141.58	-31.51	34.36	-10.98	15.83	-7.33	107.22	-20.53	125.74	-24.18	18.53	-3.65
3	519.63	-141.40	32.08	-15.82	13.93	-8.26	487.55	-125.58	505.69	-133.14	18.15	-7.56
4	120.53	-330.68	46.67	-109.62	78.84	-275.14	73.86	-221.06	41.68	-55.54	-32.18	165.52
5	12.97	-30.50	20.57	-12.24	42.31	-13.47	-7.60	-18.26	-29.34	-17.02	-21.74	1.23
6	49.06	-27.89	34.27	-42.86	19.99	-50.08	14.78	14.96	29.06	22.18	14.28	7.22
7	0.76	-1.04	25.03	-9.13	5.39	-20.03	-24.27	8.09	-4.63	18.99	19.65	10.90
8	51.75	-33.21	57.76	-17.14	242.02	-44.80	-6.01	-16.06	-190.27	11.60	-184.26	27.66
9	162.41	-231.45	84.47	-127.76	49.39	-145.15	77.94	-103.69	113.02	-86.30	35.08	17.39
10	125.17	-47.42	89.99	-33.95	117.52	-33.78	35.18	-13.47	7.65	-13.64	-27.53	-0.17
11	77.68	-68.78	56.71	-25.03	32.38	-10.24	20.97	-43.75	45.30	-58.54	24.32	-14.79
12	49.37	-50.21	10.16	-22.75	10.70	-16.02	39.20	-27.46	38.67	-34.19	-0.54	-6.73
13	36.64	-106.59	60.05	-103.69	35.77	-133.52	-23.42	-2.90	0.87	26.93	24.29	29.83
14	85.45	-174.62	108.45	-490.18	193.45	-329.54	-22.99	315.56	-107.99	154.92	-85.00	-160.64
15	128.07	-162.24	183.76	-402.32	346.12	-649.35	-55.69	240.08	-218.05	487.11	-162.36	247.04
16	90.34	-111.20	98.42	-301.19	68.73	-176.84	-8.08	189.99	21.61	65.64	29.69	-124.35
17	20.22	-53.70	8.69	-18.71	9.68	-8.58	11.53	-34.99	10.54	-45.13	-0.99	-10.13
18	154.01	-41.05	61.71	-25.80	155.71	-48.41	92.30	-15.26	-1.70	7.36	-94.00	22.62
19	40.02	-44.91	19.94	-52.56	65.39	-50.01	20.09	7.65	-25.37	5.10	-45.45	-2.55
20	61.33	-50.80	66.04	-124.13	8.04	-25.27	-4.71	73.33	53.29	-25.53	58.00	-98.86
21	504.53	-168.53	129.43	-44.28	294.25	-100.91	375.10	-124.26	210.28	-67.63	-164.82	56.63
22	57.76	-194.69	51.65	-166.06	120.74	-328.52	6.12	-28.64	-62.97	133.83	-69.09	162.46
23	96.37	-328.59	27.21	-130.19	55.24	-153.88	69.16	-198.40	41.14	-174.71	-28.02	23.69
24	144.96	-241.25	46.50	-135.08	87.01	-42.73	98.46	-106.17	57.95	-198.53	-40.51	-92.35
25	65.72	-51.73	106.85	-324.91	192.97	-399.57	-41.13	273.18	-127.26	347.84	-86.13	74.66
26	1011.43	-298.79	731.23	-240.52	664.36	-288.50	280.20	-58.27	347.07	-10.29	66.86	47.98
27	210.19	-451.15	170.81	-227.70	296.61	-359.79	39.38	-223.45	-86.42	-91.36	-125.80	132.09
28	289.78	-99.82	196.29	-84.05	49.97	-142.87	93.49	-15.77	239.81	43.05	146.32	58.82
29	31.36	-60.90	18.07	-46.88	7.62	-2.57	13.30	-14.02	23.75	-58.33	10.45	-44.32
30	29.98	-13.40	15.90	-8.52	101.58	-30.89	14.08	-4.88	-71.59	17.49	-85.67	22.37
31	52.24	-65.14	15.32	-44.31	83.40	-273.17	36.92	-20.83	-31.15	208.04	-68.08	228.87
32	89.94	-276.54	89.61	-261.01	138.73	-375.17	0.33	-15.53	-48.79	98.62	-49.12	114.16
33	261.00	-119.21	124.51	-67.02	137.45	-57.87	136.49	-52.20	123.54	-61.34	-12.95	-9.15
34	3.39	-9.36	7.27	-12.08	1.28	-2.06	-3.88	2.72	2.11	-7.29	6.00	-10.01
35	203.08	-251.30	215.84	-50.62	308.35	-68.52	-12.76	-200.69	-105.27	-182.79	-92.51	17.90
36	253.44	-491.50	142.86	-380.70	161.47	-342.14	110.58	-110.79	91.97	-149.35	-18.61	-38.56
37	3.96	-2.95	53.75	-15.28	12.57	-4.08	-49.79	12.33	-8.61	1.13	41.18	-11.20
38	11.29	-31.26	12.19	-42.00	57.14	-21.26	-0.91	10.74	-45.85	-10.00	-44.94	-20.74
39	30.90	-88.59	21.42	-73.33	8.34	-24.34	9.48	-15.27	22.56	-64.26	13.09	-48.99
40	24.93	-22.01	19.56	-6.05	5.30	-4.60	5.38	-15.96	19.64	-17.41	14.26	-1.45
41	31.51	-19.88	6.67	-5.34	47.31	-9.29	24.85	-14.54	-15.79	-10.59	-40.64	3.95
42	40.68	-18.59	10.41	-5.26	91.71	-19.52	30.27	-13.33	-51.02	0.92	-81.30	14.26
43	41.10	-13.03	17.81	-6.49	39.92	-10.59	23.29	-6.54	1.17	-2.44	-22.11	4.10
44	30.41	-7.32	12.34	-6.91	22.72	-5.76	18.07	-0.41	7.70	-1.57	-10.37	-1.15
45	9.89	-20.50	10.06	-13.42	12.91	-2.14	-0.17	-7.08	-3.02	-18.36	-2.85	-11.28
46	41.70	-34.73	58.24	-17.03	46.96	-14.11	-16.54	-17.70	-5.26	-20.62	11.28	-2.92
47	126.76	-70.31	103.33	-36.46	75.74	-59.93	23.44	-33.85	51.02	-10.38	27.58	23.47
48	63.95	-178.26	52.58	-174.42	25.38	-86.75	11.37	-3.83	38.56	-91.50	27.19	-87.67
49	275.55	-87.13	196.44	-41.83	16.26	-18.19	79.11	-45.31	259.29	-68.95	180.18	-23.64
50	245.22	-90.26	107.75	-36.03	39.61	-35.72	137.47	-54.23	205.62	-54.54	68.14	-0.31
51	85.55	-225.33	48.45	-90.21	97.47	-269.39	37.10	-135.11	-11.93	44.06	-49.03	179.18
52	843.15	-178.22	67.74	-28.88	76.05	-22.62	775.41	-149.34	767.10	-155.60	-8.31	-6.26
53	109.14	-70.77	156.05	-707.44	55.21	-22.48	-46.91	636.66	53.93	-48.30	100.84	-684.96
54	810.74	-360.62	603.67	-162.35	1067.60	-271.75	207.08	-198.27	-256.85	-88.86	-463.93	109.41
55	225.18	-517.18	146.26	-452.13	208.03	-378.76	78.93	-65.06	17.15	-138.42	-61.77	-73.36
56	85.86	-51.68	88.30	-50.53	26.82	-49.78	-2.44	-1.15	59.04	-1.90	61.48	-0.75
57	51.13	-124.24	18.95	-40.51	22.46	-23.89	32.19	-83.73	28.67	-100.34	-3.52	-16.61
58	46.07	-83.49	25.21	-65.60	21.89	-10.12	20.85	-17.88	24.17	-73.37	3.32	-55.48
59	147.51	-57.31	111.99	-29.49	40.26	-13.19	35.52	-27.81	107.25	-44.12	71.72	-16.31
60	179.98	-546.32	112.14	-331.67	101.76	-340.59	67.84	-214.66	78.21	-205.74	10.38	8.92
61	505.76	-161.97	232.23	-82.70	129.69	-50.88	273.53	-79.27	376.08	-111.10	102.54	-31.82
62	6.87	-18.62	13.28	-16.04	0.87	-0.63	-6.40	-2.58	6.00	-17.99	12.41	-15.41
63	665.42	-222.51	319.54	-104.32	100.21	-23.53	345.88	-118.19	565.20	-198.98	219.33	-80.79
64	367.65	-897.33	180.07	-573.33	136.79	-281.58	187.58	-324.00	230.86	-615.75	43.28	-291.75
65	117.67	-128.92	69.06	-39.65	25.96	-7.72	48.61	-89.26	91.71	-121.19	43.10	-31.93
66	300.75	-149.21	138.61	-64.42	502.87	-284.49	162.14	-84.79	-202.12	135.29	-364.26	220.07
67	199.00	-283.75	110.74	-204.94	64.95	-105.45	88.26	-78.82	134.05	-178.31	45.79	-99.49
68	97.88	-57.86	73.41	-61.04	7.55	-11.89	24.47	3.18	90.33	-45.97	65.86	-49.15
69	392.79	-190.70	205.45	-96.29	214.52	-70.11	187.35	-94.41	178.27	-120.60	-9.08	-26.19
70	21.83	-9.04	22.40	-8.07	7.71	-3.09	-0.58	-0.97	14.12	-5.96	14.70	-4.99

Table E.5. Maximum ($\epsilon 1$) and minimum ($\epsilon 3$) principal strain values at the location of 70 landmarks during first molar (M1) bite load for the 3 models of durophagous species, and strain differences ($\Delta \epsilon 1$ and $\Delta \epsilon 3$) at landmark locations between models. Strain values are in microstrain (μ strain).

M1 bite landmark	Cerrocebus		Lophocebus		Mandrillus		Cerrocebus-Lophocebus		Cerrocebus-Mandrillus		Lophocebus-Mandrillus	
	$\epsilon 1$	$\epsilon 3$	$\epsilon 1$	$\epsilon 3$	$\epsilon 1$	$\epsilon 3$	$\Delta \epsilon 1$	$\Delta \epsilon 3$	$\Delta \epsilon 1$	$\Delta \epsilon 3$	$\Delta \epsilon 1$	$\Delta \epsilon 3$
1	6.11	-6.06	6.58	-1.80	2.94	-2.60	-0.48	-4.26	3.16	-3.46	3.64	0.80
2	97.20	-21.25	68.14	-19.37	22.51	-7.84	29.06	-1.89	74.70	-13.41	45.64	-11.52
3	406.48	-111.44	28.54	-14.65	14.04	-8.19	377.95	-96.79	392.44	-103.25	14.50	-6.45
4	106.70	-299.00	42.48	-95.08	72.38	-256.46	64.22	-203.93	34.32	-42.55	-29.90	161.38
5	14.55	-25.55	21.07	-10.10	44.72	-14.26	-6.52	-15.45	-30.16	-11.29	-23.65	4.16
6	51.38	-34.48	34.22	-42.53	20.15	-50.46	17.16	8.04	31.23	15.98	14.07	7.93
7	1.36	-2.05	25.85	-9.42	5.40	-20.10	-24.49	7.37	-4.04	18.06	20.46	10.68
8	56.14	-28.85	54.88	-24.07	232.33	-43.53	1.26	-4.78	-176.19	14.68	-177.46	19.46
9	150.06	-199.67	78.31	-126.42	41.48	-136.06	71.75	-73.25	108.58	-63.61	36.83	9.64
10	146.78	-56.13	92.02	-34.68	119.75	-34.31	54.77	-21.45	27.03	-21.81	-27.73	-0.37
11	64.77	-42.29	65.28	-24.10	23.29	-7.88	-0.51	-18.19	41.48	-34.41	41.98	-16.22
12	34.15	-41.29	25.67	-41.77	12.16	-15.16	8.48	0.48	21.99	-26.14	13.51	-26.61
13	24.23	-70.10	7.68	-13.04	17.06	-4.83	16.55	-57.06	7.17	-65.27	-9.38	-8.21
14	41.06	-75.73	34.94	-87.85	37.35	-84.56	6.12	12.12	3.71	8.83	-2.41	-3.29
15	206.76	-417.71	65.73	-248.68	53.41	-93.10	141.03	-169.03	153.36	-324.61	12.32	-155.58
16	175.74	-205.02	107.88	-394.39	108.69	-256.66	67.86	189.37	67.05	51.64	-0.81	-137.73
17	59.39	-133.24	12.69	-30.15	13.50	-36.60	46.70	-103.09	45.89	-96.65	-0.80	6.45
18	115.37	-23.83	33.88	-12.97	83.13	-25.40	81.48	-10.85	32.23	1.57	-49.25	12.43
19	56.31	-95.39	26.86	-58.86	70.65	-69.57	29.45	-36.52	-14.34	-25.82	-43.80	10.70
20	52.01	-42.86	66.44	-122.27	5.41	-17.02	-14.43	79.41	46.60	-25.84	61.03	-105.25
21	505.35	-168.97	135.56	-47.35	310.03	-106.75	369.79	-121.62	195.32	-62.22	-174.47	59.40
22	80.73	-271.42	52.61	-169.39	125.68	-341.52	28.12	-102.03	-44.95	70.11	-73.07	172.14
23	91.07	-304.06	24.67	-113.37	52.24	-145.79	66.39	-190.69	38.82	-158.28	-27.57	32.41
24	112.57	-195.46	46.69	-124.80	102.89	-46.37	65.88	-70.65	9.69	-149.08	-56.20	-78.43
25	66.76	-59.96	106.40	-321.28	188.22	-397.09	-39.64	261.32	-121.46	337.13	-81.82	75.81
26	1043.01	-309.21	744.40	-244.96	674.39	-291.09	298.62	-64.25	368.62	-18.12	70.00	46.14
27	210.84	-467.48	171.98	-229.05	292.62	-360.95	38.86	-238.43	-81.78	-106.53	-120.64	131.90
28	314.85	-111.81	198.34	-76.95	48.40	-125.54	116.51	-34.86	266.44	13.73	149.94	48.59
29	26.77	-47.33	17.72	-45.90	7.20	-2.72	9.05	-1.43	19.57	-44.61	10.52	-43.18
30	52.94	-16.72	18.81	-9.56	104.04	-31.64	34.14	-7.16	-51.09	14.92	-85.23	22.08
31	45.34	-81.71	16.66	-44.99	86.96	-284.51	28.68	-36.72	-41.62	202.80	-70.30	239.52
32	83.73	-247.85	90.57	-263.81	138.73	-375.25	-6.85	15.97	-55.01	127.41	-48.16	111.44
33	224.57	-118.05	121.66	-68.14	131.59	-56.46	102.90	-49.91	92.98	-61.59	-9.92	-11.68
34	1.90	-3.75	6.55	-11.15	1.30	-1.50	-4.66	7.40	0.59	-2.26	5.25	-9.66
35	207.35	-270.35	216.10	-50.62	306.78	-67.95	-8.75	-219.74	-99.43	-202.40	-90.68	17.33
36	241.65	-454.54	143.04	-379.64	159.32	-337.47	98.61	-74.89	82.32	-117.07	-16.28	-42.17
37	4.99	-3.68	55.26	-15.64	12.39	-4.07	-50.26	11.96	-7.39	0.39	42.87	-11.57
38	13.17	-37.89	11.31	-38.83	55.91	-21.09	1.86	0.94	-42.74	-16.80	-44.60	-17.74
39	22.00	-62.89	19.16	-65.53	7.60	-22.74	2.84	2.64	14.41	-40.15	11.56	-42.79
40	16.06	-17.39	11.06	-4.62	4.24	-3.64	5.00	-12.77	11.81	-13.74	6.81	-0.98
41	22.41	-14.04	4.08	-2.56	49.64	-9.45	18.33	-11.48	-27.24	-4.59	-45.56	6.89
42	28.11	-10.99	7.12	-2.96	90.03	-19.11	21.00	-8.04	-61.92	8.12	-82.91	16.15
43	27.87	-8.82	10.84	-4.29	37.01	-11.08	17.02	-4.53	-9.14	2.26	-26.16	6.79
44	17.30	-6.34	8.84	-6.57	18.45	-4.65	8.46	0.23	-1.14	-1.70	-9.61	-1.93
45	8.49	-20.29	8.90	-14.04	8.96	-1.43	-0.41	-6.25	-0.47	-18.86	-0.06	-12.61
46	34.37	-30.38	54.37	-16.13	42.99	-13.06	-20.00	-14.25	-8.62	-17.32	11.37	-3.07
47	125.68	-63.35	88.83	-33.53	72.58	-57.13	36.84	-29.82	53.09	-6.22	16.25	23.60
48	62.78	-179.62	51.88	-170.17	24.19	-81.44	10.89	-9.45	38.59	-98.18	27.70	-88.73
49	250.83	-79.34	201.30	-42.69	20.79	-13.07	49.52	-36.66	230.04	-66.27	180.51	-29.62
50	278.16	-97.62	99.68	-33.58	39.71	-35.21	178.48	-64.03	238.45	-62.40	59.97	1.63
51	84.69	-197.37	44.42	-78.31	94.67	-250.93	40.27	-119.06	-9.97	53.56	-50.25	172.62
52	687.83	-144.38	62.80	-28.16	67.34	-19.95	625.03	-116.21	620.49	-124.42	-4.54	-8.21
53	110.16	-71.54	161.95	-729.16	42.29	-22.69	-51.79	657.63	67.87	-48.84	119.66	-706.47
54	807.50	-360.74	608.57	-163.34	1079.52	-269.92	198.94	-197.40	-272.02	-90.82	-470.95	106.58
55	225.01	-516.43	147.38	-452.78	202.34	-383.17	77.62	-63.65	22.66	-133.27	-54.96	-69.61
56	76.74	-43.83	91.34	-52.39	23.53	-49.02	-14.60	8.57	53.21	5.20	67.82	-3.37
57	50.37	-123.22	19.03	-41.16	21.80	-23.77	31.34	-82.06	28.57	-99.45	-2.77	-17.39
58	48.08	-88.69	24.52	-63.67	21.26	-9.75	23.57	-25.02	26.82	-78.93	3.25	-53.92
59	152.20	-59.51	110.49	-27.86	40.56	-13.31	41.71	-31.65	111.63	-46.20	69.92	-14.56
60	182.49	-554.60	111.87	-330.93	101.50	-339.89	70.63	-223.67	80.99	-214.71	10.37	8.96
61	509.43	-162.89	224.90	-80.88	125.39	-50.06	284.53	-82.01	384.04	-112.83	99.51	-30.82
62	6.45	-17.53	12.48	-15.14	0.76	-0.51	-6.04	-2.38	5.68	-17.02	11.72	-14.63
63	660.33	-220.80	316.65	-103.56	98.86	-23.09	343.68	-117.25	561.47	-197.72	217.79	-80.47
64	372.60	-908.73	178.25	-566.41	135.82	-279.09	194.35	-342.32	236.78	-629.64	42.43	-287.32
65	122.64	-120.98	70.82	-30.27	27.38	-8.66	51.82	-90.71	95.26	-112.32	43.44	-21.61
66	292.17	-143.93	144.10	-65.55	514.72	-291.01	148.06	-78.38	-222.55	147.08	-370.62	225.46
67	155.04	-253.24	79.56	-136.32	27.00	-55.71	75.48	-116.92	128.04	-197.53	52.56	-80.61
68	82.25	-48.90	70.88	-58.95	6.56	-10.83	11.37	10.05	75.69	-38.07	64.32	-48.12
69	380.21	-188.92	204.70	-96.58	219.28	-71.82	175.51	-92.34	160.92	-117.10	-14.58	-24.76
70	18.47	-6.13	23.48	-7.90	9.66	-3.79	-5.01	1.77	8.80	-2.34	13.81	-4.11

Table E.6. Maximum ($\epsilon 1$) and minimum ($\epsilon 3$) principal strain values at the location of 70 landmarks during second molar (M2) bite load for the 3 models of durophagous species, and strain differences ($\Delta \epsilon 1$ and $\Delta \epsilon 3$) at landmark locations between models. Strain values are in microstrain (μstrain).

M2 bite landmark	Cerrocebus		Lophocebus		Mandrillus		Cerrocebus-Lophocebus		Cerrocebus-Mandrillus		Lophocebus-Mandrillus	
	$\epsilon 1$	$\epsilon 3$	$\epsilon 1$	$\epsilon 3$	$\epsilon 1$	$\epsilon 3$	$\Delta \epsilon 1$	$\Delta \epsilon 3$	$\Delta \epsilon 1$	$\Delta \epsilon 3$	$\Delta \epsilon 1$	$\Delta \epsilon 3$
1	11.20	-8.76	8.81	-1.49	1.54	-1.12	2.39	-7.27	9.65	-7.64	7.27	-0.37
2	129.71	-28.01	66.47	-18.14	20.63	-6.91	63.24	-9.87	109.08	-21.10	45.84	-11.23
3	371.42	-98.75	20.64	-11.33	10.80	-6.29	350.78	-87.42	360.63	-92.47	9.85	-5.04
4	86.09	-244.42	41.92	-78.81	62.09	-229.56	44.18	-165.61	24.01	-14.87	-20.17	150.74
5	15.98	-16.43	21.78	-6.77	49.40	-15.62	-5.80	-9.66	-33.42	-0.80	-27.62	8.86
6	52.11	-36.54	34.50	-42.42	20.38	-51.06	17.61	5.88	31.73	14.51	14.12	8.63
7	2.34	-3.67	27.52	-10.00	5.42	-20.19	-25.18	6.33	-3.08	16.52	22.10	10.19
8	58.51	-22.68	53.98	-40.28	219.21	-42.39	4.53	17.60	-160.71	19.71	-165.24	2.11
9	125.67	-184.92	51.66	-104.33	21.53	-110.10	74.02	-80.59	104.14	-74.82	30.12	5.77
10	152.26	-58.19	100.93	-37.87	124.34	-35.39	51.34	-20.31	27.92	-22.80	-23.41	-2.48
11	65.42	-25.15	59.71	-22.01	15.33	-5.29	5.70	-3.14	50.08	-19.86	44.38	-16.72
12	49.74	-58.22	27.73	-39.68	10.77	-11.88	22.02	-18.54	38.98	-46.34	16.96	-27.80
13	3.32	-2.83	5.13	-5.99	64.16	-17.27	-1.81	3.17	-60.85	14.44	-59.03	11.27
14	2.56	-6.08	11.41	-31.48	5.39	-9.73	-8.85	25.40	-2.83	3.65	6.02	-21.75
15	36.26	-100.30	34.17	-68.66	3.66	-8.57	2.09	-31.64	32.60	-91.72	30.51	-60.08
16	49.58	-124.00	40.43	-95.19	35.05	-112.91	9.16	-28.82	14.53	-11.10	5.37	17.72
17	86.13	-204.99	39.32	-68.63	72.03	-202.62	46.81	-136.36	14.10	-2.37	-32.71	133.99
18	14.17	-74.42	21.38	-50.97	33.54	-104.79	-7.22	-23.45	-19.38	30.37	-12.16	53.82
19	82.45	-126.41	49.70	-76.34	83.30	-108.71	32.76	-50.07	-0.85	-17.70	-33.60	32.37
20	43.21	-36.64	66.63	-115.94	3.46	-4.57	-23.42	79.31	39.75	-32.07	63.17	-111.37
21	532.49	-178.30	140.73	-51.15	342.09	-118.46	391.76	-127.15	190.40	-59.84	-201.36	67.30
22	85.50	-286.05	59.98	-192.35	135.75	-367.80	25.52	-93.70	-50.25	81.75	-75.77	175.45
23	83.45	-269.86	23.10	-91.44	47.50	-133.81	60.35	-178.42	35.95	-136.05	-24.40	42.37
24	95.07	-146.93	36.74	-97.11	86.36	-37.75	58.33	-49.82	8.71	-109.18	-49.62	-59.36
25	76.16	-63.93	108.11	-318.78	182.23	-396.36	-31.95	254.84	-106.07	332.42	-74.12	77.58
26	1069.07	-317.26	770.00	-253.57	693.11	-295.84	299.07	-63.69	375.96	-21.42	76.89	42.27
27	214.47	-483.44	172.96	-230.85	288.04	-365.16	41.51	-252.59	-73.56	-118.28	-115.08	134.32
28	348.07	-127.80	192.99	-64.11	48.77	-104.66	155.08	-63.69	299.30	-23.14	144.22	40.55
29	24.39	-41.76	16.97	-43.36	6.42	-3.15	7.42	1.60	17.97	-38.60	10.55	-40.20
30	64.70	-20.60	31.74	-14.77	108.54	-33.01	32.96	-5.83	-43.84	12.41	-76.80	18.24
31	42.34	-86.88	21.67	-54.08	95.41	-311.51	20.66	-32.81	-53.08	224.63	-73.74	257.43
32	82.85	-240.29	90.00	-262.22	139.05	-376.22	-7.15	21.93	-56.20	135.93	-49.05	114.00
33	208.09	-119.77	111.82	-71.27	120.27	-54.01	96.26	-48.51	87.81	-65.77	-8.45	-17.26
34	3.51	-3.79	4.81	-8.85	2.18	-1.36	-1.29	5.06	1.33	-2.43	2.63	-7.49
35	209.03	-278.64	211.50	-50.07	303.93	-66.85	-2.48	-228.57	-94.90	-211.79	-92.43	16.78
36	236.85	-440.27	140.45	-365.66	154.79	-327.40	96.40	-74.60	82.07	-112.87	-14.34	-38.27
37	5.61	-4.01	58.36	-16.42	12.02	-4.06	-52.75	12.42	-6.40	0.05	46.34	-12.36
38	13.05	-36.99	11.56	-39.39	53.73	-21.38	1.49	2.39	-40.67	-15.61	-42.16	-18.01
39	15.57	-45.13	13.25	-44.51	6.02	-18.14	2.32	-0.63	9.55	-26.99	7.23	-26.36
40	23.36	-37.54	9.80	-5.13	3.01	-2.91	13.57	-32.41	20.35	-34.63	6.78	-2.22
41	20.83	-10.58	4.28	-1.68	48.43	-8.94	16.54	-8.90	-27.61	-1.64	-44.15	7.26
42	20.33	-5.86	6.44	-1.87	86.55	-18.37	13.88	-3.99	-66.22	12.51	-80.11	16.50
43	19.91	-6.72	4.76	-1.69	34.49	-11.68	15.16	-5.03	-14.58	4.97	-29.74	9.99
44	8.52	-4.80	4.37	-4.94	15.76	-4.50	4.15	0.14	-7.24	-0.31	-11.39	-0.45
45	8.23	-19.54	6.46	-13.15	4.48	-1.05	1.77	-6.39	3.75	-18.49	1.98	-12.10
46	30.96	-27.68	44.74	-13.47	34.94	-10.96	-13.77	-14.22	-3.98	-16.72	9.80	-2.50
47	88.18	-53.23	76.82	-31.71	68.78	-56.46	11.36	-21.52	19.40	3.23	8.04	24.75
48	58.95	-174.47	51.41	-166.09	22.83	-75.58	7.54	-8.38	36.12	-98.88	28.58	-90.51
49	250.27	-79.10	192.93	-40.86	21.91	-11.78	57.33	-38.25	228.36	-67.32	171.02	-29.07
50	271.93	-95.82	101.38	-34.14	45.14	-33.90	170.55	-61.68	226.79	-61.92	56.24	-0.24
51	78.46	-157.88	42.67	-59.46	92.62	-225.82	35.79	-98.43	-14.15	67.94	-49.94	166.37
52	580.26	-123.48	47.78	-22.41	44.06	-13.14	532.48	-101.07	536.20	-110.34	3.71	-9.26
53	111.59	-75.49	168.87	-752.71	31.07	-23.54	-57.28	677.21	80.52	-51.95	137.80	-729.17
54	825.81	-367.93	614.08	-164.67	1094.05	-269.88	211.73	-203.26	-268.25	-98.06	-479.97	105.20
55	232.61	-537.49	148.89	-454.92	194.75	-386.51	83.72	-82.56	37.86	-150.98	-45.86	-68.42
56	86.65	-42.49	85.66	-42.22	21.07	-46.12	0.99	-0.28	65.58	3.63	64.59	3.90
57	48.59	-119.23	19.29	-41.45	21.61	-24.45	29.30	-77.78	26.98	-94.78	-2.32	-17.00
58	46.58	-85.21	25.05	-65.12	19.69	-9.04	21.54	-20.09	26.89	-76.17	5.35	-56.08
59	143.00	-55.72	116.66	-27.76	45.60	-15.21	26.34	-27.96	97.40	-40.50	71.06	-12.54
60	180.01	-547.56	112.46	-332.82	100.90	-338.07	67.55	-214.74	79.11	-209.49	11.57	5.25
61	492.97	-158.27	219.53	-79.64	122.27	-49.34	273.44	-78.62	370.69	-108.92	97.26	-30.30
62	5.09	-13.86	11.46	-14.01	0.66	-0.38	-6.37	0.15	4.43	-13.48	10.81	-13.63
63	640.50	-214.12	314.34	-102.95	97.22	-22.56	326.17	-111.17	543.28	-191.56	217.12	-80.40
64	368.06	-895.63	177.59	-564.43	135.74	-279.52	190.47	-331.20	232.32	-616.11	41.85	-284.91
65	102.82	-62.79	70.40	-31.01	23.90	-7.29	32.43	-31.78	78.92	-55.50	46.49	-23.72
66	294.43	-141.77	151.39	-66.87	538.25	-303.36	143.04	-74.89	-243.81	161.60	-386.86	236.49
67	93.51	-149.72	46.76	-89.13	12.83	-25.63	46.74	-60.58	80.68	-124.09	33.94	-63.50
68	72.84	-41.26	56.38	-45.95	5.65	-9.23	16.46	4.68	67.19	-32.03	50.74	-36.71
69	372.27	-185.32	203.48	-96.78	221.23	-72.59	168.79	-88.55	151.04	-112.74	-17.75	-24.19
70	15.26	-8.17	22.10	-7.84	10.33	-4.00	-6.84	-0.33	4.93	-4.17	11.76	-3.84

Table E.7. Maximum ($\epsilon 1$) and minimum ($\epsilon 3$) principal strain values at the location of 70 landmarks during third molar (M3) bite load for the 3 models of durophagous species, and strain differences ($\Delta \epsilon 1$ and $\Delta \epsilon 3$) at landmark locations between models. Strain values are in microstrain (μ strain).

M3 bite landmark	Cerrocebus		Lophocebus		Mandrillus		Cerrocebus-Lophocebus		Cerrocebus-Mandrillus		Lophocebus-Mandrillus	
	$\epsilon 1$	$\epsilon 3$	$\epsilon 1$	$\epsilon 3$	$\epsilon 1$	$\epsilon 3$	$\Delta \epsilon 1$	$\Delta \epsilon 3$	$\Delta \epsilon 1$	$\Delta \epsilon 3$	$\Delta \epsilon 1$	$\Delta \epsilon 3$
1	14.19	-11.53	12.52	-4.69	2.31	-0.89	1.67	-6.84	11.88	-10.63	10.21	-3.80
2	130.49	-28.29	63.85	-16.49	18.41	-6.35	66.64	-11.80	112.08	-21.94	45.44	-10.14
3	294.34	-76.37	11.27	-7.31	6.38	-3.71	283.07	-69.06	287.96	-72.66	4.89	-3.61
4	70.46	-175.23	45.13	-60.19	47.27	-180.86	25.32	-115.03	23.18	5.63	-2.14	120.67
5	16.82	-6.97	22.31	-8.35	56.42	-18.09	-5.49	1.38	-39.60	11.12	-34.11	9.74
6	53.73	-40.46	34.95	-42.44	20.80	-52.10	18.78	1.98	32.93	11.64	14.15	9.66
7	3.88	-6.21	30.14	-10.91	5.55	-20.72	-26.26	4.70	-1.67	14.51	24.59	9.81
8	62.92	-44.16	51.89	-65.20	178.40	-38.05	11.03	21.04	-115.48	-6.11	-126.51	-27.15
9	85.84	-170.06	28.21	-86.48	15.75	-86.44	57.63	-83.59	70.09	-83.63	12.46	-0.04
10	157.43	-60.14	104.96	-39.29	128.45	-36.45	52.46	-20.84	28.97	-23.69	-23.49	-2.84
11	58.05	-17.42	48.67	-17.32	6.30	-2.17	9.38	-0.10	51.75	-15.25	42.07	-15.15
12	52.05	-58.51	28.80	-32.90	8.77	-7.55	23.25	-25.61	43.29	-50.96	20.34	-25.35
13	44.93	-13.70	22.74	-14.92	102.98	-27.58	22.20	1.22	-58.05	13.88	-80.24	12.66
14	25.70	-11.28	7.57	-6.66	67.26	-39.75	18.14	-4.63	-41.55	28.46	-59.69	33.09
15	11.71	-27.90	6.98	-11.35	31.83	-33.71	4.74	-16.55	-20.12	5.81	-24.86	22.36
16	48.68	-60.22	22.87	-30.69	23.05	-47.50	25.82	-29.53	25.64	-12.71	-0.18	16.82
17	30.57	-77.65	52.55	-88.32	42.61	-121.63	-21.98	10.66	-12.04	43.98	9.94	33.32
18	109.18	-975.79	309.48	-624.75	236.27	-675.80	-200.30	-351.04	-127.09	-299.99	73.21	51.04
19	139.23	-185.28	88.53	-93.11	99.90	-159.57	50.70	-92.17	39.33	-25.72	-11.36	66.46
20	29.59	-26.07	67.88	-108.69	28.16	-9.26	-38.29	82.62	1.43	-16.81	39.72	-99.43
21	553.70	-185.97	146.85	-55.86	370.57	-129.03	406.85	-130.11	183.13	-56.94	-223.72	73.17
22	90.97	-302.17	61.53	-197.76	139.60	-379.22	29.44	-104.41	-48.63	77.04	-78.06	181.46
23	77.19	-230.79	22.93	-69.19	39.82	-117.32	54.26	-161.60	37.37	-113.47	-16.89	48.13
24	69.95	-89.04	25.55	-61.98	61.67	-25.81	44.41	-27.06	8.28	-63.23	-36.12	-36.17
25	91.82	-72.99	110.53	-325.02	167.18	-373.31	-18.71	252.03	-75.36	300.32	-56.65	48.29
26	1107.89	-329.39	796.27	-262.33	711.39	-301.39	311.62	-67.06	396.50	-28.00	84.88	39.06
27	222.16	-510.91	175.16	-234.57	281.02	-371.31	47.00	-276.34	-58.87	-139.61	-105.87	136.74
28	383.02	-145.04	189.65	-64.82	45.80	-71.32	193.37	-80.23	337.22	-73.72	143.85	6.51
29	20.40	-32.84	15.76	-40.17	6.17	-3.73	4.64	7.33	14.23	-29.11	9.59	-36.44
30	81.21	-26.38	39.96	-18.25	115.79	-35.16	41.25	-8.13	-34.58	8.78	-75.83	16.92
31	41.85	-97.40	26.44	-55.46	88.99	-290.61	15.41	-41.94	-47.14	193.21	-62.55	235.15
32	81.74	-227.99	90.48	-263.68	138.69	-375.47	-8.74	35.70	-56.95	147.48	-48.21	111.78
33	184.65	-123.47	103.57	-75.78	108.54	-51.64	81.07	-47.70	76.11	-71.83	-4.97	-24.13
34	14.31	-8.23	2.45	-5.66	5.24	-2.39	11.86	-2.57	9.07	-5.83	-2.79	-3.26
35	211.90	-291.26	208.64	-49.85	299.74	-65.39	3.26	-241.40	-87.84	-225.87	-91.10	15.54
36	230.59	-422.17	139.13	-355.09	150.19	-317.69	91.46	-67.08	80.40	-104.47	-11.06	-37.39
37	7.12	-4.42	63.08	-17.57	11.82	-4.06	-55.95	13.15	-4.70	-0.36	51.26	-13.51
38	13.76	-38.21	11.55	-38.84	51.06	-20.79	2.21	0.63	-37.29	-17.42	-39.51	-18.05
39	6.24	-19.20	6.57	-20.63	3.71	-11.43	-0.33	1.44	2.53	-7.77	2.86	-9.20
40	25.64	-48.83	10.03	-7.11	1.48	-2.37	15.61	-41.72	24.15	-46.46	8.54	-4.74
41	20.58	-8.05	8.93	-2.95	43.89	-7.79	11.66	-5.10	-23.31	-0.27	-34.96	4.83
42	15.49	-5.15	10.56	-3.82	82.32	-17.50	4.93	-1.34	-66.83	12.35	-71.76	13.68
43	14.50	-6.77	8.02	-4.17	33.50	-13.07	6.48	-2.60	-19.00	6.30	-25.48	8.90
44	2.62	-2.60	1.81	-2.59	16.68	-6.14	0.81	-0.01	-14.06	3.54	-14.87	3.55
45	7.04	-15.92	4.48	-10.47	2.95	-1.00	2.57	-5.45	4.10	-14.92	1.53	-9.47
46	25.10	-22.76	34.56	-10.29	26.73	-9.22	-9.46	-12.46	-1.63	-13.54	7.82	-1.07
47	48.40	-41.31	55.10	-26.92	57.78	-45.44	-6.70	-14.38	-9.38	4.14	-2.68	18.52
48	54.14	-165.99	50.96	-158.31	17.94	-54.32	3.17	-7.68	36.20	-111.67	33.03	-103.99
49	238.12	-75.11	182.51	-38.49	43.14	-15.00	55.61	-36.62	194.98	-60.11	139.37	-23.49
50	276.19	-96.10	97.51	-33.01	46.51	-33.00	178.68	-63.10	229.68	-63.10	51.00	-0.01
51	78.94	-108.78	43.93	-37.87	83.88	-177.66	35.02	-70.91	-4.93	68.88	-39.95	139.79
52	407.88	-88.96	29.68	-15.82	11.92	-4.02	378.20	-73.14	395.96	-84.94	17.75	-11.80
53	113.53	-80.16	180.19	-792.76	17.09	-39.18	-66.66	712.60	96.44	-40.99	163.10	-753.58
54	850.09	-377.57	624.11	-166.87	1128.99	-265.59	225.98	-210.70	-278.90	-111.98	-504.87	98.72
55	242.27	-564.39	151.30	-457.73	184.60	-404.70	90.96	-106.66	57.66	-159.69	-33.30	-53.03
56	101.89	-38.76	80.32	-31.27	17.83	-41.97	21.57	-7.49	84.06	3.21	62.49	10.69
57	45.62	-112.61	19.33	-41.33	20.84	-25.11	26.29	-71.27	24.79	-87.50	-1.50	-16.22
58	44.98	-82.19	24.87	-64.72	18.50	-8.24	20.11	-17.47	26.47	-73.94	6.37	-56.48
59	133.88	-51.78	123.06	-26.66	49.63	-16.69	10.82	-25.12	84.25	-35.09	73.43	-9.97
60	176.67	-538.02	112.27	-332.43	100.54	-337.32	64.39	-205.59	76.12	-200.70	11.73	4.89
61	473.57	-152.84	207.21	-76.70	109.25	-47.25	266.35	-76.14	364.32	-105.59	97.97	-29.45
62	3.11	-8.55	9.64	-12.03	0.88	-0.34	-6.53	3.48	2.23	-8.20	8.76	-11.69
63	614.62	-205.40	309.35	-101.64	94.07	-21.63	305.28	-103.76	520.55	-183.77	215.28	-80.01
64	363.09	-880.82	174.83	-554.25	132.17	-270.03	188.26	-326.57	230.91	-610.79	42.66	-284.23
65	64.83	-28.60	58.37	-28.47	19.69	-9.05	6.46	-0.12	45.14	-19.55	38.68	-19.42
66	295.86	-138.32	160.80	-66.66	546.60	-294.53	135.05	-71.66	-250.75	156.21	-385.80	227.87
67	46.07	-74.91	21.69	-45.80	19.86	-31.22	24.38	-29.12	26.21	-43.69	1.83	-14.58
68	55.20	-26.74	37.74	-29.43	4.13	-6.45	17.46	2.69	51.07	-20.29	33.61	-22.98
69	360.21	-180.81	202.20	-97.03	233.00	-76.69	158.01	-83.79	127.21	-104.12	-30.80	-20.34
70	19.17	-11.51	21.13	-8.55	10.85	-4.22	-1.96	-2.95	8.32	-7.28	10.28	-4.33

Table E.8. Maximum ($\epsilon 1$) and minimum ($\epsilon 3$) principal strain values at the location of 70 landmarks during first incisor (I1) bite load for the 3 models of baboon species, and strain differences ($\Delta \epsilon 1$ and $\Delta \epsilon 3$) at landmark locations between models. Strain values are in microstrain (μ strain).

I1 bite landmark	P. anubis		P. hamadryas		T.gelada		P.anubis-P.hamadryas		P.anubis-T.gelada		P.hamadryas-T.gelada	
	$\epsilon 1$	$\epsilon 3$	$\epsilon 1$	$\epsilon 3$	$\epsilon 1$	$\epsilon 3$	$\Delta \epsilon 1$	$\Delta \epsilon 3$	$\Delta \epsilon 1$	$\Delta \epsilon 3$	$\Delta \epsilon 1$	$\Delta \epsilon 3$
1	136.04	-207.36	216.52	-238.07	646.29	-552.11	-80.48	30.70	-510.25	344.75	-429.77	314.05
2	410.20	-155.96	171.02	-133.07	208.52	-109.23	239.17	-22.89	201.68	-46.73	-37.49	-23.84
3	215.06	-63.33	32.15	-11.92	266.00	-96.64	182.91	-51.42	-50.94	33.31	-233.85	84.73
4	44.27	-284.71	59.86	-192.99	52.97	-235.65	-15.59	-91.72	-8.70	-49.07	6.89	42.66
5	5.39	-14.90	21.76	-8.05	59.08	-18.98	-16.37	-6.85	-53.69	4.08	-37.32	10.93
6	15.67	-31.19	8.67	-20.12	32.80	-99.76	7.00	-11.06	-17.13	68.58	-24.13	79.64
7	0.42	-0.80	0.03	-0.07	2.14	-0.85	0.40	-0.73	-1.71	0.05	-2.11	0.78
8	94.78	-54.09	156.41	-40.84	217.62	-70.22	-61.63	-13.26	-122.83	16.13	-61.21	29.38
9	189.49	-150.76	115.32	-109.74	153.01	-324.59	74.18	-41.02	36.48	173.83	-37.70	214.84
10	62.05	-20.13	44.90	-15.94	19.85	-14.72	17.15	-4.19	42.20	-5.41	25.05	-1.22
11	121.39	-281.97	82.57	-217.72	167.55	-489.47	38.82	-64.25	-46.16	207.50	-84.98	271.76
12	282.55	-85.58	383.44	-119.94	265.55	-158.28	-100.89	34.36	17.00	72.70	117.89	38.35
13	116.36	-33.56	167.97	-57.92	23.13	-51.89	-51.62	24.36	93.23	18.33	144.85	-6.03
14	91.96	-33.47	152.08	-40.13	222.93	-117.64	-60.12	6.66	-130.97	84.17	-70.85	77.52
15	85.85	-26.19	103.89	-34.93	149.83	-97.46	-18.04	8.74	-63.98	71.28	-45.94	62.54
16	62.78	-17.71	103.95	-26.63	110.40	-53.01	-41.17	8.92	-47.62	35.30	-6.45	26.38
17	38.53	-13.96	29.18	-9.24	102.17	-42.26	9.35	-4.72	-63.64	28.30	-72.99	33.02
18	186.20	-83.57	13.50	-12.79	161.90	-62.75	172.69	-70.78	24.29	-20.82	-148.40	49.96
19	49.76	-36.18	136.58	-49.21	44.85	-94.33	-86.82	13.03	4.91	58.15	91.73	45.12
20	49.52	-58.15	65.07	-77.33	0.79	-0.14	-15.55	19.17	48.73	-58.01	64.28	-77.18
21	254.42	-81.94	278.24	-85.70	295.63	-88.27	-23.82	3.76	-41.21	6.33	-17.39	2.57
22	170.16	-59.45	137.35	-75.52	224.28	-101.30	32.82	16.08	-54.12	41.85	-86.93	25.78
23	74.19	-227.96	61.08	-244.30	115.10	-377.12	13.11	16.35	-40.91	149.16	-54.03	132.82
24	161.83	-73.01	163.56	-67.95	125.98	-386.48	-1.73	-5.06	35.84	313.48	37.58	318.54
25	306.53	-897.05	192.00	-237.50	260.30	-265.86	114.52	-659.55	46.23	-631.19	-68.30	28.36
26	134.36	-324.32	876.44	-222.29	476.56	-203.76	-742.08	-102.03	-342.19	-120.56	399.88	-18.53
27	229.45	-205.44	355.07	-192.44	220.30	-391.01	-125.62	-13.00	9.15	185.57	134.78	198.57
28	149.01	-157.93	79.39	-105.77	342.56	-76.96	69.62	-52.17	-193.55	-80.97	-263.17	-28.80
29	22.32	-69.64	22.18	-55.51	37.35	-107.10	0.14	-14.13	-15.03	37.46	-15.17	51.59
30	8.83	-25.38	20.14	-54.56	39.68	-103.24	-11.31	29.19	-30.85	77.86	-19.54	48.68
31	10.26	-26.67	8.47	-6.75	44.71	-18.17	1.79	-19.92	-34.45	-8.50	-36.24	11.42
32	178.25	-572.73	266.89	-922.38	183.21	-647.35	-88.64	349.65	-4.96	74.62	83.68	-275.03
33	177.15	-163.96	65.02	-42.41	126.14	-42.46	112.13	-121.56	51.01	-121.51	-61.12	0.05
34	6.95	-29.98	34.52	-50.13	6.72	-17.70	-27.57	20.16	0.23	-12.28	27.80	-32.43
35	422.30	-122.53	576.40	-171.20	427.56	-134.12	-154.11	48.67	-5.26	11.59	148.84	-37.08
36	332.37	-1560.99	279.51	-376.18	161.31	-74.62	52.85	-1184.80	171.05	-1486.36	118.20	-301.56
37	4.34	-13.62	8.26	-4.37	13.83	-38.93	-3.92	-9.26	-9.49	25.30	-5.57	34.56
38	13.65	-17.62	32.08	-12.16	26.76	-8.52	-18.42	-5.46	-13.10	-9.10	5.32	-3.64
39	78.08	-285.35	64.60	-168.30	143.87	-501.44	13.49	-117.06	-65.79	216.09	-79.27	333.15
40	158.88	-70.02	382.78	-138.36	227.23	-59.49	-223.90	68.34	-68.34	-10.53	155.55	-78.87
41	70.79	-28.83	190.22	-130.02	127.80	-49.22	-119.42	101.18	-57.00	20.38	62.42	-80.80
42	62.62	-26.37	82.29	-61.68	128.08	-58.33	-19.67	35.31	-65.47	31.96	-45.80	-3.35
43	70.61	-22.47	70.75	-47.59	400.62	-97.65	-0.14	25.12	-330.01	75.18	-329.87	50.06
44	62.96	-16.58	120.46	-36.22	333.28	-85.83	-57.50	19.63	-270.32	69.25	-212.82	49.62
45	41.93	-19.15	31.19	-10.48	144.40	-47.59	10.74	-8.67	-102.47	28.44	-113.21	37.11
46	74.07	-23.00	24.00	-21.42	89.11	-42.87	50.07	-1.58	-15.03	19.88	-65.10	21.46
47	213.51	-71.66	44.24	-31.03	146.58	-36.38	169.26	-40.63	66.93	-35.28	-102.33	5.35
48	57.51	-204.22	52.05	-48.47	5.16	-13.32	5.46	-155.75	52.35	-190.90	46.89	-35.14
49	220.21	-75.27	237.24	-75.28	341.26	-108.51	-17.04	0.01	-121.05	33.24	-104.02	33.23
50	193.18	-57.31	110.35	-65.42	254.82	-89.60	82.83	8.12	-61.64	32.29	-144.47	24.18
51	75.57	-219.53	63.59	-187.97	124.96	-385.14	11.97	-31.56	-49.40	165.62	-61.37	197.17
52	155.52	-57.64	183.10	-84.42	211.00	-230.27	-27.59	26.78	-55.48	172.63	-27.89	145.85
53	195.80	-484.39	233.26	-464.55	270.84	-455.38	-37.47	-19.83	-75.04	-29.00	-37.57	-9.17
54	953.96	-361.44	651.00	-244.22	465.01	-225.92	302.96	-117.22	488.95	-135.52	185.99	-18.30
55	160.68	-164.09	249.32	-361.72	114.54	-222.35	-88.64	197.63	46.14	58.26	134.78	-139.37
56	121.21	-140.20	85.06	-149.06	149.94	-96.57	36.15	8.86	-28.73	-43.62	-64.88	-52.49
57	30.32	-58.56	18.48	-56.56	38.23	-124.15	11.84	-2.01	-7.91	65.59	-19.74	67.59
58	17.36	-58.38	9.00	-31.10	53.52	-111.50	8.36	-27.27	-36.16	53.12	-44.53	80.40
59	30.47	-40.65	6.56	-7.69	25.74	-8.83	23.91	-32.95	4.73	-31.82	-19.18	1.14
60	213.70	-739.71	289.86	-836.88	150.67	-462.22	-76.16	97.17	63.03	-277.49	139.19	-374.66
61	279.43	-121.60	42.86	-95.95	103.40	-52.50	236.58	-25.65	176.04	-69.10	-60.54	-43.44
62	8.59	-28.66	7.10	-10.30	4.22	-11.43	1.49	-18.36	4.37	-17.23	2.88	1.13
63	401.61	-139.42	452.56	-588.89	350.48	-188.64	-50.95	449.47	51.12	49.22	102.07	-400.25
64	267.53	-759.13	250.60	-633.77	282.42	-107.88	16.93	-125.36	-14.89	-651.25	-31.82	-525.89
65	71.42	-162.62	55.12	-140.42	209.70	-573.74	16.30	-22.20	-138.28	411.13	-154.59	433.33
66	324.68	-242.64	808.58	-168.48	248.95	-158.21	-483.90	-74.16	75.72	-84.44	559.62	-10.28
67	58.53	-51.05	36.33	-19.05	46.07	-178.52	22.20	-32.01	12.46	127.47	-9.74	159.48
68	43.02	-141.15	37.95	-85.65	184.64	-562.04	5.06	-55.50	-141.62	420.89	-146.68	476.40
69	381.66	-184.24	537.25	-150.55	225.95	-133.85	-155.59	-33.69	155.71	-50.39	311.30	-16.70
70	78.74	-44.02	66.83	-45.67	53.91	-117.58	11.91	1.65	24.83	73.56	12.92	71.91

Table E.9. Maximum ($\epsilon 1$) and minimum ($\epsilon 3$) principal strain values at the location of 70 landmarks during second incisor (I2) bite load for the 3 models of baboon species, and strain differences ($\Delta \epsilon 1$ and $\Delta \epsilon 3$) at landmark locations between models. Strain values are in microstrain (μ strain).

I2 bite landmark	P. anubis		P. hamadryas		T.gelada		P.anubis-P.hamadryas		P.anubis-T.gelada		P.hamadryas-T.gelada	
	$\epsilon 1$	$\epsilon 3$	$\epsilon 1$	$\epsilon 3$	$\epsilon 1$	$\epsilon 3$	$\Delta \epsilon 1$	$\Delta \epsilon 3$	$\Delta \epsilon 1$	$\Delta \epsilon 3$	$\Delta \epsilon 1$	$\Delta \epsilon 3$
1	76.02	-99.61	141.11	-207.56	147.64	-397.31	-65.08	107.95	-71.62	297.70	-6.54	189.74
2	346.34	-200.68	163.83	-177.47	273.62	-211.46	182.51	-23.21	72.72	10.77	-109.79	33.98
3	185.37	-58.21	29.75	-11.56	272.14	-100.94	155.63	-46.65	-86.77	42.73	-242.39	89.38
4	45.53	-281.51	60.10	-195.98	51.87	-231.54	-14.56	-85.53	-6.34	-49.97	8.22	35.56
5	5.32	-14.25	22.03	-8.33	59.19	-19.01	-16.70	-5.92	-53.87	4.76	-37.16	10.68
6	15.79	-31.60	8.45	-19.87	33.28	-101.32	7.34	-11.72	-17.49	69.72	-24.83	81.44
7	0.43	-0.82	0.04	-0.06	2.17	-0.88	0.39	-0.76	-1.74	0.05	-2.13	0.82
8	98.18	-54.16	153.49	-40.64	218.27	-71.04	-55.31	-13.52	-120.09	16.87	-64.78	30.39
9	191.45	-150.03	117.19	-113.29	160.63	-337.63	74.25	-36.75	30.82	187.59	-43.44	224.34
10	68.09	-19.81	49.90	-17.71	23.75	-15.70	18.19	-2.10	44.35	-4.12	26.15	-2.01
11	111.76	-253.36	84.82	-225.00	184.50	-547.32	26.93	-28.36	-72.74	293.96	-99.68	322.32
12	306.89	-172.75	424.57	-156.60	797.07	-523.21	-117.68	-16.15	-490.19	350.46	-372.50	366.61
13	144.44	-43.78	204.83	-66.36	12.79	-33.16	-60.38	22.58	131.65	-10.62	192.04	-33.20
14	112.05	-40.78	171.88	-46.65	222.47	-122.54	-59.83	5.86	-110.42	81.76	-50.59	75.89
15	107.67	-36.95	105.10	-41.69	160.55	-105.55	2.57	4.74	-52.88	68.60	-55.45	63.86
16	64.34	-17.92	103.46	-26.07	51.77	-35.72	-39.12	8.15	12.57	17.80	51.69	9.65
17	31.27	-8.86	30.94	-8.46	96.08	-42.40	0.34	-0.40	-64.80	33.55	-65.14	33.95
18	213.23	-95.48	15.41	-13.95	196.05	-76.23	197.82	-81.53	17.18	-19.25	-180.63	62.28
19	48.11	-24.81	128.46	-48.78	47.63	-113.45	-80.35	23.97	0.48	88.64	80.83	64.67
20	48.39	-56.22	64.63	-76.75	0.73	-0.14	-16.24	20.53	47.66	-56.07	63.90	-76.60
21	268.92	-83.72	297.25	-91.80	310.33	-92.77	-28.34	8.09	-41.42	9.05	-13.08	0.96
22	145.83	-53.71	105.37	-68.90	181.80	-90.14	40.46	15.18	-35.96	36.43	-76.42	21.25
23	75.86	-230.37	55.93	-239.78	118.82	-388.54	19.93	9.41	-42.96	158.16	-62.89	148.76
24	124.72	-84.15	120.02	-57.64	188.81	-581.47	4.70	-26.52	-64.09	497.32	-68.79	523.84
25	307.49	-905.93	194.87	-245.10	264.10	-272.91	112.62	-660.83	43.39	-633.02	-69.22	27.82
26	131.16	-317.64	891.27	-224.66	501.67	-212.33	-760.11	-92.97	-370.51	-105.30	389.60	-12.33
27	229.09	-209.58	354.60	-193.02	223.50	-405.38	-125.51	-16.56	5.59	195.80	131.10	212.36
28	160.05	-168.21	92.60	-112.13	367.77	-81.13	67.45	-56.08	-207.71	-87.09	-275.16	-31.00
29	21.57	-67.53	21.66	-53.27	36.86	-105.85	-0.09	-14.26	-15.29	38.32	-15.20	52.58
30	7.45	-21.32	17.81	-47.80	38.30	-98.67	-10.36	26.48	-30.85	77.34	-20.49	50.86
31	11.92	-21.98	4.89	-12.55	25.01	-12.70	7.02	-9.43	-13.10	-9.28	-20.12	0.14
32	178.58	-574.04	266.80	-921.90	184.39	-651.78	-88.22	347.86	-5.81	77.74	82.41	-270.12
33	171.90	-166.55	60.05	-44.26	101.60	-36.78	111.84	-122.29	70.30	-129.77	-41.54	-7.48
34	6.83	-29.45	34.33	-50.07	6.72	-17.69	-27.49	20.63	0.12	-11.75	27.61	-32.38
35	421.09	-121.77	576.56	-171.23	426.10	-131.93	-155.47	49.46	-5.01	10.16	150.46	-39.30
36	330.98	-1547.82	273.82	-367.98	155.48	-64.63	57.16	-1179.84	175.50	-1483.19	118.35	-303.35
37	4.21	-13.51	8.26	-4.39	13.97	-38.42	-4.05	-9.12	-9.76	24.91	-5.71	34.03
38	13.20	-22.48	27.41	-10.62	22.44	-8.30	-14.21	-11.86	-9.25	-14.18	4.96	-2.32
39	57.93	-214.93	48.29	-128.44	116.57	-407.60	9.64	-86.50	-58.65	192.66	-68.29	279.16
40	124.82	-58.96	299.67	-107.14	241.29	-72.36	-174.86	48.18	-116.47	13.41	58.39	-34.77
41	48.13	-21.19	129.13	-89.73	268.20	-41.23	-81.00	68.53	-220.06	20.04	-139.06	-48.49
42	47.58	-23.27	58.80	-52.53	123.71	-61.47	-11.22	29.26	-76.13	38.20	-64.91	8.94
43	54.04	-26.00	62.83	-43.86	349.71	-87.06	-8.79	17.86	-295.67	61.06	-286.88	43.20
44	61.91	-18.74	113.84	-33.72	409.61	-97.19	-51.93	14.98	-347.70	78.45	-295.77	63.47
45	41.26	-20.99	25.92	-10.32	152.04	-48.15	15.34	-10.66	-110.78	27.16	-126.13	37.82
46	62.46	-19.75	20.10	-18.98	62.40	-30.01	42.35	-0.78	0.06	10.25	-42.29	11.03
47	214.45	-79.76	38.67	-27.77	169.13	-40.76	175.78	-51.99	45.32	-39.00	-130.47	12.99
48	58.85	-208.78	53.07	-49.42	5.49	-14.19	5.78	-159.36	53.37	-194.59	47.59	-35.23
49	206.83	-71.95	213.24	-71.46	331.08	-105.17	-6.41	-0.49	-124.25	33.22	-117.84	33.71
50	211.29	-62.29	138.74	-66.84	276.13	-96.76	72.55	4.55	-64.84	34.47	-137.39	29.92
51	72.32	-213.75	63.20	-188.33	121.60	-372.06	9.13	-25.42	-49.27	158.30	-58.40	183.73
52	148.24	-53.27	277.08	-75.07	250.05	-147.65	-128.85	21.80	-101.81	94.37	27.03	72.58
53	195.27	-477.14	231.32	-454.38	264.36	-432.23	-36.05	-22.76	-69.09	-44.91	-33.04	-22.15
54	941.08	-361.30	647.84	-249.41	444.13	-224.23	293.25	-111.90	496.96	-137.07	203.71	-25.17
55	160.95	-162.36	249.06	-358.43	111.18	-216.52	-88.10	196.07	49.77	54.16	137.88	-141.91
56	108.02	-125.75	74.58	-131.57	138.81	-78.82	33.44	5.82	-30.78	-46.93	-64.22	-52.75
57	30.06	-57.79	19.44	-59.74	37.99	-123.68	10.62	1.95	-7.93	65.89	-18.55	63.94
58	18.08	-61.06	10.50	-36.08	54.70	-115.08	7.59	-24.98	-36.61	54.01	-44.20	78.99
59	39.43	-43.55	18.72	-8.87	45.59	-15.10	20.72	-34.69	-6.16	-28.45	-26.88	6.23
60	214.53	-742.31	288.94	-833.87	145.71	-445.86	-74.41	91.55	68.81	-296.45	143.23	-388.00
61	290.27	-123.68	41.51	-89.80	117.51	-52.86	248.76	-33.88	172.75	-70.82	-76.01	-36.94
62	8.66	-28.87	7.04	-10.17	4.10	-11.17	1.62	-18.70	4.56	-17.70	2.94	1.00
63	401.34	-139.72	454.03	-590.13	345.79	-186.96	-52.70	450.41	55.55	47.24	108.25	-403.17
64	269.85	-766.71	256.02	-649.89	285.14	-112.32	13.83	-116.82	-15.28	-654.39	-29.11	-537.57
65	75.39	-167.99	58.50	-137.72	223.38	-612.74	16.89	-30.27	-148.00	444.76	-164.89	475.02
66	342.44	-261.05	844.24	-180.57	274.91	-193.37	-501.80	-80.48	67.54	-67.68	569.33	12.80
67	43.82	-67.91	36.68	-44.88	131.93	-285.57	7.14	-23.03	-88.12	217.67	-95.25	240.70
68	36.00	-113.76	32.65	-77.43	159.67	-486.77	3.35	-36.34	-123.67	373.00	-127.02	409.34
69	362.99	-172.34	512.37	-147.20	205.31	-107.54	-149.38	-25.14	157.67	-64.79	307.05	-39.65
70	75.23	-35.66	97.31	-53.03	63.28	-156.18	-22.07	17.36	11.95	120.52	34.02	103.16

Table E.10. Maximum ($\epsilon 1$) and minimum ($\epsilon 3$) principal strain values at the location of 70 landmarks during first premolar (P3) bite load for the 3 models of baboon species, and strain differences ($\Delta \epsilon 1$ and $\Delta \epsilon 3$) at landmark locations between models. Strain values are in microstrain (μ strain).

P3 bite landmark	P. anubis		P. hamadryas		T.gelada		P.anubis-P.hamadryas		P.anubis-T.gelada		P.hamadryas-T.gelada	
	$\epsilon 1$	$\epsilon 3$	$\epsilon 1$	$\epsilon 3$	$\epsilon 1$	$\epsilon 3$	$\Delta \epsilon 1$	$\Delta \epsilon 3$	$\Delta \epsilon 1$	$\Delta \epsilon 3$	$\Delta \epsilon 1$	$\Delta \epsilon 3$
1	17.80	-18.65	5.93	-19.34	24.92	-37.60	11.87	0.69	-7.12	18.95	-18.99	18.26
2	28.66	-31.80	16.38	-49.16	73.76	-147.59	12.28	17.36	-45.10	115.79	-57.38	98.43
3	64.45	-47.61	11.16	-6.86	232.67	-90.58	53.30	-40.75	-168.21	42.97	-221.51	83.72
4	47.77	-255.96	56.35	-196.44	44.21	-197.99	-8.58	-59.52	3.56	-57.97	12.15	1.55
5	4.77	-10.30	23.99	-8.99	55.72	-18.02	-19.22	-1.31	-50.94	7.72	-31.73	9.03
6	16.60	-33.23	8.80	-20.68	35.72	-109.04	7.80	-12.55	-19.12	75.81	-26.92	88.36
7	0.50	-0.97	0.03	-0.06	3.38	-1.38	0.47	-0.91	-2.88	0.41	-3.35	1.31
8	105.02	-49.56	134.11	-37.80	199.47	-68.40	-29.09	-11.76	-94.45	18.84	-65.36	30.60
9	197.96	-152.86	121.10	-119.24	190.23	-351.20	76.86	-33.62	7.73	198.35	-69.13	231.97
10	88.88	-24.38	60.66	-21.54	34.46	-19.52	28.21	-2.84	54.42	-4.85	26.20	-2.01
11	79.54	-30.43	38.66	-21.17	73.16	-209.72	40.87	-9.26	6.37	179.29	-34.50	188.55
12	8.04	-21.73	15.57	-21.34	48.73	-44.97	-7.53	-0.39	-40.69	23.24	-33.16	23.63
13	81.84	-82.11	172.72	-339.96	246.69	-658.09	-90.88	257.85	-164.85	575.98	-73.97	318.13
14	113.01	-203.90	195.72	-165.79	423.89	-966.92	-82.71	-38.11	-310.89	763.02	-228.18	801.13
15	138.72	-119.71	115.44	-180.21	322.15	-459.34	23.29	60.51	-183.43	339.63	-206.72	279.13
16	94.53	-98.21	89.02	-103.97	66.61	-244.02	5.51	5.76	27.91	145.82	22.41	140.05
17	33.43	-46.35	24.79	-11.30	54.81	-71.97	8.64	-35.05	-21.38	25.62	-30.02	60.67
18	228.50	-102.44	17.33	-14.01	236.48	-92.54	211.17	-88.42	-7.98	-9.90	-219.15	78.52
19	92.00	-37.68	84.39	-60.47	62.25	-140.55	7.61	22.79	29.75	102.87	22.15	80.08
20	44.93	-49.30	63.50	-74.63	0.55	-0.16	-18.57	25.33	44.38	-49.14	62.95	-74.47
21	305.78	-95.03	337.34	-104.86	359.58	-108.33	-31.56	9.84	-53.81	13.30	-22.24	3.46
22	83.02	-42.42	43.03	-73.01	87.29	-70.59	39.99	30.59	-4.27	28.17	-44.26	-2.42
23	77.11	-230.96	42.88	-211.15	123.35	-403.06	34.23	-19.81	-46.24	172.10	-80.47	191.90
24	48.80	-105.05	34.33	-72.57	262.76	-801.91	14.47	-32.48	-213.96	696.87	-228.44	729.34
25	307.14	-920.00	204.47	-270.73	277.64	-289.48	102.67	-649.27	29.50	-630.52	-73.17	18.75
26	121.56	-297.42	936.66	-236.44	576.89	-238.89	-815.10	-60.98	-455.33	-58.52	359.77	2.46
27	226.43	-221.76	351.77	-193.72	231.35	-448.01	-125.34	-28.04	-4.92	226.25	120.42	254.30
28	177.34	-163.95	153.03	-113.69	411.10	-86.08	24.30	-50.26	-233.76	-77.87	-258.06	-27.61
29	19.16	-60.45	19.11	-44.18	34.31	-98.78	0.05	-16.26	-15.15	38.34	-15.20	54.60
30	4.29	-9.49	10.40	-26.87	32.62	-80.10	-6.10	17.38	-28.33	70.61	-22.23	53.23
31	19.24	-34.03	14.00	-43.69	12.33	-34.70	5.24	9.66	6.91	0.67	1.68	-8.99
32	178.55	-574.46	265.85	-918.29	185.44	-656.35	-87.31	343.82	-6.89	81.88	80.42	-261.94
33	158.09	-175.33	52.13	-55.27	47.79	-37.95	105.96	-120.05	110.30	-137.37	4.35	-17.32
34	5.92	-25.51	33.33	-49.47	6.13	-15.91	-27.41	23.96	-0.20	-9.60	27.20	-33.56
35	415.35	-119.17	572.21	-169.68	414.50	-125.60	-156.86	50.51	0.86	6.43	157.71	-44.08
36	330.86	-1515.98	258.63	-345.82	143.07	-38.22	72.22	-1170.16	187.79	-1477.76	115.57	-307.60
37	3.37	-11.75	9.41	-4.99	13.88	-29.89	-6.04	-6.76	-10.51	18.14	-4.47	24.90
38	14.46	-35.47	17.07	-7.81	12.59	-11.06	-2.60	-27.66	1.87	-24.41	4.47	3.25
39	20.11	-69.51	17.76	-41.92	37.21	-128.30	2.36	-27.58	-17.10	58.79	-19.46	86.37
40	39.39	-16.00	59.34	-19.10	81.12	-21.51	-19.95	3.10	-41.73	5.51	-21.78	2.41
41	13.33	-6.60	12.43	-8.33	236.85	-75.35	0.90	1.72	-223.52	68.74	-224.42	67.02
42	19.11	-11.85	10.51	-17.26	50.53	-38.78	8.60	5.41	-31.42	26.92	-40.02	21.52
43	26.96	-17.11	19.60	-13.69	108.15	-36.04	7.36	-3.42	-81.19	18.93	-88.55	22.35
44	37.48	-13.29	44.95	-13.16	289.04	-61.07	-7.46	-0.13	-251.56	47.78	-244.09	47.90
45	25.22	-17.44	10.51	-8.49	99.21	-28.92	14.71	-8.95	-73.99	11.48	-88.70	20.43
46	40.44	-13.17	13.04	-13.26	12.46	-5.99	27.40	0.09	27.99	-7.18	0.58	-7.27
47	206.75	-100.39	33.32	-25.70	192.07	-45.16	173.44	-74.70	14.69	-55.24	-158.75	19.46
48	59.97	-212.74	54.01	-49.91	5.84	-15.11	5.96	-162.83	54.14	-197.63	48.17	-34.80
49	175.31	-63.98	166.05	-62.96	280.86	-89.48	9.26	-1.02	-105.55	25.50	-114.82	26.53
50	239.87	-69.99	194.15	-71.14	309.20	-108.51	45.72	1.16	-69.33	38.52	-115.05	37.36
51	55.84	-176.33	55.74	-161.48	99.35	-292.82	0.10	-14.86	-43.51	116.49	-43.61	131.35
52	72.69	-32.45	304.17	-88.86	311.10	-117.41	-231.48	56.42	-238.41	84.96	-6.93	28.55
53	191.70	-466.44	232.25	-454.39	259.98	-415.41	-40.55	-12.05	-68.29	-51.03	-27.74	-38.98
54	927.36	-362.28	645.47	-253.73	425.95	-222.53	281.89	-108.55	501.40	-139.75	219.52	-31.20
55	159.03	-160.00	248.00	-356.12	109.00	-206.69	-88.97	196.11	50.03	46.69	139.00	-149.43
56	87.23	-96.17	50.41	-93.10	110.90	-44.72	36.82	-3.08	-23.67	-51.45	-60.49	-48.38
57	28.19	-53.34	20.83	-63.02	33.85	-110.51	7.36	9.68	-5.66	57.17	-13.02	47.49
58	19.24	-64.85	13.00	-44.27	52.18	-114.38	6.24	-20.59	-32.94	49.53	-39.18	70.11
59	59.56	-45.83	48.84	-17.46	91.93	-30.13	10.71	-28.37	-32.37	-15.70	-43.08	12.68
60	215.12	-743.98	285.48	-823.05	135.23	-409.95	-70.36	79.07	79.89	-334.02	150.25	-413.10
61	304.85	-126.34	39.93	-82.00	139.67	-54.32	264.93	-44.34	165.18	-72.01	-99.74	-27.67
62	8.10	-26.98	6.84	-9.88	3.35	-9.14	1.26	-17.10	4.75	-17.83	3.49	-0.73
63	397.60	-139.34	453.73	-588.50	329.22	-180.21	-56.13	449.16	68.38	40.88	124.51	-408.28
64	274.42	-779.13	263.39	-671.58	288.86	-119.34	11.03	-107.55	-14.44	-659.79	-25.48	-552.24
65	59.41	-73.39	43.74	-31.47	170.98	-530.47	15.67	-41.92	-111.57	457.08	-127.24	499.00
66	385.15	-309.25	922.53	-210.75	333.81	-289.24	-537.38	-98.50	51.34	-28.00	588.72	78.50
67	156.23	-300.98	173.72	-247.07	360.85	-539.38	-17.50	-53.91	-204.63	230.40	-187.13	292.31
68	24.98	-68.12	17.40	-47.32	90.40	-271.88	7.58	-20.80	-65.42	203.76	-73.00	224.56
69	330.35	-152.62	471.79	-141.02	169.17	-73.68	-141.44	-11.60	161.19	-78.94	302.62	-67.34
70	44.82	-20.07	78.85	-37.48	136.65	-157.82	-34.03	17.40	-91.83	137.74	-57.80	120.34

Table E.11. Maximum ($\epsilon 1$) and minimum ($\epsilon 3$) principal strain values at the location of 70 landmarks during second premolar (P4) bite load for the 3 models of baboon species, and strain differences ($\Delta \epsilon 1$ and $\Delta \epsilon 3$) at landmark locations between models. Strain values are in microstrain (μstrain).

P4 bite landmark	P. anubis		P. hamadryas		T.gelada		P.anubis-P.hamadryas		P.anubis-T.gelada		P.hamadryas-T.gelada	
	$\epsilon 1$	$\epsilon 3$	$\epsilon 1$	$\epsilon 3$	$\epsilon 1$	$\epsilon 3$	$\Delta \epsilon 1$	$\Delta \epsilon 3$	$\Delta \epsilon 1$	$\Delta \epsilon 3$	$\Delta \epsilon 1$	$\Delta \epsilon 3$
1	13.13	-15.04	4.52	-13.25	18.07	-31.83	8.61	-1.79	-4.94	16.79	-13.55	18.58
2	16.13	-29.63	13.62	-39.11	55.65	-136.71	2.51	9.48	-39.53	107.08	-42.03	97.60
3	52.89	-49.08	8.35	-6.18	216.65	-85.15	44.54	-42.90	-163.76	36.07	-208.29	78.97
4	48.03	-245.63	55.51	-195.76	42.09	-188.24	-7.48	-49.87	5.93	-57.39	13.41	-7.52
5	4.50	-8.77	24.67	-9.15	54.81	-17.79	-20.17	0.38	-50.31	9.02	-30.14	8.64
6	16.86	-33.65	8.96	-21.01	36.39	-111.16	7.91	-12.65	-19.53	77.50	-27.43	90.15
7	0.52	-1.02	0.04	-0.05	3.72	-1.52	0.48	-0.97	-3.20	0.50	-3.68	1.47
8	105.79	-47.51	128.72	-36.95	194.83	-68.22	-22.93	-10.56	-89.03	20.71	-66.10	31.26
9	196.38	-148.43	120.00	-116.67	197.41	-335.68	76.37	-31.76	-1.03	187.26	-77.41	219.02
10	94.67	-26.08	63.03	-22.38	37.57	-20.79	31.65	-3.69	57.11	-5.29	25.46	-1.60
11	73.80	-28.88	55.16	-24.42	58.11	-142.49	18.64	-4.46	15.69	113.61	-2.95	118.07
12	7.86	-24.94	8.49	-13.92	42.27	-38.65	-0.64	-11.02	-34.41	13.71	-33.77	24.73
13	54.30	-47.26	90.69	-174.50	50.70	-116.72	-36.39	127.24	3.60	69.46	39.99	-57.78
14	102.21	-183.71	152.17	-420.90	291.26	-399.59	-49.95	237.19	-189.04	215.88	-139.09	-21.31
15	139.30	-261.89	168.80	-309.05	308.18	-1197.92	-29.50	47.16	-168.88	936.03	-139.38	888.87
16	120.69	-140.33	109.04	-143.83	104.33	-373.43	11.64	3.50	16.35	233.10	4.71	229.60
17	48.17	-71.24	33.47	-21.47	63.47	-109.82	14.70	-49.77	-15.30	38.58	-30.00	88.35
18	215.48	-96.45	17.43	-13.52	245.34	-96.23	198.05	-82.93	-29.87	-0.22	-227.91	82.71
19	109.13	-45.47	73.03	-66.96	68.10	-145.97	36.09	21.49	41.02	100.51	4.93	79.02
20	44.09	-47.42	63.25	-74.08	0.54	-0.18	-19.17	26.66	43.54	-47.25	62.71	-73.91
21	314.14	-98.40	346.59	-107.87	372.26	-112.39	-32.45	9.47	-58.11	13.99	-25.66	4.52
22	70.67	-41.61	36.91	-82.12	66.87	-70.85	33.76	40.50	3.80	29.24	-29.96	-11.27
23	76.83	-230.56	41.46	-202.10	124.28	-406.41	35.37	-28.46	-47.45	175.85	-82.82	204.31
24	41.44	-99.15	30.48	-72.45	261.73	-797.17	10.95	-26.70	-220.29	698.02	-231.24	724.71
25	306.42	-920.24	206.39	-276.06	281.55	-293.63	100.03	-644.18	24.88	-626.60	-75.16	17.58
26	119.49	-293.05	946.82	-239.42	597.43	-246.28	-827.33	-53.63	-477.93	-46.77	349.40	6.86
27	225.65	-224.41	351.07	-193.78	233.50	-459.44	-125.42	-30.63	-7.85	235.03	117.57	265.67
28	178.49	-154.50	174.28	-114.11	418.43	-86.45	4.21	-40.39	-239.94	-68.05	-244.15	-27.66
29	18.61	-58.79	18.40	-41.77	33.54	-96.60	0.21	-17.02	-14.93	37.81	-15.13	54.83
30	4.54	-7.25	8.53	-21.67	31.09	-74.71	-3.99	14.42	-26.55	67.46	-22.56	53.03
31	20.59	-40.57	15.95	-50.22	15.41	-47.62	4.64	9.64	5.17	7.04	0.53	-2.60
32	178.43	-574.16	265.67	-917.60	185.68	-657.42	-87.24	343.45	-7.25	83.26	79.99	-260.19
33	155.33	-177.69	51.55	-58.76	41.59	-46.47	103.78	-118.93	113.74	-131.22	9.96	-12.29
34	5.60	-24.12	33.03	-49.24	6.00	-15.43	-27.43	25.11	-0.40	-8.69	27.03	-33.81
35	413.89	-118.59	570.93	-169.23	411.54	-124.46	-157.05	50.64	2.35	5.87	159.39	-44.77
36	331.62	-1510.01	255.46	-341.17	140.54	-31.50	76.16	-1168.84	191.08	-1478.51	114.92	-309.68
37	3.71	-11.20	9.77	-5.17	14.29	-27.88	-6.06	-6.03	-10.58	16.68	-4.52	22.71
38	14.78	-37.75	15.35	-7.55	11.26	-13.05	-0.56	-30.20	3.53	-24.70	4.09	5.50
39	17.64	-59.82	16.40	-37.94	29.63	-100.66	1.24	-21.87	-11.99	40.84	-13.23	62.72
40	31.81	-12.50	45.41	-16.42	72.51	-18.52	-13.59	3.91	-40.69	6.02	-27.10	2.10
41	10.30	-5.20	6.57	-5.93	214.57	-74.14	3.74	0.74	-204.27	68.94	-208.01	68.20
42	14.22	-9.22	6.81	-13.82	40.67	-34.95	7.41	4.60	-26.45	25.73	-33.86	21.13
43	21.00	-13.60	13.78	-10.10	79.00	-37.28	7.22	-3.50	-58.00	23.68	-65.22	27.18
44	30.13	-11.30	34.56	-10.18	249.43	-51.05	-4.44	-1.12	-219.30	39.75	-214.86	40.87
45	21.22	-16.63	9.05	-8.77	87.11	-24.78	12.17	-7.85	-65.89	8.15	-78.07	16.01
46	37.84	-12.24	12.23	-12.35	6.78	-3.35	25.62	0.10	31.06	-8.89	5.45	-9.00
47	199.85	-103.07	32.57	-28.08	192.07	-46.19	167.28	-75.00	7.78	-56.88	-159.50	18.11
48	59.76	-212.07	53.99	-49.76	5.89	-15.27	5.76	-162.31	53.87	-196.79	48.10	-34.49
49	169.92	-62.22	159.30	-61.40	264.98	-84.50	10.62	-0.82	-95.06	22.29	-105.68	23.10
50	241.29	-70.28	202.40	-71.47	314.57	-110.61	38.89	1.20	-73.28	40.34	-112.17	39.14
51	50.00	-161.94	54.16	-150.38	92.35	-267.72	-4.16	-11.56	-42.35	105.78	-38.19	117.34
52	63.69	-31.90	290.84	-86.66	307.64	-117.14	-227.15	54.76	-243.95	85.24	-16.80	30.48
53	190.45	-466.35	233.40	-458.86	260.30	-415.96	-42.96	-7.50	-69.85	-50.39	-26.89	-42.90
54	929.33	-362.73	645.86	-253.11	424.37	-222.13	283.48	-109.62	504.96	-140.60	221.49	-30.98
55	158.03	-160.12	247.73	-356.61	109.01	-204.56	-89.69	196.49	49.02	44.44	138.71	-152.05
56	86.08	-92.66	47.17	-90.98	105.05	-39.74	38.91	-1.68	-18.97	-52.92	-57.87	-51.24
57	27.51	-51.82	20.99	-63.13	32.41	-105.91	6.52	11.32	-4.90	54.10	-11.42	42.78
58	19.29	-64.88	13.38	-45.48	51.08	-113.38	5.91	-19.40	-31.79	48.50	-37.70	67.90
59	62.95	-45.00	53.80	-19.00	102.68	-33.64	9.15	-26.00	-39.73	-11.37	-48.88	14.63
60	214.89	-743.19	284.62	-820.34	132.71	-401.15	-69.73	77.15	82.18	-342.05	151.90	-419.20
61	304.17	-126.04	39.77	-81.54	144.14	-54.70	264.41	-44.50	160.03	-71.35	-104.37	-26.84
62	7.82	-26.07	6.81	-9.84	3.15	-8.60	1.01	-16.23	4.67	-17.46	3.66	-1.23
63	396.11	-138.97	452.84	-587.41	324.54	-178.23	-56.72	448.44	71.57	39.25	128.29	-409.18
64	274.84	-779.42	263.96	-673.22	289.55	-120.80	10.89	-106.20	-14.71	-658.62	-25.60	-552.43
65	56.80	-35.60	43.09	-16.04	145.21	-479.42	13.72	-19.56	-88.41	443.82	-102.12	463.38
66	393.03	-319.72	936.05	-217.15	348.71	-318.42	-543.01	-102.57	44.32	-1.30	587.34	101.26
67	139.01	-286.24	163.13	-255.61	295.75	-509.72	-24.12	-30.62	-156.74	223.48	-132.62	254.11
68	24.01	-69.72	16.29	-46.69	82.76	-243.30	7.72	-23.04	-58.75	173.58	-66.47	196.62
69	327.55	-150.82	467.65	-140.26	162.16	-68.57	-140.10	-10.56	165.39	-82.25	305.49	-71.69
70	44.48	-20.58	76.18	-36.56	141.48	-155.76	-31.70	15.98	-97.00	135.18	-65.30	119.20

Table E.12. Maximum ($\epsilon 1$) and minimum ($\epsilon 3$) principal strain values at the location of 70 landmarks during first molar (M1) bite load for the 3 models of baboon species, and strain differences ($\Delta \epsilon 1$ and $\Delta \epsilon 3$) at landmark locations between models. Strain values are in microstrain (μ strain).

M1 bite landmark	P. anubis		P. hamadryas		T.gelada		P.anubis-P.hamadryas		P.anubis-T.gelada		P.hamadryas-T.gelada	
	$\epsilon 1$	$\epsilon 3$	$\epsilon 1$	$\epsilon 3$	$\epsilon 1$	$\epsilon 3$	$\Delta \epsilon 1$	$\Delta \epsilon 3$	$\Delta \epsilon 1$	$\Delta \epsilon 3$	$\Delta \epsilon 1$	$\Delta \epsilon 3$
1	10.21	-12.10	3.77	-3.18	3.30	-9.60	6.45	-8.92	6.92	-2.50	0.47	6.42
2	22.34	-8.75	6.46	-6.32	11.12	-30.54	15.88	-2.43	11.22	21.78	-4.67	24.22
3	47.81	-43.46	7.28	-5.51	186.56	-72.97	40.53	-37.96	-138.74	29.50	-179.28	67.46
4	46.97	-231.97	52.51	-183.65	37.92	-168.81	-5.54	-48.33	9.05	-63.16	14.59	-14.84
5	4.22	-7.09	25.11	-9.22	52.95	-17.22	-20.90	2.13	-48.73	10.13	-27.83	8.00
6	17.12	-34.03	9.17	-21.68	37.36	-114.16	7.95	-12.35	-20.23	80.12	-28.18	92.47
7	0.54	-1.06	0.03	-0.05	4.46	-1.81	0.50	-1.01	-3.92	0.75	-4.42	1.76
8	103.59	-44.45	118.89	-35.07	181.47	-65.45	-15.30	-9.38	-77.88	21.00	-62.58	30.38
9	193.29	-139.81	114.04	-112.86	188.66	-303.31	79.25	-26.94	4.63	163.50	-74.62	190.44
10	98.84	-27.24	63.48	-22.57	39.79	-22.06	35.37	-4.67	59.05	-5.18	23.68	-0.51
11	65.10	-25.99	66.22	-26.66	48.75	-26.86	-1.11	0.67	16.35	0.86	17.47	0.20
12	12.58	-38.59	11.11	-14.65	2.34	-4.48	1.46	-23.95	10.23	-34.12	8.77	-10.17
13	15.51	-13.45	24.70	-18.83	21.30	-41.49	-9.19	5.38	-5.79	28.04	3.40	22.65
14	34.39	-39.74	18.61	-14.85	98.45	-60.77	15.79	-24.89	-64.06	21.03	-79.84	45.92
15	56.50	-71.03	32.81	-49.16	132.15	-79.95	23.69	-21.87	-75.65	8.91	-99.34	30.78
16	102.71	-126.60	60.05	-97.55	65.29	-247.18	42.65	-29.05	37.42	120.58	-5.23	149.63
17	44.57	-73.54	21.15	-25.09	53.59	-107.81	23.42	-48.45	-9.02	34.27	-32.44	82.72
18	160.29	-72.17	11.76	-10.10	187.22	-72.89	148.53	-62.07	-26.92	0.73	-175.45	62.79
19	121.74	-53.13	59.40	-75.58	78.87	-155.23	62.34	22.45	42.87	102.10	-19.47	79.66
20	43.51	-45.79	63.13	-73.50	0.54	-0.19	-19.62	27.71	42.97	-45.61	62.59	-73.32
21	322.87	-101.70	355.22	-110.70	402.15	-121.96	-32.35	9.00	-79.28	20.26	-46.93	11.26
22	67.40	-42.65	38.27	-86.11	62.62	-72.79	29.12	43.47	4.78	30.14	-24.34	-13.33
23	75.70	-228.91	39.94	-189.58	122.86	-402.91	35.76	-39.33	-47.16	173.99	-82.92	213.33
24	38.35	-77.05	25.35	-43.71	198.83	-604.91	13.00	-33.34	-160.48	527.86	-173.48	561.19
25	305.33	-916.87	205.07	-271.99	282.14	-290.67	100.26	-644.89	23.18	-626.20	-77.07	18.69
26	118.78	-291.34	948.32	-240.01	606.46	-249.77	-829.54	-51.33	-487.69	-41.56	341.86	9.77
27	224.99	-225.51	350.63	-193.74	234.15	-465.30	-125.65	-31.77	-9.16	239.79	116.48	271.56
28	177.03	-140.24	193.68	-112.57	428.07	-86.71	-16.65	-27.67	-251.04	-53.53	-234.39	-25.86
29	18.38	-58.01	17.88	-40.34	33.22	-95.65	0.50	-17.68	-14.83	37.64	-15.33	55.32
30	5.35	-5.87	7.51	-19.12	29.31	-68.18	-2.16	13.25	-23.96	62.30	-21.80	49.06
31	20.38	-42.53	14.79	-46.87	15.48	-48.64	5.59	4.34	4.91	6.11	-0.69	1.77
32	178.27	-573.62	265.81	-918.14	185.35	-656.37	-87.54	344.52	-7.08	82.75	80.46	-261.77
33	154.17	-178.95	51.52	-60.27	40.16	-51.94	102.65	-118.68	114.01	-127.00	11.36	-8.32
34	5.20	-22.44	32.64	-48.87	5.65	-14.24	-27.44	26.44	-0.44	-8.20	27.00	-34.63
35	412.93	-118.30	570.42	-169.04	407.86	-123.33	-157.49	50.74	5.07	5.03	162.56	-45.71
36	333.41	-1509.02	254.56	-339.82	139.60	-28.83	78.85	-1169.20	193.81	-1480.19	114.96	-310.99
37	4.10	-10.27	10.30	-5.44	14.77	-23.60	-6.20	-4.83	-10.68	13.33	-4.48	18.17
38	14.65	-38.00	15.38	-7.45	9.99	-14.34	-0.73	-30.55	4.67	-23.67	5.40	6.88
39	15.67	-54.01	14.57	-35.33	21.93	-73.66	1.10	-18.68	-6.26	19.64	-7.36	38.32
40	21.51	-8.73	22.42	-9.04	19.51	-8.24	-0.91	0.31	2.00	-0.49	2.91	-0.80
41	7.69	-4.38	4.06	-4.32	111.86	-39.29	3.63	-0.06	-104.17	34.91	-107.80	34.97
42	10.98	-5.89	4.25	-6.11	19.06	-20.21	6.73	0.21	-8.08	14.31	-14.81	14.10
43	17.68	-8.11	6.04	-3.98	35.68	-27.43	11.64	-4.13	-18.00	19.32	-29.64	23.45
44	21.60	-8.30	20.15	-6.06	140.04	-27.32	1.46	-2.24	-118.44	19.02	-119.90	21.26
45	16.93	-15.55	7.47	-9.39	59.34	-16.32	9.45	-6.15	-42.41	0.78	-51.87	6.93
46	37.18	-11.79	11.90	-11.67	9.62	-4.79	25.28	-0.12	27.56	-7.00	2.28	-6.88
47	185.89	-98.65	27.99	-23.59	175.23	-42.16	157.90	-75.06	10.67	-56.49	-147.24	18.57
48	58.77	-208.75	53.12	-48.67	5.64	-14.61	5.65	-160.09	53.12	-194.14	47.48	-34.05
49	167.68	-60.60	165.63	-59.93	247.86	-79.38	2.05	-0.66	-80.18	18.78	-82.23	19.44
50	235.35	-68.46	191.68	-68.22	305.14	-107.55	43.67	-0.24	-69.79	39.10	-113.46	39.33
51	43.46	-144.61	49.26	-130.28	80.44	-226.45	-5.80	-14.33	-36.98	81.84	-31.18	96.17
52	55.98	-27.95	258.12	-75.34	247.26	-93.30	-202.15	47.38	-191.29	65.35	10.86	17.97
53	188.91	-469.66	236.49	-473.16	267.10	-439.85	-47.58	3.50	-78.19	-29.81	-30.60	-33.31
54	938.22	-363.38	648.95	-248.09	442.85	-222.80	289.27	-115.29	495.37	-140.58	206.09	-25.29
55	156.66	-161.27	247.64	-360.33	112.95	-206.98	-90.98	199.07	43.71	45.71	134.69	-153.36
56	88.10	-90.59	46.74	-94.17	103.47	-41.06	41.36	3.58	-15.37	-49.53	-56.73	-53.11
57	26.77	-50.22	20.17	-60.50	29.97	-97.80	6.60	10.28	-3.20	47.57	-9.80	37.29
58	19.03	-63.88	12.79	-43.48	47.91	-108.29	6.24	-20.40	-28.88	44.41	-35.12	64.81
59	63.76	-42.38	50.10	-17.77	104.34	-34.13	13.66	-24.61	-40.58	-8.25	-54.24	16.36
60	214.23	-741.03	284.16	-819.01	133.15	-401.87	-69.93	77.97	81.09	-339.16	151.02	-417.13
61	297.47	-124.46	40.37	-85.88	135.66	-53.23	257.09	-38.59	161.81	-71.23	-95.29	-32.64
62	7.40	-24.64	6.81	-9.89	2.89	-7.71	0.59	-14.75	4.51	-16.93	3.92	-2.17
63	394.31	-138.36	450.10	-584.97	320.15	-176.01	-55.79	446.61	74.17	37.64	129.95	-408.96
64	274.25	-775.75	260.36	-662.37	287.45	-116.74	13.89	-113.37	-13.20	-659.01	-27.08	-545.63
65	63.48	-26.91	54.52	-24.56	134.05	-395.60	8.96	-2.35	-70.57	368.69	-79.53	371.04
66	393.64	-321.37	928.04	-215.48	347.03	-319.17	-534.40	-105.89	46.61	-2.20	581.01	103.69
67	94.56	-208.09	103.94	-163.07	165.55	-296.48	-9.38	-45.02	-70.99	88.39	-61.61	133.41
68	22.75	-75.78	16.12	-47.88	82.94	-241.86	6.63	-27.90	-60.18	166.08	-66.81	193.99
69	332.27	-153.67	480.53	-142.06	169.16	-83.08	-148.27	-11.61	163.11	-70.58	311.37	-58.98
70	52.59	-22.24	73.56	-30.58	98.25	-99.35	-20.97	8.34	-45.66	77.10	-24.69	68.76

Table E.13. Maximum ($\epsilon 1$) and minimum ($\epsilon 3$) principal strain values at the location of 70 landmarks during second molar (M2) bite load for the 3 models of baboon species, and strain differences ($\Delta\epsilon 1$ and $\Delta\epsilon 3$) at landmark locations between models. Strain values are in microstrain (μstrain).

M2 bite landmark	P. anubis		P. hamadryas		T.gelada		P.anubis-P.hamadryas		P.anubis-T.gelada		P.hamadryas-T.gelada	
	$\epsilon 1$	$\epsilon 3$	$\epsilon 1$	$\epsilon 3$	$\epsilon 1$	$\epsilon 3$	$\Delta\epsilon 1$	$\Delta\epsilon 3$	$\Delta\epsilon 1$	$\Delta\epsilon 3$	$\Delta\epsilon 1$	$\Delta\epsilon 3$
1	7.42	-7.80	9.56	-4.85	3.44	-5.75	-2.15	-2.95	3.98	-2.05	6.12	0.90
2	31.09	-9.16	19.14	-10.06	12.34	-18.20	11.95	0.89	18.75	9.03	6.80	8.14
3	36.52	-39.76	3.68	-4.11	124.32	-49.41	32.83	-35.65	-87.80	9.65	-120.64	45.30
4	47.18	-209.40	58.96	-176.20	32.13	-133.82	-11.78	-33.19	15.05	-75.58	26.83	-42.38
5	3.83	-4.31	26.44	-9.54	50.56	-16.69	-22.61	5.23	-46.73	12.39	-24.12	7.15
6	17.61	-34.84	9.51	-22.55	39.46	-120.79	8.10	-12.29	-21.84	85.96	-29.94	98.24
7	0.58	-1.15	0.04	-0.04	5.73	-2.33	0.55	-1.10	-5.15	1.19	-5.69	2.29
8	102.71	-39.62	105.50	-32.52	166.41	-66.17	-2.79	-7.10	-63.71	26.55	-60.91	33.64
9	174.44	-115.75	90.18	-95.02	151.09	-209.28	84.26	-20.73	23.35	93.54	-60.91	114.27
10	108.21	-29.99	67.43	-24.00	48.59	-25.97	40.78	-6.00	59.62	-4.03	18.84	1.97
11	50.51	-20.48	62.02	-24.25	54.71	-23.63	-11.51	3.77	-4.20	3.15	7.31	-0.62
12	14.01	-36.41	16.50	-15.89	4.15	-3.67	-2.49	-20.53	9.86	-32.74	12.35	-12.22
13	6.60	-6.42	26.08	-8.70	6.60	-20.02	-19.48	2.27	0.01	13.59	19.49	11.32
14	7.29	-13.01	12.52	-3.53	25.31	-14.57	-5.22	-9.48	-18.01	1.56	-12.79	11.04
15	19.35	-21.76	12.52	-16.06	58.67	-36.61	6.83	-5.70	-39.32	14.85	-46.16	20.55
16	12.70	-47.40	29.05	-105.54	14.50	-12.23	-16.34	58.14	-1.80	-35.16	14.55	-93.31
17	54.53	-102.18	35.09	-52.36	73.74	-175.11	19.43	-49.82	-19.21	72.93	-38.64	122.75
18	52.99	-26.31	4.36	-4.50	97.91	-37.51	48.63	-21.82	-44.93	11.20	-93.56	33.01
19	151.10	-70.52	46.97	-101.52	100.78	-184.85	104.14	31.00	50.33	114.33	-53.81	83.33
20	42.12	-42.36	62.61	-72.22	0.60	-0.27	-20.48	29.87	41.52	-42.09	62.01	-71.96
21	340.53	-108.76	380.15	-118.71	459.14	-140.20	-39.62	9.95	-118.61	31.44	-78.99	21.49
22	54.58	-44.74	36.66	-107.39	39.24	-101.47	17.93	62.64	15.34	56.73	-2.59	-5.92
23	74.34	-226.46	37.95	-167.51	122.01	-402.31	36.39	-58.95	-47.67	175.84	-84.06	234.80
24	29.94	-58.94	18.54	-41.81	147.68	-446.27	11.41	-17.14	-117.73	387.33	-129.14	404.46
25	303.92	-914.46	204.94	-271.52	286.50	-292.73	98.99	-642.94	17.43	-621.73	-81.56	21.21
26	116.37	-286.16	961.29	-243.89	654.20	-267.31	-844.92	-42.27	-537.83	-18.85	307.10	23.42
27	224.12	-229.34	349.91	-194.13	239.17	-489.67	-125.80	-35.21	-15.05	260.32	110.75	295.53
28	180.67	-116.57	230.67	-112.93	469.36	-91.82	-50.00	-3.64	-288.69	-24.74	-238.69	-21.10
29	17.61	-55.57	16.63	-36.23	31.43	-90.58	0.98	-19.34	-13.82	35.01	-14.80	54.36
30	9.32	-5.27	4.30	-10.33	25.41	-51.45	5.02	5.06	-16.09	46.18	-21.11	41.12
31	21.45	-50.43	16.56	-53.32	25.63	-79.02	4.90	2.89	-4.18	28.59	-9.08	25.71
32	178.22	-573.54	266.10	-919.06	186.76	-661.68	-87.88	345.52	-8.55	88.14	79.34	-257.38
33	150.68	-182.42	51.48	-66.70	42.15	-87.58	99.20	-115.72	108.53	-94.84	9.33	20.88
34	4.52	-19.42	31.88	-48.16	5.42	-12.57	-27.36	28.74	-0.89	-6.85	26.46	-35.59
35	411.08	-117.54	570.10	-168.92	404.80	-122.44	-159.03	51.38	6.28	4.90	165.31	-46.48
36	336.16	-1503.18	249.70	-332.71	134.90	-13.45	86.46	-1170.47	201.26	-1489.73	114.79	-319.26
37	5.45	-9.32	11.18	-5.87	17.78	-18.32	-5.73	-3.45	-12.33	9.00	-6.60	12.45
38	15.03	-40.73	13.31	-7.22	9.52	-21.72	1.72	-33.52	5.51	-19.01	3.79	14.51
39	12.35	-42.48	11.65	-27.45	11.72	-35.26	0.70	-15.03	0.62	-7.22	-0.08	7.81
40	14.87	-6.80	12.59	-6.97	8.68	-12.19	2.28	0.17	6.19	5.40	3.91	5.23
41	4.84	-3.68	7.22	-5.47	56.00	-23.20	-2.38	1.79	-51.16	19.52	-48.78	17.73
42	11.20	-4.18	7.58	-3.95	6.85	-11.47	3.62	-0.24	4.35	7.29	0.73	7.53
43	19.33	-3.65	7.03	-3.66	13.49	-29.08	12.30	0.02	5.84	25.44	-6.46	25.42
44	12.81	-4.67	11.09	-3.70	51.00	-8.70	1.71	-0.97	-38.19	4.03	-39.91	5.00
45	11.83	-13.99	5.88	-9.21	31.97	-7.99	5.95	-4.79	-20.14	-6.00	-26.09	-1.22
46	34.44	-10.65	10.72	-9.93	6.70	-3.63	23.72	-0.73	27.74	-7.02	4.01	-6.30
47	168.76	-98.05	24.15	-23.09	166.20	-43.97	144.61	-74.97	2.56	-54.08	-142.05	20.88
48	57.57	-204.74	52.49	-47.74	5.56	-14.42	5.08	-157.00	52.01	-190.31	46.93	-33.31
49	160.07	-57.58	159.86	-56.95	208.75	-67.25	0.22	-0.62	-48.68	9.68	-48.89	10.30
50	233.14	-67.65	197.79	-67.22	307.39	-109.12	35.35	-0.43	-74.24	41.47	-109.60	41.90
51	35.85	-117.46	45.74	-103.58	59.01	-143.90	-9.89	-13.88	-23.16	26.45	-13.27	40.33
52	44.64	-24.44	217.82	-64.90	191.13	-72.15	-173.17	40.46	-146.49	47.71	26.69	7.25
53	186.68	-472.44	239.81	-487.46	273.08	-460.25	-53.13	15.02	-86.40	-12.19	-33.27	-27.20
54	946.78	-364.30	651.29	-244.61	454.95	-222.74	295.49	-119.69	491.84	-141.57	196.34	-21.88
55	154.91	-162.47	247.34	-363.18	116.46	-206.04	-92.43	200.70	38.45	43.57	130.88	-157.13
56	87.80	-84.91	41.85	-90.82	94.76	-36.32	45.95	5.91	-6.95	-48.59	-52.91	-54.50
57	25.67	-47.81	20.11	-59.73	25.40	-82.87	5.56	11.92	0.27	35.06	-5.29	23.14
58	19.04	-63.65	13.11	-44.43	43.81	-102.92	5.93	-19.23	-24.77	39.27	-30.71	58.49
59	68.35	-39.20	55.04	-19.21	125.16	-40.85	13.31	-19.99	-56.81	1.65	-70.12	21.64
60	213.52	-738.64	282.83	-814.85	129.00	-386.82	-69.31	76.22	84.52	-351.82	153.83	-428.04
61	291.80	-122.99	40.56	-87.91	137.08	-52.73	251.24	-35.08	154.72	-70.26	-96.52	-35.18
62	6.73	-22.43	6.74	-9.84	2.44	-6.15	-0.01	-12.59	4.29	-16.28	4.30	-3.69
63	391.44	-137.54	447.17	-582.30	308.44	-170.71	-55.74	444.76	83.00	33.16	138.73	-411.60
64	274.71	-774.39	259.15	-658.58	287.04	-116.32	15.56	-115.81	-12.33	-658.07	-27.89	-542.25
65	87.55	-41.32	80.81	-30.63	157.91	-232.07	6.74	-10.69	-70.37	190.75	-77.11	201.43
66	401.97	-331.91	938.66	-221.63	378.86	-381.79	-536.69	-110.28	23.11	49.88	559.80	160.16
67	57.31	-141.35	54.83	-116.14	60.25	-186.83	2.48	-25.21	-2.93	45.48	-5.42	70.69
68	23.29	-77.32	15.51	-44.93	73.98	-201.72	7.77	-32.39	-50.69	124.40	-58.47	156.79
69	332.80	-154.37	482.04	-142.11	163.40	-86.20	-149.24	-12.26	169.41	-68.17	318.64	-55.91
70	58.21	-22.12	71.73	-27.25	91.52	-68.62	-13.53	5.14	-33.31	46.51	-19.78	41.37

Table E.14. Maximum ($\epsilon 1$) and minimum ($\epsilon 3$) principal strain values at the location of 70 landmarks during third molar (M3) bite load for the 3 models of baboon species, and strain differences ($\Delta \epsilon 1$ and $\Delta \epsilon 3$) at landmark locations between models. Strain values are in microstrain (μ strain).

M3 bite landmark	P. anubis		P. hamadryas		T.gelada		P.anubis-P.hamadryas		P.anubis-T.gelada		P.hamadryas-T.gelada	
	$\epsilon 1$	$\epsilon 3$	$\epsilon 1$	$\epsilon 3$	$\epsilon 1$	$\epsilon 3$	$\Delta \epsilon 1$	$\Delta \epsilon 3$	$\Delta \epsilon 1$	$\Delta \epsilon 3$	$\Delta \epsilon 1$	$\Delta \epsilon 3$
1	4.34	-3.44	13.41	-7.15	11.68	-11.03	-9.07	3.71	-7.34	7.60	1.73	3.89
2	34.61	-9.27	27.37	-13.54	35.16	-30.62	7.23	4.27	-0.56	21.35	-7.79	17.08
3	24.86	-35.39	1.55	-3.76	43.75	-19.27	23.31	-31.63	-18.90	-16.12	-42.20	15.51
4	49.83	-179.81	72.94	-168.11	39.85	-91.84	-23.10	-11.70	9.98	-87.97	33.09	-76.27
5	3.55	-2.62	27.79	-9.90	47.12	-16.06	-24.23	7.28	-43.57	13.45	-19.33	6.17
6	18.33	-36.02	10.03	-23.91	42.49	-130.32	8.30	-12.12	-24.16	94.30	-32.46	106.41
7	0.65	-1.27	0.04	-0.04	7.70	-3.13	0.61	-1.24	-7.05	1.86	-7.66	3.09
8	102.30	-32.90	90.45	-28.84	152.90	-74.63	11.85	-4.06	-50.60	41.73	-62.45	45.78
9	114.24	-85.75	51.73	-73.81	58.65	-115.08	62.52	-11.94	55.60	29.33	-6.92	41.26
10	121.32	-33.92	71.84	-25.61	59.70	-31.02	49.49	-8.31	61.62	-2.90	12.13	5.41
11	33.88	-13.93	46.60	-17.80	16.56	-7.27	-12.72	3.87	17.32	-6.66	30.05	-10.53
12	12.10	-25.80	19.41	-13.16	9.89	-5.43	-7.31	-12.63	2.22	-20.36	9.53	-7.73
13	10.56	-8.41	43.66	-13.52	2.06	-5.84	-33.10	5.11	8.49	-2.57	41.60	-7.69
14	3.77	-5.44	33.71	-10.23	17.18	-10.76	-29.94	4.79	-13.41	5.32	16.53	0.52
15	3.20	-9.99	8.27	-5.66	20.86	-17.22	-5.07	-4.34	-17.67	7.22	-12.59	11.56
16	9.46	-26.09	6.70	-27.24	29.74	-9.82	2.76	1.15	-20.28	-16.27	-23.04	-17.43
17	21.77	-68.90	26.77	-56.01	17.59	-21.43	-5.00	-12.89	4.18	-47.46	9.18	-34.58
18	164.45	-343.28	10.98	-12.37	109.64	-157.89	153.47	-330.91	54.82	-185.38	-98.66	145.53
19	194.61	-97.89	44.15	-143.03	126.07	-215.64	150.47	45.14	68.54	117.75	-81.93	72.61
20	40.35	-37.47	61.70	-70.21	0.70	-0.44	-21.35	32.74	39.65	-37.03	61.00	-69.78
21	366.26	-119.22	415.30	-130.02	545.72	-167.93	-49.04	10.80	-179.46	48.71	-130.42	37.91
22	40.45	-51.72	40.05	-134.75	45.66	-170.57	0.40	83.02	-5.21	118.85	-5.61	35.82
23	72.86	-223.90	36.57	-141.34	118.73	-395.60	36.29	-82.56	-45.86	171.71	-82.16	254.26
24	19.49	-40.03	15.25	-42.04	75.16	-221.31	4.24	2.01	-55.67	181.28	-59.91	179.27
25	302.52	-911.80	202.67	-265.18	284.74	-287.28	99.85	-646.62	17.77	-624.52	-82.07	22.11
26	114.05	-281.28	972.84	-247.34	710.93	-288.56	-858.79	-33.94	-596.88	7.27	261.92	41.22
27	224.15	-234.19	349.72	-194.93	244.29	-511.53	-125.58	-39.26	-20.14	277.34	105.43	316.60
28	191.99	-85.05	264.29	-110.03	542.86	-115.59	-72.29	24.98	-350.86	30.54	-278.57	5.56
29	16.45	-51.87	15.12	-31.46	29.42	-84.66	1.33	-20.41	-12.97	32.79	-14.30	53.20
30	17.61	-6.98	3.28	-2.72	24.15	-31.88	14.33	-4.26	-6.54	24.90	-20.87	29.17
31	23.26	-61.53	17.49	-57.25	38.89	-114.16	5.78	-4.28	-15.62	52.63	-21.40	56.91
32	178.86	-575.94	267.03	-922.22	190.02	-673.49	-88.17	346.28	-11.16	97.55	77.01	-248.73
33	146.70	-187.21	52.34	-74.70	53.91	-137.63	94.36	-112.51	92.80	-49.58	-1.57	62.93
34	3.58	-14.99	30.66	-46.88	5.77	-10.54	-27.09	31.89	-2.19	-4.46	24.89	-36.34
35	410.53	-117.05	571.99	-169.54	408.88	-123.67	-161.46	52.50	1.65	6.62	163.11	-45.88
36	339.99	-1495.10	244.32	-324.92	130.86	2.98	95.67	-1170.18	209.12	-1498.08	113.46	-327.89
37	8.25	-8.66	12.24	-6.39	25.63	-13.70	-3.98	-2.27	-17.37	5.04	-13.39	7.31
38	15.82	-45.19	11.01	-7.15	11.33	-32.97	4.81	-38.04	4.49	-12.22	-0.32	25.82
39	8.24	-27.96	7.48	-15.98	14.14	-8.60	0.76	-11.97	-5.91	-19.36	-6.66	-7.38
40	10.04	-5.30	5.79	-7.57	4.28	-17.33	4.25	2.27	5.76	12.04	1.51	9.77
41	5.14	-3.28	11.87	-7.31	10.75	-8.91	-6.73	4.04	-5.61	5.63	1.12	1.59
42	15.49	-5.28	16.33	-6.34	3.88	-7.82	-0.84	1.06	11.61	2.54	12.45	1.48
43	29.30	-6.21	15.26	-8.67	5.83	-22.11	14.04	2.47	23.47	15.90	9.43	13.44
44	9.01	-2.41	14.06	-4.60	6.53	-19.92	-5.05	2.19	2.48	17.50	7.53	15.32
45	7.61	-10.92	4.13	-6.36	8.79	-3.39	3.48	-4.55	-1.18	-7.52	-4.66	-2.97
46	30.28	-9.17	9.43	-7.69	6.74	-3.75	20.86	-1.47	23.54	-5.42	2.68	-3.94
47	148.58	-98.27	18.77	-20.32	162.99	-46.34	129.82	-77.95	-14.40	-51.93	-144.22	26.02
48	55.88	-198.96	51.30	-46.15	5.37	-13.96	4.58	-152.81	50.51	-185.00	45.93	-32.19
49	148.06	-53.30	153.08	-53.16	163.65	-53.30	-5.02	-0.14	-15.58	0.01	-10.56	0.14
50	232.66	-67.31	203.98	-65.91	309.54	-110.85	28.68	-1.41	-76.88	43.54	-105.56	44.95
51	41.54	-84.72	44.11	-72.29	50.78	-53.18	-2.58	-12.43	-9.24	-31.54	-6.66	-19.12
52	31.29	-20.54	156.14	-48.88	104.32	-37.73	-124.85	28.34	-73.04	17.20	51.81	-11.14
53	184.09	-475.49	243.91	-505.61	280.32	-485.70	-59.81	30.12	-96.23	10.21	-36.42	-19.91
54	956.28	-365.45	654.62	-239.93	474.93	-223.54	301.65	-125.52	481.34	-141.91	179.69	-16.39
55	153.10	-164.05	247.15	-367.23	121.57	-207.84	-94.04	203.18	31.53	43.79	125.58	-159.39
56	84.87	-74.74	34.34	-82.28	84.98	-33.34	50.53	7.54	-0.11	-41.39	-50.64	-48.94
57	24.28	-44.73	20.03	-58.73	19.66	-63.84	4.25	13.99	4.62	19.11	0.37	5.11
58	19.26	-63.92	13.47	-45.49	39.27	-96.79	5.79	-18.44	-20.01	32.86	-25.80	51.30
59	75.91	-34.93	60.42	-20.64	150.10	-48.84	15.49	-14.29	-74.20	13.91	-89.69	28.20
60	212.72	-735.96	281.46	-810.59	125.03	-372.07	-68.75	74.63	87.69	-363.89	156.44	-438.52
61	285.59	-121.32	41.08	-91.38	135.15	-51.58	244.51	-29.93	150.44	-69.73	-94.07	-39.80
62	5.78	-19.26	6.63	-9.74	2.27	-4.38	-0.85	-9.51	3.52	-14.88	4.36	-5.36
63	387.91	-136.57	443.25	-579.02	295.52	-164.79	-55.34	442.45	92.39	28.22	147.73	-414.23
64	275.86	-773.94	256.89	-651.48	285.65	-113.88	18.97	-122.46	-9.80	-660.06	-28.77	-537.59
65	91.49	-43.91	97.36	-32.24	188.12	-70.84	-5.87	-11.68	-96.63	26.93	-90.76	38.60
66	414.32	-347.52	942.48	-224.87	417.75	-453.07	-528.15	-122.65	-3.43	105.55	524.72	228.20
67	37.16	-95.56	31.80	-81.89	28.80	-100.55	5.36	-13.67	8.36	4.99	3.00	18.66
68	22.50	-70.72	13.04	-36.09	59.37	-144.47	9.46	-34.63	-36.87	73.75	-46.33	108.38
69	331.70	-154.55	486.56	-142.73	162.43	-96.74	-154.87	-11.83	169.26	-57.81	324.13	-45.98
70	59.95	-21.08	66.67	-22.82	76.10	-32.37	-6.72	1.74	-16.15	11.29	-9.43	9.54

Table E.15. Maximum ($\epsilon 1$) and minimum ($\epsilon 3$) principal strain values at the location of 70 landmarks during first incisor (I1) bite load for the models of male and female P. anubis and T. gelada species, and strain differences ($\Delta \epsilon 1$ and $\Delta \epsilon 3$) at landmark locations between male and female models. Strain values are in microstrain (μ strain).

I1 bite landmark	P.anubis (male)		P.anubis (female)		T.gelada (male)		T.gelada (female)		P.anubis(m)-P.anubis(f)		T.gelada(m)-T.gelada(f)	
	$\epsilon 1$	$\epsilon 3$	$\epsilon 1$	$\epsilon 3$	$\epsilon 1$	$\epsilon 3$	$\epsilon 1$	$\epsilon 3$	$\Delta \epsilon 1$	$\Delta \epsilon 3$	$\Delta \epsilon 1$	$\Delta \epsilon 3$
1	136.04	-207.36	57.76	-161.38	646.29	-552.11	253.83	-506.64	78.28	-45.98	392.46	-45.47
2	410.20	-155.96	216.46	-81.55	208.52	-109.23	89.03	-47.34	193.73	-74.41	119.49	-61.89
3	215.06	-63.33	232.92	-77.67	266.00	-96.64	85.76	-38.91	-17.86	14.34	180.24	-57.73
4	44.27	-284.71	56.55	-191.64	52.97	-235.65	32.40	-79.74	-12.29	-93.08	20.57	-155.91
5	5.39	-14.90	11.44	-14.76	59.08	-18.98	36.78	-12.04	-6.05	-0.14	22.31	-6.93
6	15.67	-31.19	5.42	-10.91	32.80	-99.76	10.28	-10.72	10.25	-20.27	22.52	-89.04
7	0.42	-0.80	0.75	-0.45	2.14	-0.85	0.54	-0.47	-0.33	-0.35	1.59	-0.38
8	94.78	-54.09	31.60	-31.01	217.62	-70.22	32.53	-23.78	63.18	-23.08	185.08	-46.44
9	189.49	-150.76	81.29	-167.69	153.01	-324.59	54.50	-112.50	108.20	16.93	98.51	-212.09
10	62.05	-20.13	10.81	-7.36	19.85	-14.72	14.54	-6.60	51.24	-12.77	5.31	-8.11
11	121.39	-281.97	82.35	-254.07	167.55	-489.47	85.88	-211.92	39.04	-27.89	81.67	-277.55
12	282.55	-85.58	261.12	-96.70	265.55	-158.28	503.18	-193.11	21.43	11.12	-237.64	34.83
13	116.36	-33.56	56.59	-29.49	23.13	-51.89	95.39	-54.56	59.77	-4.07	-72.26	2.67
14	91.96	-33.47	85.23	-29.28	222.93	-117.64	119.79	-51.59	6.74	-4.19	103.14	-66.05
15	85.85	-26.19	76.00	-23.42	149.83	-97.46	87.68	-39.22	9.85	-2.77	62.15	-58.24
16	62.78	-17.71	79.12	-21.37	110.40	-53.01	63.73	-28.97	-16.34	3.66	46.67	-24.04
17	38.53	-13.96	40.00	-20.87	102.17	-42.26	85.80	-28.11	-1.47	6.91	16.37	-14.15
18	186.20	-83.57	144.10	-44.71	161.90	-62.75	71.16	-21.21	42.10	-38.86	90.74	-41.54
19	49.76	-36.18	41.22	-18.58	44.85	-94.33	21.99	-53.53	8.54	-17.60	22.86	-40.80
20	49.52	-58.15	24.38	-69.66	0.79	-0.14	11.86	-17.50	25.14	11.51	-11.08	17.36
21	254.42	-81.94	215.60	-64.35	295.63	-88.27	99.04	-36.59	38.83	-17.59	196.59	-51.69
22	170.16	-59.45	64.02	-37.11	224.28	-101.30	90.03	-55.36	106.14	-22.33	134.25	-45.94
23	74.19	-227.96	44.76	-139.10	115.10	-377.12	41.61	-129.50	29.42	-88.86	73.49	-247.62
24	161.83	-73.01	136.86	-98.10	125.98	-386.48	76.67	-145.28	24.97	25.10	49.31	-241.20
25	306.53	-897.05	121.21	-236.73	260.30	-265.86	119.85	-200.79	185.32	-660.32	140.45	-65.07
26	134.36	-324.32	566.32	-139.69	476.56	-203.76	81.89	-146.33	-431.95	-184.62	394.67	-57.42
27	229.45	-205.44	111.52	-210.11	220.30	-391.01	195.52	-103.71	117.93	4.66	24.77	-287.30
28	149.01	-157.93	72.42	-101.11	342.56	-76.96	78.15	-60.03	76.59	-56.82	264.40	-16.94
29	22.32	-69.64	38.04	-107.99	37.35	-107.10	23.34	-56.75	-15.72	38.35	14.01	-50.35
30	8.83	-25.38	29.95	-82.91	39.68	-103.24	62.80	-18.28	-21.12	57.53	-23.12	-84.96
31	10.26	-26.67	17.97	-41.16	44.71	-18.17	40.38	-43.20	-7.72	14.49	4.33	25.03
32	178.25	-572.73	133.29	-423.47	183.21	-647.35	56.96	-196.16	44.97	-149.26	126.25	-451.19
33	177.15	-163.96	76.97	-69.30	126.14	-42.46	96.72	-45.01	100.18	-94.66	29.41	2.56
34	6.95	-29.98	5.94	-13.88	6.72	-17.70	4.78	-9.92	1.01	-16.10	1.95	-7.78
35	422.30	-122.53	216.24	-95.58	427.56	-134.12	147.55	-78.30	206.06	-26.95	280.00	-55.82
36	332.37	-1560.99	111.98	-310.51	161.31	-74.62	65.43	-184.04	220.39	-1250.48	95.88	109.42
37	4.34	-13.62	0.93	-0.49	13.83	-38.93	1.63	-1.13	3.41	-13.14	12.20	-37.80
38	13.65	-17.62	10.65	-32.16	26.76	-8.52	10.60	-8.15	3.01	14.54	16.15	-0.37
39	78.08	-285.35	68.87	-225.66	143.87	-501.44	79.06	-204.27	9.21	-59.69	64.81	-297.18
40	158.88	-70.02	84.04	-36.35	227.23	-59.49	203.25	-76.79	74.84	-33.68	23.98	17.29
41	70.79	-28.83	67.20	-23.94	127.80	-49.22	88.95	-51.17	3.60	-4.89	38.85	1.95
42	62.62	-26.37	85.88	-25.59	128.08	-58.33	86.13	-44.55	-23.27	-0.79	41.95	-13.78
43	70.61	-22.47	82.80	-19.44	400.62	-97.65	95.87	-34.62	-12.19	-3.03	304.75	-63.03
44	62.96	-16.58	66.78	-21.28	333.28	-85.83	102.39	-30.25	-3.82	4.69	230.89	-55.59
45	41.93	-19.15	65.98	-20.97	144.40	-47.59	69.33	-21.35	-24.05	1.82	75.07	-26.24
46	74.07	-23.00	239.61	-62.24	89.11	-42.87	72.55	-9.44	-165.53	39.24	16.56	-33.43
47	213.51	-71.66	110.36	-32.34	146.58	-36.38	39.11	-92.67	103.15	-39.32	107.46	56.28
48	57.51	-204.22	22.16	-81.82	5.16	-13.32	31.16	-71.93	35.35	-122.40	-26.00	58.61
49	220.21	-75.27	167.09	-53.50	341.26	-108.51	151.68	-49.69	53.11	-21.77	189.58	-58.82
50	193.18	-57.31	113.53	-43.90	254.82	-89.60	52.11	-54.01	79.65	-13.41	202.71	-35.59
51	75.57	-219.53	45.58	-159.29	124.96	-385.14	46.68	-146.06	29.99	-60.23	78.29	-239.08
52	155.52	-57.64	181.75	-70.94	211.00	-230.27	304.44	-66.63	-26.23	13.30	-93.44	-163.64
53	195.80	-484.39	170.41	-380.40	270.84	-455.38	521.60	-150.69	25.38	-103.99	-250.76	-304.70
54	953.96	-361.44	382.18	-133.00	465.01	-225.92	124.12	-161.40	571.78	-228.44	340.88	-64.52
55	160.68	-164.09	163.36	-239.49	114.54	-222.35	289.55	-129.58	-2.68	75.40	-175.01	-92.76
56	121.21	-140.20	76.69	-113.55	149.94	-96.57	92.22	-87.90	44.51	-26.65	57.72	-8.67
57	30.32	-58.56	21.39	-77.96	38.23	-124.15	16.29	-25.01	8.94	19.40	21.94	-99.14
58	17.36	-58.38	35.47	-78.31	53.52	-111.50	56.44	-17.66	-18.11	19.93	-2.91	-93.84
59	30.47	-40.65	20.11	-48.10	25.74	-8.83	44.36	-44.92	10.36	7.45	-18.62	36.09
60	213.70	-739.71	113.26	-357.70	150.67	-462.22	74.19	-247.87	100.44	-382.01	76.48	-214.36
61	279.43	-121.60	121.12	-92.42	103.40	-52.50	82.66	-41.91	158.31	-29.18	20.74	-10.59
62	8.59	-28.66	12.42	-18.33	4.22	-11.43	3.47	-7.99	-3.82	-10.33	0.75	-3.44
63	401.61	-139.42	357.03	-119.13	350.48	-188.64	212.32	-105.33	44.57	-20.29	138.16	-83.31
64	267.53	-759.13	161.52	-426.43	282.42	-107.88	86.86	-286.47	106.02	-332.70	195.56	178.59
65	71.42	-162.62	87.77	-177.53	209.70	-573.74	71.83	-229.20	-16.35	14.92	137.88	-344.55
66	324.68	-242.64	166.31	-111.07	248.95	-158.21	157.84	-65.87	158.37	-131.57	91.11	-92.34
67	58.53	-51.05	15.02	-40.46	46.07	-178.52	43.58	-85.62	43.51	-10.59	2.49	-92.90
68	43.02	-141.15	70.66	-141.47	184.64	-562.04	77.37	-190.84	-27.65	0.32	107.27	-371.21
69	381.66	-184.24	124.40	-84.35	225.95	-133.85	121.82	-80.51	257.26	-99.89	104.13	-53.34
70	78.74	-44.02	26.81	-34.91	53.91	-117.58	6.86	-18.83	51.93	-9.11	47.05	-98.75

Table E.16. Maximum ($\epsilon 1$) and minimum ($\epsilon 3$) principal strain values at the location of 70 landmarks during second incisor (I2) bite load for the models of male and female *P. anubis* and *T. gelada* species, and strain differences ($\Delta\epsilon 1$ and $\Delta\epsilon 3$) at landmark locations between male and female models. Strain values are in microstrain (μ strain).

I2 bite landmark	P.anubis (male)		P.anubis (female)		T.gelada (male)		T.gelada (female)		P.anubis(m)-P.anubis(f)		T.gelada(m)-T.gelada(f)	
	$\epsilon 1$	$\epsilon 3$	$\epsilon 1$	$\epsilon 3$	$\epsilon 1$	$\epsilon 3$	$\epsilon 1$	$\epsilon 3$	$\Delta\epsilon 1$	$\Delta\epsilon 3$	$\Delta\epsilon 1$	$\Delta\epsilon 3$
1	76.02	-99.61	48.56	-35.85	147.64	-397.31	83.27	-62.88	27.46	-63.76	64.38	-334.42
2	346.34	-200.68	172.38	-137.53	273.62	-211.46	105.53	-61.22	173.95	-63.15	168.09	-150.23
3	185.37	-58.21	186.10	-60.29	272.14	-100.94	73.59	-36.19	-0.73	2.08	198.55	-64.75
4	45.53	-281.51	56.30	-189.72	51.87	-231.54	32.15	-80.38	-10.77	-91.79	19.73	-151.16
5	5.32	-14.25	11.71	-14.89	59.19	-19.01	36.52	-11.93	-6.38	0.64	22.67	-7.08
6	15.79	-31.60	5.42	-10.96	33.28	-101.32	10.21	-10.87	10.37	-20.63	23.07	-90.45
7	0.43	-0.82	0.82	-0.49	2.17	-0.88	0.62	-0.49	-0.39	-0.34	1.55	-0.38
8	98.18	-54.16	33.23	-30.52	218.27	-71.04	34.38	-23.37	64.95	-23.64	183.89	-47.67
9	191.45	-150.03	85.25	-163.33	160.63	-337.63	59.29	-115.76	106.20	13.30	101.34	-221.86
10	68.09	-19.81	16.87	-6.60	23.75	-15.70	17.06	-6.37	51.22	-13.21	6.69	-9.33
11	111.76	-253.36	88.76	-251.96	184.50	-547.32	89.47	-222.49	23.00	-1.40	95.03	-324.83
12	306.89	-172.75	377.81	-171.14	797.07	-523.21	590.28	-238.99	-70.92	-1.61	206.79	-284.22
13	144.44	-43.78	90.87	-53.27	12.79	-33.16	123.28	-77.09	53.58	9.50	-110.49	43.94
14	112.05	-40.78	110.41	-42.32	222.47	-122.54	151.71	-71.67	1.64	1.54	70.76	-50.87
15	107.67	-36.95	89.40	-29.27	160.55	-105.55	114.44	-61.43	18.26	-7.68	46.11	-44.11
16	64.34	-17.92	80.03	-23.70	51.77	-35.72	71.86	-26.03	-15.69	5.78	-20.09	-9.69
17	31.27	-8.86	36.88	-21.26	96.08	-42.40	93.58	-26.91	-5.61	12.41	2.49	-15.49
18	213.23	-95.48	166.00	-51.33	196.05	-76.23	83.43	-24.99	47.23	-44.15	112.62	-51.24
19	48.11	-24.81	61.95	-23.40	47.63	-113.45	17.53	-43.50	-13.84	-1.41	30.11	-69.95
20	48.39	-56.22	23.23	-67.17	0.73	-0.14	11.55	-16.74	25.16	10.96	-10.82	16.59
21	268.92	-83.72	226.26	-66.93	310.33	-92.77	105.68	-36.31	42.65	-16.79	204.65	-56.46
22	145.83	-53.71	38.97	-39.28	181.80	-90.14	80.58	-56.45	106.86	-14.43	101.22	-33.70
23	75.86	-230.37	42.89	-128.06	118.82	-388.54	45.91	-140.71	32.97	-102.32	72.91	-247.82
24	124.72	-84.15	118.33	-159.27	188.81	-581.47	68.24	-186.07	6.39	75.12	120.57	-395.40
25	307.49	-905.93	122.84	-243.08	264.10	-272.91	121.67	-210.28	184.65	-662.86	142.43	-62.64
26	131.16	-317.64	579.26	-142.45	501.67	-212.33	83.03	-140.22	-448.10	-175.19	418.64	-72.11
27	229.09	-209.58	111.05	-213.04	223.50	-405.38	195.89	-106.15	118.05	3.46	27.62	-299.23
28	160.05	-168.21	89.35	-116.11	367.77	-81.13	83.70	-66.61	70.70	-52.10	284.07	-14.52
29	21.57	-67.53	40.30	-115.09	36.86	-105.85	24.42	-58.39	-18.73	47.56	12.44	-47.46
30	7.45	-21.32	27.75	-75.09	38.30	-98.67	66.66	-18.95	-20.30	53.77	-28.36	-79.72
31	11.92	-21.98	13.33	-42.68	25.01	-12.70	33.51	-40.28	-1.42	20.70	-8.50	27.59
32	178.58	-574.04	129.85	-412.46	184.39	-651.78	58.82	-202.33	48.73	-161.58	125.57	-449.45
33	171.90	-166.55	72.07	-70.65	101.60	-36.78	88.36	-44.26	99.82	-95.90	13.23	7.48
34	6.83	-29.45	5.52	-13.05	6.72	-17.69	4.54	-9.51	1.31	-16.40	2.18	-8.19
35	421.09	-121.77	209.25	-92.27	426.10	-131.93	148.03	-78.19	211.84	-29.50	278.07	-53.74
36	330.98	-1547.82	106.78	-295.68	155.48	-64.63	64.09	-178.78	224.21	-1252.14	91.38	114.15
37	4.21	-13.51	1.65	-0.76	13.97	-38.42	1.85	-1.23	2.56	-12.75	12.12	-37.19
38	13.20	-22.48	14.61	-44.43	22.44	-8.30	8.98	-9.22	-1.42	21.95	13.46	0.93
39	57.93	-214.93	52.77	-173.98	116.57	-407.60	62.65	-162.22	5.16	-40.96	53.93	-245.38
40	124.82	-58.96	87.04	-30.33	241.29	-72.36	157.33	-65.28	37.78	-28.63	83.96	-7.09
41	48.13	-21.19	55.56	-23.79	268.20	-41.23	66.27	-38.98	-7.43	2.60	201.93	-2.25
42	47.58	-23.27	67.64	-20.20	123.71	-61.47	68.43	-35.63	-20.06	-3.07	55.28	-25.84
43	54.04	-26.00	73.90	-17.70	349.71	-87.06	85.44	-29.29	-19.87	-8.30	264.27	-57.77
44	61.91	-18.74	59.90	-19.07	409.61	-97.19	102.04	-34.71	2.01	0.33	307.57	-62.49
45	41.26	-20.99	55.32	-18.41	152.04	-48.15	65.16	-21.81	-14.06	-2.58	86.89	-26.33
46	62.46	-19.75	202.16	-51.57	62.40	-30.01	54.18	-7.82	-139.70	31.81	8.22	-22.19
47	214.45	-79.76	108.03	-40.15	169.13	-40.76	45.67	-107.35	106.42	-39.61	123.46	66.59
48	58.85	-208.78	22.93	-83.71	5.49	-14.19	32.11	-74.33	35.92	-125.07	-26.63	60.14
49	206.83	-71.95	156.34	-50.32	331.08	-105.17	137.56	-45.05	50.49	-21.63	193.52	-60.12
50	211.29	-62.29	151.30	-51.39	276.13	-96.76	62.29	-50.39	60.00	-10.90	213.84	-46.37
51	72.32	-213.75	49.49	-163.58	121.60	-372.06	47.21	-140.54	22.83	-50.18	74.39	-231.52
52	148.24	-53.27	222.14	-86.12	250.05	-147.65	392.42	-89.83	-73.90	32.85	-142.37	-57.81
53	195.27	-477.14	167.96	-372.61	264.36	-432.23	521.13	-149.98	27.31	-104.53	-256.77	-282.25
54	941.08	-361.30	378.83	-130.62	444.13	-224.23	122.30	-164.83	562.25	-230.69	321.82	-59.40
55	160.95	-162.36	162.69	-236.67	111.18	-216.52	288.15	-127.30	-1.74	74.30	-176.97	-89.22
56	108.02	-125.75	56.69	-91.84	138.81	-78.82	79.05	-69.91	51.33	-33.91	59.76	-8.91
57	30.06	-57.79	18.19	-63.25	37.99	-123.68	15.80	-25.11	11.88	5.46	22.19	-98.57
58	18.08	-61.06	35.83	-79.47	54.70	-115.08	52.29	-16.29	-17.75	18.40	2.41	-98.79
59	39.43	-43.55	23.85	-48.46	45.59	-15.10	52.43	-47.33	15.58	4.91	-6.83	32.23
60	214.53	-742.31	114.76	-364.50	145.71	-445.86	72.26	-241.08	99.77	-377.81	73.45	-204.78
61	290.27	-123.68	124.99	-91.84	117.51	-52.86	85.46	-42.98	165.28	-31.85	32.05	-9.88
62	8.66	-28.87	12.81	-18.85	4.10	-11.17	3.51	-7.94	-4.15	-10.01	0.59	-3.23
63	401.34	-139.72	361.11	-120.17	345.79	-186.96	213.34	-105.53	40.23	-19.55	132.44	-81.43
64	269.85	-766.71	165.40	-438.30	285.14	-112.32	87.88	-293.40	104.46	-328.41	197.25	181.08
65	75.39	-167.99	98.73	-186.19	223.38	-612.74	85.56	-252.45	-23.35	18.21	137.83	-360.30
66	342.44	-261.05	179.41	-121.74	274.91	-193.37	165.67	-76.21	163.03	-139.31	109.24	-117.16
67	43.82	-67.91	53.88	-101.09	131.93	-285.57	85.98	-135.99	-10.06	33.18	45.95	-149.58
68	36.00	-113.76	49.19	-105.17	159.67	-486.77	66.90	-154.34	-13.19	-8.60	92.77	-332.42
69	362.99	-172.34	115.63	-76.18	205.31	-107.54	115.52	-74.47	247.36	-96.15	89.80	-33.07
70	75.23	-35.66	40.49	-30.12	63.28	-156.18	26.87	-39.49	34.74	-5.54	36.41	-116.69

Table E.17. Maximum ($\epsilon 1$) and minimum ($\epsilon 3$) principal strain values at the location of 70 landmarks during first premolar (P3) bite load for the models of male and female P. anubis and T. gelada species, and strain differences ($\Delta\epsilon 1$ and $\Delta\epsilon 3$) at landmark locations between male and female models. Strain values are in microstrain (μ strain).

P3 bite landmark	P.anubis (male)		P.anubis (female)		T.gelada (male)		T.gelada (female)		P.anubis(m)-P.anubis(f)		T.gelada(m)-T.gelada(f)	
	$\epsilon 1$	$\epsilon 3$	$\epsilon 1$	$\epsilon 3$	$\epsilon 1$	$\epsilon 3$	$\epsilon 1$	$\epsilon 3$	$\Delta\epsilon 1$	$\Delta\epsilon 3$	$\Delta\epsilon 1$	$\Delta\epsilon 3$
1	17.80	-18.65	17.24	-12.16	24.92	-37.60	18.34	-8.98	0.56	-6.48	6.58	-28.62
2	28.66	-31.80	40.88	-42.10	73.76	-147.59	47.73	-48.39	-12.21	10.30	26.03	-99.20
3	64.45	-47.61	86.39	-33.04	232.67	-90.58	53.34	-38.79	-21.94	-14.57	179.32	-51.79
4	47.77	-255.96	51.96	-171.71	44.21	-197.99	30.13	-79.75	-4.19	-84.25	14.08	-118.24
5	4.77	-10.30	13.04	-14.03	55.72	-18.02	34.94	-11.35	-8.27	3.73	20.78	-6.68
6	16.60	-33.23	6.19	-11.84	35.72	-109.04	10.44	-11.54	10.41	-21.39	25.29	-97.50
7	0.50	-0.97	1.25	-0.65	3.38	-1.38	0.91	-0.48	-0.75	-0.33	2.47	-0.90
8	105.02	-49.56	33.92	-26.75	199.47	-68.40	36.48	-20.78	71.09	-22.81	162.99	-47.62
9	197.96	-152.86	87.53	-154.68	190.23	-351.20	71.82	-114.42	110.43	1.82	118.41	-236.79
10	88.88	-24.38	28.12	-9.21	34.46	-19.52	21.57	-6.45	60.76	-15.17	12.89	-13.08
11	79.54	-30.43	35.02	-59.69	73.16	-209.72	48.40	-127.54	44.52	29.26	24.77	-82.18
12	8.04	-21.73	32.11	-76.60	48.73	-44.97	80.44	-154.40	-24.07	54.87	-31.70	109.43
13	81.84	-82.11	72.94	-126.44	246.69	-658.09	130.40	-113.53	8.90	44.33	116.29	-544.56
14	113.01	-203.90	146.61	-143.35	423.89	-966.92	272.23	-299.94	-33.61	-60.56	151.66	-666.99
15	138.72	-119.71	131.74	-85.58	322.15	-459.34	214.22	-187.40	6.98	-34.13	107.93	-271.95
16	94.53	-98.21	83.00	-40.13	66.61	-244.02	123.28	-69.72	11.53	-58.08	-56.67	-174.30
17	33.43	-46.35	24.71	-29.16	54.81	-71.97	99.59	-31.95	8.72	-17.19	-44.78	-40.02
18	228.50	-102.44	163.08	-50.39	236.48	-92.54	94.77	-28.69	65.41	-52.05	141.71	-63.85
19	92.00	-37.68	103.56	-30.40	62.25	-140.55	8.16	-22.36	-11.56	-7.28	54.08	-118.19
20	44.93	-49.30	21.42	-63.50	0.55	-0.16	10.76	-14.67	23.51	14.20	-10.20	14.50
21	305.78	-95.03	237.01	-69.83	359.58	-108.33	114.37	-36.00	68.76	-25.19	245.21	-72.32
22	83.02	-42.42	25.87	-58.89	87.29	-70.59	62.46	-58.37	57.15	16.47	24.83	-12.22
23	77.11	-230.96	37.55	-107.75	123.35	-403.06	50.64	-150.74	39.56	-123.21	72.71	-252.32
24	48.80	-105.05	70.02	-162.09	262.76	-801.91	86.02	-207.96	-21.22	57.05	176.74	-593.95
25	307.14	-920.00	124.83	-251.09	277.64	-289.48	126.66	-237.30	182.31	-668.92	150.98	-52.18
26	121.56	-297.42	603.00	-148.32	576.89	-238.89	87.82	-127.21	-481.44	-149.10	489.07	-111.69
27	226.43	-221.76	110.70	-219.29	231.35	-448.01	195.25	-111.47	115.74	-2.47	36.10	-336.54
28	177.34	-163.95	108.94	-113.39	411.10	-86.08	90.80	-71.42	68.40	-50.56	320.30	-14.66
29	19.16	-60.45	41.75	-120.20	34.31	-98.78	25.19	-58.27	-22.59	59.75	9.12	-40.51
30	4.29	-9.49	24.51	-63.86	32.62	-80.10	70.82	-19.32	-20.22	54.37	-38.20	-60.77
31	19.24	-34.03	13.32	-45.22	12.33	-34.70	19.88	-33.54	5.92	11.19	-7.56	-1.16
32	178.55	-574.46	124.72	-395.80	185.44	-656.35	63.05	-216.47	53.82	-178.66	122.39	-439.88
33	158.09	-175.33	65.40	-73.87	47.79	-37.95	71.09	-44.05	92.69	-101.46	-23.30	6.10
34	5.92	-25.51	4.48	-10.74	6.13	-15.91	3.83	-8.15	1.45	-14.76	2.30	-7.75
35	415.35	-119.17	198.03	-86.86	414.50	-125.60	148.11	-77.68	217.33	-32.30	266.39	-47.91
36	330.86	-1515.98	101.52	-277.33	143.07	-38.22	62.14	-170.04	229.33	-1238.64	80.93	131.82
37	3.37	-11.75	2.59	-1.08	13.88	-29.89	2.16	-1.46	0.78	-10.68	11.71	-28.43
38	14.46	-35.47	17.46	-53.35	12.59	-11.06	7.21	-11.68	-3.00	17.88	5.38	0.62
39	20.11	-69.51	24.91	-82.28	37.21	-128.30	29.27	-77.42	-4.80	12.78	7.94	-50.88
40	39.39	-16.00	28.23	-10.33	81.12	-21.51	64.17	-28.13	11.16	-5.67	16.95	6.62
41	13.33	-6.60	19.50	-9.82	236.85	-75.35	25.47	-18.16	-6.17	3.22	211.38	-57.18
42	19.11	-11.85	27.94	-8.69	50.53	-38.78	30.60	-19.30	-8.83	-3.17	19.93	-19.47
43	26.96	-17.11	34.08	-7.80	108.15	-36.04	45.88	-17.97	-7.12	-9.31	62.27	-18.07
44	37.48	-13.29	31.85	-9.91	289.04	-61.07	61.08	-23.76	5.64	-3.38	227.96	-37.31
45	25.22	-17.44	30.98	-10.66	99.21	-28.92	38.48	-14.39	-5.76	-6.79	60.72	-14.53
46	40.44	-13.17	153.93	-38.52	12.46	-5.99	31.13	-5.48	-113.49	25.35	-18.67	-0.51
47	206.75	-100.39	96.15	-50.70	192.07	-45.16	54.02	-131.34	110.61	-49.70	138.05	86.18
48	59.97	-212.74	22.81	-83.69	5.84	-15.11	32.68	-75.88	37.16	-129.04	-26.85	60.77
49	175.31	-63.98	140.96	-45.36	280.86	-89.48	109.13	-35.72	34.35	-18.62	171.74	-53.76
50	239.87	-69.99	179.10	-57.31	309.20	-108.51	80.62	-46.92	60.77	-12.68	228.58	-61.59
51	55.84	-176.33	50.67	-153.59	99.35	-292.82	46.29	-124.21	5.17	-22.75	53.06	-168.62
52	72.69	-32.45	177.25	-69.12	311.10	-117.41	393.52	-89.40	-104.56	36.67	-82.42	-28.01
53	191.70	-466.44	166.93	-369.27	259.98	-415.41	520.45	-148.14	24.77	-97.17	-260.46	-267.27
54	927.36	-362.28	379.93	-131.04	425.95	-222.53	121.75	-166.95	547.43	-231.24	304.20	-55.58
55	159.03	-160.00	162.92	-239.67	109.00	-206.69	284.21	-126.00	-3.90	79.66	-175.21	-80.70
56	87.23	-96.17	40.35	-67.17	110.90	-44.72	55.82	-39.95	46.89	-29.00	55.08	-4.76
57	28.19	-53.34	14.26	-45.76	33.85	-110.51	14.46	-24.21	13.92	-7.57	19.39	-86.30
58	19.24	-64.85	34.64	-77.20	52.18	-114.38	43.00	-13.44	-15.40	12.35	9.18	-100.94
59	59.56	-45.83	26.99	-46.11	91.93	-30.13	62.81	-48.77	32.57	0.28	29.11	18.64
60	215.12	-743.98	115.28	-366.93	135.23	-409.95	69.80	-232.67	99.84	-377.05	65.44	-177.29
61	304.85	-126.34	125.34	-92.03	139.67	-54.32	87.83	-43.95	179.51	-34.30	51.84	-10.37
62	8.10	-26.98	12.30	-18.02	3.35	-9.14	3.35	-7.30	-4.20	-8.95	0.00	-1.84
63	397.60	-139.34	357.32	-119.30	329.22	-180.21	213.10	-105.36	40.28	-20.03	116.12	-74.85
64	274.42	-779.13	167.75	-444.93	288.86	-119.34	89.79	-302.61	106.67	-334.20	199.08	183.27
65	59.41	-73.39	101.63	-113.77	170.98	-530.47	104.18	-253.74	-42.22	40.38	66.80	-276.73
66	385.15	-309.25	190.01	-135.19	333.81	-289.24	178.84	-96.47	195.15	-174.06	154.97	-192.77
67	156.23	-300.98	115.91	-173.79	360.85	-539.38	128.17	-177.87	40.32	-127.20	232.68	-361.51
68	24.98	-68.12	24.57	-64.14	90.40	-271.88	47.43	-96.53	0.41	-3.99	42.97	-175.35
69	330.35	-152.62	107.82	-72.63	169.17	-73.68	103.67	-64.24	222.53	-79.99	65.49	-9.43
70	44.82	-20.07	32.31	-18.78	136.65	-157.82	29.19	-43.02	12.50	-1.29	107.46	-114.80

Table E.18. Maximum ($\epsilon 1$) and minimum ($\epsilon 3$) principal strain values at the location of 70 landmarks during second premolar (P4) bite load for the models of male and female *P. anubis* and *T. gelada* species, and strain differences ($\Delta \epsilon 1$ and $\Delta \epsilon 3$) at landmark locations between male and female models. Strain values are in microstrain (μ strain).

P4 bite landmark	P.anubis (male)		P.anubis (female)		T.gelada (male)		T.gelada (female)		P.anubis(m)-P.anubis(f)		T.gelada(m)-T.gelada(f)	
	$\epsilon 1$	$\epsilon 3$	$\epsilon 1$	$\epsilon 3$	$\epsilon 1$	$\epsilon 3$	$\epsilon 1$	$\epsilon 3$	$\Delta \epsilon 1$	$\Delta \epsilon 3$	$\Delta \epsilon 1$	$\Delta \epsilon 3$
1	13.13	-15.04	11.17	-8.95	18.07	-31.83	10.66	-6.51	1.96	-6.10	7.41	-25.32
2	16.13	-29.63	24.60	-28.81	55.65	-136.71	30.80	-30.59	-8.47	-0.81	24.85	-106.12
3	52.89	-49.08	66.15	-27.12	216.65	-85.15	51.65	-37.52	-13.25	-21.97	165.00	-47.64
4	48.03	-245.63	49.81	-162.33	42.09	-188.24	29.01	-78.36	-1.78	-83.29	13.08	-109.88
5	4.50	-8.77	13.77	-13.56	54.81	-17.79	34.44	-11.17	-9.27	4.79	20.36	-6.62
6	16.86	-33.65	6.60	-12.28	36.39	-111.16	10.50	-11.75	10.27	-21.37	25.89	-99.41
7	0.52	-1.02	1.53	-0.72	3.72	-1.52	1.08	-0.50	-1.01	-0.30	2.64	-1.02
8	105.79	-47.51	34.13	-24.98	194.83	-68.22	36.69	-19.53	71.67	-22.53	158.14	-48.69
9	196.38	-148.43	86.65	-149.90	197.41	-335.68	73.89	-113.09	109.73	1.47	123.52	-222.59
10	94.67	-26.08	32.89	-10.59	37.57	-20.79	22.54	-6.56	61.78	-15.49	15.02	-14.23
11	73.80	-28.88	29.29	-23.96	58.11	-142.49	35.16	-78.71	44.51	-4.92	22.95	-63.78
12	7.86	-24.94	13.55	-30.94	42.27	-38.65	31.63	-60.63	-5.69	6.00	10.64	21.98
13	54.30	-47.26	29.90	-46.00	50.70	-116.72	47.74	-42.91	24.40	-1.25	2.96	-73.81
14	102.21	-183.71	81.97	-174.50	291.26	-399.59	139.67	-278.90	20.25	-9.21	151.58	-120.68
15	139.30	-261.89	142.92	-83.53	308.18	-1197.92	238.54	-281.34	-3.61	-178.36	69.64	-916.57
16	120.69	-140.33	98.69	-61.20	104.33	-373.43	136.53	-83.61	22.00	-79.13	-32.20	-289.82
17	48.17	-71.24	27.84	-40.47	63.47	-109.82	96.84	-33.75	20.33	-30.77	-33.37	-76.06
18	215.48	-96.45	156.17	-48.22	245.34	-96.23	89.70	-27.17	59.30	-48.23	155.64	-69.06
19	109.13	-45.47	120.61	-33.07	68.10	-145.97	6.73	-15.98	-11.49	-12.40	61.37	-130.00
20	44.09	-47.42	20.76	-62.20	0.54	-0.18	10.51	-13.93	23.33	14.78	-9.96	13.75
21	314.14	-98.40	242.16	-71.32	372.26	-112.39	117.08	-37.34	71.98	-27.08	255.18	-75.05
22	70.67	-41.61	25.72	-70.58	66.87	-70.85	59.23	-59.00	44.95	28.97	7.64	-11.85
23	76.83	-230.56	35.12	-99.77	124.28	-406.41	50.88	-150.56	41.71	-130.79	73.40	-255.84
24	41.44	-99.15	55.25	-141.68	261.73	-797.17	72.58	-179.73	-13.82	42.53	189.14	-617.44
25	306.42	-920.24	125.43	-253.67	281.55	-293.63	128.05	-245.02	180.99	-666.57	153.50	-48.61
26	119.49	-293.05	612.32	-150.70	597.43	-246.28	89.52	-124.37	-492.83	-142.35	507.90	-121.91
27	225.65	-224.41	110.67	-221.78	233.50	-459.44	194.75	-112.71	114.98	-2.63	38.75	-346.73
28	178.49	-154.50	116.36	-109.02	418.43	-86.45	93.80	-71.62	62.14	-45.48	324.62	-14.82
29	18.61	-58.79	42.34	-122.33	33.54	-96.60	25.07	-57.56	-23.73	63.54	8.47	-39.04
30	4.54	-7.25	23.45	-59.98	31.09	-74.71	72.22	-19.58	-18.92	52.73	-41.13	-55.12
31	20.59	-40.57	14.24	-46.82	15.41	-47.62	16.71	-31.26	6.34	6.24	-1.30	-16.35
32	178.43	-574.16	122.87	-389.74	185.68	-657.42	64.12	-220.09	55.57	-184.41	121.56	-437.33
33	155.33	-177.69	63.20	-75.38	41.59	-46.47	67.25	-44.41	92.13	-102.30	-25.66	-2.05
34	5.60	-24.12	4.03	-9.74	6.00	-15.43	3.55	-7.61	1.57	-14.38	2.45	-7.82
35	413.89	-118.59	193.95	-84.84	411.54	-124.46	147.90	-77.51	219.94	-33.75	263.64	-46.95
36	331.62	-1510.01	99.87	-271.03	140.54	-31.50	62.05	-168.95	231.75	-1238.98	78.49	137.46
37	3.71	-11.20	2.93	-1.20	14.29	-27.88	2.20	-1.52	0.78	-10.00	12.09	-26.37
38	14.78	-37.75	18.15	-55.53	11.26	-13.05	6.96	-12.16	-3.37	17.78	4.30	-0.89
39	17.64	-59.82	19.78	-65.55	29.63	-100.66	23.75	-63.28	-2.14	5.73	5.88	-37.38
40	31.81	-12.50	18.58	-6.95	72.51	-18.52	43.10	-19.07	13.23	-5.55	29.41	0.55
41	10.30	-5.20	12.18	-6.48	214.57	-74.14	17.06	-13.10	-1.88	1.28	197.51	-61.04
42	14.22	-9.22	19.00	-5.98	40.67	-34.95	21.55	-14.48	-4.78	-3.24	19.12	-20.47
43	21.00	-13.60	23.40	-5.02	79.00	-37.28	33.36	-13.32	-2.39	-8.58	45.64	-23.96
44	30.13	-11.30	23.40	-7.27	249.43	-51.05	46.60	-18.30	6.73	-4.03	202.83	-32.75
45	21.22	-16.63	24.19	-8.72	87.11	-24.78	30.99	-12.12	-2.96	-7.91	56.12	-12.66
46	37.84	-12.24	138.06	-34.22	6.78	-3.35	28.32	-5.10	-100.21	21.97	-21.54	1.75
47	199.85	-103.07	90.71	-54.83	192.07	-46.19	53.83	-133.70	109.14	-48.25	138.25	87.51
48	59.76	-212.07	22.66	-83.51	5.89	-15.27	32.34	-75.10	37.10	-128.55	-26.45	59.82
49	169.92	-62.22	136.32	-43.80	264.98	-84.50	103.85	-34.01	33.60	-18.41	161.13	-50.49
50	241.29	-70.28	186.30	-59.27	314.57	-110.61	83.43	-46.00	54.99	-11.01	231.14	-64.62
51	50.00	-161.94	50.41	-147.00	92.35	-267.72	45.25	-117.23	-0.42	-14.94	47.10	-150.49
52	63.69	-31.90	160.69	-62.95	307.64	-117.14	377.54	-84.57	-97.00	31.05	-69.90	-32.57
53	190.45	-466.35	166.92	-369.19	260.30	-415.96	520.39	-147.67	23.53	-97.16	-260.09	-268.29
54	929.33	-362.73	380.99	-131.66	424.37	-222.13	122.55	-165.63	548.35	-231.07	301.82	-56.50
55	158.03	-160.12	163.19	-241.75	109.01	-204.56	283.05	-126.99	-5.15	81.63	-174.03	-77.57
56	86.08	-92.66	36.96	-60.73	105.05	-39.74	52.36	-35.41	49.12	-31.94	52.68	-4.33
57	27.51	-51.82	12.93	-39.83	32.41	-105.91	14.06	-23.73	14.58	-11.99	18.36	-82.18
58	19.29	-64.88	34.04	-76.01	51.08	-113.38	40.32	-12.66	-14.75	11.13	10.76	-100.72
59	62.95	-45.00	27.80	-44.72	102.68	-33.64	63.79	-47.98	35.15	-0.29	38.89	14.34
60	214.89	-743.19	115.26	-366.97	132.71	-401.15	69.68	-232.42	99.63	-376.22	63.03	-168.73
61	304.17	-126.04	124.83	-92.20	144.14	-54.70	87.29	-43.77	179.34	-33.84	56.85	-10.93
62	7.82	-26.07	11.99	-17.53	3.15	-8.60	3.22	-6.96	-4.16	-8.53	-0.06	-1.65
63	396.11	-138.97	354.71	-118.69	324.54	-178.23	212.09	-105.06	41.40	-20.28	112.45	-73.16
64	274.84	-779.42	168.29	-446.27	289.55	-120.80	90.20	-303.29	106.55	-333.15	199.36	182.49
65	56.80	-35.60	104.51	-80.38	145.21	-479.42	107.42	-242.21	-47.71	44.78	37.79	-237.21
66	393.03	-319.72	192.63	-140.19	348.71	-318.42	180.99	-100.03	200.40	-179.53	167.72	-218.38
67	139.01	-286.24	97.56	-156.82	295.75	-509.72	95.01	-108.03	41.45	-129.42	200.74	-401.69
68	24.01	-69.72	20.12	-58.29	82.76	-243.30	42.74	-85.87	3.89	-11.43	40.02	-157.44
69	327.55	-150.82	105.29	-71.60	162.16	-68.57	101.93	-62.60	222.26	-79.22	60.23	-5.97
70	44.48	-20.58	31.55	-17.58	141.48	-155.76	20.86	-34.60	12.93	-3.00	120.62	-121.16

Table E.19. Maximum ($\epsilon 1$) and minimum ($\epsilon 3$) principal strain values at the location of 70 landmarks during first molar (M1) bite load for the models of male and female P. anubis and T. gelada species, and strain differences ($\Delta \epsilon 1$ and $\Delta \epsilon 3$) at landmark locations between male and female models. Strain values are in microstrain (μ strain).

M1 bite landmark	P.anubis (male)		P.anubis (female)		T.gelada (male)		T.gelada (female)		P.anubis(m)-P.anubis(f)		T.gelada(m)-T.gelada(f)	
	$\epsilon 1$	$\epsilon 3$	$\epsilon 1$	$\epsilon 3$	$\epsilon 1$	$\epsilon 3$	$\epsilon 1$	$\epsilon 3$	$\Delta \epsilon 1$	$\Delta \epsilon 3$	$\Delta \epsilon 1$	$\Delta \epsilon 3$
1	10.21	-12.10	4.90	-6.45	3.30	-9.60	2.58	-3.11	5.31	-5.65	0.72	-6.49
2	22.34	-8.75	22.04	-8.03	11.12	-30.54	13.34	-7.75	0.30	-0.72	-2.21	-22.79
3	47.81	-43.46	60.20	-23.68	186.56	-72.97	47.84	-33.71	-12.38	-19.78	138.71	-39.25
4	46.97	-231.97	45.67	-145.57	37.92	-168.81	26.71	-75.34	1.31	-86.40	11.21	-93.47
5	4.22	-7.09	15.02	-12.42	52.95	-17.22	33.65	-10.89	-10.80	5.33	19.29	-6.33
6	17.12	-34.03	6.79	-12.55	37.36	-114.16	10.57	-12.10	10.33	-21.48	26.79	-102.05
7	0.54	-1.06	1.97	-0.83	4.46	-1.81	1.47	-0.59	-1.44	-0.23	2.98	-1.22
8	103.59	-44.45	33.13	-22.17	181.47	-65.45	37.08	-17.18	70.46	-22.29	144.38	-48.27
9	193.29	-139.81	77.44	-147.70	188.66	-303.31	74.52	-109.40	115.85	7.89	114.15	-193.90
10	98.84	-27.24	38.03	-12.04	39.79	-22.06	24.14	-6.95	60.82	-15.20	15.65	-15.11
11	65.10	-25.99	32.16	-10.62	48.75	-26.86	29.76	-28.99	32.94	-15.38	18.99	2.13
12	12.58	-38.59	5.84	-14.52	2.34	-4.48	7.78	-18.47	6.73	-24.08	-5.43	13.99
13	15.51	-13.45	4.30	-3.13	21.30	-41.49	10.26	-3.74	11.21	-10.32	11.04	-37.75
14	34.39	-39.74	14.14	-13.85	98.45	-60.77	13.26	-5.04	20.25	-25.89	85.19	-55.73
15	56.50	-71.03	62.37	-43.68	132.15	-79.95	45.03	-82.19	-5.87	-27.35	87.12	2.24
16	102.71	-126.60	88.69	-54.44	65.29	-247.18	147.36	-122.22	14.02	-72.17	-82.07	-124.96
17	44.57	-73.54	30.62	-47.18	53.59	-107.81	89.97	-36.44	13.95	-26.36	-36.38	-71.37
18	160.29	-72.17	128.14	-39.60	187.22	-72.89	74.34	-22.49	32.15	-32.56	112.87	-50.41
19	121.74	-53.13	136.74	-35.21	78.87	-155.23	9.91	-7.91	-15.00	-17.92	68.96	-147.32
20	43.51	-45.79	20.09	-61.13	0.54	-0.19	10.07	-12.61	23.41	15.34	-9.53	12.42
21	322.87	-101.70	254.43	-74.84	402.15	-121.96	123.54	-40.40	68.44	-26.86	278.61	-81.56
22	67.40	-42.65	27.03	-79.43	62.62	-72.79	55.17	-60.38	40.37	36.78	7.44	-12.41
23	75.70	-228.91	31.81	-90.96	122.86	-402.91	51.14	-149.66	43.88	-137.95	71.72	-253.24
24	38.35	-77.05	41.38	-95.06	198.83	-604.91	46.95	-126.17	-3.03	18.01	151.88	-478.74
25	305.33	-916.87	125.65	-254.64	282.14	-290.67	130.26	-257.42	179.68	-662.23	151.88	-33.26
26	118.78	-291.34	620.65	-152.94	606.46	-249.77	92.54	-120.19	-501.88	-138.39	513.93	-129.59
27	224.99	-225.51	110.80	-224.29	234.15	-465.30	193.83	-114.70	114.19	-1.22	40.32	-350.60
28	177.03	-140.24	124.05	-97.59	428.07	-86.71	101.08	-71.74	52.99	-42.66	326.99	-14.97
29	18.38	-58.01	43.01	-124.96	33.22	-95.65	24.77	-56.23	-24.63	66.95	8.45	-39.42
30	5.35	-5.87	23.03	-58.07	29.31	-68.18	75.43	-20.37	-17.68	52.20	-46.12	-47.81
31	20.38	-42.53	14.55	-47.32	15.48	-48.64	11.78	-27.07	5.83	4.79	3.70	-21.57
32	178.27	-573.62	121.56	-385.39	185.35	-656.37	65.85	-225.92	56.71	-188.22	119.50	-430.46
33	154.17	-178.95	61.58	-77.02	40.16	-51.94	61.60	-45.38	92.59	-101.93	-21.43	-6.56
34	5.20	-22.44	3.42	-8.27	5.65	-14.24	3.05	-6.60	1.79	-14.16	2.60	-7.64
35	412.93	-118.30	190.81	-83.26	407.86	-123.33	147.48	-77.22	222.12	-35.04	260.38	-46.11
36	333.41	-1509.02	99.97	-267.53	139.60	-28.83	62.19	-167.91	233.44	-1241.49	77.41	139.08
37	4.10	-10.27	3.23	-1.30	14.77	-23.60	2.26	-1.61	0.87	-8.97	12.52	-21.99
38	14.65	-38.00	17.75	-54.47	9.99	-14.34	6.62	-12.89	-3.10	16.47	3.37	-1.45
39	15.67	-54.01	15.64	-52.70	21.93	-73.66	17.00	-45.95	0.03	-1.31	4.93	-27.71
40	21.51	-8.73	4.14	-2.75	19.51	-8.24	19.29	-7.93	17.37	-5.97	0.22	-0.31
41	7.69	-4.38	4.15	-1.92	111.86	-39.29	7.81	-6.86	3.53	-2.46	104.04	-32.43
42	10.98	-5.89	10.25	-3.31	19.06	-20.21	10.96	-7.96	0.73	-2.58	8.10	-12.24
43	17.68	-8.11	12.20	-3.36	35.68	-27.43	17.50	-6.90	5.48	-4.74	18.19	-20.53
44	21.60	-8.30	13.88	-4.39	140.04	-27.32	26.86	-10.70	7.72	-3.91	113.18	-16.62
45	16.93	-15.55	17.71	-7.05	59.34	-16.32	20.81	-9.24	-0.78	-8.49	38.53	-7.08
46	37.18	-11.79	121.58	-29.67	9.62	-4.79	24.85	-4.65	-84.40	17.89	-15.22	-0.14
47	185.89	-98.65	80.01	-54.05	175.23	-42.16	52.14	-134.54	105.88	-44.60	123.09	92.38
48	58.77	-208.75	21.99	-82.31	5.64	-14.61	31.54	-73.19	36.77	-126.44	-25.90	58.57
49	167.68	-60.60	134.24	-43.00	247.86	-79.38	97.17	-31.85	33.44	-17.60	150.69	-47.53
50	235.35	-68.46	183.56	-58.47	305.14	-107.55	87.23	-44.46	51.79	-9.99	217.91	-63.09
51	43.46	-144.61	48.00	-133.12	80.44	-226.45	43.22	-103.81	-4.54	-11.49	37.21	-122.64
52	55.98	-27.95	141.47	-55.57	247.26	-93.30	348.27	-76.62	-85.50	27.61	-101.01	-16.68
53	188.91	-469.66	167.85	-372.09	267.10	-439.85	520.42	-147.13	21.06	-97.58	-253.32	-292.72
54	938.22	-363.38	384.17	-133.80	442.85	-222.80	124.40	-162.51	554.05	-229.58	318.45	-60.29
55	156.66	-161.27	164.05	-246.79	112.95	-206.98	281.33	-129.77	-7.39	85.52	-168.37	-77.20
56	88.10	-90.59	37.34	-53.91	103.47	-41.06	48.56	-29.83	50.77	-36.68	54.91	-11.23
57	26.77	-50.22	11.92	-35.80	29.97	-97.80	13.40	-22.90	14.84	-14.42	16.57	-74.90
58	19.03	-63.88	33.03	-73.89	47.91	-108.29	35.77	-11.38	-14.00	10.01	12.14	-96.91
59	63.76	-42.38	27.05	-41.81	104.34	-34.13	64.77	-46.07	36.70	-0.57	39.57	11.93
60	214.23	-741.03	114.68	-364.45	133.15	-401.87	69.81	-233.12	99.55	-376.58	63.33	-168.75
61	297.47	-124.46	122.06	-92.94	135.66	-53.23	85.80	-43.23	175.41	-31.52	49.85	-10.01
62	7.40	-24.64	11.26	-16.47	2.89	-7.71	2.96	-6.32	-3.86	-8.17	-0.07	-1.40
63	394.31	-138.36	348.66	-117.26	320.15	-176.01	209.89	-104.43	45.65	-21.10	110.25	-71.58
64	274.25	-775.75	167.46	-443.37	287.45	-116.74	90.84	-303.52	106.79	-332.38	196.61	186.78
65	63.48	-26.91	104.55	-36.05	134.05	-395.60	112.02	-216.85	-41.07	9.14	22.03	-178.75
66	393.64	-321.37	190.72	-141.63	347.03	-319.17	183.87	-104.46	202.92	-179.74	163.17	-214.71
67	94.56	-208.09	48.66	-85.92	165.55	-296.48	38.62	-34.41	45.89	-122.17	126.93	-262.07
68	22.75	-75.78	19.14	-55.07	82.94	-241.86	35.33	-69.94	3.61	-20.71	47.61	-171.92
69	332.27	-153.67	103.59	-71.81	169.16	-83.08	100.05	-60.52	228.68	-81.86	69.11	-22.56
70	52.59	-22.24	33.02	-16.22	98.25	-99.35	10.04	-20.81	19.56	-6.03	88.21	-78.54

Table E.20. Maximum ($\epsilon 1$) and minimum ($\epsilon 3$) principal strain values at the location of 70 landmarks during second molar (M2) bite load for the models of male and female P. anubis and T. gelada species, and strain differences ($\Delta\epsilon 1$ and $\Delta\epsilon 3$) at landmark locations between male and female models. Strain values are in microstrain (μ strain).

M2 bite landmark	P.anubis (male)		P.anubis (female)		T.gelada (male)		T.gelada (female)		P.anubis(m)-P.anubis(f)		T.gelada(m)-T.gelada(f)	
	$\epsilon 1$	$\epsilon 3$	$\epsilon 1$	$\epsilon 3$	$\epsilon 1$	$\epsilon 3$	$\epsilon 1$	$\epsilon 3$	$\Delta\epsilon 1$	$\Delta\epsilon 3$	$\Delta\epsilon 1$	$\Delta\epsilon 3$
1	7.42	-7.80	6.00	-7.19	3.44	-5.75	1.82	-1.75	1.41	-0.61	1.62	-4.00
2	31.09	-9.16	26.30	-9.43	12.34	-18.20	7.99	-3.72	4.79	0.26	4.35	-14.47
3	36.52	-39.76	44.39	-18.24	124.32	-49.41	37.23	-28.38	-7.87	-21.52	87.09	-21.03
4	47.18	-209.40	40.88	-120.31	32.13	-133.82	22.70	-70.68	6.31	-89.09	9.43	-63.14
5	3.83	-4.31	16.89	-10.57	50.56	-16.69	32.22	-10.38	-13.06	6.26	18.34	-6.31
6	17.61	-34.84	7.49	-13.41	39.46	-120.79	10.77	-12.82	10.12	-21.43	28.69	-107.97
7	0.58	-1.15	2.72	-1.03	5.73	-2.33	2.29	-0.84	-2.14	-0.12	3.44	-1.49
8	102.71	-39.62	32.95	-17.65	166.41	-66.17	38.35	-13.31	69.76	-21.96	128.07	-52.85
9	174.44	-115.75	54.25	-128.70	151.09	-209.28	62.72	-94.57	120.19	12.95	88.37	-114.72
10	108.21	-29.99	47.59	-14.95	48.59	-25.97	26.57	-7.79	60.62	-15.04	22.02	-18.18
11	50.51	-20.48	31.88	-10.12	54.71	-23.63	29.70	-12.63	18.62	-10.36	25.01	-11.01
12	14.01	-36.41	7.45	-14.05	4.15	-3.67	6.89	-13.78	6.57	-22.36	-2.74	10.10
13	6.60	-6.42	7.09	-4.62	6.60	-20.02	12.25	-6.81	-0.49	-1.80	-5.66	-13.21
14	7.29	-13.01	3.92	-1.51	25.31	-14.57	13.87	-5.56	3.37	-11.51	11.43	-9.01
15	19.35	-21.76	12.34	-6.83	58.67	-36.61	6.97	-2.86	7.01	-14.93	51.70	-33.75
16	12.70	-47.40	7.40	-28.13	14.50	-12.23	22.60	-83.04	5.30	-19.26	-8.10	70.80
17	54.53	-102.18	45.76	-77.49	73.74	-175.11	88.81	-61.45	8.77	-24.68	-15.07	-113.66
18	52.99	-26.31	61.75	-19.75	97.91	-37.51	41.20	-12.32	-8.76	-6.56	56.71	-25.19
19	151.10	-70.52	171.23	-40.47	100.78	-184.85	33.50	-14.71	-20.12	-30.05	67.27	-170.14
20	42.12	-42.36	18.81	-58.97	0.60	-0.27	9.27	-10.28	23.31	16.61	-8.67	10.02
21	340.53	-108.76	272.93	-80.30	459.14	-140.20	137.24	-46.64	67.60	-28.45	321.90	-93.56
22	54.58	-44.74	30.13	-98.61	39.24	-101.47	48.40	-62.93	24.45	53.87	-9.15	-38.54
23	74.34	-226.46	26.81	-78.73	122.01	-402.31	51.68	-147.92	47.53	-147.73	70.33	-254.39
24	29.94	-58.94	26.29	-57.51	147.68	-446.27	22.80	-69.94	3.66	-1.44	124.88	-376.33
25	303.92	-914.46	126.02	-256.33	286.50	-292.73	134.12	-278.21	177.90	-658.14	152.38	-14.52
26	116.37	-286.16	637.07	-157.30	654.20	-267.31	98.51	-113.08	-520.70	-128.86	555.69	-154.23
27	224.12	-229.34	111.07	-228.75	239.17	-489.67	192.56	-118.58	113.04	-0.60	46.61	-371.09
28	180.67	-116.57	131.20	-74.16	469.36	-91.82	112.78	-67.66	49.47	-42.41	356.58	-24.17
29	17.61	-55.57	44.10	-129.24	31.43	-90.58	24.08	-53.49	-26.49	73.67	7.35	-37.09
30	9.32	-5.27	21.92	-53.26	25.41	-51.45	80.50	-21.72	-12.60	47.99	-55.09	-29.73
31	21.45	-50.43	15.67	-50.72	25.63	-79.02	5.80	-21.08	5.78	0.29	19.83	-57.94
32	178.22	-573.54	119.01	-376.99	186.76	-661.68	68.63	-235.26	59.20	-196.54	118.13	-426.42
33	150.68	-182.42	58.80	-80.02	42.15	-87.58	53.09	-48.13	91.88	-102.39	-10.94	-39.45
34	4.52	-19.42	2.33	-5.76	5.42	-12.57	2.16	-4.86	2.19	-13.66	3.25	-7.71
35	411.08	-117.54	185.19	-80.31	404.80	-122.44	146.62	-76.68	225.89	-37.23	258.18	-45.75
36	336.16	-1503.18	99.04	-259.44	134.90	-13.45	62.21	-165.36	237.12	-1243.75	72.69	151.91
37	5.45	-9.32	3.78	-1.56	17.78	-18.32	2.33	-1.77	1.67	-7.76	15.45	-16.55
38	15.03	-40.73	18.01	-55.49	9.52	-21.72	6.29	-14.34	-2.98	14.76	3.23	-7.39
39	12.35	-42.48	11.22	-37.84	11.72	-35.26	10.58	-29.43	1.13	-4.64	1.15	-5.82
40	14.87	-6.80	3.88	-3.58	8.68	-12.19	6.10	-4.34	10.99	-3.21	2.58	-7.85
41	4.84	-3.68	3.53	-1.80	56.00	-23.20	2.88	-2.77	1.30	-1.88	53.11	-20.43
42	11.20	-4.18	7.65	-3.47	6.85	-11.47	4.59	-3.16	3.55	-0.71	2.27	-8.31
43	19.33	-3.65	8.28	-5.50	13.49	-29.08	7.01	-2.41	11.05	1.86	6.48	-26.68
44	12.81	-4.67	6.59	-2.32	51.00	-8.70	10.94	-4.23	6.22	-2.35	40.06	-4.47
45	11.83	-13.99	10.69	-5.25	31.97	-7.99	11.31	-6.59	1.14	-8.74	20.66	-1.40
46	34.44	-10.65	98.77	-23.74	6.70	-3.63	20.04	-4.00	-64.33	13.09	-13.34	0.37
47	168.76	-98.05	66.30	-56.91	166.20	-43.97	49.75	-134.74	102.46	-41.14	116.45	90.77
48	57.57	-204.74	21.16	-80.94	5.56	-14.42	30.33	-70.16	36.41	-123.79	-24.76	55.74
49	160.07	-57.58	128.56	-41.03	208.75	-67.25	88.61	-29.08	31.51	-16.55	120.13	-38.18
50	233.14	-67.65	187.99	-60.02	307.39	-109.12	94.72	-43.22	45.16	-7.63	212.67	-65.90
51	35.85	-117.46	45.64	-112.79	59.01	-143.90	40.98	-83.46	-9.79	-4.67	18.03	-60.44
52	44.64	-24.44	113.00	-44.51	191.13	-72.15	286.17	-62.34	-68.36	20.07	-95.04	-9.81
53	186.68	-472.44	168.79	-375.05	273.08	-460.25	520.58	-146.95	17.89	-97.39	-247.50	-313.30
54	946.78	-364.30	388.13	-136.36	454.95	-222.74	127.06	-158.25	558.66	-227.94	327.89	-64.49
55	154.91	-162.47	165.20	-253.46	116.46	-206.04	279.33	-134.65	-10.29	90.98	-162.87	-71.39
56	87.80	-84.91	35.82	-44.20	94.76	-36.32	43.57	-22.36	51.98	-40.71	51.18	-13.96
57	25.67	-47.81	9.81	-26.61	25.40	-82.87	12.58	-21.92	15.86	-21.20	12.82	-60.95
58	19.04	-63.65	31.63	-71.02	43.81	-102.92	29.21	-9.52	-12.58	7.37	14.60	-93.40
59	68.35	-39.20	27.15	-37.57	125.16	-40.85	67.22	-43.16	41.20	-1.63	57.94	2.31
60	213.52	-738.64	114.12	-362.00	129.00	-386.82	69.99	-234.09	99.41	-376.63	59.01	-152.73
61	291.80	-122.99	118.95	-93.79	137.08	-52.73	83.76	-42.51	172.85	-29.20	53.33	-10.22
62	6.73	-22.43	10.20	-14.96	2.44	-6.15	2.53	-5.24	-3.47	-7.46	-0.09	-0.91
63	391.44	-137.54	340.74	-115.42	308.44	-170.71	206.60	-103.46	50.70	-22.13	101.84	-67.24
64	274.71	-774.39	167.12	-441.58	287.04	-116.32	91.98	-304.43	107.59	-332.81	195.06	188.11
65	87.55	-41.32	89.78	-39.17	157.91	-232.07	111.53	-169.06	-2.24	-2.15	46.38	-63.00
66	401.97	-331.91	189.04	-146.58	378.86	-381.79	188.96	-111.41	212.93	-185.33	189.89	-270.39
67	57.31	-141.35	22.83	-44.34	60.25	-186.83	20.02	-19.06	34.48	-97.01	40.23	-167.77
68	23.29	-77.32	15.21	-46.78	73.98	-201.72	25.46	-49.44	8.08	-30.54	48.52	-152.28
69	332.80	-154.37	100.14	-71.34	163.40	-86.20	97.13	-57.37	232.66	-83.04	66.27	-28.83
70	58.21	-22.12	33.65	-14.83	91.52	-68.62	4.19	-8.79	24.56	-7.29	87.33	-59.83

Table E.21. Maximum ($\epsilon 1$) and minimum ($\epsilon 3$) principal strain values at the location of 70 landmarks during third molar (M3) bite load for the models of male and female P. anubis and T. gelada species, and strain differences ($\Delta \epsilon 1$ and $\Delta \epsilon 3$) at landmark locations between male and female models. Strain values are in microstrain (μ strain).

M3 bite landmark	P.anubis (male)		P.anubis (female)		T.gelada (male)		T.gelada (female)		P.anubis(m)-P.anubis(f)		T.gelada(m)-T.gelada(f)	
	$\epsilon 1$	$\epsilon 3$	$\epsilon 1$	$\epsilon 3$	$\epsilon 1$	$\epsilon 3$	$\epsilon 1$	$\epsilon 3$	$\Delta \epsilon 1$	$\Delta \epsilon 3$	$\Delta \epsilon 1$	$\Delta \epsilon 3$
1	4.34	-3.44	5.59	-7.76	11.68	-11.03	2.22	-3.25	-1.25	4.32	9.46	-7.78
2	34.61	-9.27	27.60	-8.94	35.16	-30.62	11.65	-4.43	7.00	-0.33	23.51	-26.19
3	24.86	-35.39	26.03	-11.59	43.75	-19.27	21.07	-19.23	-1.17	-23.80	22.69	-0.04
4	49.83	-179.81	39.29	-91.05	39.85	-91.84	28.35	-63.38	10.54	-88.76	11.50	-28.47
5	3.55	-2.62	19.12	-7.68	47.12	-16.06	29.26	-9.38	-15.56	5.07	17.86	-6.69
6	18.33	-36.02	8.66	-14.97	42.49	-130.32	11.19	-14.15	9.67	-21.05	31.30	-116.17
7	0.65	-1.27	3.89	-1.33	7.70	-3.13	3.81	-1.34	-3.24	0.05	3.89	-1.80
8	102.30	-32.90	33.03	-13.50	152.90	-74.63	40.14	-25.18	69.27	-19.39	112.76	-49.44
9	114.24	-85.75	31.66	-101.10	58.65	-115.08	28.95	-74.19	82.59	15.34	29.70	-40.89
10	121.32	-33.92	59.56	-18.74	59.70	-31.02	28.67	-8.57	61.76	-15.18	31.04	-22.45
11	33.88	-13.93	24.00	-8.13	16.56	-7.27	21.03	-8.24	9.88	-5.80	-4.47	0.97
12	12.10	-25.80	12.35	-10.09	9.89	-5.43	18.46	-11.54	-0.25	-15.70	-8.57	6.11
13	10.56	-8.41	10.16	-5.99	2.06	-5.84	13.22	-8.05	0.39	-2.42	-11.16	2.22
14	3.77	-5.44	12.14	-5.70	17.18	-10.76	18.24	-8.62	-8.38	0.26	-1.06	-2.14
15	3.20	-9.99	12.48	-6.11	20.86	-17.22	15.00	-9.32	-9.28	-3.88	5.87	-7.90
16	9.46	-26.09	14.19	-16.47	29.74	-9.82	11.85	-4.29	-4.73	-9.62	17.89	-5.53
17	21.77	-68.90	26.65	-46.82	17.59	-21.43	33.42	-152.44	-4.88	-22.08	-15.82	131.01
18	164.45	-343.28	58.25	-180.85	109.64	-157.89	36.78	-111.80	106.20	-162.42	72.86	-46.10
19	194.61	-97.89	223.07	-50.19	126.07	-215.64	83.86	-35.11	-28.45	-47.70	42.22	-180.53
20	40.35	-37.47	16.91	-55.50	0.70	-0.44	8.22	-6.41	23.45	18.03	-7.52	5.97
21	366.26	-119.22	292.81	-86.45	545.72	-167.93	160.42	-56.31	73.45	-32.77	385.30	-111.62
22	40.45	-51.72	34.48	-120.99	45.66	-170.57	40.00	-65.29	5.97	69.26	5.66	-105.28
23	72.86	-223.90	22.20	-70.48	118.73	-395.60	51.98	-144.17	50.66	-153.42	66.75	-251.43
24	19.49	-40.03	13.90	-25.51	75.16	-221.31	13.78	-22.03	5.59	-14.52	61.38	-199.28
25	302.52	-911.80	126.36	-257.89	284.74	-287.28	140.70	-311.78	176.16	-653.91	144.04	-24.50
26	114.05	-281.28	657.32	-162.74	710.93	-288.56	109.93	-103.18	-543.27	-118.55	600.99	-185.38
27	224.15	-234.19	111.57	-234.24	244.29	-511.53	190.95	-125.39	112.57	0.05	53.34	-386.15
28	191.99	-85.05	125.10	-42.12	542.86	-115.59	123.35	-51.56	66.89	-42.94	419.51	-64.04
29	16.45	-51.87	44.56	-132.07	29.42	-84.66	22.19	-47.71	-28.12	80.20	7.23	-36.95
30	17.61	-6.98	20.40	-46.61	24.15	-31.88	86.01	-23.56	-2.79	39.63	-61.86	-8.32
31	23.26	-61.53	17.94	-56.90	38.89	-114.16	5.69	-19.32	5.32	-4.63	33.20	-94.84
32	178.86	-575.94	115.73	-366.18	190.02	-673.49	72.45	-248.08	63.14	-209.76	117.57	-425.41
33	146.70	-187.21	55.72	-83.69	53.91	-137.63	43.52	-55.09	90.99	-103.51	10.39	-82.54
34	3.58	-14.99	0.71	-2.09	5.77	-10.54	0.86	-2.14	2.87	-12.90	4.91	-8.40
35	410.53	-117.05	178.39	-76.53	408.88	-123.67	144.70	-75.69	232.14	-40.52	264.18	-47.98
36	339.99	-1495.10	97.86	-248.19	130.86	2.98	62.42	-161.58	242.13	-1246.91	68.44	164.56
37	8.25	-8.66	4.57	-2.01	25.63	-13.70	2.32	-2.01	3.69	-6.64	23.31	-11.69
38	15.82	-45.19	18.85	-58.37	11.33	-32.97	6.08	-16.80	-3.03	13.18	5.25	-16.17
39	8.24	-27.96	6.53	-21.45	14.14	-8.60	4.80	-12.83	1.71	-6.51	9.35	4.22
40	10.04	-5.30	3.43	-6.60	4.28	-17.33	2.29	-5.42	6.61	1.30	1.98	-11.91
41	5.14	-3.28	5.28	-3.15	10.75	-8.91	1.12	-0.92	-0.14	-0.13	9.63	-7.99
42	15.49	-5.28	8.15	-4.80	3.88	-7.82	2.67	-1.47	7.34	-0.47	1.21	-6.34
43	29.30	-6.21	8.79	-7.79	5.83	-22.11	5.03	-2.88	20.52	1.58	0.80	-19.23
44	9.01	-2.41	7.07	-1.58	6.53	-19.92	3.92	-1.87	1.94	-0.83	2.61	-18.05
45	7.61	-10.92	5.28	-3.32	8.79	-3.39	3.95	-3.53	2.34	-7.59	4.85	0.14
46	30.28	-9.17	75.66	-18.11	6.74	-3.75	14.11	-2.87	-45.38	8.94	-7.36	-0.88
47	148.58	-98.27	51.08	-59.58	162.99	-46.34	45.21	-128.33	97.50	-38.69	117.78	81.99
48	55.88	-198.96	19.72	-78.41	5.37	-13.96	28.15	-64.24	36.16	-120.56	-22.78	50.28
49	148.06	-53.30	118.74	-37.72	163.65	-53.30	78.15	-25.68	29.32	-15.58	85.50	-27.62
50	232.66	-67.31	198.38	-63.84	309.54	-110.85	106.55	-42.77	34.28	-3.48	202.99	-68.08
51	41.54	-84.72	44.22	-87.75	50.78	-53.18	40.15	-57.00	-2.68	3.03	10.63	3.82
52	31.29	-20.54	73.89	-29.19	104.32	-37.73	177.60	-38.52	-42.61	8.65	-73.28	0.79
53	184.09	-475.49	169.62	-377.74	280.32	-485.70	520.85	-147.73	14.47	-97.75	-240.53	-337.97
54	956.28	-365.45	392.92	-139.44	474.93	-223.54	131.00	-151.62	563.36	-226.01	343.93	-71.92
55	153.10	-164.05	166.65	-261.33	121.57	-207.84	277.62	-143.19	-13.55	97.27	-156.05	-64.65
56	84.87	-74.74	31.61	-30.30	84.98	-33.34	36.71	-13.24	53.26	-44.44	48.27	-20.10
57	24.28	-44.73	6.77	-12.93	19.66	-63.84	11.67	-20.83	17.51	-31.80	7.99	-43.01
58	19.26	-63.92	29.61	-66.94	39.27	-96.79	20.60	-7.03	-10.35	3.01	18.67	-89.76
59	75.91	-34.93	28.15	-32.23	150.10	-48.84	71.78	-38.50	47.75	-2.69	78.32	-10.34
60	212.72	-735.96	113.48	-358.92	125.03	-372.07	70.38	-235.90	99.23	-377.04	54.65	-136.17
61	285.59	-121.32	115.66	-94.61	135.15	-51.58	80.68	-41.43	169.93	-26.71	54.46	-10.15
62	5.78	-19.26	8.55	-12.62	2.27	-4.38	1.72	-3.19	-2.76	-6.63	0.55	-1.19
63	387.91	-136.57	331.76	-113.34	295.52	-164.79	201.46	-101.93	56.15	-23.22	94.06	-62.86
64	275.86	-773.94	166.77	-439.45	285.65	-113.88	93.74	-304.69	109.09	-334.49	191.91	190.81
65	91.49	-43.91	57.90	-32.23	188.12	-70.84	94.63	-95.84	33.59	-11.68	93.49	25.00
66	414.32	-347.52	185.41	-152.05	417.75	-453.07	193.82	-116.88	228.91	-195.47	223.93	-336.19
67	37.16	-95.56	15.05	-23.46	28.80	-100.55	15.71	-14.44	22.11	-72.10	13.09	-86.11
68	22.50	-70.72	9.91	-31.85	59.37	-144.47	13.59	-25.63	12.59	-38.87	45.78	-118.83
69	331.70	-154.55	96.73	-71.08	162.43	-96.74	92.75	-52.97	234.96	-83.47	69.68	-43.78
70	59.95	-21.08	29.36	-12.12	76.10	-32.37	6.17	-2.81	30.59	-8.96	69.93	-29.55

Table E.22. Maximum ($\epsilon 1$) and minimum ($\epsilon 3$) principal strain values at the location of 70 landmarks during first incisor (I1) bite load for the models of a durophagous, a graminivorous and *Macaca* species, and strain differences ($\Delta\epsilon 1$ and $\Delta\epsilon 3$) at landmark locations between the two models. Strain values are in microstrain (μstrain).

I1 bite landmark	Cerrocebus		Theropithecus		Cerrocebus-Theropithecus		Macaca fascicularis	
	$\epsilon 1$	$\epsilon 3$	$\epsilon 1$	$\epsilon 3$	$\Delta\epsilon 1$	$\Delta\epsilon 3$	$\epsilon 1$	$\epsilon 3$
1	511.69	-672.17	646.29	-552.11	-134.60	-120.06	310.42	-583.26
2	628.19	-376.16	208.52	-109.23	419.67	-266.93	442.05	-182.16
3	980.40	-272.94	266.00	-96.64	714.40	-176.29	38.45	-97.38
4	151.60	-399.15	52.97	-235.65	98.64	-163.51	134.86	-437.00
5	22.71	-43.94	59.08	-18.98	-36.38	-24.96	75.85	-24.57
6	49.58	-17.26	32.80	-99.76	16.78	82.50	37.57	-73.66
7	2.15	-1.05	2.14	-0.85	0.01	-0.20	8.55	-3.60
8	59.50	-46.18	217.62	-70.22	-158.12	24.04	54.38	-24.43
9	158.86	-249.21	153.01	-324.59	5.85	75.37	91.64	-95.31
10	61.43	-27.62	19.85	-14.72	41.57	-12.91	255.61	-79.12
11	178.19	-629.68	167.55	-489.47	10.64	-140.21	151.73	-532.50
12	307.09	-162.59	265.55	-158.28	41.55	-4.31	419.89	-154.09
13	275.53	-83.70	23.13	-51.89	252.40	-31.81	144.27	-44.18
14	134.68	-48.31	222.93	-117.64	-88.26	69.33	143.65	-77.60
15	222.70	-79.11	149.83	-97.46	72.87	18.36	83.05	-54.18
16	68.05	-23.21	110.40	-53.01	-42.35	29.80	95.22	-39.19
17	43.65	-19.81	102.17	-42.26	-58.52	22.45	47.98	-35.24
18	154.64	-44.07	161.90	-62.75	-7.26	18.68	9.89	-18.29
19	147.25	-64.01	44.85	-94.33	102.39	30.32	298.95	-127.48
20	87.70	-72.09	0.79	-0.14	86.91	-71.95	120.71	-216.57
21	434.19	-145.77	295.63	-88.27	138.56	-57.50	372.94	-115.98
22	121.87	-84.47	224.28	-101.30	-102.41	16.83	183.86	-114.15
23	97.39	-342.43	115.10	-377.12	-17.72	34.69	134.31	-439.12
24	268.26	-336.33	125.98	-386.48	142.27	50.16	65.31	-203.99
25	64.20	-32.69	260.30	-265.86	-196.10	233.17	431.85	-823.53
26	931.55	-272.48	476.56	-203.76	454.99	-68.73	1073.09	-471.38
27	235.65	-426.34	220.30	-391.01	15.35	-35.33	435.77	-897.15
28	193.54	-65.28	342.56	-76.96	-149.02	11.68	228.68	-104.93
29	43.04	-93.35	37.35	-107.10	5.70	13.75	36.82	-114.09
30	29.75	-68.35	39.68	-103.24	-9.92	34.89	142.77	-54.41
31	113.49	-55.90	44.71	-18.17	68.78	-37.73	141.34	-57.13
32	124.63	-365.61	183.21	-647.35	-58.58	281.74	276.04	-828.75
33	380.03	-134.90	126.14	-42.46	253.89	-92.44	449.03	-182.14
34	9.47	-25.92	6.72	-17.70	2.75	-8.22	8.43	-18.69
35	192.17	-197.38	427.56	-134.12	-235.39	-63.26	121.75	-151.46
36	291.88	-611.14	161.31	-74.62	130.57	-536.52	153.80	-167.12
37	1.79	-1.03	13.83	-38.93	-12.04	37.90	16.52	-5.61
38	15.03	-11.97	26.76	-8.52	-11.73	-3.45	94.58	-28.01
39	170.42	-501.43	143.87	-501.44	26.55	0.01	167.41	-464.35
40	578.06	-181.77	227.23	-59.49	350.84	-122.28	1086.34	-257.07
41	275.97	-128.02	127.80	-49.22	148.18	-78.80	201.36	-86.56
42	194.16	-63.31	128.08	-58.33	66.08	-4.98	224.54	-98.86
43	171.66	-55.58	400.62	-97.65	-228.96	42.07	113.32	-100.44
44	123.32	-30.65	333.28	-85.83	-209.96	55.18	96.95	-39.01
45	49.89	-41.71	144.40	-47.59	-94.52	5.88	59.84	-42.87
46	98.13	-58.39	89.11	-42.87	9.02	-15.52	29.39	-36.13
47	122.90	-114.71	146.58	-36.38	-23.67	-78.33	246.99	-130.42
48	68.09	-171.89	5.16	-13.32	62.93	-158.57	97.04	-300.35
49	393.05	-125.02	341.26	-108.51	51.79	-16.51	512.38	-189.01
50	124.36	-93.91	254.82	-89.60	-130.46	-4.30	182.97	-161.48
51	102.75	-349.71	124.96	-385.14	-22.21	35.43	134.49	-517.54
52	1203.18	-286.31	211.00	-230.27	992.19	-56.04	1396.94	-358.52
53	108.02	-70.59	270.84	-455.38	-162.81	384.79	391.12	-397.37
54	815.71	-357.81	465.01	-225.92	350.70	-131.89	1328.88	-378.10
55	225.86	-520.69	114.54	-222.35	111.32	-298.34	333.32	-706.58
56	87.20	-120.58	149.94	-96.57	-62.74	-24.01	235.82	-147.01
57	58.60	-137.25	38.23	-124.15	20.37	-13.10	37.32	-99.45
58	43.15	-66.56	53.52	-111.50	-10.37	44.94	146.79	-48.22
59	121.87	-46.01	25.74	-8.83	96.13	-37.18	135.77	-52.98
60	172.82	-522.74	150.67	-462.22	22.15	-60.52	326.01	-1104.85
61	494.29	-158.98	103.40	-52.50	390.89	-106.47	220.50	-104.01
62	8.01	-21.52	4.22	-11.43	3.78	-10.09	4.61	-16.21
63	681.47	-227.83	350.48	-188.64	330.99	-39.19	622.88	-355.82
64	352.98	-862.32	282.42	-107.88	70.56	-754.44	250.79	-390.35
65	94.21	-171.60	209.70	-573.74	-115.50	402.15	172.24	-156.84
66	314.26	-163.75	248.95	-158.21	65.31	-5.54	539.60	-192.09
67	35.05	-66.91	46.07	-178.52	-11.02	111.62	16.95	-19.15
68	129.36	-120.16	184.64	-562.04	-55.28	441.88	159.02	-152.69
69	446.75	-201.70	225.95	-133.85	220.80	-67.85	806.79	-307.85
70	26.13	-59.38	53.91	-117.58	-27.78	58.20	52.90	-18.56

Table E.23. Maximum ($\epsilon 1$) and minimum ($\epsilon 3$) principal strain values at the location of 70 landmarks during second incisor (I2) bite load for the models of a durophagous, a graminivorous and *Macaca* species, and strain differences ($\Delta\epsilon 1$ and $\Delta\epsilon 3$) at landmark locations between the two models. Strain values are in microstrain (μstrain).

I2 bite landmark	Cerrocebus		Theropithecus		Cerrocebus-Theropithecus		Macaca fascicularis	
	$\epsilon 1$	$\epsilon 3$	$\epsilon 1$	$\epsilon 3$	$\Delta\epsilon 1$	$\Delta\epsilon 3$	$\epsilon 1$	$\epsilon 3$
1	192.44	-348.01	147.64	-397.31	44.79	49.29	158.95	-278.35
2	561.70	-327.76	273.62	-211.46	288.08	-116.31	470.02	-213.53
3	889.70	-245.11	272.14	-100.94	617.56	-144.16	35.53	-83.83
4	149.96	-398.13	51.87	-231.54	98.09	-166.59	132.07	-425.34
5	21.63	-42.32	59.19	-19.01	-37.56	-23.31	71.43	-22.90
6	47.99	-19.03	33.28	-101.32	14.71	82.28	38.00	-73.68
7	1.66	-0.81	2.17	-0.88	-0.51	0.07	9.27	-3.83
8	52.14	-44.88	218.27	-71.04	-166.13	26.16	52.40	-23.23
9	166.13	-256.02	160.63	-337.63	5.50	81.61	102.90	-107.06
10	80.53	-30.02	23.75	-15.70	56.78	-14.32	279.13	-85.33
11	181.46	-640.56	184.50	-547.32	-3.04	-93.24	142.22	-499.51
12	483.26	-369.87	797.07	-523.21	-313.82	153.33	498.43	-260.56
13	365.72	-109.36	12.79	-33.16	352.93	-76.21	137.98	-80.82
14	171.06	-60.09	222.47	-122.54	-51.41	62.44	136.53	-99.98
15	237.59	-88.69	160.55	-105.55	77.04	16.85	32.11	-57.76
16	48.04	-16.80	51.77	-35.72	-3.72	18.92	57.10	-23.27
17	33.85	-14.92	96.08	-42.40	-62.22	27.49	35.34	-34.84
18	194.63	-46.29	196.05	-76.23	-1.42	29.94	9.77	-18.94
19	109.40	-45.70	47.63	-113.45	61.77	67.76	245.71	-104.35
20	82.10	-66.63	0.73	-0.14	81.37	-66.49	114.76	-202.40
21	463.14	-155.28	310.33	-92.77	152.81	-62.52	412.91	-128.00
22	74.72	-89.70	181.80	-90.14	-107.07	0.45	130.49	-110.88
23	105.33	-365.46	118.82	-388.54	-13.49	23.08	149.53	-478.83
24	251.66	-373.83	188.81	-581.47	62.85	207.64	-12.22	-135.41
25	61.55	-36.01	264.10	-272.91	-202.55	236.91	435.91	-873.97
26	945.72	-277.22	501.67	-212.33	444.05	-64.88	1085.01	-475.83
27	225.75	-426.33	223.50	-405.38	2.25	-20.96	435.36	-892.77
28	212.14	-67.56	367.77	-81.13	-155.62	13.57	224.54	-104.69
29	41.12	-87.41	36.86	-105.85	4.26	18.44	30.57	-93.68
30	25.17	-49.49	38.30	-98.67	-13.13	49.18	162.78	-61.84
31	93.68	-55.95	25.01	-12.70	68.67	-43.25	117.89	-48.69
32	114.44	-340.64	184.39	-651.78	-69.94	311.14	278.68	-835.01
33	349.74	-129.48	101.60	-36.78	248.14	-92.69	422.11	-175.14
34	8.03	-22.67	6.72	-17.69	1.31	-4.97	7.10	-16.19
35	194.79	-210.87	426.10	-131.93	-231.32	-78.94	122.13	-151.53
36	281.26	-577.87	155.48	-64.63	125.78	-513.24	152.57	-165.69
37	2.15	-1.44	13.97	-38.42	-11.82	36.98	18.52	-6.35
38	9.59	-16.95	22.44	-8.30	-12.85	-8.65	45.78	-19.26
39	122.20	-354.75	116.57	-407.60	5.63	52.85	123.43	-340.81
40	377.49	-111.89	241.29	-72.36	136.20	-39.52	741.70	-177.07
41	166.88	-89.25	268.20	-41.23	-101.32	-48.02	148.00	-63.11
42	146.86	-66.12	123.71	-61.47	23.15	-4.64	159.71	-80.05
43	134.34	-42.86	349.71	-87.06	-215.36	44.20	95.00	-79.12
44	108.25	-26.94	409.61	-97.19	-301.36	70.25	76.19	-29.77
45	37.26	-32.79	152.04	-48.15	-114.78	15.36	52.82	-32.19
46	73.67	-50.37	62.40	-30.01	11.27	-20.37	28.36	-33.11
47	150.38	-112.54	169.13	-40.76	-18.75	-71.78	261.03	-130.79
48	68.80	-176.67	5.49	-14.19	63.31	-162.48	99.21	-308.04
49	353.31	-112.19	331.08	-105.17	22.24	-7.02	443.30	-163.64
50	172.57	-85.65	276.13	-96.76	-103.57	11.11	218.63	-154.25
51	98.28	-314.94	121.60	-372.06	-23.32	57.12	115.78	-441.68
52	1259.53	-281.32	250.05	-147.65	1009.48	-133.68	1330.29	-340.29
53	107.46	-66.98	264.36	-432.23	-156.90	365.25	384.94	-383.68
54	801.35	-354.05	444.13	-224.23	357.22	-129.82	1319.79	-375.28
55	220.46	-505.30	111.18	-216.52	109.28	-288.78	331.25	-704.03
56	79.00	-96.92	138.81	-78.82	-59.81	-18.09	206.04	-114.13
57	57.24	-135.92	37.99	-123.68	19.25	-12.24	41.62	-111.33
58	45.08	-76.07	54.70	-115.08	-9.62	39.01	124.17	-42.77
59	139.49	-53.46	45.59	-15.10	93.89	-38.36	153.19	-58.53
60	177.48	-537.28	145.71	-445.86	31.77	-91.42	324.10	-1098.17
61	509.64	-163.26	117.51	-52.86	392.13	-110.40	231.78	-106.29
62	8.23	-22.21	4.10	-11.17	4.13	-11.04	5.32	-17.55
63	688.99	-230.35	345.79	-186.96	343.20	-43.39	621.45	-354.66
64	361.94	-885.14	285.14	-112.32	76.80	-772.82	254.25	-396.21
65	70.65	-184.75	223.38	-612.74	-152.73	428.00	128.46	-140.01
66	313.41	-161.65	274.91	-193.37	38.50	31.72	557.14	-200.16
67	50.51	-111.26	131.93	-285.57	-81.43	174.32	34.99	-84.43
68	155.95	-111.43	159.67	-486.77	-3.72	375.34	164.27	-123.82
69	433.24	-200.85	205.31	-107.54	227.93	-93.30	785.69	-290.96
70	61.60	-60.31	63.28	-156.18	-1.69	95.88	59.08	-18.74

Table E.24. Maximum ($\epsilon 1$) and minimum ($\epsilon 3$) principal strain values at the location of 70 landmarks during first premolar (P3) bite load for the models of a durophagous, a graminivorous and *Macaca* species, and strain differences ($\Delta\epsilon 1$ and $\Delta\epsilon 3$) at landmark locations between the two models. Strain values are in microstrain (μstrain).

P3 bite landmark	Cercopithecus		Theropithecus		Cercopithecus-Theropithecus		Macaca fascicularis	
	$\epsilon 1$	$\epsilon 3$	$\epsilon 1$	$\epsilon 3$	$\Delta\epsilon 1$	$\Delta\epsilon 3$	$\epsilon 1$	$\epsilon 3$
1	6.17	-7.74	24.92	-37.60	-18.76	29.85	23.29	-22.45
2	141.43	-32.20	73.76	-147.59	67.67	115.39	136.95	-49.14
3	563.54	-154.45	232.67	-90.58	330.88	-63.87	21.92	-44.90
4	129.72	-353.13	44.21	-197.99	85.52	-155.14	116.55	-348.74
5	15.08	-33.89	55.72	-18.02	-40.63	-15.87	67.94	-22.32
6	48.53	-25.93	35.72	-109.04	12.81	83.11	39.19	-72.52
7	0.41	-0.48	3.38	-1.38	-2.97	0.90	13.26	-5.35
8	50.23	-36.12	199.47	-68.40	-149.24	32.29	48.81	-16.27
9	167.44	-241.04	190.23	-351.20	-22.78	110.16	120.19	-123.57
10	117.24	-44.24	34.46	-19.52	82.78	-24.71	321.52	-98.79
11	81.52	-96.94	73.16	-209.72	8.35	112.78	99.60	-96.14
12	49.97	-42.04	48.73	-44.97	1.24	2.92	15.70	-35.15
13	130.81	-317.42	246.69	-658.09	-115.87	340.67	208.04	-291.28
14	111.72	-49.47	423.89	-966.92	-312.17	917.45	326.73	-854.50
15	148.01	-124.74	322.15	-459.34	-174.15	334.60	231.77	-790.27
16	74.99	-86.43	66.61	-244.02	8.37	157.60	87.02	-218.25
17	11.05	-29.71	54.81	-71.97	-43.76	42.27	31.57	-101.50
18	194.79	-45.04	236.48	-92.54	-41.69	47.50	10.16	-16.61
19	34.43	-24.85	62.25	-140.55	-27.81	115.70	28.79	-22.89
20	66.00	-54.35	0.55	-0.16	65.44	-54.19	91.55	-149.35
21	494.25	-165.15	359.58	-108.33	134.67	-56.82	474.64	-143.95
22	53.50	-169.92	87.29	-70.59	-33.79	-99.34	65.51	-202.87
23	100.99	-345.32	123.35	-403.06	-22.35	57.73	157.66	-496.69
24	161.36	-273.41	262.76	-801.91	-101.40	528.50	28.18	-234.01
25	63.57	-48.63	277.64	-289.48	-214.07	240.85	478.91	-1112.34
26	996.95	-294.11	576.89	-238.89	420.06	-55.21	1133.77	-493.47
27	210.95	-444.13	231.35	-448.01	-20.40	3.89	437.95	-870.26
28	271.92	-91.38	411.10	-86.08	-139.18	-5.30	250.32	-105.93
29	33.29	-66.12	34.31	-98.78	-1.02	32.67	11.65	-22.42
30	24.08	-15.34	32.62	-80.10	-8.54	64.76	197.83	-74.51
31	58.05	-61.93	12.33	-34.70	45.72	-27.23	38.74	-22.14
32	93.25	-286.89	185.44	-656.35	-92.18	369.46	288.39	-856.65
33	276.50	-120.16	47.79	-37.95	228.71	-82.21	325.38	-153.82
34	4.29	-12.53	6.13	-15.91	-1.83	3.37	1.86	-5.57
35	201.55	-244.09	414.50	-125.60	-212.94	-118.49	125.27	-152.62
36	258.12	-505.89	143.07	-38.22	115.05	-467.68	149.54	-165.50
37	3.60	-2.65	13.88	-29.89	-10.28	27.24	26.65	-9.48
38	10.80	-29.67	12.59	-11.06	-1.80	-18.61	25.07	-83.47
39	35.56	-101.81	37.21	-128.30	-1.65	26.48	39.99	-110.10
40	27.95	-15.28	81.12	-21.51	-53.17	6.24	200.73	-46.86
41	37.88	-24.46	236.85	-75.35	-198.96	50.89	58.56	-24.74
42	49.39	-24.12	50.53	-38.78	-1.14	14.66	62.23	-28.44
43	50.08	-15.99	108.15	-36.04	-58.06	20.05	34.34	-27.48
44	38.86	-8.78	289.04	-61.07	-250.18	52.29	17.30	-12.01
45	11.39	-20.49	99.21	-28.92	-87.82	8.43	41.72	-21.27
46	44.84	-36.53	12.46	-5.99	32.38	-30.54	24.81	-25.33
47	139.41	-76.35	192.07	-45.16	-52.66	-31.20	294.95	-125.92
48	65.31	-178.93	5.84	-15.11	59.48	-163.82	102.48	-319.89
49	281.96	-89.16	280.86	-89.48	1.10	0.32	282.91	-105.05
50	238.03	-88.88	309.20	-108.51	-71.17	19.63	302.88	-147.07
51	88.49	-243.38	99.35	-292.82	-10.86	49.44	87.48	-248.08
52	918.22	-193.90	311.10	-117.41	607.11	-76.48	846.10	-215.36
53	108.57	-69.51	259.98	-415.41	-151.42	345.89	367.60	-388.42
54	807.32	-358.85	425.95	-222.53	381.37	-136.32	1308.25	-371.66
55	223.37	-512.29	109.00	-206.69	114.37	-305.60	330.46	-698.58
56	86.32	-54.08	110.90	-44.72	-24.58	-9.36	125.27	-51.52
57	51.77	-125.41	33.85	-110.51	17.91	-14.90	50.76	-135.64
58	45.89	-82.98	52.18	-114.38	-6.29	31.40	72.11	-33.50
59	148.69	-57.68	91.93	-30.13	56.76	-27.54	187.67	-64.90
60	179.80	-545.45	135.23	-409.95	44.57	-135.50	320.63	-1085.64
61	508.89	-162.90	139.67	-54.32	369.22	-108.57	251.62	-110.31
62	7.31	-19.79	3.35	-9.14	3.96	-10.65	6.52	-18.53
63	671.82	-224.66	329.22	-180.21	342.60	-44.45	614.13	-351.32
64	367.36	-897.26	288.86	-119.34	78.49	-777.93	260.27	-406.74
65	112.50	-155.05	170.98	-530.47	-58.48	375.42	144.49	-97.19
66	302.93	-151.58	333.81	-289.24	-30.88	137.66	611.16	-276.80
67	211.27	-320.96	360.85	-539.38	-149.58	218.42	200.85	-300.49
68	104.95	-61.60	90.40	-271.88	14.54	210.29	106.17	-54.97
69	398.40	-192.19	169.17	-73.68	229.23	-118.51	741.71	-261.96
70	26.42	-12.17	136.65	-157.82	-110.23	145.65	17.23	-10.10

Table E.25. Maximum ($\epsilon 1$) and minimum ($\epsilon 3$) principal strain values at the location of 70 landmarks during second premolar (P4) bite load for the models of a durophagous, a graminivorous and *Macaca* species, and strain differences ($\Delta \epsilon 1$ and $\Delta \epsilon 3$) at landmark locations between the two models. Strain values are in microstrain (μ strain).

P4 bite landmark	Cercopithecus		Theropithecus		Cercopithecus-Theropithecus		Macaca fascicularis	
	$\epsilon 1$	$\epsilon 3$	$\epsilon 1$	$\epsilon 3$	$\Delta \epsilon 1$	$\Delta \epsilon 3$	$\epsilon 1$	$\epsilon 3$
1	7.63	-6.83	18.07	-31.83	-10.44	25.00	23.34	-18.46
2	141.58	-31.51	55.65	-136.71	85.92	105.20	115.46	-43.17
3	519.63	-141.40	216.65	-85.15	302.98	-56.25	19.09	-39.48
4	120.53	-330.68	42.09	-188.24	78.44	-142.44	110.93	-320.98
5	12.97	-30.50	54.81	-17.79	-41.83	-12.71	68.77	-24.37
6	49.06	-27.89	36.39	-111.16	12.67	83.26	39.74	-72.17
7	0.76	-1.04	3.72	-1.52	-2.96	0.48	14.62	-5.88
8	51.75	-33.21	194.83	-68.22	-143.08	35.01	50.52	-19.39
9	162.41	-231.45	197.41	-335.68	-35.00	104.24	113.87	-115.77
10	125.17	-47.42	37.57	-20.79	87.60	-26.63	327.59	-101.25
11	77.68	-68.78	58.11	-142.49	19.57	73.71	94.25	-72.26
12	49.37	-50.21	42.27	-38.65	7.10	-11.56	17.86	-45.45
13	36.64	-106.59	50.70	-116.72	-14.07	10.13	78.53	-101.31
14	85.45	-174.62	291.26	-399.59	-205.80	224.97	164.88	-558.33
15	128.07	-162.24	308.18	-1197.92	-180.11	1035.68	404.73	-1632.31
16	90.34	-111.20	104.33	-373.43	-13.99	262.24	188.29	-457.10
17	20.22	-53.70	63.47	-109.82	-43.25	56.11	60.62	-213.24
18	154.01	-41.05	245.34	-96.23	-91.33	55.18	10.59	-16.21
19	40.02	-44.91	68.10	-145.97	-28.08	101.06	46.31	-98.93
20	61.33	-50.80	0.54	-0.18	60.79	-50.62	84.47	-133.01
21	504.53	-168.53	372.26	-112.39	132.27	-56.15	469.39	-141.76
22	57.76	-194.69	66.87	-70.85	-9.11	-123.84	75.49	-260.68
23	96.37	-328.59	124.28	-406.41	-27.91	77.82	151.78	-479.64
24	144.96	-241.25	261.73	-797.17	-116.76	555.91	21.16	-193.87
25	65.72	-51.73	281.55	-293.63	-215.83	241.90	503.07	-1203.05
26	1011.43	-298.79	597.43	-246.28	414.01	-52.51	1152.39	-499.90
27	210.19	-451.15	233.50	-459.44	-23.31	8.29	441.25	-863.65
28	289.78	-99.82	418.43	-86.45	-128.65	-13.37	264.72	-105.59
29	31.36	-60.90	33.54	-96.60	-2.18	35.70	18.42	-12.02
30	29.98	-13.40	31.09	-74.71	-1.11	61.31	202.05	-75.89
31	52.24	-65.14	15.41	-47.62	36.83	-17.52	26.83	-20.64
32	89.94	-276.54	185.68	-657.42	-95.74	380.88	291.47	-863.17
33	261.00	-119.21	41.59	-46.47	219.41	-72.75	295.42	-149.31
34	3.39	-9.36	6.00	-15.43	-2.61	6.07	0.98	-2.41
35	203.08	-251.30	411.54	-124.46	-208.46	-126.85	126.45	-153.06
36	253.44	-491.50	140.54	-31.50	112.90	-460.00	149.42	-166.42
37	3.96	-2.95	14.29	-27.88	-10.33	24.94	28.62	-10.24
38	11.29	-31.26	11.26	-13.05	0.03	-18.22	29.44	-103.26
39	30.90	-88.59	29.63	-100.66	1.27	12.07	32.57	-89.65
40	24.93	-22.01	72.51	-18.52	-47.57	-3.49	158.50	-36.79
41	31.51	-19.88	214.57	-74.14	-183.06	54.25	46.60	-19.75
42	40.68	-18.59	40.67	-34.95	0.01	16.36	47.09	-22.03
43	41.10	-13.03	79.00	-37.28	-37.90	24.25	26.53	-20.66
44	30.41	-7.32	249.43	-51.05	-219.01	43.73	13.25	-12.90
45	9.89	-20.50	87.11	-24.78	-77.22	4.28	41.18	-23.27
46	41.70	-34.73	6.78	-3.35	34.93	-31.38	24.13	-23.91
47	126.76	-70.31	192.07	-46.19	-65.31	-24.12	308.32	-126.83
48	63.95	-178.26	5.89	-15.27	58.06	-162.98	103.34	-322.96
49	275.55	-87.13	264.98	-84.50	10.57	-2.63	256.04	-95.07
50	245.22	-90.26	314.57	-110.61	-69.35	20.35	322.72	-148.43
51	85.55	-225.33	92.35	-267.72	-6.80	42.40	86.54	-210.20
52	843.15	-178.22	307.64	-117.14	535.51	-61.08	722.80	-183.77
53	109.14	-70.77	260.30	-415.96	-151.16	345.19	363.67	-389.38
54	810.74	-360.62	424.37	-222.13	386.37	-138.49	1305.12	-370.67
55	225.18	-517.18	109.01	-204.56	116.17	-312.63	330.09	-697.18
56	85.86	-51.68	105.05	-39.74	-19.19	-11.94	112.91	-45.91
57	51.13	-124.24	32.41	-105.91	18.72	-18.32	52.95	-141.33
58	46.07	-83.49	51.08	-113.38	-5.01	29.90	63.78	-33.06
59	147.51	-57.31	102.68	-33.64	44.83	-23.67	195.37	-65.47
60	179.98	-546.32	132.71	-401.15	47.26	-145.18	319.96	-1083.17
61	505.76	-161.97	144.14	-54.70	361.62	-107.28	256.86	-111.48
62	6.87	-18.62	3.15	-8.60	3.72	-10.02	6.82	-18.67
63	665.42	-222.51	324.54	-178.23	340.87	-44.29	612.75	-350.69
64	367.65	-897.33	289.55	-120.80	78.10	-776.53	261.94	-409.73
65	117.67	-128.92	145.21	-479.42	-27.54	350.50	144.82	-83.83
66	300.75	-149.21	348.71	-318.42	-47.96	169.21	627.65	-305.92
67	199.00	-283.75	295.75	-509.72	-96.75	225.97	168.62	-254.50
68	97.88	-57.86	82.76	-243.30	15.12	185.44	91.65	-46.89
69	392.79	-190.70	162.16	-68.57	230.63	-122.13	732.13	-256.53
70	21.83	-9.04	141.48	-155.76	-119.65	146.71	12.05	-7.79

Table E.26. Maximum ($\epsilon 1$) and minimum ($\epsilon 3$) principal strain values at the location of 70 landmarks during first molar (M1) bite load for the models of a durophagous, a graminivorous and *Macaca* species, and strain differences ($\Delta\epsilon 1$ and $\Delta\epsilon 3$) at landmark locations between the two models. Strain values are in microstrain (μstrain).

M1 bite landmark	Cercopithecus		Theropithecus		Cercopithecus-Theropithecus		Macaca fascicularis	
	$\epsilon 1$	$\epsilon 3$	$\epsilon 1$	$\epsilon 3$	$\Delta\epsilon 1$	$\Delta\epsilon 3$	$\epsilon 1$	$\epsilon 3$
1	6.11	-6.06	3.30	-9.60	2.81	3.54	39.57	-16.41
2	97.20	-21.25	11.12	-30.54	86.08	9.29	143.62	-59.99
3	406.48	-111.44	186.56	-72.97	219.93	-38.48	19.99	-44.09
4	106.70	-299.00	37.92	-168.81	68.77	-130.19	101.90	-287.05
5	14.55	-25.55	52.95	-17.22	-38.39	-8.33	69.92	-24.14
6	51.38	-34.48	37.36	-114.16	14.02	79.67	39.09	-70.92
7	1.36	-2.05	4.46	-1.81	-3.10	-0.23	16.11	-6.49
8	56.14	-28.85	181.47	-65.45	-125.33	36.60	47.87	-23.94
9	150.06	-199.67	188.66	-303.31	-38.60	103.64	110.41	-120.62
10	146.78	-56.13	39.79	-22.06	106.99	-34.07	328.08	-101.38
11	64.77	-42.29	48.75	-26.86	16.02	-15.43	91.46	-56.35
12	34.15	-41.29	2.34	-4.48	31.81	-36.81	32.88	-60.53
13	24.23	-70.10	21.30	-41.49	2.94	-28.61	26.86	-23.22
14	41.06	-75.73	98.45	-60.77	-57.39	-14.96	42.81	-131.13
15	206.76	-417.71	132.15	-79.95	74.61	-337.76	147.77	-589.02
16	175.74	-205.02	65.29	-247.18	110.45	42.17	241.80	-568.63
17	59.39	-133.24	53.59	-107.81	5.80	-25.43	66.71	-234.51
18	115.37	-23.83	187.22	-72.89	-71.85	49.07	10.34	-13.96
19	56.31	-95.39	78.87	-155.23	-22.56	59.85	69.44	-170.60
20	52.01	-42.86	0.54	-0.19	51.48	-42.68	81.49	-123.54
21	505.35	-168.97	402.15	-121.96	103.20	-47.01	464.07	-141.13
22	80.73	-271.42	62.62	-72.79	18.11	-198.63	77.44	-268.64
23	91.07	-304.06	122.86	-402.91	-31.79	98.85	139.86	-448.89
24	112.57	-195.46	198.83	-604.91	-86.26	409.45	-0.09	-138.47
25	66.76	-59.96	282.14	-290.67	-215.39	230.71	505.97	-1217.28
26	1043.01	-309.21	606.46	-249.77	436.55	-59.44	1157.05	-502.44
27	210.84	-467.48	234.15	-465.30	-23.31	-2.18	442.94	-861.10
28	314.85	-111.81	428.07	-86.71	-113.22	-25.10	265.07	-104.44
29	26.77	-47.33	33.22	-95.65	-6.45	48.32	22.45	-12.06
30	52.94	-16.72	29.31	-68.18	23.63	51.46	205.91	-77.31
31	45.34	-81.71	15.48	-48.64	29.86	-33.08	28.56	-18.09
32	83.73	-247.85	185.35	-656.37	-101.62	408.52	292.47	-865.49
33	224.57	-118.05	40.16	-51.94	184.41	-66.11	287.30	-148.56
34	1.90	-3.75	5.65	-14.24	-3.75	10.48	1.22	-1.61
35	207.35	-270.35	407.86	-123.33	-200.50	-147.02	126.93	-153.25
36	241.65	-454.54	139.60	-28.83	102.05	-425.71	149.53	-166.69
37	4.99	-3.68	14.77	-23.60	-9.78	19.92	32.49	-11.81
38	13.17	-37.89	9.99	-14.34	3.18	-23.55	28.00	-95.38
39	22.00	-62.89	21.93	-73.66	0.07	10.77	30.83	-84.59
40	16.06	-17.39	19.51	-8.24	-3.45	-9.15	133.69	-30.69
41	22.41	-14.04	111.86	-39.29	-89.45	25.25	45.34	-18.86
42	28.11	-10.99	19.06	-20.21	9.06	9.21	46.72	-19.38
43	27.87	-8.82	35.68	-27.43	-7.82	18.61	23.34	-18.37
44	17.30	-6.34	140.04	-27.32	-122.74	20.98	11.40	-13.24
45	8.49	-20.29	59.34	-16.32	-50.85	-3.97	40.52	-23.65
46	34.37	-30.38	9.62	-4.79	24.75	-25.59	23.02	-22.77
47	125.68	-63.35	175.23	-42.16	-49.55	-21.19	285.23	-117.70
48	62.78	-179.62	5.64	-14.61	57.14	-165.01	101.16	-314.23
49	250.83	-79.34	247.86	-79.38	2.97	0.03	275.88	-102.57
50	278.16	-97.62	305.14	-107.55	-26.98	9.94	314.10	-146.42
51	84.69	-197.37	80.44	-226.45	4.26	29.08	83.88	-184.10
52	687.83	-144.38	247.26	-93.30	440.57	-51.08	710.16	-179.82
53	110.16	-71.54	267.10	-439.85	-156.93	368.32	360.86	-410.02
54	807.50	-360.74	442.85	-222.80	364.65	-137.94	1312.36	-372.87
55	225.01	-516.43	112.95	-206.98	112.05	-309.46	333.11	-698.35
56	76.74	-43.83	103.47	-41.06	-26.73	-2.77	122.80	-52.00
57	50.37	-123.22	29.97	-97.80	20.40	-25.42	52.23	-139.41
58	48.08	-88.69	47.91	-108.29	0.17	19.61	64.54	-32.48
59	152.20	-59.51	104.34	-34.13	47.86	-25.38	193.75	-61.71
60	182.49	-554.60	133.15	-401.87	49.34	-152.73	321.28	-1087.51
61	509.43	-162.89	135.66	-53.23	373.77	-109.66	249.56	-109.50
62	6.45	-17.53	2.89	-7.71	3.56	-9.81	6.15	-16.14
63	660.33	-220.80	320.15	-176.01	340.18	-44.80	610.98	-350.72
64	372.60	-908.73	287.45	-116.74	85.15	-791.99	259.91	-406.33
65	122.64	-120.98	134.05	-395.60	-11.41	274.62	136.08	-61.70
66	292.17	-143.93	347.03	-319.17	-54.87	175.24	623.59	-300.32
67	155.04	-253.24	165.55	-296.48	-10.51	43.24	131.88	-142.38
68	82.25	-48.90	82.94	-241.86	-0.69	192.96	92.42	-44.26
69	380.21	-188.92	169.16	-83.08	211.05	-105.84	734.85	-261.13
70	18.47	-6.13	98.25	-99.35	-79.78	93.22	15.01	-9.17

Table E.27. Maximum ($\epsilon 1$) and minimum ($\epsilon 3$) principal strain values at the location of 70 landmarks during second molar (M2) bite load for the models of a durophagous, a graminivorous and *Macaca* species, and strain differences ($\Delta\epsilon 1$ and $\Delta\epsilon 3$) at landmark locations between the two models. Strain values are in microstrain (μstrain).

M2 bite landmark	Cerocebus		Theropithecus		Cerocebus-Theropithecus		Macaca fascicularis	
	$\epsilon 1$	$\epsilon 3$	$\epsilon 1$	$\epsilon 3$	$\Delta\epsilon 1$	$\Delta\epsilon 3$	$\epsilon 1$	$\epsilon 3$
1	11.20	-8.76	3.44	-5.75	7.76	-3.01	45.32	-12.74
2	129.71	-28.01	12.34	-18.20	117.37	-9.82	149.78	-60.66
3	371.42	-98.75	124.32	-49.41	247.10	-49.34	17.33	-40.57
4	86.09	-244.42	32.13	-133.82	53.96	-110.60	85.43	-212.32
5	15.98	-16.43	50.56	-16.69	-34.58	0.27	67.63	-23.90
6	52.11	-36.54	39.46	-120.79	12.66	84.25	38.91	-69.44
7	2.34	-3.67	5.73	-2.33	-3.39	-1.34	19.84	-8.00
8	58.51	-22.68	166.41	-66.17	-107.90	43.48	49.19	-43.09
9	125.67	-184.92	151.09	-209.28	-25.42	24.36	78.32	-103.17
10	152.26	-58.19	48.59	-25.97	103.68	-32.22	319.95	-99.35
11	65.42	-25.15	54.71	-23.63	10.71	-1.52	71.15	-37.06
12	49.74	-58.22	4.15	-3.67	45.59	-54.55	38.99	-52.83
13	3.32	-2.83	6.60	-20.02	-3.28	17.19	29.14	-20.66
14	2.56	-6.08	25.31	-14.57	-22.74	8.49	17.45	-7.67
15	36.26	-100.30	58.67	-36.61	-22.41	-63.68	21.59	-8.34
16	49.58	-124.00	14.50	-12.23	35.09	-111.77	87.94	-199.13
17	86.13	-204.99	73.74	-175.11	12.39	-29.88	197.84	-696.71
18	14.17	-74.42	97.91	-37.51	-83.74	-36.91	12.21	-9.13
19	82.45	-126.41	100.78	-184.85	-18.33	58.43	146.24	-390.87
20	43.21	-36.64	0.60	-0.27	42.61	-36.37	72.20	-95.66
21	532.49	-178.30	459.14	-140.20	73.34	-38.10	442.10	-138.58
22	85.50	-286.05	39.24	-101.47	46.26	-184.58	87.43	-310.11
23	83.45	-269.86	122.01	-402.31	-38.56	132.45	116.80	-384.10
24	95.07	-146.93	147.68	-446.27	-52.61	299.34	2.68	-91.01
25	76.16	-63.93	286.50	-292.73	-210.34	228.79	531.37	-1318.13
26	1069.07	-317.26	654.20	-267.31	414.87	-49.95	1183.96	-513.93
27	214.47	-483.44	239.17	-489.67	-24.70	6.23	451.51	-852.69
28	348.07	-127.80	469.36	-91.82	-121.28	-35.97	213.62	-95.67
29	24.39	-41.76	31.43	-90.58	-7.04	48.83	43.03	-16.46
30	64.70	-20.60	25.41	-51.45	39.29	30.85	205.11	-76.82
31	42.34	-86.88	25.63	-79.02	16.70	-7.86	40.03	-28.59
32	82.85	-240.29	186.76	-661.68	-103.91	421.39	296.31	-873.32
33	208.09	-119.77	42.15	-87.58	165.94	-32.19	251.76	-146.68
34	3.51	-3.79	5.42	-12.57	-1.90	8.78	9.47	-5.27
35	209.03	-278.64	404.80	-122.44	-195.77	-156.20	128.70	-153.91
36	236.85	-440.27	134.90	-13.45	101.95	-426.82	149.90	-168.49
37	5.61	-4.01	17.78	-18.32	-12.17	14.31	43.18	-16.19
38	13.05	-36.99	9.52	-21.72	3.53	-15.27	31.53	-110.19
39	15.57	-45.13	11.72	-35.26	3.84	-9.88	21.32	-58.26
40	23.36	-37.54	8.68	-12.19	14.68	-25.35	87.34	-20.25
41	20.83	-10.58	56.00	-23.20	-35.17	12.62	40.54	-15.98
42	20.33	-5.86	6.85	-11.47	13.47	5.61	42.51	-15.02
43	19.91	-6.72	13.49	-29.08	6.42	22.37	15.89	-12.50
44	8.52	-4.80	51.00	-8.70	-42.48	3.90	10.00	-15.95
45	8.23	-19.54	31.97	-7.99	-23.74	-11.55	38.27	-25.34
46	30.96	-27.68	6.70	-3.63	24.26	-24.05	20.31	-19.66
47	88.18	-53.23	166.20	-43.97	-78.02	-9.26	262.68	-106.46
48	58.95	-174.47	5.56	-14.42	53.39	-160.04	98.39	-302.00
49	250.27	-79.10	208.75	-67.25	41.52	-11.85	266.94	-99.41
50	271.93	-95.82	307.39	-109.12	-35.46	13.30	325.72	-145.63
51	78.46	-157.88	59.01	-143.90	19.45	-13.98	95.56	-137.01
52	580.26	-123.48	191.13	-72.15	389.13	-51.33	567.75	-143.10
53	111.59	-75.49	273.08	-460.25	-161.48	384.76	354.33	-436.21
54	825.81	-367.93	454.95	-222.74	370.86	-145.20	1319.78	-375.16
55	232.61	-537.49	116.46	-206.04	116.15	-331.44	337.14	-699.18
56	86.65	-42.49	94.76	-36.32	-8.11	-6.17	119.44	-50.12
57	48.59	-119.23	25.40	-82.87	23.18	-36.36	53.96	-143.99
58	46.58	-85.21	43.81	-102.92	2.77	17.71	56.58	-31.43
59	143.00	-55.72	125.16	-40.85	17.84	-14.87	203.65	-64.47
60	180.01	-547.56	129.00	-386.82	51.01	-160.74	322.13	-1089.94
61	492.97	-158.27	137.08	-52.73	355.88	-105.54	243.74	-107.76
62	5.09	-13.86	2.44	-6.15	2.65	-7.71	5.71	-12.27
63	640.50	-214.12	308.44	-170.71	332.07	-43.42	606.81	-349.91
64	368.06	-895.63	287.04	-116.32	81.02	-779.31	258.25	-403.55
65	102.82	-62.79	157.91	-232.07	-55.09	169.28	94.76	-62.86
66	294.43	-141.77	378.86	-381.79	-84.43	240.03	628.54	-299.71
67	93.51	-149.72	60.25	-186.83	33.26	37.11	73.99	-44.40
68	72.84	-41.26	73.98	-201.72	-1.14	160.46	79.12	-31.34
69	372.27	-185.32	163.40	-86.20	208.87	-99.12	730.15	-261.08
70	15.26	-8.17	91.52	-68.62	-76.26	60.46	22.27	-11.12

Table E.28. Maximum ($\epsilon 1$) and minimum ($\epsilon 3$) principal strain values at the location of 70 landmarks during third molar (M3) bite load for the models of a durophagous, a graminivorous and *Macaca* species, and strain differences ($\Delta\epsilon 1$ and $\Delta\epsilon 3$) at landmark locations between the two models. Strain values are in microstrain (μstrain).

M3 bite landmark	Cerocebus		Theropithecus		Cerocebus-Theropithecus		Macaca fascicularis	
	$\epsilon 1$	$\epsilon 3$	$\epsilon 1$	$\epsilon 3$	$\Delta\epsilon 1$	$\Delta\epsilon 3$	$\epsilon 1$	$\epsilon 3$
1	14.19	-11.53	11.68	-11.03	2.51	-0.49	44.72	-11.39
2	130.49	-28.29	35.16	-30.62	95.33	2.34	143.05	-54.06
3	294.34	-76.37	43.75	-19.27	250.58	-57.10	13.99	-34.43
4	70.46	-175.23	39.85	-91.84	30.60	-83.39	73.21	-126.70
5	16.82	-6.97	47.12	-16.06	-30.30	9.09	62.08	-21.52
6	53.73	-40.46	42.49	-130.32	11.24	89.86	38.23	-67.57
7	3.88	-6.21	7.70	-3.13	-3.83	-3.08	24.77	-10.00
8	62.92	-44.16	152.90	-74.63	-89.98	30.46	54.50	-72.87
9	85.84	-170.06	58.65	-115.08	27.19	-54.98	40.75	-70.01
10	157.43	-60.14	59.70	-31.02	97.72	-29.12	302.37	-93.92
11	58.05	-17.42	16.56	-7.27	41.49	-10.15	53.03	-22.52
12	52.05	-58.51	9.89	-5.43	42.16	-53.08	42.62	-40.51
13	44.93	-13.70	2.06	-5.84	42.87	-7.87	34.22	-28.40
14	25.70	-11.28	17.18	-10.76	8.53	-0.52	41.88	-31.28
15	11.71	-27.90	20.86	-17.22	-9.15	-10.69	17.04	-37.72
16	48.68	-60.22	29.74	-9.82	18.94	-50.40	51.32	-129.52
17	30.57	-77.65	17.59	-21.43	12.98	-56.22	167.42	-246.85
18	109.18	-975.79	109.64	-157.89	-0.46	-817.90	119.13	-36.81
19	139.23	-185.28	126.07	-215.64	13.16	30.36	236.22	-678.40
20	29.59	-26.07	0.70	-0.44	28.89	-25.63	67.70	-70.43
21	553.70	-185.97	545.72	-167.93	7.98	-18.04	446.07	-144.44
22	90.97	-302.17	45.66	-170.57	45.31	-131.60	85.41	-303.59
23	77.19	-230.79	118.73	-395.60	-41.53	164.81	90.21	-302.92
24	69.95	-89.04	75.16	-221.31	-5.21	132.27	26.82	-79.05
25	91.82	-72.99	284.74	-287.28	-192.92	214.29	555.27	-1422.79
26	1107.89	-329.39	710.93	-288.56	396.97	-40.83	1206.68	-525.35
27	222.16	-510.91	244.29	-511.53	-22.13	0.62	464.24	-847.07
28	383.02	-145.04	542.86	-115.59	-159.84	-29.45	163.51	-90.44
29	20.40	-32.84	29.42	-84.66	-9.02	51.82	49.92	-18.32
30	81.21	-26.38	24.15	-31.88	57.06	5.50	197.22	-73.83
31	41.85	-97.40	38.89	-114.16	2.96	16.76	56.35	-26.08
32	81.74	-227.99	190.02	-673.49	-108.28	445.50	301.42	-884.88
33	184.65	-123.47	53.91	-137.63	130.74	14.16	221.95	-148.86
34	14.31	-8.23	5.77	-10.54	8.54	2.31	20.08	-9.93
35	211.90	-291.26	408.88	-123.67	-196.98	-167.59	132.77	-155.80
36	230.59	-422.17	130.86	2.98	99.73	-425.14	148.34	-170.91
37	7.12	-4.42	25.63	-13.70	-18.51	9.28	59.74	-23.10
38	13.76	-38.21	11.33	-32.97	2.43	-5.24	36.12	-129.77
39	6.24	-19.20	14.14	-8.60	-7.91	-10.59	10.70	-28.82
40	25.64	-48.83	4.28	-17.33	21.36	-31.49	45.36	-12.14
41	20.58	-8.05	10.75	-8.91	9.83	0.86	40.40	-14.27
42	15.49	-5.15	3.88	-7.82	11.61	2.66	46.63	-15.59
43	14.50	-6.77	5.83	-22.11	8.67	15.34	9.84	-9.95
44	2.62	-2.60	6.53	-19.92	-3.91	17.32	12.36	-21.02
45	7.04	-15.92	8.79	-3.39	-1.75	-12.52	34.35	-26.31
46	25.10	-22.76	6.74	-3.75	18.35	-19.01	15.95	-15.21
47	48.40	-41.31	162.99	-46.34	-114.58	5.03	221.34	-89.41
48	54.14	-165.99	5.37	-13.96	48.77	-152.03	93.62	-280.47
49	238.12	-75.11	163.65	-53.30	74.48	-21.81	260.32	-97.19
50	276.19	-96.10	309.54	-110.85	-33.35	14.75	337.24	-143.95
51	78.94	-108.78	50.78	-53.18	28.16	-55.60	134.00	-112.00
52	407.88	-88.96	104.32	-37.73	303.56	-51.23	419.84	-105.11
53	113.53	-80.16	280.32	-485.70	-166.79	405.54	348.94	-472.61
54	850.09	-377.57	474.93	-223.54	375.16	-154.03	1333.02	-379.41
55	242.27	-564.39	121.57	-207.84	120.70	-356.55	343.57	-701.91
56	101.89	-38.76	84.98	-33.34	16.91	-5.42	117.75	-50.18
57	45.62	-112.61	19.66	-63.84	25.96	-48.77	56.05	-149.64
58	44.98	-82.19	39.27	-96.79	5.70	14.60	47.51	-30.10
59	133.88	-51.78	150.10	-48.84	-16.22	-2.94	218.25	-76.94
60	176.67	-538.02	125.03	-372.07	51.64	-165.95	323.30	-1093.17
61	473.57	-152.84	135.15	-51.58	338.42	-101.26	231.84	-104.61
62	3.11	-8.55	2.27	-4.38	0.84	-4.16	6.47	-7.60
63	614.62	-205.40	295.52	-164.79	319.10	-40.61	600.75	-348.73
64	363.09	-880.82	285.65	-113.88	77.44	-766.94	254.40	-396.77
65	64.83	-28.60	188.12	-70.84	-123.29	42.24	78.00	-54.73
66	295.86	-138.32	417.75	-453.07	-121.90	314.75	624.16	-273.89
67	46.07	-74.91	28.80	-100.55	17.27	25.64	47.29	-19.48
68	55.20	-26.74	59.37	-144.47	-4.17	117.72	66.69	-25.34
69	360.21	-180.81	162.43	-96.74	197.78	-84.07	729.56	-262.90
70	19.17	-11.51	76.10	-32.37	-56.93	20.86	32.12	-14.41